

i|C|P|S 19

International Conference on Polygeneration Strategies

PROCEEDINGS



TECHNISCHE
UNIVERSITÄT
WIEN
Vienna | Austria



November 18 – 20 | 2019
Vienna | Austria
www.icps-conference.org

International Conference on Polygerneration Strategies 19

18th of November to 20th of November 2019
Schönbrunn Palace | Apothecaries' Wing
Vienna, Austria

Proceedings

Hermann Hofbauer · Stefan Müller
Editors

Proceedings of the ICPS 19

International Conference on Polygerneration Strategies 19

18th of November to 20th of November 2019

Schönbrunn Palace | Apothecaries' Wing
Vienna, Austria

2nd Edition 2019



TECHNISCHE
UNIVERSITÄT
WIEN
Vienna | Austria



Univ. Prof. Dipl.-Ing. Dr. Hermann Hofbauer
hermann.hofbauer@tuwien.ac.at

Dipl.-Ing. Dr. Stefan Müller
stefan.mueller@tuwien.ac.at

Technische Universität Wien
Institut für Verfahrenstechnik, Umwelttechnik und technische Biowissenschaften
Zukunftsfähige Energietechnik

TU Wien
Institute of Chemical, Environmental and Bioscience Engineering
Future Energy Technology

Getreidemarkt 9/166
1060 Vienna
Austria

ISBN: 978-3-9503671-1-9

© Technische Universität Wien

© Verein zur Förderung zukunftsfähiger Energietechnik auf Basis der Poly-generationsstrategie aus Biomasse

ZVR-Zahl: 384062498

Getreidemarkt 9/166
1060 Vienna
Austria

Cover Design: DerHiasl

Preface



The ICPS series started 10 years ago with four successful conferences in a row showing the possibilities of polygeneration concepts for an efficient use of biomass to generate various bio-products via gasification. After a break of 6 years it is now urgently necessary to show again the progress made in these years in this field. The introduction to the first conference is still valid and today even much more important:

"Biomass gasification is a key technology for biomass utilization in the future. By conversion of solid biomass into a product gas or syngas all important energy forms currently used in our energy system can be produced: heat, electricity, synthetic biofuels, and chemicals. [...] Syngas production, syngas cleaning and syngas utilization are subject of large research programs in several countries worldwide and enormous progress have been achieved in this field in the recent years."

This was the statement 10 years ago and it is valid even more today. The climate targets set in the Paris Agreement need urgent actions and gasification based polygeneration can help to mitigate these problems. Now we are interested in the outcome and the results of the scientific research as well as in the experience gained from industrial implementations in the last years.

The trend in the last years are characterized by the use of bio-waste, application of different gasification agents (among those also CO₂), advanced gasifier design, optimized gas cleaning and upgrading systems, and a broad variety of synthesis processes. Furthermore, integrated concepts for bio-refineries, bio-based circular economies, combined with carbon capture and utilization (CCU) are as well part of these polygeneration strategies.

Therefore, the main aim of the conference was to present the current state-of-the-art of these developments and successes during the last years. National and international researchers, industrial representatives from the manufacturer and utility side were invited and welcome to contribute to the success of the conference. The conference offers a platform for the exchange of innovative ideas, unconventional concepts, new conversion processes, optimized process combinations, integrated plant concepts and also surprising measurement results.

We hope that we could fulfill your expectations in this event, in an organizational and scientific perspective. It was a pleasure and honor for me, beside of the explained scientific focus of this conference, to grant for true Austrian hospitality in these three days, which I hope you enjoyed during the International Conference on Polygeneration Strategies 19. We hope that you will remember nice and interesting experiences when taking this book to hand in future.

Vienna, August 2019

Hermann Hofbauer

Scientific Committee

	Univ.-Prof. Hermann Hofbauer DI Dr. Stefan Müller Univ.-Prof. Markus Lehner Univ.-Prof. Robert Scharler Univ.-Prof. Tobias Pröll DI Dr. Andrés Anca-Couce DI Dr. Michael Fuchs, MBA DI Dr. Matthias Kuba DI Dr. Markus Luisser DI Dr. Gerhard Schöny DI Dr. Gerald Weber	TU Wien - Chair TU Wien - Co-Chair Montanuniversität Leoben TU Graz BOKU TU Graz Bundesministerium Nachhaltigkeit und Tourismus BEST - Bioenergy and Sustainable Technologies BEST - Bioenergy and Sustainable Technologies TU Wien BEST - Bioenergy and Sustainable Technologies
	Ass.-Prof. Dr. Kawnish Kirtania	Bangladesh University of Engineering and Technology
	Univ.-Prof. Martin Kaltschmitt Univ.-Prof. Jürgen Karl Univ.-Prof. Reinhard Rauch	Technische Universität Hamburg Friedrich-Alexander Universität Erlangen-Nürnberg Karlsruhe Institute of Technology
	Univ.-Prof. Umberto Arena Assoc. Prof. Fabrizio Scala	Università degli Studi della Campania “Luigi Vanvitelli” Università degli Studi di Napoli Federico II
	Ir. Berend Vreugdenhil	TNO
	Univ.-Prof. Joanna Łojewska	Uniwersytet Jagielloński W Krakowie
	Univ.-Prof. Joakim Lundgren Assoc. Prof. Martin Seemann Univ.-Prof. Marcus Öhman	Luleå tekniska universitet Chalmers University of Technology Luleå tekniska universitet
	Dr. Massimiliano Materazzi	University College London
	Univ.- Prof. Kevin J. Whitty	The University of Utah

Junior Committee

DI Anna Mauerhofer	TU Wien
DI Florian Benedikt	TU Wien
DI Josef Fuchs	TU Wien

Powered by



Contents

Experimental test in a lab-scale fluidized bed reactor to investigate agglomeration behavior under real conditions

S. Diem, S. Müller, F. Benedikt, H. Hofbauer

TU Wien, Institute of Chemical Environmental and Bioscience Engineering - Future Energy Technology,
Getreidemarkt 9/166, 1060 Vienna, Austria

Influence of fuel ash and bed material on the water-gas-shift equilibrium in DFB biomass steam gasification

K. Fürsatz^{1,2}, J. Fuchs², A. Bartik², M. Kuba^{1,2}, H. Hofbauer²

1. BEST – Bioenergy and Sustainable Technologies GmbH, Inffeldgasse 21b, 8010 Graz, Austria

2. TU Wien, Institute of Chemical, Environmental and Bioscience Engineering (ICEBE), Getreidemarkt 9/166, 1060 Vienna, Austria

Catalytic effect of potassium in thermochemical gasification of biogenic resources in a floating fixed bed gasifier

A. Hofmann, H. Füssl-Le, B. Hupfauf

MCI Management Center Innsbruck – The Entrepreneurial School, Dpt. Environmental, Process & Energy
Engineering, Maximilianstrasse 2, 6020 Innsbruck, Austria

Development of a new method for investigation of the ash melting behavior in the fluidized bed conversion processes

J. Priscak^{1,2}, M. Kuba^{1,2}, H. Hofbauer²

1. BEST – Bioenergy and Sustainable Technologies GmbH, Inffeldgasse 21b, A-8010 Graz, Austria

2. TU Wien, Institute of Chemical, Environmental and Bioscience Engineering (ICEBE), Getreidemarkt 9/166, 1060 Vienna, Austria

Steam gasification of sewage sludge for synthesis processes

J.C. Schmid¹, A. Bartik³, F. Benedikt³, A.M. Mauerhofer³, J. Fuchs³,
E. Schanz¹, S. Reisinger¹, B. Nowak¹, F. Bühler¹, M. Österreicher¹,
A. Lunzer², C. Walcher², S. Müller², M. Fuchs², H. Hofbauer³

1. SMS group Process Technologies GmbH, Daffingergasse 4, 1030 Vienna, Austria

2. Energy & Chemical Engineering GmbH, Pappelstraße 13, 1140 Vienna, Austria

3. TU Wien, Inst. of Chem., Environ. & Bioscience Eng., Getreidemarkt 9/166, 1060 Vienna, Austria

Spectroscopic in situ methods for the evaluation of the active centers on ash-layered bed materials from gasification in a fluidized bed reactor

D. Chlebda¹, K. Aziaba², D. Janisch², M. Kuba^{2,3}, H. Hofbauer³, J. Łojewska¹

1. Jagiellonian University, Faculty of Chemistry, Gronostajowa 2, Krakow, Poland

2. Bioenergy 2020+ GmbH, Wiener Straße 49, A-7540 Güssing, Austria

3. Vienna University of Technology, Institute of Chemical Engineering - Future Energy Technology, Getreidemarkt 9/166, 1060 Vienna, Austria

Structure analysis with relevance for complex materials – an outlook to X-ray absorption spectroscopy on phosphorus

N. Skoglund

Thermochemical Energy Conversion Laboratory, Umeå University, SE-901 87 Umeå, Sweden

Gasification - Advanced Reactor Systems: Full Papers 57

Evaluation of sorption enhanced reforming in combination with oxyfuel combustion fo the sequestration of CO₂

M. Hammerschmid, S. Müller, J. Fuchs, H. Hofbauer

TU Wien, Institute of Chemical Environmental and Bioscience Engineering - Future Energy Technology,
Getreidemarkt 9/166, 1060 Vienna, Austria

58

Gasification - Advanced Reactor Systems: Abstracts 69

Syngas production for DME synthesis from sorption enhanced gasification of biomass: A pilot plant-based case study

S. Hafner, M. Schmid, G. Scheffknecht

University of Stuttgart, Institute of Combustion and Power Plant Technology (IFK),
Pfaffenwaldring 23, 70569 Stuttgart, Germany

70

Syngas Applications - Production of Biofuels: Full Papers

72

Dual fluidized bed biomass gasification: Temperature variation using pure CO₂ as gasification agent

A. M. Mauerhofer, S. Müller, F. Benedikt, J. Fuchs, A. Bartik, M. Hammerschmid,
H. Hofbauer

TU Wien, Institute of Chemical Environmental and Bioscience Engineering - Future Energy Technology,
Getreidemarkt 9/166, 1060 Vienna, Austria

73

Aviation biofuels: an economic and environmental assessment with an outlook on cost reduction potentials

U. Neuling, M. Kaltschmitt

Hamburg University of Technology, Institute of Environmental Technology and Energy Economics,
Eissendorfer Strasse 40, 21073 Hamburg, Germany

83

Syngas Applications - Production of Biofuels: Abstracts

96

Continuous hydrodeoxygenation of liquid phase pyrolysis oil with biogenous hydrogen enriched synthesis gas for fuel production

K. Treusch^{1,2}, A. M. Mauerhofer³, N. Schwaiger², P. Pucher¹,
E. Ahn¹, S. Müller³, D. Painer², H. Hofbauer³, M. Siebenhofer²

1. BDI-BioEnergy International GmbH, Parkring 18, 8074 Raaba-Grambach, Graz, Austria

2. Graz University of Technology, Institute of Chemical Engineering and Environmental Technology,
Inffeldgasse 25c, 8010 Graz, Austria

3. TU Wien, Institute of Chemical, Environmental and Bioscience Engineering, Getreidemarkt 9/166, 1060 Vienna, Austria

97

Syngas Applications - Electricity and Heat: Full Papers

100

Investigation of SOFC operation with steam gasifier product gases as a basis for enhancing its performance

G. Pongratz¹, V. Subotić¹, H. Schroettner², B. Stoeckl¹, C. Hochenauer¹,
A. Anca-Couce¹, R. Scharler¹

1. Graz University of Technology, Institute of Thermal Engineering, Inffeldgasse 21, 8010 Graz, Austria

2. Graz University of Technology, Institute for Electron Microscopy and Nanoanalysis, Steyrergasse 17, 8010 Graz, Austria

101

Syngas Applications - Electricity and Heat: Abstracts

113

Demonstrative installation for cogeneration of heat and power from biomass gasification process

T. Iluk, M. Szul, A. Sobolewski

1. Institute for Chemical Processing of Coal, Zamkowa 1, 41-803 Zabrze, Poland

114

From wood to biogas – a small-scale demonstrationN. B. K. Rasmussen¹, C. L. Höffner^{1,2}

1. Danish Gas Technology Centre, Dr Neergaards Vej 5B, 2970 Hørsholm, Denmark

2. Technical University of Denmark, Chemical and Biochemical Engineering, 2800 Kgs Lyngby, Denmark

Experimental performance of a trickle-bed reactor for biological methanation

T. Weidlich, T. Trabold, M. Neubert, P. Treiber, J. Karl

Friedrich-Alexander-Universität Erlangen-Nürnberg, Chair of Energy Process Engineering,
Fürther Str. 244f, 90429 Nürnberg, Germany**Dynamic methanation of by-product gases from integrated steelworks**

P. Wolf-Zoellner, A. R. Medved, A. Krammer, K. Salbrechter, M. Lehner

Chair of Process Technology and Industrial Environmental Protection, Montanuniversität Leoben, Austria

1 MW scale-up of the advanced fuel flexible dual fluidized bed steam gasification process by process simulation

F. Benedikt, S. Müller, H. Hofbauer

TU Wien, Institute of Chemical Environmental and Bioscience Engineering - Future Energy Technology,
Getreidemarkt 9/166, 1060 Vienna, Austria**131****Investigating tar formation at low pressures in wood gasification systems, applying a novel thermo-chemical simulation model**G. Boiger¹, V. Buff¹, A. Zubiaga¹, A. Fassbind², P. Cael³

1. Zurich University of Applied Sciences, Institute of Computational Physics, Wildbachstrasse 21, 8409 Winterthur, Switzerland

2. Zurich University of Applied Sciences, Zentrum für Produktentwicklung, Lagerplatz 22, 8400 Winterthur, Switzerland

3. Aberta Nova S.A., Rua da Fonte n 5, 7570-622 Melides, Portugal

140**Thermochemical equilibrium study of ash transformation during combustion and gasification of sewage sludge mixtures with agricultural residues with focus on the phosphorus speciation**T. K. Hannl¹, H. Sefidari¹, M. Kuba^{1,2,3,4}, M. Öhman¹

1. Energy Engineering, Division of Energy Science, Luleå University of Technology, SE-971 87 Luleå, Sweden

2. Bioenergy2020+ GmbH, Wiener Straße 49, AT-7540 Güssing, Austria

3. Institute of Chemical, Environmental & Bioscience Engineering, TU Vienna, AT-1060 Vienna, Austria

4. Department of Applied Physics and Electronics, Umeå University, SE-901 87 Umeå

149**CPFD simulation of a dual fluidized bed cold flow model**A. Lunzer¹, S. Kraft^{2,3}, S. Müller², H. Hofbauer²

1. Verto Engineering GmbH, Franz-Josefs Kai 53/13, 1010 Vienna, Austria

2. TU Wien, Institute of Chemical, Environmental and Bioscience Engineering, Getreidemarkt 9/166, 1060 Vienna, Austria

3. Bioenergy 2020+ GmbH, Wiener Strasse 49, 7540 Güssing, Austria

160**Molecular dynamics simulations of the molten CaO-K₂O-SiO₂ system to study viscosity of woody biomass ash slags**C. Ma¹, N. Skoglund¹, M. Carlborg¹, M. Broström¹

1. Department of Applied Physics and Electronics, Thermochemical Energy Conversion Laboratory, Umeå University, SE 901 87, Umeå, Sweden

172

Kinetic Modeling of Industrial Plastic Pyrolysis

A. E. Lechleitner¹, T. Schubert¹, M. Lehner¹, W. Hofer²

1. Chair for Process Technology and Industrial Environmental Protection, Montanuniversitaet Leoben,
Franz-Josef-Str. 18, 8700 Leoben, Austria

2. OMV Refining & Marketing GmbH, Mannswoerther Straße 28, 2320 Schwechat, Austria

Developing an adsorption-based gas cleaning system for a dual fluidized bed gasification process

J. Loipersböck¹, G. Weber¹, R. Rauch², H. Hofbauer³

1. BEST - Bioenergy and Sustainable Technology, Inffeldgasse 21b, 8010 Graz, Austria

2. Karlsruhe Institute of Technology, Institute of Chemical, Environmental and Biological Engineering
Engler-Bunte-Ring 1, 76131 Karlsruhe, Germany

3. TU Wien, Institute of Chemical, Environmental and Bioscience Engineering, Getreidemarkt 9/166, 1060 Vienna, Austria

184

Secondary tar conversion in a char bed with a real producer gas reducing char deactivation

D. Fuentes-Cano¹, L. von Berg², I. Pardo-Arias¹, R. Scharler², A. Gómez-Barea¹,
A. Anca-Couce²

1. Universidad de Sevilla, Chemical and Environmental Engineering Department, Bioenergy Group, Camino de
los Descubrimientos s/n, 41092 Seville, Spain

2. Graz University of Technology, Institute of Thermal Engineering, Inffeldgasse 21, 8010 Graz, Austria

197

Decomposition of tars in dual fluidized bed gasification – mechanisms of formation and decomposition in long-term operation

K. Umeki¹, J. Priscak^{2,3}, M. Kuba^{2,3}

1. Luleå University of Technology, Energy Engineering, Division of Energy Science, SE-971 87 Luleå, Sweden

2. Bioenergy 2020+ GmbH, Wienerstraße 49, 7540 Güssing, Austria

3. TU Wien, Institute of Chemical, Environmental and Bioscience Engineering (ICEBE), Getreidemarkt 9/166, 1060 Vienna, Austria

199

Industrial Implementations - CCU, Greening the Gas: Full Papers

201

Dual fluidized bed based technologies for carbon dioxide reduction

J. Fuchs, A. M. Mauerhofer, S. Penthör, F. Benedikt, A. Bartik, M. Hammerschmid, S. Müller, H. Hofbauer

TU Wien, Institute of Chemical Environmental and Bioscience Engineering (ICEBE), Getreidemarkt 9/166, 1060 Vienna, Austria

202

Evaluation of two sorbents for the sorption-enhanced methanation in a dual fluidized bed system

A. Coppola¹, F. Massa¹, P. Salatino^{1,2}, F. Scala^{1,2}

1. Dipartimento di Ingegneria Chimica, dei Materiali e della Produzione Industriale, Università degli Studi di Napoli Federico II, Piazzale V. Tecchio 80, 80125 Napoli, Italy

2. Istituto di Ricerche sulla Combustione, CNR, Piazzale V. Tecchio 80, 80125 Napoli, Italy

210

Industrial Implementations - CCU, Greening the Gas: Abstracts

217

Technoeconomic study of cost driving factors of a gas greening system for steel making based on power-to-gas and biomass gasification

D. C. Rosenfeld, J. Lindorfer, H. Böhm

Energy Institute at the Johannes Kepler University Linz – Department of Energy Technology, Altenberger Straße 69, 4040 Linz, Austria

218

Industrial Implementations - Industrial Demonstration: Full Papers

220

Thermodynamic investigation of SNG production based on dual fluidized bed gasification of biogenic residues

A. Bartik¹, F. Benedikt¹, A. Lunzer², C. Walcher², S. Müller², H. Hofbauer¹

1. TU Wien, Institute of Chemical, Environmental and Bioscience Engineering,

Getreidemarkt 9/166, 1060 Vienna, Austria

2. Energy & Chemical Engineering GmbH, Pappelstraße 13, 1140 Vienna, Austria

221

Evaluating the efficiency of power-to-x technologies by adapting the VDI-guideline 4663

N. Eggers¹, J. Böttger¹, L. Kerpen², B. Sankol², T. Birth¹

1. Fraunhofer Institute for Factory Operation and Automation, Department for Convergent Infrastructures,
Sandtorstraße 22, 39106 Magdeburg, Germany

2. Hamburg University of Applied Sciences, Faculty of Engineering and Computer Science,
Berliner Tor 11, 20099 Hamburg, Germany

232

Industrial Implementations - Industrial Demonstration: Abstracts

242

Dynamic methanation of by-product gases from the steel industry in the scope of the project i³upgrade

A. Hauser, M. Weitzer, S. Gunsch, M. Neubert, J. Karl

Friedrich-Alexander University Erlangen-Nürnberg, Chair of Energy Process Engineering,
Fürther Str. 244f, 90429 Nürnberg, Germany

243

Industrial Implementations - Integrated Concepts: Full Papers

245

Hybridization of biomass steam gasification in dual fluidized bed reactor with concentrated solar energy

A. Gomez-Barea^{1,5}, M. Suarez-Almeida^{1,5}, M. Silva², C. Pfeifer³, J. Karl⁴, A. Ghoniem⁵

1. Chemical and Environmental Engineering Department, Escuela Técnica Superior de Ingeniería, University of Seville, Camino de los Descubrimientos s/n, 41092 Seville, Spain

2. Energy Engineering Department, Escuela Técnica Superior de Ingeniería, University of Seville, Camino de los Descubrimientos s/n, 41092 Seville, Spain

3. Department of Material Sciences and Process Engineering, University of Natural Resources and Life Sciences, 1190 Vienna, Austria

4. Department of Chemical and Biological Engineering, Friedrich-Alexander Universität Erlangen-Nürnberg, Fürther Strasse 244f, 90429 Nuremberg, Germany

5. Department of Mechanical Engineering, Massachusetts Institute of Technology, 77 Massachusetts Avenue, Cambridge, Massachusetts 02139-4307, United States

246

Integrated concept for municipal solid waste valorization: Pre-pilot experience

**K. Kirtania¹, K. B. Kabir¹, A. K. M. K. Aurnob¹, A. Arnob¹, U. Salma¹, M. S. Islam²,
M. M. Rahman¹**

1. Department of Chemical Engineering, Bangladesh University of Engineering and Technology, Dhaka – 1000, Bangladesh

2. Department of Glass and Ceramic Engineering, Bangladesh University of Engineering and Technology, Dhaka – 1000, Bangladesh

256

Industrial Implementations - Operational Experience: Full Papers

261

Laser-based deposit diagnostic in biomass-fired power plants

F. Graube-Kühne, S. Grahlf, D. Bernhardt, M. Beckmann

Dresden University of Technology, Institute of Process Engineering and Environmental Technology –
Energy Process Engineering, George-Bähr-Str. 3b, 01069 Dresden, Germany

262

Industrial Implementations - Operational Experience: Abstracts

271

A review study on Chinese domestic gasification technologies

Y. Pang, D. Müller, J. Karl

Chair of Energy Process Engineering, Friedrich-Alexander-University Erlangen-Nürnberg,
Fuerther Str. 244f, 90429 Nuremberg, Germany

272

Heat-to-Fuel Workshop: Full Papers

274

Influence of pressure and CO₂ in fluidized bed gasification of waste biomasses

M. Szul, K. Słowik, K. Głów, T. Iluk

Instytut Chemicznej Przeróbki Węgla, Zamkowa 1, 41-803 Zabrze, Poland

275

Heat-to-Fuel Workshop: Abstracts

285

Modeling, design and assessment of a milli structured reactor for Fischer Tropsch reaction

G. Geffraye, A. Bengaouer, A. Chappaz, M. Jouve

CEA, Commissariat à l'Energie Atomique et aux Energies Alternatives
LITEN, DTBH 17 avenue des Martyrs, 38000 Grenoble Cedex 9, FRANCE

286

Aqueous phase reforming of Fischer-Tropsch water fraction

G. Zoppi¹, G. Pipitone¹, H. Gruber^{2,3}, G. Weber², A. Reichhold³, R. Pirone¹, S. Bensaïd¹

1. Department of Applied Science and Technology, Politecnico di Torino, Corso Duca degli Abruzzi 24, 10129, Turin, Italy

2. Bioenergy 2020+ GmbH, Wienerstraße 49, Güssing, 7540, Austria

3. Institute of Chemical, Environmental & Biological Engineering, TU Wien, Vienna, Austria, Getreidemarkt 9/166, 1060 Vienna, Austria

289

Investigation of the upgrading of Fischer-Tropsch waxes through hydroprocessing

P. Neuner, N. Netsch, R. Rauch

Karlsruhe Institute of Technology, Engler-Bunte-Institute – Fuel Chemistry and Technology,
Engler-Bunte-Ring 1, 76131 Karlsruhe, Germany

292**Concept for the ideal 16MW_{th} biomass gasification system to feed a synthetic natural gas production process**

C. Walcher^{1,2}, S. Müller³, H. Hofbauer³, M. Fuchs⁴

1. Verto Engineering GmbH, Franz-Josefs Kai 53/131010 Vienna, Austria
2. Energy & Chemical Engineering GmbH, Pappelstrasse 13, 1140 Vienna, Austria
3. TU Wien, Institute of Chemical, Environmental and Bioscience Engineering,
Getreidemarkt 9/166, 1060 Vienna, Austria
4. Federal Ministry for Sustainability and Tourism, Stubenring 1, 1010 Wien

299

Poster Session: Abstracts

308

Hot Metal Production with Reduced Fossil Carbon Usage

S. Müller¹, L. Theiss¹, M. Hammerschmid¹, J. Fuchs¹, D. C. Rosenfeld²,
M. Lehner³, H. Hofbauer¹

1. TU Wien, Institute of Chemical Environmental and Bioscience Engineering

2. Johannes Kepler Universität Linz, Department of Energy Technology

3. Montanuniversität Leoben, Department of Environmental and Energy Process Engineering

309

Biogas to SNG demonstration plant

K. Salbrechter, A. R. Medved, A. Krammer, P. Wolf-Zöllner, M. Lehner

Montanuniversität Leoben, Chair for Process Technology and Industrial Environmental Protection

Franz-Josef-Strasse 18, 8700 Leoben, Austria

312

Optimization of industrial bio-SNG production from low-grade fuels

M. Veress, A. Bartik, F. Benedikt, S. Müller, H. Hofbauer

Vienna University of Technology, Institute of Chemical Engineering - Future Energy Technology,
Getreidemarkt 9/166, 1060 Vienna, Austria

314

Modeling steam gasification of biomass with Mathcad 15 via two reaction stages

B. Wojnicka¹, M. Ściążko², J. C. Schmid³

1. AGH University of Science and Technology, 30 Mickiewicza Av., 30-0589 Cracow, Poland

2. Institute for Chemical Processing of Coal, ul. Zamkowa 1, 41-803 Zabrze

3. SMS group Process Technologies GmbH, Daffingerstraße 4, 1030 Vienna, Austria

315

Gasification Feedstock and Agents Full Papers

Experimental test in a lab-scale fluidized bed reactor to investigate agglomeration behavior under real conditions

S. Diem^{1*}, S. Müller¹, F. Benedikt¹, H. Hofbauer¹

1. TU Wien, Institute of Chemical Environmental and Bioscience Engineering - Future Energy Technology,
Getreidemarkt 9/166, 1060 Vienna, Austria
*corresponding author: sebastian.diem@tuwien.ac.at

Abstract

This paper presents first results of experimental test runs in a lab-scale fluidized bed reactor at TU Wien to predict the agglomeration temperature of exhausted olive pomace. The controlled fluidized bed agglomeration test indicates an agglomeration temperature of approximate 945 °C by the occurrence of a pressure drop in the fluidized bed. The agglomeration phenomena is explained by the mechanism of initial low melting layer formation around burning char particles. The goal is to establish a standard prediction method based on other performed tests in similar lab-scale reactors.

1. Introduction:

Considering the current European regulations, the major contribution of bioenergy to the overall Renewable Energy Sources and current status of conversion technologies, biomass will play a major role in reducing greenhouse gases [1]. In Germany up to 40 % of forest wood is used for energy production [2] and about 18 % of the agricultural productive land is claimed for cultivation of energy crops. It is considered that this ratio will rise further [3]. These facts provoke the public food versus fuel debate. To avoid land-use conflicts, new alternative sources as municipal, industrial or agricultural by-products are in focus of research.

A practical problem in thermal conversion of substitutes of woody biomass in fluidized bed reactors is bed agglomeration caused by low melting ash components containing potassium. The interaction between ash particles and bed material at low ash melting temperatures

leads to defluidization and in the worst case to a shutdown of the reactor [4]. Two mechanisms of bed agglomeration are described in literature, coating-induced- and melt-induced agglomeration [5].

There are existing different biomass ash melting predictions tools. The Standard ash fusion test (AFT) according CEN/TS 15370-1 for determination of ash melting behavior for biomass is commonly applied by most laboratories providing fuel analyses. Ternary diagrams are used for classifying biomasses and prediction of the ash melting temperature.

Based on the elementary ash composition solidus and liquidus curves are shown in a K₂O-CaO-SiO₂-, CaO (+ MgO)-K₂O (+ Na₂O)-P₂O₅ -, or in a K₂O-SiO₂-Al₂O₃- System [6], [7], [8], [9], [10]. In a study a complex multicomponent ternary diagram is established in which all major ash forming elements are included. The data of 55 types of biomass ash compositions are used to define three areas of different deformation temperatures (low

< 1000 °C, medium 1000 - 1300 °C and high > 1300 °C) [11].

Fuel indices based on standardized chemical fuel analyses like the molar Si / (Ca + Mg) ratio for P-poor fuels [12] and the molar (Si + P + K) / (Ca + Mg) ratio for P-rich fuels can provide also indications regarding the ash-melting tendencies [13].

Empirical equations applied for biomass with the same data basis necessary for fuel indices, are a further approach [14], [15]. Advanced methods, like, simultaneous thermal analysis (STA) and thermodynamic high temperature equilibrium calculations (TEC), are used also in scientific researches related to ash melting investigations [16], [17], [18].

All previously mentioned ash melting predictions tools have in comparison their own advantages and disadvantages summarized by [19].

[20], [21] and [22] developed a controlled fluidized bed agglomeration test with a lab scale bench reactor. This method enables the detection of the event of defluidization by monitoring the pressure drop in the fluidized bed caused by forming of agglomerates. More comparable lab-scale appliances are existing, see for example [23], [24] and [25].

However, a suitable standard prediction method for real fluidized bed utilization is still missing. The present study deals with the first test run of a lab-scale fluidized bed reactor at TU Wien to predict the agglomeration temperature similar to performed test runs described in literature.

2. Experimental set up:

The schematic of the lab scale fluidized bed reactor at TU Wien is shown Fig 1. The fuel is fed on top of the bubbling bed from a fuel hopper by a screw feeder driven by a variable frequency drive. To avoid the entrance of flammable flue gases the hopper is nitrogen-purged. Preheated

air (200 °C) is forced through a stainless-steel distributor plate perforated with 31 holes (diameter 1 mm) into the stainless-steel reactor tube (height 1089 mm, diameter 54.5 mm) with a freeboard section (diameter 82.5 mm). Electrical wall heating elements with an associated temperature control system in the lower preheating section and fluidized bed reactor section enables steady state conditions. From the distributor plate up to the top the test rig is covered with thermal insulation. The reactor is equipped with a flue gas cleaning system, which consists of a cyclone and a downstream filter section for fine particle removal. The measuring instruments coupled with a digital data recording system includes an Emerson Rosemount NGA2000 multicomponent gas analyzer for detection of O₂, CO₂, CO, NO in the flue gas. The bed temperature is measured by a thermocouple (type K) and the bed pressure by a pressure transducer to monitor continuously the physical behavior of the bed. Additionally, the fluidization gas can be premixed by a mixing control desk. N₂, H₂, CO and CO₂ are able to pass via individual flowmeters to the mixing inlet valve into the preheater to produce specific reaction conditions for gasification.

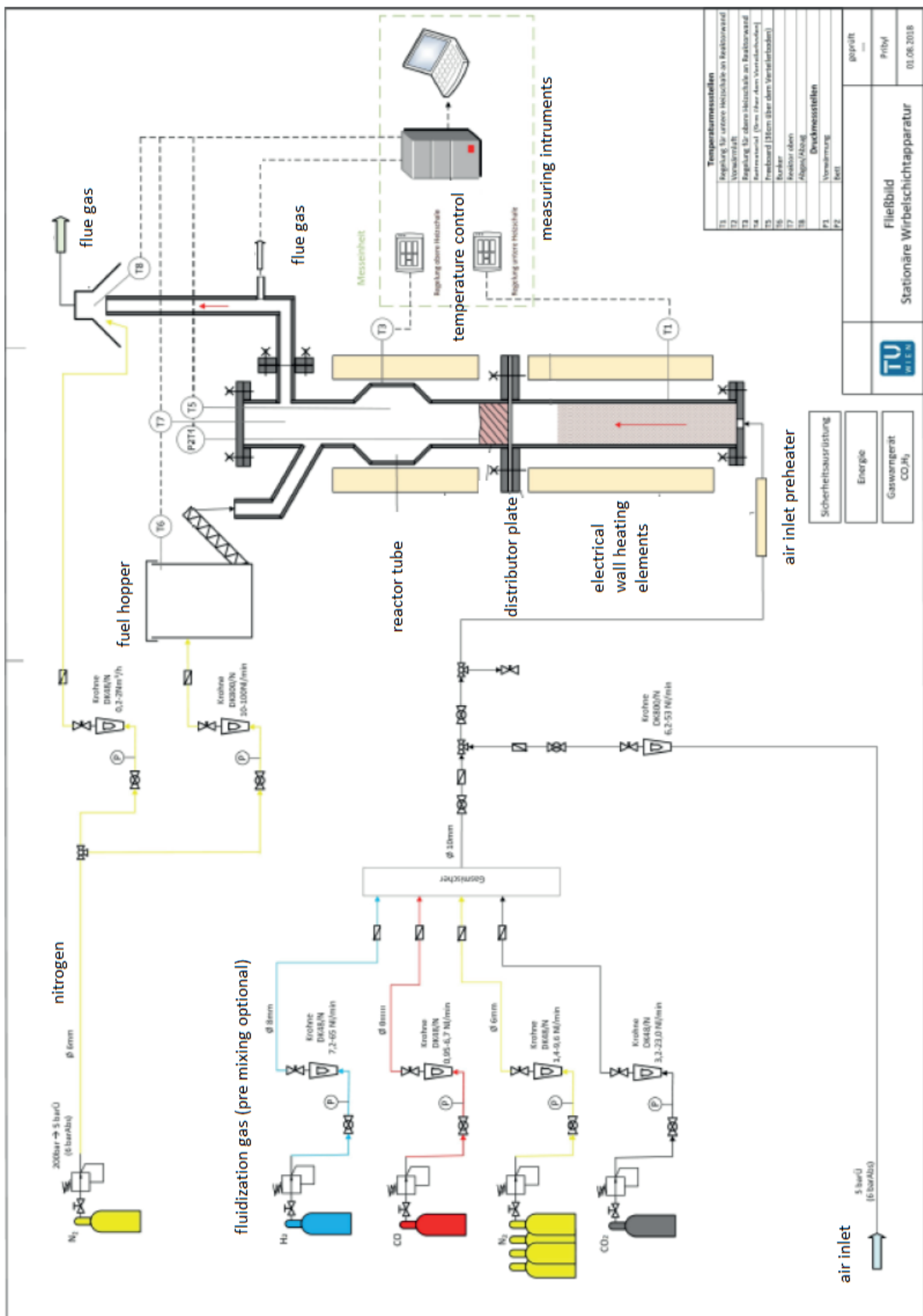


Fig.1: Fluidized bed-lab scale reactor [26]

3. Fuels and bed material:

Pellets (diameter 6 mm, length 20 – 30 mm) of olive residue (exhausted olive pomace, EOP) were used as feedstock for the first experiments. Exhausted olive pomace is a by-product of the olive oil production, after extraction of its oil. Sewage sludge granulate (SSG) was used as benchmark fuel.

The proximate and ultimate analyses of the used fuels are shown in Tab. 1. The deformation temperature (DT) of EOP was 840 °C, determined by the standard ash fusion test. This fact underlines the critical usage as a fuel in fluidized bed applications, because operation temperatures are usually above 850 °C. The deformation temperature of SSG was 1160 °C and therefore was used as comparative fuel with relatively low agglomeration propensity.

The bed material used was quartz sand with a sauter diameter of 0.299 mm to ensure the bubbling properties of the bed. For each testing, 350 g of bed material was put into the reactor. The ash compositions with the main components are summarized in Tab. 2.

	unit	EOP fuel	SSG fuel
Water content	mass.-%	8.6	10.1
Ash content	mass.-% _{db}	4.7	28.3
Carbon (C)	mass.-% _{db}	49.4	34.3
Hydrogen (H)	mass.-% _{db}	5.9	4.0
Nitrogen (N)	mass.-% _{db}	1.0	5.7
Sulfur (S)	mass.-% _{db}	0.1	1.0
Chlorine (Cl)	mass.-% _{db}	0.1	0.1
Oxygen (O)	mass.-% _{db}	43.5	54.9

Volatile matter	mass.-% _{db}	75.8	61.0
LHV, dry	MJ/kg _{db}	18.9	15.3
Ash deformation temperature (DT)	°C	840	1160
Ash fusion temperature (FT)	°C	1440	1300

Tab.1: Proximate and ultimate analyses of olive residue and sewage sludge

	unit	EOP ash	SSG ash
CaO	wt%	11.9	23.8
K ₂ O	wt%	42.5	1.4
SO ₃	wt%	5.3	3.0
P ₂ O ₅	wt%	8.1	16.9
SiO ₂	wt%	12.9	28.3
Al ₂ O ₃	wt%	2.5	10.4
MgO	wt%	6.1	7.0
NaO ₂	wt%	4.1	1.1
Fe ₂ O ₃	wt%	1.2	5.7

Tab.2: Ash compositions

4. Performing the test:

At first the quantity of EOP fuel inserted into the reactor was identified by a calibrated feeding system with flowrates at three different motor frequencies (15 Hz, 25 Hz and 50 Hz). The quantification was done at a time period of 15 min each.

The fuel rate was set to 147 g/h (10 Hz) for complete combustion (air-fuel equivalence ratio $\lambda = 1.5$). To enable bubbling fluidization conditions, the air flowrate was fixed to 16 l/min during the test run with a fluidization velocity $U = 0.54$ m/s.

The bed was heated progressively to 635 °C, afterward the fuel addition was started. Bed temperature, wall heating system temperatures and bed pressure

were recorded every five seconds by a digital recording system over the time of testing. The detection of O₂, CO₂, CO, NO was done continuously and recorded within the same time rate. Controlled external heating and heat release from fuel combustion increased the bed temperature from 635 °C up to approximate 900 °C. Then the bed temperature was raised 2 °C per minute till agglomeration occurred. At the point of agglomeration, the bed pressure dropped, and temperature raised above the bed, then the fuel load was stopped shortly after, and all heating systems were shut off. The fluidization was sustained until the appliance was cooled down to ambient temperature to avoid overheating of the test rig over 1050 °C. Finally, the remained ash and bed material were collected from the reactor by opening the distributor flange and were weighed. The mentioned flue gas cleaning system was not yet installed during the performing of the test.

5. Results and discussion:

For the first test with EOP fuel the progress of the bed temperature and bed pressure is shown in Fig. 2. The dotted vertically line in the diagram indicates the beginning of the decrease of the pressure and the associated bed temperature signifies the agglomeration temperature. The determined agglomeration temperature for EOP fuel at the first run is 945 °C and 942 °C at the second run, they are in comparison between the characteristic temperatures of the standard ash fusion test (DT 840 °C and FT 1440 °C). This range can be explained by the different ash preparation temperatures, 550 °C versus 900 °C and neglecting interactions with bed material under fluidized conditions.

A theoretical ash content in the bed can be calculated based on the fuel rate and time period of fuel load. The first test run lasted

5 h with a resulting ash to bed ratio of 10 % considering the 4,7 % ash content of the fuel and a total remaining mass of 385 g. To reach the half of ash to bed ratio, the second run lasted 2 h 30 min with a remaining mass of 367 g. There was a difference of 11 % relative to the calculated total mass at the first and 5 % at the second test. This is caused by the abrasion of tinder from the reactor interior hot surfaces and errors related to the calibration of the fuel feeding system. At both tests, the pressure drop occurred after 30 min during the controlled bed temperature increase, which was started at approximate 900 °C. This indicates in comparison that even the half amount of accumulated ash in the bed is enough to enable bed agglomeration. The collected agglomerates includes entirely with surface melt coated unburned fuel particles. This phenomenon of bed agglomeration started from around burning char particles is described by [24]. There are two possible explanations for agglomeration described: First, a certain time is necessary to build up a critical thickness of bed particle coatings with low melting alkali phases. In this case, the bed temperature is higher than the eutectic temperature of the coatings. Second, if the bed temperature is lower than the specific eutectic temperature, an accumulation of coatings is prevented, but agglomerates can still formed by the local heat release near burning char, where the local temperature peak is higher than the bed temperature. This supports the formation of a surface melting. These formed agglomerates can resist collisions within the fluidized bed and their amount increases progressively.



Fig.3: Formed Agglomerates and bed material after a test run [27]

The result is a buildup of a defluidized layer in the bed. Fig.3 shows such layer in the upper section from the second run. However, the relative small diameter of the reactor tube heated by the electrical wall elements has to take into account, because of the temperature gradient between the heated wall and the middle of the bed. At the reactor surface there is a relative higher temperature compared to the center of it. Therefore, agglomeration can also facilitated at the exterior of the fluidized bed.

It can be stated that the agglomeration occurred at the half amount of ash in the bed under the same conditions as the first run, is a consequence of the presence of a

relatively high ratio intact agglomerates around char particles to bed material, compared to the first test. A third test run with SSG fuel was performed under the same conditions as the second run with EOP fuel with an fuel feeding time of 2 h 30 min. At a maximum operating bed temperature of 950 °C no pressure drop occurred. The absent of an act of agglomeration results in the relatively low amount of K₂O, 1.4 wt% in SSG ash compared to 42.5 wt% in EOP ash, see Tab. 2.

6. Conclusion:

The first tests with the new lab-scale fluidized bed reactor at TU Wien shows applicable performances to detect the agglomeration temperature of biomass fuels. To approve the applicability in comparison with other existing agglomeration test rigs further problematic ash melting behavior related fuels have to be investigated. The agglomeration nearby the reactor surface and consequently a uniform temperature ambience in the fluidized bed has to be achieved. Additionally, a harmonization to other existing lab-scale units in terms of test procedure have to be done to archive a optimum of comparability.

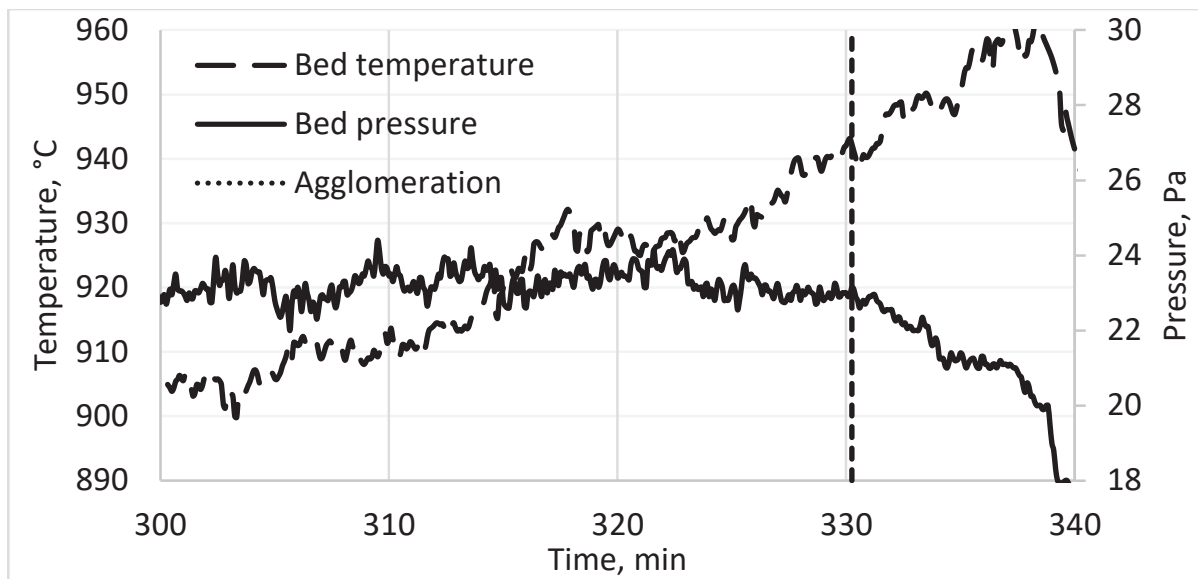


Fig.2: Bed temperature and bed pressure profile, first test run

Acknowledgements

This work is part of the project „CEMphos“ and is funded by the Austrian Federal Ministry of Transport, Innovation and Technology (BMVIT) and the Austrian Research Promotion Agency (FFG) and carried out under the “Produktion der Zukunft” program.

7. References

- [1] A. Bauen, G. Berndes, M. Junginger, F. Vuille, and M. Londo, “Bioenergy – a Sustainable,” *Structure*, pp. 1–108, 2009.
- [2] Statistisches Bundesamt, “Bericht zu den Umweltökonomischen Gesamtrechnungen,” Wiesbaden, 2014.
- [3] M.-L. F.-L. F. Majer Stefan, Stecher Kitty, Adler Philipp, Thrän Daniela, “Biomassepotenziale und Nutzungskonkurrenz,” 2013.
- [4] M. Hupa, O. Karlström, and E. Vainio, “Biomass combustion technology development - It is all about chemical details,” *Proc. Combust. Inst.*, 2017.
- [5] H. J. M. Visser, “The influence of Fuel Composition on Agglomeration Behaviour in Fluidised-Bed Combustion,” *ECN Biomass*, no. September, p. 44, 2004.
- [6] B. M. Jenkins, R. R. Bakker, and J. B. Wei, “On the properties of washed straw,” *Biomass and Bioenergy*, 1996.
- [7] S. Q. Turn, C. M. Kinoshita, and D. M. Ishimura, “Removal of inorganic constituents of biomass feedstocks by mechanical dewatering and leaching,” *Biomass and Bioenergy*, 1997.
- [8] L. A. Hansen, F. J. Frandsen, K. Dam-Johansen, H. S. Sørensen, and B. J. Skrifvars, “Characterization of ashes and deposits from high-temperature coal-straw co-firing,” *Energy and Fuels*, vol. 13, no. 4, pp. 803–816, 1999.
- [9] M. Öhman and A. Nordin, “The role of kaolin in prevention of bed agglomeration during fluidized bed combustion of biomass fuels,” *Energy and Fuels*, vol. 14, no. 3, pp. 618–624, 2000.
- [10] A. Grimm, “Doctoral Thesis: Experimental studies of ash transformation processes in combustion of phosphorus-rich biomass fuels,” 2012.

- [11] S. V. Vassilev, D. Baxter, and C. G. Vassileva, “An overview of the behaviour of biomass during combustion: Part II. Ash fusion and ash formation mechanisms of biomass types,” *Fuel*, vol. 117, no. PART A, pp. 152–183, 2014.
- [12] E. Lindström, M. Sandström, D. Boström, and M. Öhman, “Slagging characteristics during combustion of cereal grains rich in phosphorus,” *Energy and Fuels*, vol. 21, no. 2, pp. 710–717, 2007.
- [13] P. Sommersacher, T. Brunner, and I. Obernberger, “Fuel indexes: A novel method for the evaluation of relevant combustion properties of new biomass fuels,” *Energy and Fuels*, vol. 26, no. 1, pp. 380–390, 2012.
- [14] L. M. Hans Hartmann, Thorsten Böhm, “Naturbelassene biogene Festbrennstoffe – umweltrelevante Eigenschaften und Einflussmöglichkeiten,” 2000.
- [15] V. K. Friedl A., Padouvas E., Rotter H., “Prediction of heating value of biomass fuel and ash melting behaviour using elemental compositions of fuel and ash,” 2004.
- [16] N. Evic, T. Brunner, and I. Obernberger, “Prediction of Biomass Ash Melting Behaviour – Correlation Between the Data Obtained from Thermodynamic Equilibrium Calculations and Simultaneous Thermal Analysis (STA),” *20th Eur. Biomass Conf. Exhib.*, no. October 2015, pp. 807–813, 2012.
- [17] L. E. Fryda, K. D. Panopoulos, and E. Kakaras, “Agglomeration in fluidised bed gasification of biomass,” *Powder Technol.*, 2008.
- [18] M. Zevenhoven-Onderwater *et al.*, “The ash chemistry in fluidised bed gasification of biomass fuels. Part I: Predicting the chemistry of melting ashes and ash-bed material interaction,” *Fuel*, vol. 80, no. 10, pp. 1489–1502, 2001.
- [19] P. Sommersacher, T. Brunner, I. Obernberger, N. Kienzl, and W. Kanzian, “Application of novel and advanced fuel characterization tools for the combustion related characterization of different wood/kaolin and straw/kaolin mixtures,” *Energy and Fuels*, vol. 27, no. 9, pp. 5192–5206, 2013.
- [20] M. Öhman and A. Nordin, “A new method for quantification of fluidized bed agglomeration tendencies: A sensitivity analysis,” *Energy and Fuels*, vol. 12, no. 1, pp. 90–94, 1998.
- [21] E. Natarajan, M. Öhman, M. Gabra, A. Nordin, T. Liliedahl, and A. N. Rao, “Experimental determination of bed agglomeration tendencies of some common agricultural residues in fluidized bed combustion and gasification,” *Biomass and Bioenergy*, vol. 15, no. 2, pp. 163–169, 1998.
- [22] B. J. Skrifvars, M. Öhman, A. Nordin, and M. Hupa, “Predicting bed agglomeration tendencies for biomass fuels fired in FBC boilers: A comparison of three different prediction methods,” *Energy and Fuels*, vol. 13, no. 2, pp. 359–363, 1999.
- [23] M. Zevenhoven-Onderwater, R. Backman, B. J. Skrifvars, and M. Hupa, “The ash chemistry in fluidised bed gasification of biomass fuels. Part II: Ash behaviour prediction versus bench scale agglomeration tests,” *Fuel*, 2001.
- [24] F. Scala and R. Chirone, “Characterization and early detection of bed agglomeration during the fluidized bed combustion of olive husk,” *Energy and Fuels*, vol. 20, no. 1, pp. 120–132, 2006.
- [25] W. Lin, K. Dam-Johansen, and F. Frandsen, “Agglomeration in bio-fuel fired fluidized bed combustors,” *Chem. Eng. J.*, 2003.
- [26] M. Pribyl, “Phosphorrückgewinnung aus Klärschlamm in den Prozessstrukturen eines Zementwerks,” TU Wien, 2019.
- [27] C. Jezierski, “Prediction of biomass slagging behaviour in fluidized bed reactors based on ternary diagrams,” TU Wien, 2018.

Influence of fuel ash and bed material on the water-gas-shift equilibrium in DFB biomass steam gasification

K. Fürsatz^{1,2*}, J. Fuchs², A. Bartik², M. Kuba^{1,2} and H. Hofbauer²

1. BEST – Bioenergy and Sustainable Technologies GmbH, Inffeldgasse 21b, 8010 Graz, Austria

2. TU Wien, Institute of Chemical, Environmental and Bioscience Engineering (ICEBE),
Getreidemarkt 9/166, 1060 Vienna, Austria

*corresponding author, katharina.fuersatz@best-research.eu

Abstract

The bed material chosen for dual fluidized bed steam gasification has an important effect on the performance of gasification. Depending on their characteristics and properties, bed materials can have either a higher or lower catalytic activity, which influences the product gas composition as well as the tar content in the product gas. More catalytically active bed materials, like limestone and olivine, improve the quality of the product gas by e.g. promoting the water-gas-shift reaction and tar reforming reaction. The layers formed on the bed material are another aspect influencing the product gas composition. These layers are formed by the interaction of bed material and fuel ash. The deviation from the water-gas-shift equilibrium was chosen to quantify the effect of several bed materials and ash layers on the catalytic activity. The bed materials tested were K-feldspar, limestone, and activated olivine, while the used fuels were softwood, chicken manure, a bark – chicken manure mixture, and a bark – straw – chicken manure mixture. The performed experiments showed that an increased catalytic activity can be achieved by either using a catalytically active bed materials or ash-rich fuels.

1. Introduction:

Biomass can be used as CO₂-neutral carbon source for thermo-chemical conversion processes. One possible technology that can be applied is gasification. An advantage of gasification is the fact that not only power and heat can be produced but it is additionally possible to obtain a nitrogen-free product gas as intermediate energy carrier, which can be used as feed stream for further synthesis processes.

The dual fluidized bed (DFB) steam gasification is an especially suitable gasification technology, if synthesis is the major focus of the utilization of biomass, since a H₂:CO ratio of 2:1 or higher can already be achieved in the product gas before further gas upgrading. The

synthesis of Fischer-Tropsch products [1], mixed alcohols [2], [3], and synthetic natural gas [4] are some of the possible syntheses that can be performed with product gas from biomass gasification. Furthermore, separation of H₂ from the product gas [5] can be conducted for the production of H₂ of high purity for use in fuel cells.

Steam is used as gasification agent in this technology, leading to a nearly nitrogen free product gas. The DFB steam gasification technology applies two fluidized bed reactors, seen in Fig. 1: one gasification and one combustion reactor. The fuel is fed into the gasification reactor where it is devolatilized and gasified. A fraction of the remaining char is transferred to the combustion reactor,

together with the bed material. The combustion reactor is fluidized with air and char is combusted to heat up the bed material. The heated-up bed material is transported back to the gasification reactor to supply the energy needed for the endothermal gasification reactions in form of heat.

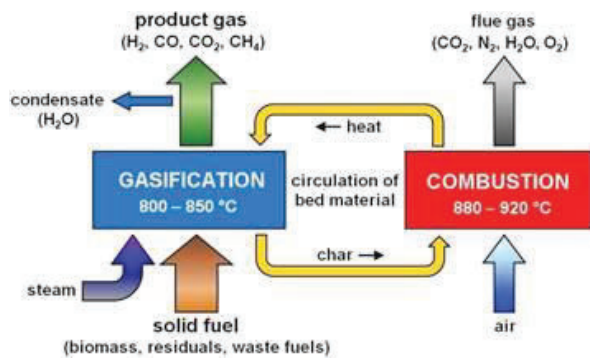


Fig. 1: Basic principle of DFB steam gasification [6]

Apart from transporting heat between combustion and gasification the bed material is also used for catalyzing gasification reactions. Olivine is currently applied in industrial plants due to its catalytic activity [7].

Current research is focused on the substitution of olivine, since it contains traces of heavy metals, which necessitate the deposition of the accruing ash [8]. K-feldspar [9]–[11] and limestone [12], [13] are some of the most promising bed materials currently investigated to substitute olivine. K-feldspar ($KAlSi_3O_8$) has similar mechanical properties compared to olivine, making it a suitable bed material for fluidized bed application. A disadvantage of K-feldspar is its catalytic inactivity in its unused state [9]. However, even inactive materials can be activated through interaction with fuel ash [9]. Limestone, on the other hand, is a catalytically active bed material but, due to its low abrasion resistance, leads to high dust contents in the product gas [12].

The interaction between fuel ash and bed materials is another aspect greatly

influencing the catalytic activity inside the DFB steam gasification system. Layers observed on olivine during the operation at the DFB steam gasification plant Güssing were proven to be responsible for reduced tar contents in the product gas [14]. Further research has shown, that layers formed on quartz [15] and K-feldspar [9] as well and also have a positive catalytic effect on the water-gas-shift (WGS) equilibrium.

A detailed comparison of the effect of bed material choice to the effect of ash layers on the surface of the bed particles on the catalytic activity has not been performed so far. Therefore, this work focuses on the combination of those two effects and tries to quantify the catalytic activity for an objective comparison. This is done by analyzing several gasification experiments with a wide array of fuels and bed materials and comparing those experiments for their deviation from the WGS equilibrium. Complementary elemental analyses of the formed layers were performed in addition for better insight into bed material – fuel ash interactions.

2. Concept and methodology:

2.1 Bed material

The bed materials used in this study were K-feldspar, limestone and activated olivine obtained from HGA Senden. K-feldspar was sieved with a 400 μm sieve to remove all coarse particles, resulting in a d_{sv} of 287 μm . The activated olivine (Mg, Fe, Ca// SiO_4) had to be sieved as well, since the pilot plant uses a smaller bed material size due to fluid dynamic reasons. Using a sieve with a mesh size of 514 μm and removing all bigger particles led to a d_{sv} of 329 μm . The limestone (mainly CaCO_3) could be used as delivered with a d_{sv} of 480 μm .

2.2 Fuel preparation

Several fuels were used throughout this work. Tab. 1 gives the ash content, as well as the lower heating value of all used fuels. Softwood (SW) and chicken manure (CM) were available as pellets with a diameter of 6 mm. All other fuels had to be milled, mixed according to the needed fuel blends and pelletized to 6 mm pellets without any binder.

Fuels (mixtures) used	Ash content mass fraction in % (db ¹)	Lower heating value in MJ kg ⁻¹ (db ¹)
SW	0.2	18.943
Bark (0.7) - CM (0.3)	13.5	16.430
CM	25.4	13.900
Bark (0.595) – Straw (0.15) – CM (0.255)	12.5	16.780

¹dry basis

Tab. 1: Ash content and lower heating value of the used fuels and fuel blends

2.3 100 kW_{th} pilot plant

Several experimental campaigns (see Tab. 2) have been conducted with the advanced 100 kW_{th} pilot plant at TU Wien to investigate the influence of different bed materials and fuel ash. According to the basic principle (Fig. 1) the pilot plant consists of two reactors (gasification reactor and combustion reactor) with an overall height of about 7 m. More details about the reactor-design can be seen in Fig. 2 and were described by Benedikt et al. [16]. The pilot plant facility including fuel supply equipment, a control room and equipment for gas cooling, cleaning and measurement, covers two floors of around 35m².

No	Bed material (blend)	Fuel (blend)
#1	K-FS (0.9) – Limestone (0.1)	SW
#2	K-FS (0.9) – Limestone (0.1)	Bark (0.7) – CM (0.3)
#3	K-FS (0.9) – Limestone (0.1)	CM
#4	K-FS	SW
#5	K-FS	Bark (0.595) – Straw (0.15) – CM (0.255)
#6	K-FS (0.5) – Limestone (0.5)	SW
#7	Activated olivine	SW
#8	Activated olivine	Bark (0.7) – CM (0.3)

Tab. 2: Summary of all experiments performed. The blend ratios are given as dry mass fractions.

Following the DFB principle, a nitrogen-free product gas is produced under gasification atmosphere and steam as gasification agent. At the exit of both reactors the gas streams are separated from the bed material via gravity separators and cyclones afterwards. The advanced 100 kW_{th} pilot plant is equipped with an enhanced gasification reactor system, which increases the product gas quality significantly. This advanced design exhibits an upper gasification reactor with geometrical constrictions that leads to an increased hold-up of hot bed material and increases the contact time between product gas and hot bed material. The enhanced gas-solid contact in these turbulent fluidized zones promotes tar cracking and reforming reactions by the use of a catalytic bed material. Thus, the conversion efficiency is increased [17]. Further, the advanced reactor system allows for the usage of different fuels [13], [16], bed materials [18]–[21] and gasification agents [22].

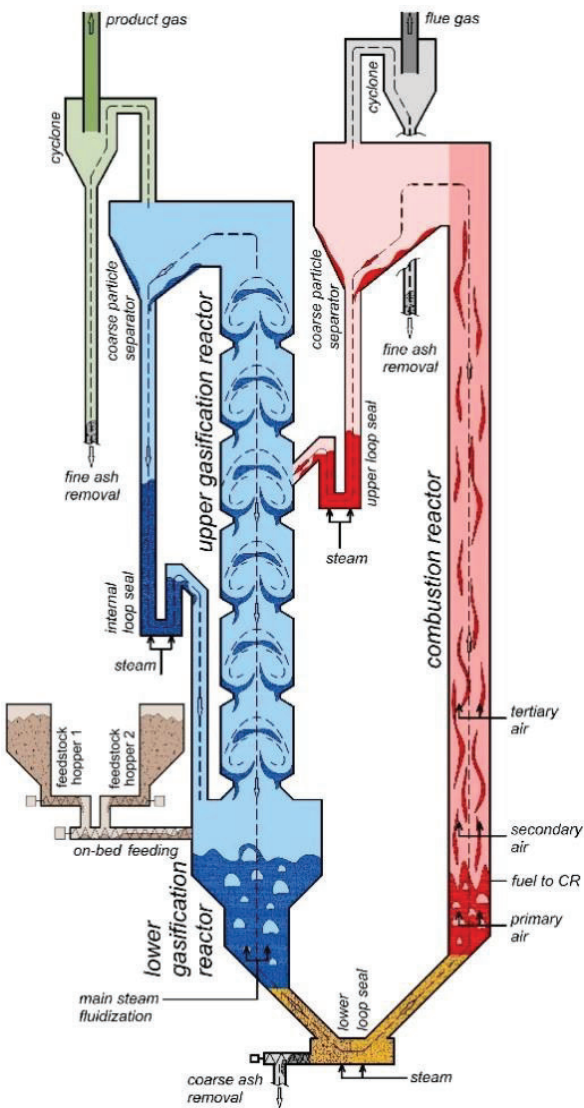


Fig. 2: Scheme of the advanced 100 kW_{th} pilot plant.

During a test run the pilot plant is controlled with a programmable logic controller (PLC). The PLC continuously measures and records data of all relevant flow rates, temperatures, pressures as well as the main gas composition of the product gas (H_2 , CO , CO_2 , CH_4) with Rosemount NGA 2000 measurement devices. Additionally, C_2H_4 and other higher hydrocarbons are analyzed every 12 min by a gas chromatograph (Perkin Elmer ARNEL - Clarus 500). Further, a standardized arrangement of sampling equipment is used to analyze the tar content in the product gas. Single tar components are determined by gas chromatography coupled with mass

spectrometry (GCMS). For tar measurements at the advanced pilot plant, toluene is used as solvent instead of isopropanol, because the solubility for tar in toluene is higher and the water content in the gas can be measured at the same time in a simple way.

2.4 Elemental analysis

Collected bed material samples were embedded in an epoxy-based resin. The epoxy disc was subsequently polished to obtain cross-sections of the bed particles, consisting of both ash and bed material, which could be used for determination of layer growth and composition. Elemental analysis of the bed material layers was carried out with a Carl Zeiss Evo LS15 scanning electron microscope (SEM) equipped with an Oxford X-Max 80 energy dispersive X-ray spectrometer (EDS). The measurements conducted were area analyses to obtain a distribution of elements.

3. Results and discussion

3.1 Product gas composition and catalytic activity

The gas compositions measured throughout the experiments are summarized in Fig. 3. The deviation from the WGS equilibrium was chosen as parameter to quantify the catalytic activity. This deviation was calculated according to the following equation [20]:

$$p\delta_{eq,WGS}(p_i, T) = \log_{10} \left[\frac{\prod_i p_i^{\nu_i}}{K_P(T)} \right]$$

It can be seen in Fig. 3 that two independent parameters, namely the type of bed material and the fuel ash content, have an influence on the gas composition.

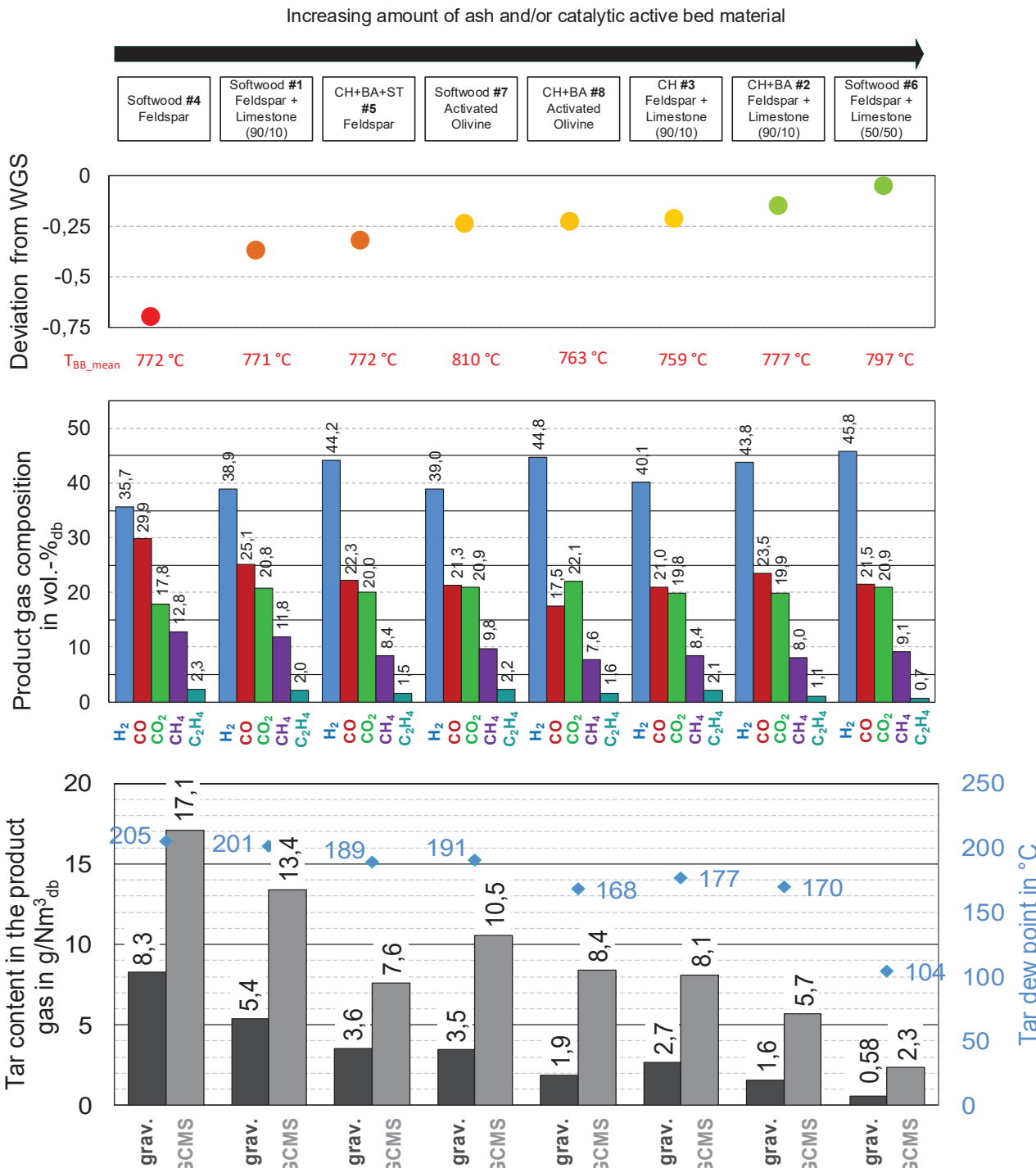


Fig. 3: Gas composition dependency of the catalytic activity of bed material and fuel ash. Upper image: Deviation of the product gas composition from the WGS equilibrium (T_{BB_mean}: bubbling bed mean temperature). Middle image: Product gas composition observed. Lower image: gravimetric and GCMS tar in the product gas as well as the tar dew point of the GCMS components calculated according to the calculation tool from the Energy Research Centre of the Netherlands (ECN) [23]

The activity of the bed material, which has been the focus of extensive research [12], [24], [25], has a clear effect on the obtained gas composition. When K-

feldspar is used as bed material the product gas composition highly deviates from the WGS equilibrium. The deviation from the WGS equilibrium correlates with low H₂

contents in the product gas as well as higher tar contents and a higher tar dew point. High contents of limestone, which is calcined (mainly CaO) at the temperature level in the system, led to increased H₂ contents in the gas and a smaller deviation from the WGS equilibrium. These results are in accordance with literature stating the high catalytic activity of CaO [12], [18]. The activated olivine shows an intermediate catalytic activity between K-feldspar and limestone. This order of catalytic activity of the studied bed materials was also observed by Kuba et al. who showed that K-feldspar is an inactive bed material, followed by fresh olivine and layered (activated) olivine. Limestone showed the highest catalytic activity in the study [26].

The fuel ash content is the second parameter influencing the catalytic activity. This is obvious when comparing experiments #4 and #5. Pure K-feldspar was used for both experiments. When softwood (low ash content) was used, the product gas highly deviated from the WGS equilibrium. Using a fuel with elevated contents of ash increased the H₂ content in the product gas considerably. Further, the tar content in the gas could be reduced by more than half. This is a promising result for the further use of residual biomass, since residual biomass tends to contain higher ash contents compared to wood and woody biomass. It should be possible to activate even inactive bed materials during operation, making it possible to use a broader range of bed materials for DFB steam gasification. The in-situ activation of feldspars in DFB steam gasification was already observed in literature [9], [10].

3.2 Ash layer analysis

Exemplary EDS mappings will be presented in the following section. Due to the short experimental time of a few hours it was not possible to develop layers thick enough for a quantitative analysis.

Though, it was still possible to observe thin layers forming on the bed materials. Fig. 4 shows EDS mappings of bed material samples from experiments #2, #3, and #5. The brightness indicates the concentration of a certain element, in this case the concentration of K, Ca, Si and P. Layers are indicated by thin contours around a bed particle with a different composition compared to the layer. K-feldspar particles are indicated by high concentrations of K, Si and Al (not depicted). The layers formed on K-

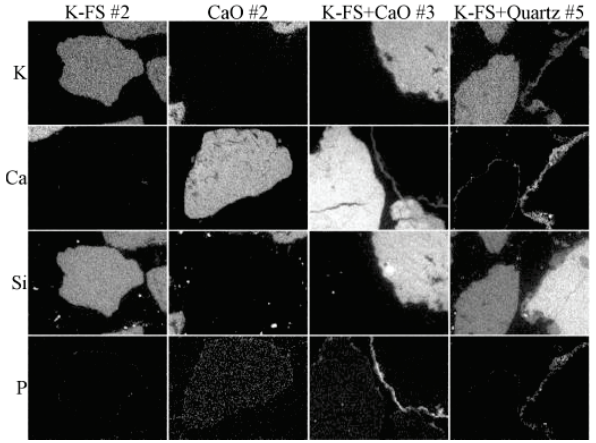


Fig. 4: EDS mappings of selected bed material samples.

feldspar particles are containing Ca and P, which is discernible in varying degrees for the different samples. The most pronounced layers formed after the gasification of chicken manure, while the thinnest layers developed during the gasification of bark (0.7) – CM (0.3). Limestone particles are indicated by high concentrations of Ca. No layer formation is recognizable for those limestone particles. This could be due to the low abrasion resistance of limestone.

The quartz particle (rich in Si) observed for experiment #5, which is a contamination stemming from the bed material, formed layers rich in K, Ca, and P. The layers observed for K-feldspar and quartz are in accordance with already observed layer formation for P-rich fuels [27], [28].

The layer formation observed for these experiments is assumed to be one reason for the increased catalytic activity compared to the gasification of softwood (experiments #1 and #4, respectively). The increased ash contents in the fuel led to an accelerated accumulation of ash inside the system, enhancing the layer formation tendency.

The catalytic activity of bed material layers is frequently described in literature [7], [9], [26], [29]. In literature, special focus is given to Ca-rich ash layers [15], [30] and alkali-rich layers [25], [31], which are both attributed with a positive influence on the catalytic activity. Both Ca and K were found in the layers, as seen in Fig. 4, correlating to the increased catalytic activity during DFB steam gasification (Fig. 3).

4. Conclusion and outlook

The product gas composition and the tar content were determined for several gasification campaigns at the 100 kW_{th} pilot plant. The deviation from the WGS equilibrium was introduced as a parameter to quantify the catalytic activity inside the gasification reactor. The results showed that it was possible to enhance the catalytic activity either by a catalytically active bed material or by an ash-rich fuel, which lead to the formation of an ash-rich layer on the bed material.

6. Acknowledgements

This study was carried out within the Bioenergy2020+ GmbH projects N200560 and C200410. Bioenergy2020+ GmbH is funded within the Austrian COMET program, which is managed by the Austrian Research Promotion Agency (FFG) and promoted by the federal government of Austria as well as the federal states of Burgenland, Niederösterreich, and Steiermark. We are grateful for the support of our project partner, the Institute of Chemical Engineering, Environmental and Bioscience Technology at the TU Wien. The Kempe Foundation is thanked for their financial support of the post-doctoral research of Matthias Kuba at Umeå University and Luleå University of Technology. The authors acknowledge the facilities and technical assistance from Cheng Choo Lee of the Umeå Core Facility for Electron Microscopy (UCEM - NMI node) at the Chemical Biological Centre (KBC), Umeå University.

Especially Ca and K in layers are known for their positive influence on the catalytic activity. Both elements were observed in the layers, further explaining the observed increase in catalytic activity.

5. Abbreviations

CM	chicken manure
db	dry basis
DFB	dual fluidized bed
FS	feldspar
K-FS	Potassium-feldspar
GCMS	gas chromatography coupled with mass spectrometry
PLC	programmable logic controller
SW	softwood
WGS	water gas shift

Symbols

d_{sv}	diameter of spherical volume
$K_p(T)$	equilibrium constant of a specific chemical reaction (dependent on T)
p	pressure
p_i	partial pressure of component i
T	temperature
T_{BB_mean}	bubbling bed mean temperature
$\delta_{eq,WGS}$	logarithmic equilibrium deviation of the WGS reaction
v_i	stoichiometric factor of component i

7. References

- [1] A. Sauciuc, A. Potetz, G. Weber, R. Rauch, H. Hofbauer, and L. Dumitrescu, ‘Synthetic diesel from biomass by Fischer - Tropsch synthesis’, *Renew. Energy Power Qual. J.*, pp. 337–342, May 2011.
- [2] M. Binder, R. Rauch, and H. Hofbauer, ‘Improving the propanol yield of mixed alcohol synthesis based on wood gas derived from biomass steam gasification’, presented at the 5th International Symposium on Gasification and its Applications (iSGA-5), Busan, Korea, 2016.
- [3] M. Binder, R. Rauch, M. Koch, M. Summers, C. Aichernig, and H. Hofbauer, ‘Influence of Sulfur Components on the Catalytic Mixed Alcohol Synthesis Based on Wood Gas Derived from Biomass Steam Gasification’, 2017.
- [4] M. Kraussler, F. Pontzen, M. Müller-Hagedorn, L. Nenning, M. Luisser, and H. Hofbauer, ‘Techno-economic assessment of biomass-based natural gas substitutes against the background of the EU 2018 renewable energy directive’, *Biomass Convers. Biorefinery*, vol. 8, no. 4, pp. 935–944, Dec. 2018.
- [5] M. Kraussler, M. Binder, and H. Hofbauer, ‘2250-h long term operation of a water gas shift pilot plant processing tar-rich product gas from an industrial scale dual fluidized bed biomass steam gasification plant’, *Int. J. Hydrg. Energy*, vol. 41, no. 15, pp. 6247–6258, Apr. 2016.
- [6] J. C. Schmid, U. Wolfesberger, S. Koppatz, C. Pfeifer, and H. Hofbauer, ‘Variation of feedstock in a dual fluidized bed steam gasifier— influence on product gas, tar content, and composition’, *Environ. Prog. Sustain. Energy*, vol. 31, no. 2, pp. 205–215, Jul. 2012.
- [7] F. Kirnbauer and H. Hofbauer, ‘Investigations on Bed Material Changes in a Dual Fluidized Bed Steam Gasification Plant in Güssing, Austria’, *Energy Fuels*, vol. 25, no. 8, pp. 3793–3798, Jul. 2011.
- [8] M. Kuba *et al.*, ‘Mechanism of Layer Formation on Olivine Bed Particles in Industrial-Scale Dual Fluid Bed Gasification of Wood’, *Energy Fuels*, vol. 30, no. 9, pp. 7410–7418, Sep. 2016.
- [9] K. Wagner, A. M. Mauerhofer, M. Kuba, and H. Hofbauer, ‘Suitability of K-feldspar as Alternative Bed Material in Dual Fluidized Bed Steam Gasification in Combination with Ash-Rich Feedstocks’, in *23rd International Conference on FBC*, Seoul, Korea, 2018, pp. 967–976.
- [10] N. Berguerand and T. Berdugo Vilches, ‘Alkali-Feldspar as a Catalyst for Biomass Gasification in a 2-MW Indirect Gasifier’, *Energy Fuels*, vol. 31, no. 2, pp. 1583–1592, Feb. 2017.
- [11] N. Berguerand, J. Marinkovic, T. Berdugo Vilches, and H. Thunman, ‘Use of alkali-feldspar as bed material for upgrading a biomass-derived producer gas from a gasifier’, *Chem. Eng. J.*, vol. 295, pp. 80–91, Jul. 2016.
- [12] A. M. Mauerhofer, F. Benedikt, J. Christian Schmid, and H. Hofbauer, ‘Mixtures of Silica Sand and Calcite as Bed Material for Dual Fluidized Bed Steam Gasification’, in *Proceedings of SEEP2017*, 2017, pp. 253–266.
- [13] F. Benedikt, J. Fuchs, J. C. Schmid, S. Müller, and H. Hofbauer, ‘Advanced dual fluidized bed steam gasification of wood and lignite with calcite as bed material’, *Korean J. Chem. Eng.*, vol. 34, no. 9, pp. 2548–2558, Sep. 2017.
- [14] F. Kirnbauer, V. Wilk, H. Kitzler, S. Kern, and H. Hofbauer, ‘The positive effects of bed material coating on tar reduction in a dual fluidized bed gasifier’, *Fuel*, vol. 95, pp. 553–562, May 2012.

- [15] M. Kuba, F. Havlik, F. Kirnbauer, and H. Hofbauer, ‘Influence of bed material coatings on the water-gas-shift reaction and steam reforming of toluene as tar model compound of biomass gasification’, *Biomass Bioenergy*, vol. 89, no. Supplement C, pp. 40–49, Jun. 2016.
- [16] F. Benedikt, J. C. Schmid, J. Fuchs, A. M. Mauerhofer, S. Müller, and H. Hofbauer, ‘Fuel flexible gasification with an advanced 100 kW dual fluidized bed steam gasification pilot plant’, *Energy*, vol. 164, pp. 329–343, Dec. 2018.
- [17] A. M. Mauerhofer, J. C. Schmid, F. Benedikt, J. Fuchs, S. Müller, and H. Hofbauer, ‘Dual fluidized bed steam gasification: Change of product gas quality along the reactor height’, *Energy*, vol. 173, pp. 1256–1272, Apr. 2019.
- [18] A. M. Mauerhofer, F. Benedikt, J. C. Schmid, J. Fuchs, S. Müller, and H. Hofbauer, ‘Influence of different bed material mixtures on dual fluidized bed steam gasification’, *Energy*, vol. 157, pp. 957–968, Aug. 2018.
- [19] J. Fuchs, J. C. Schmid, S. Müller, and H. Hofbauer, ‘Dual fluidized bed gasification of biomass with selective carbon dioxide removal and limestone as bed material: A review’, *Renew. Sustain. Energy Rev.*, vol. 107, pp. 212–231, Jun. 2019.
- [20] J. Fuchs, J. C. Schmid, S. Müller, A. M. Mauerhofer, F. Benedikt, and H. Hofbauer, ‘The impact of gasification temperature on the process characteristics of sorption enhanced reforming of biomass’, *Biomass Convers. Biorefinery*, May 2019.
- [21] J. Fuchs *et al.*, ‘The impact of bed material cycle rate on in-situ CO₂ removal for sorption enhanced reforming of different fuel types’, *Energy*, vol. 162, pp. 35–44, Nov. 2018.
- [22] A. M. Mauerhofer, J. Fuchs, S. Müller, F. Benedikt, J. C. Schmid, and H. Hofbauer, ‘CO₂ gasification in a dual fluidized bed reactor system: Impact on the product gas composition’, *Fuel*, vol. 253, pp. 1605–1616, Oct. 2019.
- [23] ‘Energy research center of The Netherlands (ECN)’. [Online]. Available: <http://www.thersites.nl/completemodel.aspx>. [Accessed: 12-Jul-2019].
- [24] K. Göransson, U. Söderlind, P. Engstrand, and W. Zhang, ‘An experimental study on catalytic bed materials in a biomass dual fluidised bed gasifier’, *Renew. Energy*, vol. 81, pp. 251–261, Sep. 2015.
- [25] T. Berdugo Vilches, J. Marinkovic, M. Seemann, and H. Thunman, ‘Comparing Active Bed Materials in a Dual Fluidized Bed Biomass Gasifier: Olivine, Bauxite, Quartz-Sand, and Ilmenite’, *Energy Fuels*, vol. 30, no. 6, pp. 4848–4857, Jun. 2016.
- [26] M. Kuba, F. Kirnbauer, and H. Hofbauer, ‘Influence of coated olivine on the conversion of intermediate products from decomposition of biomass tars during gasification’, *Biomass Convers. Biorefinery*, vol. 7, no. 1, pp. 11–21, Mar. 2017.
- [27] K. Wagner, M. Kuba, G. Häggström, N. Skoglund, M. Öhman, and H. Hofbauer, ‘Influence of Phosphorus on the Layer Formation on K-feldspar During Fluidized Bed Combustion and Gasification’, *Eur. Biomass Conf. Exhib. Proc.*, vol. 26th EUBCE-Copenhagen 2018, pp. 486–492, 2018.
- [28] K. Wagner *et al.*, ‘Layer formation mechanism of K-feldspar in bubbling fluidized bed combustion of phosphorus-lean and phosphorus-rich residual biomass’, *Appl. Energy*, vol. 248, pp. 545–554, Aug. 2019.
- [29] T. Berdugo Vilches, M. C. Seemann, and H. Thunman, ‘Influence of in-bed catalysis by ash-coated olivine on tar formation in steam gasification of biomass’, *Energy Fuels*, Aug. 2018.
- [30] J. Kryca, J. Priščák, J. Łojewska, M. Kuba, and H. Hofbauer, ‘Apparent kinetics of the water-gas-shift reaction in biomass gasification using ash-layered olivine as catalyst’, *Chem. Eng. J.*, vol. 346, pp. 113–119, Aug. 2018.

- [31] K. Umeki, G. Häggström, A. Bach-Oller, K. Kirtania, and E. Furusjö, ‘Reduction of Tar and Soot Formation from Entrained-Flow Gasification of Woody Biomass by Alkali Impregnation’, *Energy Fuels*, vol. 31, no. 5, pp. 5104–5110, May 2017.

Catalytic effect of potassium in thermochemical gasification of biogenic resources in a floating fixed bed gasifier

A. Hofmann^{1*}, H. Füssl-Le¹, B. Hupfauf¹

1. MCI Management Center Innsbruck – The Entrepreneurial School, Dpt. Environmental, Process & Energy Engineering

Maximilianstrasse 2, 6020 Innsbruck, Austria

*corresponding author: angela.hofmann@mci.edu

Abstract

The floating fixed bed wood gasifier has a potential to use low-cost residues from agriculture and forestry. Those feedstocks often contain relevant amounts of potassium salts that are known to lower the ash melting point and to catalytically accelerate the Boudouard reaction, which is one of the main reactions in the gasification process. The influence of varying amounts and types of potassium salts on the reaction rate of the Boudouard reaction was quantified in previous works. Basing on these findings, an ASPEN-Plus®-based tool (SBR-Sim 3.0) was developed to simulate the product gas composition and temperature profile in the floating fixed bed gasifier, caused by potassium-induced changes of the reaction kinetics of the Boudouard reaction.

The main findings from the simulations were that the CO content of the product gas and the carbon conversion rate can be increased when increasing the reaction rate of the Boudouard reaction up to a factor of two, thus improving product gas quality. With a higher enforcement of the reaction rate of the endothermic Boudouard reaction, the reaction lowers the overall temperature in the reactor, thus leading to undesirably increased CO₂ output. Conclusions are drawn on how the potassium content of potassium-containing feedstock will influence product gas quality and temperature profile in the reactor to predict gasification behavior by analyzing the chemical composition of the raw material.

1. Introduction

Biogenic residues for gasification

The floating fixed bed gasification technology was developed for the energetic use of woodchips in the range of 1 to 5 MW of fuel power. In this staged co-current process, the gravity force of the bulk bed is balanced by the force of the ascending pyrolysis gas flow, which leads to low pressure loss across the bed and avoids the generation of gas channels in the bulk bed. The comparatively long residence time of the pyrolysis gas in the charcoal bed allows an efficient conversion of tars, hence producing

constant gas qualities with tar contents below 50 mg m⁻³ (u.s.c) [1].

The use of biogenic residues is of relevance both from an ecological and from an economic point of view. As woodchips represent a high value feedstock that is exposed to high competition regarding its usage (building material, pulp industry), their replacement as a feedstock for energy production by biogenic residues (straw, corn husks etc.) or biogenic wastes (sewage sludge, biogas digestate, waste wood etc.) is desirable. Many of those alternative biogenic raw materials (ABR) are characterized by the following properties:

- The raw material is more inhomogenic than woodchips
- The calorific value is lower than in woodchips
- The ash content is higher than in woodchips
- An increased level of potassium in the ash increases slagging tendencies

These unfavorable properties are contrasted with a lower purchase price, which might increase the economic interest in using ABR. The adaptation of a wood gasification plant to ABR requires considering not only altered fluidic properties caused by varying particle shapes and an altered situation for gas purification but also the slagging properties of raw materials with high potassium content.

The influence of potassium on reaction kinetics, mainly the Boudouard reaction as a representative of heterogenous gasification reaction, was described in previous work [2][3]. The main findings are summarized in this paper. Basing on these findings, an ASPEN Plus ® based simulation tool, SBR-Sim 3.0, was developed [4] to simulate the influence of the enhanced reaction rate of the Boudouard reaction on the product gas composition as well as on the temperature profile in the floating fixed bed reactor. [5]

Floating fixed bed gasification

The floating fixed bed gasification is a two-stage autothermal process. In the first stage, the feed material is dried and pyrolyzed at temperatures of 450 to 500 °C. The resulting pyrolysis gas and pyrolysis char are fed to the second stage, the core part of the gasification plant. In this conic reactor, the oxidation and

reduction reactions take place. The floating fixed bed is established by feeding both the gas and the char from the reactor bottom, against gravity. Below the lower edge of the bed, the gasification air is introduced, creating a highly turbulent and partly oxidative zone that provides the required heat for the process. The widening of the reactor towards the top helps to keep the bed floating, saves the need for a grate and avoids sintering of constructive elements. The char particles are thermo-chemically reduced while moving upward in the bed. The product gas is collected at the reactor top and subject to downstream treatment. The basic product gas composition is 17-19 % H₂, 14-16 % CO, 14-16 % CO₂, 1,0-2,5 % CH₄, 47-49 % N₂ (result of > 100 test runs; %vol). Total BTEX range < 100 ppm, total PAH < 10 ppm and total gravimetric tars < 100 ppm.

The constructive design of the reactor allows for low pressure loss (<100 mbar), even material distribution across the cross-section, relatively long gas residence times (5-6 s), and thus avoids local hot spots, material compaction, gas channeling, wall flow and resulting tar creation.

Ash melting behavior

According to Kahn et al. [6], biomass can be classified in six categories following biomass composition, its combustion pattern and ash composition. [7] defines four categories of fuels, based on the oxides of their main ash components, see figure 1. While calcium and magnesium dominate in woody ashes (1), waste materials (3) contain relevant amounts of ferrous oxides. However, it has to be noted that in biogenic materials, in general the component composition distribution may vary substantially.

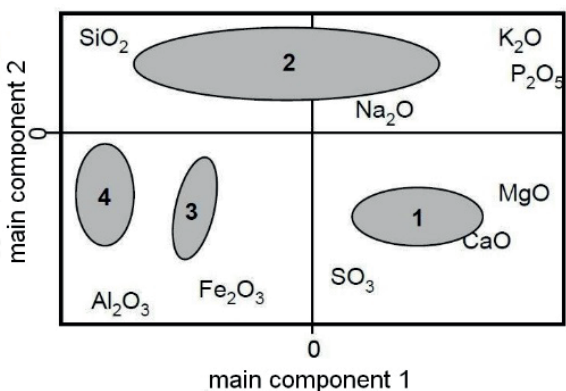


Figure 1: Fuel categories, according to their main ash components (1 = woody biomass, 2 = culmiferous (straw-based) biomass, 3 = waste materials, 4 = chars) [7]

Ash melting patterns are characterized by four standardized specific temperatures (shrinking starting temperature, initial deforming temperature, hemisphere temperature, flow temperature). The complex reaction schemes of biogenic feedstock ash components are difficult to predict. Several authors, such as [7][8][9], made efforts to conclude the ash melting pattern from the ash composition. However, most findings are basing on ashes from combustion plants. With gasification, also a high carbon content can be found in the ash. The remaining carbon influences the ash melting [5], and due to the diversity of biomass compositions, a defined ash melting point does not exist.

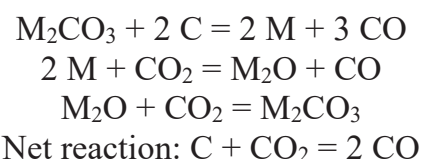
Potassium as a catalyst

Potassium has a history of use as a catalyst in coal gasification for acceleration of heterogenic reactions [10][11]. Numerous publications confirm the catalytic properties of potassium in coal gasification reactions. It catalyzes the heterogeneous water-gas reaction of activated carbon in the same way as a metal oxide catalyst [10]. It improves the oxygen transfer from the gas phase to the carbon surface, thus increasing the number of adsorptive bonds of carbon to oxygen and to carbon monoxide. Hence, the

carbon-carbon bonds are weakened and reactivity is enhanced [12]. Potassium and sodium carbonate catalyze the Boudouard reaction mainly at temperatures below 1000 °C, while above 1000 °C non-catalytic mechanisms are effective [13]. The reaction rate of the heterogenous water-gas reaction is enhanced by a factor of 10 when adding 10 %m potassium carbonate to a char gasification with steam and CO₂. At a constant carbon conversion rate, the gasification temperature could be lowered below 700 °C [14].

At steam gasification of spruce, a 3.0 mmol alkali supplement of potassium carbonate per g spruce increased carbon turnover from 77 to 93 % [15]. At examinations of potassium in various biomass ashes it was found that the catalytic activity of potassium is decreased by silicon. It is assumed that potassium silicates are formed, which deactivate the catalytic mechanisms [16].

At the Boudouard reaction, the catalytic effect of potassium is described by two mechanisms. One of those is relevant for this paper and restricted to temperatures below 800 °C. The reaction steps are described as follows with M representing any alkali metal [17]:



The mechanism shows that the reaction steps could run infinitely without the alkali carbonate being depleted [18].

In the context of gasification of low melting raw materials it was investigated if and to what extent the gasification temperature in the reactor can be lowered in order to achieve a carbon conversion rate that is equivalent to wood gasification,

considering the temperature-dependent longer residence time in the floating fixed bed reactor [5]. Therefore, various biogenic raw materials with varying potassium contents as well as potassium-added spruce wood samples were gasified in the lab under CO₂ and steam atmospheres, respectively, to determine the carbon turnover reaction velocity compared to raw spruce wood. The data base for the ASPEN Plus®-based simulation tool SBR-Sim 3.0 was fed with the results of those examinations. Carbon turnover and relative reaction velocity were investigated by thermogravimetric analysis (TGA) [3]. Pyrolyzed pellets of wood (partly supplemented by various potassium salts) and biogenic residues were gasified under CO₂ atmosphere. It was found that by adding up to 5 %m of potassium, at 850 °C, the reaction velocity multiplies up to the quadruple. The catalytic effect of potassium could not be quantified exactly because of strong dependency on the type of potassium salt used. However, it is concluded that the raw material's composition already suggests its reactivity [2][3]. As the possibility exists that potassium silicates (eutectica) are formed that may further lower the melting point [16][19] and as well back-influence the catalytic effect of potassium, the effect of silicon content in samples is highlighted in [3].

2. Concept and methodology

The standard model of ASPEN Plus® does not cover kinetics and residence time data. The calculations result from thermodynamic equilibria. The heterogeneous water-gas reaction is a rather slow reaction, and it can be assumed that the residence time in the respective temperature zone in the reactor is not long enough to achieve equilibrium. Thus, kinetics had to be programmed additionally by Fortran modules. Hence,

the following reactions were completed by kinetic data [4]:

- Carbon oxidation
- Hydrogen oxidation
- Boudouard reaction
- Heterogeneous water-gas reaction
- Hydrogenating gasification reaction
- Water-gas shift reaction

Starting from the version SBR-Sim 2.x that still produced strong deviances in the gas composition, the model was refined by kinetic data from literature and the reactivity of pyrolysis char via the CRF (char reactivity factor) [20]. The updated SBR-Sim 3.0 shows only small deviations from real experimental data of the pilot gasification plant with a fuel power of 250 kW. The comparative results are shown in figure 2.

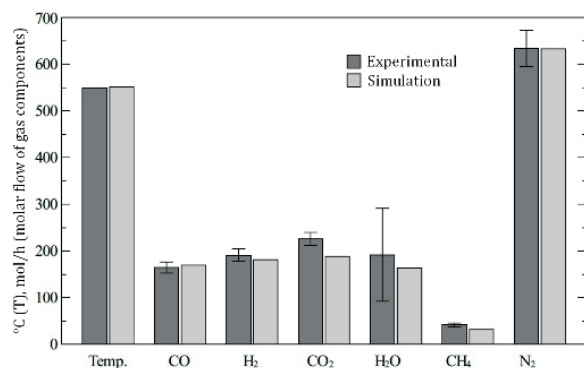


Figure 2: Product gas temperature and composition: Experimental (VL CW Alpha) and Simulation (SBR-Sim 3.0)

The simulation design covers the particularities of operation and reactor type. Phase ratios, temperature control and residence time patterns cannot be reproduced through one of the standard appliances provided by the simulation software. Due to the strong variations of temperature and concentrations across the reactor height, the floating fixed bed reactor may best be compared to a plug flow reactor.

In addition to temperature and concentration changes of all reactants, also particle sizes, bulk and particle porosities as well as particle surface areas change as particles move through the reactor. Due to the conic reactor geometry, also the gas-particle residence time and the inflow velocity vary across the reactor height. This is why a cascade of stirred tank reactors is chosen for the simulation model. It is assumed to reflect the prevalent reaction conditions in relation to the respective site in the reactor. It also allows to assign higher definition to more relevant zones of the reactor such as the inlet or the lower edge of the charcoal bed, and to simplify less relevant parts. 14 continuously stirred tank reactors (RED-1 to RED-14) were defined, starting at the reactor bottom where the feed and gas inlets are located (see figure 3).

In the simulation model, the following assumptions were made:

- The simulation covers only the main floating fixed bed reactor, i.e. oxidation and reduction processes. Upstream drying and pyrolysis and downstream dust filtering, gas washing etc. are neglected.
- The feed stream is composed of pyrolysis gas and char and based on empirical data.
- Due to its special structure and the inherent several reaction zones, the reactor is modeled as a series of cascading stirred tank reactors.
- Only the steady state is investigated. Radial temperature and concentration gradients are neglected.
- The main reactions are given with the relevant kinetic data. Any further

intermediate and side reactions will be calculated by the simulation software.

- Particles are handled according to the shrinking core model.

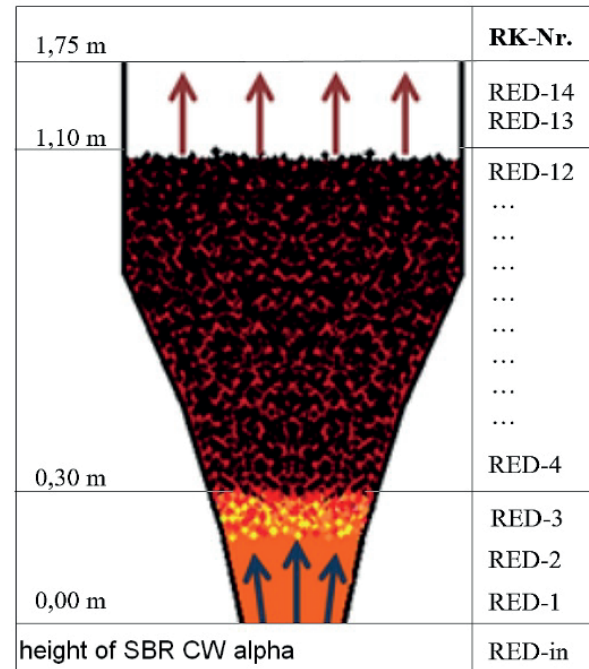


Figure 3: Modeling the reactor segmentation

For the simulation, the Boudouard reaction is considered a pseudo first order reaction (carbon is a solid available in excess). In this case, the reaction velocity r_i is a product of reaction velocity constant k_i and the concentration of carbon dioxide, and hence a factor to increase the reaction velocity equates to a factor of k_i (see eq. 1-3).

$$r_{C-CO_2} = k_{C-CO_2} \cdot c_C \cdot (p_{CO_2} - p_{CO_2}^*) \cdot V_{ST} \quad (1)$$

$$k_{C-CO_2} = k_{0, C-CO_2} \cdot e^{-\frac{E_{A, C-CO_2}}{RT}} \quad (2)$$

$$p_{CO_2}^* = \frac{p_{CO_2}}{e^{20,92 + \frac{20280}{T}}} \quad (3)$$

with

r_{C-CO_2} reaction rate in $\frac{mol}{s}$

k_{C-CO_2} reaction velocity constant in $\frac{1}{atm \cdot s}$

c_C molar carbon concentration in $\frac{mol}{m^3}$

p_{CO_2} partial pressure of carbon dioxide in atm

$$\begin{aligned}
 V_{ST} & \text{ stirred tank volume in m}^3 \\
 k_{0, C\text{-CO}_2} & = 930 \frac{1}{\text{atm} \cdot \text{s}} \\
 E_A & = 45.000 \frac{\text{cal}}{\text{mol}} \\
 R & = 8,314 \frac{\text{J}}{\text{mol K}} \\
 T & \text{ temperature in K}
 \end{aligned}$$

A schematic description of the routine of the simulation model can be retrieved from figure 4.

At constant temperature, k_i depends of the frequency factor k_0 and the activation energy E_A . By setting that parameter in ASPEN Plus® via Fortran code, the underlying kinetics can be influenced. It is assumed that the catalytic activity of potassium does not influence the steric factor significantly but intervenes only in activation energy.

Thus, the respective activation energy can be calculated. The parameters of the simulation runs are listed in table 1. For the intervention in the underlying kinetics,

the Fortran code has to be adapted and compiled before each simulation run.

Table 1: Kinetic parameter of simulation runs K 1.1 to K 1.6

	Factor of k_i	E_A in $\frac{\text{cal}}{\text{mol}}$
K 1.1	1,00	45.000
K 1.2	1,25	42.955
K 1.3	1,50	41.285
K 1.4	2,00	38.648
K 1.5	3,00	36.606
K 1.6	5,00	34.932

Material streams are marked red, calculation modules black and energy loss streams green. The main input stream is split to PYRO-GAS and CHAR streams. The PYRO-GAS stream is defined by real pilot test data. Tars contained in pyrolysis gas are referred to as benzene.

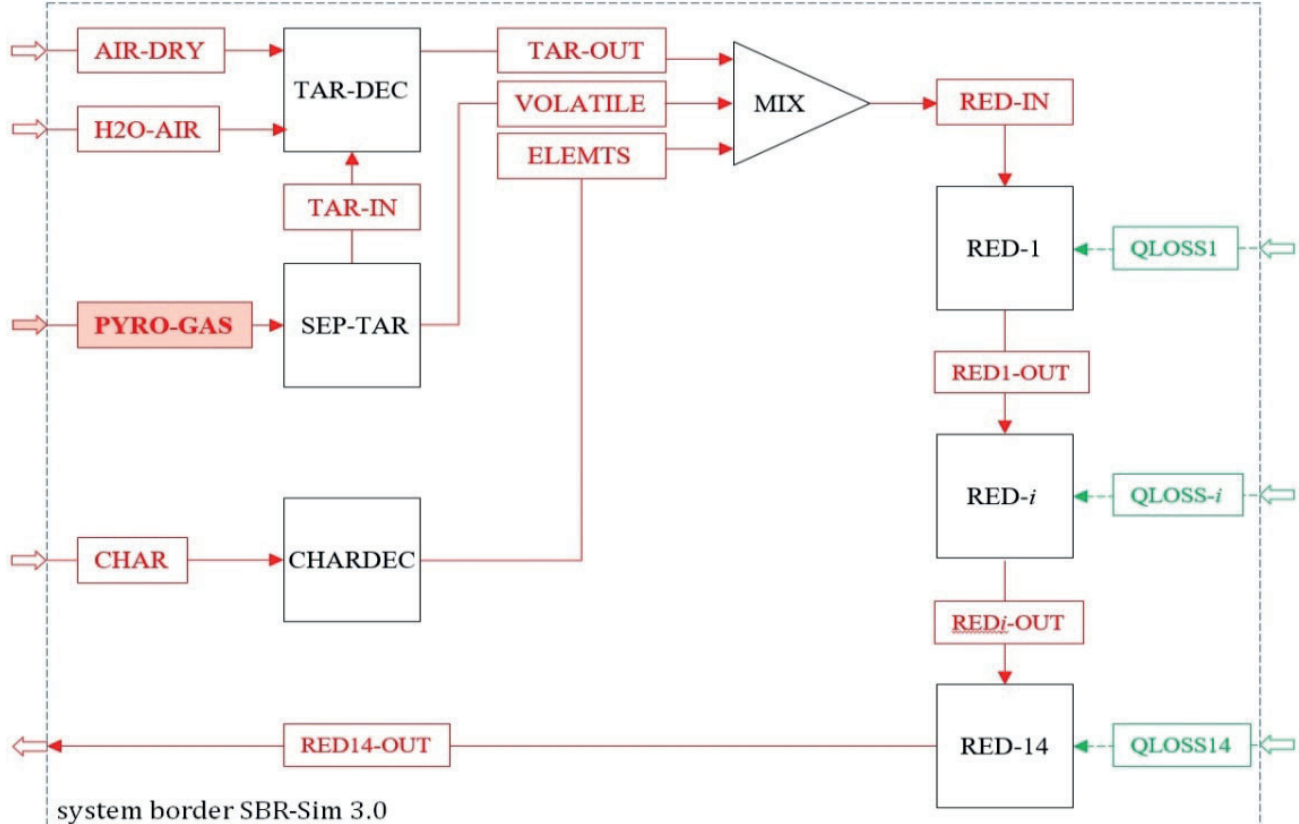


Figure 4: Process, modelled in SBR-Sim 3.0

According to pilot test results, tar cracking is an upstream process of the TAR-IN (benzene) stream, effected in TAR-DEC at air/750°C. The resulting product stream is TAR-OUT. The solids stream CHAR is defined a non-conventional solids stream that does not participate in chemical equilibrium. CHAR is decomposed into its components at CHARDEC. The resulting ELEMITS stream contains a conventional elemental stream of reaction partners.

The gasification air consists of a mixture of AIR-DRY and H₂O-AIR.

The streams resulting from those upstream processes are mixed (MIX) and fed to the reactor as RED-IN. The reactor is segmented into a cascade of 14 separately parametrized continuous stirred tank reactors (CSTR, RED-*i*) that the streams pass and leave as RED14-OUT. Heat losses are referred to as negative input streams QLOSS-*i*.

Based on the simulation of the VL CW Alpha [20] and the kinetics proposed in [21] for the Boudouard reaction, the reaction velocity is varied by the factor of 1 to 5.

The profiles of temperature, gas composition and calorific value of the product gas are displayed in relation to the height of the reactor. The achievable carbon conversion rate and cold gas efficiency of the respective simulation runs are compared. The cold gas efficiency rate η signifies the heating value H_i of the product gas mass flow \dot{m} in relation to the energy content of the biomass per time unit (eq. 4):

$$\eta_{CG} = \frac{H_i, \text{product gas} \cdot \dot{m}_{\text{product gas}}}{H_i, \text{biomass} \cdot \dot{m}_{\text{biomass}}} \quad (4)$$

All experimental raw data can be retrieved from the authors on request.

3. Results and discussion

The following figures 5 and 6 show the characteristics of material flow temperature and mole flows of product gas components over the reactor height of the respective simulation runs at standard reaction velocity (factor = 1, figure 5) and 5 times increased reaction velocity (factor = 5, figure 6). The figures show that both the gas composition and the temperature at the outlet of the reactor are more or less in the same range in both cases. The big difference can be seen in the concentration and the temperature profile over the height of the reactor. With the standard reaction rate, the resulting maximum temperature in the lower zone of the reactor is at 870 °C. When rising the reaction rate by factor 5, the maximum achievable temperature is lower than 700 °C due to the enhanced endothermic reaction, and the temperature profile is more homogeneous with the standard reaction velocity. In contrast, the gas composition, mainly the mole fractions of CO and CO₂, are more homogeneous over the height in case of the higher reaction rate of the Boudouard reaction.

Figure 7 shows the temperature and dry gas heating value graphs over the reactor height of all simulation runs. The desired maximum temperature of 800 °C to avoid slagging in the reactor is indicated as a vertical line.

The simulation results demonstrate that an increase in Boudouard reaction velocity at first lowers the temperature in the whole reactor, as expected. When increasing the reaction velocity by a factor of 2, the critical temperature of 800 °C is not exceeded at any site in the reactor.

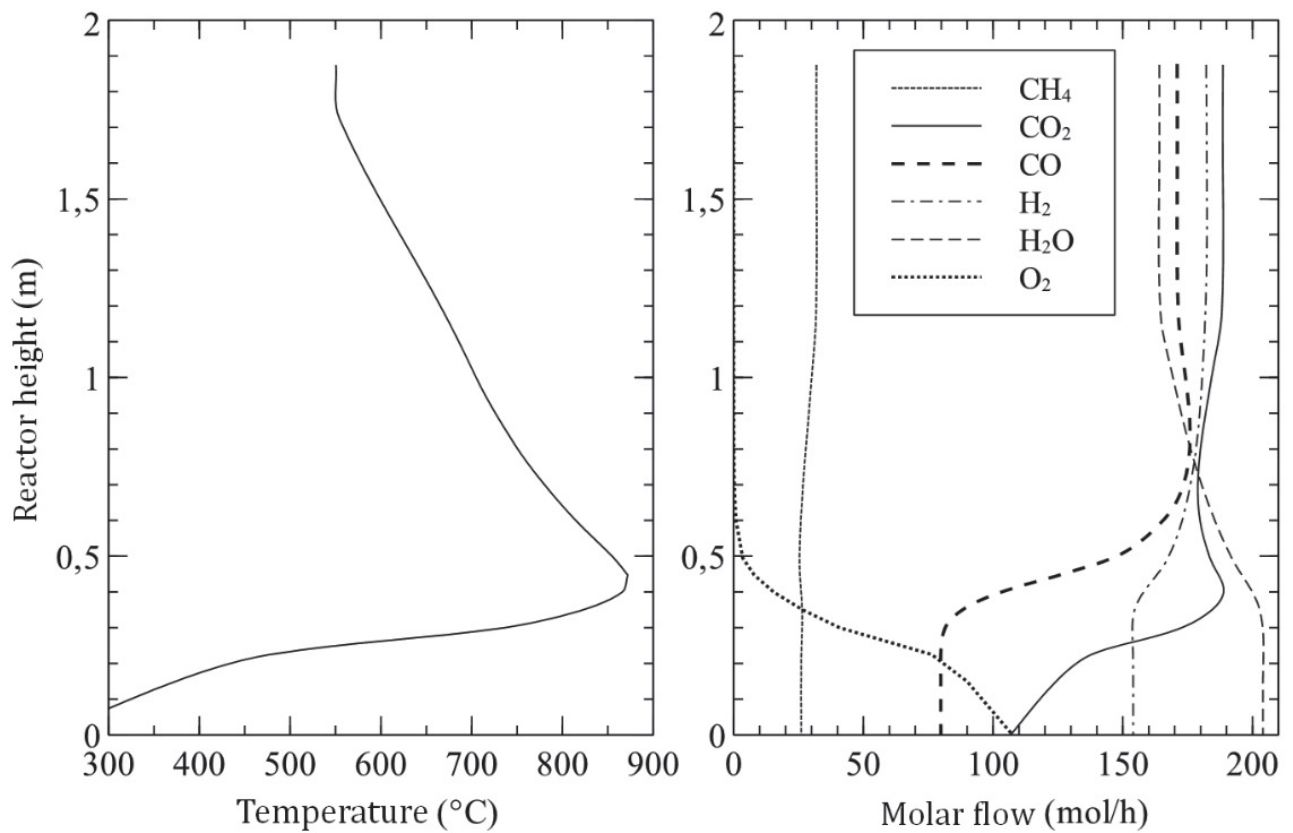


Figure 5: Temperature, \dot{n}_{gas} at respective reactor height - K 1.1, factor = 1

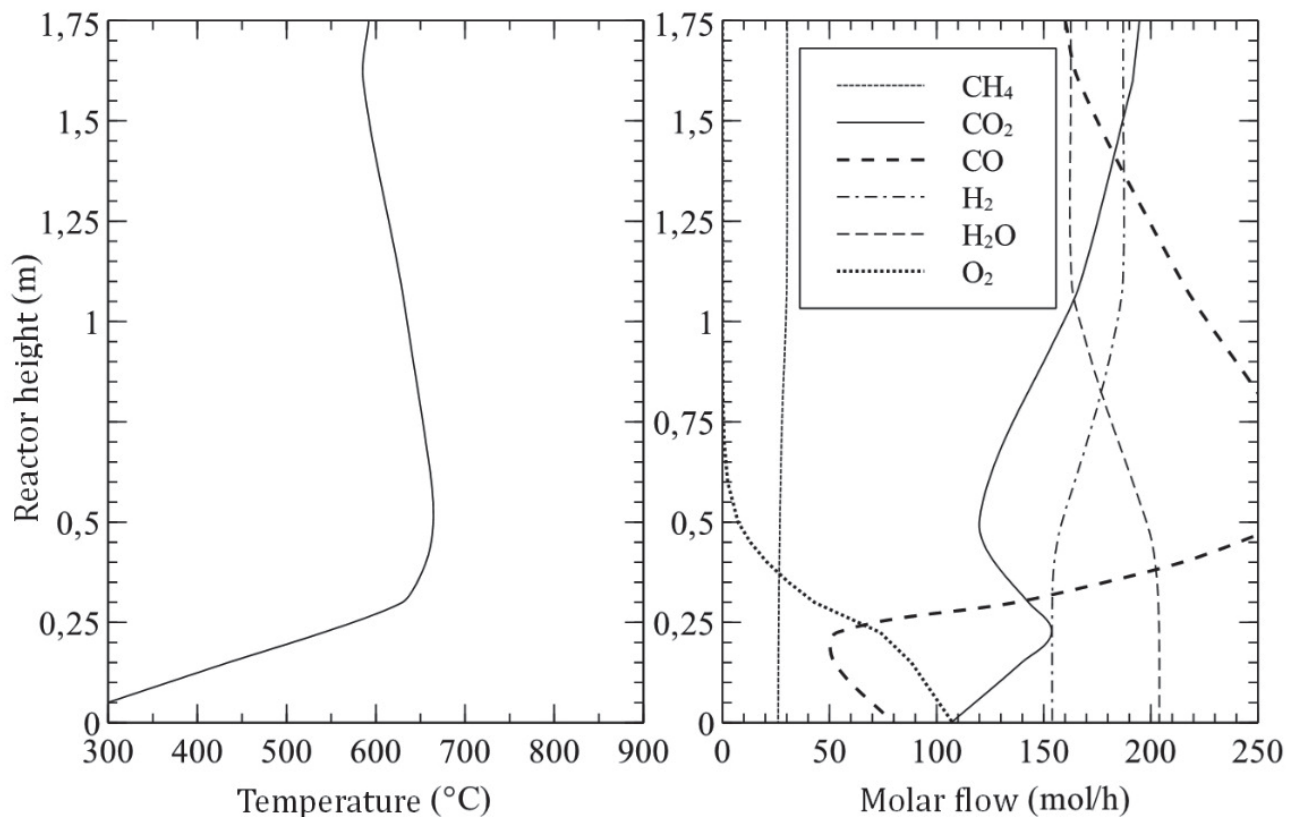


Figure 6: Temperature, \dot{n}_{gas} at respective reactor height - K 1.6, factor = 5

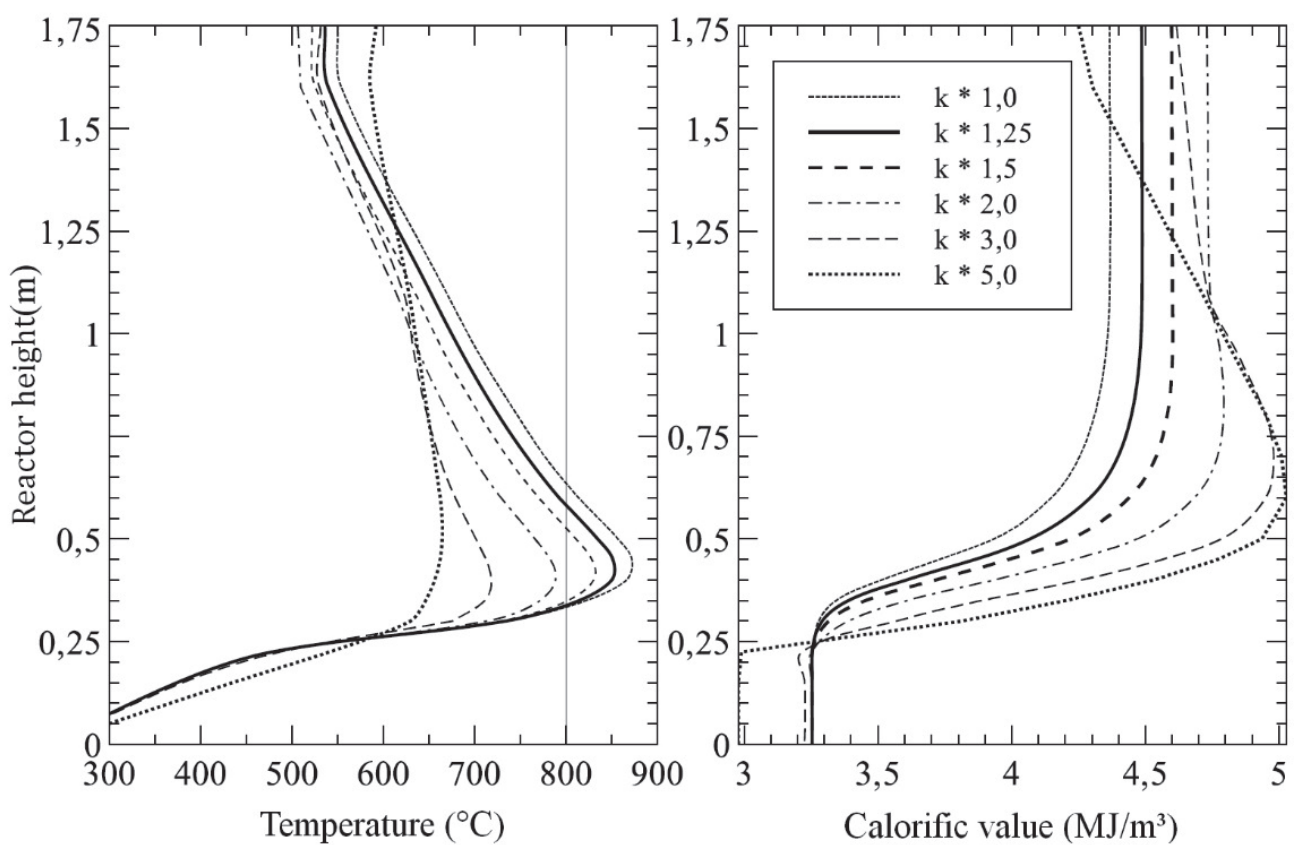


Figure 7: Temperature and heating value as a function of reaction velocity

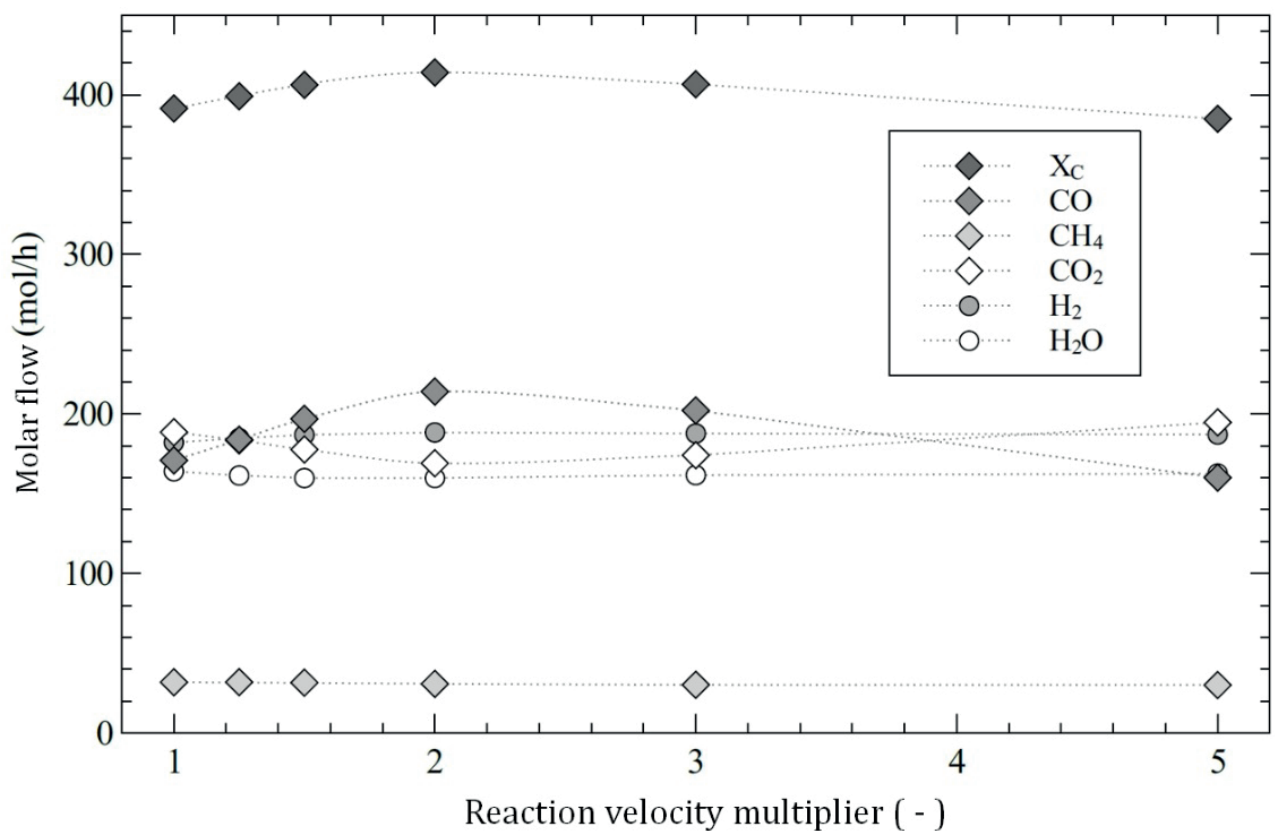


Figure 8: carbon conversion rate X_C and mole flows of product gas components

With increasing reaction velocities, the temperature profile changes: In the lower reactor segments RED-1 to RED-10 the temperature continues to drop with the factor of the reaction speed, while in higher segments (real reactor height $> 0,8$ m), the temperature is rising with a factor of 5. This might be due to a shift of Boudouard reaction equilibrium at the point where the originally endothermal reaction to carbon monoxide is inverted towards an exothermal reaction to carbon dioxide. The phenomenon can be deducted from the product gas composition, as the carbon monoxide content declines strongly while the CO₂ content increases accordingly.

Figure 8 shows the product gas composition at the reactor exit as well as the carbon conversion rate X_C in mol h⁻¹ as a function of reaction velocities.

The maximum of CO and the minimum of CO₂, respectively, can be found at the velocity factor of 2. This also leads to a maximum carbon conversion rate at the same point.

The results confirm that the potassium-induced increase of reaction velocity of the Boudouard reaction influences the carbon conversion, the reaction temperature and the product gas composition. Increasing the reaction velocity up to a factor of 2, which corresponds to a potassium content of 2.5 %m in the ash, benefits the gasification process in the chosen simulation model. At higher potassium contents, which lead to higher reaction velocity, endothermal reactions get more relevant and thus, temperatures in the reactor drop. Hence, the CO/CO₂ equilibrium is pushed towards CO₂, leading to a deterioration of product gas quality.

Although there are also catalytic effects described on the heterogeneous

water gas reaction [14], these influence could not be observed in the setup of the floating fixed bed gasification reactor, neither with experiments on the pilot plant nor in the simulation. A reason therefore could be the lower reaction speed of this reaction in combination with the low gas residence time at temperatures higher than 750 °C [4][20].

4. Conclusion and Outlook

Residues from agriculture and forestry have a high potential to be used as secondary raw materials in the energy industry. Due to their high potassium content and resulting low ash melting point, the utilization in thermo-chemical processes is restricted by technical viability. Economic advantages resulting from low procurement prices are diminished by higher cost for pretreatment and for technical adaptations of the processing plant.

The thermochemical gasification in the floating fixed bed reactor offers a certain potential to benefit from the catalytic properties of potassium containing ABR by lowering the maximum temperature in the reactor and thus avoiding the slagging temperature range. The gasification simulation by means of the SBR-Sim 3.0 simulation tool confirmed the literature data regarding the effects of potassium-enhanced reaction kinetics of the Boudouard reaction. Thus, a raw material's chemical ash composition allows to estimate if and to what extent the Boudouard reaction will be accelerated. However, an exact prediction is not possible due to the complexity of ash transformation reactions. Any potential raw material has to be analyzed by thermogravimetric analyses for a reliable statement on the extent of catalytic effects.

It has to be considered that at lower reaction temperatures, the tar reduction by

thermal cracking across the bulk material is influenced. The residence time is slightly reduced in segments above 700 °C. For the moment, it is impossible to quantify the fraction of thermal cracking on total tar reduction in the floating fixed bed reactor. It is assumed that the main fraction of tars is directly oxidized at the entrance site of the gasification air, and that the final elimination takes place across the bulk material [22]. Thus, it is possible that the remaining tar content is still much lower than at other gasification processes, even if the process is running at low temperature. However, a rise in tar content compared to standard operation mode has to be expected.

The results show that the increased reaction velocity of the Boudouard reaction to some extent positively affects the product gas quality in the floating fixed bed gasification process. The simulation tool will support further process improvements. For the future development, a model validation using real test data is indispensable. The simulation results can be considered as plausible, and they can be understood as a possible trend, as it was not yet possible to

match the simulation to real test operation results. For validation purposes, the pilot plant CW Alpha has to be adapted to meet the simulation parameters.

The low temperature gasification of potassium containing raw materials with the floating fixed bed gasification process is technically viable. However, losses in product gas quality and cold gas power have to be expected. The final decision will be an economic decision that has to be taken specifically for each raw material.

Abbreviations

ABR	Alternative biogenic raw materials
BTEX	benzene, toluene, ethylbenzene, xylene
CRF	char reactivity factor
CSTR	continuous stirred tank reactor
CW	CraftWERK, trade name
PAH	polycondensed aromatic carbohydrates
TGA	thermogravimetric analysis
u.s.c.	under standard conditions
VL	test run (Versuchslauf)
%m	mass fraction
%vol	volume fraction

5. References

- [1] M. Prantauer, A. Hofmann, M. Huber, G. Kreutner: Tar reduction mechanisms on non-catalytic hot gas filters in biomass gasification plants. Proceedings of the ICPS 11, Vienna, Austria (2011) pp 115–122.
- [2] A. Hofmann, M. Huemer, D. Bozic, M.B. Huber: Investigations on the catalytic effects of potassium and silicon in the thermo-chemical gasification of agricultural residues. Poster Presentation, International Conference of Chemical Kinetics, Ghent, 06/2015
- [3] D. Bozic: Einfluss des Kalium- und Siliziumgehaltes auf den stofflichen Abbau von Biomasse. Master Thesis, Management Center Innsbruck, Innsbruck, 2015.
- [4] R. Thaler: Erstellung eines simulationsbasierten Optimierungstools für einen Schwebebettvergaser mit Aspen Plus. Master thesis, Management Center Innsbruck, Innsbruck, 2016.
- [5] A. Hofmann: Untersuchungen zur thermochemischen Vergasung von biogenen Rohstoffen mit niedrigem Ascheschmelzpunkt im Schwebefestbett-Vergaser. Thesis, Technische Universität Wien, 2018.

- [6] A. A. Kahn, W. de Jong, P. J. Jansens, H. Spliethoff: Biomass combustion in fluidized bed boilers: potential problems and remedies. *Fuel Processing Technology* **90** (2009) pp 21–50.
- [7] B. Gatternig, U. Hohenwarter, J. Karl: Ascheproblematik in biomassegefeuerten Wirbelschichtanlagen. 11tes Symposium Energieinnovation Graz 2010.
- [8] R. Aeckersberg: Analyse des Ascheschmelzverhaltens von Holzpellets in Abhängigkeit ausgewählter Aschekomponenten. Thesis, Rheinisch-Westfälische Technische Hochschule Aachen, Aachen, 2011.
- [9] H. Li, N. Yoshihiko, Z. Dong, M. Zhang: Application of the FactSage to Predict the Ash Melting Behavior in Reducing Conditions. *Chinese Journal of Chemical Engineering* **14** (2006) pp 784–789.
- [10] K. J. Hüttlinger, B. Masling, R. Minges: Katalytische Wirkung von Kalium bei der Konvertierung und Methanisierung von Kohlenmonoxid. *Chem.-Ing.-Tech.* **58** (1986) pp 409–412
- [11] K. H. van Heek, H.-J. Mühlen, H. Jüntgen: Progress in the kinetics of coal and char gasification. *Chem. Eng. Technol* **10** (1987) pp 411–419.
- [12] P. C. Koenig, R. G. Squires, N. M. Laurendeau: Effect of potassium carbonate on char gasification by carbon dioxide. *Journal of Catalysis* **100** (1986) pp 228–239.
- [13] S. Li, Y. Cheng: Catalytic gasification of gas-coal char in CO₂. *Fuel* **74** (1995) pp 456–458.
- [14] J. Kopyscinski, J. Lam, C. A. Mims, J. M. Hill: K₂CO₃ catalyzed steam gasification of ash-free coal. Studying the effect of temperature on carbon conversion and gas production rate using a drop-down reactor. *Fuel* **128** (2014) pp 210–219.
- [15] D. C. Elliott, R. T. Hallen, J. L. Sealock: Alkali catalysis in biomass gasification. *Journal of Analytical and Applied Pyrolysis* **6** (1984) pp 299–316.
- [16] K. Umeki, A. Moilanen, A. Gómez-Barea, J. Konttinen: A model of biomass char gasification describing the change in catalytic activity of ash. *Chemical Engineering Journal* **207–208** (2012) pp 616–624.
- [17] D. W. McKee, C. L. Spiro, P. G. Kosky, E. J. Lamby: Catalytic effects of alkali metal salts in the gasification of coal char. *Symposium on coal gasification*, Argonne National Laboratory, Ed., Las Vegas, 1982.
- [18] D. A. Sams, F. Shadman: Mechanism of potassium-catalyzed carbon/CO₂ reaction. *AIChE Journal* **7** (1986) pp 1132–1137.
- [19] R. Backmann: High temperature equilibrium calculations of ash forming elements in biomass combustion / gasification systems - state-of-the-art, possibilities and applications. in Obernberger, I. (Ed.s): *Ashes and particulate emissions from biomass combustion - formation, characterisation, evaluation, treatment*. Graz: dbv-Verlag für die Technische Universität Graz (1998) pp 105–117.
- [20] F. Bekerthy: Optimierung eines Simulationsmodells zur Abschätzung der Produktgaszusammensetzung am Beispiel eines Schwebebettvergasers. Master thesis, Management Center Innsbruck, Innsbruck, 2017.
- [21] C. Y. Wen, H. Chen, M. Onozaki: Users manual for computer simulation and design of the movingbed coal gasifier: Final report. Department of Chemical Engineering, 1982.
- [22] S. Dumfort, M. Huemer, A. Hofmann, M.B. Huber, J. Krueger: Tar decomposition at low temperatures within staged gasification reactors – first approach towards mechanisms and background, *GSTF Journal of Engineering Technology (JET)* **3** (2015)

Development of a New Method for Investigation of the Ash Melting Behavior in the Fluidized Bed Conversion Processes

J.Priscak^{1,2*}, M.Kuba^{1,2}, H.Hofbauer²

1. BEST – Bioenergy and Sustainable Technologies GmbH, Inffeldgasse 21b, A-8010 Graz, Austria

2. TU Wien, Institute of Chemical, Environmental and Bioscience Engineering (ICEBE),

Getreidemarkt 9/166, 1060 Vienna, Austria

*corresponding author, juraj.priscak@best-research.eu

Abstract

The suitability of woody biomass for thermochemical conversion process using fluidized bed technology has already been successfully demonstrated in the last decades. However in lower-rank biomass (e.g. crops and agriculture residues), the ash-forming matter differs from the one in the woody biomass and can cause operational problems such as agglomeration, sintering, fouling, or eventually total defluidization of the fluidized bed. These problems are common for both – combustion and gasifying reactors. Hence the understanding of the ash behavior, as well as creating of a reliable method for the prediction of the ash melting in the fluidized bed is necessary. Several methods such as the ash fusion test, the compression- strength- based test or the controlled fluidization bed agglomeration test can be used to determine the ash melting temperature in the fluidized bed. However none of the test takes into account the influence of the local overheating caused by burning char particles. The following paper focuses on developing a new reliable method to investigate the ash behavior in the fluidized bed.

1. Introduction:

According to the [1], the predicted average annual percent change of the world energy consumption will increase in the next 15 years by 1.5%. In order to meet this increasing demand for energy and also to minimize the air and nature pollution connected to its production, replacing fossil fuels with renewable energy sources is necessary. Already today, renewable energy resources like wind, sun, and water show great potential to compensate a relevant share of fossil fuels as a primary energy source. The most widespread of the renewable energy resources is however biomass, which covers more than 10% of the world primary energy consumption. Especially utilization of waste biomass (agriculture residues, municipal wastes) gained more focus in last years. However,

in this type of biomass the ash-forming matter differs from woody biomass and can cause operational problems such as sintering, agglomeration or eventually total defluidization of the fluidized bed. These problems are common for both – combustion and gasification reactors. Hence, the understanding of the ash melting behavior, as well as the creating a reliable method for predicting the operational problems in fluidized bed systems is necessary. There are number of techniques to predict ash behavior during thermochemical conversion processes, focused mostly on bed agglomeration. The ASTM ash fusion test is a standard method based on the visual indication of the softening and melting behavior of the test sample [2]. Although it has been repeatedly reported as a poor method for determination of ash related problems

[3],[4],[5] it is still widely used due to its simplicity. Skrifvars et al. proposed a method for the prediction of the biomass sintering, based on the compression strength tests and the thermodynamic equilibrium calculations [4]. The method highlights the importance of the bed sintering due to partially ash melting and its contribution to the bed agglomeration and to the deposit formation. However, both methods suffer from exclusion of the interaction between ash and bed material. Öhman and Nordin developed a more reliable method for prediction of bed agglomeration tendencies in fluidized bed combustion (FBC) boilers [6]. According to the method, the fuel is first combusted in oxidizing atmosphere in a fluidized bed (FB) reactor until sufficient amount of ash is produced. Afterwards the fuel feeding is stopped and the bed temperature is linearly increased by applying external heat to the primary air and to the reactors walls. The initial agglomeration temperature is determined by a sudden temperature and pressure drop in the bed. However, since the local overheating of the burning char particles is absent in the test, it remains unclear, how well the results reproduce the bed agglomeration in a full-scale FB reactor [3]. Moreover, the progressive accumulation of ash in the bed is not accounted for either, which can be problematic in the case of fuels like e.g. lignin or rice husk, in which coherent ash particles are formed during steady state combustion and can cause serious operational problems. As the experiments with lignin showed, the stability and morphology of the ash particles depends not only on the combustion temperature, but on the combustion regime as well, and therefore above-mentioned methods may not simulate the real behavior of the ash during combustion of such fuels. For example, rapid combustion of lignin in the fluidized bed at temperatures above 700°C leads to an extensive formation of such

particles, which accumulates at the top of the bed. Such combustion regime is present in the fluidized bed reactor, where the fuel particle is introduced into the reactor already at elevated temperature and rapidly heated. On the other hand, if the ash is being produced with a technique, which involves a preheating step at lower temperature followed by a slow increase in temperature (without char burnout), the result is a loose ash, which will be in FB carried out as a fly ash. Therefore in order to fully investigate the biomass ash melting behavior during combustion in the fluidized bed reactor at different bed temperatures, it is necessary to develop a method, which includes burning of the char particle as well. Such method has been proposed and tested in the lab-scale reactor with wheat straw and wheat straw lignin.

2. Concept and methodology:

2.1. Fuel characterization

Wheat straw and wheat straw lignin have been pelletized prior to the experiments in the FB reactor and the furnace oven. **Fehler! Verweisquelle konnte nicht gefunden werden.** shows fuels properties, obtained by corresponding norm methods (water content by DIN 51718; ash content by EN ISO 18022; volatiles by EN ISO 18023; lower heating value by DIN 51900 T2; initial deformation temperature (IDT) by CEN/TS 15370-1).

	Wheat straw	Lignin
Moisture (wt.%)	7.2	6.06
Ash content (wt.% _{d.b})	7.5	15.47
Volatiles (wt.% _{d.b})	74.7	64.88
LHV (kJ/kg)	16860	18779
IDT (°C)	830	1430

Tab. 1: Important combustion parameters of wheat straw and lignin

Furthermore, a XRF analysis of the fuel ashes was performed by Test Laboratory for Combustion Systems at TU Vienna with the Axios Advanced Analyser from company Panalytical. The mass of individual elements were measured and afterwards recalculated to oxides (Tab. 2).

Oxide	Wheat straw	Lignin
Fe ₂ O ₃	1.81	0.71
CaO	4.43	3.76
K ₂ O	12.26	3.08
P ₂ O ₅	2.71	1.23
SiO ₂	60.88	84.46
Al ₂ O ₃	1.52	2.62
MgO	4.32	0.35
Na ₂ O	2.56	1.48

Tab. 2: Ash composition of fuels (wt.%)

Low alkali content of lignin (compared to wheat straw) origins in a leaching step of the process, where lignin is extracted as a byproduct. **Fehler! Verweisquelle konnte nicht gefunden werden.** shows results from an elemental analysis, performed at Microanalytical Laboratory at Institute for Physical Chemistry at TU Vienna. Total sulfur and chlorine content was determined by the norm method EN ISO 16994.

Element	Wheat straw	Lignin
Carbon	45.09	51.67
Hydrogen	5.75	3.49
Nitrogen	0.55	1.43
Sulfur	0.12	0.123
Chlorine	0.09	0.025

Tab. 3: Elemental analysis of wheat straw and lignin (wt.%)

2.2. Experiments in the lab-scale reactor

Experiments with both fuels have been performed in the lab-scale reactor with an electric power of 1.5kW. **Fehler! Verweisquelle konnte nicht gefunden werden.** shows a schematic of the reactor, including the positioning of the temperature and pressure measurement. The reactor has an inner diameter of 5.3 cm and a bed height of 10 cm and is made of stainless steel. Before the air is distributed into the reactor through a perforated plate, it is heated with a temperature regulator and with a cylindrical electrical furnace with the power of 750 W. The fluidized bed section is heated up using a uniform cylindrical electrical furnace with the same power output. Air volume flow of 20 Nl/min has been used, what corresponds to a U/U_{mf} ratio of approx. 20. In total, five K-type thermocouples monitor the temperatures of the fluidized bed, the freeboard, the fuel bunker, the flange sealing as well as the temperatures of the wall of preheater and reactor heater. The pressure sensor is situated before the distribution plate, so the pressure drop across the bed can be calculated from the difference between atmospheric and measured pressure. Feedstock pellets are transported from the feedstock bunker into the reactor with a screw conveyor. The used method consists of two parts. In the first part the ash is produced in the reactor through the fuel combustion. Approximately 300 g/h of the fuel have been continuously supplied into the reactor by the screw conveyor. Quartz sand (300 g) with a particle diameter between 400-500 µm has been used as a bed material. The bed material has been fluidized with 20 Nl/min of air and temperature held at 650 °C by adjusting the external heaters power. After approx. 1 hour of the ashing phase, the bed temperature is increased in steps of 50 °C (part 2) by external electrical heater (while maintaining constant fuel supply of 300

g/h) until reaching the bed temperature of 950-1000 °C.

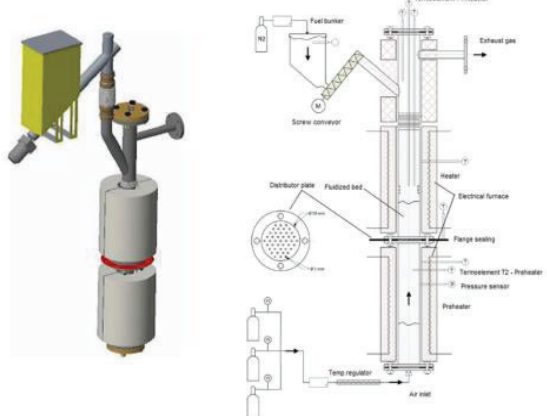


Fig. 1: Scheme of the lab-scale fluidized bed reactor [7]

2.3. Experiments in the furnace oven

In order to further investigate the formation of coherent ash particles during lignin combustion (Chapter 3.1), additional experiments in the furnace oven have been performed. During the experiments, lignin pellets have been burned in an electrical furnace oven in two regimes. Air has been used as an oxidizing agent in both cases. The first regime (combustion at low heating rate) included preheating phase, where the sample was at first continuously heated to 250 °C in 30 min. The temperature in the furnace oven has been then kept constant at 250 °C for 120 min. Afterwards the sample was heated up to 600 °C (Sample 1), 700 °C (Sample 3) and 800 °C (Sample 5) and burnt at constant temperature for another 210 min. During the second regime (without preheating; combustion at high heating rate) the sample was inserted into the furnace oven already at combustion temperature (600 °C, 700 °C and 800 °C for Sample 2, 4, 6 accord.) for 210 min. Afterwards the samples have been cooled down to a room temperature and further examined by XRF and XRD analysis.

2.4. Chemical equilibrium calculations

Thermochemical equilibrium calculations have been performed using the software Factsage 7.3 in the Equilib module, which employs the Gibbs energy minimization algorithm and thermochemical functions. The fuel ash composition (Tab. 2) has been used as a reactant stream. The amount of air, necessary for total combustion, has been subsequently calculated in Factsage. FactPS, FToxid and FTsalt have been chosen as databases. Solutions FToxide-SLAGA and FTsalt-SALTB have been used in calculations for both fuels.

3. Results and discussion

3.1. Behavior of wheat straw and lignin in fluidized bed combustion

Fehler! Verweisquelle konnte nicht gefunden werden. shows the results of the experiment with wheat straw. As can be seen from temperature and pressure measurement, the bed collapses approx. at 03:30 (overall operating time, including the initial heating of the reactor).

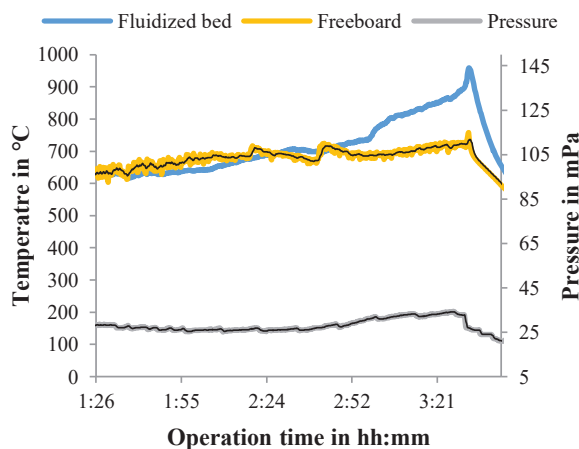


Fig. 2: Temperature and pressure profile of the wheat straw combustion in the FB reactor

This time corresponds to the bed temperature of 865 °C and the ash content of 20 wt.%_{d.b.} (with no regards on the ash that has been carried out from the reactor). The melting temperature of wheat straw based on thermodynamic equilibrium calculations (Fig. 6) is 750 °C, what exceeds measured value by 100 °C.

Although the melting phase occurs already at 650 °C, at least 15-30 wt.% of the ash needs to be molten in order for an ash particle to be sticky [8]–[10]. After the reactor was cooled down and opened, agglomerates were found in the bed (Fig. 3).



Fig. 3: Bed agglomerates from combustion of wheat straw in the FB reactor

The experiment with lignin started with the ashing phase (approx. 1 hour) as well. The amount of ash in the reactor after 1 hour corresponds to approx. 7 wt.%_{db}. The temperature of the bed has been afterwards continuously increased with an electrical heater. At approx. 4:22 pressure fluctuations occurred and the fuel supply was turned off.

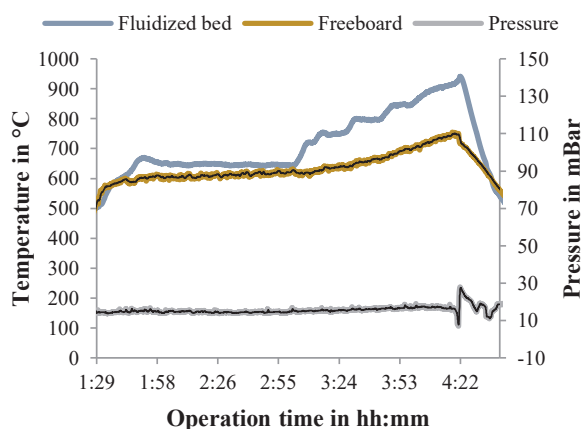


Fig. 4 : Temperature and pressure profile of lignin combustion in the FB reactor

As have been found later, the bed collapse was caused by coherent ash residues (Fig. 5), which were accumulated at the top of the bed.



Fig. 5: Coherent ash particles from combustion of lignin in the FB reactor

No bed agglomeration occurred, what has been also supported by equilibrium calculations. As can be seen at **Fehler! Verweisquelle konnte nicht gefunden werden.**, the amount of molten ash does not exceed 30 wt.%. However partially molten ash is responsible for the mechanical stability of the ash particles, which increases above 850 °C. Therefore if the method is used, where ash is prepared at temperature under 700 °C and then continuously heated up, such problematic behavior of the fuel ash may not be detected.

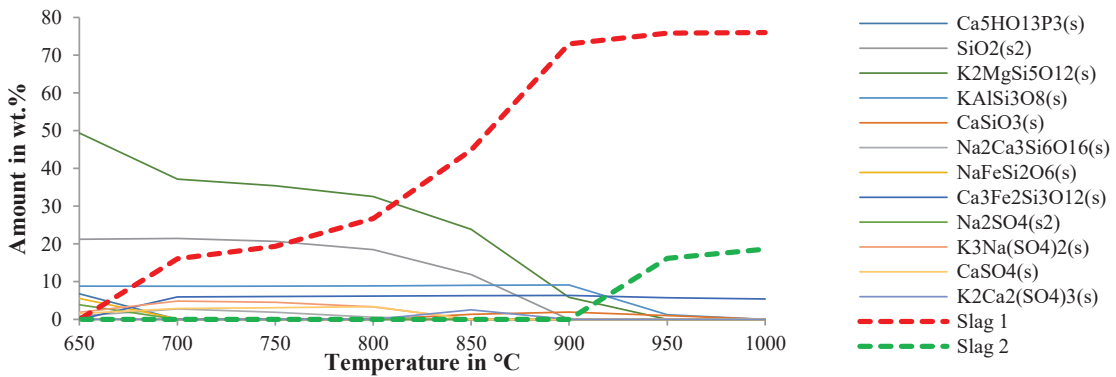


Fig. 6: Equilibrium calculations based on wheat straw ash composition

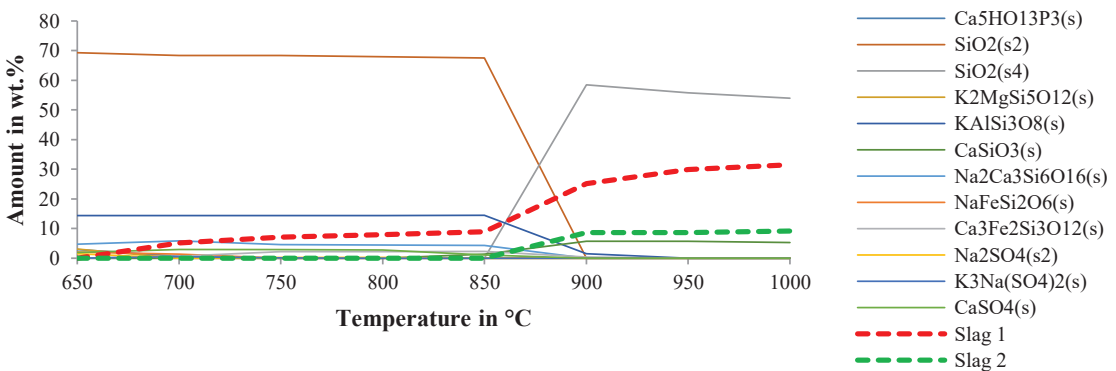


Fig. 7: Equilibrium calculations based on lignin ash composition

3.2. Behavior of lignin ash at different combustion regimes

Experiments in the furnace oven at different combustion temperatures show strong dependence between the formation of dimensionally stable ash particles and the combustion regime. Combustion of particles without preheating, where the sample is introduced into the furnace oven at typical operating temperatures (Fig. 8, left column), leads to a formation of dimensionally stable or coherent ash particles. On the other hand, if the samples are first dried at 250°C and then continuously heated up to typical operating temperatures (Fig. 8, right column), the result will be a formation of more fragile ash particles.

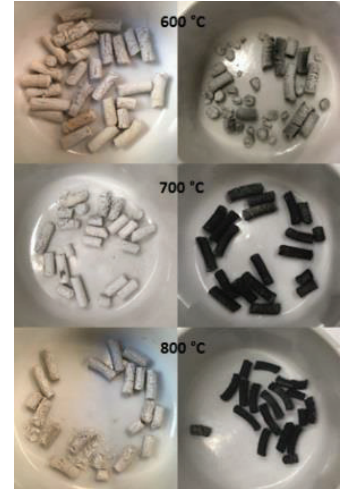


Fig. 8: Samples 1-6; Combustion with (left) and without (right) preheating step

Samples from the experiments in the furnace oven were further analyzed with an X-ray diffraction (Fig. 9). In all 6 cases, majority of the sample is present in the amorphous phase. Crystalline phase is composed mainly of cristobalite, quartz and arcanite. Up to 700 °C, quartz is the dominant silica polymorph in the crystalline phase. Above 700 °C,

crystallization of cristobalite (with peak at 21-22 °2Theta) from amorphous phase occurs.

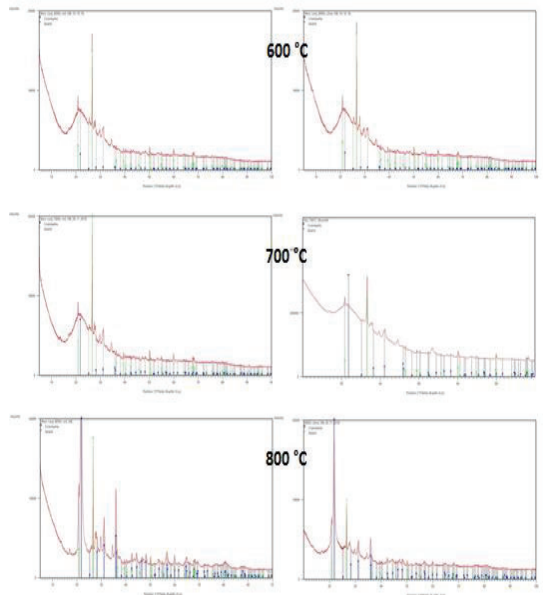


Fig. 9: XRD Analysis of the samples 1-6; Combustion with (left) and without (right) preheating step

From comparison of XRD patterns is apparent, that crystallization of cristobalite and quartz from amorphous phase

dependent on combustion temperature and is practically independent of combustion regime. Similar observations have been made by combustion of rice hulls [11]–[14], [15]. Venezia et al. [11] examined effects of alkali ions on these transitions and concluded, that both Na^+ and K^+ ions destabilize the amorphous silica and support crystallization of silica polymorphs like quartz, cristobalite and tridymite. Moreover, Nakata et al. [15] found, that potassium contained in the rice hull ash accelerate the crystallization of amorphous SiO_2 to cristobalite. Hence, more extensive crystallization of cristobalite is connected to the potassium content in the ash and its availability for the chemical reaction. As can be seen in **Fehler! Verweisquelle konnte nicht gefunden werden.**, the potassium content in the examined samples 1-6 is comparable. However, different heating regimes lead to variant reaction pathways of alkali ions during combustion and gasification.

Sample	1	2	3	4	5	6
Temperature	600 °C	600 °C	700 °C	700 °C	800 °C	800 °C
Heating rate	Low	High	Low	High	Low	High
Fe_2O_3	0.90	0.82	0.77	0.91	0.87	0.95
CaO	6.87	7.14	6.41	6.70	6.88	7.23
K_2O	3.87	3.54	3.36	3.95	3.81	4.34
P_2O_5	2.88	3.01	2.85	2.85	2.84	2.86
SiO_2	79.2	80.0	79.4	80.2	79.5	76.4
Al_2O_3	1.26	2.15	2.86	1.85	1.41	2.81
MgO	1.06	0.93	0.86	1.03	1.04	1.17
Na_2O	1.12	0.65	0.95	0.85	0.91	2.44
SO_3	2.22	1.36	2.09	1.14	2.23	1.00

Tab. 4: XRF Analysis of Sample 1-6

Sulfur, which concentrations vary in the different samples, may play an important role in these pathways. Sulfur and potassium behavior during the combustion of biomass were investigated by Knudsen

et al.[16]. According to the authors, 40-50 % of total sulfur is released into the gas phase in the interval between 500-800 °C. On the contrary, only a little (<10%) or none potassium is released below 700 °C.

In their other paper [17] Knudsen et al. have observed, that sulfur is upon heating not released directly into the gas phase, but rather transformed into another form of solid sulfur, such as alkali sulfate [18]. Consequently potassium sulfates will be formed at lower heating rates and preserved in the crystal form during char burn-off, since the melting point of potassium sulfate reaches \sim 1300 °C. However, upon rapid heating (gasification, combustion) potassium and sulfur are released into the gas phase simultaneously, enabling the reaction between potassium and silica which leads to a formation of alkali silicates with low melting point. Without reaction partner from a solid state,

sulfur will be released into gas phase, decreasing its content in e.g. Sample 4 (700 °C, high HR), in comparison to Sample 3 (700 °C, low HR). Equilibrium calculations in Factsage 7.3 also predicted formation of $K_2SO_4(s2)$ in both cases. In the case of sample 2, 4 and 6 considerably lower amounts of $K_2SO_4(s2)$ leads to a formation of $K_2Si_4O_9(s)$ which is further transformed into liquid Slag 1 (Fig. 11). On the other hand, if enough sulfur is available for capturing potassium in the form of $K_2SO_4(s2)$, potassium silicates will not form and consequently liquid slag (Slag 1 and Slag 2) will form earliest at temperatures above 900 °C (Fig. 10).

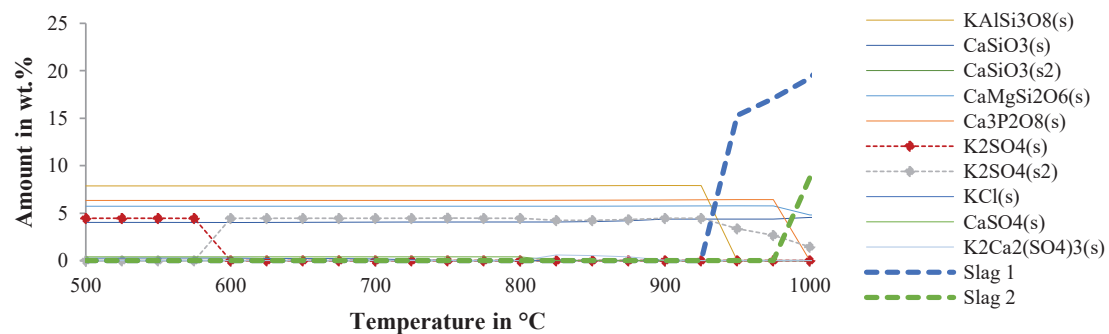


Fig. 10: Equilibrium calculations based on ash composition of Sample 3

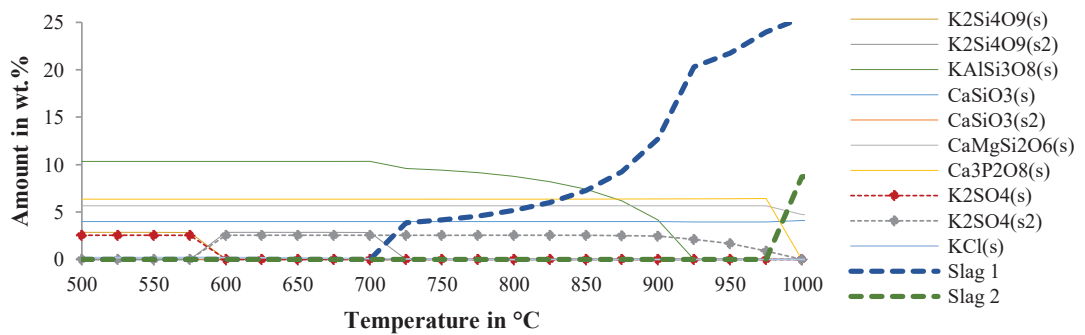


Fig. 11: Equilibrium calculations based on ash composition of Sample 4

3.3. Comparison of ash behavior methodologies

*bed collapse caused by accumulation of ash residues
Tab. 5 shows comparison of the ash melting temperatures acquired by the

standard ASTM fusion test, equilibrium calculations in Factsage and the experiments in the FB reactor.

	Wheat Straw	Lignin
ASTM	830 °C	1430 °C
Factsage	800 °C	900 °C
FB reactor	865 °C	900 °C*

*bed collapse caused by accumulation of ash residues

Tab. 5: Comparison of ash melting temperatures from the ASTM test, equilibrium calculations and the experiment in FB reactor

In the case of wheat straw, the temperature determined by the ASTM test is comparable with agglomeration temperature from the experiments in the FB reactor, at which bed particles adhere together due to molten ash (so called “melt-induced” agglomeration). However, as already established by several authors, the ASTM fusion test fails to predict the agglomeration temperature in most cases, since the interactions between ash particles and bed material are excluded from the test. These interactions may lead to a formation of a uniform coating on the bed material surface, which at elevated temperatures may initiate agglomeration (“coating-induced agglomeration”). On the other hand, the method proposed by Öhman and Nordin [6] is suitable for determination of both agglomeration types. However it may not be able to detect other problematic ash behavior – formation and accumulation of the coherent ash particles in the fluidized bed. As have been showed in Chapter 3.2, the formation of such particles is due to

reaction pathways enhanced above certain temperature. Therefore it is necessary, in order to detect such problematic ash behavior, to include char particle burning in the used method. Such method has been proposed and tested with wheat straw and wheat straw lignin. The developed method is capable to determine the bed agglomeration temperature (“melt-induced agglomeration”), as well as formation and accumulation of coherent ash particles. Suitability of the proposed method for determination of “coating-induced” agglomeration is however still subject for further investigation.

4. Conclusion and Outlook

A new method for investigation of the ash behavior in the fluidized bed combustion, which besides ash-bed material interactions also accounts for the influence of local overheating caused by burning char particles has been developed and tested. In the case of wheat straw, agglomeration temperature of 865 °C has been determined, what is in good agreement with the results of chemical equilibrium calculations (800 °C). The developed method has been also able to detect another problematic ash behavior – formation of coherent ash particles during combustion of wheat straw lignin. These ash particles were accumulated at the top of the fluidized bed and caused bed collapse. Formation of the particles was caused by molten phase, what was predicted by equilibrium calculations as well.

5. Acknowledgements

This study was carried out within the Bioenergy2020+ GmbH project C200410. Bioenergy2020+ GmbH is funded within the Austrian COMET program, which is managed by the Austrian Research Promotion Agency (FFG) and promoted by the federal government of Austria as well as the federal states of Burgenland, Niederösterreich, and Steiermark. We are grateful for the support of our project partners HGA Senden (Stadtwerke Ulm), Bertsch Energy, Quarzwerke and Institute of Chemical, Environmental and Bioscience Engineering (ICEBE).

6. References

- [1] S. C. Davis, W. Hay, und J. Pierce, Biomass in the energy industry: An introduction, London (GB): BP plc, 2014.
- [2] D. ASTM, 87: Standard Test Method for Fusibility of Coal and Coke Ash, 1985 Annual Book of Standards, Bd. 5, 1857.
- [3] F. Scala, Particle agglomeration during fluidized bed combustion: Mechanisms, early detection and possible countermeasures, Fuel Processing Technology, Bd. 171, S. 31–38, März 2018.
- [4] B.-J. Skrifvars, R. Backman, und M. Hupa, Characterization of the sintering tendency of ten biomass ashes in FBC conditions by a laboratory test and by phase equilibrium calculations, Fuel Processing Technology, Bd. 56, Nr. 1, S. 55–67, Juli 1998.
- [5] B.-J. Skrifvars, M. Öhman, A. Nordin, und M. Hupa, Predicting Bed Agglomeration Tendencies for Biomass Fuels Fired in FBC Boilers: A Comparison of Three Different Prediction Methods, Energy Fuels, Bd. 13, Nr. 2, S. 359–363, März 1999.
- [6] M. Öhman und A. Nordin, A New Method for Quantification of Fluidized Bed Agglomeration Tendencies: A Sensitivity Analysis, Energy Fuels, Bd. 12, Nr. 1, S. 90–94, Jan. 1998.
- [7] D. Eßletzbichler, Auslegung, Aufbau und Inbetriebnahme einer Wirbelschichtapparatur im Labormaßstab für thermische Umwandlungsprozesse von Biomasse, S. 161, 2017.
- [8] N. Evic, T. Brunner, und I. Obernberger, „Prediction of biomass ash melting behavior“, S. 8, 2012.
- [9] M. Zevenhoven-Onderwater, J.-P. Blomquist, B.-J. Skrifvars, R. Backman, und M. Hupa, The prediction of behaviour of ashes from five different solid fuels in fluidised bed combustion, Fuel, Bd. 79, Nr. 11, S. 1353–1361, Sep. 2000.
- [10] D. Lundmark, C. Mueller, B.-J. Skrifvars, und M. Hupa, „Computational fluid dynamic model of combustion and ash deposition in a biomass-cofired bubbling fluidized bed boiler, Clean Air: International Journal on Energy for a Clean Environment, Bd. 8, Nr. 2, S. 155–169, 2007.
- [11] A. M. Venezia, V. La Parola, A. Longo, und A. Martorana, Effect of Alkali Ions on the Amorphous to Crystalline Phase Transition of Silica, Journal of Solid State Chemistry, Bd. 161, Nr. 2, S. 373–378, Nov. 2001.
- [12] Y. Shinohara und N. Kohyama, Quantitative Analysis of Tridymite and Cristobalite Crystallized in Rice Husk Ash by Heating, Ind Health, Bd. 42, Nr. 2, S. 277–285, 2004.
- [13] T. Okutani, Utilization of silica in rice hulls as raw materials for silicon semiconductors, Journal of Metals, Materials and Minerals, Bd. 19, Nr. 2, Apr. 2017.
- [14] S. Chandrasekhar, K. G. Satyanarayana, P. N. Pramada, P. Raghavan, und T. N. Gupta, Review Processing, properties and applications of reactive silica from rice husk—an overview, Journal of Materials Science, Bd. 38, Nr. 15, S. 3159–3168, Aug. 2003.
- [15] Y. Nakata, M. Suzuki, T. Okutani, M. Kikuchi, und T. Akiyama, Preparation and Properties of SiO₂ from Rice Hulls, J. Ceram. Soc. Japan, Bd. 97, Nr. 1128, S. 842–849, Aug. 1989.
- [16] J. N. Knudsen, P. A. Jensen, und K. Dam-Johansen, Transformation and Release to the Gas Phase of Cl, K, and S during Combustion of Annual Biomass, Energy Fuels, Bd. 18, Nr. 5, S. 1385–1399, Sep. 2004.
- [17] J. N. Knudsen, P. A. Jensen, W. Lin, F. J. Frandsen, und K. Dam-Johansen, Sulfur Transformations during Thermal Conversion of Herbaceous Biomass, Energy Fuels, Bd. 18, Nr. 3, S. 810–819, Mai 2004.

- [18] P. Glarborg und P. Marshall, „Mechanism and modeling of the formation of gaseous alkali sulfates“, Combustion and Flame, Bd. 141, Nr. 1, S. 22–39, Apr. 2005.

Steam gasification of sewage sludge for synthesis processes

J.C. Schmid^{1*}, A. Bartik³, F. Benedikt³, A.M. Mauerhofer³, J. Fuchs³,
E. Schanz¹, S. Reisinger¹, B. Nowak¹, F. Bühler¹, M. Österreicher¹,
A. Lunzer², C. Walcher², S. Müller², M. Fuchs², H. Hofbauer³

1. SMS group Process Technologies GmbH, Daffingergasse 4, 1030 Vienna, Austria

2. Energy & Chemical Engineering GmbH, Pappelstraße 13, 1140 Vienna, Austria

3. TU Wien, Inst. of Chem., Environ. & Bioscience Eng., Getreidemarkt 9/166, 1060 Vienna, Austria

*corresponding author, johannes.schmid@smsgroup.at

Abstract

The paper presents measurement results of a gasification test run. Municipal sewage sludge from a digestion tower is gasified in an advanced dual fluidized bed reactor system. Steam is used as gasification agent and an olivine-limestone mixture as bed material. The fuel analysis shows a very high ash content and a low heating value of the dried sewage sludge. In addition, a significant amount of nitrogen in the fuel is present, leading to a high ammonia content in the product gas. Sintering effects caused by the high ash content do not occur. Thus, a gasification process without limitation is achieved. The fuel input is located in the lower gasification reactor operating as bubbling fluidized bed, whereas the upper gasification reactor is designed as a column of turbulent fluidized zones for tar cracking. The results show an efficient in-situ tar reduction. With a look on the product gas composition a comparatively high carbon dioxide and a low carbon monoxide content is surprising. It is obvious that an iron oxide reduction of the initial fuel ash occur in the gasification reactor. In addition, it is assumed that the significant iron content in the fuel ash also leads to a transport of oxygen from the combustion reactor to the gasification reactor. Thus, carbon monoxide and hydrogen are oxidized in the gasification reactor by the circulating iron-rich ash particles (chemical looping effect).

1. Introduction

The thermochemical conversion of biomass is a promising option for the environmentally friendly production of valuable renewable products. Fuels from biogenic sources are particularly relevant, as these fuels constitute the only practical carbon source available within the range of renewables. Fluidized bed steam gasification of solid fuels is a promising technology to produce a nearly nitrogen-free and hydrogen-rich product gas. After gas cleaning processes, the utilization of the product gas as syngas for various synthesis processes is auspicious. [1]

In the case of industrial utilization, high quality wood chips are a comparatively expensive fuel [2]. Waste material and biogenic residues as fuel, like sewage sludge, are of interest for gasification processes and for the future energy supply. However, alternative low-cost fuels often have difficult chemical and physical properties. A risk that higher hydrocarbons such as tar will not convert sufficiently is present. In addition, undesired substances, high contents of fuel ash and disadvantageous ash sintering behavior lead to limitations regarding fluidized bed gasification. This may affect the plant availability in a critical way. [3]

To face these challenges, an advanced gasification reactor design was developed and a pilot plant with 100 kW fuel power was put in operation at TU Wien in 2014. Fig. 1 shows the basic idea of the advanced gasification process. The special design of the gasification reactor aims at supporting gasification reactions, improving conversion rates, and minimizing the tar content of the product gas. Fig. 2 shows an illustration of the pilot plant at TU Wien. The upper part of the gasification reactor features a column of fluidized bed zones with counter-current flow of the raw product gas flowing upwards and hot bed material introduced from the combustion reactor flowing downwards. Thus, the increased contact between the introduced fuel, the volatiles, and the bed material provides for a significant reduction of undesired product gas components like tar [4,5]. The 100 kW fuel power pilot plant enables gasification test runs with a relevant plant size. This is indispensable to gather meaningful results.

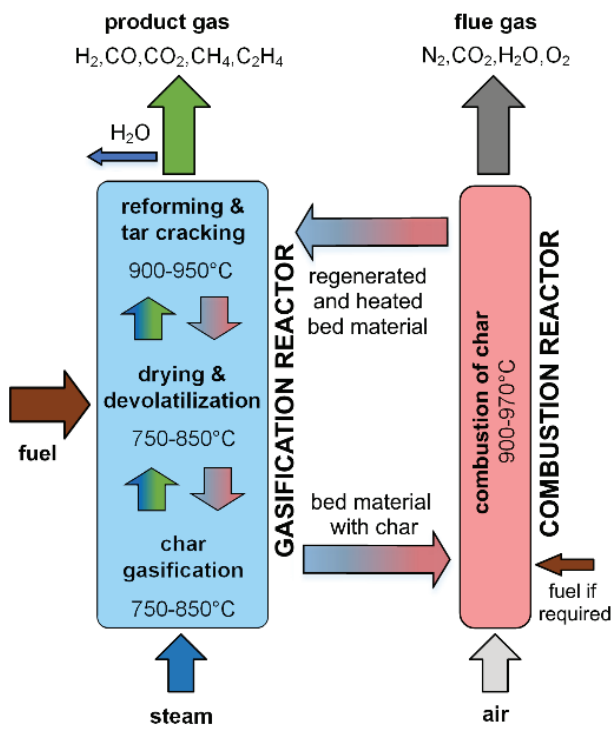


Fig.1: Basic principle of dual fluidized bed steam gasification at TU Wien

2. Methodology

The investigations base on experimental research with the advanced 100 kW pilot plant at TU Wien. Fig. 2 shows the inner dimensions and heights of the used dual fluidized bed gasifier. All pressure and temperature measurement points of the reactor system are visible. A screw conveyor feeds the solid fuel onto the bubbling bed of the lower gasification reactor. A special feeding system enables the utilization of a broad range of fuels without limitations.

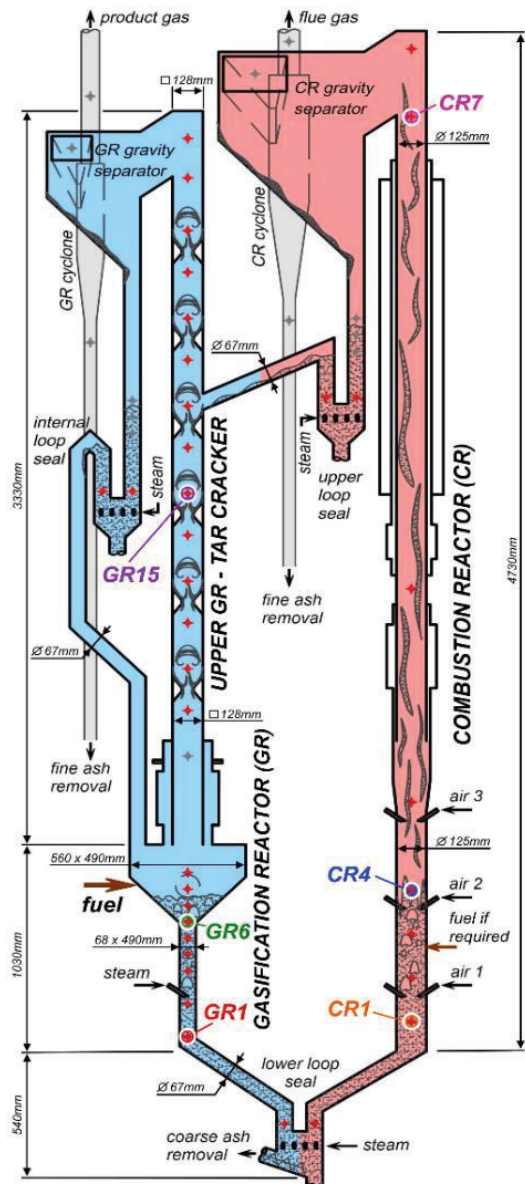


Fig.2: Dimensions, media inputs and measurement points of the gasifier

The pilot plant is equipped with a programmable logic controller (PLC), which continuously gathers and records all measured data. The installation of more than 20 media flows, 100 temperatures, and 70 pressures ensure an insight into the gasification process. Different Rosemount NGA2000 gas analyzers continuously measure the main product gas and flue gas components like hydrogen (H_2), carbon monoxide (CO), carbon dioxide (CO_2), methane (CH_4) and oxygen (O_2). Perkin Elmer ARNEL – Clarus 500 gas chromatograph measures further product gas components, like ethylene (C_2H_4) and ethane (C_2H_6) every 15 minutes. The setup of the product gas and flue gas measurement can be seen in Fig. 3. The product gas has to be filtered and washed with rapeseed methyl ester (RME) in advance to eliminate fine dust particles and condensable components like water and tar.

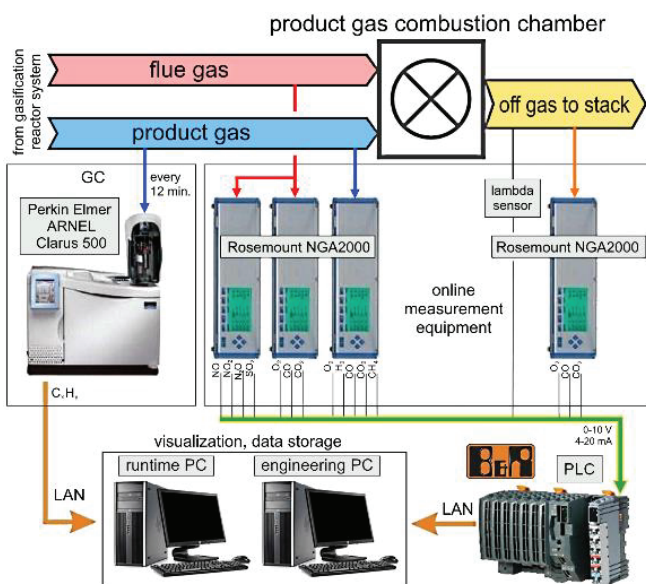


Fig.3: Online measurement of gases [4]

Other product gas components like tar, water, char and dust are detected discontinuously (Fig. 4). Solid particles, like char and dust are sampled with a small cyclone and a quartz wool stuffed filter cartridge. Water and tar is sampled with impinger bottles and toluene as solvent.

Following, the gravimetric tar content as well as tar components detected by gas chromatography coupled with mass spectrometry (GCMS) are determined. The measurement method is based on CEN/TS 15439. The sampling procedure for the detection of ammonia (NH_3) and hydrogen sulfide (H_2S) in the product gas is very similar, but with the use of different solvents.

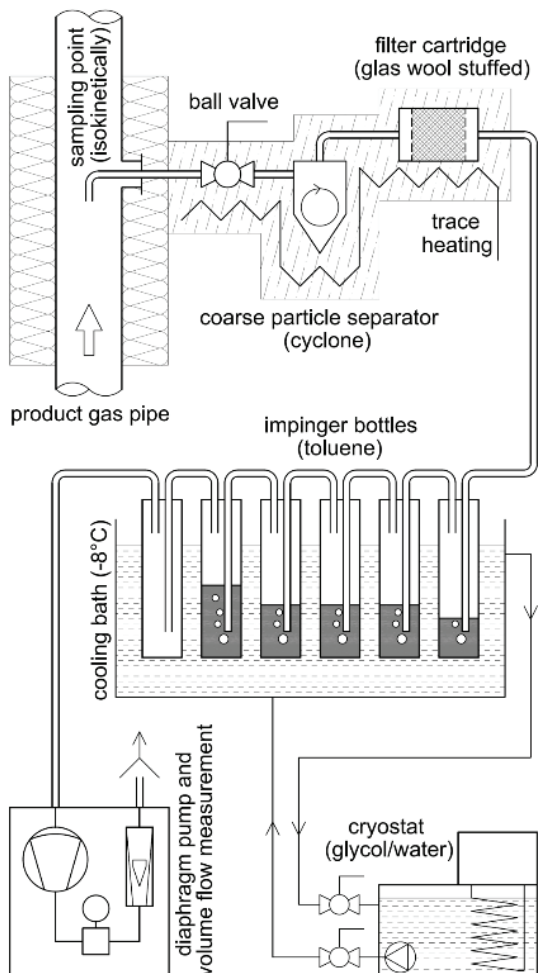


Fig.4: Tar, dust, char and water sampling [6]

This paper presents the measurement results of a steam gasification test run with municipal sewage sludge from digestion towers as fuel and a mixture of olivine and limestone as bed material. The extensive scientific equipment gathers measurement values of the experiment. A detailed description of the pilot plant at TU Wien is available in literature [6,7,8].

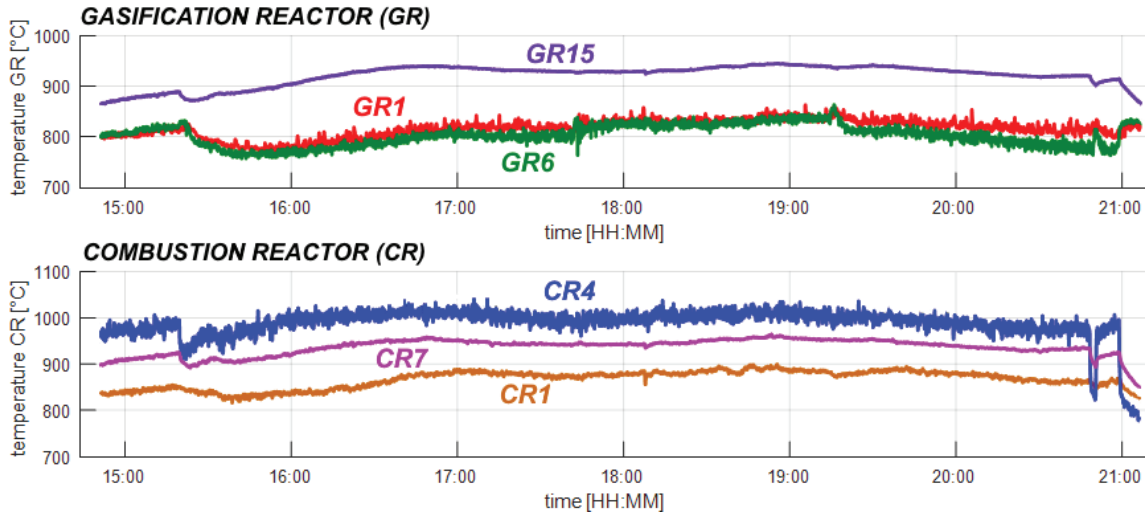


Fig.5: Courses of specific temperatures during the gasification test run over time

This paper focuses on the visualization of pure measurement data visualized with Tables and Figures. For the evaluation of measurements, typically the mean values of a defined steady-state operation phase are used. Fig. 5 shows the courses of temperatures over time of the test run. It is shown that a uniform operation was achieved. For the heat-up procedure of the pilot plant softwood was used. The gasification of 100 % sewage sludge pellets took place between 15:30-17:40 and 19:20-20:45. Softwood pellets were gasified in between due to limited amount of pelletized sewage sludge and the preparation work for measurement procedures of ammonia (NH_3) and hydrogen sulfide (H_2S). Fig. 6 shows the temperature profiles along the reactor height for the steady-state phase 17:10-17:40. A simulation with the software tool IPSEpro is in progress. It will enable calculations of mass and energy balances and will give a deep insight into the test run in future.

3. Results and Discussion

Table 1 presents main process parameters of the gasification test run for two defined steady-state operation phases. Table 2 shows the fuel analysis of sewage sludge. The fuel was dried and pelletized to guarantee a constant fuel feeding into the

gasification reactor via a screw conveyor. The high ash content causes a low heating value. A high amount of nitrogen is present in sewage sludge as fuel.

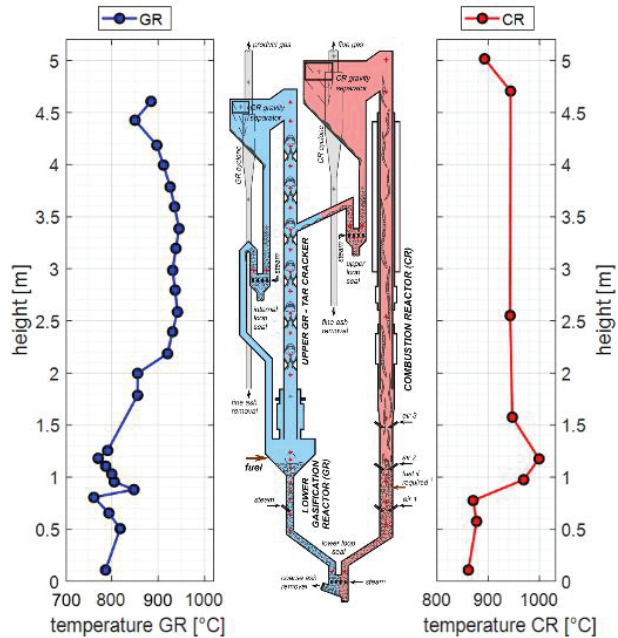


Fig.6: Temperature profiles of the gasification and combustion reactor (mean 17:10-17:40)

High ash melting temperatures predict an operation without sintering effects of the bed material particles caused by the fuel ash. In addition, Table 3 shows the XRF-analysis of the fuel ash. Attention should be paid on the relatively high content of iron oxide as an integral part of the ash. Iron (iron oxide) is a suitable oxygen carrier in dual fluidized beds at high temperatures [9].

Table 1: General process parameters of the sewage sludge gasification test run

parameter	unit	mean value	
bed material	wt.-%	80% olivine, 20% limestone	
steam/fuel ratio	kg _{H2O} / kg _{fuel,daf}	1.45	
steam/carbon ratio	kg _{H2O} / kg _C	2.72	
fuel input GR	kW (kg/h)	69.8 (28.1)	
steady-state phase	hh:mm	16:10- 16:40	17:10- 17:40
additional fuel input CR	kW	76.3	51.7
temp. in lower GR (GR6-GR1)	°C	780-800	800-815
temp. in upper GR (GR15)	°C	925-935	935-940
temp. in CR (CR7)	°C	930-940	940-950

Table 2: Fuel analysis of municipal sewage sludge from a digestion tower from Krems/Austria

parameter	unit	value
water content	wt.-%	8.7
ash content	wt.-% _{db}	52.3
carbon (C)	wt.-% _{db}	25.48
hydrogen (H)	wt.-% _{db}	3.02
nitrogen (N)	wt.-% _{db}	3.46
sulfur (S)	wt.-% _{db}	1.18
chlorine (Cl)	wt.-% _{db}	0.106
oxygen (O)*	wt.-% _{db}	14.45
volatile matter	wt.-% _{db}	44.55
lower heating value, moist	MJ/kg	8.94
ash deformation temp. (A)	°C	1140
ash flow temp. (D)	°C	1230

* calculated by difference to 100 wt.-%_{db}

Fig. 7 shows a section of the main product gas components of the experimental test run over time. The mean values of the product gas composition and the content of different minor components in the product gas are presented in Table 4. The results present the product gas composition without nitrogen from purging the fuel hoppers and the measurement points. Therefore, only the nitrogen in the fuel

causes the presented nitrogen (N₂) and ammonia (NH₃) content in the product gas. It is assumed that the not measured hydrogen cyanide (HCN) is a product gas component, approximately ca. 8-9 % of the ammonia value [10].

Table 3: XRF-analysis of sewage sludge ash

oxide	content wt.-%	oxide	content wt.-%
MoO₃	n.d.	Cr₂O₃	0.04
Nb₂O₅	n.d.	V₂O₅	n.d.
ZrO₂	0.06	TiO₂	0.83
SrO	0.11	CaO	13.18
PbO	0.01	K₂O	1.29
As₂O₃	0.01	Cl	0.14
ZnO	0.29	SO₃	4.80
CuO	0.11	P₂O₅	14.85
NiO	0.02	SiO₂	33.23
Co₃O₄	n.d.	Al₂O₃	17.59
Fe₂O₃	8.50	MgO	3.52
MnO	0.07	Na₂O	1.37

n.d. not detected

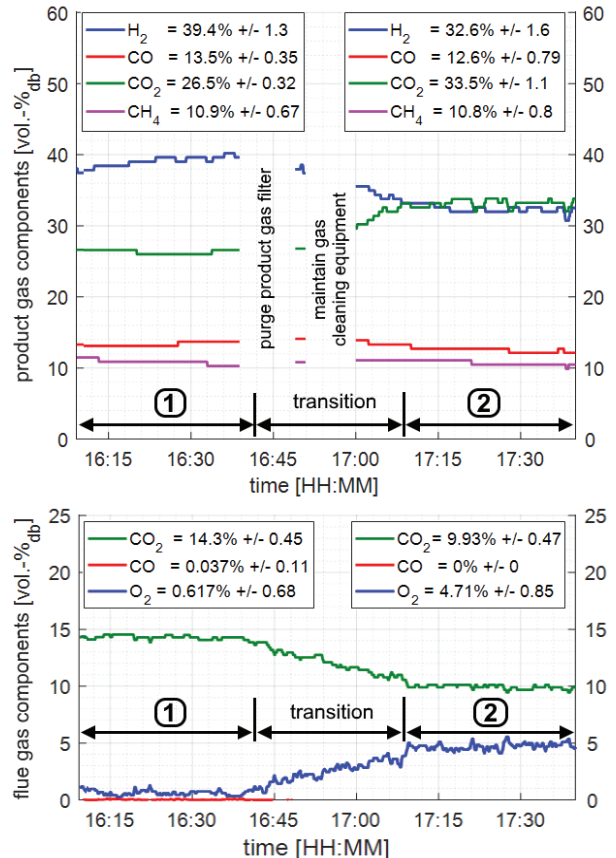


Fig.7: Courses over time of product gas and flue gas components during the gasification test run

Table 4: Product gas components of sewage sludge steam gasification

parameter	unit	before upper GR (before tar cracker)	after upper GR (after tar cracker)	
			16:10-16:40	17:10-17:40
hydrogen (H₂)	vol.-% _{db}	n.p.	39.4	32.6
carbon monoxide (CO)	vol.-% _{db}	n.p.	13.5	12.6
carbon dioxide (CO₂)	vol.-% _{db}	n.p.	26.5	33.5
methane (CH₄)	vol.-% _{db}	n.p.	10.9	10.8
ethylene (C₂H₄)	vol.-% _{db}	n.p.	3.0	2.3
ethane (C₂H₆)	vol.-% _{db}	n.p.	0.19	0.11
nitrogen (N₂)*	vol.-% _{db}	n.p.	0.2-0.9	2.1-2.2
ammonia (NH₃)	vol.-% _{db}	n.p.	n.p.	4.6
hydrogen sulfide (H₂S)	vol.-% _{db}	n.p.	n.p.	1.4
fly char	g/Nm ³ _{db}	26.3	n.p.	1.1
dust	g/Nm ³ _{db}	1350	n.p.	8.1
water content	vol.-%	55	n.p.	62
benzene (B)	mg/Nm ³ _{db}	21650	n.p.	7300
toluene (T)	mg/Nm ³ _{db}	n.m.	n.p.	n.m.
ethyl-benzene (E)	mg/Nm ³ _{db}	840	n.p.	51
xylanes (X)	mg/Nm ³ _{db}	2340	n.p.	12
GCMS tar (without BTEX)	g/Nm ³ _{db}	27.5	n.p.	16.3
grav. tar	g/Nm ³ _{db}	35.5	n.p.	4.75

n.p.: measurement not performed, n.m.: not measureable (toluene is solvent for tar sampling procedure), * nitrogen from purging fuel hoppers and measurement points excluded

The results show that the special design of the gasification reactor is favorable to decrease undesired components in the product gas. Detectable tar contents in the product gas (GCMS, grav. tar, BTEX) decrease significantly during the flow through the upper gasification reactor. Especially, the reduction of the gravimetric tar by 87 % has to be mentioned, because gravimetric tar represents the problematic heavy polycyclic aromatic hydrocarbons in the product gas. Heavy polycyclic aromatic hydrocarbons are the main reason for fouling and clogging effects inside product gas pipes and apparatuses of gasification

plants. Toluene is used as solvent for the tar sampling procedure. Thus, it is not possible to detect the toluene content in the product gas. Experience shows that typical toluene contents are in the range of 20-50 % of the benzene value.

Fig. 7 has to be discussed in detail. The measurement values show that a reduction of the iron oxide of the fuel ash is present in the gasification reactor. It is assumed that an oxygen transport from the combustion to the gasification reactor occurred, which has to be validated by the use of process simulation. Two different steady-state operation phases were

reached during the gasification test run with sewage sludge as fuel. Phase 1 represents an operation where oxygen, introduced into the combustion reactor with the air, is fully utilized for the combustion reactions of char from the gasifier and additional fuel. After a transition period the steady-state phase 2 is reached. Phase 2 represents an operation with lower additional fuel input and/or higher air input into the combustion reactor. In that point, oxygen is present in sufficient amounts for an efficient oxidation of fuel ash iron (iron oxide). The reducing atmosphere and the high temperature in the gasification reactor promote the discharge of oxygen from the fuel ash. The release of oxygen results in lower hydrogen (H_2) and carbon monoxide (CO) and higher carbon dioxide (CO_2) and water contents (H_2O) in the product gas. It is obvious that the transport of oxygen from the combustion reactor to the gasification reactor is significantly higher in phase 2 in comparison to phase 1. This so-called chemical looping process is limited by the availability of oxygen in the combustion reactor. For phase 2 the high availability of oxygen (O_2) is visible with a look on the flue gas composition of Fig. 7.

It has to be mentioned, that the advanced reactor concept was designed for the reduction of tar in gasification applications

and the possibility to produce CO_2 with chemical looping applications [11, 12]. Thus, a chemical looping active ash or bed material have significant higher effect and influence in the pilot plant at TU Wien compared to other dual fluidized bed designs. Actual experimental results show that the advanced fluidized bed reactor concept is predestinated for chemical looping combustion of solid fuels, especially biogenic residues and lignocellulosic biomass [13].

It is possible to present pictures (Fig. 8) of samples of the “oxidized” ash and bed material mix from the combustion reactor entering the gasification reactor, and the “reduced” ash and bed material mix leaving the gasification reactor in the lower part of the reactor system. The samples were taken after 4 hours of operation. The accumulation of bed ash from the sewage sludge in the bed material circulation is visible. Fig. 8 shows that a significant difference of the oxidation state of the iron content is present. The difference of the brown-red colored bed material entering the gasification reactor and the grey colored bed material leaving the gasification reactor is clearly visible. The presented results seem to confirm the theoretical discussion and the assumption of a possible chemical looping effect in dual fluidized bed gasifier systems if sewage sludge is utilized as fuel [14].



Fig.8: Bed material ash mixture from the combustion reactor entering the gasification reactor (left: brown-red colored) and leaving the gasification reactor (right: gray colored)

Additionally, also continuously introduced calcium carbonate from the fuel ash has to be considered as possible source of carbon dioxide in the product gas. Calcium carbonate (CaCO_3) forms calcium oxide (CaO) and releases carbon dioxide (CO_2) at high temperatures in the gasification reactor.

4. Conclusion and Outlook

Economic reasons lead to a rising interest to use alternative low-cost fuels for gasification processes. At the same time, products that are more valuable should be generated via gas upgrading or syntheses instead of heat and power generation. Thus, the focus is the production of hydrogen–methane gas mixtures [15], pure hydrogen [16], synthetic natural gas (SNG) [3,17,18], Fischer-Tropsch liquids [19] or mixed alcohols [20]. In addition, the direct utilization of the product gas as fuel gas is promising, directly substituting fossil fuels for high-temperature processes in industry [2,17].

In Austria approx. 236 000 t municipal sewage sludge (dry substance) were produced in 2017 from municipal sewage treatment plants with a capacity of at least 2000 PE60 (Population equivalent with a biochemical oxygen demand of 60g/day and person). 20% is introduced onto agricultural areas, 55% are treated thermally, and 25% are treated in another way (e.g. composting, mechanical-biological treatment) [21]. Therefore, sewage sludge has the utilization potential as fuel for dual fluidized bed steam gasification plants with a cumulative fuel power of 92 MW (7000 hours of operation per year). The 55% of sewage sludge already used in thermal processes would lead to 50 MW. Furthermore, sewage sludge is a promising fuel since currently municipal sewage treatment plants have to pay for disposal.

The measurement results of the pilot plant at TU Wien enable the generation of meaningful knowledge. This is especially relevant since the gasification of alternative and ash-rich fuel types is technologically challenging. The novel reactor design shows advantages to produce a product gas with comparable low tar contents. A chemical looping effect of the iron rich fuel ash could be responsible for the high carbon dioxide content in the product gas. The more oxygen is available in the combustion reactor, the higher is the transport of oxygen with the fuel ash from the combustion reactor to the gasification reactor. The product gas composition is influenced significantly. Nevertheless, a constant operation without problems was achieved with sewage sludge as fuel for a total period of nearly 4 hours. Important plant equipment like coarse ash output and fine/fly ash cyclones allowed a steady-state operation. Therefore, measures such as ash sieving procedures, hot bed material reuse, fuel blends variations, and varying bed material mixtures should be considered in future. To improve gasification efficiency or increase the hydrogen content in the product gas sorption enhanced gasification/reforming [4, 22] or a general operation with lower temperatures are promising options.

The pursuing research deals with detailed calculations regarding the presented sewage sludge test run. Performance indicating key figures have to be supported by the detailed validation of measurement values via mass and energy balance. The use of the simulation software IPSEpro enables the calculation of these figures. In addition, the presence of the chemical looping effect can be mathematically verified. Thus, the gained results and future calculations will generate knowledge for the up-scaling and design of industrial-sized dual fluidized bed gasifiers.

5. Acknowledgement

The present work is part of the research project “ReGas4Industry” and receives financial support from the research program “Energieforschung” funded by the Austrian Climate and Energy Fund.

6. References

- [1] M. Kaltschmitt. Energy from Organic Materials (Biomass). A Volume in the Encyclopedia of Sustainability Science and Technology, Second Edition (2019), Springer New York.
- [2] J.C. Schmid. Technoökonomische Fallstudien als Entscheidungsunterstützung für das strategische Management. Master Thesis (2016), Austrian Institute of Management.
- [3] M. Materazzi, P.U. Foscolo. Substitute Natural Gas from Waste – Technical Assessment and Industrial Applications of Biochemical and Thermochemical Processes. First Edition (2019), Elsevier, Academic Press.
- [4] J.C. Schmid et al. Syngas for biorefineries from thermochemical gasification of lignocellulosic fuels and residues – 5 years’ experience with an advanced dual fluidized bed gasifier design. Biomass Conversion and Biorefinery (2019).
- [5] A.M. Mauerhofer et al. Dual fluidized bed steam gasification: Change of product gas quality along the reactor height. Energy 173 (2019) p1256-1272.
- [6] A.M. Mauerhofer et al. Influence of different bed material mixtures on dual fluidized bed steam gasification. Energy 157 (2018) p957–968.
- [7] C. Pfeifer et al. Next generation biomass gasifier. In: Proc. 19th Europ. Biom. Conf. (2011), Berlin, Germany.
- [8] F. Benedikt et al. Fuel flexible gasification with an advanced 100 kW dual fluidized bed steam gasification pilot plant. Energy 164 (2018) p329-343.
- [9] T. Pröll, H. Hofbauer. Chemical Looping Combustion and Reforming. In. Proc. 9th Europ. Conf. on Ind. Furnaces and Boilers (2011), Estoril, Portugal.
- [10] V. Wilk, H. Hofbauer. Conversion of fuel nitrogen in a dual fluidized bed steam gasifier. Fuel 106 (2013) p793-801.
- [11] T. Proell, et al. Design considerations for direct solid fuel chemical looping combustion systems. IEA GHG: 2nd High Temperature Solid Looping Cycles Network Meeting (2010), Alkmaar, Netherlands.
- [12] T. Proell, J. Schmid, C. Pfeifer, H. Hofbauer. Fluidized Bed Reactor System. United States Patent, Patent No.: US 9,089,826 B2, (2015).
- [13] S. Penthor et al. First results from an 80 kW dual fluidized bed pilot unit for solid fuels at TU Wien. 5th Int. Conf. on Chemical Looping (2018), Park City, Utah, USA.
- [14] D. Schweitzer. Experimentelle und simulative Untersuchungen der Wasserdampfvergasung von Klärschlamm und weiteren biogenen Brennstoffen. Doctoral thesis (2018), IFK University Stuttgart.
- [15] M. Kraussler et al. An experimental approach aiming the production of a gas mixture composed of hydrogen and methane from biomass as natural gas substitute in industrial applications. Bioresource Technology 237(2017) p39-46
- [16] S. Müller. Hydrogen from biomass for industry - Industrial application of hydrogen production based on dual fluid gasification. Doctoral thesis (2013), TU Wien, Austria.
- [17] D.C. Rosenfeld et al. Scenario analysis of implementing a power-to-gas and biomass gasification system in an integrated steel plant: A techno-economic and environmental study. Renewable Energy 147 (2020), p.1511-1524
- [18] L. Malek. Renewable gas in a Swedish context. Doctoral thesis (2018), Lund University, Sweden.
- [19] Gruber et al. Fischer-Tropsch products from biomass-derived syngas and renewable hydrogen. Biomass Conversion and Biorefinery (2019).
- [20] G. Weber. Production of mixed alcohols using MoS₂ catalyst from biomass derived synthesis gas. Dissertation (2018), TU Wien, Austria.
- [21] Bundesministerium für Nachhaltigkeit und Tourismus. Die Bestandsaufnahme der Abfallwirtschaft in Österreich - Statusbericht 2019, Wien.
- [22] J. Fuchs et al. Dual fluidized bed gasification of biomass with selective carbon dioxide removal and limestone as bed material: A review. Renewable and Sustainable Energy Reviews 107 (2019) p212-231.

Gasification Feedstock and Agents Abstracts

Spectroscopic *in situ* methods for the evaluation of the active centers on ash-layered bed materials from gasification in a fluidized bed reactor

D. Chlebda¹, K. Aziaba², D. Janisch², M. Kuba^{2,3}, H. Hofbauer³,
J. Łojewska^{1,*}

1. Jagiellonian University, Faculty of Chemistry, Gronostajowa 2, Krakow, Poland

2. Bioenergy 2020+ GmbH, Wiener Straße 49, A-7540 Güssing, Austria

3. Vienna University of Technology, Institute of Chemical Engineering - Future Energy Technology,
Getreidemarkt 9/166, 1060 Vienna, Austria

*corresponding author, corresponding.author@tuwien.ac.at

1. Introduction:

One of the more promising energy alternatives is the use of inedible feed stocks and biomass for carbon dioxide capture as well as biofuel. Amongst various solutions for biomass utilization is steam gasification towards fuels and valuable chemicals in a dual fluidized bed (DFB).

Interaction between biomass ash of different origin and bed material in a fluidized bed leads to the formation of modified bed particles with catalytic properties towards the water gas shift reaction and the reduction of tars. It has already been known that the active layer formed on the ash grains is a result of the enrichment of components as well as segregation of the phases upon high temperature exposure in the reactor (around 850°C).

In order to better control the whole process of biomass conversion and gasification it seem important to find the fundamental structure-activity relationships of the catalytic material composed of ash-enriched bed. The purpose of this study was thus to employ various surface sensitive and *in situ* spectroscopic methods

to investigate the active centers formed on the surface of the material.

2. Methodology, Results and Discussion

The materials used were ash enriched particles of olivine and feldspar processed in a biomass reactor filled with different kinds of feedstocks. The samples were examined for BET surface area.

The samples activity was studied for WGS reaction of CO in a CATALAB instrument (Hiden).

The *in situ* Raman, FTIR and UV/Vis methods utilizing various probe molecules such as CO, CH₃COOH, NH₃, MeOH were chosen to study chemical properties of the surface of the material.

The outer layer was studied by XPS and XRD utilizing low angle diffractional analysis.

3. Conclusions

It has been shown that the ash layer is composed mainly of CaO. The chemical composition of the surface was characterized by the *in situ* spectroscopic methods. Through analytically testing model compounds, such as pure CaO, with

specific reaction molecules, the activity of active centers could be described. Furthermore, detailed characterization of the surface properties of the particles was conducted showing the activation through ash layer formation. Additionally, the results also show the limitations of the analytical method in detecting active sites directly when no pure model compounds are used for benchmarking. Thus, an

evaluation of the suitability of different analysis methods will be presented.

Structure analysis with relevance for complex materials – an outlook to X-ray absorption spectroscopy on phosphorus

N. Skoglund¹

1.Thermochemical Energy Conversion Laboratory, Umeå University, SE-901 87 Umeå, Sweden
*corresponding author, nils.skoglund@umu.se

1. Introduction and Short Description:

Several challenges in thermal energy conversion of biomass are directly linked to so-called ash transformation reactions. These reactions are responsible for interactions between fuel ash and bed material, issues arising from melt formation, fouling and deposit formation. The current strategy to understand these complex reactions are mainly related to methods such as scanning electron microscopy with energy-dispersive X-ray spectroscopy (SEM—EDS), chemical fractionation, or powder X-ray diffraction (XRD).

These methods, respectively, have advantages and draw-backs. SEM-EDS provides spatial information concerning elements but is limited by penetration depth and sample morphology. Chemical fractionation on the other hand may alter the chemical composition of the sample during analysis due to changes induced by using a solvent that may cause new compounds to form and precipitate or dissolve. XRD can provide information concerning which compounds has actually formed but is limited to crystalline compounds only and depends on a relevant reference library.

Ash and material interactions in thermochemical processes has been successfully studied through these methods but several questions remain. For instance, the chemical composition in

phosphorus-rich ash fractions that could be suitable for recovery. If these contain significant amounts of amorphous material the cat-ions surrounding the phosphate anions cannot be accurately described. This has severe implications for the recycling of nutrients from ashes which should be a part of a circular bioeconomy.

This lack of analytical information could be addressed using synchrotron-based X-ray absorption spectroscopy (XAS), which directly probes the average chemical environment of a selected element. This is made possible by fine-tuning the incoming X-ray beam energy and scanning the absorption with fine resolution. Further, if coupled X-ray fluorescence, it is possible to not only produce an elemental map similar to that from SEM-EDS, but also determine the chemical environment of selected elements in specific points.

The aim of the present work is to show some examples from on-going work on phosphate structures in ash particles from beamline 10.3.2 at the synchrotron Advanced Light Source, Lawrence Berkeley National Laboratory, USA. Importantly, it is demonstrated that ashes from biomass combustion are valid sample types for this analysis technique.

2. Methodology, Results and Discussion

Measurements with X-ray absorption spectroscopy at the phosphorus K-edge were performed at beamline 10.3.2 at the synchrotron Advanced Light Source, Lawrence Berkeley National Laboratory, USA. A library of reference phosphate compounds was prepared based on compounds previously identified in literature. Emphasis was placed on the anionic state when prioritizing samples as orthophosphates were found to be most common. Additionally, phosphorus-rich ash particles from bubbling fluidized bed combustion of rapeseed cake were analysed.

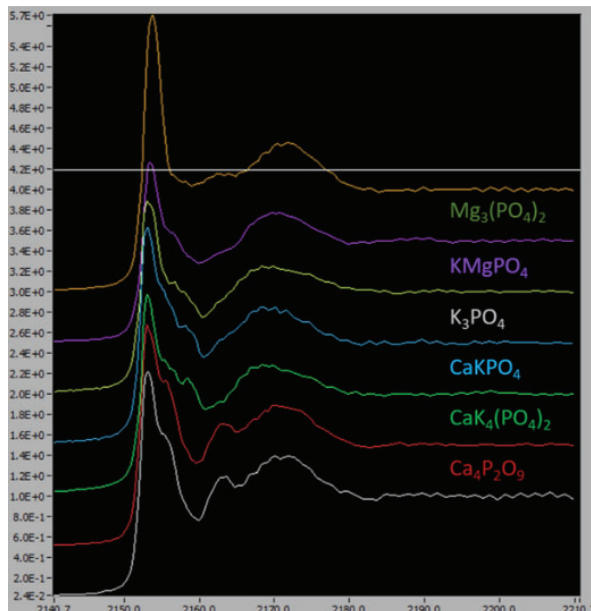


Fig. 1 X-ray absorption spectroscopy from phosphates standards plotted as a function of energy vs detector counts.

The results obtained display that the local structure surrounding cations are different

enough to allow linear combination fitting even in amorphous samples. Further, the biomass ash did yield a spectra proving the feasibility of analyzing biomass ash types with synchrotron-based XAS. This also shows that such materials could be used with other elements in focus which opens up new possibilities.

3. Conclusion and Outlook

The full paper will contain initial results from measurements on phosphate references and a phosphorus-rich biomass ash sample. This highlights the potential of this advanced analytical method for application in the field of energy technology, where analytical challenges such as material interactions and oxidation state of interesting elements could be analysed in detail.

4. Acknowledgements

This research was funded by Swedish Research Council (Grant No. 2017-05331) and FORMAS (Grant No. 2017-01613), and used the resources of the Advanced Light Source (ALS), at Lawrence Berkeley National Laboratory, Berkeley, California, which is a DOE Office of Science User Facility under contract no. DE-AC02-05CH11231 (ALS08232 T.A.L.). ALS Beamline 10.3.2 is acknowledged and I thank research scientist Dr Sirine Fakra for valuable assistance with the analyses at ALS.

Gasification
Advanced Reactor Systems
Full Papers

Evaluation of Sorption Enhanced Reforming in Combination with Oxyfuel Combustion for the Sequestration of CO₂

M. Hammerschmid^{1*}, S. Müller¹, J. Fuchs¹ and H. Hofbauer¹

1. TU WIEN, Institute of Chemical Engineering, Environmental and Bioscience Engineering,
Getreidemarkt 9/166, 1060 Vienna, Austria
* corresponding author, martin.hammerschmid@tuwien.ac.at

Abstract

Traditional dual fluid gasification enables a favorable product gas comprising hydrogen, carbon monoxide, carbon dioxide, and methane. This paper focus on Sorption Enhanced Reforming combined with Oxyfuel combustion, which constitutes an additional opportunity for CO₂ sequestration. First experimental results in the test plants at TU Wien (100 kW) and at University Stuttgart (200 kW) have been implemented. Based on these results, the functionality of OxySER could be demonstrated and a concept for the commercial-scale use is developed. Furthermore, the profitability of OxySER, by application in a raw iron production plant for the generation of reduction gas, within a techno-economic assessment is investigated. The results of the techno-economic assessment show that the production of reduction gas via Sorption Enhanced Reforming in combination with Oxyfuel combustion can definitely compete with the natural gas route. The biggest potential to increase the profitability of the OxySER process offers the use of low-grade fuels like bark or sugarcane bagasse to decrease the fuel costs, which is the main cost driver.

1. Introduction:

Since industrialized nations consume more energy per capita than developing countries as well as the increasing standard of living in general raise the future challenges for developing a sustainable economic system based on renewable technologies. Additionally, future challenges of climate change and the exorbitant carbon dioxide (CO₂) emissions from fossil fuels lead to a high demand of CO₂-neutral technologies in future. Since biomass releases the same amount of CO₂ as it aggregates during its growth, the utilization of biogenic fuels can contribute significantly to a reduction of CO₂ emissions. Further, several technologies provide the possibility of additional carbon-emission reduction by

sequestration of CO₂ from industrial processes.

Fig. 1 represents the way towards **CO₂ sequestration** within an industrial plant in the context of a combustion process and further CO₂ utilization or storage. The biggest potential for the sequestration of CO₂ are in the raw iron production, refinery, cement production and the natural gas processing. [1] Within these plants, a sequestration process can be implemented. Post combustion capture, Pre combustion capture, Oxyfuel combustion and Separated combustion are several possibilities for industrial CO₂ sequestration. Further explanations regarding CO₂ sequestration can be found in [1], [2] and [3].

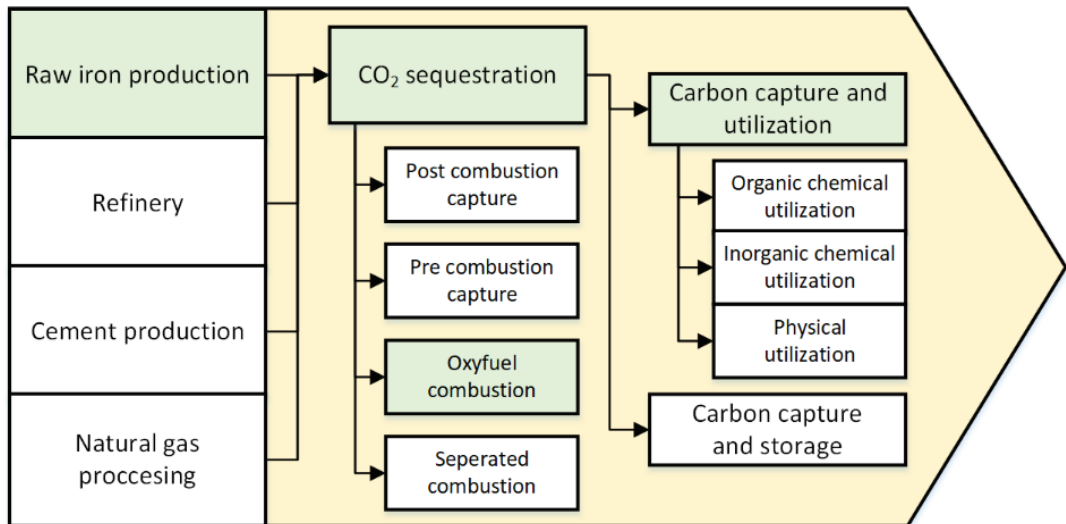


Fig. 1: Possibilities for CO₂ sequestration [2]

The main focus of the paper lies on Oxyfuel combustion. This CO₂ sequestration technology uses as fluidization agent a mix of pure oxygen and recirculated flue gas. Therefore, the nitrogen from the air is excluded from the combustion system. [2]

Furthermore, the sequestered and purified CO₂ could be used in further process steps as raw material, **Carbon capture and utilization (CCU)**, or stored in underground deposits, **Carbon capture and storage (CCS)**. [3], [4]

Today around 130 million tons of carbon dioxide are utilized materially. 110 million tons are used as product and 20 million tons as industry gas. [4]

Beside the CCU technologies, CO₂ can also be stored in underground deposits. CCS is banned in Austria except research projects up to a storage volume of 100 000 t of CO₂. [6]

1.1 Sorption Enhanced Reforming

A promising option for the sequestration of CO₂ from biomass and the generation of a hydrogen-rich product gas at the same time is the Sorption Enhanced Reforming process in combination with Oxyfuel combustion (**OxySER**).

The Sorption Enhanced Reforming (SER) is based on the dual fluidized bed steam gasification process. Detailed information regarding the dual fluidized bed steam gasification process can be found in literature. [5]–[7] Fig. 2 demonstrates the basic principle of SER.

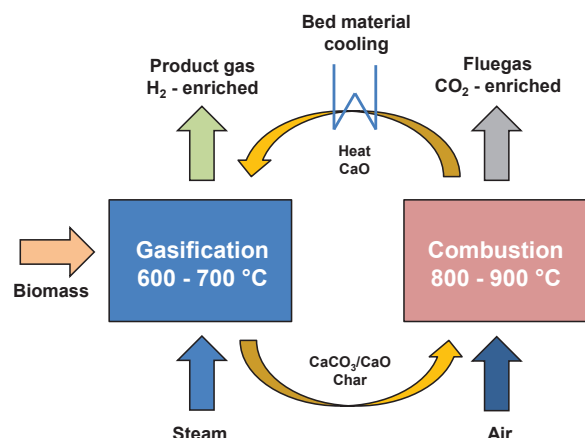
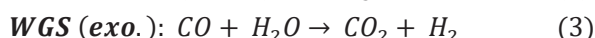
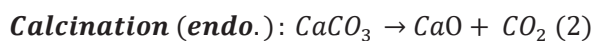


Fig. 2: Concept of Sorption Enhanced Reforming [8]

First of all, biomass, residues or waste materials are introduced in the gasification reactor. Limestone is used as bed material which serves as transport medium for heat, but also as carrier for CO₂ from the gasification reactor (GR) to the combustion reactor (CR) by adjusting the temperature levels in the reactors correctly. Within the SER process, steam serves as fluidization and gasification

agent in the GR. Therein, several endothermic gasification reactions take place in a temperature range between 600-700°C. [5] Residual char is transferred with the bed material from the GR to the CR. The CR is operated within a temperature range between 800-900°C and with the fluidization agent air. By combustion of residual char in the CR, heat is released. This suitable temperature profiles in the GR and CR ensure that the bed material (limestone) is first calcined to calcium oxide (CaO) at high temperatures in the CR (2). Then the CaO is carbonized in the GR with the carbon dioxide from the product gas (1). Thus, in this cyclic process a transport of CO₂ from the product gas to the flue gas appears. [9] The use of steam in the gasification reactor and the water gas shift reaction (3) in combination with in-situ CO₂ sorption via the bed material system CaO/CaCO₃ enables the production of a nitrogen free and hydrogen enriched product gas as showed in **Tab. 1**. [5], [10]



Parameter	Unit	Conventional gasification (100 kW)	Gasification by SER (100 kW)
Fuel		wood pellets	wood pellets
Bed material		olivine	limestone
Particle size	mm	0.4 - 0.6	0.5 - 1.3
Water (H ₂ O)	vol.-%	30 - 45	50 - 65
Hydrogen (H ₂)	vol.-%dry	36 - 42	55 - 75
Carbon monoxide (CO)	vol.-%dry	19 - 24	4 - 11
Carbon dioxide (CO ₂)	vol.-%dry	20 - 25	6 - 20
Methane (CH ₄)	vol.-%dry	9 - 12	8 - 14
Non cond. hydrocarbons (C _x H _y)	vol.-%dry	2.3 - 3.2	1.5 - 3.8
Dust particles	g/Nm ³	10 - 20	20 - 50
Tar	g/Nm ³	4 - 8	0.3 - 0.9

Tab. 1: Comparison product gas composition of conventional gasification and SER [5]

The decrease of the gasification temperature in comparison to the conventional gasification, leads to increasing demands on the bed material cooling. [11]

Tab. 1 represents a comparison between the product gas compositions of conventional gasification and SER. As mentioned above, the carbon dioxide content of the product gas could be reduced through the SER method. Furthermore, the hydrogen content is higher in comparison to the conventional gasification. The catalytic activity of limestone enables a reduction of tar at the same time. [4], [5], [12]

1.2 Oxyfuel combustion

The Oxyfuel combustion is characterized by the use of a mixture of pure oxygen and recirculated flue gas as oxidation agent.

Fig. 3 represents the concept of Oxyfuel combustion. The reason for the flue gas recirculation is the related possibility of temperature regulation in the combustion chamber. In case of application of Oxyfuel combustion on dual fluidized bed steam gasification, a mixture ($\dot{m}_{O_2,\text{fluid}}$) of 30 vol.-%_{dry} pure oxygen ($\dot{m}_{O_2,\text{clean}}$) and 70 vol.-%_{dry} flue gas ($\dot{m}_{O_2,\text{recirc}}$) has been determined based on a variety of tests on the pilot plant at the TU Wien. [2] This is a good compromise between safety, efficiency and technical requirements. [2]

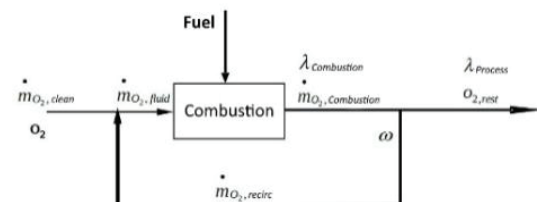


Fig. 3: Concept of Oxyfuel combustion [2]

After condensation of steam, a CO₂ enriched flue gas stream is produced. An important operating parameter is the oxygen surplus ($\lambda_{\text{Combustion}}$). The aim

of this technology is to reach low oxygen contents and high CO₂ contents in the flue gas. The recirculation of flue gas ($m_{O_2,recirc}$) implies also the recirculation of surplus oxygen. Therefore, the stoichiometric combustion ratio of the combustion step ($\lambda_{Combustion}$) is always higher than the stoichiometric combustion ratio of the overall process ($\lambda_{process}$). [2]

1.3 Combination of Oxyfuel combustion and Sorption Enhanced Reforming

The combination of Oxyfuel combustion and Sorption Enhanced Reforming (OxySER) combines the advantages of both technologies. **Fig. 4** represents the concept of the combined technology. [4] Compared with **Fig. 2**, which shows the SER process, the combustion part is now operated as Oxyfuel combustion as explained in Chapter 1.2.

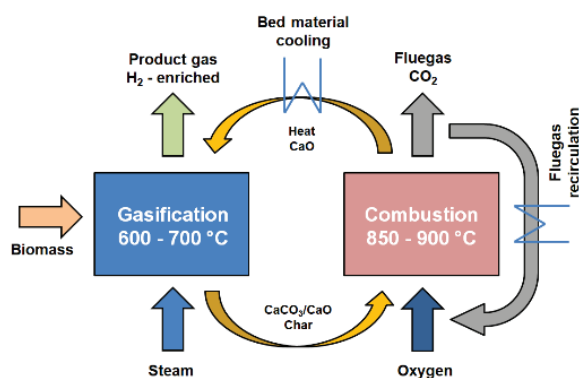


Fig. 4: Concept of OxySER [8]

By the use of renewable fuels and a continuous sequestration and storage or utilization of CO₂, an improved CO₂ balance can be achieved. [4], [13] **Tab. 2** represents test results of the 200 kW pilot plant at University Stuttgart. Therein, product gas compositions from the SER and OxySER gasification technology are compared. The comparison illustrates that a CO₂ enriched flue gas in the OxySER test rig in Stuttgart was obtained.

Parameter	Unit	Gasification by SER (200 kW)	Gasification by OxySER (200 kW)
Fuel		wood pellets	wood pellets
Bed material		limestone	limestone
Particle size	mm	0.3 - 0.7	0.3 - 0.7
Product gas composition			
Water (H ₂ O)	vol.-%	50	50
Hydrogen (H ₂)	vol.-%dry	69 - 72	70
Carbon monoxide (CO)	vol.-%dry	8 - 11	8
Carbon dioxide (CO ₂)	vol.-%dry	5 - 7	8
Methane (CH ₄)	vol.-%dry	11 - 12	11
Non cond. hydrocarbons (C _x H _y)	vol.-%dry	2 - 3	3
Tar	g/Nm ³	14	6
Flue gas composition			
Water (H ₂ O)	vol.-%	14	30
Oxygen (O ₂)	vol.-%dry	7	9
Nitrogen (N ₂)	vol.-%dry	46	-
Carbon dioxide (CO ₂)	vol.-%dry	47	91

Tab. 2: Comparison product gas and flue gas composition of SER and OxySER [13]

However, OxySER implies the following advantages in comparison to the conventional gasification:

- selective CO₂ transport to flue gas,
- decrease of tar content in product gas,
- high CO₂ content in flue gas > 90 vol.-%dry [13],
- smaller flue gas stream because of flue gas recirculation,
- nitrogen free flue gas.

These assumptions serve as a basis for the conception of an industrial application.

2. Concept and methodology:

With regard to the techno-economic assessment of the CO₂ sequestration technology OxySER, a plant concept for the integration in an existing industrial plant has been developed.

2.1 Concept of CO₂ sequestration with OxySER

The OxySER plant concept for integration in an existing raw iron production plant is illustrated in **Fig. 5**. The plant shows a

product gas power of 10 MW. For the production of 10 MW product gas, 5000 kg/h of wood chips with a water content of 40 wt.-% are required. [5] The wood chips are treated in a biomass dryer. Afterwards the biomass is fed in the gasification reactor. The bed material inventory (limestone) of the system contains 2500 kg. In the gasification

reactor, a H₂ enriched product gas with a temperature of 680 °C is produced. Subsequently, the dust particles are removed out of the product gas by a cyclone. Besides ash, these dust particles contain still carbon. This is the reason why the particles are recirculated to the combustion reactor. [4]

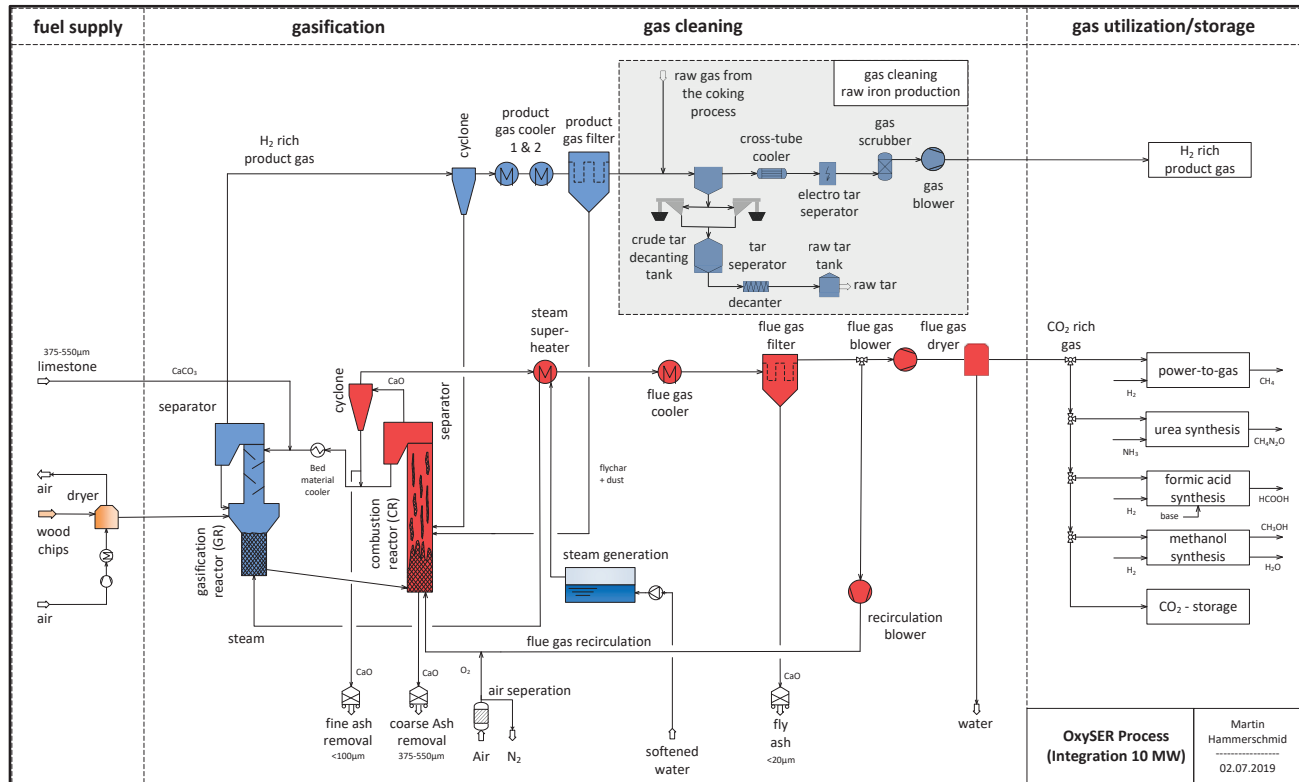


Fig. 5: OxySER plant concept with 10 MW product gas power for the integration in an existing industry plant [5]

Afterwards, the product gas is cooled down to 180°C. The released heat can be used for preheating of the biomass dryer air. [4] Furthermore, the product gas filter separates further fine dust particles out of the product gas stream and conveys them back to the combustion reactor. In the gas cleaning system of the existing raw iron plant, tar is separated in a scrubber and water is condensed. Biodiesel is used as solvent. The product gas exits the scrubber with a temperature of 40°C. Afterwards, it is compressed in a blower and subsequently used as reduction gas in a blast furnace. The CO₂ enriched flue gas leaves the combustion reactor with a

temperature of 900°C. The flue gas is cooled down to 180°C by the steam superheater and a flue gas cooler. Steam is heated up to 450°C in a countercurrent heat exchanger. Fly ash is removed out of the system by a flue gas filter. A partial flow from the flue gas is recirculated and mixed with pure oxygen. Pure oxygen is produced by an air separation unit. The remaining flue gas stream is compressed in the flue gas blower and water is condensed in a flue gas dryer. The cleaned CO₂ rich gas can be used in different CCU processes. [4]

The integration approach offers the advantage to use existing equipment, like gas cleaning steps and air separation units from industrial plants. Furthermore, the produced product gas can be used directly in the industrial plant, for example as reduction gas in raw iron production plants. [4]

2.2 Simulation of mass- & energy balances with IPSEpro

Mass and energy balances of the concept of CO₂ sequestration in combination with OxySER, based on model libraries, which were developed on the TU Wien, has been calculated in IPSEpro. For further information regarding IPSEpro a reference is made to [14] and [15].

2.3. Techno-economic assessment with net present value calculation

The techno-economic assessment regarding the net present value (NPV) calculation serves as decision-making tool for the valuation of upcoming investments. The NPV is a function of the investment and operating costs. The operating costs are multiplied by the cumulative present value factor, which includes the interest rate and the plant lifetime. Therefore, the NPV calculation helps to compare expected payments in the future with current payments. Further information can be found in [16] and [7].

3. Results and discussion

Based on experiences of the pilot plant from the TU Wien and the University of Stuttgart, combined with the previously described concept, the mass- and energy balances were calculated. Furthermore, the mass- and energy balances are the basis for a techno-economic assessment. **Tab. 3** and **Tab. 4** represents the plant utilities and operating parameters of an OxySER plant.

Parameter	Unit	Value	Ref.
Bed material inventory	kg	2500	[5]
Fuel (wood chips)	kg/h	5040	[5]
Fresh bed material	kg/h	177	[16]
Cooling capacity in % of fuel power (kW/kW _{th})	%	5 - 20	[11]
Oxygen	Nm ³ /h	1102	[5]
Fresh water	kg/h	37.8	[5]
RME	kg/h	20	[5]
Flushing gas	Nm ³ /h	50	[5]

Tab. 3: Plant utilities of an OxySER plant with 10 MW product gas energy

Tab. 5 shows the exiting mass- and volume flows of an OxySER plant with 10 MW product gas energy. It can be seen, that 5040 kg/h of wood chips and 1102 Nm³/h of pure oxygen are required for the production of 2880 Nm³/h product gas. The product gas is used as reduction gas in the raw iron production route. Furthermore, 3610 kg/h of CO₂ can be produced for further utilization. The costs for final disposal of 105 kg/h of ash and dust have been taken into account.

Parameter	Unit	Value	Ref.
Lower heating value (wood chips)	MJ/kg	9.53	[5]
Water content (wood chips)	wt.-%	40	[5]
Combustion temperature	°C	900-950	[17]
Gasification temperature	°C	625-680	[17]
Particle size (bed material)	µm	375-550	Assumption
Coarse ash	µm	375-550	Assumption
Fine ash	µm	< 100	Assumption
Very fine ash	µm	< 20	Assumption
Water content (product gas)	vol.-%	7.81	[5]
Lower heating value (product gas)	MJ/kg	22.88	[5]

Tab. 4: Operating parameters of an OxySER plant with 10 MW product gas energy

Parameter	Unit	Value	Ref.
Product gas	Nm ³ /h	2880	IPSE
Flue gas	Nm ³ /h	5300	IPSE
Ash and dust	kg/h	105	[5]
Bed material	kg/h	100	[4]
Carbon dioxide (for CCU)	kg/h	3610	[5]

Tab. 5: Output flow streams of an OxySER plant with 10 MW product gas energy

The techno-economic assessment relies on the results of the IPSEpro simulation. **Tab. 6** represents the fuel prices for chosen fuel types. It is thus evident that natural gas is with 25 €/MWh (see **Tab. 6**) the most expensive fuel within this analysis and sugarcane bagasse with 6 €/MWh the cheapest fuel.

Fuel type	Unit	Value	Ref.
Wood chips	€/MWh	22.5	[4]
Natural gas	€/MWh	25	[18]
Bark	€/MWh	19.2	[16]
Sugarcane bagasse	€/MWh	6	Assumption

Tab. 6: Fuel prices for techno-economic assessment

In **Tab. 7** and **Tab. 8** cost rates for utilities and for the NPV calculation are listed. Exemplary, the costs for one employee per year are assumed to 57 000 €/a and the expected plant lifetime of an OxySER plant is 20 years. (see **Tab. 8**)

Parameter	Unit	Value	Ref.
Electricity	€/kWh	0.04	[16]
Limestone	€/t	35	[16]
Nitrogen	€/Nm ³	0.003	[16]
Fresh water	€/t	0.02	[16]
Solvent (RME)	€/t	960	[16]
Oxygen (air separator)	€/Nm ³	0.02	Assumption
Oxygen (external purchase)	€/Nm ³	0.07	[5]
Emission allowances certificate	€/tCO ₂	23	[19]
Costs for ash disposal	€/t	90	CHP Güssing
CO ₂ expenses	€/Nm ³	0.06	Assumption

Tab. 7: Cost rates for utilities

Parameter	Unit	Value	Ref.
Maintenance costs per year	%/a	2.00	[7]
Insurance, administration & tax per year	%/a	2.50	[7]
Number of employees (Integration)	-	3	Assumption
Costs of one employee per year	€/a	57000	[16]
Expected plant life time	a	20	Assumption
Interest rate	%	4	Assumption

Tab. 8: Cost rates for NPV calculation

The techno-economic analysis is based on the following **business case** that an operator of a raw iron production plant would like to build a new reduction gas supply unit driven by biogenic feedstock. The NPV calculation, which is shown in **Tab. 9**, serves as decision-making tool. The goal to produce 10 MW reduction gas, should be achieved with regard to CO₂ emissions. The reference option (Option 0) is the production of reduction gas by steam reforming of natural gas. Furthermore, various alternative options (Options 1-4) are compared with the reference option:

- **Option 0** (reference case): Production of 10 MW reduction gas through steam reforming of natural gas,
- **Option 1:** Production of 10 MW reduction gas through gasification of wood chips by SER,
- **Option 2:** Production of 10 MW reduction gas through gasification of wood chips by OxySER,
- **Option 3:** Production of 10 MW reduction gas through gasification of bark by OxySER,
- **Option 4:** Production of 10 MW reduction gas through gasification of sugarcane bagasse by OxySER.

The SER process in Option 1 requires no pure oxygen for operation. However, the flue gas of the SER process cannot be exploited in further utilization steps because of the high nitrogen content in the flue gas. The alternative Options 2-4 are

based on the SER process in combination with Oxyfuel combustion. The shared use of gas cleaning and utility preparation steps already existing in steel industry, like air separation, decrease the investment costs by 50% (assumption). The OxySER process is based on the assumption that the CO₂ is sold as product for utilization. **Tab. 9** represents the Net present value

calculation for the production of 10 MW reduction gas. Therein, the fuel energy per year, the investment costs including interest and fuel costs per year are listed. Furthermore, **Tab. 9** shows beside the fuel costs also all other consumption related costs. Costs for CO₂ emission certificates are paid only for the use of fossil fuels (reference case).

Parameter	Unit	Natural gas	SER wood chips (Integration)	OxySER wood chips (Integration)	OxySER bark (Integration)	OxySER bagasse (Integration)
		Reference	Option 1	Option 2	Option 3	Option 4
Product gas energy	MW	10	10	10	10	10
Fuel energy natural gas	MWh/a	70 000				
Fuel energy wood chips	MWh/a		93 100	93 100		
Fuel energy bark	MWh/a				93 100	
Fuel energy sugarcane bagasse	MWh/a					93 100
Investment costs incl. interest	€	8 000 000	10 000 000	10 000 000	10 000 000	10 000 000
Fuel costs natural gas	€/a	1.750.000				
Fuel costs wood chips	€/a		2 094 750	2 094 750		
Fuel costs bark	€/a				1 787 520	
Fuel costs sugarcane bagasse	€/a					558 600
CO ₂ emission certificates	€/a	322 000				
Maintenance, insurance, etc.	€/a	360 000	450 000	450 000	450 000	450 000
Employee costs	€/a	57 000	171 000	171 000	171 000	171 000
Auxiliaries	€/a	33 215	177 770	177 770	177 770	177 770
Disposal costs	€/a		66 150	66 150	66 150	66 150
Oxygen costs	€/a			154 280	154 280	154 280
Sum of Expenses per year	€/a	2 522 215	2 959 670	3 113 950	2 806 720	1 577 800
Earnings CO ₂	€/a			765 758	765 758	765 758
Sum of Earnings per year	€/a			765 758	765 758	765 758
Investment costs incl. interest	€	8 000 000	10 000 000	10 000 000	10 000 000	10 000 000
Expenses - Earnings	€/a	2 522 215	2 959 670	2 348 193	2 040 963	812 043
Additional investment costs (compared to reference option)	€	0	2 000 000	2 000 000	2 000 000	2 000 000
Operating expenses savings	€/a	0	- 437 455	174 022	481 252	1 710 172
Relative Net Present Value	€	0	- 7 945 017	364 963	4 540 219	21 241 241

Tab. 9: Net present value calculation for the production of 10 MW reduction gas

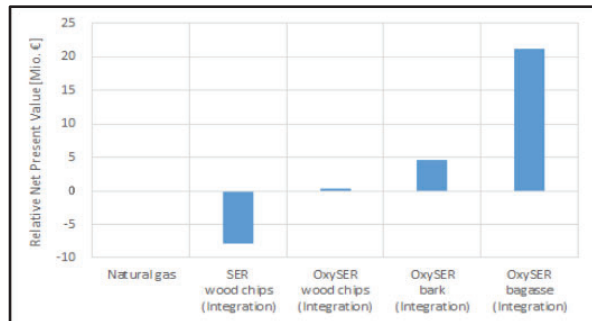


Fig. 7: Relative Net Present Value

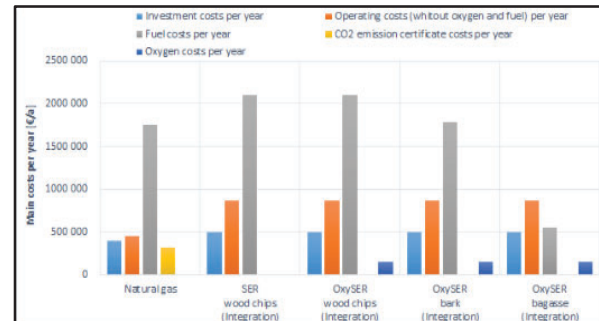


Fig. 6: Main costs per year

The Relative NPV represents the profitability of alternative production routes in comparison to the reference route. The NPV of Option 1 shows a negative value. This means that the operation of SER with wood chips based on the expected plant lifetime of 20 years is less profitable than the reference option. The techno-economic comparison between SER and OxySER shows that the earnings through carbon dioxide are much higher than the oxygen costs. This is the reason for the positive NPV and thereby profitable operation in Option 2. Due to less fuel costs in the alternative Options 3 and 4, the profitability increase. **Fig. 7** represents the main costs of all options per year. It can be seen, that the fuel costs are the main cost driver in the process.

Additionally, a sensitivity analysis of fuel prices, cost rates for utilities and cost rates for NPV have been created. **Tab. 10** represents the sensitivity analysis based on Option 3 of the techno-economic assessment. The cost rates are calculated for the case that the NPV for Option 3 is equal to the reference option.

Parameter	Unit	Initial Value	Sensitivity Value NPV = 0	Dev.
Bark	€/MWh	19.2	22.8	19%
Natural gas	€/MWh	25.0	20.2	-19%
Investment costs	€	10.0 Mio	12.8 Mio	28%
Oxygen (air separator)	€/Nm ³	0.02	0.06	200%
Solvent (RME)	€/t	960	3350	249%
Costs for ash disposal	€/t	90	544	504%
Limestone	€/t	35	304	769%
Fuel costs (very sensitive)				
Investment costs (sensitive)				
Utility costs (not sensitive)				

Tab. 10: Sensitivity analysis cost rates

The sensitivity values, shown in **Tab. 10**, are the limit values for the profitability of Option 3 compared with the reference option. This means for example that Option 3 is favourable compared to the reference option if the investment costs does not exceed 12.8 Mio €.

4. Conclusion and Outlook

The gasification via SER allows the in-situ CO₂ sorption via the bed material system CaO/CaCO₃. Therefore, the selective transport of carbon dioxide to the flue gas stream is reached. The use of a mix of pure oxygen and recirculated flue gas as fluidization agent in the CR results in a nearly pure CO₂ flue gas stream. The CO₂ could be used for further synthesis processes like e.g. the urea synthesis.

The results of the techno-economic assessment show that the production of reduction gas via Sorption Enhanced Reforming in combination with Oxyfuel combustion can definitely compete with the natural gas route. Especially, low-grade fuels like bark or sugarcane bagasse increase the profitability of the OxySER process. Furthermore, the sensitivity analysis of the cost rates show that the fuel and investment costs have more influence on the profitability of the OxySER plant than the utility costs. This means, to increase the profitability of a DFB plant, further research work should focus on the development of additional integration process routes with the use of low-grade fuels.

Summing up, the shown integration concept indicates valuable data for the design of the proposed concept. Beforehand a demonstration at a reasonable scale is recommended.

5. Acknowledgements

The present work contains results of the project ERBA II which is being conducted within the “Energieforschung” research program funded by the Austrian Climate and Energy Fund and processed by the Austrian Research Promotion Agency (FFG). The work has been accomplished in cooperation with voestalpine Stahl GmbH, and voestalpine Stahl Donawitz GmbH.

LIST OF ABBREVIATIONS

CCS	Carbon Capture and Storage
CCU	Carbon Capture and Utilization
CaCO ₃	calcium carbonate
CaO	calcium oxide
CH ₄	methane
CO	carbon monoxide
CO ₂	carbon dioxide
CR	combustion reactor
C _x H _y	non condensable hydrocarbons
Dev.	deviation
dry	dry basis
GR	gasification reactor
H ₂	hydrogen
H ₂ O	water
NPV	Net Present Value
OxySER	Sorption Enhanced Reforming in combination with Oxyfuel combustion
Ref.	reference
SER	Sorption Enhanced Reforming
vol.-%	volumetric percent
wt.-%	weight percent
WGS	water gas shift reaction

LIST OF SYMBOLS

$\lambda_{Combustion}$	stoichiometric combustion ratio of the combustion step
$\lambda_{Process}$	stoichiometric combustion ratio of the overall process
$\dot{m}_{O_2,clean}$	mass flow of pure oxygen
$\dot{m}_{O_2,combustion}$	mass flow of oxygen in the flue gas
$\dot{m}_{O_2,fluid}$	mass flow of oxygen in the oxidation agent
$\dot{m}_{O_2,recirc}$	mass flow of oxygen in recirculated flue gas
$O_{2,rest}$	remaining oxygen in the flue gas after recirculation
ω	recirculation rate

6. References

- [1] P. Markewitz, L. Zhao, and M. Robinius, “Technologiebericht 2.3 CO₂-Abscheidung und Speicherung (CCS),” Wuppertal, Karlsruhe, Saarbrücken, 2017.
- [2] G. Tondl, “Oxyfuel Verbrennung von Klärschlamm,” Institute of Chemical, Environmental and Bioscience Engineering, 2013.
- [3] W. Kuckshinrichs *et al.*, “Weltweite Innovationen bei der Entwicklung von CCS-Technologien und Möglichkeiten der Nutzung und des Recyclings von CO₂,” Berlin, 2010.
- [4] M. Hammerschmid, “Evaluierung von Sorption Enhanced Reforming in Kombination mit Oxyfuel-Combustion für die Abscheidung von CO₂,” TU Wien, 2016.
- [5] S. Müller, “Hydrogen from Biomass for Industry-Industrial Application of Hydrogen Production Based on Dual Fluid Gasification,” TU Wien, 2013.
- [6] J. C. Schmid, M. Kolbitsch, J. Fuchs, F. Benedikt, S. Müller, and H. Hofbauer, “Steam gasification of EXHAUSTED OLIVE POMACE with a dual fluidized bed pilot plant at TU Wien,” TU Wien, 2016.
- [7] M. Hammerschmid, “Entwicklung eines virtuellen Planungsraums anhand des Basic Engineering einer Zweibettwirbelschichtanlage,” TU Wien, Vienna, 2019.
- [8] J. Fuchs, K. Wagner, M. Kuba, S. Müller, J. C. Schmid, and H. Hofbauer, “Thermische Vergasung minderwertiger Reststoffe zur Produktion von Wertstoffen und Energie,” Vienna, 2017.
- [9] J. Fuchs, J. C. Schmid, S. Müller, and H. Hofbauer, “Dual fluidized bed gasification of biomass with selective carbon dioxide removal and limestone as bed material: A review,” *Renew. Sustain. Energy Rev.*, vol. 107, no. August 2018, pp. 212–231, 2019.
- [10] S. Koppatz, “In – situ Produktgaskonditionierung durch selektive CO₂ – Abscheidung bei Wirbelschicht – Dampfvergasung von Biomasse : Machbarkeitsnachweis im industriellen Maßstab,” TU Wien, 2008.
- [11] R. Jentsch, “Modellierung des SER-Prozesses in einem Neuen-Zweibettwirbelschicht-Dampfvergaser-System,” TU Wien, 2015.
- [12] G. Soukup, “Der AER – Prozess , Weiterentwicklung in einer Technikumsanlage und Demonstration an einer Großanlage,” TU Wien, 2009.
- [13] D. Schweitzer *et al.*, “Pilot-scale demonstration of oxy-SER steam gasification: Production of syngas with pre-combustion CO₂ capture,” *Energy Procedia*, vol. 86, pp. 56–68, 2016.
- [14] S. Müller, J. Fuchs, J. C. Schmid, F. Benedikt, and H. Hofbauer, “Experimental development of sorption enhanced reforming by the use of an advanced gasification test plant,” *Int. J. Hydrogen Energy*, vol. 42, no. 50, pp. 29694–29707, 2017.
- [15] T. Pröll and H. Hofbauer, “Development and Application of a Simulation Tool for Biomass Gasification Based Processes,” *Int. J. Chem. React. Eng.*, vol. 6, no. 1, 2008.
- [16] J. C. Schmid, “Technoökonomische Fallstudien als Entscheidungsunterstützung für das strategische Management,” Fachhochschule Burgenland, 2016.
- [17] J. Fuchs *et al.*, “The impact of bed material cycle rate on in-situ CO₂ removal for sorption enhanced reforming of different fuel types,” *Energy*, vol. 162, pp. 35–44, 2018.
- [18] “Industriegaspreis E-Control - Preisentwicklungen,” 2019. [Online]. Available: <https://www.e-control.at/statistik/gas/marktstatistik/preisentwicklung>. [Accessed: 04-Jul-2019].
- [19] “European Emission Allowances (EUA),” 2019. [Online]. Available: <https://www.eex.com/en/market-data/emission-allowances/spot-market/european-emission-allowances#/!2016/05/26>. [Accessed: 04-Jul-2019].

Gasification Advanced Reactor Systems Abstracts

Syngas production for DME synthesis from Sorption Enhanced Gasification of Biomass: A Pilot Plant-based Case Study

S.Hafner^{1*}, M.Schmid¹, G.Scheffknecht¹

1. University of Stuttgart, Institute of Combustion and Power Plant Technology (IFK), Pfaffenwaldring 23, 70569 Stuttgart, Germany

*corresponding author, selina.hafner@ifk.uni-stuttgart.de

1. Introduction and Short Description:

For fulfilling the climate targets of the European Union, it will be necessary to reduce the use of fossil fuels significantly. Therefore, the development and optimization of technologies for the production of transport fuels such as Dimethyl Ether (DME) from renewable sources and waste streams is of main importance.

A very promising process for the production of the syngas that is needed for the synthesis of Dimethyl Ether is the sorption enhanced gasification (SEG). In this process, biomass is gasified in a dual fluidized bed reactor using a CaO-based CO₂ sorbent as bed material. The CaO absorbs the CO₂ (CaO + CO₂ ⇌ CaCO₃) that is formed during gasification, shifting the water-gas-shift reaction (CO + H₂O ⇌ CO₂ + H₂) towards the product side, leading to an enhanced hydrogen output. By adjusting the operational parameters (e.g. gasification temperature), a syngas with a Module M ($M = (y_{H_2} - y_{CO_2})/(y_{CO} + y_{CO_2})$) equal to 2 that is optimal for DME synthesis, can be produced. The heat that is required for the endothermic gasification reactions is provided by hot circulating bed material from the combustion reactor and heat generated from the exothermic carbonation and water-gas-shift reactions. In the combustor, temperatures above 850 °C are achieved through burning unconverted char from the gasifier (and

additional fuel if required) with air. Due to the high temperatures in the combustor, CaCO₃ is regenerated to CaO (CaCO₃ ⇌ CaO + CO₂), which is essential for CO₂ capture in the gasifier.

2. Methodology, Results and Discussion

The investigations were conducted in a pilot scale facility which consists of a bubbling (gasifier) and a circulating (combustor) fluidized bed reactor that are connected to each other. SEG experiments were performed with two different biomasses: wood pellets and pellets made out of the organic fraction of municipal solid waste (MSW). The composition of both biomasses is presented in Table 1.

Table 1. Chemical composition of wood pellets and pellets made out of the organic fraction of MSW

			Wood	MSW
Proximate analysis	γ _{H2O}	wt%,ad	6.0	8.0
	γ _{ash}	wt%,db	0.2	33.2
	γ _V	wt%,daf	82.7	90.0
	γ _{FC}		17.3	10.0
Ultimate analysis	γ _C	wt%,daf	50.8	53.9
	γ _H		6.1	6.4
	γ _N		0.2	2.5
	γ _S		0.1	0.6
	γ _{Cl}		0.0	1.0
	H _u	MJ/kg	17.4	11.6

Limestone with a nominal particle size distribution of 0.1 – 0.3 mm was used as bed material.

The experiments with both biomasses were conducted at a gasification temperature of 635 °C and a steam-to-carbon ratio of 1.5 mol/mol.

Standard gas components such as H₂, CO₂, CO and CH₄ and lower hydrocarbons (C₂-C₄) were measured continuously after fine filtration, washing in isopropanol (for tar removal) and condensation.

Tars were measured wet chemically according to the tar protocol [1].

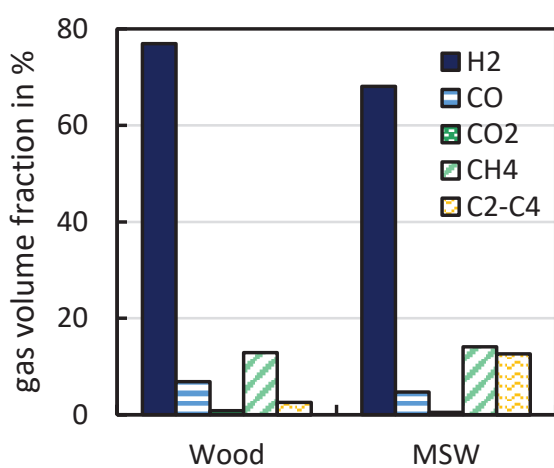


Fig. 1. Gas volume fractions of the syngas (N₂-free, dry basis) for SEG with wood and MSW

In Fig. 1, the N₂-free gas volume fractions on dry basis for H₂, CO, CO₂, CH₄ and C₂-C₄ are plotted for SEG with wood and MSW pellets. For SEG with wood pellets, a hydrogen concentration of 77 % has been reached, while the concentration for SEG with MSW was much lower with only 68 %. Another difference between the syngas obtained from the two biomasses is the C₂-C₄ concentration, which is much

lower for SEG with wood pellets compared to SEG with MSW pellets (2.5 vs. 12.6 %). The same accounts for the gravimetric tar concentration. For SEG with wood, a gravimetric tar concentration of 19 g/m³ (STP) was measured, which is much lower than the 31 g/m³ (STP) that have been measured while using MSW. Both tar values have been measured at a gasification temperature of about 655 °C.

3. Conclusion and Outlook

The presentation covers results achieved from SEG with wood pellets and pellets made out of the organic fraction of municipal solid waste. Results are presented comprehensively focusing on syngas composition, considering standard gases (H₂, CO, CO₂ and CH₄), lower hydrocarbons (C₂-C₄) and tars. It is shown that the facility can be operated stably with both investigated fuels and that both fuels are suitable for the production of a syngas with a Module M equal to 2 that is required for downstream DME synthesis.

4. Acknowledgement

The FLEDGED project has received funding from the European Union's Horizon 2020 research and innovation programme under grant agreement No 727600 .

5. References

- [1] DIN CEN/TS 15439:2006-08, Biomass gasification - Tar and particles in product gases - Sampling and analysis.

Syngas Applications
Production of Biofuels
Full Papers

Dual fluidized bed biomass gasification: Temperature variation using pure CO₂ as gasification agent

A.M. Mauerhofer^{1*}, S. Müller¹, F. Benedikt¹, J. Fuchs¹, A. Bartik¹, M. Hammerschmid¹, and H. Hofbauer¹

1. TU Wien, Institute of Chemical, Environmental and Bioscience Engineering (ICEBE),

Getreidemarkt 9/166, 1060 Vienna, Austria

*corresponding author, anna.mauerhofer@tuwien.ac.at

Abstract

In many industrial processes, the climate-damaging gas CO₂ is produced as undesired by-product. The dual fluidized bed biomass gasification technology offers the opportunity to solve this problem by using the produced CO₂ within the process as gasification agent. Therefore, a 100 kW pilot plant at TU Wien was used to investigate the use of CO₂ as gasification agent by converting softwood as fuel and olivine as bed material into a product gas. A temperature variation from 740 to 840°C was conducted to investigate the change of the main product gas components over the gasification temperature. With increasing temperature, CO and H₂ increased and CO₂ decreased. Additionally, another parameter variation was conducted, where the typically used gasification agent steam was substituted stepwise by CO₂. Thereby, the amount of CO and CO₂ increased and the content of H₂ decreased. These trends resulted in a declining H₂/CO ratio and a decreasing lower heating value when CO₂ was increased as gasification agent.

1. Introduction

The increasing visible and noticeable effects of the climate change, require the development of efficient and feasible strategies to be able to meet the targets of the Paris Agreement. To achieve these targets, the research on efficient energy technologies with low greenhouse gas emissions and the possibility to recycle undesired by-products within the process is urgent. A possible technology could be the thermochemical conversion process of biomass gasification. In this way, fossil energy sources like crude oil or lignite are substituted by renewable, alternative feedstock to produce a highly- valuable product gas. This product gas could be further upgraded in different synthesis processes to produce fuels or other chemicals [1], [2]. Additionally, the

recycling of produced carbon dioxide (CO₂) within the gasification process could reduce greenhouse gas emissions and contribute to the overall carbon cycle in a positive way. The dual fluidized bed (DFB) biomass gasification using steam as gasification agent has been developed successfully for more than 20 years at TU Wien [3]. However, the use of CO₂ as gasification agent presents a novel research topic at TU Wien. In contrast to pure steam biomass gasification, where a hydrogen (H₂)-enriched product gas is generated, a carbon monoxide (CO)-rich product gas is created, when CO₂ is used as gasification agent. In this way, the H₂/CO ratio, which presents an important factor for different synthesis processes, is influenced. With the DFB biomass gasification system, the adjustment of the H₂/CO ratio in a range of 0.6:1 to 10:1 is

possible [4], [5]. This presents a huge flexibility in the generation of the product gas for different synthesis processes.

In this publication, the influence of the gasification temperature on pure CO₂ as gasification agent is investigated. Additionally, a second parameter variation, the stepwise substitution of steam by CO₂ as gasification is discussed.

2. Concept and methodology

2.1 DFB CO₂/steam gasification reactor system

For the experimental test campaigns, a 100 kW_{th} DFB pilot plant, which was built at TU Wien, was used. The principle of the DFB gasification pilot plant is shown in Fig. 1. The pilot plant is composed of two reactors: a gasification reactor (GR, blue rectangle) and a combustion reactor (CR, red rectangle), which are connected by loop seals (horizontal arrows). The GR is divided in a lower part, where the devolatilization and gasification reactions take place and an upper part, where reforming and gasification reactions occur.

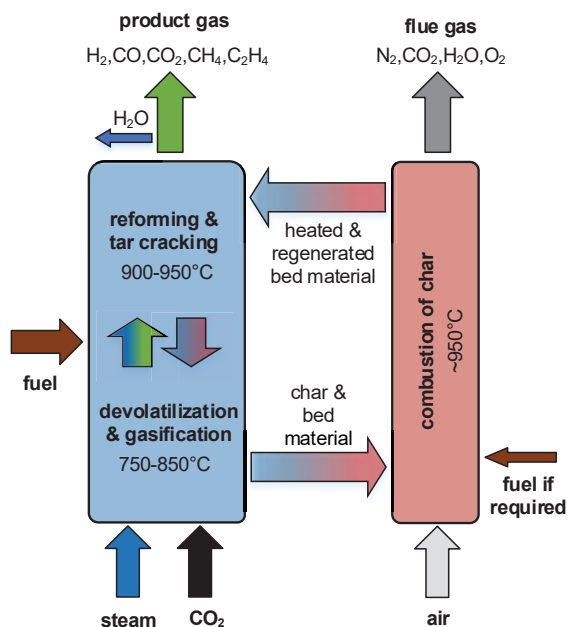


Fig. 1: Principle of the DFB CO₂/steam biomass gasification

The GR is fluidized with CO₂ and/or steam and the CR with air. Biomass is introduced into the GR. In the GR, a product gas, which is composed of CO, H₂, CO₂, methane (CH₄), ethylene (C₂H₄), water (H₂O) and other minor components, is generated. In the CR, a flue gas, which mainly contains CO₂, H₂O, nitrogen (N₂) and oxygen (O₂) is produced.

The 100 kW_{th} DFB biomass gasification pilot plant went into operation in 2014 [6]. Fig. 2 shows the upper part of the pilot plant with three fuel hoppers and the lower part of the reactor system with some ash removal containers. The GR of the pilot plant is operated as bubbling bed in the lower part and as counter-current column with turbulent fluidized bed zones in the upper part. In the upper part of the gasification reactor, constrictions are implemented, which enable an increased interaction of hot bed material particles with the product gas. Thus, the residence time as well as the conversion efficiency is increased [7], [8].



Fig. 2: Upper part and lower part of the DFB biomass gasification system

2.2 Investigated materials

For the presented test campaigns, softwood (SW) pellets were used as fuel and olivine as bed material. The proximate and ultimate analysis of SW is shown in **Tab. 1** and the composition of olivine is presented in **Tab. 2**. Olivine was used as bed material because it is known as state-of-the-art bed material and is typically used in industrial-sized biomass gasification plants [9].

Tab. 1: Proximate and ultimate analysis of softwood pellets

parameter	unit	value
proximate analysis		
water content	wt.-%	7.2
volatiles	wt.-% _{db}	85.4
fixed C	wt.-% _{db}	14.6
LHV (dry)	MJ/kg _{db}	18.9
LHV (moist)	MJ/kg	17.4
ultimate analysis		
ash content	wt.-% _{db}	0.2
carbon (C)	wt.-% _{db}	50.7
hydrogen (H)	wt.-% _{db}	5.9
oxygen (O)	wt.-% _{db}	43.0
nitrogen (N)	wt.-% _{db}	0.2
sulphur (S)	wt.-% _{db}	0.005
chloride (Cl)	wt.-% _{db}	0.005
ash content	wt.-% _{db}	0.2
carbon (C)	wt.-% _{db}	50.7
ash melting behaviour		
deformation temperature (A)	°C	1335

Tab. 2: Composition of olivine

parameter	unit	value
Fe ₂ O ₃	wt.-%	8.0 - 10.5
MgO	wt.-%	48 - 50
SiO ₂	wt.-%	39 - 42
CaO	wt.-%	≤ 0.4
trace elements (< 0.4 per element)	wt.-%	≤ 4.6
hardness	Mohs	6 - 7
sauter mean diameter	mm	0.243
particle density	kg/m ³	2850

2.3 Validation of process data with IPSE

To close the mass and energy balances of the experimental data recorded during the presented test campaigns, the software simulation tool IPSEpro was used. For this purpose, a detailed model library, which was developed at TU Wien over many years, was used. [10], [11]. The following key parameters were selected to describe the operation of the presented test campaigns. All input and output streams, which were used for the calculation of the key parameters are presented in **Fig. 3**. The carbon to CO conversion $X_{C \rightarrow CO}$ describes the amount of CO in the product gas to the total amount of introduced C as fuel and gasification agent (see **Eq. 1**). **Eq. 2** shows the CO₂ conversion rate X_{CO_2} , which gives the ratio of consumed CO₂ during gasification to the amount of CO₂ introduced into the GR. Detailed information about the calculation of X_{CO_2} can be found in [12]. X_{H_2O} is defined as the steam-related water conversion. It presents water consumed for e.g. CO and H₂ production in relation to the sum of water, which is fed to the GR as gasification agent and fuel water (see **Eq. 3**). To describe the efficiency of the test campaigns, the overall cold gas efficiency $\eta_{CG,o}$ is given in **Eq. 4**. It shows the amount of chemical energy in the product gas in relation to the fuel introduced into the gasification and combustion reactor minus appearing heat losses.

$$X_{C \rightarrow CO} = \frac{x_{CO,PG} \times \dot{m}_{PG}}{x_{C,fuel} \times \dot{m}_{fuel,db} + x_{C,CO_2,fluid} \times \dot{m}_{CO_2,fluid}} \quad (1)$$

$$X_{CO_2} = \frac{\dot{m}_{CO_2,fluid} + k_{CO_2} \times \dot{m}_{fuel,daf} - x_{CO_2,PG} \times \dot{m}_{PG}}{\dot{m}_{CO_2,fluid} + \dot{m}_{fuel,daf} \times k_{CO_2}} \quad (2)$$

$$X_{H_2O} = \frac{\dot{m}_{steam} + x_{H_2O,fuel} \times \dot{m}_{fuel} - x_{H_2O,PG} \times \dot{m}_{PG}}{\dot{m}_{steam} + x_{H_2O,fuel} \times \dot{m}_{fuel}} \quad (3)$$

$$\eta_{CG,o} = \frac{\dot{V}_{PG} \times LHV_{PG}}{\dot{m}_{GR,fuel} \times LHV_{GR,fuel} + \dot{m}_{CR,fuel} \times LHV_{CR,fuel} - \dot{Q}_{loss}} \cdot 100 \quad (4)$$

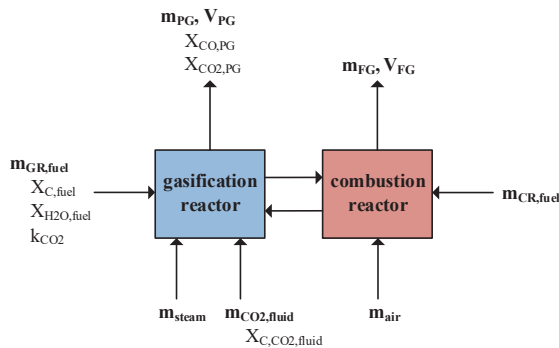


Fig. 3: Input and output streams for the calculation of the key parameters

In Eq. 5, a very important gasification reaction, namely the reverse water gas shift (RWGS) reaction, is shown and used for the discussion of the results. Additionally, the deviation of this reaction from thermodynamic equilibrium is shown in Eq. 6. The RWGS reaction is a homogeneous gas-gas reaction, which favors the CO production. The equilibrium constant $K_p,RWGS(T)$ was calculated using the software tool HSC [13]. If the deviation is zero, it means that the equilibrium state of the equation is reached. A negative value would indicate, that the gas composition is on the side of the reactants, which would mean, that a further reaction is thermodynamically possible. A positive sign would imply that the actual state is on the side of the products. However, this state can not be reached thermodynamically through the RWGS reaction alone. Additional reactions are required as stated in [14].



$$p\delta_{eq,RWGS} = \log_{10}\left[\frac{\prod_i p_i^{v_i}}{K_p,RWGS(T)}\right] \quad (6)$$

2.4 Thermodynamic calculations

To compare the experimental results with theory, thermodynamic calculations were carried out beforehand. Therefore, the product gas compositions were calculated in their thermodynamic equilibrium with the software tool HSC Chemistry [13] based on the minimization of the Gibbs free energy. At the equilibrium state, the Gibbs free energy of the investigated system was minimized, which is explained in detail in [15].

3. Results and discussion

In Tab. 3, the main operational parameters of 5 test campaigns are shown. In these 5 test campaigns, the gasification agent was changed from pure H_2O to pure CO_2 . Softwood was used as fuel and olivine as bed material for all test campaigns. The CO_2/H_2O ratio of the gasification agent was changed from 0/100 to 100/0 vol.-% in five steps. The temperatures in the gasification and the combustion reactor were in the same range. In the following, the experimental results are presented. To compare the experimental results with theory, thermodynamic calculations were carried out beforehand.

Tab. 3: Main operational parameters

parameter	unit	test campaign				
		1	2	3	4	5
fuel	-	SW	SW	SW	SW	SW
bed material	-	olivine	olivine	olivine	olivine	olivine
CO_2/H_2O fluidization	vol.-%	0/100	32/68	45/55	68/32	100/0
fuel to GR	kW	95	92	86	87	83
fuel to CR	kW	68	59	53	53	56
T GR _{lower}	°C	827	833	838	838	837
T GR _{upper}	°C	935	936	938	934	947
T CR _{outlet}	°C	947	944	944	941	964

Fig. 4 shows the course of the main product gas components depending on the gasification agent in the thermodynamic equilibrium for the 5 test campaigns. In the thermodynamic equilibrium, the H₂ content decreased and the CO content increased. The CO₂ content showed an increasing trend as well, but decreased abruptly when 100 vol.-% CO₂ was theoretically used as gasification agent. CH₄ remained almost 0 vol.-%_{db} for all operating points in the thermodynamic equilibrium.

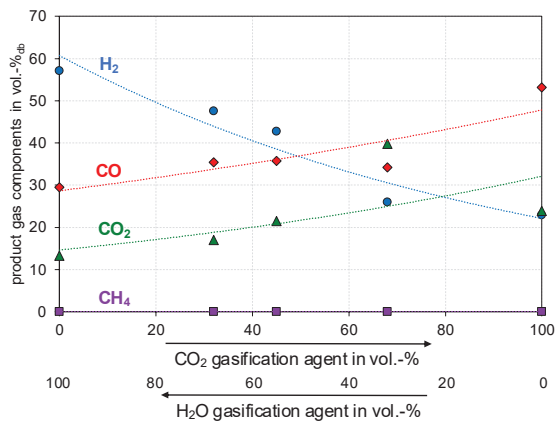


Fig. 4: Change of product gas composition over CO₂ input as gasification agent in the thermodynamic equilibrium

Fig. 5 presents the experimental results of the 5 test campaigns, where steam was substituted stepwise by CO₂.

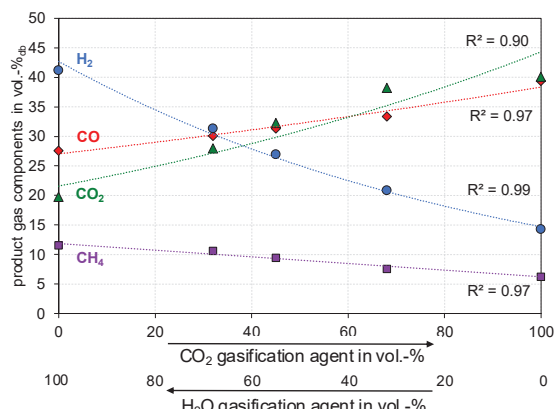


Fig. 5: Change of product gas composition over CO₂ input as gasification agent

CO₂ and CO showed an increasing trend with increasing CO₂ content as gasification agent. The opposite phenomenon was seen for H₂, which was decreasing with increasing CO₂ input. CH₄ slightly declined, but remained relatively stable. However, this declining trend could also be an effect of dilution. The best fitting trend lines with quite high coefficients of determination were calculated for H₂, CO and CO₂ with an exponential approach and for CH₄ with a linear approach. The trends of the experimental results were in accordance with the trends of the thermodynamic calculations for H₂, CH₄ and CO. However, for CO₂ there was a declining trend in the thermodynamic calculations, when 100 vol.-% CO₂ was theoretically used as gasification agent, which doesn't reflect the results of the experiments. In general, the values of CO were higher and the values of CO₂ and H₂ lower in the thermodynamic equilibrium compared to the experimental results. The content of CH₄ was almost 0 vol.-%_{db} along the increasing CO₂ gasification input. Although, there are quite high deviations between the amount of the product gas components, the thermodynamic calculations provide a good insight, what theoretically would be possible.

Fig. 6 shows the deviation from the RWGS reaction over increasing CO₂ input. Regarding the RWGS reaction, the equilibrium between 827 - 838°C lies on the side of the products in the thermodynamic equilibrium [16], which was the case for test campaign 1. With increasing CO₂ as gasification agent, the gas composition was shifted towards the educt side. When pure CO₂ was used as gasification agent, the gas composition was completely on the side of the educts, which objected to the predictions of the thermodynamic equilibrium.

One of the reasons for the huge deviations from the thermodynamic equilibrium and the high contents of CO₂ in the product gas of the test campaigns, could be a too low residence time in the gasification reactor. It is well known, that the reaction rate of the Boudouard reaction is much slower than the reaction rate of the RWGS reaction [17]. Longer residence times would improve the conversion efficiency. [18] Due to the inefficient conversion of CO₂, a certain amount of it maybe took not place on any chemical reaction, which diluted the whole product gas. Additionally, higher temperatures would have also been favorable for the progress of the chemical reactions and thus the conversion efficiency.

One can conclude from these findings, that using pure CO₂ as gasification agent is not efficient for the biomass gasification process in such temperature ranges. However, using mixtures of steam and CO₂ like in test campaigns 2 and 3, present a promising approach for recycling CO₂ within this process. Additionally, a moderate H₂/CO ratio was generated and the deviation from the chemical equilibrium was close to 0.

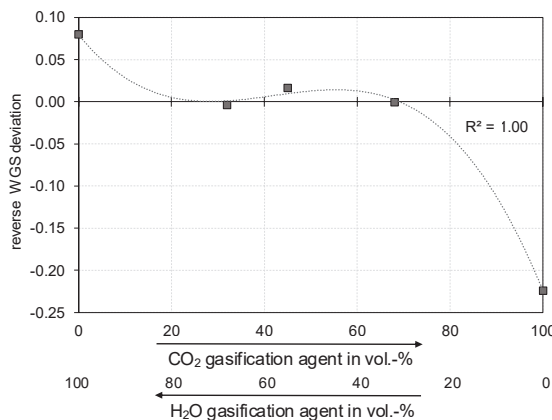


Fig. 5: Change of the deviation from the reverse WGS equilibrium over CO₂ input as gasification agent
3.1 Temperature variation

When fluidizing the gasification reactor with pure CO₂ as gasification agent, a

temperature variation from 740 to 840°C was conducted. Beforehand, thermodynamic calculations were carried out as well. The results of these calculations are displayed in **Fig. 6**. In the thermodynamic equilibrium, CO contents of 48 - 55 vol.-%_{db} were possible, while the amount of CO₂ ranged between 23 - 27 vol.-%_{db}. The H₂ content was about 23 vol.-%_{db} in average and CH₄ accounted for almost 0 vol.-%_{db}.

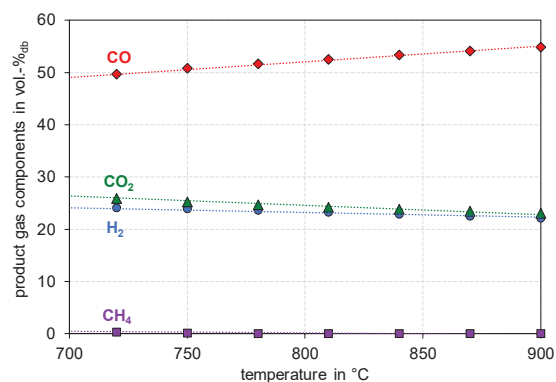


Fig. 6: Change of product gas composition over gasification temperature in the thermodynamic equilibrium

Fig. 6 shows the experimental results of the temperature variation over the gasification temperature TGR_{lower} when pure CO₂ was used as gasification agent. The best fitting trend lines of the experimental results with quite high coefficients of determination were calculated for H₂, CO and CO₂ with an exponential approach and for CH₄ with a linear approach. The trends of CO₂ and CO of the thermodynamic calculations were equal to that of the experimental results, however, the amounts showed quite high deviations. The CO content showed an increase from 23 to 37 vol.-%_{db} and the CO₂ content a decrease from 58 to 40 vol.-%_{db} in the experimental investigations. In contrast to the slightly decreasing trend of H₂ in the thermodynamic calculations along the increasing gasification temperature, the experimental results

showed an increasing course of H₂. CH₄ remained relatively stable with a slight decrease over the increase in temperature during the test campaigns, but accounted for almost 0 vol.-%_{db} in the thermodynamic calculations. In general, there are deviations in the amounts of the product gas components between the thermodynamic calculations and the experimental results, but the trends of CO and CO₂ correspond to the trends of the experimental investigations.

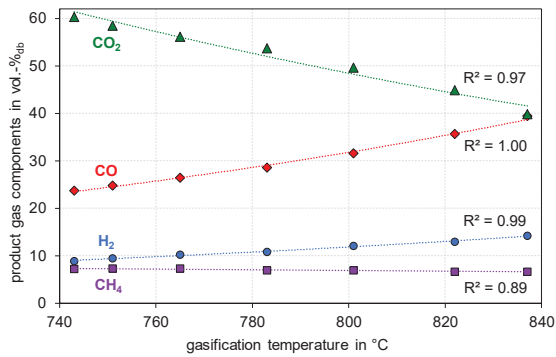


Fig. 7: Change of product gas composition over gasification temperature of test campaign 5

Based on the trends of CO and CO₂ in Fig. 7, one can conclude, that higher temperatures, over 840°C would be favorable for using pure CO₂ as gasification agent. At higher temperatures, the RWGS reaction as well as the Boudouard reaction, which both favor the production of CO, would take place to a higher extent (see [16], [18]). Fig. 8 depicts the deviation from the RWGS reaction equilibrium calculated with Eq. 6 of the different operating points of the temperature variation. In general, the state of equilibrium was on the side of the educts over the whole temperature range. This could be traced back to too short residence times in the gasification reactor, which decreased the conversion efficiency of CO₂. This excess CO₂ maybe diluted to whole product gas as explained before. Based on these assumptions, following hypotheses can be proposed: From 740°C

to around 780 - 800°C the gas composition was on the educt side. This can be seen in the increasing negative deviation of the RWGS reaction. At around 800°C, the RWGS reaction seemed to be in equilibrium, which was also stated by [19] and [20]. From 800°C, the deviation from the RWGS reaction showed a decreasing course towards the product side. This indicated, that from 800°C, the production of CO and in parallel the conversion of CO₂ was favored. Comparable results for temperatures over 800°C using steam as gasification agent can be found in literature [21].

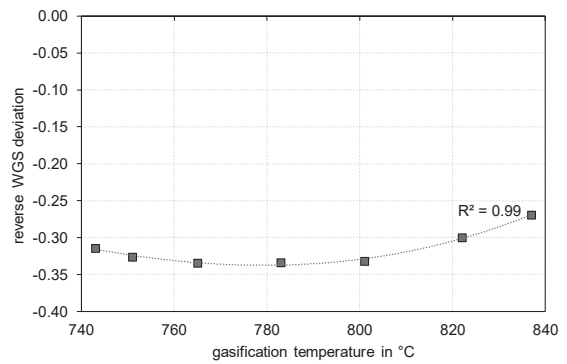


Fig. 8: Change of the deviation from the reverse WGS equilibrium over gasification temperature of test campaign 5

Tab. 5 shows the performance indicating key parameters of validated data with IPSEpro of test campaigns 1 to 5. It is visible, that the CO₂ conversion increased with increasing CO₂ input. Contrarily, the water conversion decreased. This could be explained by the RWGS reaction, where H₂O was formed (see Eq. 5 in the opposite direction) at temperatures over 800°C. The carbon to CO conversion had a maximum, when the GR was fluidized with pure steam. For this case, the lowest total amount of carbon (C) was introduced into the GR compared to test campaigns 2 to 5, where also the amount of C in the gasification agent accounted to the total C input into the GR. Overall cold gas efficiencies around 70 % were reached for

all test campaigns. The H₂/CO ratio was lowered from 1.49 for pure steam as gasification agent to 0.39 for pure CO₂ gasification. The same declining trend was seen for the lower heating value (LHV). Both trends could be explained by the increasing amount of the inert gas CO₂ in the product gas. The gravimetric tar contents of pure steam and pure CO₂ gasification were higher than the one, which was produced when a mixture of steam and CO₂ was used as gasification agent. This could be explained by the combined effect of steam and dry

reforming reactions, when a mixture of steam and CO₂ was used as gasification agent [4]. The dust contents were in the range of 0.3 to 1.0 g/m³_{stp} and are typical values for gasification with olivine as bed material. The char contents were lower, when CO₂ was present in the gasification and higher when only steam was used as gasification agent. This could be explained by a higher amount of fuel, which was introduced into the CR for test campaign 1.

Tab. 5: Performance indicating key parameters

key figure	unit	test campaign				
		1	2	3	4	5
X _{CO₂}	kg _{CO₂} /kg _{CO₂}	0	-0.25	-0.05	0.09	0.29
X _{H₂O}	kg _{H₂O} /kg _{steam}	0.28	0.18	0.06	-0.16	-0.54
X _{C→CO}	kg _{C,CO} / kg _{C,fuel&fluid}	0.38	0.34	0.33	0.32	0.34
η _{CG,o}	%	72	70	67	66	69
H ₂ /CO	-	1.49	1.04	0.86	0.63	0.39
LHV ^a	MJ/m ³ _{stp}	12.7	11.2	10.6	9.2	8.7
grav. tar ^b	g/m ³ _{stp}	6.7 ^c	n.m.	n.m.	4.1	6.2
dust ^b	g/m ³ _{stp}	0.3 ^c	n.m.	n.m.	1.0	0.6
char ^b	g/m ³ _{stp}	2.4 ^c	n.m.	n.m.	1.5	0.5

^a free of tar and char;

^b measured by the Test Laboratory for Combustion Plants a TU Wien;

^c values from another comparable test run with SW as fuel and olivine as bed material;

n.m. not measured;

4. Conclusion and Outlook

The results with CO₂ as gasification agent instead of steam showed, that the product gas was shifted towards higher CO and lower H₂ contents. The stepwise substitution of steam by CO₂ indicated, that it is not beneficial to use pure CO₂ as gasification agent for the biomass gasification process with the investigated process conditions. Mixtures of steam and CO₂ as gasification would be much more efficient regarding the achievement of an appropriate H₂/CO ratio for different syntheses like the dimethyl ether or the Fischer-Tropsch syntheses. Additionally,

the destruction of higher hydrocarbons like tar is also much more efficient when using mixtures of steam and CO₂ as gasification agent. The temperature variation indicated, that higher temperatures, over 840°C would be favorable for pure CO₂ gasification, because the RWGS reaction as well as the Boudouard reaction could take place to a higher extent at higher temperatures. Furthermore higher residence times in the gasification reactor would affect the conversion efficiency of CO₂ in a positive way. In general, the trends of the thermodynamic calculations reflect the trends of the experimental results.

Concluding from the results, the admixture of CO₂ between 0 and 50 vol.-% to the gasification agent mixture is reasonable. An advantageous effect of using CO₂ as gasification or fluidization agent is the possibility to recycle produced CO₂ within the process and therefore reducing CO₂ emissions.

An extended version of this publication would include the presentation of

hydrogen balances around the GR and a more detailed discussion of the results. Future investigations could focus on a temperature variation up to temperatures of 900°C. Additionally, an optimized concept of the current reactor design could be carried out for CO₂ gasification in the DFB reactor system.

LIST OF ABBREVIATIONS

C	carbon
CR	combustion reactor
DFB	dual fluidized bed
GR	gasification reactor
LHV	lower heating value
PGY	product gas yield
SW	softwood
vol.-%	volumetric percent
WGS	water gas shift
wt.-%	weight percent

LIST OF SUBSCRIPTS

C	carbon
CO ₂	carbon dioxide
CR	combustion reactor
daf	dry and ash-free
db	dry basis
fuel	fuel to gasification reactor
GR	gasification reactor
H ₂ O	water
PG	product gas
steam	steam input in GR

5. Acknowledgements

This work was supported by the European Union's Horizon 2020 research and innovation programme under grant agreement number 764675 (Heat-to-Fuel).

6. References

- [1] Weber G. Production of mixed alcohols using MoS₂ catalyst from biomass derived synthesis gas. Doctoral thesis, TU Wien, 2017.
- [2] Gruber H, Groß P, Rauch R, Weber G, Loipersböck J, Niel J, et al. Fischer-tropsch Synthesis – Effects of Feedstock Load Changes Regarding Product Quality and Catalyst Attrition. Proc. 25th Eur. Biomass Conf. Exhib. Stock. Sweden, 2017. doi:10.5071/25thEUBCE2017-3AO.9.4.
- [3] Hofbauer H. Biomass Gasification for Electricity and Fuels, Large Scale. Encycl. Sustain. Sci. Technol., Springer; 2017, p. 459–78. doi:10.1007/978-1-4614-5820-3.
- [4] Mauerhofer AM, Fuchs J, Müller S, Benedikt F, Schmid JC, Hofbauer H. CO₂ gasification in a dual fluidized bed reactor system: Impact on the product gas composition. Fuel 2019.
- [5] Fuchs J, Schmid JC, Müller S, Hofbauer H. Dual fluidized bed gasification of biomass with

stp	standard temperature and pressure
th	thermal

LIST OF SYMBOLS

\dot{m}	mass flow	kg/s
\dot{V}_{PG}	dry volumetric prod. gas flow	m ³ /s
X_{CO_2}	CO ₂ conversion	%
X_{H_2O}	steam-related water conversion	kg _{H2O} /kg _{H2O}
$X_{C \rightarrow CO}$	Carbon to CO conversion	kg _{C,co} /kg _{C,fuel&fluid}
$\eta_{CG,o}$	overall cold gas efficiency	%
\dot{Q}_{loss}	heat loss	kW
LHV	lower heating value	MJ/m ³ _{stp,db}

- selective carbon dioxide removal and limestone as bed material: A review. *Renew Sustain Energy Rev* 2019;107:212–31. doi:10.1016/j.rser.2019.03.013.
- [6] Schmid JC. Development of a novel dual fluidized bed gasification system for increased fuel flexibility. TU Wien, doctoral thesis, 2014.
- [7] Schmid JC, Pröll T, Kitzler H, Pfeifer C, Hofbauer H. Cold flow model investigations of the countercurrent flow of a dual circulating fluidized bed gasifier. *Biomass Convers Biorefinery* 2012;2:229–44. doi:10.1007/s13399-012-0035-5.
- [8] Mauerhofer AM, Schmid JC, Benedikt F, Fuchs J, Müller S, Hofbauer H. Dual fluidized bed steam gasification: Change of product gas quality along the reactor height. *Energy* 2019;173:1256–72. doi:10.1016/j.energy.2019.02.025.
- [9] Benedikt F, Kuba M, Christian J, Müller S, Hofbauer H. Assessment of correlations between tar and product gas composition in dual fluidized bed steam gasification for online tar prediction. *Appl Energy* 2020;238:1138–49. doi:10.1016/j.apenergy.2019.01.181.
- [10] Müller S, Fuchs J, Schmid JC, Benedikt F, Hofbauer H. Experimental Development of Sorption Enhanced Reforming by the Use of an Advanced Gasification Test Plant. *Int J Hydrogen Energy* 2017;42:29697–707. doi:10.1016/j.ijhydene.2017.10.119.
- [11] Pröll T, Hofbauer H. Development and Application of a Simulation Tool for Biomass Gasification Based Processes. *Int J Chem React Eng* 2008;6:Article A89. doi:10.2202/1542-6580.1769.
- [12] Mauerhofer AM, Müller S, Benedikt F, Fuchs J, Bartik A, Hofbauer H. CO₂ GASIFICATION OF BIOGENIC FUELS IN A DUAL FLUIDIZED BED REACTOR SYSTEM. *Biomass Convers Biorefinery* 2019. doi:<https://doi.org/10.1007/s13399-019-00493-3>.
- [13] Outokumpu HSC Chemistry Thermochemical Database, ver 6.1 A Roine - Finland: Outokumpu Research Oy, 2018.
- [14] Kuba M, Kirnbauer F, Hofbauer H. Influence of coated olivine on the conversion of intermediate products from decomposition of biomass tars during gasification. *Biomass Convers Biorefinery* 2017;7:11–21. doi:10.1007/s13399-016-0204-z.
- [15] Jarunghammachote S, Dutta A. Equilibrium modeling of gasification: Gibbs free energy minimization approach and its application to spouted bed and spout-fluid bed gasifiers. *Energy Convers Manag* 2008;49:1345–56. doi:10.1016/j.enconman.2008.01.006.
- [16] Poboß N. Experimentelle Untersuchung der sorptionsunterstützten Reformierung. University Stuttgart, doctoral thesis, 2016.
- [17] Ahmed II, Gupta AK. Kinetics of woodchips char gasification with steam and carbon dioxide. *Appl Energy* 2011;88:1613–9. doi:10.1016/j.apenergy.2010.11.007.
- [18] Lahijani P, Alimuddin Z, Mohammadi M, Rahman A. Conversion of the greenhouse gas CO₂ to the fuel gas CO via the Boudouard reaction : A review. *Renew Sustain Energy Rev* 2015;41:615–32. doi:10.1016/j.rser.2014.08.034.
- [19] Aghaalikhani A, Schmid JC, Borello D, Fuchs J, Benedikt F, Hofbauer H, et al. Detailed modelling of biomass steam gasification in a dual fluidized bed gasifier with temperature variation. *Renew Energy* 2019;143:703–18. doi:10.1016/j.renene.2019.05.022.
- [20] Callaghan CA. Kinetics and Catalysis of the Water-Gas-Shift Reaction: A Microkinetic and Graph Theoretic Approach. Worcester Polytechnic Institute, doctoral thesis, 2006.
- [21] Schmid JC, Benedikt F, Fuchs J, Mauerhofer AM, Müller S, Hofbauer H. Syngas for biorefineries from thermochemical gasification of lignocellulosic fuels and residues - 5 years' experience with an advanced dual fluidized bed gasifier design. *Biomass Convers Biorefinery* 2019. doi:<https://doi.org/10.1007/s13399-019-00486-2> REVIEW ARTICLE Syngas.

Aviation biofuels: an economic and environmental assessment with an outlook on cost reduction potentials

U. Neuling^{1*}, M. Kaltschmitt¹

1. Hamburg University of Technology, Institute of Environmental Technology and Energy Economics,
Eissendorfer Strasse 40, 21073 Hamburg, Germany
*corresponding author, ulf.neuling@tuhh.de

Abstract

The global awareness to reduce greenhouse gas (GHG) emissions from aviation and thereby make the overall aviation sector more environmentally friendly has increased in recent years. In this context, one main driver is seen in the development of advanced renewable jet fuels for aviation, which have already been used for some regular flights by various air carrier. Therefore, this paper compares four different production processes for biokerosene located in northern Germany, investigating two different types of biomass feedstock for each process. These conversion processes are then assessed in terms of technical, economic and environmental criteria based on data retrieved from an extensive process simulation. Main outcome of this analysis are mass and energy balances, kerosene production costs and GHG emissions for the investigated conversion routes, including a rough analysis of future cost reduction potentials.

The results of the investigated criteria are scattering significantly; i.e. no “silver bullet” can be seen based on these findings. Nevertheless, the significant influence of the provision of the biomass feedstock becomes obvious. Generally spoken the more environmentally sound and economic viable the feedstock provision can be realized, the more promising is the resulting biokerosene related to the economic and environmental criteria assessed here. This result is more or less independent from the respective conversion route.

1. Introduction:

Today the aviation industry is emitting about 820 million tCO₂/a representing a total share of 2.5 % of the global CO₂ emissions [1]. These emissions are most likely to increase in the years to come, since the ascending living standards in emerging countries like China, India and Brazil (and thus the accelerating travel activities) as well as the strongly rising world trade flows will induce even more and longer flight operations per year. With regard to this development, the international aviation industry has developed a challenging self-commitment related to the further development of global CO₂ emissions from civil aviation. This includes a carbon neutral growth starting from 2020 leading to CO₂ emission reductions by

50 % in 2050 related to the year 2005 [2]. These ambitious goals have to be realized via more efficient aircrafts, optimized flight operations (e.g. single European sky) and renewable aviation fuels with a significantly reduced carbon footprint. According to these goals the largest CO₂ emission reduction is expected to be realized based on the market introduction of advanced bio- and/or power fuels for aviation.

Today civil aviation depends basically fully on Jet A-1 (kerosene) produced from crude oil. While for land transportation various alternative options are possible and partly already market mature from a technical point of view (e.g. biofuels, e-mobility, hydrogen and fuel cells, switch to rail roads and/or water ways) this is not

the case for aviation (in a large scale) yet. Here research has just recently started to develop alternatives. These activities focus mainly on the development of the provision of alternative aviation fuels with low GHG emissions fulfilling the Jet A-1 specifications (so-called “drop-in” fuels). So far, most of these activities are strongly dedicated to fuels based on biogenic feedstock; but some early activities are carried out to use CO₂ (e.g. extracted from air) and electricity from renewable sources of energy for the provision of a synthetic kerosene (power to liquid (PtL) fuels).

The reason for this strong focus is that civil airplanes in commercial use today are usually operated with Jet A-1 kerosene and that their average technical lifetime is approximately 25 years and longer. Additionally, fuels used within airplanes should have a high energy density to minimize the necessary volume needed to operate a long-haulflight and a good combustion quality to allow for a highly efficient use. Beside this they should be characterized by a widespread or even global availability, fulfill numerous safety requirements, and have to be transported, stored and pumped easily. Kerosene resp. Jet A-1 fulfills all these requirements. Thus it is most likely that this fuel will stay in place also in the years to come especially due to the fact that the fuel characteristics of Jet A-1 are well adapted to the demands of an airplane turbine as well as the harsh conditions during a long distance flight roughly 10,000 m above ground.

So far, numerous options to produce kerosene from organic matter (i.e. biomass) have been and still are under investigation globally (see also [3]). Among these various options, no silver bullet has been identified for the time being. To get a better understanding of the various conversion processes, four conversion routes have been analyzed in more detail, regarding technical, economic and environmental criteria. Therefore a detailed process modelling

simulation of these various processes is realized. Based on these results an overall economic assessment following the annuity method as well as a life cycle assessment (LCA) is conducted. Additionally cost reduction potentials are analyzed by extrapolating the process efficiency as well as the equipment cost reduction due to a large scale application to the medium (2030) and long-term future (2045). The results, i.e. mainly the kerosene production costs and the GHG emissions within the overall life cycle, are then compared to each other and to a fossil reference to draw some conclusions.

2. Concept and methodology:

The overall conceptual process designs for the four investigated process routes are given in Fig. 1 to 4 (see also [4] for more details on the process design). In the following section the main input parameters, as well as the applied methodology will be given.

The four different processes in combination with the two different feedstock given below, whereby the acronym for each combination will also be used in the following sections (see also Fig. 1 to 4).

AtJ-WS: Alcohol-to-Jet using wheat straw

AtJ-WG: Alcohol-to-Jet using wheat grains

Bio-GtL-SM: Biogas-to-Liquids using biogas produced from the German product mix

Bio-GtL-Ma: Biogas-to-Liquids using biogas produced from manure

BtL-WS: Biomass-to-Liquids using wheat straw

BtL-Wi: Biomass-to-Liquids using willow wood chips from short rotation coppice

HEFA-JO: Hydrogenated Esters and Fatty Acids using jatropha oil

HEFA-PO: Hydrogenated Esters and Fatty Acids using palm oil

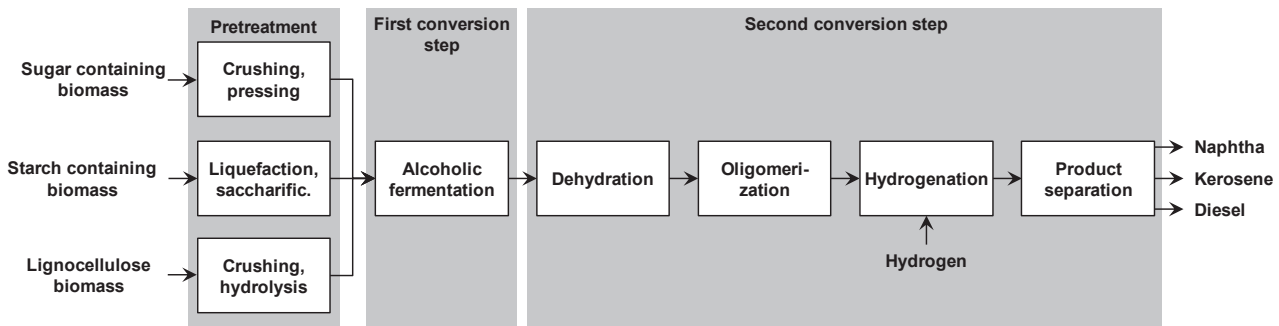


Fig.1 Process conversion chain for an alcohol-to-jet (AtJ) process

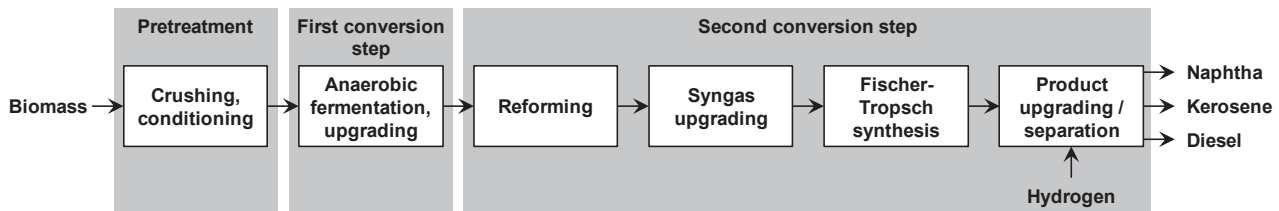


Fig.2 Process conversion chain for a biogas-to-liquids (Bio-GtL) process

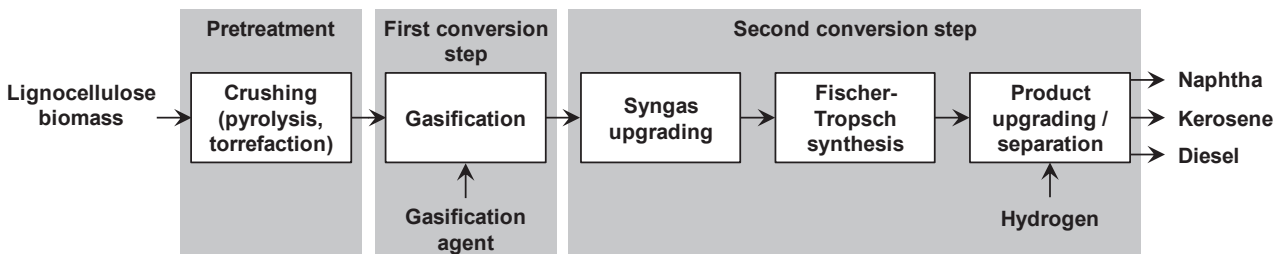


Fig.3 Process conversion chain for a biomass-to-liquids (BtL) process

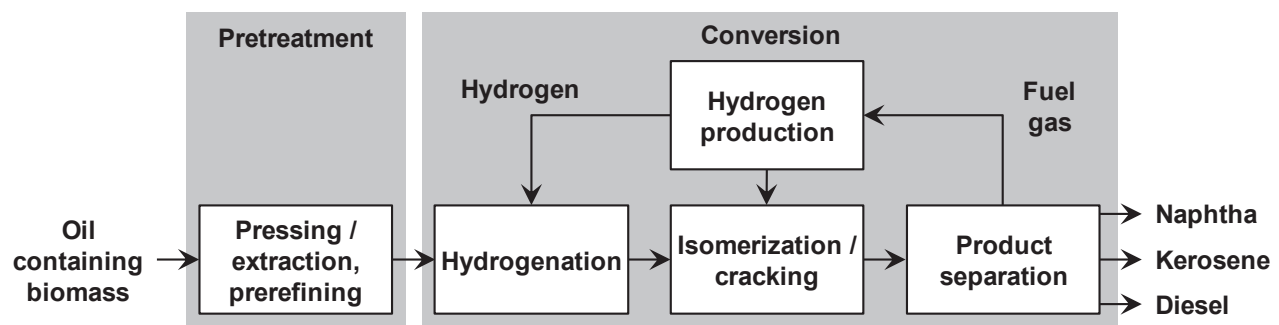


Fig.4 Process conversion chain for a hydrogenated esters and fatty acids (HEFA) process

All process concepts are designed with an annual production capacity of 800 000 t/a of liquid products and include a decentralized biomass pretreatment to increase the energy density of the feedstock and thereby decrease the transportation intensity. This includes the production of isobutanol via a fermentation process for AtJ, biomethane production via anaerobic di-

gestions for Bio-GtL, pyrolysis respectively torrefaction for BtL and vegetable oil pre-refining for the HEFA concepts (see [4] for a detailed concept description). The conversion plants as well as all pretreatment steps are located and operated in northern Germany, next to a port. The same is true for the biomass cultivation; the only exception are jatropha and palm

oil, which are imported from Mozambique resp. Malaysia via ship

For the techno-economic analysis, mass and energy balances of all processes have to be provided. This is done by modelling and simulating all processes in Aspen Plus V8.6 [5]. Heat integration was carried out via pinch analysis using the Aspen Energy Analyzer V8.6 [6]. Details about the included methodology, simulation structure and databases of Aspen can be found in the respective manuals. Based on these results the overall process efficiency for each process is calculated using Eq. 1.

$$\eta_{tot} = \frac{\sum \dot{W}_{Products} + P_{el}}{\sum \dot{W}_{Educts} + P_{el,own}} \quad \text{Eq. 1}$$

with η_{tot}

$$\sum \dot{W}_{Products}$$

Overall process efficiency

$$P_{el}$$

Sum of product energy flows

$$\sum \dot{W}_{Products}$$

Generated electrical power

$$P_{el,own}$$

Sum of educt energy flows

Consumed electrical power

All investigated conversion plants have been modelled and assessed using the n^{th} plant theory. According to this theory, plant economics are to be interpreted as the costs for a commercial scaled technology. That implies that several commercial plants have been built and are operational; i.e. the overall conversion pathway is market mature. This allows a fair comparison of technologies from different development stages. The economic analysis is based on the annuity method, following [7] and using the general assumptions giving in Table 1. All costs are calculated for the year 2017, using the chemical engineering plant cost index (CEPCI) for annualization [8].

Parameter	Unit	Value
Base year	-	2017
Plant availability	h/a	7 500
Plant lifetime	a	20
Rate of interest	%	4

Tab.1: Overall financial frame assumptions

Biomass prices are based on published data including all aspects of the feedstock provision. The assumed prices are given in Table 2. Prices for all other auxiliary material or energy flows (e.g. process water, chemical and bio-catalysts as well as electricity) included in the calculations are given in [4].

Parameter	Price	Source
Biomethane from grid	0.070 €/kWh resp. 913 €/t	[9]
Biomethane from manure	0.055 €/kWh resp. 717 €/t	[9]
Jatropha oil	1 250.0 €/t	[10]
Palm oil	639.9 €/t	[11]
Wheat grain	160.0 €/t	[12]
Willow wood chips	50.0 €/t	[13]
Straw	85.0 €/t	[14]

Tab.2: Assumed feedstock prices

To give a rough overview of the potential future cost reduction potential of the investigated production routes results of the techno-economic assessment are extrapolated to the near future (2030 and 2045). Therefore the result of the technical assessment, i.e. the calculated process efficiency is extrapolated following a saturation model, based on research and industry developments. In a second step the potential cost reduction due to learning and scaling effects is calculated using learning curves based on comparable process developments, leading to reduced capital costs. The described approach is visualized Figure 1.

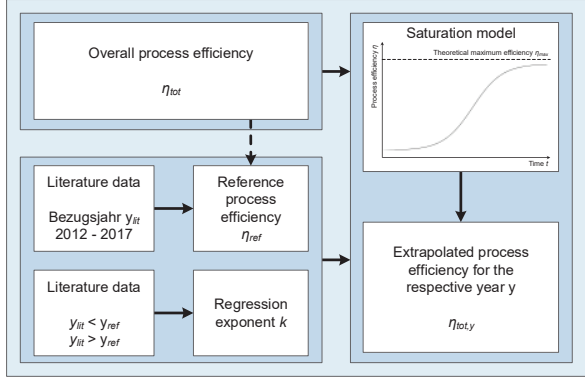


Fig.1: Methodological approach for the technical process extrapolation

Based on this approach, the results of the process assessment for the year 2017 can be extrapolated to 2030 and 2045 using Eq. 2. The respective regression exponent is calculated according to Eq. 3 and Eq. 4 according to the base year of the comparative literature case

$$\eta_{tot,y} = \eta_{max} - (\eta_{max} - \eta_{ref}) \cdot e^{-k \cdot (y - y_{ref})} \quad \text{Eq. 2}$$

with $\eta_{tot,y}$ Extrapolated process efficiency for the respective year
 η_{max} Theoretical maximum efficiency
 η_{ref} Process efficiency for the reference year
 k Regression exponent
 y Extrapolated year
 y_{ref} Reference year

$$k = \frac{-1}{y_{ref} - y_{lit}} \cdot \ln \left(\frac{\eta_{max} - \eta_{ref,m}}{\eta_{max} - \eta_{lit}} \right), \quad \text{Eq. 3}$$

$$y_{lit} < y_{ref} \\ k = \frac{-1}{y_{lit} - y_{ref}} \cdot \ln \left(\frac{\eta_{max} - \eta_{lit}}{\eta_{max} - \eta_{ref,m}} \right), \quad \text{Eq. 4}$$

$$y_{lit} > y_{ref}$$

with y_{ref} Reference year
 y_{lit} Base year of the literature source

η_{max}	Theoretical maximum efficiency
$\eta_{ref,m}$	Mean reference efficiency
η_{lit}	Efficiency of the literature source

The detailed applied methodology is described in [4].

To determine the GHG emissions of the different processes a lifecycle analysis (LCA) of the overall conversion process is conducted. Following the common procedure within such an LCA defined by the International Organization for Standardization different alternatives of a product or service can be compared related to their environmental impacts [15, 16]. This includes the conversion or production process as well as the respective pre-chains (e.g. biomass cultivation and transportation); additionally, recycling processes are taken into consideration if they are realized. For such a total product life cycle the terminology “from cradle to grave” is widely used.

Therefore, the system boundary includes the cultivation of the feedstock, its transportation, all pretreatment and conversions steps as well as the distribution and use of the final product (see Figure 2). The respective biokerosene production plant is located in Germany, the functional unit all upstream emissions are related to is 1 MJ kerosene. The overall emissions assessed here are allocated; i.e. they are subdivided on the main product kerosene and all other byproducts on an energy basis.

For calculation the environmental impacts of the pre-chains prior to the biokerosene production data from the ecoinvent database V3.5 is used [17]. Additional data from [18] was used for enzyme production, from [19] for alpha and gluco-amylase production and from [20] for jatropha cultivation and oil prerefining. The catalyst production has not been included in the inventory analysis, since information

about the detailed composition of the catalyst material is not available due to IP reasons.

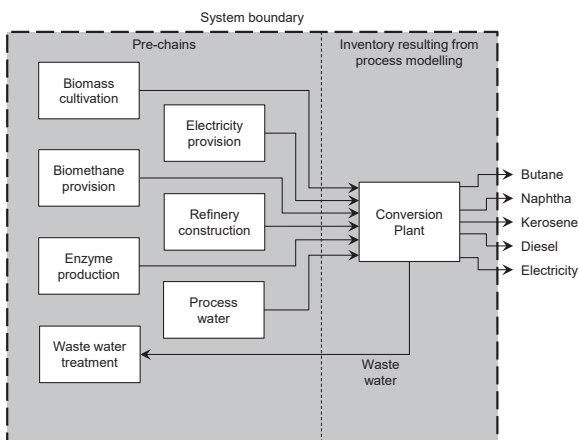


Fig.2: System boundary for the life cycle assessment

During the impact assessment, the results from the inventory analysis are allocated to different impact categories. Here the impact category “global warming potential” with a time scope of 100 years (GWP100) is applied, using the ReCiPe 2016 Mid-point (H) method [21]. The results for the different biofuels are compared to the fossil reference defined by the European Renewable Energy Directive II (EU RED II) of 94.0 gCO_{2eq}/MJ [22].

3. Results and discussion

The results based on the process modeling of the four investigated processes are discussed below. This includes the general mass and energy balances for each process, the overall costs related to the defined calculation method leading to the biokerosene production costs as well as the CO_{2eq} emissions resulting from the life cycle analysis performed according to the frame conditions and methodology defined above. Additionally the cost reduction potential for the years 2030 and 2045 due to the process extrapolation is discussed briefly.

The mass flow of the main input and output parameters as well as the related energy flows and the resulting process efficiencies calculated via the lower heating

value are shown in Table 3. The overall mass flow of the kerosene fraction shows the lowest values for the Fischer-Tropsch processes (i.e. Bio-GtL and BtL) with approx. 58 to 60 t/h followed by the AtJ route resulting in a kerosene production of approx. 66 t/h and the HEFA option with the highest kerosene mass fraction of approx. 72 t/h.

In terms of energy efficiency the results show a much higher deviation. Again the HEFA processes show the highest overall efficiencies of 90 to 91 % as well as a kerosene efficiency of 58 to 60 %.

All other processes are characterized by significantly lower values, starting with the Bio-GtL route (with 57 % resp. 26 %) followed by the AtJ-WG process showing an overall efficiency of 53 % and a kerosene specific efficiency of 32 %. The three process alternatives using lignocellulosic feedstock (i.e. AtJ-WS and both BtL concepts) are characterized by the lowest energy efficiencies; the overall efficiency ranges from 35 to 38 % and the kerosene efficiency varies between 19 and 24 %. The comparatively low process efficiencies regarding the BtL concepts is mainly related to the high energy demand of the air separation unit, needed to provide pure oxygen as gasification agent, significantly reducing the overall efficiency.

All in all it can be said, that the more the natural synthesis performance (by the different plants) can be used, the higher is the overall processes efficiency. E.g. the chain length of vegetable oils and the one of kerosene are relatively close to each other. As a result, only minor modifications in the biopolymers are necessary and a large part of the vegetable oil molecules synthesized by the plants is found almost unchanged in the fuel. This leads to the high overall efficiencies of HEFA the concepts. If, on the other hand, the biopolymers of the biomass are initially decomposed thermally into very small molecules (hydrogen and car-

bon monoxide) in order to then be reassembled with the appropriate technical effort to the desired fuel molecules, this leads to lower overall efficiencies, as e.g. in the BtL process.

Based on the process simulation results stated above the various process routes can be analyzed economically. The results of

this economic assessment are presented in Figure 3. All details regarding the calculation of the equipment costs can be found in [4]. Following these data large variations can be seen, with the largest bandwidth in terms of total investment costs as well as operation-linked costs.

	AtJ		Bio-GtL	BtL		HEFA	
	AtJ-WS	AtJ-WG		BtL-WS	BtL-Wi	HEFA-JO	HEFA-PO
Mass flow [kg/h]							
Feedstock	-675 000	-510 000	-204 900	-875 000	-650 000	-127 500	-129 000
Methane ^a	-5 104	-5 179	0	0	0	-11 398	-10 340
Butane/Naphtha	9 317	9 405	25 478	25 269	24 916	27 322	27 323
Kerosene	66 208	66 628	59 359	58 806	57 663	69 666	71 863
Diesel	31 725	32 186	22 190	23 569	23 122	9 676	7 481
Energy flow [MW]							
Feedstock	-3 300	-2 414	-2 676	-3 636	-3 233	-1 322	-1 333
Methane ^a	-67	-68	0	0	0	-149	-135
Electricity ^b	-17	-13	-83	-132	-152	-7	-8
Electricity ^c	0	0	260	0	0	19	25
Butane/Naphtha	112	113	309	306	302	338	338
Kerosene	797	809	729	723	709	855	882
Diesel	385	391	271	288	282	118	91
Energy efficiency [%]							
Overall process	38	53	57	35	38	90	91
Kerosene fraction	24	32	26	19	21	58	60

^a: Methane is used for hydrogen production via steam methane reforming

^b: Gross electricity consumption of the conversion process

^c: Electricity production due to implementation of excess process heat in a steam power process

Tab.3: Mass and energy flows as well as resulting energy efficiencies for the investigated conversion routes (Negative values are related to input parameters, positive values are output parameters)

This is especially true for the biokerosene production costs for the different processes as well as for the same process with a different feedstock.

- The highest production costs are calculated for both Bio-GtL processes, resulting in 2 854 €/t for the Bio-GtL-GSM concept and 2 178 €/t for Bio-GtL-Ma under the given constraints and assumptions.
- The lowest production costs could be achieved with the HEFA-PO, the BtL-

Wi and the AtJ-WS process, resulting in 978 €/t, 992 €/t and 1 016 €/t, respectively.

- The AtJ-WG route results in production costs of 1 249 €/t, more or less in the middle of the overall cost bandwidth calculated here.
- With costs of 1 687 €/t and 2 096 €/t for BtL-WS and HEFA-JO these options are located in the upper half of the cost bandwidth opened up by all investigated options

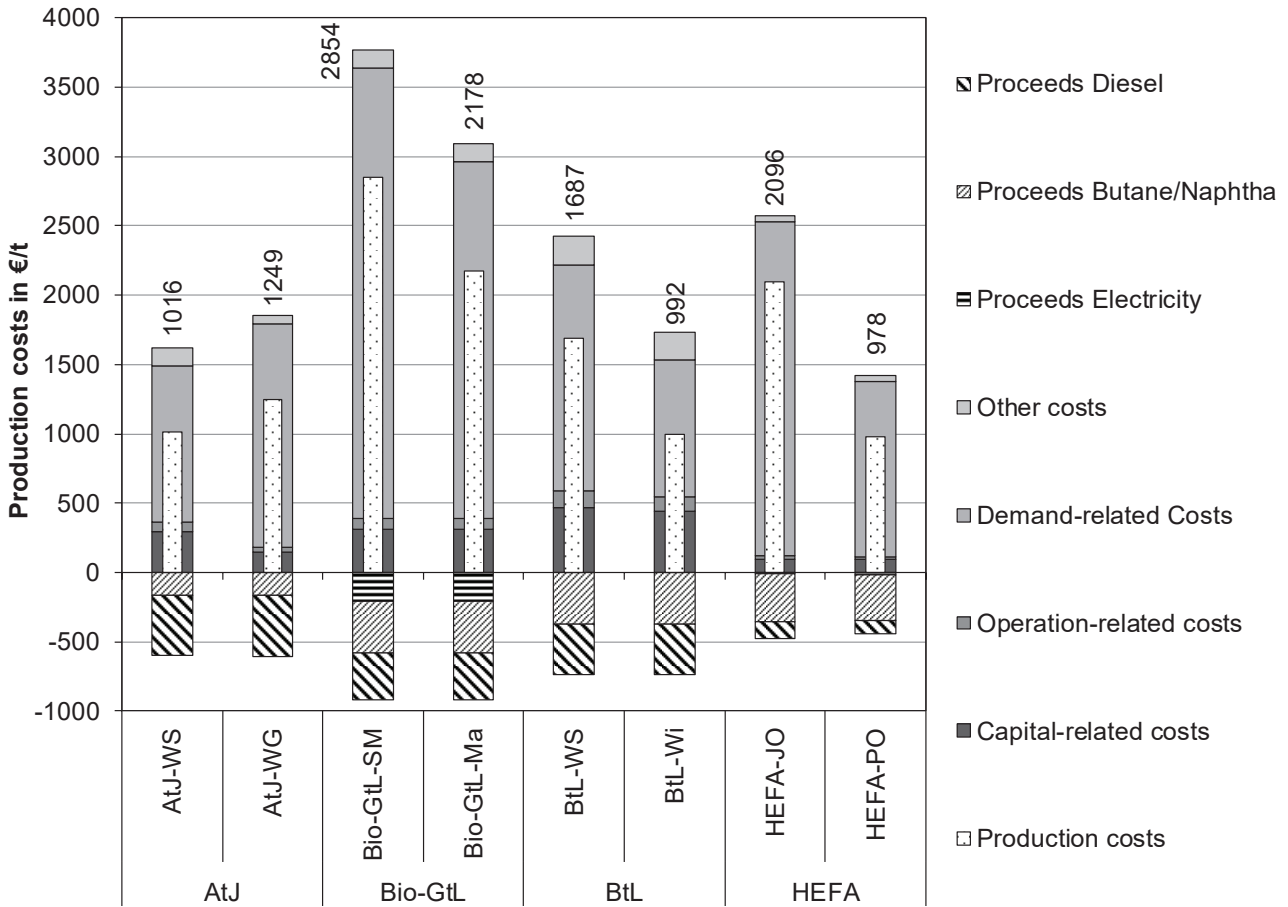


Fig.3: Production costs for the four different investigated biokerosene production routes with two different biomass resources for each route

Under the given assumptions and conversion routes none of the investigated pathways could produce biokerosene cost competitive to fossil kerosene with a price of roughly 560 €/t for the first half of 2019 [23]. Therefore, on the one hand side the production costs have to be reduced; the most important option to do so is to realize lower feedstock costs due to an optimized agricultural production. On the other hand side, the price for fossil fuel might increase as it has been the case in the beginning of this century. Additionally and/or alternatively, compensation payments or penalties for CO₂ emissions from fossil fuel energy might be used to compensate at least a part of this considerable price gap.

In comparison to the cost analysis, the overall greenhouse gas (GHG) emissions for all investigated processes are given in Figure 4 and are discussed below.

Following these results the GHG emissions of the different production routes show a very broad bandwidth. For most processes the emissions from biomass cultivation dominate the overall GHG emissions; this is not true for the processes based on lignocellulosic biomass. Due to the optimized, decentralized biomass pre-treatment emissions resulting from biomass or intermediate product transportation are rather low compared to previous calculations [24].

The lowest GHG emissions can be realized with the AtJ-WS concept, resulting in total emissions of roughly 17 gCO_{2eq}/MJ_{Kerosene} or an emission reduction potential of roughly 80 % compared to the fossil reference. The BtL and HEFA concepts are related to GHG emissions between 28 and 38 gCO_{2eq}/MJ_{Kerosene} respectively emission reductions between 60 and 70 %. The

highest emissions are related to both Bio-GtL processes as well as the AtJ concept using wheat grains, only resulting in emission reductions between 10 and 32 %.

Huge deviations related to the emissions of the actual biofuel production, i. e. the conversion of the biomass into final fuels can be seen. Although the Bio-GtL processes show the highest overall emissions, the emissions related conversion process are marginal. Both AtJ and HEFA concepts

show higher emissions for the conversion step, which are mainly related to the use of methane for hydrogen production via steam reforming. Again, the high electricity demand for the air separation unit included in the BtL concepts results in comparatively high emissions for the conversion step. These emissions may be reduced by using renewable electricity instead of grid electricity, as assumed for this analysis.

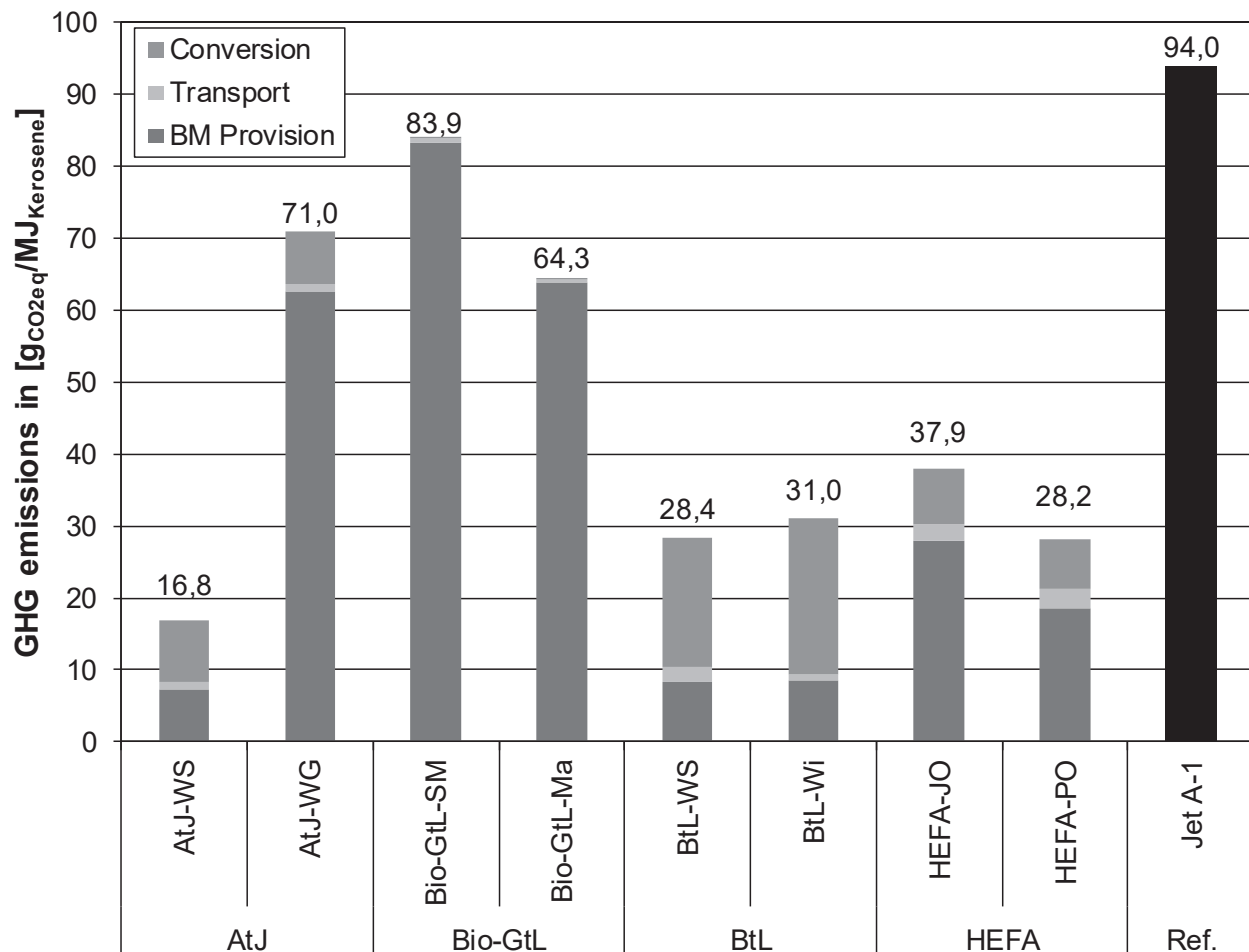


Fig.4: GHG emissions of the investigated biokerosene production routes in comparison to a fossil Jet A-1 reference (BM = biomass; fossil Jet A-1 reference according to the EU RED II [22])

Interpreting the GHG emissions one always has to keep in mind, that they result from a rather rough estimation of the overall life cycle emissions and might therefore be connected with high uncertainties. This is especially true for the comparatively good results of the HEFA processes, since the production of (especially tropical) vegetable oils like jatropha or palm oil might

come in hand with land-use change (LUC) effects leading to much higher emissions than calculated here. As such effects are very sensitive to the related assumptions and may strongly vary for different plantation locations, they have not been investigated here in detail.

To give a rough estimation of the future development of the investigated processes,

the potential cost reduction is shown in Figure 5, mainly resulting from two different effects, applied to estimate future developments. On the one hand side, a potential efficiency increase due to a large scale implementation of the production technology calculated following a saturation model including assumed increasing production capacities for the next years has

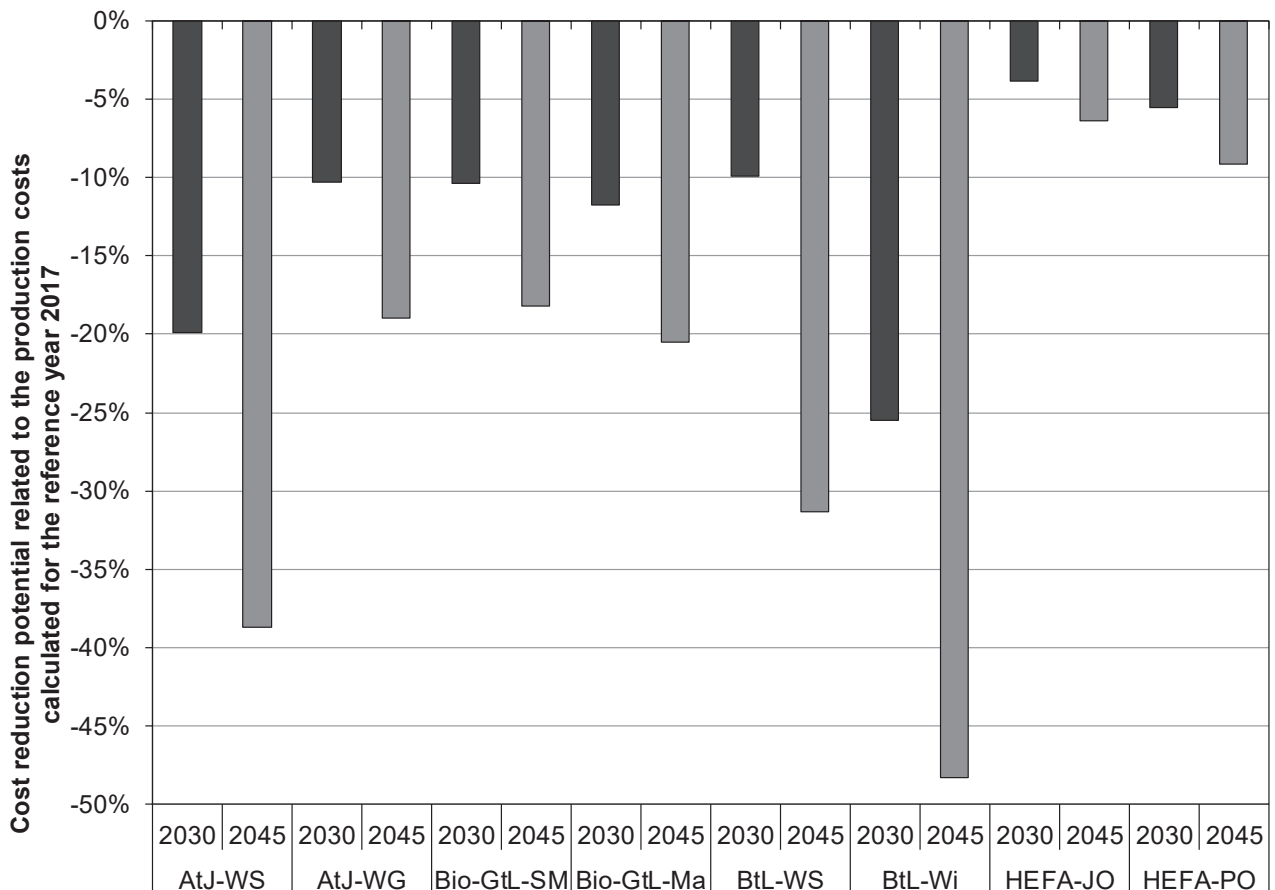


Fig.5: Relative cost reduction potential of the kerosene production costs related to the reference year 2017

Already in the medium term (2030), significant production cost reductions can be observed. The lowest cost reduction of approx. 4 % is calculated for the HEFA concept with jatropha oil (HEFA-JO), the highest reduction of approx. 25 % can be observed for the BtL process based on willow wood as raw material (BtL-Wi). The influence of the reduced investment becomes particularly clear in the case of the BtL processes, since they contribute to a higher share of the production costs than for the other concepts (see Figure 2).

been implied. Additionally equipment costs and thereby the overall investments might decrease due to learning effects coming along with the capacity build up, estimated by applying experience curves and the corresponding progress ratios.

For the long-term concepts (2045) an even greater reduction in production costs is to be expected. The lowest cost reductions of approx. 6 and 9 % respectively are expected for the HEFA concepts. This is due to the already very efficient conversion of raw materials and the comparatively low mass-based demand for raw materials. For the Bio-GtL processes, the cost reduction is calculated to be between 18 to 21 %. Depending on the feedstock and the combination with the corresponding pretreatment processes, the AtJ and BtL processes can

result into significantly different reduction potentials.

For the AtJ process based on wheat grain (AtJ-WG) the predicted reduction is roughly 19 %, for the AtJ-WS concept, the kerosene production costs can be reduced by almost 40 %. Although the BtL process based on wheat straw (BtL-WS) is expected to show the lowest absolute costs by 2045, the relative cost reduction of 31 % is significantly lower than the expected reduction of 48 % for the BtL process using willow wood (BtL-Wi) as.

4. Conclusion and Outlook

The overall goal of this paper is to present an extensive assessment of different production pathways for biokerosene in terms of technical, economic and environmental aspects. Therefore, four different processes with two kinds of biogenic feedstock each have been modelled using a commercially available process simulation software. The results have been assessed based on the overall process efficiency (technical parameter), the biokerosene provision costs (economic parameter) and the GHG emissions occurring within the overall life cycle (environmental parameter). As an outlook, the production cost reduction potential has been investigated, based on a rough process extrapolation. The presented overall results show a broad variety for the different conversion routes and assessed criteria.

- In terms of energy efficiency the HEFA processes seem to have the best performance characteristics (91 % overall and 60 % kerosene efficiency). In addition, the HEFA process based on palm oil results in comparatively low production costs (978 €/t) and relatively low GHG emissions of 28 gCO_{2eq}/MJ_{Kerosene}. Nevertheless, it is most unlikely that large-scale palm oil production will be realized in an environmental friendly and sustainable way in the future since this would most

likely lead to a clearing of virgin land to meet the increasing plant oil demand, which would be connected with LUC effects resulting in way higher GHG emissions.

- All processes based on lignocellulosic biomass (namely AtJ-WS and both BtL concepts) show good results from a GHG-reduction point of view (17 to 31 gCO_{2eq}/MJ_{Kerosene}). At least two of these process routes, namely BtL-Wi and AtJ-WS additionally result in comparatively low production costs (992 resp. 1 016 €/t). But they show rather poor energy efficiencies due to high losses during the overall conversion process induced by the manifold of chemical conversion reactions each characterized by obligatory losses.
- Considering the potential future cost reduction, except for the HEFA concepts all processes show a high reduction potential above 18 %. Again, the conversion routes using lignocellulosic biomass show the highest potential to be cost competitive in the near future, resulting into cost reductions roughly varying between 30 and 50 %.

Following these results, an ideal production process for biokerosene cannot be identified solely based on the assessed criteria. According to the current state, the combination of the AtJ process with straw and the BtL process with willow wood and thus two processes using lignocellulosic biomass as feedstock seem to have the greatest economic potential. Thus, in the future, kerosene might be produced at almost the same cost using two different processes with different and thus non-competitive raw materials under the given assumptions, which can have a positive effect on the market stability. However, this is always strongly linked to the actual local raw material availability and further (partly political) framework conditions. For all processes, the selected raw materials determine the results of the assessed

criteria. This applies to the technical efficiency of the different conversion processes, to the great influence of raw material costs on the kerosene production costs as well as on the GHG emissions related to the fuel production. This is due to the different characteristics, growing conditions, and the logistical challenges for the provision of biomass. Therefore, sustainable and efficient biomass provision is essential for the cost-effective production of biofuels.

5. References

1. International Energy Agency (IEA): World Energy Outlook 2016. World energy outlook. OECD/IEA, Paris (2016)
2. The International Air Transport Association (IATA): IATA Technology Roadmap 2013. 4th Edition. The International Air Transport Association (IATA), Montreal, Genf (2013)
3. Kaltschmitt, M., Neuling, U. (eds.): Biokerosene. Status and Prospects. Springer Berlin Heidelberg, Berlin, Heidelberg (2018)
4. Neuling, U.: Biokerosinherstellung. Verfahrensidentifikation, Simulation und Bewertung. Schriftenreihe Technische Forschungsergebnisse, vol. 34. Kovac, Dr. Verlag, Hamburg (2019)
5. Aspen Technology: Aspen Plus V8.6. part of Aspen Process Modelling V8.6. Aspen Technology Inc., Cambridge, MA, USA (2016)
6. Aspen Technology: Aspen Energy Analyzer V8.6. part of Aspen Process Modelling V8.6. Aspen Technology Inc., Cambridge, MA, USA (2016)
7. Verein Deutscher Ingenieure (VDI): Wirtschaftlichkeit gebäudetechnischer Anlagen - Grundlagen und Kostenberechnung, VDI 2067. Beuth-Verlag, Berlin (2012). Accessed 15 May 2014
8. Chemical Engineering: The Chemical Engineering Plant Cost Index. <http://www.chemicalengineering.com/pci-home>. Accessed 9 November 2017
9. Scholwin, F., Grope, J., Schüch, A., Daniel-Gromke, J., Beil, M., Holzhammer, U.: Dossier Ist-Stand der Biomethannutzung. Kosten – Klimawirkungen – Verwertungswege. KWK aus Biogas, Biomethan und Erdgas im Vergleich. Bundesministerium für Wirtschaft und Energie (BMWi), Berlin (2014)
10. Zschocke, A.: BurnFair Abschlussbericht. Deutsche Lufthansa, Frankfurt. http://air-reg.de/images/downloads/Abschlussbericht_BurnFAIR.pdf (2014)
11. IndexMundi: Palm oil - Monthly Price - Commodity Prices - Price Charts, Data, and News - IndexMundi. <http://www.indexmundi.com/commodities/?commodity=palm-oil&months=60>. Accessed 2 February 2017
12. finanzen.net GmbH: Weizenpreis. <https://www.finanzen.net/rohstoffe/weizenpreis>. Accessed 1 August 2016

Under current regulatory conditions, the use of biokerosene in aviation does not seem realistic from an economic point of view. In addition, if a reduction in greenhouse gas emissions from aviation is desired, appropriate framework conditions must be enacted to create an economic incentive for the use of biokerosene in order to make it competitive with fossil kerosene.

13. Kuppens, T., van Dael, M., Vanreppelen, K., Thewys, T., Yperman, J., Carleer, R., Schreurs, S., van Passel, S.: Techno-economic assessment of fast pyrolysis for the valorization of short rotation coppice cultivated for phytoextraction. *Journal of Cleaner Production* (2015). <https://doi.org/10.1016/j.jclepro.2014.07.023>
14. Trippe, F.: Techno-ökonomische Bewertung alternativer Verfahrenskonfigurationen zur Herstellung von Biomass-to-Liquid (BtL) Kraftstoffen und Chemikalien. Dissertation, Karlsruhe Institute of Technology [KIT] (2013). Accessed 16 June 2015
15. Deutsches Institut für Normung e.V.: Umweltmanagement – Ökobilanz – Grundsätze und Rahmenbedingungen. Beuth Verlag GmbH, Berlin, Germany(14040) (2009)
16. Deutsches Institut für Normung e.V.: Umweltmanagement – Ökobilanz – Anforderungen und Anleitungen. Beuth Verlag GmbH, Berlin, Germany(14044) (2006)
17. Wernet, G., Bauer, C., Steubing, B., Reinhard, J., Moreno-Ruiz, E., Weidema, B.: The ecoinvent database version 3 (part I). Overview and methodology. *Int J Life Cycle Assess* (2016). <https://doi.org/10.1007/s11367-016-1087-8>
18. Liptow, C., Tillman, A.-M., Janssen, M., Wallberg, O., Taylor, G.A.: Ethylene based on woody biomass—what are environmental key issues of a possible future Swedish production on industrial scale. *Int J Life Cycle Assess* (2013). <https://doi.org/10.1007/s11367-013-0564-6>
19. Nielsen, P.H., Oxenbøll, K.M., Wenzel, H.: Cradle-to-Gate Environmental Assessment of Enzyme Products Produced Industrially in Denmark by Novozymes A/S. *Int J Life Cycle Assess* (2007). <https://doi.org/10.1065/lca2006.08.265.1>
20. Meyer, K., Weinberg, J., Kaltschmitt, M.: GHG emissions from jatropha-based bioderived synthetic paraffinic kerosene. *Biofuels* (2012). <https://doi.org/10.4155/bfs.12.57>
21. Huijbregts, M.A.J., Steinmann, Z.J.N., Elshout, P.M.F., Stam, G., Verones, F., Vieira, M., Zijp, M., Hollander, A., van Zelm, R.: ReCiPe2016: a harmonised life cycle impact assessment method at midpoint and endpoint level. *Int J Life Cycle Assess* (2017). <https://doi.org/10.1007/s11367-016-1246-y>
22. European Parliament and Council: Directive (EU) 2018/2001 of the European Parliament and of the Council of 11 December 2018 on the promotion of the use of energy from renewable sources (2018)
23. The International Air Transport Association (IATA): Jet Fuel Price Monitor. <https://www.iata.org/publications/economics/fuel-monitor/Pages/index.aspx> (2019). Accessed 08-07.2019
24. Neuling, U., Kaltschmitt, M.: Techno-economic and environmental analysis of aviation biofuels. *Fuel Processing Technology* (2018). <https://doi.org/10.1016/j.fuproc.2017.09.022>

Syngas Applications Production of Biofuels Abstracts

Continuous hydrodeoxygenation of liquid phase pyrolysis oil with biogenous hydrogen enriched synthesis gas for fuel production

Klara Treusch^{1,2*}, Anna Magdalena Mauerhofer³, Nikolaus Schwaiger², Peter Pucher¹, Edgar Ahn¹, Stefan Müller³, Daniela Painer², Hermann Hofbauer³, Matthäus Siebenhofer²

1. BDI-BioEnergy International GmbH, Parkring 18, 8074 Raaba-Grambach, Graz, Austria
2. Graz University of Technology, Institute of Chemical Engineering and Environmental Technology, Inffeldgasse 25c, 8010 Graz, Austria
3. TU Wien, Institute of Chemical, Environmental and Bioscience Engineering, Getreidemarkt 9/166, 1060 Vienna, Austria

*corresponding author, klara.treusch@bdi-bioenergy.com

1. Introduction and Short Description:

Science is racing against time to stop global warming. Since the Kyoto protocol [1], published in the mid-90s, climate policy was set in motion. Different protocols, the most common ones being the Paris agreement [2] in 2015 and the renewable energy directive [3] (RED) in 2009 of the European Union with a recast in 2018 [4], have evolved. According to the Paris agreement, the climate change is to hold significantly below 2°C. Experts are not sure if this goal is still achievable. [5] In all agreements it is clearly stated,

that significant reduction of GHGs has to occur in order to achieve CO₂ neutrality eventually. This ambitious goal can only be achieved if all feasible sources for renewable energy production are exploited.

From this point of view, the concept of biofuel production via the bioCRACK process and subsequent hydrodeoxygenation (HDO) of liquid phase pyrolysis (LPP) oil with synthesis gas (syngas) from renewable feed has been developed (Figure 1).

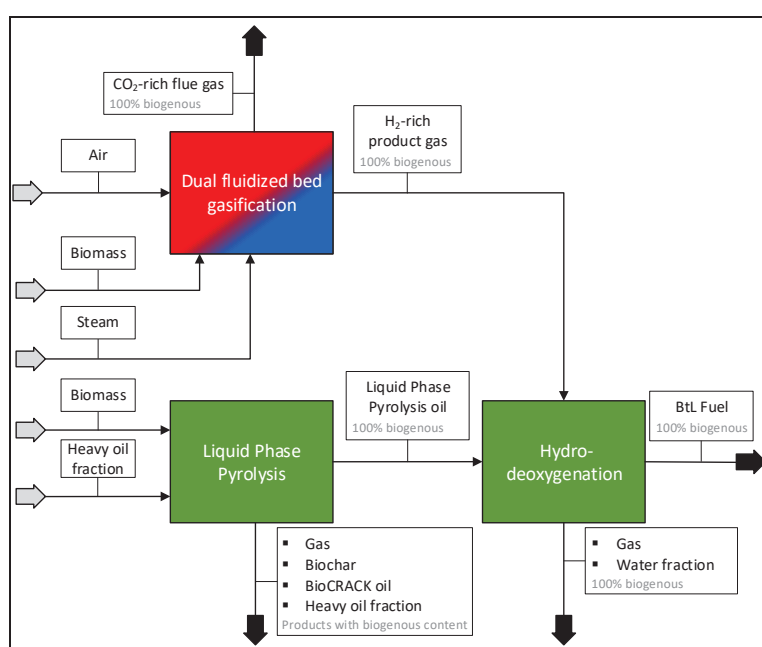


Figure 1: Combined biofuel production route

It combines two major pathways for biomass liquefaction: indirect liquefaction through gasification [6] with subsequent synthesis and direct liquefaction through pyrolysis [7] and HDO.

In the **bioCRACK process** [8], biomass is liquefied through pyrolysis in a heavy oil refinery stream; whereas non-polar biomass fragments are then dissolved in the heat carrier oil and polar biomass constituents build up LPP oil together with the water of reaction. The heat carrier oil, which is also partly cracked during this process, is afterwards upgraded in existing refinery units. LPP oil needs a more extensive upgrade such as HDO.

In order to replace fossil hydrogen and prevent extensive gas cleaning concepts, LPP oil was subsequently hydrotreated with a hydrogen rich synthesis gas, produced via **sorption enhanced reforming (SER)** [9], by making use of the water-gas shift (WGS) reaction. The combined biofuel production concept of LPP and SER is shown in Figure 1.

2. Process design and methodology

Liquid phase pyrolysis was performed in the bioCRACK pilot plant, which was designed for a maximum throughput of 100 kg/h biomass.

Gasification was carried out in a 100 kW_{th} **dual fluidized bed (DFB) steam gasification reactor** in technical scale.

The HDO experiments were performed in a lab scale plug flow reactor with a throughput of 10 g/h LPP oil, equivalent to a liquid hourly space velocity of 0.5 h⁻¹, at 350°C and 120 bar. The reaction was catalyzed heterogeneously with a sulfided metal oxide catalyst.

3. Results and Discussion

For HDO, a test gas bomb with the composition of the SER produced syngas, as shown in Table 1, was used.

Table 1: Composition of the syngas test gas bomb

Product gas composition	Test gas bomb
H ₂ [vol% _{db}]	70.5
CO [vol% _{db}]	8
CO ₂ [vol% _{db}]	5.5
CH ₄ [vol% _{db}]	14
C ₂ H ₄ [vol% _{db}]	1
C ₂ H ₆ [vol% _{db}]	1

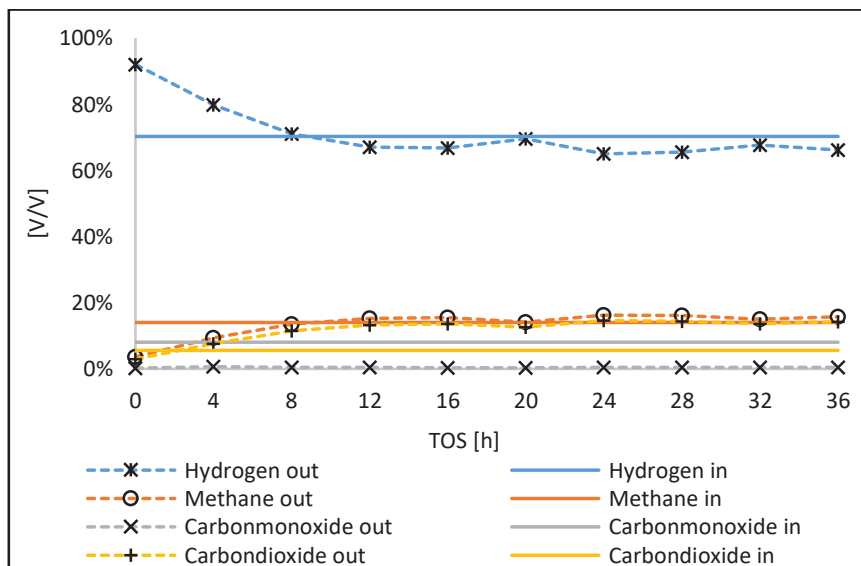


Figure 2: Gas phase composition of HDO inlet (syngas) and outlet gas

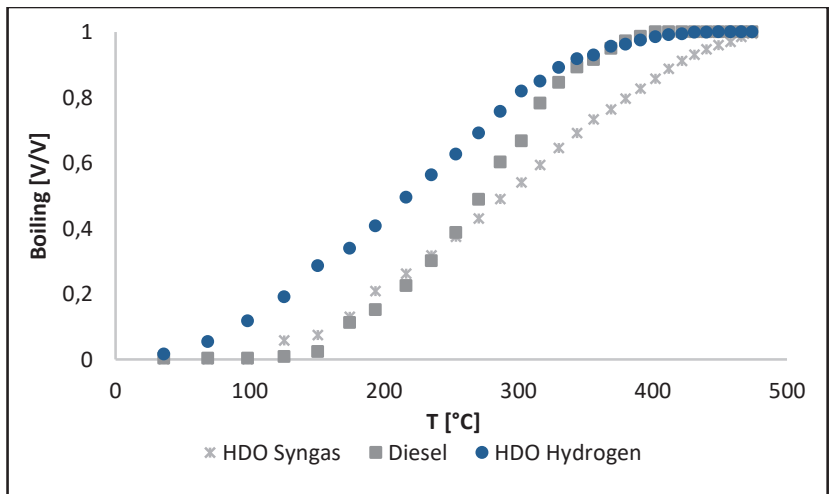


Figure 3: Boiling range of the HDO syngas product compared to HDO with pure hydrogen as well as diesel

In Figure 2, the composition of the HDO inlet gas phase is compared with the HDO outlet gas phase. In the first 8 hours, pure hydrogen, which was used for sulfidation, was replaced by syngas. Afterwards, a stable outlet gas phase composition was achieved. CO was nearly fully converted into CO_2 with a stoichiometric factor of one, Methane was not converted. The net hydrogen content decreased slightly. Thus, a product with close to diesel properties, comparable to HDO with pure hydrogen, was produced, which reflects in the boiling range in Figure 3.

Literature

- [1] United Nations, *Kyoto Protocol to the United Nations Framework Convention on Climate Change*. United Nations, 1998, p. 20.
- [2] UNFCCC, “ADOPTION OF THE PARIS AGREEMENT: Proposal by the President to the United Nations Framework Convention on Climate Change,” vol. 21932, no. December, pp. 1–32, 2015.
- [3] “Directive 2009/28/EC of the European Parliament and the Council of 23 April 2009 on the promotion of the use of energy from renewable sources and amending and subsequently repealing Directives 2001/77/EC and 2003/30/EC,” *Off. J. Eur. Union*, pp. 16–62, 2009.
- [4] “Directive (EU) 2018/2001 of the european parliament and of the council of 11 December 2018 n the promotion of the use of energy from renewable sources (recast),” *Off. J. Eur. Union*, pp. 82–209, 2018.
- [5] IPPC, “Climate Change 2014: Synthesis Report. Contribution of Working Groups I, II and III to the Fifth Assessment Report of the Intergovernmental Panel on Climate Change [Core Writing Team, R.K. Pachauri and L.A. Meyer (eds.)],” Geneva, Switzerland, 2014.
- [6] H. Hofbauer, “Biomass Gasification for Electricity and Fuels, Large Scale,” in *Encyclopedia of Sustainability Science and Technology*, Springer, 2017, pp. 459–478.
- [7] A. V Bridgwater, D. Meier, and D. Radlein, “An overview of fast pyrolysis of biomass,” *Org. Geochem.*, vol. 30, pp. 1479–1493, 1999.
- [8] K. Treusch, J. Ritzberger, N. Schwaiger, P. Pucher, and M. Siebenhofer, “Diesel production from lignocellulosic feed : the bioCRACK process,” *R.Soc.open sci.*, vol. 4, no. 171122, 2017.
- [9] J. Fuchs *et al.*, “The Impact of Bed Material Cycle Rate on In-Situ CO_2 Removal for Sorption Enhanced Reforming of Different Fuel Types,” *Energy*, vol. 162, pp. 35–44, 2018.

Syngas Applications Electricity and Heat Full Papers

Investigation of SOFC operation with steam gasifier product gases as a basis for enhancing its performance

G. Pongratz^{1*}, V. Subotić¹, H. Schroettner², B. Stoeckl¹, C. Hochenauer^{1,3},
A. Anca-Couce¹, R. Scharler^{1,3}

1. Graz University of Technology, Institute of Thermal Engineering, Inffeldgasse 21, 8010 Graz, Austria
2. Graz University of Technology, Institute for Electron Microscopy and Nanoanalysis, Steyrergasse 17, 8010 Graz,
Austria
3. BEST – Bioenergy and Sustainable Technologies GmbH, Inffeldgasse 21b, 8010 Graz, Austria
*corresponding author, gernot.pongratz@tugraz.at

Abstract

Solid oxide fuel cells (SOFC) represent a promising technology to increase the electrical efficiency of biomass-based combined-heat-power systems in comparison to state-of-the-art gas engines, additionally providing high temperature heat. To identify favorable gas compositions and operating conditions for an efficient coupling with gasifiers at low degradation risk is of major importance to ensure stability, reliability and durability of the systems used. Therefore, this study presents a comprehensive analysis on the influence of main gas components on the performance of an industrial-size SOFC relevant for the use with product gases from biomass gasification. Recommendations for concentrations of H_2O , CO , CH_4 and CO_2 in a H_2+N_2 gas mixture for enhancing cell performance are presented. Moreover, the degradation stability of a loaded cell fueled with a modeled steam-gasifier product gas is investigated showing no performance- or substrate degradation.

1. Introduction

Gasifiers coupled with gas engines increasingly replace steam turbine cycles as state-of-the-art systems for converting solid biomass to power because they provide higher thermodynamic efficiencies, especially for small- to medium-scale plants. However, also in this case, the electrical efficiency is limited by the thermodynamic cycle. Combined with high prices for biomass feedstocks, this reduces the attractiveness of electricity production from biomass. Coupling gasifiers with high temperature SOFCs instead of gas engines would increase the electrical efficiency from around 30% to values up to over 40%, in addition to providing high temperature heat and therefore increasing the attractiveness of power production from solid biomass. [1]

As SOFCs are based on heterogeneous catalytic reaction processes, the main drawback of their use with gasifiers in comparison to combustion engines is the higher sensitivity to degradation. This is caused by the components of the derived product gas, which includes impurities like tars, dust, sulfur- and chlorine compounds that can act either as catalyst poison or lead to depositions in the porous fuel electrode, deteriorating SOFC performance [2]. SOFC operating conditions like temperature, electrical load, but especially the concentration of the main components of the employed fuel gas can also induce fuel electrode degradation, e.g. a low steam-to-carbon ratio (SCR) can lead to carbon deposition and a high steam concentration to re-oxidation of the nickel catalyst used in state-of-the-art SOFC anode substrates [3]. To investigate

favorable gas compositions and operating conditions for an efficient coupling of SOFCs with gasifiers at low degradation risk is of major importance to ensure stability, reliability and durability of the systems used.

1.1. SOFC operation with gas components from a product gas

Several studies have already been published investigating the influence of main gas components of biomass gasification product gases on SOFC characteristics. It is argued in [4], that in case of CO/H₂ mixtures, a performance decrease of an anode-supported cell (ASC) with nickel/yttria-stabilized zirconia (Ni/YSZ) anode and 25 cm² active surface can be observed at high CO fractions (>90 vol%). In [5], the impact of bio-syngas and its components on the anode of a nickel/gadolinium-doped ceria (Ni/GDC) electrolyte-supported cell (ESC) is investigated with the outcome that increasing amounts of N₂ and CO in dry H₂ lead to an increase of diffusion losses and therefore a decrease in cell performance. However, the addition of CO₂ to dry H₂ leads to the production of H₂O according to the water gas shift (WGS) reaction (1). As H₂O is the product of the hydrogen oxidation reaction (2), even small amounts of water decrease the voltage losses at low electrical load (activation polarization), thus linearizing the current-voltage correlation of a SOFC, as experimentally shown in [6] and theoretically described in [7]. This linear current-voltage correlation results in a more stable operation behaviour due to better controllability of the cell.



The results of a detailed electrochemical characterization of a Ni/YSZ ASC with 25 cm² active surface over a broad measuring range of temperature and

hydrogen/carbon/oxygen-ratios of the fuel is presented in [8]. The authors claim that although kinetic parameters for the oxidation of H₂-CO-CO₂-N₂-H₂O mixtures are the same as for pure H₂ operation, only H₂ is directly electrochemically oxidized in a Ni/YSZ SOFC. The opposite is claimed by the authors of [9]. In this work, the role of CO and CO₂ on the performance of a Ni/YSZ ASC with 10 cm² active surface is investigated with the outcome that the electrochemical reactivity of CO is comparable to H₂ as long as the amount of fuel in a fuel/N₂ mixture does not exceed 27 vol%. Higher CO concentrations would decrease the cell performance due to higher diffusion losses of CO in comparison to H₂.

In [10] it is also highlighted that a higher performance for the oxidation of H₂ than of CO can be achieved in Ni/YSZ anodes. Moreover, the importance of the WGS reaction was highlighted, as in H₂-CO mixtures the produced H₂O (reaction (2)) reacts with CO to form H₂ as long as the H₂ content is greater than ca. 50 vol%. The higher diffusion resistivity of CO in comparison to H₂ is also claimed as a reason for a lower oxidation rate of CO in [11]. In [12], the cell performance as well as polarization losses of a Ni/YSZ ASC with 25 cm² active surface was investigated when using CO/CO₂/N₂ and H₂/H₂O/N₂ mixtures revealing lower performance levels when using CO as oxidant. A more comprehensive study on the influence of varying mixtures of H₂, H₂O, CO, CO₂, CH₄ and N₂ on the current-voltage correlation of a Ni/YSZ button cell was conducted by [13] to develop a black box model of the cell, however, without a detailed description of the loss mechanisms.

Summing up, the literature review revealed that H₂ is a more preferable oxidant than CO due to better diffusivity and electrochemical reactivity. Moreover, dilution with N₂ and CO₂ should be

minimized to avoid an increase of diffusion losses for all reactive gas components to the active centers of the substrate. Furthermore, the importance of the WGS reaction was highlighted as CO_2 would shift the water gas equilibrium to a side where more CO than H_2 will be formed, thus increasing losses due to worse electrochemical activity. However, in dry $\text{H}_2\text{-CO}_2$ mixtures H_2O can be formed via WGS reducing the activation polarization, thus linearizing the current-voltage correlation of a SOFC.

1.2. Coupling gasification and SOFCs

Anode substrate: The literature review revealed that in general cells with Ni/GDC or Ni/YSZ substrate have been investigated for the use with product gases relevant for biomass gasification. Significantly more publications deal with cells based on Ni/YSZ anodes, possibly due to their better performance in electrochemically oxidizing hydrogen and being closer to a broad commercialization [3]. However, as comprehensively reviewed in [2] and [14], cells with Ni/GDC anode show the highest potential for the use with bio-syngases due to their higher tolerance against contaminants like H_2S and HCl in comparison to cells with Ni/YSZ anode. Moreover, this anode substrate is less prone to the formation of solid carbon deposits when fuelled with carbonaceous gases, especially at a low SCR [15]. Thus, cells with Ni/GDC anode were used for the experiments presented in this paper, especially considering future experiments with fuel gases containing contaminants as well as real product gases from biomass gasifiers.

Cell design: Moreover, the differences in the structure of the layers between an ESC and an ASC as shown in Figure 1 have to be considered to find a suitable design for the use with bio-syngases. In an ASC, most of the mechanical support is applied by the anodic substrate. Thus, the risk for

gas leakages from the cathode to the anode side through cracks and therefore cell malfunction induced by anode degradation is higher for ASCs than for ESCs. Degradation can result from solid carbon depositions or forming of nickel oxide. This has to be considered when cells are operated in environments favouring carbon deposition or nickel re-oxidation, both possible when using product gases from biomass gasification.

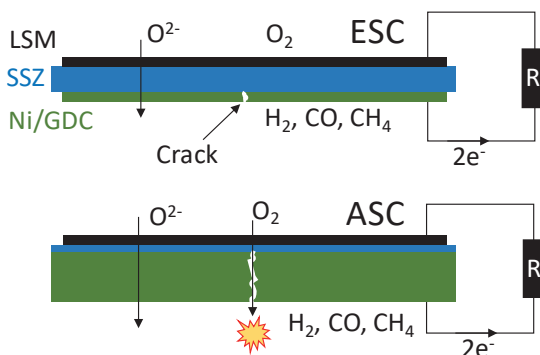


Figure 1 Comparison of ESC (top) and ASC (bottom) SOFC structure

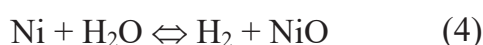
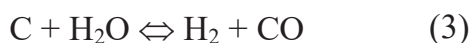
To increase the relevance of test results for industrial applications, the use of cells with an active surface of at least 80 cm^2 is beneficial as macroscopic effects like uneven gas and temperature distribution and furthermore fuel utilization can be reproduced more easily.

Gasifier, gasification agent and gas cleaning: Considering gasifier technologies, there are big differences in product gas compositions depending on feedstock, operating conditions and gasification agent. Table 1 shows examples of typical product gas compositions from common gasifier designs, both having high potential for the coupling with SOFCs [16]: a fixed-bed downdraft gasifier with air (FDA) and a fluidized bed gasifier with steam (FBS) as gasification agent.

vol% w.b.	FDA	FBS
H ₂	16	24
H ₂ O	15	37
CO	17	15
CO ₂	13	13
CH ₄	3	7
N ₂	36	4
SCR	0.75	1.68
H ₂ /CO	0.94	1.6
LHV [MJ/Nm ³ w.b.]	4.6	6.5

Table 1 Product gas compositions of common gasifier designs (values based on [17], [18], [19] and internal data)

To find out the most promising gasifier type for the experimental investigations, the following issues were considered: The lower heating value (LHV) of the FBS gasifier product gas is higher than that of a FDA gasifier. Besides, considering the higher H₂/CO ratio of the FBS gasifier and the before mentioned better reactivity of H₂ in comparison to CO, a better performance can be expected. Moreover, the significantly lower N₂ content is supposed to result in a lower diffusion resistivity of the reactants to the anode. Finally, due to the higher SCR, solid carbon depositions in the anode substrate can be avoided [20] as carbon reacts with steam to form H₂ and CO according reaction (3). Nevertheless, high steam contents might lead to re-oxidation of the nickel catalyst (reaction (4)), resulting not only in a decrease of active sites and therefore performance losses but also in the growth of nickel grains resulting in mechanical substrate degradation. This degradation behaviour is described in [21] for a direct coupling of a SOFC with a gasifier as well as theoretically in [22].



Furthermore, a hot/dry gas cleaning is suggested as the most promising, which improves the system efficiency avoiding steam condensation as shown for the FDA

case in an Ni/YSZ ASC SOFC in [16]. With this cleaning option, all contaminants beside tars could be removed. Besides, literature suggests that cell degradation can be avoided with the expected tar concentrations for cells with Ni/GDC anode [2]. Nevertheless, the high steam content of a FBS producer gas with hot/dry gas cleaning can be as well a risk for the cell as stated in [16].

Summing up, to the best of the authors' knowledge a comprehensive study on the influence of main gas components (H₂, CO, CH₄, CO₂, H₂O, N₂) on the performance of an industrial-size SOFC relevant for the use with product gases from biomass gasification is missing in literature. Therefore, this work deals with the results of an electrochemical characterization of a Ni/GDC ESC when using synthetic fuel gas mixtures with generally high amounts of water vapor, as product gases from steam gasifiers seem to be most promising for the use with SOFCs. Moreover, the possible risk of degradation caused by fuel electrode re-oxidation in a steam-rich atmosphere is evaluated. The obtained results will enable defining advantageous operating conditions in order to achieve an efficient coupling of gasifiers with SOFCs whilst avoiding cell degradation.

2. Materials and methods

An industrial-size ESC SOFC with 80 cm² active surface was used for the experimental investigations. The cell consisted of a 40 µm Ni/GDC anode and a 45 µm lanthanum strontium manganite (LSM) cathode on both sides of an 165 µm electrolyte out of scandia stabilized zirconia (SSZ), manufactured by IKTS [23].

The cell was placed in an alumina housing developed in-house with nickel- and platinum meshes used for the electrical contacting of anode and cathode. This

assembly enables electrochemical impedance spectroscopy (EIS) measurements with minimal cross influences from the periphery to ensure accurate representation of cell characteristics. The cell holder was placed in a test rig shown in Figure 2, which enabled fuelling the SOFC with dry or humidified gas mixtures.

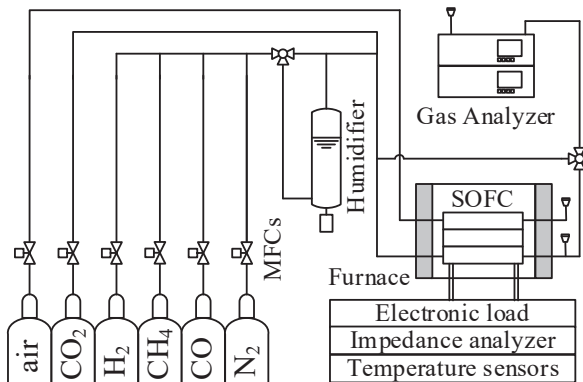


Figure 2 Test rig scheme based on [12]

Current-voltage curves as well as EIS measurements were conducted using a Bio-Logic SAS SP-150 analyser. A Bio-Logic SAS VMP3B-80A/3V booster was used to perform experiments up to 80 A electrical load. The maximum load was restricted by a minimum cell voltage of 0.7 V. At higher loads nickel re-oxidation is thermodynamically possible due to a sufficient high oxygen partial pressure at the anode, as described in [24]. The frequency range for EIS measurements was varied between 100 mHz and 10 kHz with a current amplitude increasing with the DC-current load. Temperatures on the anode side were recorded in the centre and the border area of the flow field at 3 points along the flow direction within the alumina housing, therefore not representing a punctual but an area-averaged cell temperature for each measurement point. Moreover, a continuous off-gas and temporary feed-gas analysis was conducted using an ABB Advanced Optima 2000 gas analyzer with

a Uras 14 and Caldos 17 module. To investigate microstructural phenomena, post-mortem analyses were performed with a Zeiss Ultra 55 equipped with a field emission scanning electron microscope (SEM) and an energy-dispersive X-ray spectroscope (EDX).

To investigate the influence of gas components on the cell performance, each component was varied as shown in Table 2 at 850°C regulated oven temperature and 2 slpm anodic and cathodic gas flow rates. The variation of the N₂ compound is neglected in this paper due to less relevance for FBS systems in comparison to FDA systems. Moreover, it is generally known that an increase of the nitrogen compound leads to a performance decrease due to a lower LHV of the fuel gas and higher diffusion losses for the reactive species to the active centres as described in [6]. To investigate the influence of carbonaceous species on the cell characteristics, the N₂ content of a reference mixture containing 50 vol% H₂, 25 vol% H₂O and 25 vol% N₂ was replaced by CO, CH₄ and CO₂ thus simulating steam gasifier product gases and enabling WGS- as well as Methane-Steam-Reforming (MSR) reactions (5) in comparable extents.



At each operating point, a detailed electrochemical analysis was conducted by means of current-voltage curves as well as EIS at open circuit voltage (OCV) and several load levels. Temperatures on the anode side within the ceramic cell holder were measured at OCV, full-load and intermediate load after a stabilization period.

ID	850°C 2 slpm	H ₂	H ₂ O	CO	CH ₄	CO ₂	N ₂	LHV MJ/Nm ³
vol%								
1	Influence H ₂ O	50	5			45		5.54
2		50	10			40		5.54
3		50	25	Reference		25		5.54
4		50	50					5.54
5	Influence CO	50	25	5		20		6.17
6		50	25	10		15		6.79
7		50	25	25				8.68
8	Influence CH ₄	50	25		5	20		7.33
9		50	25		10	15		9.12
10		50	25		25			14.49
11	Influence CO ₂	50	25			15	10	5.54
12		50	25	5		15	5	6.17
13		50	25		5	15	5	7.33
14		50	25	5	5	15		7.96
15	FBS 800°C	22	36	11	5	11	15	5.61

Table 2 Operating points of parameter study (ID1-14) and long-term experiment (ID15)

To analyse changes in the cell performance for each gas composition, the following four parameters were compared between the operating points. Except for the OCV, all comparison parameters were taken at a constant current density of $i = 300 \text{ mA/cm}^2$ representing a high load for all supplied gas compositions (see Figure 4):

- The cell voltage U as an indicator for the electrical power output as well as the OCV representing the electrochemical potential for the applied gas mixture.
- The area specific resistance (ASR) representing the sum of all voltage losses within the cell according to equation (6) [7].

$$ASR = \frac{OCV - U}{i} [\Omega \text{cm}^2] \quad (6)$$

- The electrical efficiency η_{el} according equation (7).

$$\eta_{el} = \frac{U * i * ActiveSurface}{\dot{V}_{Anode} * LHV_{Mixture}} [\%] \quad (7)$$

- A parameter defined by the authors as conversion efficiency η_{conv} according equation (8), which is assumed to represent the efficiency of the cell for converting chemical energy in

electrical energy neglecting spare fuel by considering the fuel utilization U_f . This parameter enables to compare cell performances between different fuel-gas energy contents.

$$\eta_{conv} = \eta_{el} \frac{1}{U_f} [\%] \quad (8)$$

In addition to experiments with varying fuel gas composition the cell was run on a simulated product gas from an in-house FBS gasifier at a lower temperature of 800°C for 500 h. The gas composition is shown as ID15 in Table 2. The higher N₂ content in comparison to the FBS mixture presented in Table 1 results from pressurizing the fuel tank with N₂ necessary for the operation of the in-house FBS gasifier. A constant load of 300 mA/cm² was applied and current-voltage-curves as well as EIS-spectra were recorded every 2 hours to track the degradation behavior as a result of possible nickel re-oxidation within the anode substrate in this steam-rich environment. Afterwards, SEM and EDX analyses were conducted to investigate changes in the anode substrate.

3. Results and discussion

In Figure 3, the abovementioned parameters U, OCV, ASR, η_{el} and η_{conv} are illustrated for the following operating conditions: current density of 300 mA/cm² (except OCV), gas compositions as shown in Table 2, 850°C regulated oven temperature and 2 slpm for both anodic and cathodic gas flow rates. Furthermore, Figure 4 shows current-voltage correlations for the reference gas mixture and mixtures without N₂. A parameter analysis was performed to reveal recommendations for gas compositions to increase cell performance. A thorough explanation of the specific loss mechanisms considering impedance data would exceed the scope of this paper and is therefore only briefly discussed.

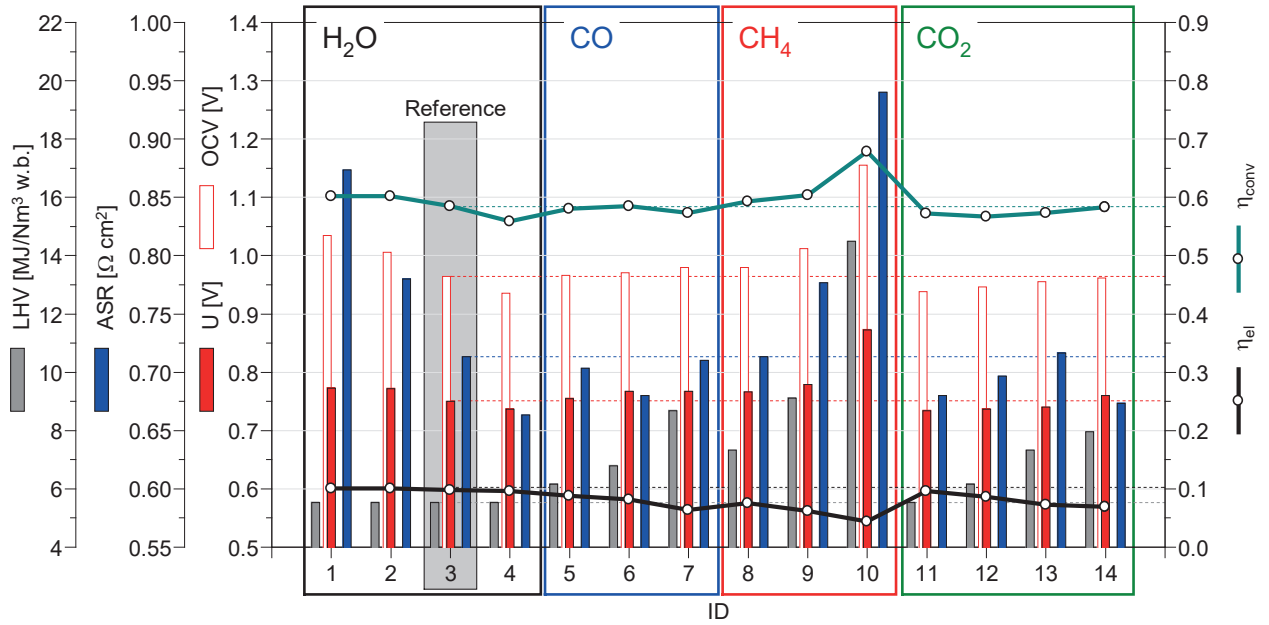


Figure 3 U, ASR and efficiencies at 300 mA/cm² electrical load and OCV

H_2O : The steady decrease of the cell voltage can be explained as follows: Higher concentrations of H_2O , which is the reaction product of the hydrogen oxidation reaction (2), lowers the OCV and therefore leads to a decrease of cell voltage despite constant LHV as shown in Figure 3. However, the increasing water content from 5 to 50 vol% leads to a strong decrease of the ASR due to lower voltage losses at low load levels (activation polarization), which is also described in [6]. A decrease of voltage losses is in general desirable for an efficient operation of SOFCs. Nevertheless, considering the before mentioned necessary comparability of the reference gas mixture to a FBS gasifier product gas, a mixture of 50 vol% H_2 and 25 vol% H_2O in N_2 is employed as reference mixture for further experiments, whereas N_2 will be substituted by carbonaceous species. This mixture shows the best comparability to FBS product gases at a passable cell performance reduction.

CO : Increasing the CO concentration in the reference gas mixture results in an increase of the fuel-gas LHV and moreover the cell voltage at decreasing

ASR. However, no voltage increase can be observed between 10 and 25 vol% CO, despite constantly increasing LHV. At a certain CO concentration above 10 vol% (H_2/CO ratio smaller 5), it seems that CO electrochemically oxidizes before taking part in WGS reactions (1) to form electrochemically more reactive H_2 , resulting in an increasing ASR. Therefore, also considering the peak of η_{conv} at 10 vol% CO, substituting N_2 of the reference gas mixture with CO concentrations higher than 10 vol% should be avoided.

CH_4 : In comparison to an increasing CO concentration, an increase of CH_4 concentration results in a 3 times higher H_2 production rate when comparing WGS reaction (1) with MSR reaction (5). The obtained higher volume flow and therefore lower fuel utilization in combination with a higher H_2 concentration within the cell results in an increase of the OCV [7]. Nevertheless, the ASR increases with increasing CH_4 concentration, leading to a stronger decrease of electrical efficiency. This can be argued as a result of a measured temperature decrease of ca. 15 K from fuel inlet to fuel outlet due to endothermic MSR reactions (5). A

decrease in temperature results in a higher ohmic resistance of the electrolyte according to [7], which could be confirmed by analyzing impedance data. Considering the nearly full conversion of CH₄ into CO and H₂ measured with the gas analyzer, no water will be left in the gas when the electrochemical oxidation of H₂ takes place. This leads to a higher activation polarization as described in the introduction chapter. As a result, the current-voltage curve for ID10 at 25 vol% CH₄ loses its linearity as shown in Figure 4. In conclusion, a H₂O/CH₄ ratio higher than 1 is strongly recommended to avoid high polarization losses and ensure linearity of the current-voltage correlation.

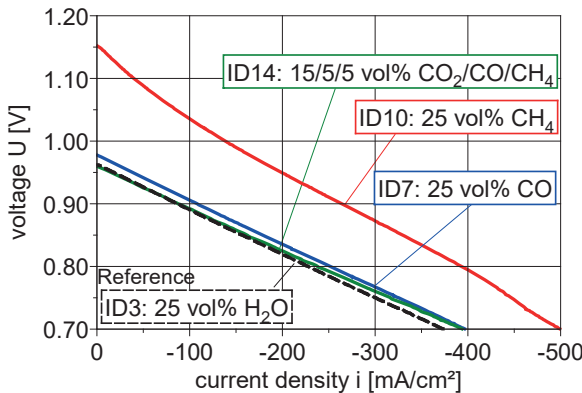


Figure 4 Current-voltage correlations of gas compositions without N₂

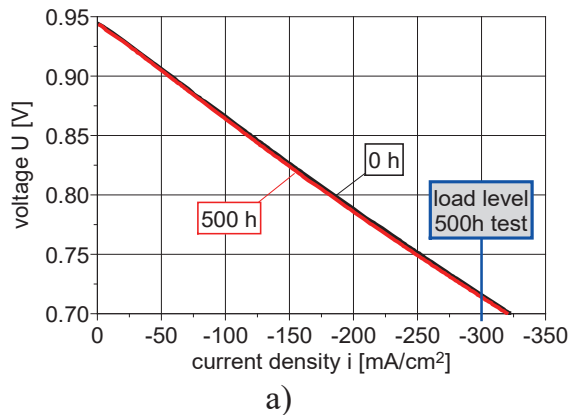
CO₂: When adding 15 vol% CO₂ to the reference gas mixture, a fraction of CO₂ reacts via WGS with H₂ to produce H₂O and CO. As described in the introduction chapter, CO has a lower electrochemical activity than H₂ explaining the voltage decrease, also lowering the OCV. This also might explain the ASR decrease. When adding the reactive species CO and CH₄ even in small extents of 5 vol%, this negative impact gets partly compensated. Nevertheless, voltage measured while feeding the anode with gas mixtures of 5 vol% N₂ (ID7: 10 vol% CO or ID10: 10 vol% CH₄) is not achievable when using gas mixture ID14, despite a lower ASR. For this reason, it can be concluded that the

amount of CO₂ in the gas mixture should always be as low as possible, especially to avoid conversion of electrochemically high-reactive H₂ with CO₂ to CO and H₂O via WGS and to keep diffusion resistances low for electrochemically active species.

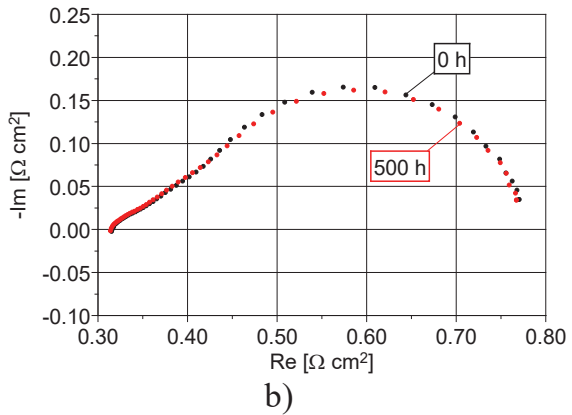
Considering the results of the parameter study, the gas composition of an in-house FBS gasifier fueled with wood pellets presented as ID15 in Table 2 is confirmed as suitable for the use as fuel gas for the 500 h degradation experiment due to following reasons:

- It shows a comparable composition to the FBS mixture presented in Table 1, besides a higher N₂ concentration thus lowering the power output but not influencing WGS and MSR reactions.
- The steam content of 36 vol% shows a risk for degradation due to nickel re-oxidation (4) according to [21] which is relevant to investigate for industrial applications. Nevertheless, it is far below 50 vol% to avoid a strong ASR increase and therefore higher polarization losses as well as it ensures a H₂O/CH₄ ratio higher than 1.
- Although the H₂/CO ratio of 2 is smaller than 5, which was not recommended before, the higher H₂O content might also increase WGS reactions and therefore a higher production rate of H₂ from CO and H₂O. Besides, it is a much more favorable ratio than for FDA gasifiers (see Table 1).

Long term test with typical composition of FBS: In Figure 5, the results of the 500 h experiment at 800°C oven temperature and 300 mA/cm² with simulated product gas from an in-house FBS gasifier (see Table 2 - ID15) are presented. Current-voltage curves as well as impedance spectra show no degradation of the cell performance.



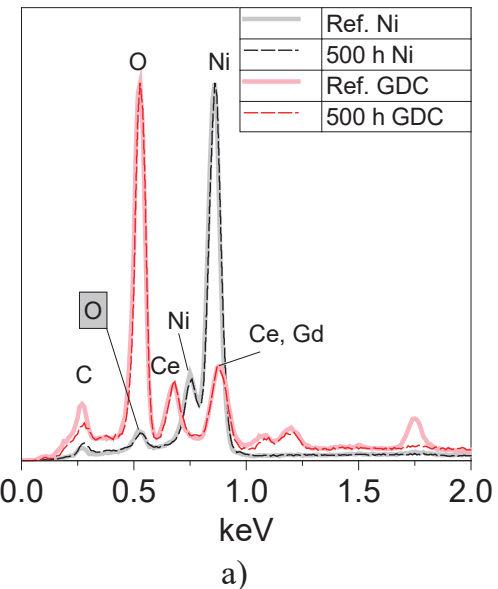
a)



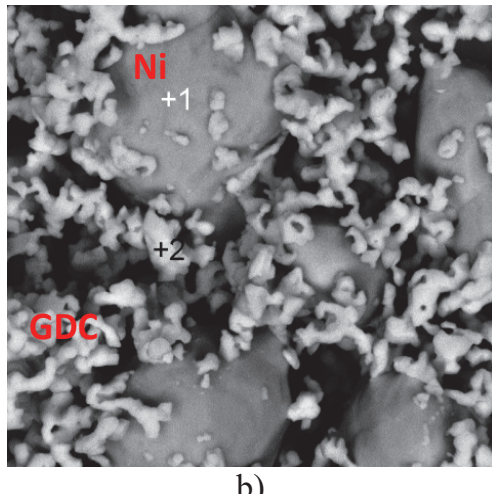
b)

Figure 5 a) Current-voltage curves and **b)** impedance spectra comparison of cell before and after 500h long term experiment

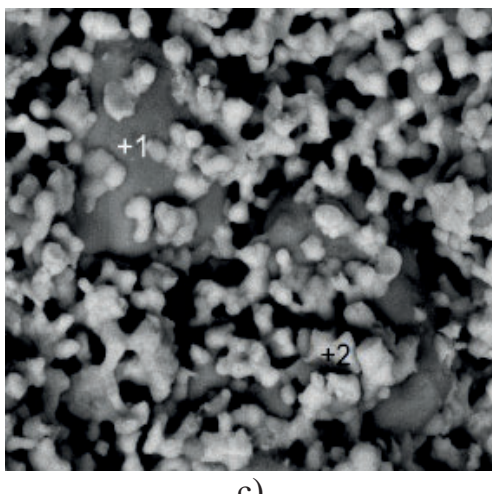
Nevertheless, performance degradation analyses do not deliver information about possible local changes in the microstructure of the anode substrate, which could cause a fast cell degradation after longer operation periods. Therefore, SEM and EDX analyses were used to investigate if the anode structure changed during the operating time. The results of these analyses are presented in Figure 6.



a)



b)



c)

Figure 6 a) EDX comparison with marked oxygen peak of **b)** reduced reference anode substrate with **c)** substrate after 500 h experiment

A reduced but unloaded cell was used as reference, with definitely no oxidized

nickel. When comparing Figure 6 b) with c), no significant differences in nickel grainsize or shape can be detected. Also considering the EDX spectra, no difference between the substrate composition can be assumed as the oxygen peak representing nickel oxide (marked and grey-colored) stays at the same size and shape. The different distribution of GDC on nickel grains cannot be argued as a result of the 500 h experiment but of manufacturing tolerances. Summing up, nickel re-oxidation after 500 h loaded operation in a gas mixture with 36 vol% H₂O could not be detected. However, slight changes in the distribution of substrate components might be possible but do not influence cell performance.

In conclusion, it can be claimed that fueling Ni/GDC anodes with a FBS gasifier product gas containing 36 vol% H₂O does not result in performance- or substrate degradation at a high electrical load.

4. Conclusion and Outlook

This work presents a comprehensive study on the influence of main gas components on the performance of an industrial-size SOFC relevant for the use with product gases from biomass gasification.

First, a literature review on the most promising cell configuration and biomass gasifier product gas compositions was done. ESC-SOFCs with Ni/GDC anode showed the highest potential for the use with biomass gasifiers due to (i) their higher tolerance against catalyst contaminants and thus better resistivity to solid carbon deposits than cells with Ni/YSC anode, as well as (ii) their lower risk of failure resulting from cracks in the anodic structure in comparison to ASC-SOFCs. Product gases from FBS gasifiers were rated as most promising for the use with SOFCs and are focused in this work. Second, changes in cell characteristics when adding carbonaceous species CO,

CH₄ and CO₂ while decreasing the N₂ content in a reference gas mixture of 50-25-25 vol% H₂-H₂O-N₂ representing a steam gasifier product gas were investigated: CO concentrations higher than 10 vol% result in an increase of the ASR and stagnating cell voltage and should be avoided. For the same reference mixture, CH₄ concentrations should not exceed 10-20 vol% to avoid CH₄/H₂O ratios smaller one and furthermore a strong increase of the ASR. The amount of CO₂ in the gas mixture should be aimed as low as possible, especially to avoid conversion of electrochemically high reactive H₂ with CO₂ to CO via WGS and to keep diffusion resistances low. Detailed electrochemical analyses of the presented results as well as experiments with higher fuel utilizations will help to further understand processes within the cell. The presented results from the parameter study confirm FBS product gas compositions as most suitable for the use with SOFCs.

Third, the 500 h degradation stability of a loaded cell fueled with steam-rich simulated FBS gasifier product gas was investigated showing no performance or substrate degradation, especially considering re-oxidation of anodic nickel. Experiments with higher fuel utilizations will increase degradation risks and therefore industrial relevance of presented results.

5. Acknowledges

The financial support by the Austrian Ministry for Transport, Innovation and Technology (bmvit) for the BIO-CCHP project (FFG number 869036) within the framework of the 11th Joint Call of ERA-NET Bioenergy is gratefully acknowledged.

6. Abbreviations

ASC	anode supported cell
ASR	area specific resistance
EDX	energy-dispersive X-ray spectroscope
EIS	electrochemical impedance spectroscopy
ESC	electrolyte supported cell
FBS	fluidized bed steam
FDA	fixed-bed downdraft air
LHV	lower heating value
LSM	lanthanum strontium manganite
MSR	methane steam reforming
Ni/GDC	nickel/gadolinium-doped ceria
Ni/YSZ	nickel/yttria-stabilized zirconia

OCV	open circuit voltage
SCR	steam to carbon ratio
SEM	scanning electron microscopy
SOFC	solid oxide fuel cell
SSZ	scandia stabilized zirconia
WGS	water gas shift

7. List of symbols

U	cell voltage [V]
i	current density [mA/cm^2]
η_{el}	electrical efficiency [%]
η_{conv}	conversion efficiency [%]

8. Literature

- [1] S. Heidenreich and P. U. Foscolo, *Prog. Energy Combust. Sci.*, vol. 46, pp. 72–95, 2015.
- [2] Z. Ud Din and Z. A. Zainal, *Renew. Sustain. Energy Rev.*, vol. 72, pp. 1050–1066, 2017.
- [3] J. Hanna, W. Y. Lee, Y. Shi, and A. F. Ghoniem, *Prog. Energy Combust. Sci.*, vol. 40, pp. 74–111, 2014.
- [4] A. Weber, B. Sauer, A. C. Müller, D. Herbstritt, and E. Ivers-Tiffée, *Solid State Ion.*, vol. 152–153, pp. 543–550, 2002.
- [5] P. V. Aravind, J. P. Ouweertjes, E. de Heer, N. Woudstra, and G. Rietveld, *ECS Proc. Vol.*, vol. 2005–07, pp. 1459–1467, 2005.
- [6] V. Subotić, B. Stoeckl, V. Lawlor, J. Strasser, H. Schroettner, and C. Hochenauer, *Appl. Energy*, vol. 222, pp. 748–761, 2018.
- [7] S. C. Singhal and K. Kendall, Eds., New York: Elsevier Advanced Technology, 2003.
- [8] A. Kromp, A. Leonide, A. Weber, and E. Ivers-Tiffée, *J. Electrochem. Soc.*, vol. 158, no. 8, pp. B980–B986, 2011.
- [9] M. Lebreton, B. Delanoue, E. Baron, F. Ricoul, A. Kerihuel, A. Subrenat, O. Joubert, and A. Le Gal La Salle, *Int. J. Hydrot. Energy*, vol. 40, no. 32, pp. 10231–10241, 2015.
- [10] Y. Jiang and A. V. Virkar, *J. Electrochem. Soc.*, vol. 150, no. 7, pp. A942–A951, 2003.
- [11] Y. Matsuzaki and I. Yasuda, *J. Electrochem. Soc.*, vol. 147, no. 5, pp. 1630–1635, 2000.
- [12] B. Stoeckl, V. Subotić, M. Preininger, H. Schroettner, and C. Hochenauer, *Electrochimica Acta*, vol. 275, pp. 256–264, 2018.
- [13] A. Baldinelli, L. Barelli, and G. Bidini, *Energy*, vol. 90, pp. 2070–2084, 2015.
- [14] P. V. Aravind and W. de Jong, *Prog. Energy Combust. Sci.*, vol. 38, no. 6, pp. 737–764, 2012.
- [15] M. Ihara, K. Matsuda, H. Sato, and C. Yokoyama, *Solid State Ion.*, vol. 175, no. 1, pp. 51–54, 2004.
- [16] V. Subotić, A. Baldinelli, L. Barelli, R. Scharler, and A. Anca-Couce, in *Energy Procedia*, 2018, p. 6.
- [17] A. V. Bridgwater, *Fuel*, vol. 74, no. 5, pp. 631–653, 1995.
- [18] A. V. Bridgwater, H. Hofbauer, and Sjaak. Van Loo, Newbury : CPL Press, 2009.
- [19] C. Pfeifer, S. Koppatz, and H. Hofbauer, *Biomass Convers. Biorefinery*, vol. 1, no. 1, pp. 39–53, 2011.
- [20] B. Stoeckl, V. Subotić, D. Reichholz, H. Schroettner, and C. Hochenauer, *Electrochimica Acta*, vol. 256, pp. 325–336, 2017.

- [21] Ph. Hofmann, K. D. Panopoulos, L. E. Fryda, A. Schweiger, J. P. Ouveltjes, and J. Karl, *Int. J. Hydrot. Energy*, vol. 33, no. 11, pp. 2834–2844, 2008.
- [22] L. Holzer *et al.*, *J. Power Sources*, vol. 196, no. 3, pp. 1279–1294, 2011.
- [23] N. Trofimenko, M. Kusnezoff, and A. Michaelis, *ECS Trans.*, vol. 78, no. 1, pp. 3025–3037, 2017.
- [24] D. Larrain, J. Van herle, and D. Favrat, *J. Power Sources*, vol. 161, no. 1, pp. 392–403, 2006.

Syngas Applications Electricity and Heat Abstracts

Demonstrative Installation for Cogeneration of Heat and Power from Biomass Gasification Process

T. Iluk^{1*}, M. Szul¹, A. Sobolewski¹

1. Institute for Chemical Processing of Coal,
Zamkowa 1, 41-803 Zabrze, Poland
*corresponding author, tiluk@ichpw.pl

1. Introduction and Short Description

Biomass is a key feedstock utilized by energy sector as a source of renewable energy. Due to its characteristics and

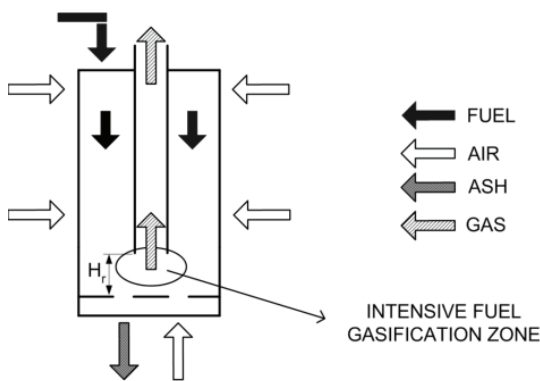


Fig. 1: Schematic representation of GazEla fixed bed reactor.

possibility for procurement, it finds applications in particular in small and medium size distributed energy systems. In the range of 5-25MW of thermal power, gasification systems find their highest efficiency advantage over conventional combustion systems. From economical perspective, important is utilization of biomass from waste sources that often are generated during wood processing, in agriculture or are wastes from food industries. These feedstocks differ greatly in physicochemical properties, hence reactors used for their conversion need to be flexible.

Tab. 1: Proximate and ultimate analysis of feedstock

IChPW has developed a construction of a fixed-bed reactor dedicated for operation in Combined Heat and Power units based on piston engines. The reactor (Fig. 1) together with gas cleaning system and piston engine has been realized in a pilot scale (ca. 60 kW_t) and demonstrative scale (1.5MW_t).

Nominal parameters of the demonstrative installation are:

- fuel stream: 400 kg/h,
- process gas stream: 1300 kg/h,
- LHV of syngas: 4.5 ÷ 5 MJ/Nm³,
- Cold gas efficiency: 60 ÷ 65%,
- output 800kW of heat and 350kw of power.

Results from gasification of waste wood

Parameter	Symbol	Value
Total water content (as received)	W _t ^r	24.8%/ 37.9%
Water content (a - analytical state)	W ^a	2.5%
Ash content	A ^a	2.9.%
Volatile organic compounds content (dry-ashless fuel)	V ^{daf}	76.0%
Carbon content	C _t ^a	51.02%
Hydrogen content	H _t ^a	6.38%
Nitrogen content	N ^a	1.11%
Sulfur content	S _t ^a	0.14%
Calculated oxygen content	O _d ^a	35.95%
Lower heating value	Q _i ^r	15.37kJ/g

chips of varied moisture content in the

	Parameter	Symbol	Unit	Wood chips 1	Wood chips 2
Reactor operational parameters	Minimal temperature (drying-pyrolysis)	T_{\min}	°C	512	512
	Gasification temperature (syngas outlet)	T_{gas}	°C	856	833
	Char combustion temperature	$T_{\text{comb.}}$	°C	1054	600
	Equivalence ratio	ER	-	0.29	0.34
	Cold gas efficiency	CGE	%	62.8	60.1
Syngas parameters	CO	X_{CO}	%	24.66	15.04
	CO_2	X_{CO_2}	%	12.91	15.75
	H_2	X_{H_2}	%	11.27	10.34
	CH_4	X_{CH_4}	%	3.82	2.99
	Lower Heating Value	LHV	MJ/Nm^3	5.70	3.73
Syngas contaminants	Volatile Organic Carbon	VOC	g/Nm^3	10.6	13.9
	Water Vapour	H_2O	g/Nm^3	186.0	350.0
	Particle content (after cyclone)		g/Nm^3	1.012	1.515
	Tar content		g/Nm^3	0.802	13.3

Tab. 2: Results of gasification experiments.

demonstrative installation are presented herein.

2. Methodology, Results and Discussion

The gasification research was done on feedstock of 24.8 (wood chips 1) and 37.9% (wood chips 2) moisture content. Hence, the first batch represented a nominal fuel for the reactor while batch 2 was a boundary case (Tab. 1).

Process gas cleaning was performed in a dry configuration consisting of a cyclone a high temperature filter, two steps of heat exchangers and a demister. This configuration ensured removal of 99% of solids, i.e. from 4-6 g/Nm^3 in raw syngas

down to 40 mg/Nm^3 at engine manifold. When gravimetric tar content is concerned, the cleaning efficiency reached 90% (reduction from 2-1 g/Nm^3 down to 200 mg/Nm^3) and was satisfactory from the perspective of engine operation.

During the research special attention has been paid towards determination of appropriate total volumetric stream of gasifying agent fed, its division between different process zones, temperature profiles. Finally, the research verified the possibility for combustion of the cleaned process gas in the piston engine, thus providing data necessary for determination of mass and energy balances of the installation and calculation of its total efficiency.

3. Conclusion and Outlook

Fixed bed reactors are a viable option of gasification applications where fluidized bed reactors cannot be applied. In particular they are advantageous for feedstocks which are costly to prepare (homogenization, densification, drying) or have high ash and moisture contents. During the research it has been shown that feedstock of very high moisture contents can be successfully gasified in fixed bed reactors with only small drop in to the CGE and syngas quality. Importantly though, start-up procedure is advised to always be done on a high calorific value, dry fuel to assure longevity of process gas cleaning equipment and the piston engine.

Syngas Applications
SNG
Full Papers

From wood to biogas – a small-scale demonstration

N.B.K. Rasmussen^{1,*}, C.L. Høffner^{1,2}

1. Danish Gas Technology Centre, Dr Neergaards Vej 5B, 2970 Hørsholm, Denmark
2. Technical University of Denmark, Chemical and Biochemical Engineering, 2800 Kgs Lyngby, Denmark
^{*}corresponding author, nbr@dtu.dk

1. Introduction

In Denmark, greening the natural gas grid is developing fast. Starting in 2012 with 0%, the share of biomethane (upgraded biogas to natural gas quality) in the grid is now (2019) about 10%. It is still increasing, but to end at the future goal of 100% it is necessary to include other sources, which could be gasification of biomasses followed by methanation.

2. Demonstration plant setup

Allothermal gasification of biomass coupled with ex situ tar removal was shown to be a viable method of producing tar-free syngas well suited for subsequent

biomethanation. The gasification was performed in a fluid bed packed with olivine particles as bed material, operated at 1 barg and at isothermal conditions at 900°C furnace temperature corresponding to 800°C reactor temperature.

Steam is used as both the fluidization and gasification agent and is added from the bottom of the gasifier. A flow of wood pellets of 320 g/h, corresponding to a thermal input of approximately 1.55 kW based on the net heating value, and a CO₂ flow of 2 l/min at 1 barg are continuously added to the gasifier from the top. The gasifier uses 5.5 kW electricity, which covers the steam generation, furnace heating and losses.

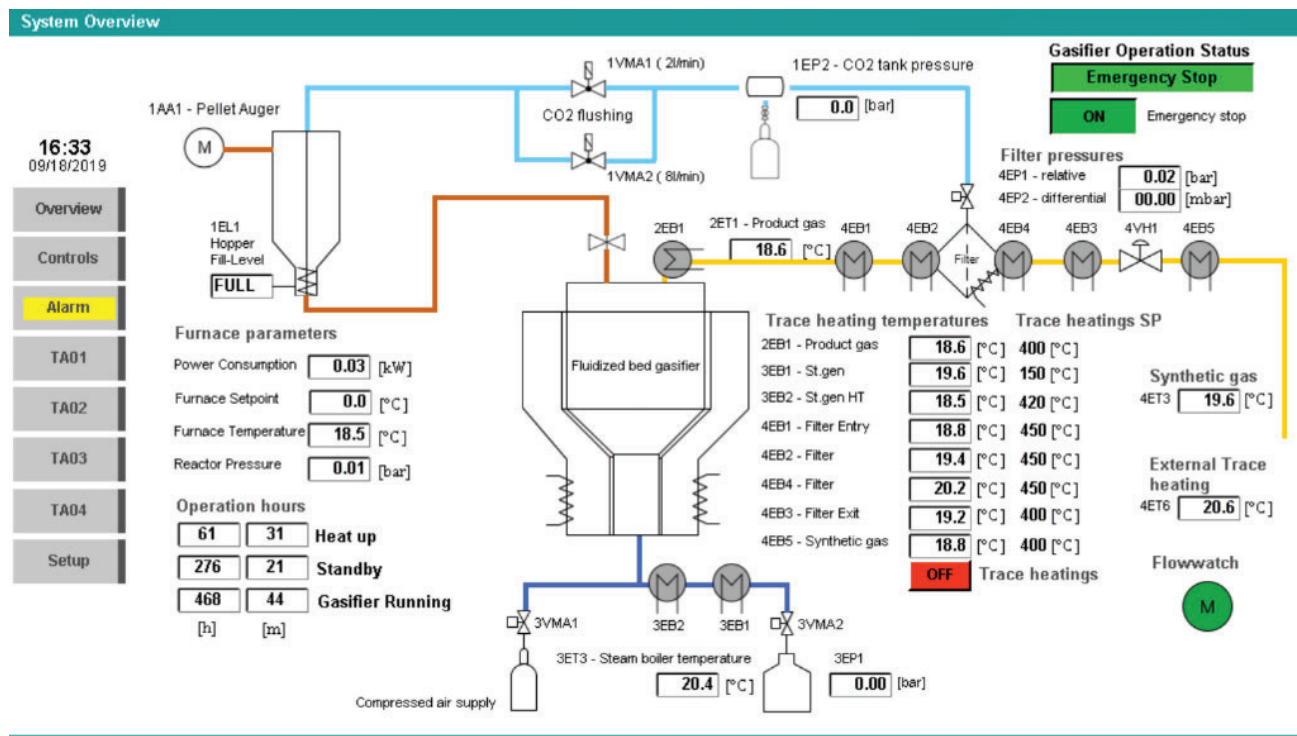


Fig. 1: System overview of the gasifier (not in operation)

Figure 1 shows a system overview of the gasifier (not in operation) including fuel hopper, fluidized bed gasifier, exit filter, steam supply and CO₂ tank for filter cleaning and CO₂ flushing [1].

3. Steam reforming

Post the gasification furnace, the temperature is kept above 350°C in order to avoid tar condensation in the pipes. Ex situ tar removal was performed through catalytic steam reforming at a temperature of approximately 700 to 800°C reached by internal heat exchange and external electrical heating. The principle is based on an internal heat exchanger packed with three distinct catalysts catalyzing the endothermic steam reforming reactions, the exothermic methanation reactions and water gas shift, respectively. The internal heat exchanger is designed in a way that more energy is released through the exothermic methanation reactions than is consumed through the endothermic steam reforming reactions. Through this concept, it is possible to raise the temperature of the tar containing syngas from 350°C up to 700-800°C where the steam reforming reactions take place. A minor amount of electricity is needed to keep the max temperature at 800°C and to account for the heat losses of the tar reformer. The observed conversion rates were 100% for tar, 89% for ethylene and 62% for propane.

Figure 2 shows the combined steam reforming and pre-methanation unit. It includes a pre-cleaning part consisting of dolomite pellets only, which also starts a WGS process and heating up syngas from about 400°C to 700°C. Then follows a steam reforming part working at 800°C and reducing tar and methane to a minimum and exchanging heat with the incoming gas. The catalyst is the “TARGET” catalyst from NEXCERIS, USA. The last part of the heat exchanger consists of catalyst, which is a mixture of

dolomite pellets and methanation pellets. The methanation pellets consist of “Methanation Catalyst META-J103” from China, including >18% Ni. In this part, the concentration of H₂O is still high and there are two parallel reactions taking place here: WGS and methanation, while the temperature drops from 600°C to around 400°C by heat exchange. The gas from the tar cracker and pre-methanation then passes through an active carbon filter to remove any remaining pollutants and from there even through a water scrubber. We never found any tar in the water scrubber.

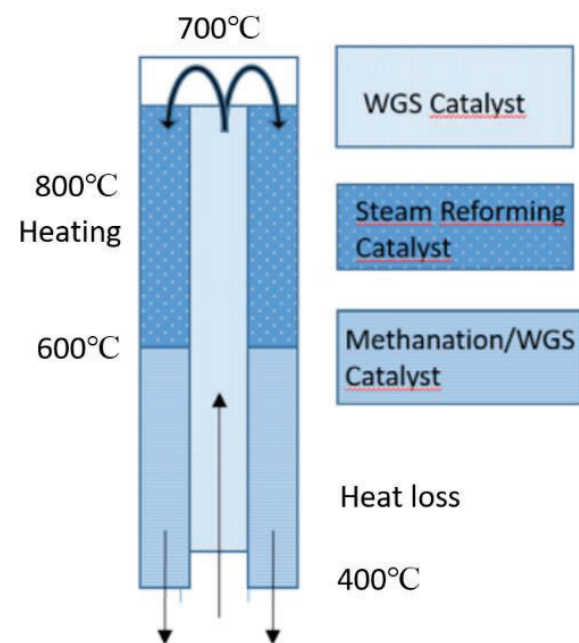


Fig. 2: Steam reforming and pre-methanation unit; the tar cracker

4. Biomethanation

The thermal fuel input of 1.55 kW coupled with the electricity consumption and allothermal operations results in a thermal output from the gasifier of 1.78 kW. As expected, most of the electricity is wasted as losses in this small lab-scale gasifier. When adding a biomethanation unit, which has an energy conversion efficiency of 80%, calculations indicate that it is possible to produce methane with an energy efficiency (based on thermal input to the gasifier) of approximately 100%.

The biomethanation unit developed at the Technical University of Denmark (DTU) was installed, and the exit gas composition from the tar reformer is exactly suited for the subsequent methanation. It consists of a trickle bed reactor with a total electronic control system for addition of nutrients, pH-control, etc. A part stream of the syngas from the gasifier and tar cracker is added to the bioreactor, which converts all gasses to a biogas only containing CO₂ and CH₄. The input gas to the biomethanation

unit contains around 48% CO₂, 11% CO, 31% H₂ and 10% CH₄, while the output gas contains around 64% CO₂ and 36% CH₄ (dry basis). Figure 3 shows the composition of the main components throughout the total system from the gasifier to the biomethanation output; all values were measured except the tar. Figure 4 shows the steam consumption, the tar reduction and the energy content in the gas flow throughout the system [2].

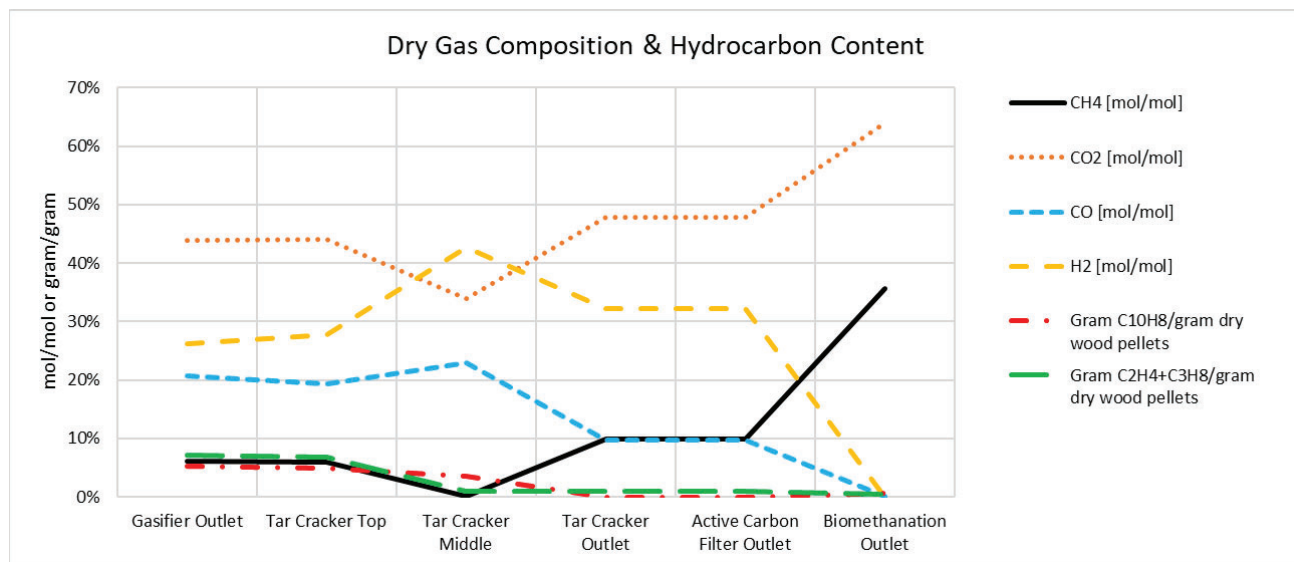


Fig. 3: The composition of the main components throughout the total reactor system

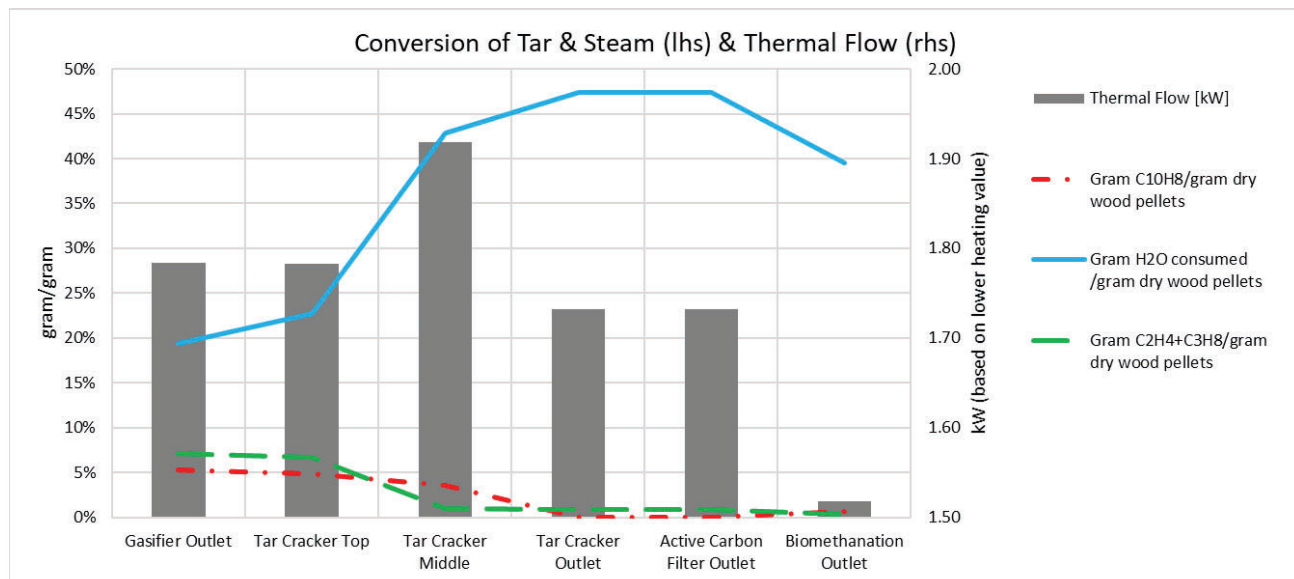


Fig. 4: The steam consumption, tar reduction and energy content in the gas flow

5. Tar modelling and mass balance

Tar from the gasifier is represented by Naphthalene ($C_{10}H_8$). According to literature, Naphthalene contributes to a large part of all the compounds in tar from gasification, and furthermore taking the average C/H ratio in tars it usually ends at 10/8 [3,4]. Hence, in this work we assume Naphthalene to represent all tars. We did not measure the tar, and we used the following method of modelling the tar content:

The mass balance was performed based on the fuel supplied to the gasifier and on measurements. The mass flow of fuel and CO_2 were continuously measured. N_2 and O_2 were always zero during the measurement, which is a test of correct

measurements as no air is supplied. The mass balance was performed based on the input and output sources of the gasification process. The gasification process input stream includes fuel material (wood pellets) and steam for fluidization (including moisture present in fuel) and CO_2 flushing to maintain the pressure in the fuel tank and prevent syngas backflow into the fuel tank. The output stream includes syngas, tar and steam. The elemental composition of input and output of gasification was balanced as shown below.

The empirical stoichiometric mass balance was done based on the stoichiometric molar flow of fuel at inlet compared to outlet, as shown in equation (1) and (2).



Equation (1) is developed as shown below:



Equation (2) is explained as follows:

$C_{13}H_{19}O_8$ represents wood that gives the correct relation of masses of C, H and O. The known amount of moisture in the fuel is represented by bH_2O and “ b ” is a calculated variable. The relation between flushing CO_2 and fuel is known, which determines variable “ a ”. The inflow of CO_2 flushing was measured using a flowmeter. The fluid bed of the gasifier is fluidized by steam and yH_2O represents the amount of steam converted to other gases during the gasification process. Only a part of the H_2O is converted. “ x ” is the stoichiometric amount of fuel in inlet. On the right side of the equation, all the measured molar concentrations of the output gases are assumed to be the

arbitrarily chosen stoichiometric amounts. As mentioned, in this work we assume Naphthalene to represent all tars. “ z ” is then the stoichiometric amount of $C_{10}H_8$ in the outlet. With these assumptions it is possible to calculate the three unknowns, x , y and z from the three elemental balance equations for C, O and H using Problem Solver in Microsoft Excel. The elemental material mass balance calculations were performed from volume basis to molar basis using the measured gas composition. Then the molar composition of dry gas and fuel was calculated with respect to its individual elements to form empirical stoichiometric equation for the gasification of wood. The calculations were made based on measurements of gas

compositions throughout the whole system from gasifier inlet to biomethanation outlet.

6. Conclusion

In a small-scale demonstration plant, we succeeded in converting wood pellets into biogas ($\text{CO}_2 + \text{CH}_4$).

The gasifier was an electrically heated lab-scale fluid-bed and the conversion efficiency of the biomass was about 100% caused by the added electricity.

The tar was converted 100% to syngas in a steam reformer. The syngas from the gasifier and tar cracker was converted into biogas in a biomethanation unit.

We have shown that instead of measuring, it is possible to calculate the steam conversion and the tar content from the gasifier based on measurements of input mass flows and output composition of the gasses.

7. Future developments

The obvious future developments in connection with the gasifier are as follows:

- Testing new fuels, e.g. separated manure fibers, separated biogas fermented fibers, washed and dried straw, etc.
- Testing the present system, but using thermal methanation instead of biomethanation
- Testing more efficient biomethanation systems (more production/liter reactor)
- Investigating how to scale up all the good results from this laboratory-

scale system to a full-scale system keeping the high conversion efficiency and minimizing the electricity consumption.

The last point is going on now in a pre-project, but the developments will depend on funding for the continuation.

8. Acknowledgements

The following are acknowledged for making this project possible: Innovation Fund Denmark, The SYNFERON project, Technical University of Denmark, Danish Gas Technology Centre and the Danish Gas Distribution Companies.

9. References

- [1] Entrade Energiesysteme AG. Operation Manual, Synferon - Fluid Bed Gasifier 2017 v.4.0.
- [2] Höffner CL. From Wood to Biogas. Internship report 2019, Technical University of Denmark.
- [3] Rapagna S, Jand N, Kiennemann A, Foscolo PU. Steam-Gasification of Biomass in a Fluidized-Bed of Olivine Particles. *Biomass and Bioenergy* 2000;19:187–197.
- [4] Devi L, Ptasinski KJ, Janssen FJJG. Pretreated olivine as tar removal catalyst for biomass gasifiers: Investigation using naphthalene as model biomass tar. *Fuel Processing Technology* 2005;86:707–730.

Syngas Applications SNG Abstracts

Experimental Performance of a Trickle-Bed Reactor for Biological Methanation

T. Weidlich^{1*}, T. Trabold¹, M. Neubert¹, P. Treiber¹, J. Karl¹

1. Friedrich-Alexander-Universität Erlangen-Nürnberg, Chair of Energy Process Engineering,
Fürther Str. 244f, 90429 Nürnberg, Germany
*corresponding author, tobias.weidlich@fau.de

1. Introduction and Short Description:

Methanogenic archaea are able to produce methane through metabolism of CO₂ or CO and H₂ [1]. Therefore, they present a second technological option, besides catalytic methanation, for the synthesis of substitute natural gas (SNG) [2]. A major challenge for the implementation of this process is supplying and dissolving the feed gases to the aqueous environment of the microorganisms. It is still unclear, whether the dissolving of the hydrogen in the liquid phase or the kinetic of the reaction of the biological system is the kinetic limitation of the process. The project ORBIT addresses this question and develops a new trickle-bed reactor for biological methanation, which runs experiments at OTH Regensburg (Fig. 1). Finally, its demonstration will take place at an existing power-to-gas site in Ibbenbüren and feed the gas grid. One goal of the ORBIT project is also the standardization of the biological methanation [3]. Furthermore, some experimental results from a second existing lab-scale reactor are shown.

2. Methodology, Results and Discussion

The most important parameter to characterize and compare the performances of these reactors is the normalized methane production rate (MPR_R). The MPR_R reports the methane produced in the system in standard cubic meters per hour, normalized to the reactor volume V_R and provides information on the productivity of the plant (equation 1). [3]

$$MPR_R = \frac{\dot{V}_{CH_4,out} - \dot{V}_{CH_4,in}}{V_R} \left[\frac{m^3}{h \cdot m^3} \right] \quad (1)$$

Figure 2 illustrates the working principle of the trickle-bed reactor. The fluid and the microorganisms are pumped to the top where they trickle downwards to the bottom of the reactor. The feed gases are injected at the reactor bottom, flow upwards and leave the reactor at the top. The resulting large two-phase interface of the trickles enables the dissolution of the feed gas in the liquid. In batch mode the reactor is filled with H₂ and CO₂ at the beginning of the batch-experiment. While the reaction takes place, the pressure decreases. If the pressure falls below 2 bar(a), the reactor is refilled with H₂ and CO₂. After the time of the batch-experiments the product gas is analyzed and the average MPR_R is calculated. In continuous mode the reactant gases flow constantly into the reactor, are converted to methane and the product gas flows constantly out of the reactor. In the past the reactor was running on a pure biological culture. That means that there is only one specific kind of microorganism. The operation mode for the pure culture experiments were batch mode. Now the reactor runs on a

mixed culture, which was created by adding dissolved waste sludge of a biogas plant to the system. The sludge contains a bright variety of different microorganism in a changing composition. As the mixed culture shows much better results, this is preferred. The here shown mixed culture experiments are in continuous operation mode.

The trickle-bed reactor operates 24/7 to get extensive results and a wide parameter analysis. It was shown, that the pressure and the recirculation rate has an impact on the performance, and that it is strongly important to feed the archaea with nutrition media. Fig. 3 shows a variation of pressure at the trickle-bed reactor with better methane production rate (MPR_R) at higher pressure. Fig. 4 shows the dependence of new nutrition media. After feeding new media (red) the performance raises up to $9.55 \text{ l}\cdot(\text{l}\cdot\text{d})^{-1}$. The maximum purity of methane is up to 96% in continuous mode. The maximum MPR_R is $31 \text{ l}\cdot(\text{l}\cdot\text{d})^{-1}$.

3. Conclusion and Outlook

This work proves that a TBR for the biological methanation is a functional reactor concept. The mixed culture worked better than the pure culture and achieved a MPR_R of $31 \text{ l}\cdot(\text{l}\cdot\text{d})^{-1}$ and a methane purity of up to 96%. The presentation at the 19 International Conference on Polygeneration Strategies will further show a broad analysis of various impacts on the biological methanation in lab-scale experiments with focusing on reactor parameter as pressure, trickles and recirculation rate. Furthermore, the influence of microorganisms, pure vs. mixed culture, and the media is going to be discussed.

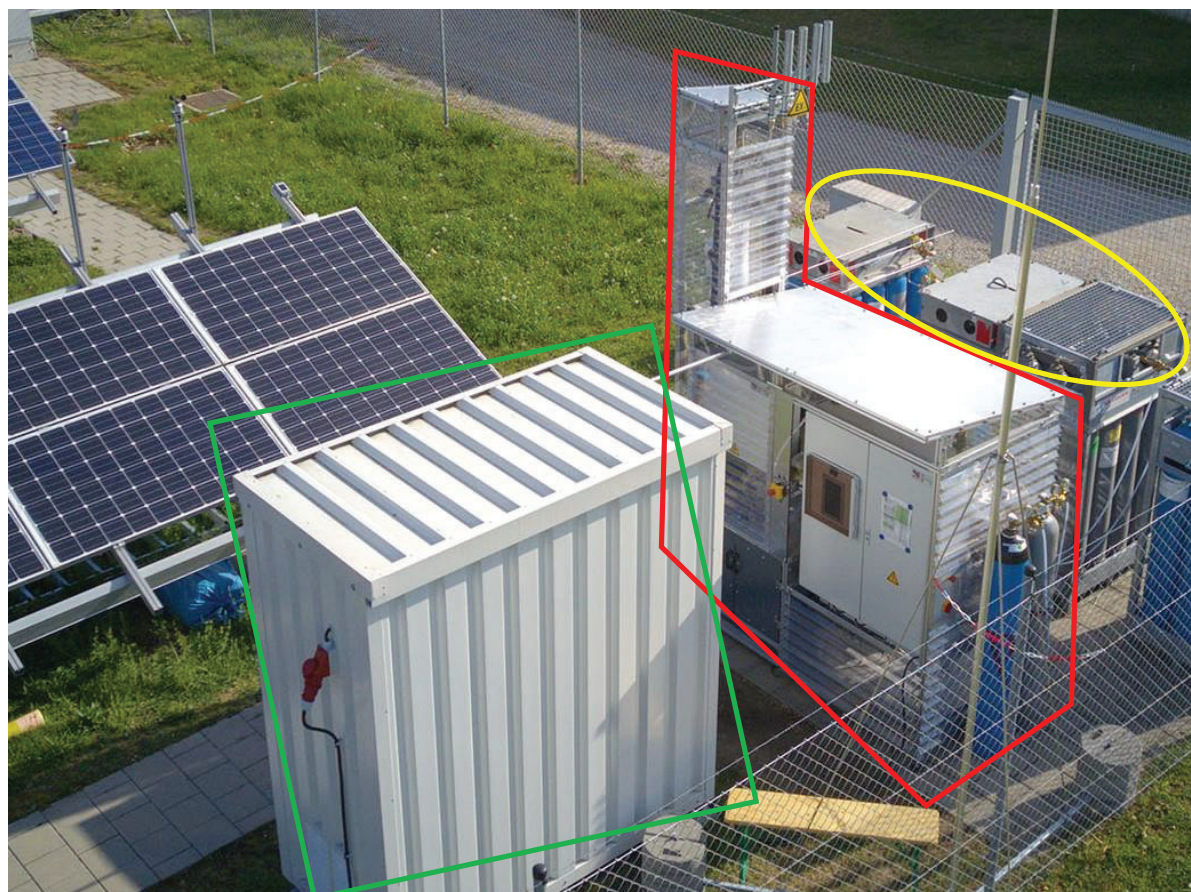


Figure 1: ORBIT reactor for biological methanation; red: trickle-bed reactor system with periphery, yellow: reactant gases, green: container with gas analyzer © Michael Heberl

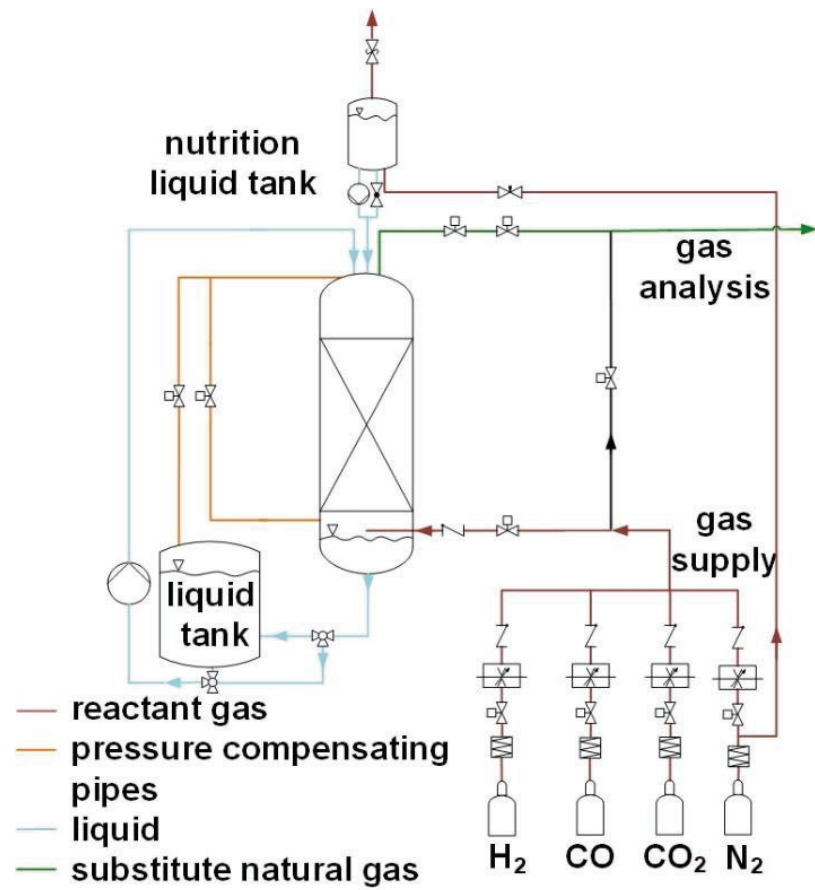


Figure 2: Existing lab-scale trickle-bed reactor at the EVT

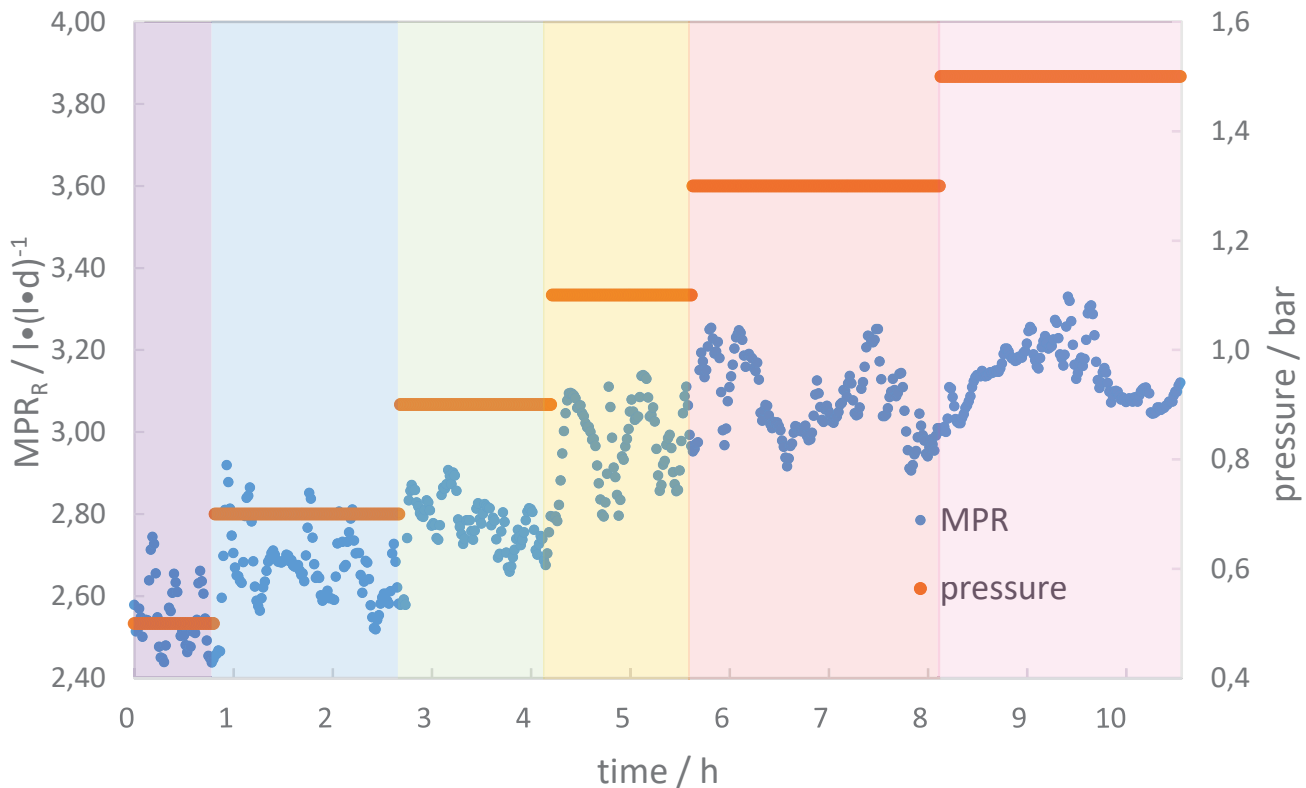


Figure 3: MPR_R over pressure at continuous operation mode with a mixed culture

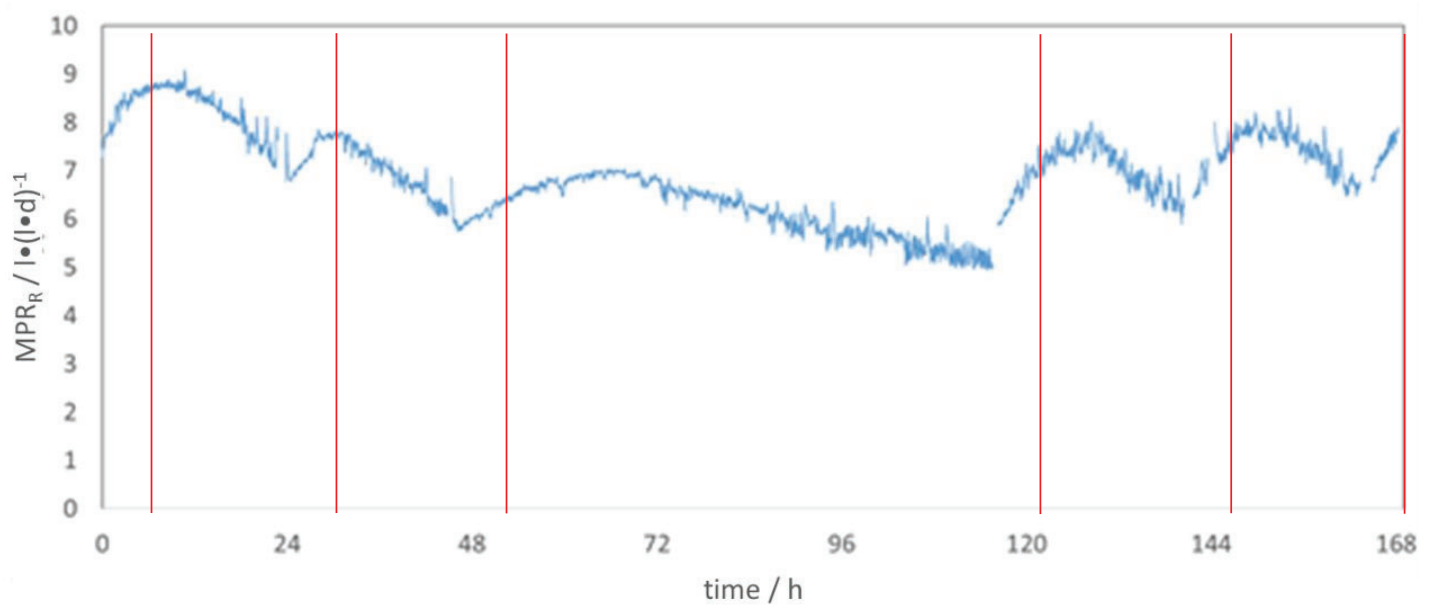


Figure 4: Influence of new media for the MPR_R at continuous operation mode using a mixed culture

- [1] H. Sahm, "Biologie der Methan-Bildung," *Chemie Ing. Tech.*, vol. 53, no. 11, pp. 854–863, 1981.
- [2] K. Bär et al. „Vergleich der biologischen und katalytischen Methanisierung für den Einsatz bei PtG_Konzepten, Fachbericht Power-to-Gas, 2016
- [3] Thema, M.; Weidlich, T.; Hörl, M.; Bellack, A.; Mörs, F.; Hackl, F.; Kohlmayer, M.; Gleich, J.; Stabenau, C.; Trabold, T.; Neubert, M.; Ortloff, F.; Brotsack, R.; Schmack, D.; Huber, H.; Hafenbradl, D.; Karl, J.; Sterner, M. Biological CO₂-Methanation: An Approach to Standardization. *Energies* 2019, 12, 1670.

Acknowledgements

The project this report is based on was supported with the help of the Federal Ministry for Economic Affairs and Energy under the project number 03ET6125B (ORBIT). The sole responsibility for the report's contents lies with the author.

Dynamic Methanation of By-product Gases from Integrated Steelworks

P. Wolf-Zoellner^{1*}, A. R. Medved¹, A. Krammer¹, K. Salbrechter¹, M. Lehner¹

1. Chair of Process Technology and Industrial Environmental Protection, Montanuniversität Leoben, Austria,
*corresponding author: philipp.wolf-zoellner@unileoben.ac.at

1. Introduction and Motivation:

Integrated steelworks are major contributors to global emissions of carbon sources such as carbon dioxide (CO_2). About 27 to 30% of any industrial CO_2 -emissions result from such integrated steelworks. [1, 2] In order to achieve the challenging goals of the Paris climate agreement it is key to work on ways to rigorously reduce these CO_2 -emissions and to incorporate green energy source in the steelmaking process.

The by-product gases accumulating in a steelworks plant, such as the blast furnace gas (BFG), basic oxygen furnace gas (BOFG) and coke oven gas (COG) have a very rich content of CO_2 and CO (carbon monoxide). At the current stage, these by-product gases are stored and utilized internally, but additional fossil energy sources are needed to cover the whole energy demand for any auxiliary energy conversion. (Fig. 1) [3]

One way of re-using certain gas streams and substitute the need of fossil fuels would be through synthesis processes like **methanation** where CO_2 and CO react with hydrogen (H_2), gathered from green energy sources, to methane (CH_4) and vapor.

Although these reactions are well-known, the kinetics and behavior under **dynamic and transient conditions** are yet to be investigated. This is especially important for steelworks processes, as the concentrations and the total volume flow

of the by-product gases vary frequently based on to the related operational working step. Even more, the amount of available hydrogen required for the methanation synthesis is only dynamically available too. It is based on an economically driven electrolyzing unit and the electricity price consequently.

The reaction behavior of a dynamically driven **power to gas** plant needs to be investigated to provide a fundamental base for its implementation in an integrated steelworks plant.

2. Methodology and Experiments

The above-mentioned investigation is carried out within the EU-funded project “*i3upgrade*”. For the necessary experiments under dynamic conditions, the existing pilot rig at the Chair of Process Technology and Industrial Environmental Protection at the Montanuniversitaet Leoben is used, which consists of three reactors, each filled with a commercial Ni-based bulk catalyst, or Ni/ Al_2O_3 wash-coated **honeycomb catalysts**. (Fig. 2) [4]

A series of experiments with synthetic BFG and BOFG has been carried out. To achieve the reaction goal of 100% CO_x conversion, an optimum hydrogen excess rate to stoichiometry was evaluated and applied for dynamic situations as they occur in an integrated steelworks plant. This includes variations in total volume flow of by-product gases, hydrogen

availability as well as dynamic cycle frequency and duration.

3. Conclusion and Outlook

The presentation will contain broad results of lab-scaled methanation experiments conducted under steady state and dynamic conditions representing the cases from an integrated steelwork. The influences on the synthesis, reactor behavior as well as the degradation of the catalyst due to the frequent load changes will be addressed. Furthermore, the performance of the commercial bulk catalyst will be compared with the newly developed wash-coated honeycombs.

4. References

- [1] A review of thermochemical processes and technologies to use steelworks off-gases, W. Uribe-Soto et al., Renewable and Sustainable Energy Reviews 74 (2017), pp. 809-823
- [2] A. Hasanbeigi, 2017, URL: <https://www.globalefficiencyintel.com/new-blog/2017/nfographic-steel-industry-energy-emissions>
- [3] Hauser, A. "i3upgrade – intelligent integrated industries". URL: <https://www.i3upgrade.eu>, 02.04.2019.
- [4] Bieger, P. „Keramische Wabenkatalysatoren zur chemischen Methanisierung von CO₂“. PhD thesis; Austria, 2017.

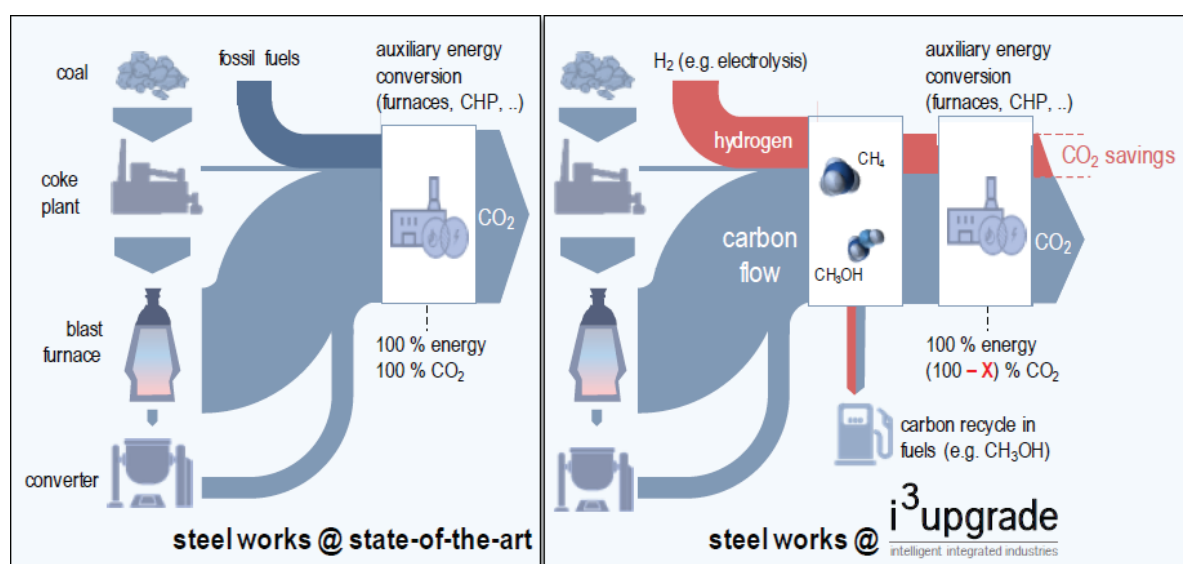


Fig. 1: Upgraded carbon flow in an integrated steelworks plant as anticipated with i3upgrade

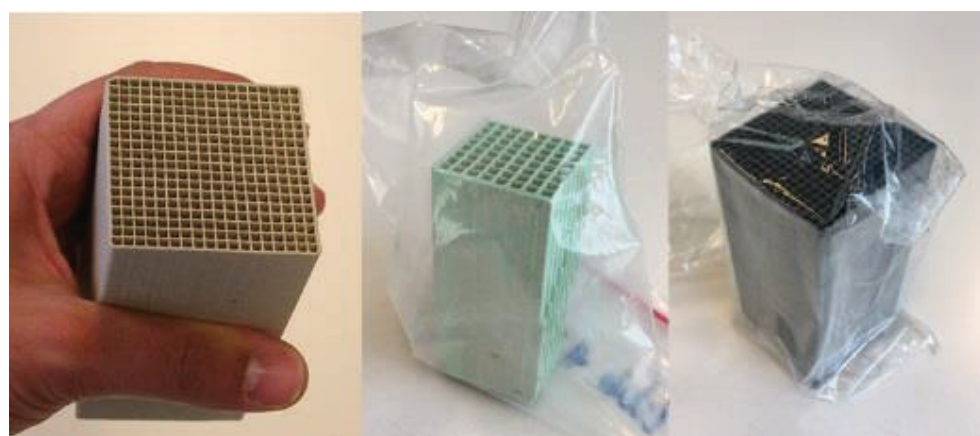


Fig. 2: Honeycomb monoliths (from left to right: raw, wash-coated, used)

Modelling and Simulation Full Papers

1 MW Scale-up of the Advanced Fuel Flexible Dual Fluidized Bed Steam Gasification Process by Process Simulation

F. Benedikt^{1,*}, S. Müller¹, H. Hofbauer¹

1. TU Wien, Institute of Chemical, Environmental and Bioscience Engineering,
Getreidemarkt 9/166, 1060 Vienna, Austria

*corresponding author: florian.benedikt@tuwien.ac.at

Abstract

Through the dual fluidized bed (DFB) steam gasification process, solid feedstock can be converted into a nitrogen-free product gas. Thereby, the DFB steam gasification offers a well-proven technology to produce heat, electricity, secondary liquid or gaseous energy carriers and valuable chemicals from wood as feedstock. DFB steam gasification was demonstrated for the gasification of wood at industrial scale between 8-32 MW fuel power at several sites. However, some of these plants suffered from difficult economic conditions if high-grade wood chips or even pellets were used as solid fuel. During the last years, a main research topic has been the utilization of low-cost residual and waste derived feedstocks. Therefore, a fuel flexible advanced reactor design was developed and constructed with 100 kW fuel power at TU Wien and tested since 2014. On the one hand, utilizing residues and waste fractions as feedstock provides a high potential to produce energy carriers, or commodities in a sustainable, eco-friendly and economic way. On the other hand, these feedstocks often have challenging fuel properties for thermo-chemical conversion processes. Although, various feedstocks were already tested at 100 kW fuel power, further investigations need to be done to prove or disprove operation stability at long-term test runs. For this reason, a scale-up to 1 MW fuel power is suggested to further study the long-term behavior of selected promising feedstock. The aim of this study is to provide design data for a basic engineering and to calculate key indicating parameters of a 1 MW fuel flexible plant.

1. Introduction

Through the dual fluidized bed steam gasification process, solid feedstock can be converted into a nitrogen-free product gas (PG). The medium calorific dry PG consists mainly of hydrogen, carbon monoxide, carbon dioxide, methane and ethylene. Basic information on the DFB process can be found in [1]. The DFB steam gasification offers a proven technology to produce heat, electricity, secondary liquid or gaseous energy carriers and valuable chemicals from wood as feedstock [2].

DFB steam gasification was demonstrated for the gasification of wood at industrial scale between 8-32 MW fuel power at several sites [3]. However, some of these plants suffered from difficult economic conditions if high-grade wood chips or even pellets were used as solid fuel - especially because the wood prices increased significantly over the last decade. **Figure 1** shows the development of wood chip prices in Germany between 2003 and 2018. As indicated, the price for woodchips increased in Germany until 2015 by roughly 110 %. However, the green feed-in tariffs for electricity and district heat from biomass were not adapted accordingly to that price increase, which led to uneconomical operation and plant shut down for many plant operators depending on wood-based fuels. It seems that the last three years of the considered timespan the strong constant upward trend leveled.

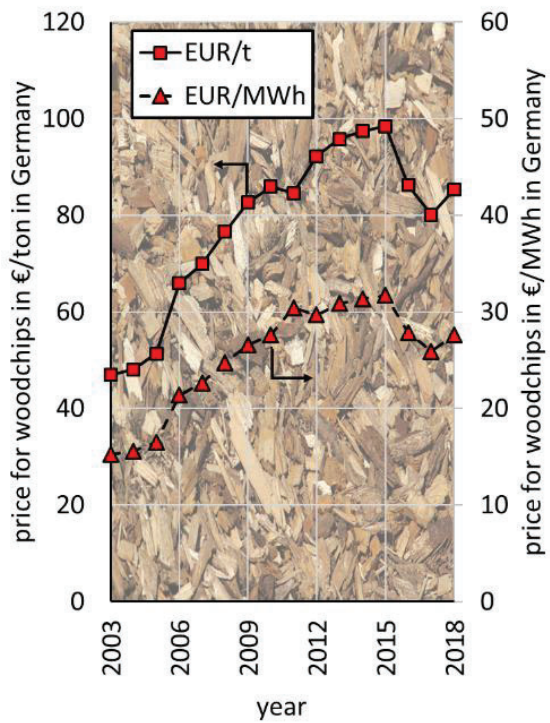


Fig.1: Development of wood chip prices with 35 wt.-% water content in Germany between 2003 and 2018 [4]

Considerations on the DFB steam gasification process showed, that the fuel costs have a significant impact on the economic efficiency [5,6]. **Figure 2** was redrawn from estimations on fuel and product prices and relevant efficiencies for their generation to the current situation for DFB steam gasification at industrial scale in 2018 in Austria, presented by Müller and Hofbauer at the Katowice Climate Change Conference [7]. These rough estimations make it obvious, that the use of wood as fuel currently leads to uneconomic operation and fuel flexible operation with low-cost fuels is a key aspect to deal with.



Fig.2: Rough estimation on fuel and product prices for DFB steam gasification

Therefore, during the last years, a main research topic at TU Wien has been the utilization of low-cost residual and waste derived feedstocks. For this reason, a fuel flexible advanced reactor design was developed and constructed with 100 kW fuel power at TU Wien and tested since 2014. An extensive review on the 100 kW pilot plant is given in [8]. On the one hand, utilizing residues and waste fractions as feedstock provides a high potential to produce energy carriers, or commodities in a sustainable, eco-friendly and economic way. On the other hand, these feedstocks often have challenging fuel properties for thermo-chemical conversion processes. Challenges arising with feedstock properties are mainly caused by:

- a high ash content and/or an undesirable ash melting behavior ,
- a high content of volatile matter, or
- other undesired impurities.

Ash-related problems can lead to poor behavior of the fluidized bed itself or to negative effects on downstream equipment. High contents of volatile matter increase the tar content in the product gas, which can lead to tar condensation during cooling of the product gas in heat exchangers. Both effects can result in reduced operating hours and more intensive maintenance efforts. In addition, higher amounts of sulfur, nitrogen and chlorine in the fuel composition may decrease the product gas quality. Although, various feedstock were already tested at 100 kW fuel power, further investigations need to be done to prove or disprove long-term operation stability. For this reason, a scale-up to 1 MW fuel power is suggested to further study the long-term behavior of selected promising feedstock to minimize the risk for further scale-up considerations.

The aim of this study is to provide design data for a basic engineering and to calculate key indicating parameters of a 1 MW fuel flexible plant.

2. Concept and methodology

The simulation work is based on an intensive literature study, operational data from industrial scale plants [5, 9] and experimental results from the advanced and the classic 100 kW pilot plant [10, 11]. The data are simulated by the use of the process simulation software IPSEpro. Thereby, following fuels were investigated:

- softwood (SW) as standard fuel,
- a waste fuel (WF) with a high share of volatile matter, and
- sewage sludge (SS) as fuel with a high ash content.

The fuel composition as well as test runs at the 100 kW pilot plants are documented in detail in [10, 11]. The use of the simulation software IPSEpro regarding the DFB process and thereby adjusted or calculated performance indicating key figures are explained by Müller et al. [12]. Equation 1 gives the steam-to-fuel ratio (φ_{SF}) and equation 2 the steam-to-carbon ratio (φ_{SC}). Equation 3 gives the product gas yield (PGY), equation 4 the steam-related water conversion (X_{H2O}), and equation 5 the cold gas efficiency (η_{CG}). As no additional fuel is fed into the combustion reactor (CR) the introduction of an overall cold gas efficiency is omitted.

$$\varphi_{SF} = \frac{\dot{m}_{steam,GR} + \dot{m}_{H2O,GR,fuel}}{\dot{m}_{GR,fuel,daf}} \quad (1)$$

$$\varphi_{SC} = \frac{\dot{m}_{steam,GR} + \dot{m}_{H2O,GR,fuel}}{\dot{m}_{C,GR,fuel}} \quad (2)$$

$$PGY = \frac{\dot{V}_{PG}}{\dot{m}_{GR,fuel,daf}} \quad (3)$$

$$X_{H2O} = \frac{\dot{m}_{steam,GR} + \dot{m}_{H2O,GR,fuel} - \dot{m}_{H2O,PG}}{\dot{m}_{steam,GR} + \dot{m}_{H2O,GR,fuel}} \quad (4)$$

$$\eta_{CG} = \frac{\dot{V}_{PG} \times LHV_{PG}}{\dot{m}_{GR,fuel} \times LHV_{GR,fuel}} \cdot 100 \quad (5)$$

In contrast to gasification test runs at the 100 kW pilot plant, the key figures are referenced on the product gas after coarse gas cleaning instead of the outlet of the gasification reactor (GR).

3. Results and discussion

The fuel composition used for simulation is shown in **Table 1**. For softwood, data from fuel analyses from 100 kW test runs [10] were the basis and have been matched with data according to Müller [5] for higher ash, sulfur and nitrogen contents for wood chips instead of pellets. The fuel composition of the waste fraction is a mixture of a shredder light fraction and a municipal solid waste fraction from [10]. The composition of sewage sludge is from [11]. During this study, chlorine was not considered and the remaining species were equalized to 100 wt.-%_{db}.

Figure 3 shows the process flow diagram, which was the basis for the calculations of the DFB gasification system with coarse gas cleaning, redrawn and modified from [5,9]. The applied fuel is dried to 20 wt.-% water content and fed into the gasification reactor, where it is gasified with steam. The water content before drying of softwood and the waste fraction was set to 40 wt.-% and to 65 wt.-% for sewage sludge according to mechanical dewatering.

Tab.1: Fuel composition for simulation

parameter	unit	SW	WF	SS
Water (H ₂ O)	wt.-%	40 (20)	40 (20)	65 (20)
Ash	wt.-% _{db}	1.0	10.1	41.5
Carbon (C)	wt.-% _{db}	50.7	71.5	29.7
Hydrogen (H)	wt.-% _{db}	5.9	10.7	3.7
Oxygen (O)	wt.-% _{db}	42.2	7.0	20.2
Nitrogen (N)	wt.-% _{db}	0.2	0.49	3.9
Sulfur (S)	wt.-% _{db}	0.01	0.15	1.0
Chlorine (Cl)	wt.-% _{db}	n.c.	n.c.	n.c.
LHV*	MJ/kg	14.4	26.9	9.1

* based on 20 wt.-% water content as fed into GR calculated with IPSEpro, n.c.: not considered

The exiting product gas is led through a separator with 80% particle separation efficiency. Downstream the PG is cooled and cleaned with a fabric baghouse filter for particle removal at 180°C with a particle separation efficiency of 99.9%. In the fabric filter, also a tar reduction of 30% was approximated according to measured data from Wolfesberger [13]. After that, a scrubber operated at 40°C with rapeseed methyl ester (RME) as solvent cleans the product gas of its major tar content. The tar separation efficiency was estimated with 80% and no particles are present in the gas exiting the scrubber. Within the scrubber, also 50% of NH₃ is separated. Further gas cleaning is not considered within this study.

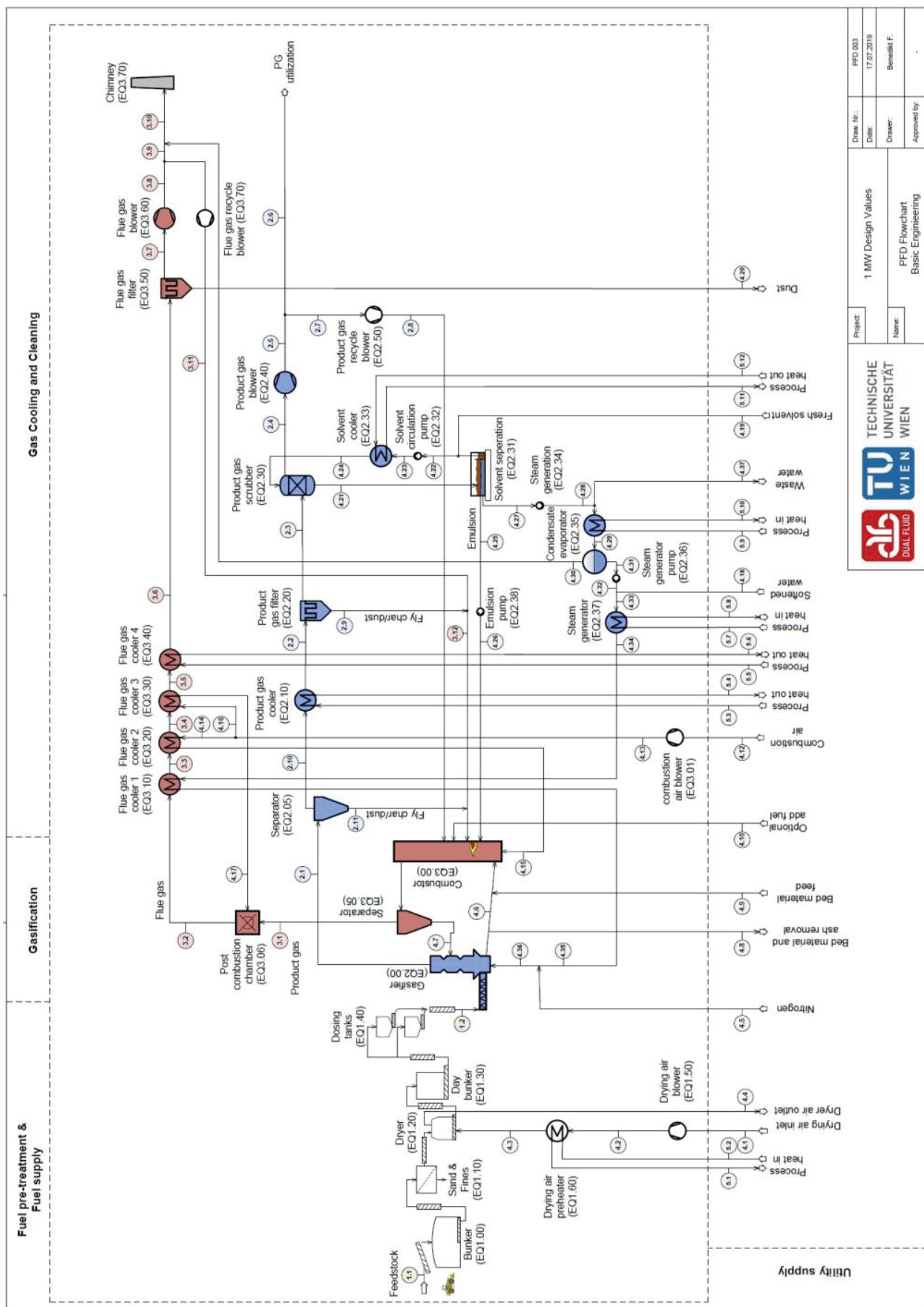


Fig.3: Process flow diagram of the fuel flexible 1 MW advanced DFB steam gasification process

The RME saturated with tar is converted as additional fuel in the combustion reactor. 10% of the evaporated water is removed via the flue gas and the rest is used as gasification agent after steam generation and internal superheating within the flue gas line to 400°C. In addition, the combustion air for the combustion reactor and the post combustion chamber is heated by heat exchangers from the flue gas to 400°C.

Tab.2: Operation parameters

parameter	unit	SW	WF	SS
GR temp.	°C	800	800	800
CR temp.	°C	950	950	950
fuel to GR	MW	1.0	1.0	1.0
fuel to GR	kg/h	249	134	396
fuel to CR	MW	0.0	0.0	0.0
heat losses*	%	5	5	5
fresh RME	kg/h	2	2	2
fresh bed material	kg/h	5	5	5
nitrogen**	Nm³/h	5	5	5
φ_{SF}	kg/kg _{daf}	0.55	1.20	1.0
φ_{SC}	kg/kg	1.07	1.51	1.97
air ratio λ in CR	kg/kg	1.25	1.25	1.25

*based on fuel input into GR,

**nitrogen used for purging of the fuel hopper system and PG filter

Tab.3: Product gas composition and impurities after the gasification reactor

parameter	unit	SW	WF	SS
H ₂ O	vol.-%	28.8	34.1	51.1
H ₂	vol.-% _{odb}	46.3	46.6	39.1
CO	vol.-% _{odb}	21.0	12.5	16.5
CO ₂	vol.-% _{odb}	21.1	14.7	20.9
CH ₄	vol.-% _{odb}	8.8	19.2	7.9
C ₂ H ₄	vol.-% _{odb}	0.50	3.1	2.4
C ₂ H ₆	vol.-% _{odb}	0.05	0.35	0.09
C ₃ H ₈	vol.-% _{odb}	0.0	0.0	0.56
N ₂	vol.-% _{odb}	2.2	3.1	4.1
H ₂ S	ppm _v	58	684	11540
NH ₃	ppm _v	475	4375	73913
tar	g/Nm ³	5	100	5
char	g/Nm ³	20	20	20
dust	g/Nm ³	20	100	300

The outlet temperatures of process heat from flue gas cooler 4 and the product gas cooler are set to a difference of 10°C to the entering flue gas or product gas, respectively. The flue gas from the combustion reactor is fed to a post combustion chamber to ensure complete combustion and then cooled to 150°C prior to the flue gas filter. Particles removed by the flue gas filter exit the system. The main operation parameters and input values applied for calculation of the 1 MW plant are shown in **Table 2**.

Table 3 shows the product gas composition, which was calculated via IPSEpro and impurities of the PG: tar, fly char and dust, which are set values. High amounts of sulfur and nitrogen in the fuel led to a low product gas quality with high amounts of ammonia and hydrogen sulfide. **Table 4** shows the performance indicating key figures, which were calculated with IPSEpro.

Tab.4: Performance indicating key figures

parameter	unit	SW	WF	SS
PGY	Nm ³ _{db} /kg _{waf}	1.2	1.7	1.0
X _{H2O}	kg _{H2O} /kg _{H2O}	0.29	0.41	0.13
η_{CG}	%	73.4	70.8	63.3

Figure 4 shows the energy flow diagram based on the lower heating value for the gasification of 1 MW softwood with 20 wt.% water content and coarse gas cleaning calculated by IPSEpro and compiled with the software e!Sankey pro. The continuous addition of fresh rapeseed methyl ester (RME) of 2 kg/h, which accounts for 20.5 kW of chemical energy flow, is depicted as additional fuel input. Besides, the steam input is from an external source with 44.7 kW. Thereby, a product gas with 734.4 kW of chemical energy and 93 kW of thermal energy was calculated. Downstream of the coarse gas cleaning 2.5 kW of chemical energy are

present in the tar within the PG. After internal steam superheating and pre-heating of the combustion air to 400°C, 101.3 kW of heat are left over within the flue gas cooler 4 (cf. **Figure 3**) at 657°C. The product gas cooler can provide 92.7 kW of heat at 790°C. Thus, an internal steam generation could be provided and 149.6 kW of thermal energy flow would still be available. For the drying of the feedstock from 40 wt.-% to 20 wt.-%, 59.3 kW of heat flow would be needed for water evaporation, which is not depicted within **Figure 4**. For this, also a part of the low temperature heat from the

solvent cooler at 55°C with 59.1 kW could be used. However, at state-of-the-art combined heat and power plants with the DFB process the low-temperature heat from solvent cooling is not utilized. Losses of chemical and thermal energy derived from the DFB reactor system, flue gas leaving the plant at 150°C, ash and bed material attrition, ammonia and waste water account for 74.8 kW.

Figure 5 & 6 show the energy flow diagrams for the use of waste fraction and sewage sludge, respectively.

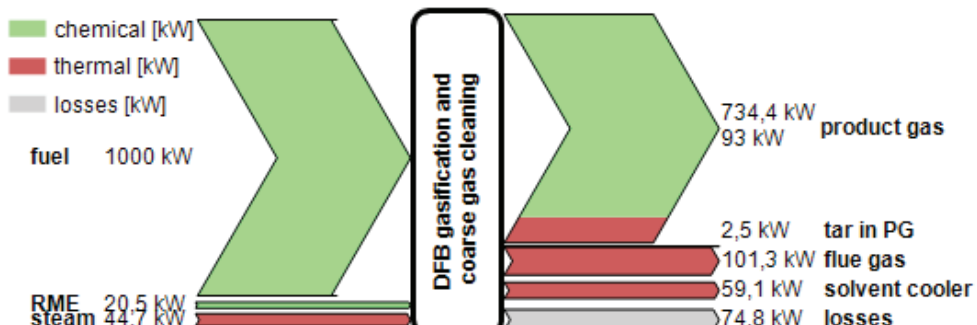


Fig.4: Energy flow diagram 1 MW softwood

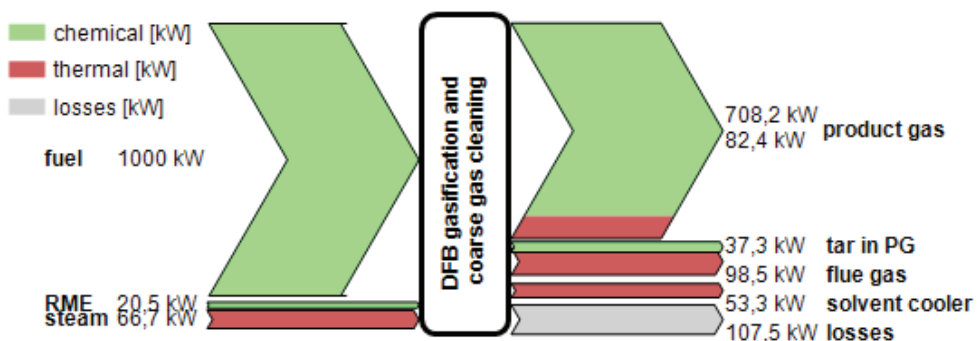


Fig.5: Energy flow diagram 1 MW waste fraction

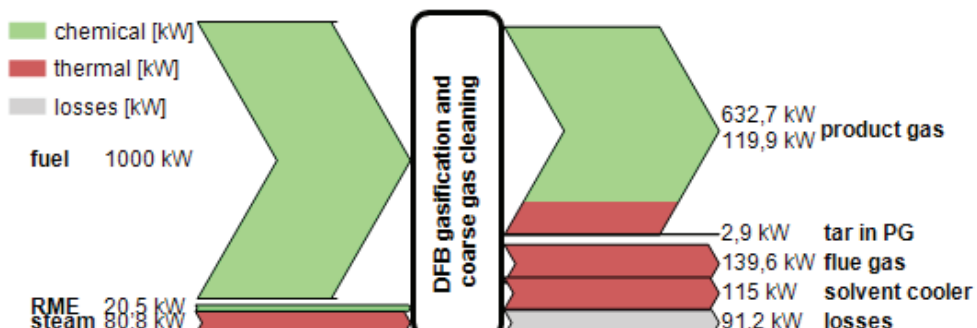


Fig.6: Energy flow diagram 1 MW sewage sludge

Due to higher amounts of steam necessary for the more challenging fuels, increased energy inputs for steam production are needed. However, also for these fuels, an internal steam generation would be feasible. The higher tar yield in the PG for the gasification of the waste fraction is obvious.

The amount of energy flow for drying, which is not presented within the figure was calculated with 31.8 kW for the waste fraction and 350.1 kW for the sewage sludge. As for the waste fraction, an internal utilization of thermal energy for drying is applicable, for the sewage sludge an external heat source or a partly utilization of the product gas needs to be applied.

4. Summary, Conclusion and Outlook

DFB systems were used for energy conversion technologies to supply electricity and heat or synthetic natural gas at industrial scale between 8-32 MW fuel input power. However, most plants suffered from difficult economic conditions due to the increasing fuel prices for woody biomass over the last decades and static green feed-in tariffs. Therefore, the investigation of fuels with low prices was a major focus over the last years at TU Wien. However, some fuels have challenging properties for thermochemical conversion. While test runs for several hours at a 100 kW fuel input scale did not lead to operational problems, it is difficult to make reliable statements on long-term operation for some of the investigated fuels. Therefore, a scale-up to 1 MW fuel input is suggested to minimize the risk for further scale-up considerations.

Experimental data and extensive knowledge of process simulation offered the basis for this study to provide the data for the gasification of 1 MW softwood as standard fuel, a waste fraction as fuel with a high volatile matter content and sewage

sludge as fuel with a high ash content. With the use of process simulation, mass- and energy balances were calculated and performance indicating key figures are presented. Hence, design data for a basic engineering of an advanced fuel flexible 1 MW DFB steam gasification plant including coarse gas cleaning are presented. An extensive gas cleaning for other synthesis routes is not part of this study but should be investigated in the future.

Abbreviations

CR	combustion reactor
daf	dry and ash-free
db	dry basis
DFB	dual fluidized bed
GR	gasification reactor
IPSEpro	equation-oriented process simulation software
LHV _{GR,fuel}	lower heating value of fuel to GR (kJ/kg)
LHV _{PG}	lower heating value of dry and char- and tar-free PG (kJ/Nm ³ _{db})
$\dot{m}_{GR,fuel}$	mass flow of fuel to GR (kg/s)
$\dot{m}_{C,GR,fuel}$	mass flow of carbon in fuel to GR (kg/s)
$\dot{m}_{GR,fuel,daf}$	mass flow of dry and ash-free fuel to GR (kg _{daf} /s)
$\dot{m}_{H2O,GR,fuel}$	mass flow of water in fuel to GR (kg/s)
$\dot{m}_{H2O,PG}$	mass flow of water in PG (kg/s)
$\dot{m}_{steam,GR}$	mass flow of steam to GR (kg/s)
PG	product gas
PGY	product gas yield (Nm ³ _{db} /kg _{fuel,daf})
ppm _v	parts per million by volume
Q _{loss}	radiative heat losses (kW)
RME	rapeseed methyl ester, bio-diesel
SS	sewage sludge
SW	softwood
TU Wien	Vienna University of Technology
vol.-% _{db}	percent by volume on dry basis
vol.-%	percent by volume
\dot{V}_{PG}	dry volumetric product gas flow (Nm ³ _{db} /s)
wt.-%	percent by weight, percent by mass
X _{H₂O}	steam-related water conversion (kg _{H2O} /kg _{H2O})
η_{CG}	cold gas efficiency (%)
λ	air-fuel equivalence ratio (kg/kg)
φ_{SC}	steam to carbon ratio (kg _{H2O} /kg _C)
φ_{SF}	steam to fuel ratio (kg _{H2O} /kg _{fuel,daf})

5. Acknowledgements

The presented study did not receive any specific funding

6. References

- [1] J. Karl, T. Pröll. Steam gasification of biomass in dual fluidized bed gasifiers: A review. *Renewable and Sustainable Energy Reviews.* **98** (2018) p64-78
- [2] R. Rauch, J. Hrbek, H. Hofbauer. Biomass gasification for synthesis gas production and application oft he syngas. *Wiley Interdisciplinary Reviews: Energy and Environment.* **3** (2013) p343–62
- [3] M. Kuba, H. Hofbauer. Experimental parametric study on product gas and tar composition in dual fluid bed gasification of woody biomass. *Biomass and Bioenergy.* **115** (2018) p35-44
- [4] www.carmen-ev.de/infothek/preisindizes/hackschnitzel/jahresmittelwerte accessed on 10.07.2019
- [5] S. Müller. Hydrogen from Biomass for Industry - Industrial Application of Hydrogen Production Based on Dual Fluid Gasification. Doctoral thesis, TU Wien (2013)
- [6] J. Corella, J.M. Toledo, G. Molina. A review on dual fluidized-bed biomass gasifiers. *Ind. Eng. Chem. Res.* **46** (2007) p. 6831–9
- [7] S. Müller, H. Hofbauer. Thermochemical conversion of biomass residues to green fuels , electricity and heat. COP24, Katowice: (2018) p. 15.
- [8] J.C. Schmid, F. Benedikt, J. Fuchs, A.M. Mauerhofer, S. Müller, H. Hofbauer. Syngas for biorefineries from thermochemical gasification of lignocellulosic fuels and residues - 5 years' experience with an advanced dual fluidized bed gasifier design. *Biomass Conversion and Biorefinery*, first online: 16 August 2019, <https://doi.org/10.1007/s13399-019-00486-2>
- [9] V. Wilk, H. Hofbauer. Analysis of optimization potential in commercial biomass gasification plants using process simulation. *Fuel Processing Technology* **141** (2016) p.138-47
- [10] F. Benedikt, J.C. Schmid, J. Fuchs, A.M. Mauerhofer, S. Müller, H. Hofbauer. Fuel flexible gasification with an advanced 100 kW dual fluidized bed steam gasification pilot plant. *Energy* **164** (2018) p. 329-43
- [11] J.C. Schmid, U. Wolfesberger, S. Koppatz, C. Pfeifer, H. Hofbauer. Variation of feedstock in a dual fluidized bed steam gasifier—fluence on product gas, tar content, and composition. *Environmental Progress & Sustainable Energy* **31** (2012) p. 205-15
- [12] S. Müller, J. Fuchs, J.C. Schmid, F. Benedikt, H. Hofbauer. Experimental Development of Sorption Enhanced Reforming by the Use of an Advanced Gasification Test Plant. *International Journal of Hydrogen Energy* **42** (2017), p. 29694-707
- [13] U. Wolfesberger. Profiling tar behavior in dual fluidized bed biomass steam gasification. Doctoral thesis, TU Wien (2013)

Investigating tar formation at low pressures in wood gasification systems, applying a novel thermo-chemical simulation model

G. Boiger^{1*}, V. Buff¹, A.Zubiaga¹, A.Fassbind², P.Caels³

1. Zurich University of Applied Sciences, Institute of Computational Physics, Wildbachstrasse 21, 8409 Winterthur, Switzerland
2. Zurich University of Applied Sciences, Zentrum für Produktentwicklung, Lagerplatz 22, 8400 Winterthur, Switzerland
3. Aberta Nova S.A., Rua da Fonte n 5, 7570-622 Melides, Portugal

*Corresponding author, gernot.boiger@zhaw.ch

Abstract

Even-though wood gasification remains a promising technology regarding de-centralized sustainable energy supply, its main limitations, namely the issues of unsteady operation, excessive tar-formation and consequential high maintenance requirements, have never been fully overcome. In order to tackle these deficiencies and to increase the understanding of thermo-chemical wood-gas phase reaction dynamics, a numerical model has been created. After validating the simulator against comparable software, it has been applied to predict and thus understand tar-formation phenomena within a small experimental co-current gasification system. This work particularly focuses on the investigation and minimization of tar-formation phenomena within low-pressure zones (e.g. downstream of valves) at temperatures $T \leq 500\text{K}$. Model-based analysis has led to a range of recommended measures, which reduce the occurrence of tars in low-pressure zones. Said recommendations are: i) Decrease gas residence time and ii) increase temperatures in low-pressure zones; iii) Increase hydrogen to carbon ratio as well as iv) oxygen to carbon ratio in the wood gas. While measures i) and ii) require modifications to the plant and/or process itself (e.g. by installing modified pipes or by re-circulating thermal energy via heat-exchangers), measures iii) and iv) can be implemented either by removing coal from the reaction zone or by adding either water or process air to the process.

1. Introduction

The method of gasifying wood via drying, pyrolysis, reduction, consequential partial oxidation to combustible *wood-gas*, gas purification, feeding a gas motor and producing electricity via a generator, has been applied for decades. Still wood gasification remains a promising technology regarding future, de-centralized, sustainable energy supply. However, the main limitations of the technology, namely the issue of excessive tar formation and consequential high maintenance requirements, have never

been fully overcome. In the course of a long term effort aiming to develop a low-tar, low-maintenance gasification device, capable of sustainably gasifying any wood-based cellulose, it has become obvious that a thorough understanding of thermo-chemical gas-phase reaction dynamics within the reactor, as well as within the gas-purification system is imperative. Thus a numeric model to account for wood-gas-phase dynamics as well as thermo-chemical equilibrium states has been considerably advanced from an original version presented in [1].

After validating the simulator based on results derived from comparable well-known thermo-dynamic solvers, it has been applied to explain, predict and thus understand tar-formation phenomena within an experimental wood-gasification plant yielding approximately 15kW of thermal- as well as approximately 3kW of electrical energy. A particular focus within this work is laid on the investigation and minimization of tar formation as well as condensation phenomena, in the light of gradually reducing temperatures as well as sudden pressure drops. Phenomena of the latter kind have been observed extensively within the mentioned experimental gasification-device, downstream of valves, bents or any gas-flow obstacles within temperature zones below 500K. These condensation events impeach the stationary function of the whole process, such that ultimately frequent maintenance stops are required. Said observations correspond to reports from other small- to large-scale gasification systems all over the world.

Model based analysis of tar condensation in low-temperature, low-pressure zones has now lead to: i) The assurance that a theoretical framework based on dynamically simulating thermo-chemical reactions thus minimizing the Gibbs Free Energy of wood-gas systems, can predict the very same qualitative increase in tar formation at low-pressure, which is observed in real-life; ii) A thorough understanding of these effects; iii) The recommendation of a range of constructive and process-based measures to reduce the occurrence of tars, in order to considerably prolong maintenance periods.

2. Concept and Methodology

Basic Modeling Concept

Based on system-dynamic principles, the newly developed wood-gas phase

simulator is inspired by a unifying perspective on general physical phenomena as basically described within Gibbs Fundamental Equation (Eqn.1), where a change in global energy of any system dE is attributed to the sum of any physical potentials φ_j times the change of respectively attributed conservative quantities $d\Psi_j$, [6]. In the face of thermo-chemical investigation, the global energy change becomes a change of total Gibbs Free Energy per chemical species ΔG_i , the driving potential specializes to the species-specific molar Gibbs Free Energy \underline{G}_i and the conservative property becomes the total amount of moles per chemical species N_i (Eqn.1).

$$dE = \sum_j \varphi_j d\Psi_j = dG_i = - \sum_i \underline{G}_i dN_i \quad \text{Eqn.1}$$

In addition the local temperature T , the molar gas-phase composition x_i and local pressure p have an impact on the molar Gibbs Free Energies of each species and will cause deviations from their standard states $^\ominus$ (see Eqn.2).

$$\Delta \underline{G}_i(T, p, x_i) = \Delta \underline{G}_i^\ominus(T, p^\ominus) + TR \ln(p \cdot x_i / p^\ominus) \quad \text{Eqn.2}$$

The knowledge of molar Gibbs Free Energies of formation in standard state $\Delta \underline{G}_i^\ominus$ calls for a calculation of molar standard entropies- and enthalpies of formation, which in turn require the implementation of the proper thermodynamic coefficients for each species. The latter were extracted from [8].

A balance of species specific molar Gibbs Free Energies with respect to stoichiometric constants γ_{ji} for species i and reaction j , is the basis for calculating prevailing molar Gibbs Free Energies of reaction $\Delta \underline{G}_{R,j}$ according Eqn. 3.

$$\Delta \underline{G}_{R,j}(T, p, x_i) = \Delta \underline{G}_{R,j}^\ominus(T, p^\ominus) + TR \sum_i \ln(p \cdot x_i^{\gamma_{ji}} / p^\ominus) \quad \text{Eqn. 3}$$

Any modeled chemical reaction j is driven by a non-zero molar Gibbs Free Energy of reaction and is governed in speed by approximate models based on Arrhenius Kinetics as provided in [2] and [4]. The chosen approach rather relies on relative inter-reaction-comparison than on absolute reaction rates, whereby a more detailed description is provided in [1] and [3].

Fig.1 presents a graphical interpretation as well as a very condensed and generalized version of the underlying modeling scheme. Hereby the rectangular containers represent conservative quantities Ψ_j , the filling heights of these containers are driving potentials φ_j and their cross sectional floor areas are system-capacities κ_j . In addition the arrows with solid dots are fluxes of the conservative quantities I_{Ψ_j} , single dots are information processing units (e.g. equations) and the dashed arcs are conveyors of information. Furthermore N_{tot} and N_i are total- and species-specific amounts of molecules respectively.

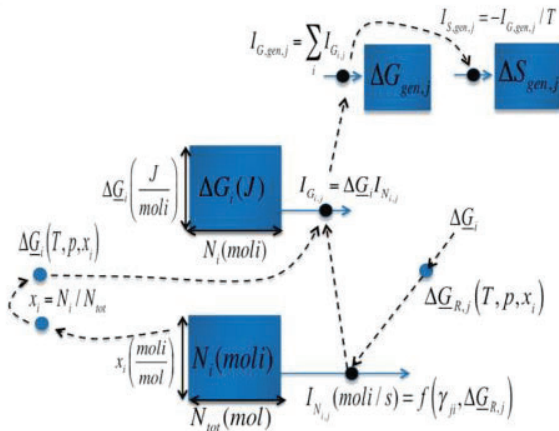


Fig.1: Graphic interpretation of the essentials of the underlying modelling scheme where i is any chemical species and j any chemical reaction.

A mathematical interpretation of the graphic solver concept within Fig.1 amounts to a series of coupled ordinary 1st order differential equations according

Eqn.4 and Eqn.5, which combine with the coupling relations within Eqn.2 and Eqn.3.

$$\frac{dN_i}{dt} = \sum_j I_{N_{i,j}} (\gamma_{ji}, \Delta G_{R,j}) \quad \text{Eqn.4}$$

$$\frac{dG_i}{dt} = \sum_j I_{G_{i,j}} = \sum_j \Delta G_i \cdot I_{N_{ij}} \quad \text{Eqn.5}$$

The differential equations are discretized with respect to time; a linear system of equations is assembled and numerically solved by a four-step Runge-Kutta scheme [9].

Chemical Species and Reactions

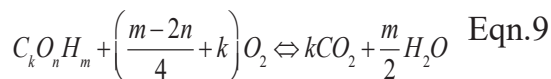
The simulation model considers the following interacting chemical species: coal C(s), water H₂O(g), methane CH₄(g), carbon-dioxide CO₂(g), carbon-monoxide CO(g), hydrogen H₂(g) and naphthalene C₁₀H₈(g). Thereby naphthalene is used to represent any tar components. The reason for choosing naphthalene, as representative for a wide range of tar-molecules, is its relatively high condensation temperature. If a gasification system is designed such that occurring naphthalene will not condensate, then it is likely that other tar components with lower condensation temperatures will not condensate either.

Within the simulation model the above mentioned chemical species interact in terms of the following chemical reactions: heterogeneous- i) Boudouard (Eqn.6), ii) Methanation (Eqn.7) and iii) Steam-Carbon (Eqn.8) reactions.

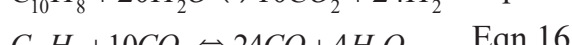
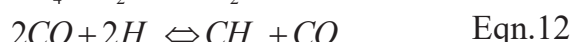


Those mechanisms occur in combination with a iv) variety of possible oxidation reactions, which can be summarized as

seen in Eqn.9, where k, n and m are the relative stoichiometric amounts of carbon-, oxygen- and hydrogen atoms respectively.



While the gasification-reactions cited in Eqn.6 to Eqn.9 correspond to approaches for modelling wood-gas equilibria found in standard literature (e.g. [2]), the hereby-presented model considerably extends this spectrum by a series of gas phase- as well as naphthalene reactions, namely: homogeneous- v) Steam-Carbon (Eqn.10), vi) Methanation (Eqn.11) and vii) Boudouard (Eqn.12) reactions as well as naphthalene-based viii) Methanation (Eqn.13), ix) Steam-Carbon (Eqn.14, Eqn.15) and x) CO₂/CO-conversion (Eqn.16, Eqn.17) reactions.



Solver Validation

The solver has been validated by comparing its results to a well-known approach based on calculating chemical equilibria by minimization of global Gibbs Free Energy as well as minimizing deviations in atomic balances by the introduction and consequential minimization of a LaGrange function L (see Eqn.18), [1], [5], [7].

$$L = \sum_i \Delta G_i + \sum_j \lambda_j \sum_i (a_{i,j} N_i - b_j^0) \quad \text{Eqn.18}$$

The LaGrange function consists of two components: one expresses the sum of all Gibbs Free Energies of formation ΔG_i of all molecular species i, while the other stands for the j atomic species balances. Thereby λ_j and b_j^0 are the LaGrangian Multiplier and the input rate of atomic species j respectively, $a_{i,j}$ is the number of atoms j per molecular species i and N_i is the total number of molecules per molecular species.

Fig.2 compares the results of the LaGrange approach to the hereby presented system-dynamic solver in terms of calculated tar-free homogeneous wood-gas equilibria compositions at $p=10^5\text{Pa}$, an oxygen to hydrogen ratio of $R_{O/H}= 1$ and a temperature range of $375\text{K} \leq T_p \leq 1350\text{K}$. It clearly shows 1:1 correspondence of the results. Additional validation has been presented in [1] and has been observed when comparing hereby-recommended measures to reduce tar in low-pressure zones (see chapter 3), with an experimental wood-gasification system.

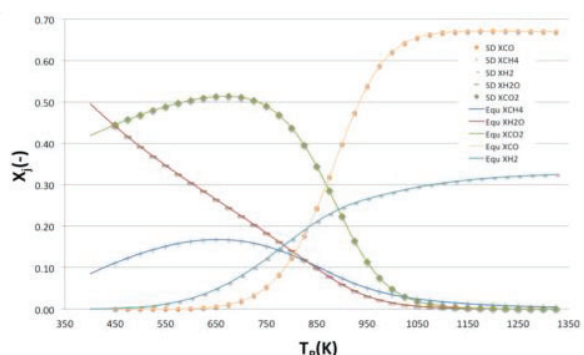


Fig.2: Wood-gas equilibria compositions $x_i(-)$ at $p=10^5\text{Pa}$, $R_{O/H}= 1$ versus process temperature $375\text{K} \leq T_p \leq 1350\text{K}$, calculated by LaGrangian equilibrium solver (“Equi x_i ”) and system dynamic solver (“SD x_i ”).

3. Results and Discussion

Based on the, thus validated, thermochemical model, a dimensionless time-line

of wood-gas being produced, purified and sucked towards the engine can be simulated. The solver qualitatively predicts shifts in species concentration as temperature- and pressure decrease along the wood-gas flow path. On this basis the following measures are recommended to minimize tar occurrence in low-pressure zones: i) Decrease gas residence time and ii) increase temperatures; iii) increase hydrogen to carbon ratio $R_{H/C}$ as well as iv) oxygen to carbon ratio $R_{O/C}$ in the wood gas. While measures i) and ii) require modifications to the plant- and process design itself (e.g. smaller pipes or re-circulation of thermal energy via heat-exchangers), measures iii) and iv) can be implemented by either removing coal from the reaction zone or by adding either water or process air to the process.

In the following, simulation results are presented, which lead to the recommended measures formulated above.

Measure i): Decrease gas residence time

The model does not depict chemical reaction kinetics quantitatively but qualitatively and in relative relation to each other. Still, simulations are able to show that lower-pressure can enhance naphthalene production according Eqn.13 to Eqn.17 significantly. Fig.3 demonstrates an exemplary simulation run, where lower pressures lead to faster creation of naphthalene as compared to a high-pressure case. However, the simulation-run behind Fig.3 also demonstrates that pressure differences do not necessarily have to yield a change in final equilibrium composition of naphthalene.

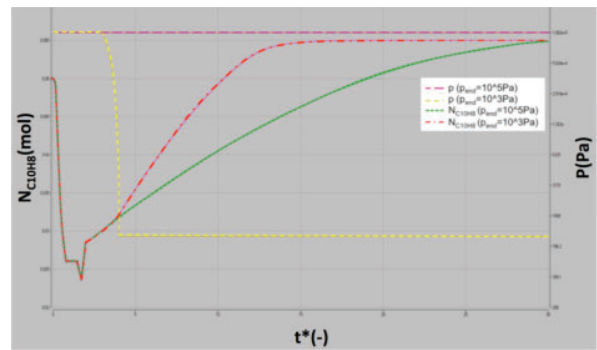


Fig. 3: Simulated absolute amount of naphthalene N_{C10H8} (mol) (case i: green; case ii: red) in wood-gas reactions versus dimensionless time $t^*(-)$, for two cases where i) pressure (purple) remains at 10^5 Pa and ii) pressure (yellow) drops from 10^5 Pa to 10^3 Pa within dimensionless residence time window $3 \leq t^* \leq 4$. In both cases temperature drops from $T=1200K$ to $T=500K$ within dimensionless residence time window $1.5 \leq t^* \leq 2$. In the low-pressure case ii) (purple), naphthalene is more readily produced along the wood-gas flow path than in the high-pressure case i) (green), while the final equilibrium state remains the same in terms of naphthalene content.

On the basis of being able to simulate exemplary outcomes like this, it is fair to assume that process condition windows exist in real-life, which lead to similar effects in actual gasification systems. The obvious counter measure to avoid tar-condensation within piping systems in the context of this phenomenon is: de-increase gas residence time in critical low-pressure zones.

Measure ii): Increase temperatures

The recommendation to reduce tar condensation in low-pressure zones by increasing local temperatures does not require simulation but is an obvious counter-measure to prevent any condensation. However, increasing temperatures is just a remedy to prevent existing tars from condensation, while

measures i), iii) and iv) are meant to prevent or at least reduce tar formation itself.

Measure iii): Increase hydrogen to carbon ratio $R_{H/C}$

Selected case studies were made to simulate the effect of varying hydrogen to carbon ratios within the fuel-input (e.g. cellulose plus additives) on the naphthalene content of the wood-gas. Fig.4 shows the comparison of three simulation runs where wood-gas with varying $R_{H/C}$ ratios was exposed to temperature- and pressure drop. According to this prediction the amount of naphthalene in equilibrium decreases with increasing $R_{H/C}$. The case with the lowest $R_{H/C}$ yields highest amounts of naphthalene in the final equilibrium state. Furthermore the pressure drop causes a clearly discernable spike in naphthalene content (see $t^* \geq 4$), which points to the correspondence between calculated results and experimentally observed effects.

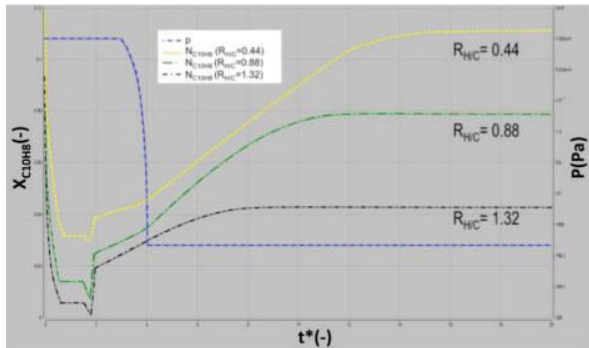


Fig. 4: Simulated relative amount of naphthalene $x_{C10H8}(-)$ in wood-gas versus dimensionless time $t^*(-)$, for three cases where $R_{H/C}$ is set to 0.44 (yellow), 0.88 (green) and 1.32 (black) respectively, $R_{O/C}=0.706$, prescribed pressure (blue) drops from $p=10^5\text{Pa}$ to $p=10^3\text{Pa}$ within dimensionless residence time window $3 \leq t^* \leq 4$ and temperature drops from $T=1200\text{K}$ to $T=500\text{K}$ within $1.5 \leq t^* \leq 2$.

Fig.5 depicts a broader perspective on expected gas-phase compositions including naphthalene content, with increasing $R_{H/C}$. The study reveals that naphthalene content in equilibrium shows a peak at $R_{H/C} \approx 0.49$ and decreases continuously with further increase of the hydrogen to carbon ratio $R_{H/C} > 0.49$. Said peak shall hereby be referred to as *methane-emergence-threshold* since it corresponds with the appearance of methane, which is only present in equilibria compositions featuring $R_{H/C} > 0.49$. Above this threshold, additional hydrogen is apparently used rather for the formation of additional methane, than for naphthalene. Below the *methane-emergence-threshold* however, additional hydrogen will favor naphthalene formation.

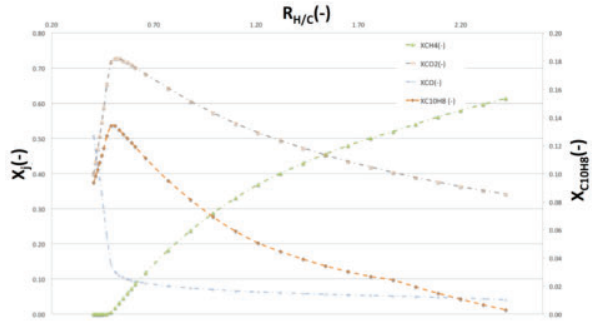


Fig. 5: Simulated wood gas equilibrium composition $x_j(-)$ with the molar fraction of naphthalene $x_{C10H8}(-)$ being highlighted on the right axes and with $x_{H_2}(-)$ and $x_{H_2O}(-)$ being omitted because they are below $1e-3$, versus ratio of hydrogen to carbon $R_{H/C}$. In all cases ratio of oxygen- to carbon $R_{O/C}=0.706$, prescribed pressure drops from $p=10^5\text{Pa}$ to $p=10^3\text{Pa}$ within dimensionless residence time window $3 \leq t^* \leq 4$ and temperature drops from $T=1200\text{K}$ to $T=500\text{K}$ within $1.5 \leq t^* \leq 2$.

Based on these results the authors recommend the increase of $R_{H/C}$ in the gasification reactor well beyond 0.49 in order to reduce tar content in low-pressure zones. This could be achieved e.g. by

either removing coal, which would otherwise continue to participate in gasification reactions (see Eqn.6 to Eqn.8) from the reaction zone, or by adding controlled amounts of water.

Measure iv): Increase oxygen to carbon ratio $R_{O/C}$

Selected case studies were also made to simulate the effect of varying oxygen to carbon ratios within the fuel-input on naphthalene content of the wood-gas. Fig.6 shows the comparison of three simulation runs where wood-gas with varying $R_{O/C}$ ratios is exposed to temperature- and pressure drop. According to this prediction the amount of naphthalene in equilibrium decreases with increasing $R_{O/C}$. As with $R_{H/C}$ the case with the lowest $R_{O/C}$ yields highest amounts of naphthalene in the final equilibrium state. Again the pressure drop causes a clearly discernable spike in naphthalene content, just as observed in real-life gasification systems.

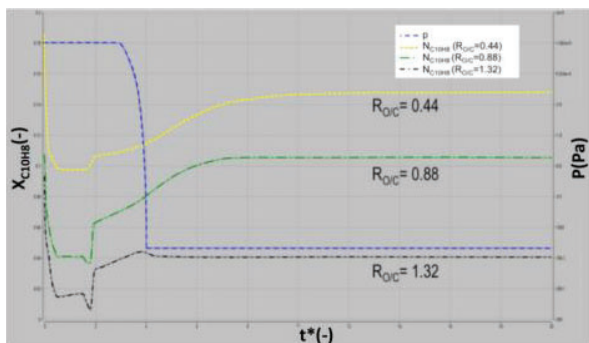


Fig. 6: Simulated relative amount of naphthalene $x_{C10H8}(-)$ in wood-gas versus dimensionless time $t^*(-)$, for three cases where $R_{O/C}$ is set to 0.44 (yellow), 0.88 (green) and 1.32 (black) respectively, $R_{H/C}=0.706$, prescribed pressure (blue) drops from $p=10^5\text{Pa}$ to $p=10^3\text{Pa}$ within dimensionless residence time window $3 \leq t^* \leq 4$ and temperature drops from $T=1200\text{K}$ to $T=500\text{K}$ within $1.5 \leq t^* \leq 2$.

Fig.7 depicts a broader perspective on expected gas-phase compositions including naphthalene content, with increasing $R_{O/C}$. The study shows that naphthalene content in equilibrium continuously decreases with increasing $R_{O/C}$. At $R_{O/C} \approx 0.55$ methane content reaches a minimum, causing a steeper decline in naphthalene content for $R_{O/C} > 0.55$.

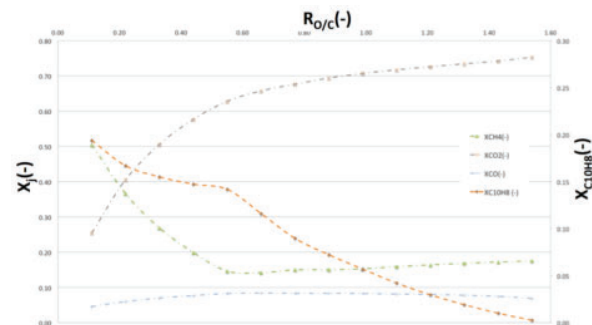


Fig. 7: Simulated wood gas equilibrium composition $x_j(-)$ with the molar fraction of naphthalene $x_{C10H8}(-)$ being highlighted on the right axes and with $x_{H2}(-)$ and $x_{H2O}(-)$ being omitted because they are below 1e-3 , versus ratio of oxygen to carbon $R_{O/C}$. In all cases the ratio of hydrogen to carbon $R_{H/C}=0.706$, prescribed pressure drops from $p=10^5\text{Pa}$ to $p=10^3\text{Pa}$ within dimensionless residence time window $3 \leq t^* \leq 4$ and temperature drops from $T=1200\text{K}$ to $T=500\text{K}$ within $1.5 \leq t^* \leq 2$.

Based on these results, the authors recommend the increase of $R_{O/C}$ in the gasification reactor as a measure to reduce tar content in low-pressure zones. This could be achieved e.g. by either removing coal from the reaction zone, by adding more process-air, or by adding controlled amounts of water.

4. Conclusion and Outlook

This work has presented insights into the physical-, methodical- and numerical principles behind a dynamic, thermochemical simulation model for the

prediction of wood-gas reactions as well as compositions under conditions of varying temperatures and pressures. Besides smaller molecular species, the model includes naphthalene in order to represent the behavior of tars with high-temperature condensation points. Following its validation, the value of the software was demonstrated by deriving four concrete measures that would help to minimize tar condensation in low-pressure, low-temperature zones within real-life gasification systems. Several exemplary simulation-case studies were presented to demonstrate the existence of process-parameter windows, which would require those very measures to ensure longer maintenance intervals and smoother, tar-

reduced operation of any gasification plant.

The hereby-presented dynamic thermochemical model is currently being converted into an easy to use, cloud-based design- and process optimization tool for wood-gasification plants. Under the name *Biogassim* and in combination with the cloud-based HPC technology *KaleidoSim®* [10], it will be free to use and accessible from anywhere in the world by the middle of 2020.

5. References

- [1] G. Boiger, (2015). System Dynamic modelling approach for resolving the thermo-chemistry of wood gasification processes, (2015), Int.Journal of Multiphysics, Vol.9, (No.2), (2015), pp. 137-155;
- [2] T.B. Reed, M. Markson, (2009). A Predictive Model for Stratified Downdraft Gasification, Progress in Biomass Conversion, Academic Press, New York; Vol.4, (1983), pp. 217–254;
- [3] G. Boiger, (2014). A thermo fluid dynamic model of wood particle gasification and combustion processes, Institute of Computational Physics (ICP), School of Engineering, Zurich University of Applied Sciences (ZHAW), Winterthur, Switzerland, Int.Journal of Multiphysics, Vol.8, (No.2), (2014), pp. 203-230;
- [4] N. Prakash, T. Karunanithi, (2008). Kinetic Modeling in Biomass Pyrolysis – A Review, Department of Chemical Engineering, Annamalai University, Annamalai Nagar. INSInet Publication, Journal of Applied Sciences Research; Vol.4, (No.12), (2008), pp. 1627-1636;
- [5] S. Shabbar, I. Janajreh, (2012). Thermodynamic equilibrium analysis of coal gasification using Gibbs energy minimization method, Masdar Institute of Science and Technology (MIST), Abu Dhabi. Energy Conversion and Management; Vol.65, (2013), pp. 755-763;
- [6] G. Job, F. Herrmann, (2005). Chemical potential – a quantity in search of recognition, Institut fuer Physikalische Chemie, Universitaet Hamburg, Abteilung fuer Didaktik der Physik, Universitaet Karlsruhe. European Journal of Physics; Vol.27, (2006), pp. 353-371;
- [7] S. Jarunghammachote, A. Dutta, (2008). Equilibrium modeling of gasification: Gibbs free energy minimization approach and its application to spouted bed and spout – fluid bed gasifiers, Energy Field of Study, School of Environment, Resources and Development, Asian Institute of Technology, Thailand. Energy Conversion and Management, 01/2008; DOI: 10.1016/j.enconman.2008.01.006;
- [8] B.J. McBride, S. Gordon, M.A. Reno, (1993). Coefficients for Calculating Thermodynamic Transport Properties, Lewis Research Center, Cleveland, Ohio, Sanford Gordon and Associates, Cleveland Ohio, Heidelberg College, Triffin, Ohio. NASA Technical Memorandum 4513, 1993;
- [9] M. Hazewinkel, et.al., (2008). Runge Kutta method, Encyclopedia of Mathematics, Springer Science+Business Media B.V./Kluwer Academic Publishers; ISBN 978-1-55608-010-4, 1994;
- [10] www.kaleidosim.com

Thermochemical equilibrium study of ash transformation during combustion and gasification of sewage sludge mixtures with agricultural residues with focus on the phosphorus speciation

Thomas Karl Hannl^{1*}, Hamid Sefidari¹, Matthias Kuba^{1,2,3,4}, Marcus Öhman¹

1. Energy Engineering, Division of Energy Science, Luleå University of Technology, SE-971 87 Luleå, Sweden
2. Bioenergy2020+ GmbH, Wiener Straße 49, AT-7540 Güssing, Austria
3. Institute of Chemical, Environmental & Bioscience Engineering, TU Vienna, AT-1060 Vienna, Austria
4. Department of Applied Physics and Electronics, Umeå University, SE-901 87 Umeå

*corresponding author, thomas.karl.hannl@ltu.se

Abstract

The necessity of recycling anthropogenically used phosphorus due to depleting quantities of available phosphate ores encouraged recent research to identify potential alternative resource pools. One of these resource pools is the ash derived from the thermochemical conversion of sewage sludge. This ash is rich in phosphorus, although most of it is chemically associated in a way where it is not plant available. The purpose of this work was to identify the P-recovery potential of ashes from sewage sludge co-conversion processes with two types of agricultural residues, namely wheat straw (rich in K and Si) and sunflower husks (rich in K), employing thermodynamic equilibrium calculations. The results indicate that both the melting behavior and the formation of plant available phosphates can be enhanced by using these feedstock mixtures in comparison to pure sewage sludge feedstock. This enhanced bioavailability of phosphates was mostly due to the predicted formation of K-bearing phosphates in the mixtures instead of Ca/Fe/Al-phosphates in the pure sewage sludge ash. According to the calculations, gasification conditions could have a negative effect on the melting behavior of the mixtures dominated by the sewage sludge ash. Furthermore, the possibility of precipitating phosphates from ash melts could be shown. It is essential to emphasize that the results of this theoretical study ought to be used with caution since non-equilibrium influences were not investigated. Nevertheless, the applicability of thermodynamic calculations in the prediction of molten and solid phases may motivate experimental research in the future.

1. Introduction:

Depleting natural resources and the ongoing growth of population require major changeovers in the future concepts of resource consumption and recycling. Phosphorus (P) is one of the resources, for which it is crucial to find ways of recycling soon, due to the limited amount of extractable phosphate rock in the Earth's crust as well as the irreplaceability of phosphorus in a variety of organisms such as plants and creatures¹. A way of decreasing the dependence on mined P-minerals is

to recycle P and thereby decrease the P-losses in the phosphorus balance. These losses have been identified to be mainly associated with accumulation in soils, landfilling and transfer of P into the hydro-sphere². Feasible options for minimizing the P-losses are, therefore, the reduction of fertilizer application, the recovery of P from P-rich wastes and the centralized gathering of P-rich streams in specific facilities. The focus of this work is the potential of P-recovery from sewage sludge wastes. Increasing the recycling rate of P for a sustainable use means returning the P

in sewage sludge back to the plants, where it originated.

Sewage sludge represents a suitable source for P-recovery because of its high P-content. However, the association of P in sewage sludge ash derived from mono-combustion plants³ and the high content of environmentally harmful elements and substances^{4,5} limit the application of sewage sludge as fertilizer on arable land. A way of separating beneficial from harmful fractions in sewage sludge is combustion and gasification, followed by the use of the sewage sludge ash as fertilizer or fertilizer precursor. Through the thermochemical conversion of sewage sludge, harmful fractions can be destroyed (e.g., hormones or pathogens) or separated (e.g., heavy metals) from the coarse ash fraction that contains the main P-fraction⁶⁻⁸.

Sewage sludge ashes contain P-amounts in a similar range as in mined phosphate rocks, i.e., up to 30 wt% P₂O₅^{9,10}. Nevertheless, the association of P in the sewage sludge ash tends to be little plant available and requires additional preparation before being used as fertilizer¹¹. Potential methods to create plant available P-compounds from sewage sludge ash are subsequent thermochemical treatment with alkali-salts¹² and acidic or basic extraction³. Through the addition of alkali-salts, the compounds whitlockite (Ca₃(PO₄)₂) and apatite (Ca₅(PO₄)₃OH) in sewage sludge ash from mono-combustion plants, which are poorly plant available, may be transferred into alkali-phosphates such as CaNaPO₄, which are more readily taken up by plants¹². The formation of K-bearing phosphates during combustion processes, where K and P are available, was shown previously^{13,14}, as was the effect of K on the solubility and plant availability of P in the ashes¹⁵.

A possibility of forming plant available P-species directly during the thermochemical conversion is the co-conversion of sewage sludge with alkali-rich feedstock, which may produce alkali-containing

phosphates. The incorporation of alkali elements in the phosphates could potentially render additional thermochemical treatment redundant and might have the potential to extract fertilizer material directly from the thermochemical conversion process, provided that the previously mentioned separation of heavy metals could be achieved. However, the composition of these feedstock mixtures in the co-combustion systems might worsen the operational performance due to enhanced ash melt formation. The use of such feedstock mixtures in industrial plants should be preceded by a theoretical and experimental analysis of the main benefits and drawbacks, to guarantee process stability and predict the chemical association of P in the ash fraction.

The objective of this work is to predict the ash transformation chemistry focusing on the P-speciation in combustion and gasification processes using sewage sludge mixtures with agricultural residues, namely, wheat straw (K- and Si-rich) and sunflower husks (K-rich) by thermodynamic equilibrium calculations. The applicability of employed thermodynamic calculation databases (GTOX, FactPS) to predict the melting behavior of the feedstock ash is presented. The potential of altering the speciation of P towards the formation of more plant available phosphates using feedstock mixtures in comparison to pure sewage sludge is studied. The predicted influence of the gas atmosphere and the process temperature on the type of phosphates and the melt formation in the coarse ash fraction is investigated.

2. Methodology

Feedstock:

The input data for the thermodynamic calculations represent the molar ash fraction of a typical sewage sludge sample (SS), wheat straw (WS), and sunflower husks (SH). The SS-feedstock was precipitated

with both iron sulfate (FeSO_4 , $\text{Fe}_2(\text{SO}_4)_3$) and poly aluminum chloride ($\text{Al}_n(\text{OH})_m\text{Cl}_{3n-m}$). For the application in the thermodynamic calculations, the compositions are converted into mol of elements per kg of dry feedstock substance and standardized, since most mixing ratios based on dry feedstock would be dominated by the SS-ash, due to the high ash content of sewage sludge. The elemental ash compositions of the three feedstocks are given in Table 1.

	SS (mol /kg df)	WS (mol /kg df)	SH (mol /kg df)
Na	0.061	0.002	0.000
Mg	0.152	0.032	0.079
Al	0.482	0.005	0.001
Si	1.068	0.337	0.017
P	1.291	0.021	0.024
K	0.066	0.216	0.191
Ca	0.873	0.071	0.095
Fe	1.182	0.002	0.001
Σ	5.175	0.686	0.408

Table 1: Ash-forming elements in the feedstocks sewage sludge (SS), wheat straw (WS) and sunflower husks (SH) given in mol per kg of dry feedstock (df)

Thermodynamic Modelling:

The thermodynamic equilibrium calculations are performed with the software

FactSage 7.3. The principle of calculations in this software is based on the assumption of global equilibrium between all input elements with formation of compounds and solutions according to the minimization of Gibbs energy in the system. The databases GTOX (stoichiometric compounds, solutions, gas species) and FactPS (stoichiometric compounds, gas species) are used. The applicability of GTOX for the modeling of ash chemistry in P-rich systems has been shown previously^{16,17}. The FactPS database is implemented to allow the formation of H-bearing stoichiometric compounds and gases. In the case of compound duplicates, the priority is given to GTOX, and the FactPS compound is suppressed. The calculations are focused on the description of an oxide melt formation. Therefore, the presence of a salt melt is neglected, and the elements S and Cl are omitted.

The input data in the FactSage Equilib-tool represents the ash composition of sewage sludge, wheat straw, and sunflower husks and mixtures of sewage sludge with wheat straw and sunflower husks individually. The sensitivity of the calculations to the number of different elements in the input data is investigated by adding both alkali elements Na and K as K. This simplification was made due to the small amounts of

Elements	
H, C, N, O, Mg, Al, Si, P, K, Ca, Fe	
Database – GTOX (solution models)	
MeO: <i>CaO, MgO, K₂O, Al₂O₃, FeO</i> OLIV: <i>(Ca,Fe,Mg)(Ca,Fe,Mg)SiO₄</i> Garn: <i>(Al,Fe)₂Ca₃Si₃O₁₂</i> MULL: <i>Al₂(Al,Fe,Si)O₅</i> CAO: <i>Ca(Al,Fe)₂O₄</i> LEUC: <i>K(Al,Fe)Si₂O₆</i> FSPA: <i>K(Al,Fe)Si₃O₈</i> MELM: <i>Ca₂Si(Al,Mg)(Al,Si)O₇</i> NAFH: <i>K(Al,Fe)O₂</i> Stoichiometric solid compounds	LIOS – <i>oxide melt containing: Mg, Al, Si, P, K, Ca, Fe, O</i> C3PL: <i>(Ca, Mg)₃(PO₄)₂</i> CMP: <i>(Ca,Mg)CaP₂O₇</i> C2F: <i>Ca₂(Al,Fe)₂O₅</i> ALPM: <i>(Al,Si)(P,Si)O₄</i> SIOM: <i>(Al,Si)(P,Si)O₄</i> K3PM: <i>K₄(Ca,Mg)P₂O₈</i> CORU: <i>(Al, Fe)₂O₃</i> Gases: CO ₂ , H ₂ O, O ₂
Database – FactPS (stoichiometric compounds)	
Gas compounds	Stoichiometric solid compounds

Table 2: Elements, compounds, and solution models used for the thermodynamic equilibrium calculations in FactSage. Database compounds are given in italics.

Na in the feedstock ashes and to focus on the speciation of the more dominant elements. Since Na is mainly found in SS-ash and the availability of alkali elements is rather low in these ashes, Na and K are summed to simulate a total availability of alkali elements instead of both K and Na individually. For the modeling of the combustion system, the gas atmosphere is set to guarantee fully oxidized conditions in the ash (20 vol% CO₂, 15 vol% H₂O, 4 vol% O₂, N₂). Due to the lack of information on the exact atmosphere in gasification systems, the gasification calculations are performed at O₂-partial pressures of 10-12 atm. This guarantees the presence of non-fully oxidized ash compounds, but it is just a benchmark for future analyses. The ratios of CO₂/CO and H₂O/H₂ are set by the equilibrium in the gasification calculations. The elements and databases used in conjunction with the considered solution models are given in Table 2.

3. Results

Melt Formation:

The formation of melt was calculated and evaluated for the pure feedstocks and the feedstock mixtures (SS+WS, SS+SH) in the temperature range from 700 to 1400 °C. Due to the methodology, the calculated and therefore evaluated melt refers solely to the oxide melt in equilibrium. This oxide melt varies in composition depending on the feedstock mixtures. Pure SS-ash and ashes dominated by SS form a melt dominated by Si, P, and Fe. Towards higher shares of WS in the mixture, the dominance of especially Fe and P in the melt decreases and the melt is dominated by K-silicates. Towards higher shares of SH in the mixture, the dominance of Fe and P decreases as well, although the levels are significantly higher than those calculated for the WS-mixtures. The melt of SH-mixtures is dominated by K, Mg, and P, whereas Si represents a minor fraction

of the melt composition. Both the mixtures with WS and SH individually show a trend towards higher levels of K. The only significant difference between combustion and gasification conditions was observed for the ashes dominated by SS-ash. Under gasification conditions, the shares of Fe and Al in the melt composition are expected to increase in comparison to the combustion conditions, whereas the shares of P and K are expected to decrease.

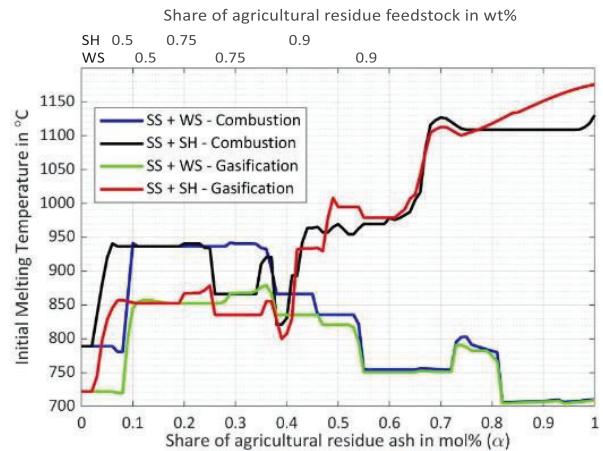


Figure 1: Initial Melting Temperature (IMT) of sewage sludge (SS) ash mixtures with wheat straw (WS) or sunflower husks (SH) under combustion and gasification conditions.

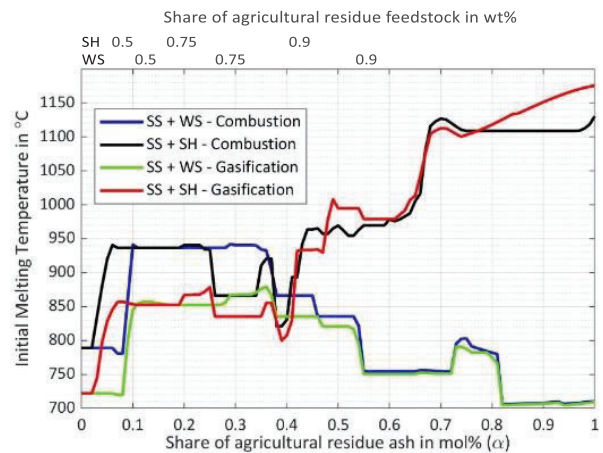


Figure 1 shows the calculated initial melt temperature (IMT) as a function of the feedstock ash mixture. The influence of the feedstock ash and the gas atmosphere can be seen. Starting from pure SS ($\alpha=0$), the IMT only depends on the gas atmosphere, with a significantly lower IMT under gasification conditions. The IMT increases for all mixtures and conditions when the share of SS-ash is decreased to

90 mol% (approx. 50 wt.% SS in dry feedstock mixture). Towards higher shares of each agricultural residue respectively, the trends for combustion and gasification conditions converge for WS and SH respectively. Around 40 mol% of agricultural feedstock share (approx. 15 wt.% SS in dry feedstock mixture), the trends for SH and WS diverge, and the difference in atmospheric conditions becomes negligible. Towards the pure agricultural residues, the IMT mostly depends on the type of agricultural residue, whereas the gas atmosphere has an impact on the SH-mixture solely.

The melting behavior of specific feedstock mixtures is further analyzed to deepen the understanding of the melting behavior at higher temperatures. This analysis again showed a significant difference in both the feedstock mixtures and the influence of the gas atmosphere. The temperatures at which a certain fraction of the ash is present as a melt is shown in Table 3 for the pure feedstocks and specific mixtures under combustion conditions. The molar shares of the melt are given in terms of all condensed ash compounds excluding oxygen to set the focus on the chemical activity of the melt.

Feedstock	IMT (°C)	25 mol% Melt (°C)	50 mol% Melt (°C)	75 mol% Melt (°C)	100 mol% Melt (°C)
Pure SS	790 (725)	990 (860)	1100 (885)	1120 (900)	1355 (>1200)
Pure WS	715 (710)	715 (710)	725 (725)	740 (740)	900 (895)
Pure SH	1135 (1180)	1185 (>1200)	1400 (>1200)	1400 (>1200)	1400 (>1200)
80% SS 20% WS	940 (855)	940 (855)	990 (880)	1135 (905)	1305 (>1200)
60% SS 40% WS	870 (840)	870 (840)	870 (840)	1075 (905)	1255 (>1200)
40% SS 60% WS	755 (755)	755 (755)	820 (795)	980 (860)	1095 (980)
20% SS 80% WS	780 (765)	785 (780)	835 (825)	860 (845)	990 (945)
80% SS 20% SH	945 (870)	945 (870)	980 (880)	1075 (890)	1165 (980)
60% SS 40% SH	885 (815)	945 (935)	975 (945)	985 (995)	1020 (1080)

Table 3: Initial Melting Temperature (IMT) and the temperatures at which certain degrees of the condensed phases are present in the melt for the pure feedstocks and specific feedstock ash mixtures. The temperatures are given under combustion conditions and (in parenthesis) under gasification conditions. The analyzed T-increment was $\Delta T=5$ °C.

Comparing the pure feedstocks, WS had the lowest IMT, followed by SS and SH. An important characteristic of WS-ash was that a large fraction of the ash melted in a small temperature interval. In case of the SS-ash, the temperature gap until the majority of the ash melted was significantly larger. For the pure SH, the melt formation, including more than 50% of the

condensed phases was above the analyzed temperature interval (700-1400 °C). Notably, gasification conditions showed little effect on the melt formation in pure WS-ash, but at higher temperatures increasing negative effect on the melt formation in pure SS-ash. For the pure SH-ash, the effect of gasification conditions could not be

determined properly, because most melting processes occurred above the analyzed temperature interval. The negative impact of gasification conditions on feedstock ash mixtures dominated by SS-ash on one side and the negligible effect of gasification conditions on feedstock ash mixtures dominated by WS-ash are consistent with the findings for the pure feedstock ashes.

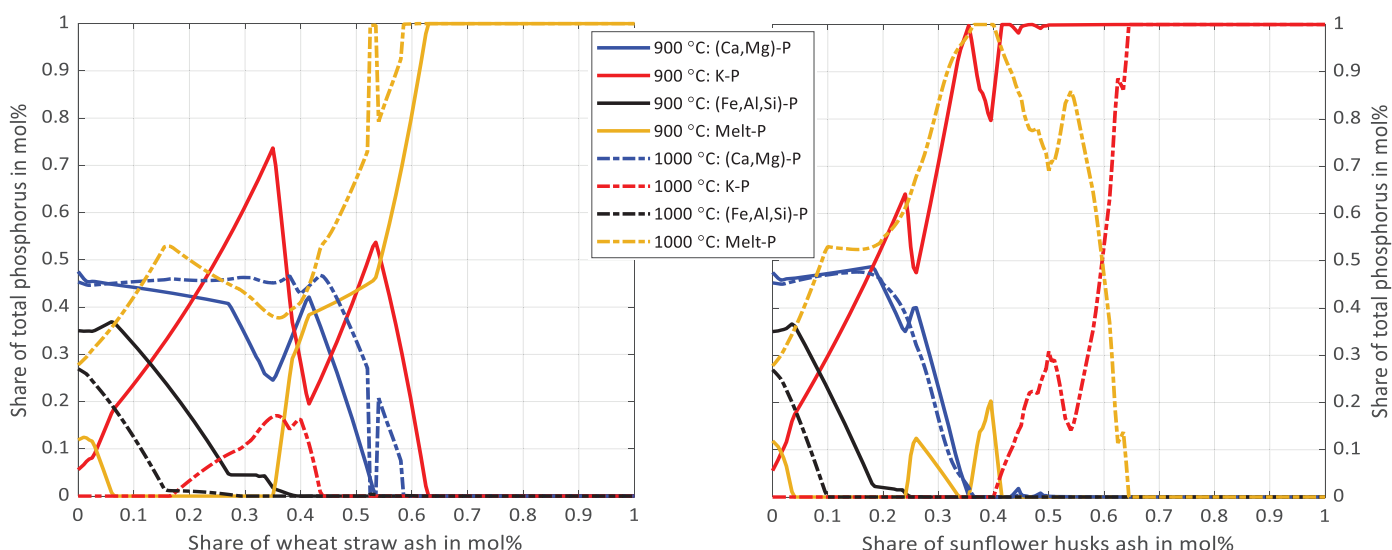


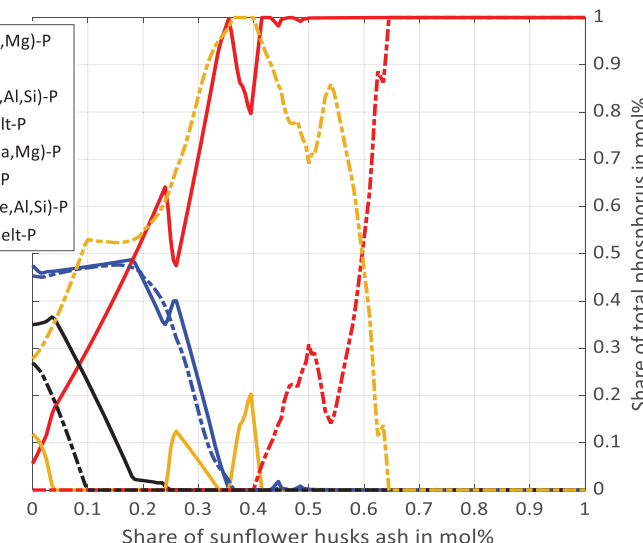
Figure 2: P-speciation for sewage sludge-mixtures with wheat straw (left) and sunflower husks (right) at 900 °C (continuous line) and at 1000 °C (dashed line) under combustion conditions.

Phosphorus Speciation:

The fate of P at specific process temperatures was analyzed in terms of the P-association with different groups of elements (Ca/Mg, K, Fe/Al/Si) and in the melt fraction. These groups may facilitate the determination of plant available P-fractions in future analyses. The grouping is focused on the accentuation of K-bearing phosphates, which means that the groups (Ca,Mg)-P and (Fe,Al)-P may incorporate additional elements such as Si but no K. All the K-bearing phosphates in the calculation, e.g., KMgPO_4 , $\text{CaK}_2\text{P}_2\text{O}_7$, CaKPO_4 , are subsumed under the term K-P. The P-speciation was analyzed for all feedstock ash mixing ratios in a temperature range of 700 to 1200 °C. A depiction of the P-association at 900 and 1000 °C for the mixtures with WS and SH respectively under combustion conditions is shown in

Figure 2. The figure and result presentation neglect all the compounds that do not contain P.

The results show that the P-speciation is strongly dependent on the temperature and the feedstock ash mixture. Pure SS-ash is dominated by phosphates incorporating Ca, Fe, and Al with minor amounts of P in the melt and K-rich phosphates. Along the WS-mixtures, the share of K-phosphates and molten P-compounds increases,



whereas feedstock ashes dominated by WS-ash contain just molten P-compounds. A similar trend can be seen for mixtures with SH-ash, although the ashes dominated by SH-ash do not contain molten P-compounds but only K-phosphates. The most significant difference in terms of the molten P-fraction is in mixtures with SH, where the share of melt-P is significantly higher at 1000 °C due to the formation of a K-, P-, and Si-rich melt. The influence of combustion and gasification conditions on the P-speciation was insignificant in the calculations.

Melt Precipitation:

As shown previously, a significant amount of P can be contained in the molten ash fraction depending on the conditions and the feedstock mixtures. Since these ashes will undergo a cooling process before any

further processing may be performed, it is of interest, which compounds precipitate from the melt under equilibrium cooling. Representative for this analysis, the molten fractions of SS-mixtures with 50 mol% SH ash and 50 mol% WS ash, respectively at 1000 °C under combustion conditions are shown in Figure 3.

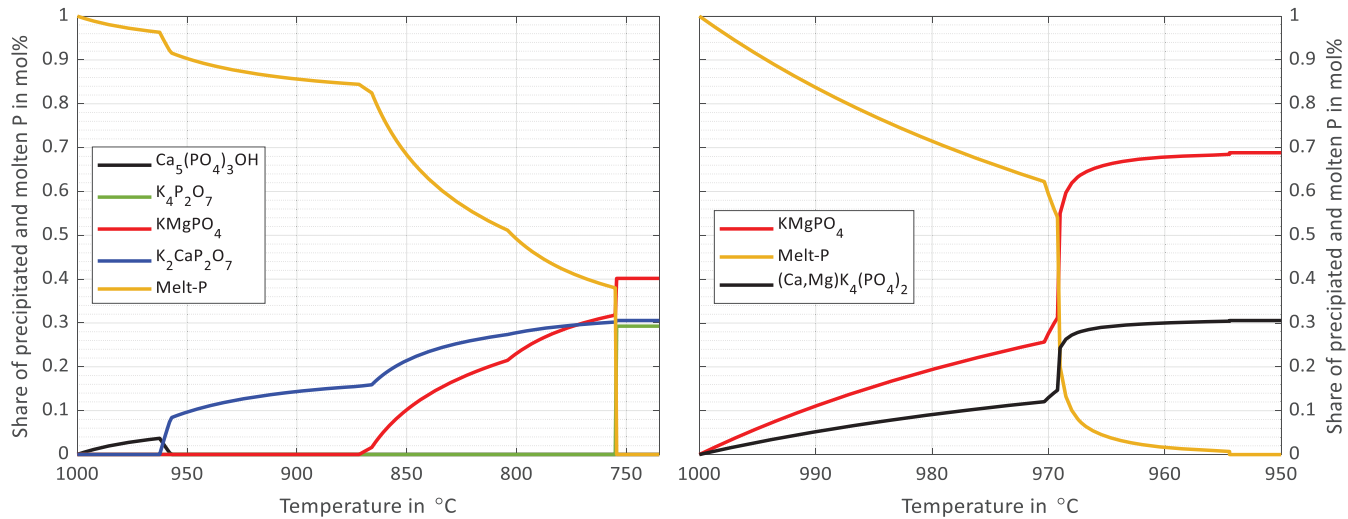


Figure 3: Precipitation of the melt fraction formed at 1000 °C under combustion conditions for mixtures of sewage sludge with wheat straw (left) and sunflower husks (right).

The outcome of the equilibrium precipitation analysis suggests that P in the melt precipitates almost solely as K-containing phosphate if sufficient K is available in the melt. For both of the presented feedstock mixtures, the melt is K-rich and phosphates are precipitated as K-bearing phosphates. Calculations of ashes dominated by SS-ash show that Ca-phosphates are expected to form if insufficient K is available. The data also shows that K-phosphates are preferred over K-silicates when K is the limiting factor in the melt composition. Precipitation under gasification conditions showed little impact on the P-speciation in the precipitated compounds.

4. Discussion

Melt Formation:

Interpretation of the results for the initial melting temperature (IMT) shown in Figure 1 is focused on the influence of the gas

atmosphere and the different feedstock compositions. The decreased IMT for all ash mixtures dominated by SS is correlated to the state of Fe-phosphates in the ash. The abrupt rise in IMT when approximately 10 mol% agricultural residue ash is present may be attributed to the formation of more stable phosphates and Fe-

oxides, which inhibits the incorporation of Fe and P into the melt. The decrease of Fe accompanied by the increase of K as the share of SS-ash decreases seems to favor the formation of more stable K-phosphates (e.g., KMgPO₄). Based on the different compound formation between combustion and gasification conditions, the oxidation state of the Fe-oxides (Fe²⁺, Fe³⁺) and formation of vivianite (Fe₃(PO₄)₂) may be the dominating factor for the decreased IMT under gasification conditions. This case is important to consider since a large fraction of P in precipitated SS can be bound to Fe²⁺ as vivianite ¹⁸, an important resource for P-recovery ¹⁹. The difference in IMT towards the pure SH and WS may be explained by the formation of low-melting K-silicates in the WS-ash, which has been documented in previous studies ^{14,20}. In the equilibrium calculations, the Si-lean SH-ash tends to form ash enriched in CaO and MgO, which are highly stable up to higher

temperatures. Notably, the gasification atmosphere increased the IMT for high SH-shares in comparison to the combustion atmosphere because K was bound as carbonate, and higher amounts of K were volatilized as KOH. The presence of carbonates indicates that the calculations solely based on the formation of an oxide melt are insufficient at high shares SH-ash, and the formation of a salt melt should be considered. Previous research stated higher stability of K_2CO_3 in a Si-lean and CO_2 -rich environment²¹. Detailed studies for the gaseous release of K would need to include Cl in the calculations^{22,23}.

The analysis of the melting behavior provided in Table 3 indicates several effects of the feedstock mixing and the gas atmosphere, which may influence the thermochemical conversion process. The mixtures with sunflower husks and wheat straw melt up to 50 mol% in a small temperature interval. The composition data suggests that this result is caused by excessive inclusion of K and P in the melt, which is enhanced by further addition of K-rich agricultural feedstock. Previous research found that excess of P and K promoted the formation of low-melting phosphates¹⁴. Although the initial melt formation was shifted towards higher temperatures, the melt starts to dissolve and incorporate a large fraction of silicates and phosphates soon thereafter. Total melting of SH-rich mixtures was inhibited by the formation of stable alkaline oxides (CaO, MgO).

In reality, the melting behavior of these feedstock mixtures might be significantly different from these theoretical equilibrium calculations due to various reasons. The assumption that in a feedstock mixture, every individual ash element is readily available to react or be associated in the melt is not reflecting the real capability of mixing technology. Even under perfect mixing parameters, the original feedstock will maintain its structure partially within

the mixture particles, which means that elements present in different pure feedstocks might not interact as freely as the calculations suggest. This interaction barrier should also be considered when highly stable solid compounds are incorporated in the melt in theory. Another aspect is that the interaction between solid compounds is considered to have no kinetic limitations in equilibrium calculations. The reactivity of the ash elements, in reality, will be defined by their state of matter. It needs to be considered that an individual pure feedstock fraction in the ash could melt or volatilize to enhance the interaction with the other feedstocks ash.

Phosphorus Speciation and Precipitation: The results of the thermodynamic calculations at specific temperatures over the entire range of mixture ratios show the potential of using SS-mixtures with agricultural residues for the creation of K-bearing phosphates. The desired shift from Ca/Mg-phosphates and Fe/Al/Si-phosphates towards K-phosphates when using feedstock mixtures was identified. It could be shown that K-bearing phosphates are thermodynamically favored in a P-limited ash environment. Therefore, the calculations indicate that the entire P was present in K-bearing phosphates (or as molten P-compounds) when the agricultural residue ash was the dominating ash fraction. The results obtained for the P-association in this work are in accordance with previous findings of the possibility to change the P-speciation in sewage sludge ashes by adding alkali-rich additives¹². Modeling a function of the P-species in dependence of a feedstock mixture, process temperature and gas atmosphere has shown its applicability in this theoretic approach. In conjunction with experiments, it would be possible to verify the results and obtain an approximation of how far experimental data deviate from equilibrium data.

Knowledge about the deviating factors between theory and experiment could establish a baseline to repeat such a methodology for other feedstock mixtures to investigate their potential of P-recovery.

The thermodynamic modeling of the P-speciation has to be evaluated critically too. First, the groups in terms of the P-associates (Ca/Mg, K, Fe/Al/Si) were selected subjectively to show the transition of the elements associated with P in the ash depending on the feedstock ash mixture and depending on the temperature. Furthermore, it was assumed that an individual group of phosphates shows similar behavior when applied as fertilizer. This approach neglects the role of the plant, the soil, and also the varying plant availability within one group²⁴. Additionally, the assumption of equilibrium in the calculations gives a simplified picture of the potential P-associations in the feedstock mixtures. The shift from Ca, Fe, and Al-phosphates towards K-phosphates is assumed to occur without kinetic limitations as a solid-solid reaction. In reality, the formation of K-phosphates will probably be enhanced by volatilized or K and P in the melt, whereas solid-solid reaction might be inhibited significantly. Furthermore, the calculations suggest that K-phosphates such as KMgPO₄ are the most stable phosphate form in this system. Therefore, the only phosphates occurring in P-lean feedstock mixtures are K-phosphates or, at higher temperatures, molten phosphates. This equilibrium assumption proposes that several other stable phosphates, which may have formed previously, e.g., Ca₃(PO₄)₂ would disintegrate to make P available for the reaction with excess-K. Considering the occurrence and stability of Ca-phosphates, this is probably not always the case in practice.

The potential of P-compounds precipitated from the molten ash fraction was identified in the equilibrium precipitation. Although the calculations indicate that molten ashes

of feedstock mixtures may precipitate mainly as K-phosphates, real precipitation cases might differ significantly. A major aspect that is lost in equilibrium cooling is the formation of amorphous material due to non-equilibrium phase transitions. Previous studies showed that amorphous material might represent a large fraction of condensed ash phases and the presence of other stable phosphates such as whitlockite (Ca₃(PO₄)₂), hydroxyapatite (Ca₅(PO₄)₃OH) or tridymite polymorphs of aluminum phosphate (AlPO₄) has been shown previously and needs to be considered^{11,25}.

5. Conclusion

Thermodynamic equilibrium calculations were performed to predict the ash transformation chemistry of sewage sludge mixtures with both sunflower husks or wheat straw under combustion and gasification conditions. Focusing on the melting behavior of the ashes and the speciation of P in the ash, the following conclusion may be drawn:

- The low initial melting temperature of sewage sludge ash, dominated by P, Fe, Si, Ca, and Al, increased significantly when the share of agricultural feedstock was above 50 wt% (approx. 10 mol% ash).
- Wheat straw (K- and Si-rich) and sunflower husks (K-rich) showed significantly different melting behavior when mixed with sewage sludge for thermochemical conversion. This difference is mainly attributed to the high shares of Si in wheat straw, forming a low melting K-silicate melt.
- Gasification conditions had the most detrimental effect on ashes dominated by sewage sludge ash. The melting tendencies during gasification were shifted towards lower temperatures for all feedstock mixtures where sewage sludge ash was dominant. The appearance of melt at lower temperatures was found to correlate with the

presence of Fe²⁺-compounds, especially vivianite.

- P in sewage sludge ashes in the calculations was mostly associated with Ca, Fe, and Al. When mixed with wheat straw or sunflower husks, the thermodynamic equilibrium shifted towards K-bearing and molten phosphates
- The precipitation of molten ashes showed high stability of K-bearing phosphates formed through equilibrium cooling.
- Alteration of the P-speciation in by co-conversion of sewage sludge with agricultural residues to-wards plant available phosphates was thermodynamically favored due to the high stability of K-bearing phosphates.

6. Acknowledgements

The financial support from the Swedish Research Council for Environment, Agricultural Sciences and Spatial Planning (Formas), project 942-2015-619, and from the Swedish Research Council, project 2016-04380, is gratefully acknowledged. Additionally, the Kempe Foundation is thanked for their financial support of the post-doc research of Matthias Kuba at Umeå University and Luleå University of Technology.

7. References

- (1) Nese, T.-S. S.; Cordell, D. Global Phosphorus Scarcity: Identifying Synergies for a Sustainable Future. *J. Sci. Food Agric.* **2012**, *92* (1), 2–6.
- (2) Ott, C.; Rechberger, H. The European Phosphorus Balance. *Resour. Conserv. Recycl.* **2012**, *60*, 159–172.
- (3) Shiba, N. C.; Ntuli, F. Extraction and Precipitation of Phosphorus from Sewage Sludge. *Waste Manag.* **2017**, *60*, 191–200.
- (4) Harrison, E. Z.; Oakes, S. R.; Hysell, M.; Hay, A. Organic Chemicals in Sewage Sludges. *Sci. Total Environ.* **2006**, *367* (2–3), 481–497.
- (5) Donatello, S.; Tyrer, M.; Cheeseman, C. R. EU Landfill Waste Acceptance Criteria and EU Hazardous Waste Directive Compliance Testing of Incinerated Sewage Sludge Ash. *Waste Manag.* **2010**, *30* (1), 63–71.
- (6) Marani, D.; Braguglia, C. ; Mininni, G.; Maccioni, F. Behaviour of Cd, Cr, Mn, Ni, Pb, and Zn in Sewage Sludge Incineration by Fluidised Bed Furnace. *Waste Manag.* **2003**, *23* (2), 117–124.
- (7) Liu, J.; Fu, J.; Ning, X.; Sun, S.; Wang, Y.; Xie, W.; Huang, S.; Zhong, S. An Experimental and Thermodynamic Equilibrium Investigation of the Pb, Zn, Cr, Cu, Mn and Ni Partitioning during Sewage Sludge Incineration. *J. Environ. Sci.* **2015**, *35*, 43–54.
- (8) Steckenmesser, D.; Vogel, C.; Böhm, L.; Heyde, B.; Adam, C. Fate of Heavy Metals and Polycyclic Aromatic Hydrocarbons (PAH) in Sewage Sludge Carbonisates and Ashes – A Risk Assessment to a Thermochemical Phosphorus-Recycling Process. *Waste Manag.* **2018**, *78*, 576–587.
- (9) Gorazda, K.; Tarko, B.; Wzorek, Z.; Kominko, H.; Nowak, A. K.; Kulczycka, J.; Henclik, A.; Smol, M. Fertilisers Production from Ashes after Sewage Sludge Combustion – A Strategy towards Sustainable Development. *Environ. Res.* **2017**, *154*, 171–180.

The occurrence of such an alteration of the P-speciation might be highly limited by kinetic aspects, especially when the transition is suggested to be solely between solid compounds. Furthermore, the occurrence of amorphous ash material has to be considered under real (non-equilibrium) conditions. Therefore, this theoretical approach must be validated by an experimental setup to find the kinetic limitations and the non-equilibrium factors that are of relevance for the P-speciation in the ash.

- (10) Krüger, O.; Adam, C. Recovery Potential of German Sewage Sludge Ash. *Waste Manag.* **2015**, *45*, 400–406.
- (11) Nanzer, S.; Oberson, A.; Huthwelker, T.; Eggenberger, U.; Frossard, E. The Molecular Environment of Phosphorus in Sewage Sludge Ash: Implications for Bioavailability. *J. Environ. Qual.* **2014**, *43* (3), 1050.
- (12) Stemann, J.; Peplinski, B.; Adam, C. Thermochemical Treatment of Sewage Sludge Ash with Sodium Salt Additives for Phosphorus Fertilizer Production – Analysis of Underlying Chemical Reactions. *Waste Manag.* **2015**, *45*, 385–390.
- (13) Li, H.; Han, K.; Wang, Q.; Lu, C. Influence of Ammonium Phosphates on Gaseous Potassium Release and Ash-Forming Characteristics during Combustion of Biomass. *Energy Fuels* **2015**, *29* (4), 2555–2563.
- (14) Grimm, A.; Skoglund, N.; Boström, D.; Boman, C.; Öhman, M. Influence of Phosphorus on Alkali Distribution during Combustion of Logging Residues and Wheat Straw in a Bench-Scale Fluidized Bed. *Energy Fuels* **2012**, *26* (5), 3012–3023.
- (15) Kumpiene, J.; Brännvall, E.; Wolters, M.; Skoglund, N.; Čirba, S.; Aksamituskas, V. Č. Phosphorus and Cadmium Availability in Soil Fertilized with Biosolids and Ashes. *Chemosphere* **2016**, *151*, 124–132.
- (16) Arnout, S.; Nagels, E. Modelling Thermal Phosphorus Recovery from Sewage Sludge Ash. *Calphad* **2016**, *55*, 26–31.
- (17) Yazhenskikh, E.; Jantzen, T.; Hack, K.; Muller, M. A New Multipurpose Thermodynamic Database for Oxide Systems. *РАСПЛАВЫ* **2019**, No. 2, 116–124.
- (18) Wilfert, P.; Mandalidis, A.; Dugulan, A. I.; Goubitz, K.; Korving, L.; Temmink, H.; Witkamp, G. J.; Van Loosdrecht, M. C. M. Vivianite as an Important Iron Phosphate Precipitate in Sewage Treatment Plants. *Water Res.* **2016**, *104*, 449–460.
- (19) Wilfert, P.; Dugulan, A. I.; Goubitz, K.; Korving, L.; Witkamp, G. J.; Van Loosdrecht, M. C. M. Vivianite as the Main Phosphate Mineral in Digested Sewage Sludge and Its Role for Phosphate Recovery. *Water Res.* **2018**, *144*, 312–321.
- (20) Mac an Bhaird, S. T.; Walsh, E.; Hemmingway, P.; Maglinao, A. L.; Capareda, S. C.; McDonnell, K. P. Analysis of Bed Agglomeration during Gasification of Wheat Straw in a Bubbling Fluidised Bed Gasifier Using Mullite as Bed Material. *Powder Technol.* **2014**, *254*, 448–459.
- (21) Anicic, B.; Lin, W.; Dam-Johansen, K.; Wu, H. Agglomeration Mechanism in Biomass Fluidized Bed Combustion – Reaction between Potassium Carbonate and Silica Sand. *Fuel Process. Technol.* **2018**, *173*, 182–190.
- (22) Wei, X.; Schnell, U.; Hein, K. Behaviour of Gaseous Chlorine and Alkali Metals during Biomass Thermal Utilisation. *Fuel* **2005**, *84* (7–8), 841–848.
- (23) Boström, D.; Skoglund, N.; Grimm, A.; Boman, C.; Öhman, M.; Broström, M.; Backman, R. Ash Transformation Chemistry during Combustion of Biomass. *Energy Fuels* **2012**, *26* (1), 85–93.
- (24) Kratz, S.; Schick, J.; Øgaard, A. F. P Solubility of Inorganic and Organic P Sources. In *Phosphorus in Agriculture: 100 % Zero*; Schnug, E., De Kok, L. J., Eds.; Springer Netherlands: Dordrecht, 2016; pp 127–154.
- (25) Lynn, C. J.; Dhir, R. K.; Ghataora, G. S.; West, R. P. Sewage Sludge Ash Characteristics and Potential for Use in Concrete. *Constr. Build. Mater.* **2015**, *98*, 767–779.

CPFD simulation of a dual fluidized bed cold flow model

A. Lunzer^{1*}, S. Kraft^{2,3}, S. Müller², H. Hofbauer²

1. Verto Engineering GmbH, Franz-Josefs Kai 53/13, 1010 Vienna, Austria
2. TU Wien, Institute of Chemical, Environmental and Bioscience Engineering, Getreidemarkt 9/166, 1060 Vienna, Austria
3. Bioenergy 2020+ GmbH, Wiener Strasse 49, 7540 Güssing, Austria

*corresponding author, al@vertö-engineering.com

Abstract

The present work was carried out to simulate a cold flow model of a biomass gasification plant. The fluid dynamical behavior depends heavily on the particles' properties like the particle size distribution (PSD). For the simulation an Eulerian-Lagrangian approach, in particular by the multi-phase particle in cell (MP-PIC) method, was used to simulate particles with a defined PSD. Therefore, Barracuda VR, a software tool with an implemented MP-PIC method specifically designed for CPFD (computational particle fluid dynamics) simulations, was the software of choice. The simulation results were verified with data of previously conducted experiments on a physical cold flow model. The cold flow model was operated with air and bronze particles. The simulations were conducted with different drag laws: an energy-minimization multi-scale (EMMS) approach, a blended Wen-Yu and Ergun (WYE) drag law, and a drag law of Ganser. Furthermore, a focus was set onto the normal particle stress (P_s value variation), which is significant in close-packed regions, and the loop seals' fluidization rate was varied to influence the particle circulation rate. The settings of the simulation were optimized, flooding behavior did not occur in advanced simulations, and the simulations reached a stable steady state behavior. The Ganser drag law combined with an adjusted P_s value with ($P_s = 30$ Pa) or without ($P_s = 50$ Pa) increased loop seal fluidization rates provided the best simulation results.

Keywords: Computational fluid dynamics, CPFD simulation, Cold flow model, Fluidized bed

1. Introduction

The demand for energy independency and renewable energy is increasing. Therefore, gasification technology is becoming more important. Dual fluid gasification is a promising technology to produce a product gas with a favorable gas composition which can be used for different products like synthetic natural gas and Fischer-Tropsch fuel.

Classical dual fluidized bed (DFB) gasification design in a bubbling bed without narrowings in the fuel reactor (FR) works well for conventional wood chips. There is

an increased interest from industry to utilize alternative low-cost fuels, but those fuels can lead to higher tar concentrations in the product gas stream. The design with narrowings in the FR column increases the solid gas interaction above the bubbling bed. This measure led to lower tar contents in the product gas and overall increased product gas quality [1].

CFD (computational fluid dynamics) is a diverse tool for applications in research and industry. The application of CFD in gas-solid multi-phase systems does face new challenges compared to traditional

simulations solely focusing on fluids. Therefore, Barracuda VR, a software tool with an implemented MP-PIC (multi-phase particle in cell) method specifically designed for CFD (computational particle fluid dynamics) simulation, was the software of choice. Because of the high particle number, the MP-PIC approach is an efficient option for larger plants and applications.

CFD simulations turned out to be very useful for the investigation of mixing behavior of fuel and bed material in dual fluidized bed plants. Optimal contact between fuel and bed material ensures low tar content which is favorable for long and stable operation of such plants. Better mixing can be achieved with additional fluidization agent as Kuba et al. have shown [2]. With CFD simulations the effect of such additional fuel nozzles can be investigated and their impact on overall mixing process in the gasification or fuel reactor.

In the present work the CFD simulation of a cold flow model used for the up-scaling and dimensioning of a biomass gasification plant is the object of interest. Cold flow models are an important tool to study fluid dynamical behavior, scale up small plants, and offer the possibility to optimize and test the design of a plant on a small scale.

A verified CFD model can reflect trends and predict the process in a plant with a certain degree of accuracy as well as allow fast testing of different plant modifications and optimization.

The goal of this work was to create a working CFD model in Barracuda which predicts the behavior of the real cold flow model accurately and to gain deeper understanding of the behavior of the DFB gasification as well as simulations of fluidized beds.

The following questions were subject of interest:

- How do the different settings (e.g. drag law, particle normal stress, etc.) in the CFD software influence the particle behavior?
- What settings lead to the best performance at a specific operating point?
- Do the optimal settings predict reliable results at different operating points in the same system?

Barracuda has already been used for studies over a broad range of fluidization regimes, ranging from bubbling beds [3]–[5], spouting beds [6], risers [7]–[12], and full loop circulating fluidized beds (CFBs) [13]–[18]. A brief literature review of already conducted simulations of CFBs is given subsequently.

A full loop CFB was simulated by Clark et al. [13] with a Wen and Yu drag law approach. The flow behavior matched well with video recordings. The pressure drops were reasonable accurate.

Wang et al. [14] simulated a CFB to investigate the influence of various modeling parameters. They simulated the CFB with the Wen-Yu drag model, which predicted the particle circulation rate best, two configurations of the WYE drag model, which predicted the total pressure drop best, and the Ganser drag model, which overestimated both the pressure drop and particle circulation rate.

Hamilton et al. [15] simulated a CFB using the Wen-Yu drag model, which overpredicted the drag force in the simulation, with higher circulation rates but with good predictions of the trend.

Adkins et al. [16] simulated a CFB with the WYE and a Parker drag model. The WYE

drag model overestimated drag forces, while a modified drag correlation with an increased P_S value, derived by Parker, improved the correlation of the data.

Ma et al. [17] used the EMMS drag model to simulate a high-density CFB. The predicted pressure distribution deviated from experimental data in dense regions of the riser, while the particle circulation rate was predicted with relative errors less than 10%.

Kraft et al. [18] simulated a dual fluidized bed with EMMS, Ganser, Turton-Levenspiel, and WYE drag laws. The EMMS drag law predicted the pressure distribution best, while the others underestimated the pressure at the bottom. The best particle circulation rates were achieved with the Ganser drag law, while EMMS's were notable lower.

Based on the literature review the EMMS, Ganser, and WYE drag laws have been tested. Generally spoken the WYE and Ganser drag law cover both dense and dilute flow but seem to overpredict the drag force in some cases. The EMMS had a promising performance, predicted the pressure distribution well, but underpredicted the particle circulation rate in some cases.

1.1. Governing equations

1.1.1. Equation for fluid phase

Continuity equation for the fluid without mass transport [19]:

$$\frac{\partial(\varepsilon_f \rho_f)}{\partial t} + \nabla \cdot (\varepsilon_f \rho_f \mathbf{u}_f) = \delta \dot{m}_p = 0$$

Eq. 1: Continuity equation

where ε_f is the fluid volume fraction, ρ_f is the fluid density, \mathbf{u}_f the fluid velocity, and $\delta \dot{m}_p$ the gas mass production rate per volume from particle-gas chemistry. Momentum equation for the fluid with interphase momentum transfer function \mathbf{F} [19]:

$$\begin{aligned} & \frac{\partial(\varepsilon_f \rho_f \mathbf{u}_f)}{\partial t} + \nabla \cdot (\varepsilon_f \rho_f \mathbf{u}_f \mathbf{u}_f) \\ &= -\nabla p + \mathbf{F} + \varepsilon_f \rho_f \mathbf{g} + \nabla \cdot (\varepsilon_f \boldsymbol{\tau}_f) \end{aligned}$$

Eq. 2: Momentum equation

where p is the pressure, \mathbf{g} the gravitational acceleration, and with the fluid stress tensor in index notation [19]:

$$\tau_{f,ij} = \mu \left(\frac{\partial u_{f,i}}{\partial x_j} + \frac{\partial u_{f,j}}{\partial x_i} \right) - \frac{2}{3} \mu \delta_{ij} \frac{\partial u_{f,k}}{\partial x_{f,k}}$$

Eq. 3: Stress tensor

where μ is the sum of laminar shear and turbulence viscosity, δ_{ij} is the Kronecker delta, $u_{f,i}$ the fluid's velocity, and x_i is the spatial variable.

1.1.2. Equations for particulate phase

The particle acceleration \mathbf{a}_p , as described in Eq. 4, was extended with an additional term, the modified acceleration due to contact stress. The particle acceleration is calculated using a blended particle acceleration model developed by O'Rourke and Snider [20].

$$\begin{aligned} \mathbf{a}_p = & D(\mathbf{u}_f - \mathbf{u}_p) - \frac{1}{\rho_p} \nabla p + \mathbf{g} \\ & - \frac{1}{\varepsilon_p \rho_p} \nabla \tau_p + \frac{\bar{\mathbf{u}}_p - \mathbf{u}_p}{2 * \tau_D} \end{aligned}$$

Eq. 4: Particle acceleration

$\bar{\mathbf{u}}_p$ is the particle mean velocity, the particle density ρ_p , and τ_D is a damping time due to inelastic particle collisions (see [20]).

The particle normal stress, τ_p , models the particle-particle interactions and is important near close-pack and has little effect elsewhere [21].

$$\tau_p = \frac{P_S * \varepsilon_p^\beta}{\max[\varepsilon_{cp} - \varepsilon_p, \alpha(1 - \varepsilon_p)]}$$

Eq. 5: Particle normal stress

ε_p is the particle volume fraction, ε_{cp} is the close-pack particle volume fraction, and P_S is a constant with the unit Pa. The constants

α , a small number to avoid dividing by zero, and β are dimensionless.

The MP-PIC method used in Barracuda describes the dynamics of the particle phase using the particle probability distribution function $f(x, u_p, \rho_p, V_p, t)$ and the evolution of the particle phase is determined by solving the Liouville equation for f [22]:

$$\frac{\partial f}{\partial t} + \nabla \cdot (f \mathbf{u}_p) \nabla_{\mathbf{u}_p} \cdot (f \mathbf{a}_p) = 0$$

Eq. 6: Liouville equation for f

where $\nabla_{\mathbf{u}_p}$ is the divergence operator with respect to particle velocity.

The particle volume fraction is related to f by [22]:

$$\varepsilon_p = \iint f \frac{m_p}{\rho_p} dm_p d\mathbf{u}_p$$

Eq. 7: Particle volume fraction

The interphase momentum transfer function per volume is defined as [22]:

$$\mathbf{F} = - \iint f \left(m_p \left[D(\mathbf{u}_f - \mathbf{u}_p) - \frac{\nabla p}{\rho_p} \right] \right) dm_p d\mathbf{u}_p$$

Eq. 8: Interphase momentum transfer

where D is the drag function.

1.2. Drag laws

In this paper the EMMS, Ganser, and WYE drag laws were used. All of those drag laws are already implemented and available in Barracuda. The EMMS drag law is based on an energy-minimization multi-scale approach and the drag coefficient is calculated from structure parameters of the gas solid interactions. For further information it is referred to Yang et al. [23]. The Ganser drag law is based on studies of Chhabra et al. [24] and Wen and Yu [25]. In this work the sphericity of the particles is 1. The WYE drag law was introduced by Gidaspow [26] and is a blend of the Wen and

Yu drag law, which is appropriate for more dilute systems and the Ergun equation [27], which is appropriate at higher packing fractions. For the formulas implemented in Barracuda for the drag laws it is referred to the Barracuda Virtual Reactor version 17.3.0 user manual [28] which can also be found in [29].

2. Concept and methodology

The simulations were based on an existing cold flow model located at TU Wien. Martinovic [30] conducted cold flow experiments on this model. Those results were used to verify and rate the performance of the simulation. A 3D model of the cold flow model was designed in Autodesk Inventor Professional 2018, as depicted in Fig. 1, and used for this work. The model has a total height of 1.57 m.

The main parts of the model are the air reactor (AR) column, the fuel reactor (FR) column, with four built-ins to narrow the cross-section, the FR bubbling bed (FR BB), a separator on top of the AR (AR SEP) and one on top of the FR column (FR SEP), and a total of three loop seals (Upper (ULS), Inner (ILS), and Lower loop seal (LLS)), which connect the separators with the AR and FR column respectively and the columns with each other.

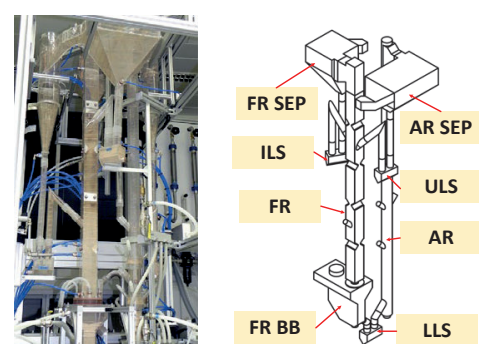


Fig. 1: Cold flow model (left) [30], 3D model for simulation (right)

The diameter of the AR was 52 mm, the width of the square FR column 62 mm and 16 mm at the narrowing (as depicted in Fig. 1).

For the cold flow model investigations bronze particles as bed material and air as fluidization agent were used. During operation the bronze particles were carried up in the riser, separated from the fluid in the separator by gravity and transported through a loop seal into the FR column. Most of the particles traveled downwards, while forming smaller fluidized beds, to the FR bubbling bed. The upwards moving particles were recirculated over a separator and a loop seal to the FR column. In the bubbling bed the particles traveled through a loop seal back to the riser.

For the simulation several settings were tested in order to accurately predict the particle behavior in the cold flow model. A focus was put on the drag law, the particle normal stress properties and influence of the fluidization rate.

The best set-up was determined in a step-by-step approach.

The simulations were conducted using Barracuda VR version 17. The hardware infrastructure was a workstation with an Intel Core i5-3570, 16 GB RAM, and a GeForce TITAN X graphics card.

2.1. General settings

The general settings for the simulation are listed in Tab. 1. The PSD of the particles is depicted in Fig. 2.

Real cell number	483 338
Total number of particles	$\sim 1.16 \times 10^{10}$
Number of numerical particles	$\sim 2.19 \times 10^6$
Particle density [30]	8800 kg/m ³
Bulk density [30]	5100 kg/m ³
Drag law	EMMS, WYE, Ganser
P _s	1 Pa (default), up to 100 Pa
Turbulence model	LES

Tab. 1: General settings overview

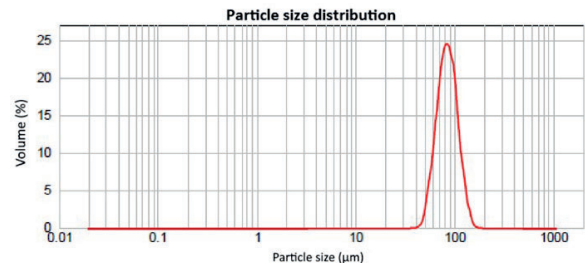


Fig. 2: Particle size distribution (PSD) of particles with a Sauter diameter of 81.7 μm [30]

2.2. Boundary conditions

In order to simulate a fluidizing bed, air had to be introduced and removed from the system. The air was able to exit the model at the pressure boundary conditions and was introduced into the system at the flow boundary conditions (see Fig. 3).

At each separator a pressure boundary condition with 1 atm was defined, permeable for air but not for particles.

In each loop seal one flow boundary condition, in the AR four (AR1_{lower}, AR1_{upper}, AR2_{lower}, AR2_{upper}) and in the bubbling bed of the FR two flow boundary conditions (FR1 and FR2) were defined. The flow boundary conditions were set as injection points (“jets”) split up in several individual flow boundary conditions. The boundary conditions in the loop seal consisted of 4 jets each, the conditions in the FR of 5 each, the conditions in the AR of 8 each. Therefore, a total of 54 active flow boundary conditions were used in the simulation to inject air into the system.

The mass flow into the system was regularly set to 24 Nm³/h into the AR, 12 Nm³/h into the FR, and 0.6 to 0.8 Nm³/h in each loop seal (see Tab. 2). This mass flow was split up equally between the jets. An overview of the flow boundary conditions is given in Tab. 2.

Furthermore, the fluidization rate was altered in the loop seals in certain simulations to investigate its influence.

	No. of jets	Position/ Height [mm]	Vol. flow [Nm ³ /h]
FR1	5	889	2
FR2	5	1999	10
AR1 _{lower}	8	111	3.69
AR1 _{upper}	8	326	8.31
AR2 _{lower}	8	425	8.31
AR2 _{upper}	8	601	3.69
LLS	4	11	0.8
ULS	4	1045	0.8
ILS	4	1045	0.6

Tab. 2: Flow conditions overview

2.3. Pressure measurement

The pressure was measured over time to evaluate the pressure profile, therefore, a total of 25 pressure measurement points were defined in the FR, AR, and LLS.

2.4. Evaluation

The performance of the simulation was rated qualitatively, by visual observation of the rendered animation of the simulation and the generated graphs (see Fig. 3). The performance was quantitatively rated based on the mass flow rate and the pressure profile including defined parameters. The defined parameters were the pressure profile parameter (P_{PP}) and the pressure gradient parameter (P_{PG}).

The P_{PP} value was defined as the pressure difference measured in the experiment and the simulation at the bottom of the FR column, which indicated the total amount of particles in the FR column. Therefore, the target value for P_{PP} is zero.

$$P_{PP} = p_{Simulation} - p_{Experiment}$$

Eq. 9: Pressure profile parameter

The P_{PG} value was calculated by adding up the squared difference, between measured and simulated values, of the pressure gradient values in the FR column. Therefore, the target value for P_{PG} is zero and it

indicated the quality of the distribution in the FR column.

$$P_{PG} = \sum_i \left(|p'(H_i)_{Simulation} - p'(H_i)_{Experiment}|^2 \right)$$

Eq. 10: Pressure gradient parameter

The circulation rate of the particles was measured with the mass flow of the particles in the AR column. If the simulation is in a steady state and no flooding occurred, this value will reflect the circulation rate of the particles. The measured value on the cold flow model in experiments was 823 kg/h (marked as a dashed line in Fig. 4, Fig. 5, and Fig. 6) with an AR fluidization rate of 24 Nm³/h.

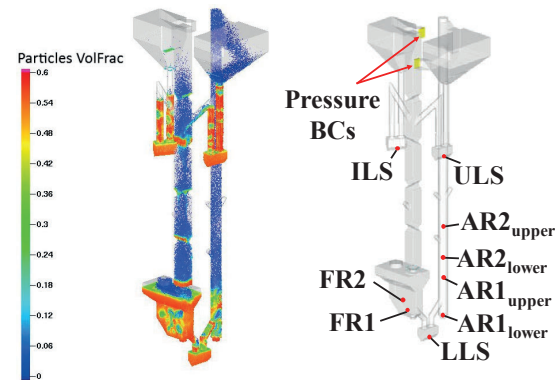


Fig. 3: Visualization of the CPFD simulation (left), boundary conditions (BCs) for simulation (right)

3. Results and discussion

Overview of simulations

Abbreviation	Drag Law	Mesh	PS [Pa]	LLS Fluidization rate [Nm³/h]	AR Fluidization rate [Nm³/h]
E300	EMMS	300k	1	0.8	24
G300	WYE	300k	1	0.8	24
W300	WYE	300k	1	0.8	24
G500	Ganser	500k	1	0.8	24
W500	WYE	500k	1	0.8	24
PS1	Ganser	500k	1	0.8	24
PS30	Ganser	500k	30	0.8	24
PS50	Ganser	500k	50	0.8	24
PS65	Ganser	500k	65	0.8	24
PS100	Ganser	500k	100	0.8	24
G1n	Ganser	500k	1	0.8	24
G1a	Ganser	500k	1	1.4	24
G30n	Ganser	500k	30	0.8	24
G30a	Ganser	500k	30	1.4	24
G30b	Ganser	500k	30	2	24
W1n	WYE	500k	1	0.8	24
W30n	WYE	500k	30	0.8	24
W30a	WYE	500k	30	1.4	24
E30n	EMMS	500k	30	0.8	24
E30a	EMMS	500k	30	1.4	24
16a	Ganser	500k	30	1.4	16
16b	Ganser	500k	50	0.8	16
20a	Ganser	500k	30	1.4	20
20b	Ganser	500k	50	0.8	20
24a	Ganser	500k	30	1.4	24
24b	Ganser	500k	50	0.8	24

Tab. 3: Overview of simulations

Drag law pre-selection

In order to find a suitable drag law for the simulation the three drag laws: Ganser, WYE, and EMMS were tested. First simulations were conducted with a coarser grid, with about 300 000 (“300k”) cells (Fig. 4: “E300”, “W300”, “G300”), to investigate the general trend of the drag laws. Subsequent simulations were conducted as described previously with a mesh with approximately 500 000 (“500k”) cells (Fig. 4: “G500” and “W500”). The defined parameters in Fig. 4 show a similar performance of both the Ganser and WYE drag laws, but with both drag laws and chosen settings flooding of the AR SEP was observed in the rendered animation. The AR SEP flooding occurred slower with the

Ganser drag law compared to the WYE drag law in the simulation with 500k cells.

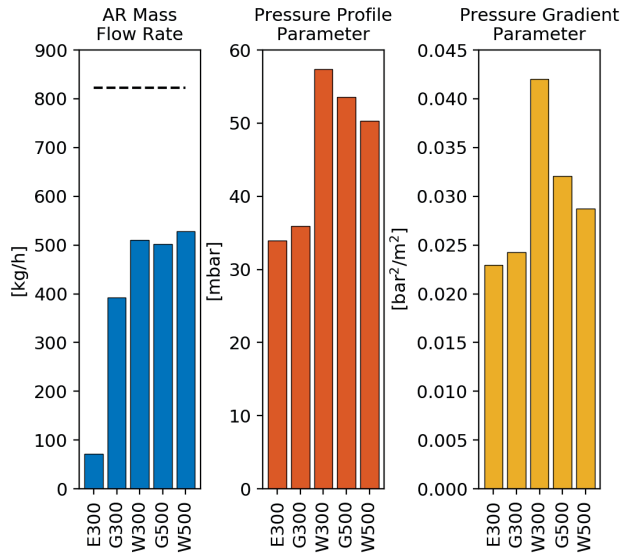


Fig. 4: Drag law variation with 300k and 500k cells

The other parameters, P_s and LLS fluidization rate, were tested with all three drag laws to find the best settings. In general, the EMMS drag law did perform worse compared to the other drag laws. An explanation for those results could be found by looking at the conditions on which the implemented EMMS model (“EMMS-Yang-2004 model”) in Barracuda was based on. Among other conditions, the model was generated for a particle density of 930 kg/m^3 and a solid flux of $14.3 \text{ kg/m}^2\text{s}$. The particle density of the bronze particles is 8800 kg/m^3 and considering a diameter in the AR column of 52 mm, the mass flux is approx. $107 \text{ kg/m}^2\text{s}$.

P_s variation

In first simulations of the cold flow model it was observed from graphs and rendered animations, that the pressure drop and bed’s height building up in the FR column are significantly higher than the measured values of the cold flow experiments. Additionally, it was a high particle volume fraction close to close-pack observed in the simulation. In order to reduce the number of particles in the FR column the P_s value was varied to influence the particle normal stress and particle acceleration (see Eq. 4). The P_s value variation was conducted from 1 Pa (default) to 100 Pa with the Ganser drag law. The simulation results are shown in Fig. 5.

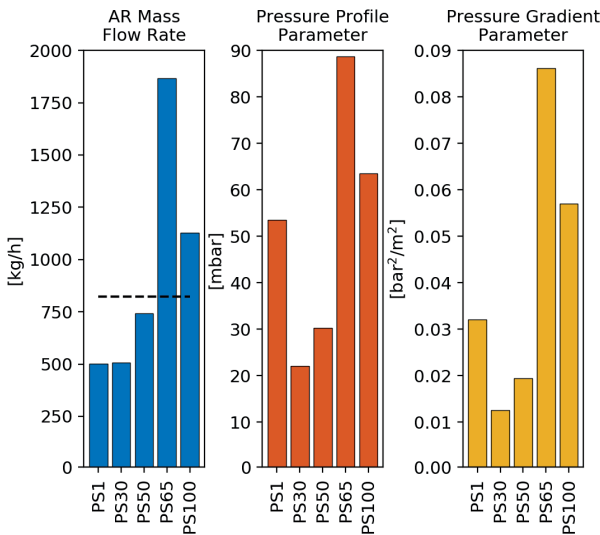


Fig. 5: P_s constant variation with Ganser

The increased P_s value to 30 and 50 Pa improved the pressure drop and pressure gradient in the FR column (see Fig. 5) while improving the particle circulation rate.

Loop seal fluidization rate variation and different drag laws

The influence of the LLS fluidization rate on particle circulation rate was observed and if the LLS fluidization rate is limiting the particle circulation rate. If the LLS limits the particle circulation a small error would impact the whole simulation on the one hand. On the other hand, adjustments to the LLS fluidization rate would allow more realistic results by adjusting the model and knowing this possible error.

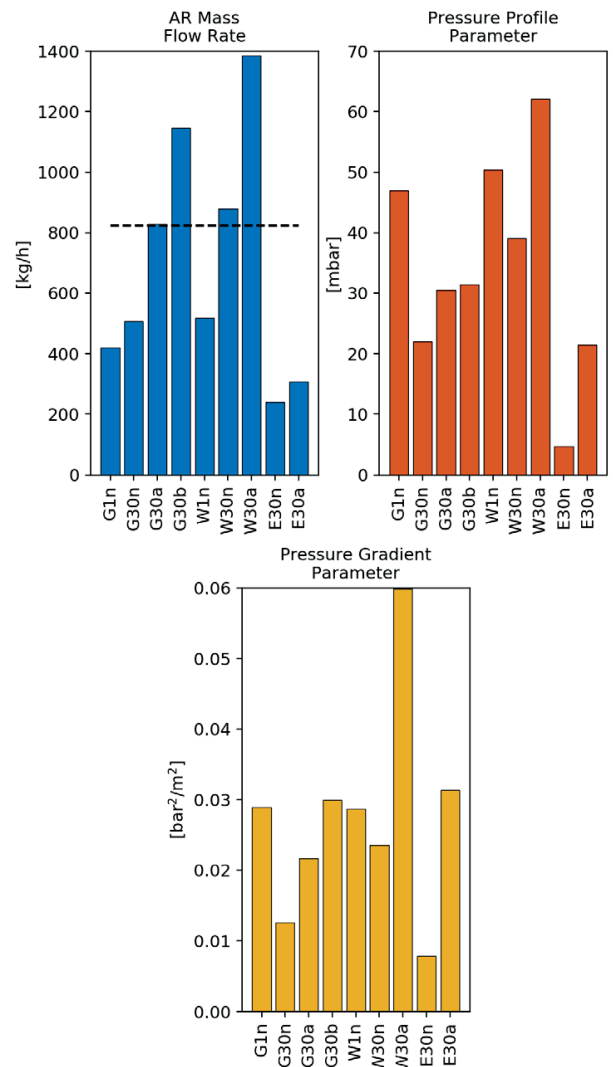


Fig. 6: Variation of loop seal fluidization rate - Simulations with non-increased loop seal fluidization rates labeled as “n”, increased by the factor 1.75 as “a”, and increased by the factor 2.5 as “b”

The simulations with Ganser and an adjusted P_s value to 30 Pa reached a stable steady state (Fig. 6). They improved further with 1.75 times increased loop seal fluidization rates. The WYE drag law predicted an AR mass flow larger than the ULS mass flow rate in all tested cases, which led to flooding of the AR SEP and an unsteady state. The EMMS drag law underestimated the mass flows with all adjustments. Those trends reflected the behavior observed previously during drag law variation. Therefore, Ganser had the best performance for the simulations. The WYE and EMMS drag laws were tested further.

Different operating points

Different operating points of the cold flow model were tested, with set AR fluidization rates from 16 to 24 Nm³/h. The results are visualized in Fig. 7 and Fig. 8. The operating points were simulated with $P_s = 30$ Pa and altered loop seal fluidization rates, which are labeled with "a", and with $P_s = 50$ and non-altered loop seal fluidization rates which are labeled as "b". The AR fluidization rate is indicated by the prefixed number in Fig. 7.

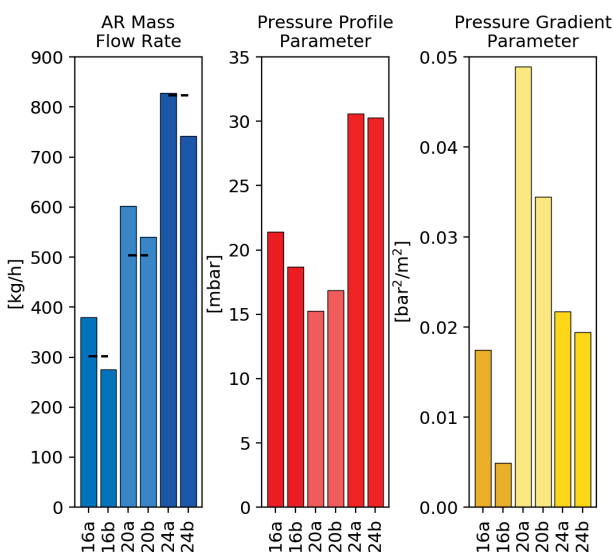


Fig. 7: Simulations of different operating point - Simulations with altered loop seal fluidization rates and $P_s = 30$ Pa are labeled as "a", with non-altered loop seal fluidization rates and $P_s = 50$ Pa are labeled as "b"

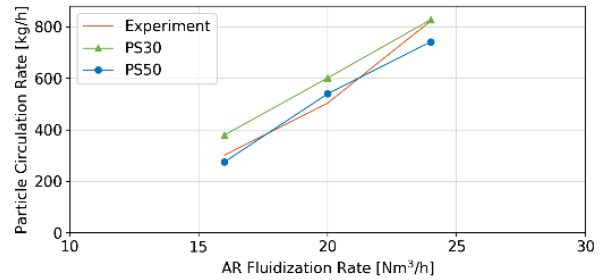


Fig. 8: Particle circulation rates at different operating points

The simulations with altered loop seal fluidization rates and P_s of 30 Pa predicted larger mass flow rates compared to the cases with normal loop seal fluidization rates and P_s of 50 Pa. The pressure difference over the FR column is in both cases very similar. The biggest was observed in particle distribution in the FR column represented as the pressure gradient. The pressure gradient deviation (P_{PG} value) visualized in Fig. 7 reflects the observation, that the cases with P_s set to 50 Pa are predicting the real particle distribution of the cold flow model better. Subsequently, the settings with P_s of 30 Pa and increased loop seal fluidization rates will be referred to as case "A", the settings with P_s of 50 Pa and normal loop seal fluidization rates will be referred to as case "B". The particle circulations rates of the simulation compared to the measured experimental circulation rates by Martinovic [30] are depicted in Fig. 8. The simulation with an AR fluidization rate of 16 Nm³/h overpredicted the particle circulation rate (302 kg/h) in case A by 26% and underpredicted in case B by 9%. The simulation with an AR fluidization rate of 20 Nm³/h overpredicted the particle circulation rate (504 kg/h) in case A by 19% and overpredicted in case B by 7%. The simulation with an AR fluidization rate of 24 Nm³/h overpredicted the particle circulation rate (823 kg/h) in case A by 1% and underpredicted in case B by 10%.

Overall the simulation with P_s set to 50 Pa and regular loop seal fluidization had a better performance due to the pressure parameters and sufficient mass flow rates. The simulations with P_s set to 30 Pa and increased loop seal fluidization rates tended to overpredict the mass flow rates and accumulated too many particles in the upper part of the FR column. The dependence of the particle circulation rate from the AR fluidization rate of the real case and the simulated cases is depicted in Fig. 8. Latter shows the clear trend of increasing particle circulation rates with increased AR fluidization rates. Based on those investigations, the best results on various operating points are calculated with a P_s value of 50 Pa.

4. Conclusion and outlook

The most important settings for the simulation are the drag law and the P_s constant. In particular the P_s constant played a significant role to achieve a steady state behavior, reduce bed heights in the FR column, and to achieve realistic particle circulation rates. The Ganser drag law and a P_s value of 50 Pa led to the best results overall. The loop seal fluidization rate had also a significant influence. Comparable results were achieved with a P_s value of 30 Pa and increased loop seal fluidization by 1.75, which led to a worse particle distribution but to a similar particle circulation rate. Different operating points were successfully simulated with those settings.

The ideal P_s value could be further investigated by repeating the simulation with slightly varied P_s values. Although good results were achieved by only adjusting the P_s value the variation of the β constant could further improve the simulation and should be considered in future simulations. In the next stage the settings of the cold flow model could be used to simulate a pilot plant. After simulating the

cold flow operation of a pilot plant successfully, heat transfer and chemical reactions should be modeled and implemented. A reliable and robust CFD model allows faster and cost-effective testing. Different set-ups of the actual gasification plant can be tested without physical modifications to optimize the geometry. Furthermore, a computational simulation allows deeper insight into the plant itself and is not limited by sight or measuring points. Therefore, fluid dynamical behavior can be investigated at any desired location. This could lead to faster implementation of the technology and improved quality of the product gas with a reduced tar content.

5. List of abbreviations

abbreviation	meaning
AR	air reactor
BB	bubbling bed
BCs	boundary conditions
CFB	circulating fluidized bed
CFD	computational fluid dynamics
CPFD	computational particle fluid dynamics
DFB	dual fluidized bed
e.g.	exempli gratia
etc.	et cetera
EMMS	energy-minimization multi- scale (EMMS drag model)
Eq.	equation
FR	fuel reactor
IC	initial condition
ILS	inner loop seal
LES	large eddy simulation
LLS	lower loop seal
MP-PIC	multi phase particle in cell
PSD	particle size distribution
SEP	separator
ULS	upper loop seal
WYE	Wen-Yu and Ergun (WYE drag model)

symbol	meaning	SI unit
a_p	particle acceleration	m/s^2
D	drag function	$1/s$
F	interphase momentum transfer function	N/m^3
p	pressure	Pa
g	gravitational acceleration	m/s^2
t	time	s
P_s	constant to calculate τ_p	Pa
u_f	fluid velocity	m/s
u_p	particle velocity	m/s
\bar{u}_p	particle mean velocity	m/s
x_i	spatial variable	m
α	constant to calculate τ_p	-
β	constant to calculate τ_p	-
ε_{cp}	close-pack particle volume fraction	-
ε_f	fluid volume fraction	-
ε_p	particle volume fraction	-
δ_{ij}	Kronecker delta	-
m_p	particle mass	kg
μ	viscosity	$kg/m * s$
∇	nabla operator	$1/m$
ρ_f	fluid density	kg/m^3
τ_D	damping time due to inelastic particle collisions	s
τ_f	fluid stress tensor	N/m^2
τ_p	particle normal stress	N/m^2

6. References

- [1] J. Schmid, ‘‘Development of a novel dual fluidized bed gasification system for increased fuel flexibility,’’ *TU Wien, Dr. thesis*, 2014.
- [2] M. Kuba, S. Kraft, F. Kirnbauer, F. Maierhans, and H. Hofbauer, ‘‘Influence of controlled handling of solid inorganic materials and design changes on the product gas quality in dual fluid bed gasification of woody biomass,’’ *Appl. Energy*, vol. 210, pp. 230–240, 2018.
- [3] F. Fotovat, A. Abbasi, R. J. Spiteri, H. de Lasa, and J. Chaouki, ‘‘A CFD model for a bubbly biomass-sand fluidized bed,’’ *Powder Technol.*, vol. 275, pp. 39–50, 2015.
- [4] Y. Liang, Y. Zhang, T. Li, and C. Lu, ‘‘A critical validation study on CFD model in simulating gas-solid bubbling fluidized beds,’’ *Powder Technol.*, vol. 263, pp. 121–134, 2014.
- [5] J. M. Weber, K. J. Layfield, D. T. Van Essendelft, and J. S. Mei, ‘‘Fluid bed characterization using electrical capacitance volume tomography (ECVT), compared to CFD software’s barracuda,’’ *Powder Technol.*, vol. 250, pp. 138–146, 2013.
- [6] L. Zhang, Z. Wang, Q. Wang, H. Qin, and X. Xu, ‘‘Simulation of oil shale semi-coke particle cold transportation in a spouted bed using CFD method,’’ *Powder Technol.*, vol. 301, pp. 360–368, 2016.
- [7] X. Shi, R. Sun, X. Lan, F. Liu, Y. Zhang, and J. Gao, ‘‘CPFD simulation of solids residence time and back-mixing in CFB risers,’’ *Powder Technol.*, vol. 271, pp. 16–25, 2015.
- [8] X. Shi, Y. Wu, X. Lan, F. Liu, and J. Gao, ‘‘Effects of the riser exit geometries on the hydrodynamics and solids back-mixing in CFB risers: 3D simulation using CPFD approach,’’ *Powder Technol.*, vol. 284, pp. 130–142, 2015.
- [9] S. S. Rodrigues, A. Forret, F. Montjovet, M. Lance, and T. Gauthier, ‘‘CFD modeling of riser with Group B particles,’’ *Powder Technol.*, vol. 283, pp. 519–529, 2015.
- [10] Q. Wang *et al.*, ‘‘Particle size distribution in CPFD modeling of gas-solid flows in a CFB riser,’’ *Particuology*, 2015.
- [11] X. Shi, X. Lan, F. Liu, Y. Zhang, and J. Gao, ‘‘Effect of particle size distribution on hydrodynamics and solids back-mixing in CFB risers using CPFD simulation,’’ *Powder Technol.*, vol. 266, pp. 135–143, 2014.
- [12] C. Chen, J. Werther, S. Heinrich, H. Y. Qi, and E. U. Hartge, ‘‘CPFD simulation of circulating fluidized bed risers,’’ *Powder Technol.*, vol. 235, pp. 238–247, 2013.
- [13] S. Clark, D. M. Snider, and J. Spenik, ‘‘CO₂ adsorption loop experiment with eulerian-lagrangian simulation,’’ *Powder Technol.*, vol. 242, pp. 100–107, 2013.
- [14] Q. Wang *et al.*, ‘‘Application of CPFD method in the simulation of a circulating fluidized bed with a loop seal, part I-Determination of modeling parameters,’’ *Powder Technol.*, vol. 253, pp. 814–821, 2014.
- [15] M. A. Hamilton, K. J. Whitty, and J. S. Lighty, ‘‘Numerical Simulation Comparison of Two Reactor Configurations for Chemical Looping Combustion and Chemical Looping With Oxygen Uncoupling,’’ *J. Energy Resour. Technol.*, vol. 138, no. 4, p. 042213, 2016.
- [16] B. D. Adkins, N. Kapur, T. Dudley, S. Webb, and P. Blaser, ‘‘Experimental validation of CFD hydrodynamic models for catalytic fast pyrolysis,’’ *Powder Technol.*, vol. 316, pp. 725–739, 2017.
- [17] Q. Ma, F. Lei, X. Xu, and Y. Xiao, ‘‘Three-dimensional full-loop simulation of a high-density CFB with standpipe aeration experiments,’’ *Powder Technol.*, vol. 320, pp. 574–585, 2017.
- [18] S. Kraft, F. Kirnbauer, and H. Hofbauer, ‘‘Influence of drag laws on pressure and bed material recirculation rate in a cold flow model of an 8 MW dual fluidized bed system by means of CPFD,’’ *Particuology*, vol. 36, pp. 70–81, 2017.
- [19] D. M. Snider, S. M. Clark, and P. J. O’Rourke, ‘‘Eulerian-Lagrangian method for three-dimensional thermal reacting flow with application to coal gasifiers,’’ *Chem. Eng. Sci.*, vol. 66, no. 6, pp. 1285–1295, 2011.
- [20] P. J. O’Rourke and D. M. Snider, ‘‘A new blended acceleration model for the particle contact forces induced by an interstitial fluid in dense particle/fluid flows,’’ *Powder Technol.*, vol. 256, pp. 39–51, 2014.
- [21] D. M. Snider, ‘‘An Incompressible Three-Dimensional Multiphase Particle-in-Cell Model for Dense Particle Flows,’’ *J. Comput. Phys.*, 2001.
- [22] M. J. Andrews and P. J. O’Rourke, ‘‘The multiphase particle-in-cell (MP-PIC) method for dense particulate flows,’’ *Int. J. Multiph. Flow*, vol. 22, no. 2, pp. 379–402, 1996.
- [23] N. Yang, W. Wang, W. Ge, L. Wang, and J. Li, ‘‘Simulation of heterogeneous structure in a circulating fluidized-bed riser by combining the two-fluid model with the EMMS approach,’’ *Ind. Eng. Chem. Res.*, vol. 43, no. 18, pp. 5548–5561, 2004.
- [24] R. P. Chhabra, L. Agarwal, and N. K. Sinha, ‘‘Drag on non-spherical particles: an evaluation of available methods,’’ *Powder Technol.*, vol. 101, no. 3, pp. 288–295, 1999.
- [25] C. Y. Wen, ‘‘YH Yu. Mechanics of fluidization,’’ in *Chemical Engineering Progress Symposium Series*, 1966, vol. 62, no. 62, pp. 100–111.
- [26] D. Gidaspow, *Multiphase flow and fluidization: continuum and kinetic theory descriptions*. Academic press, 1994.
- [27] S. Ergun, ‘‘Fluid flow through packed columns,’’ *Chem. Eng. Prog.*, vol. 48, pp. 89–94, 1952.
- [28] CFD Software LLC., ‘‘Barracuda Virtual Reactor User Manual.’’ 2018.
- [29] S. Kraft, ‘‘Investigation of particle mixing in dual fluidized bed gasification systems by means of cold flow modelling and computational methods,’’ *PhD Thesis, TU Wien*, no. August 2017, 2017.
- [30] D. Martinovic, ‘‘Kaltmodellversuche und MSR-Konzept einer Zweibett-Wirbelschicht-Vergasungsanlage,’’ Technische Universität Wien, 2013.

Molecular dynamics simulations of the molten CaO-K₂O-SiO₂ system to study viscosity of woody biomass ash slags

C. Ma^{1*}, N. Skoglund¹, M. Carlborg¹, M. Broström¹

1. Department of Applied Physics and Electronics, Thermochemical Energy Conversion Laboratory, Umeå University, SE 901 87, Umeå, Sweden

*corresponding author, charlie.ma@umu.se

Abstract

Compositions in the CaO-K₂O-SiO₂ system have been simulated with molecular dynamics in order to elucidate aspects of structural characteristics that correlate to molten slag viscosity. Focus was placed on the structural characteristics of the Si and O atoms, which included pair distribution and coordination number functions, angular relationships, Q^n values, and oxygen types. Principal component analysis was used to reveal correlations between reported viscosity values and attributes of the structural characteristics. The simulations indicated that silicate tetrahedral units were prevalent and angular and atomic mobility attributes between these units correlate with viscosity. Viscosity also tends to increase with increasing shares of Q³ or higher, and tends to decrease with increasing shares of Q² or lower, as expected.

1. Introduction

Silicate slags often form during thermal conversion processes that use solid fuels and can create problems for operations. For example, their viscosity has a critical role in causing accumulative depositions within furnaces and other thermochemical reactors that can often lead to shutdowns [1]. The slags are characterised by the ordering of Si and O atoms such that SiO₄/silicate tetrahedral units of can exhibit extensive formations of inter-tetrahedral networks that influence viscosity. Accurate knowledge of molten slag viscosities can contribute towards more robust and reliable processes. This may be achieved by attaining an understanding of the structural characteristics of molten slags at the molecular level. Obtaining such information in-situ at high temperature can be difficult, but such characteristics have the possibility of being elucidated via

molecular dynamics (MD) simulations [2]. A number of recent studies have already applied this method towards studying slag viscosity. Dai et al.[3] performed MD simulations of coal ash compositions to study the effects that fluxants have upon viscosity. Oxygen atoms were found to have different numbers of Si atoms in close proximity, where free (FO), non-bridging (NBO), bridging (BO), and tricluster (TO) O atoms have 0, 1, 2, and 3, network-forming atoms (e.g., Si) within close proximity, respectively. A stability coefficient based on this distribution was defined to form relations with viscosity values as predicted by thermodynamic modelling. In a similar manner, diffusion coefficients from MD simulations of blast furnace slag by Zhang et al.[4] were applied to the Stokes-Einstein equation to produce viscosity values comparable to those as predicted by thermodynamic modelling. Another example was reported by Xuan et al.[5], who analysed synthetic

coal ashes both experimentally and with MD simulations. They found a logarithmic relationship between the degree of polymerization, as defined by Q^n values, from the MD simulations and their measured viscosity values of the different slag compositions. In these three studies, selective parametrization were necessary and only the latter compared results with experimental values. They do, nonetheless, suggest prospects of good correlations between quantities extracted from MD simulations and slag viscosity. Others have also used MD simulations to study structural features like pair distribution functions and bond/bridging angles between atoms [6-8]. Such common structural characteristics may be closely correlated to the viscosity of slags because they are indicators of atomic mobility in the silicate network. As such, it is the aim of this study to elucidate how quantities that are commonly extracted from MD simulations correlate with experimentally reported viscosity values. To this end, compositions within the CaO-K₂O-SiO₂ system at various temperatures were simulated. For conciseness, the focus was restricted to the Si and O atoms. Principal component analysis (PCA) was carried out to elucidate correlations between characteristic quantities and measured viscosity values found in the literature [9]. The results further the understanding of molten ash slag viscosity in this system by indicating structural characteristics that are most directly linked.

2. Method

Slag compositions

Six CaO-K₂O-SiO₂ compositions based on those used by Chen and Zhao [9] in their viscosity measurements were used as inputs in the simulations (Table 1). They are labelled according to their study, from K1 to K6. Up to eight different

temperatures were simulated for each composition, giving a total of 39 cases.

Label	SiO ₂ [mol%]	K ₂ O [mol%]	CaO [mol%]
K1	70	21.1	8.9
K2	77.7	15.1	7.2
K3	52.6	29.5	17.9
K4	49.8	17	33.2
K5	70	10.5	19.5
K6	78.2	7.7	14.2

Tab.1: Slag compositions

Simulation

LAMMPS (Version 8 Feb 2019)[10, 11] was the simulation tool used. The simulation method followed that of Li et al. [12] and is briefly described here. The potential function used as the basis for interatomic forces between atoms i and j separated by distance r_{ij} is based on the Born-Mayer-Huggins function augmented with the Morse potential between cation-anion pairs [12-14]. A constant number of approximately 5000 point ion atoms were simulated at 1 femtoseconds (10^{-15} s) timesteps within constant volumes and temperatures. Slag densities were obtained from the relationship by Lange [15]. Random initial positions and velocities were assigned to atoms before simulations at 5000 K were run for 100000 timesteps (0.1 ns) to relax and randomize the system. The system temperature was then ramped to the specified values at cooling rates no greater than 10^{13} K/s, in order to avoid formation of locked-in local structures. The simulation was then run for another 4×10^5 timesteps before data files for analysis were dumped periodically during an additional 10^6 timesteps. For each simulation, characteristic structural quantities were extracted from over 10^5 atoms within the files and averaged using scripts written in R (Table 2). The mean squared displacements of each atomic species was monitored to check that a

liquid phase prevailed. The tilt angle characteristic is as defined by Yuan and Cormack [16].

Structural characteristic	Atomic pair/unit	Attribute(s)
Pair distribution functions	Si-O, O-O, Si-Si	Nearest neighbor distance [\AA] median, FWHM [\AA]
Angles	O-Si-O, Si-O-Si, Silicate tetrahedral unit tilt	Median [°], Interquartile range [°]
Q^n values	Si-O	Distribution [%]
Oxygen types	Si-O	Distribution [%]

Tab.2: Structural characteristics extracted from simulation

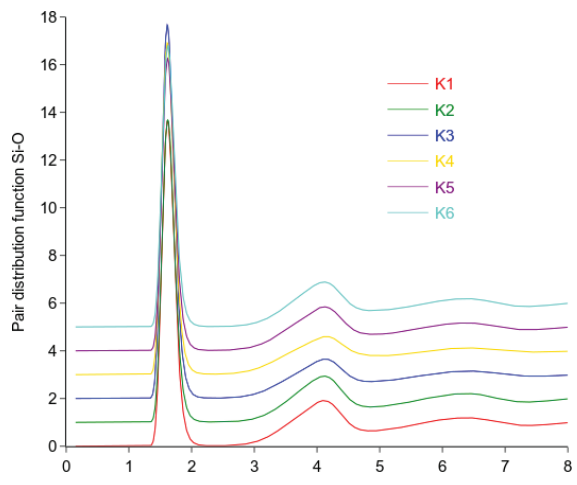
Attributes that possibly reflect atomic mobility were also quantified so that their correlations with viscosity could be assessed. SIMCA 16 facilitated the multivariate principal component analysis (PCA).

3. Results and discussion

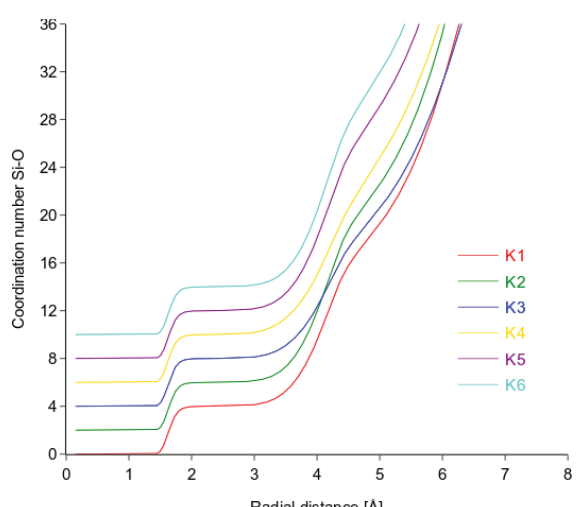
Pair distribution and coordination number functions

The Si-O pair distribution function (PDF) for each simulation in Fig.1a show the relative atomic density of O atoms that surround Si atoms. They are characterised by a major peak at a radial distance of approximately 1.6 \AA , which is a Si-O distance typical for silicate glasses and melts. Based on the valley position after the major peak in the Si-O PDFs, a cutoff radius of 2.4 \AA was set as the criterion for Si and O pairs to be considered as coordinated with each other. This value was used to evaluate Q^n values and to classify O atom types. The coordination number (CN) curves in Fig.1b show

plateaus when Si atoms are coordinated with four O atoms.



(a) PDF



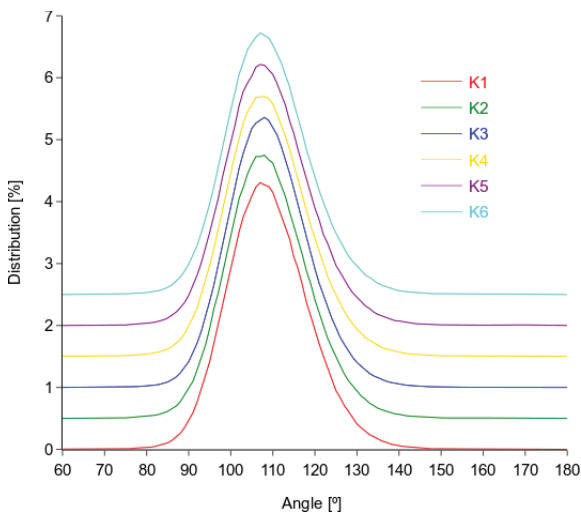
(b) CN

Fig.1: Example PDFs and CNs of Si-O pairs extracted from MD simulations at approximately 1573 K. Curves are consecutively elevated for clarity.

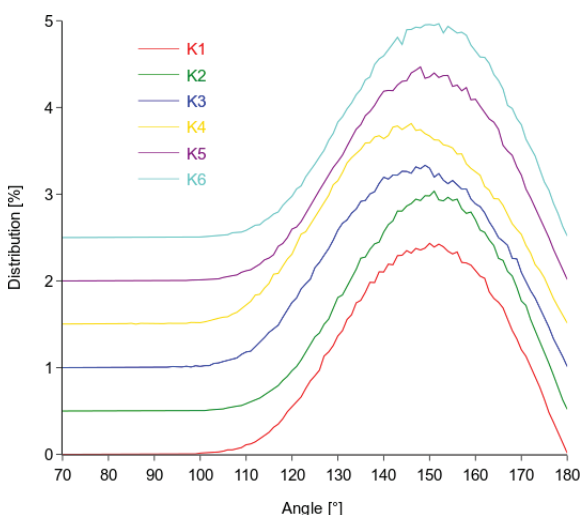
This highlights the stability of these coordinated units as it is a region in which predominately four, and only four, O atoms are located.

Angles

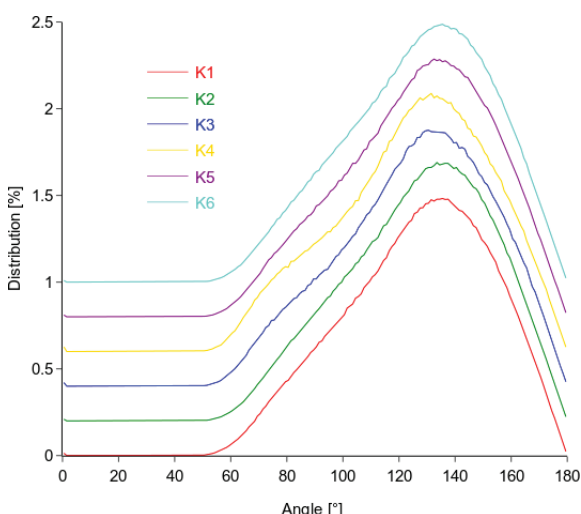
Angles formed by coordinated O-Si-O chains have similar median values (108.2 – 108.7°) for all compositions and temperatures as demonstrated in Fig.2a.



(a) O-Si-O angle



(b) Si-O-Si angle



(c) Tilt angle

Fig.2: Distributions of angles extracted from MD simulations at 1573 K. Curves are elevated for clarity.

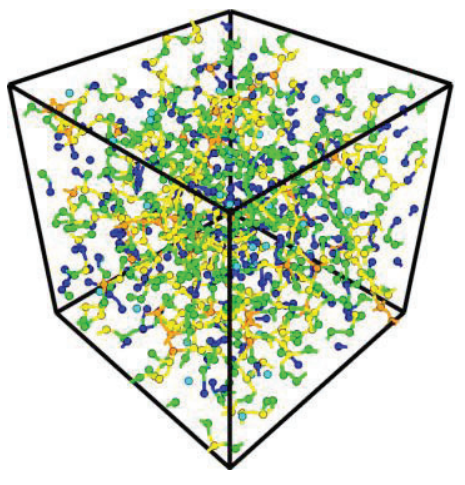
This is close to the tetrahedral angle (109.47°) and, along with the coordination number mentioned previously, indicates the prevalence of silicate tetrahedral units. The interquartile range varies between $11 - 15^\circ$, which is lower compared to those of the Si-O-Si and tilt angles. The distribution of Si-O-Si angles, which constitutes the link between silicate tetrahedral units, have median values between $143 - 151^\circ$ and interquartile ranges of $20 - 25^\circ$ (Fig.2b). The distribution of tilt angles (Fig.2c) show some variation in the median values ($126 - 130^\circ$) and the interquartile range is relatively broad ($37 - 39^\circ$). Taken together, these values indicate the presence of relatively rigid silicate tetrahedral units that are linked in a relatively flexible manner at their O atom vertices.

Q^n values

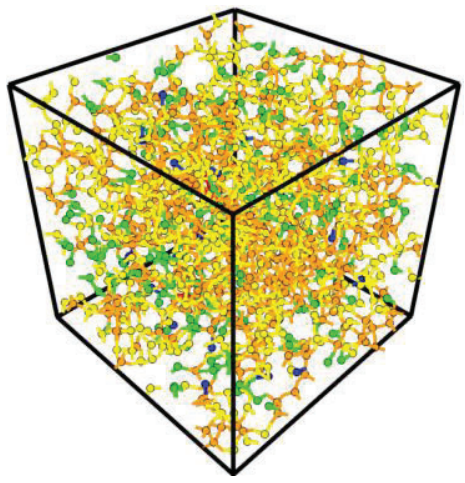
Fig.3a to 3c shown simulation snapshots of Si atoms with bridges to O atoms coloured according to their Q^n value for each composition (O atoms are omitted for the sake of clarity). This distribution did not vary significantly with temperature but is clearly affected by the differences in composition. The sparsity of K3 and K4 (Fig.3a) and their higher shares of low Q^n values is attributed to their relatively low contents of Si atoms. This restricts the formation of extensive networks with high Q^n values that are exemplified by K2 and K6 (Fig.3c).

Oxygen types

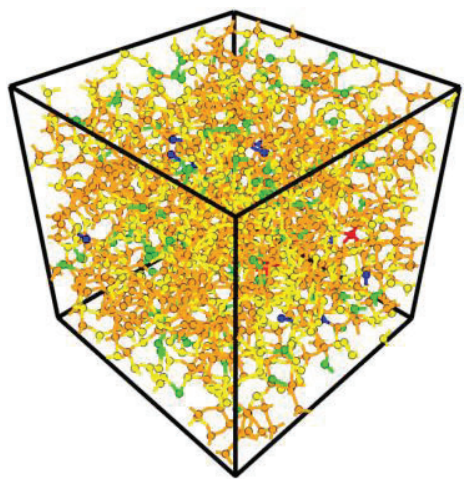
The distribution of oxygen types shown in Fig.4 indicates that BOs and NBOs dominated almost completely. The distributions did not show much variation with respect to temperature but the ratio of BO:NBO differed significantly between the compositions. In line with the Q^n values, the share of BOs is greater for compositions with greater Si content.



(a) K4



(b) K1



(c) K6

The scarcity of TOs (below 0.1 % in all cases) is consistent with the stability of the silicate tetrahedral unit; TOs instead tend to be more apparent in systems containing e.g., Al [7].

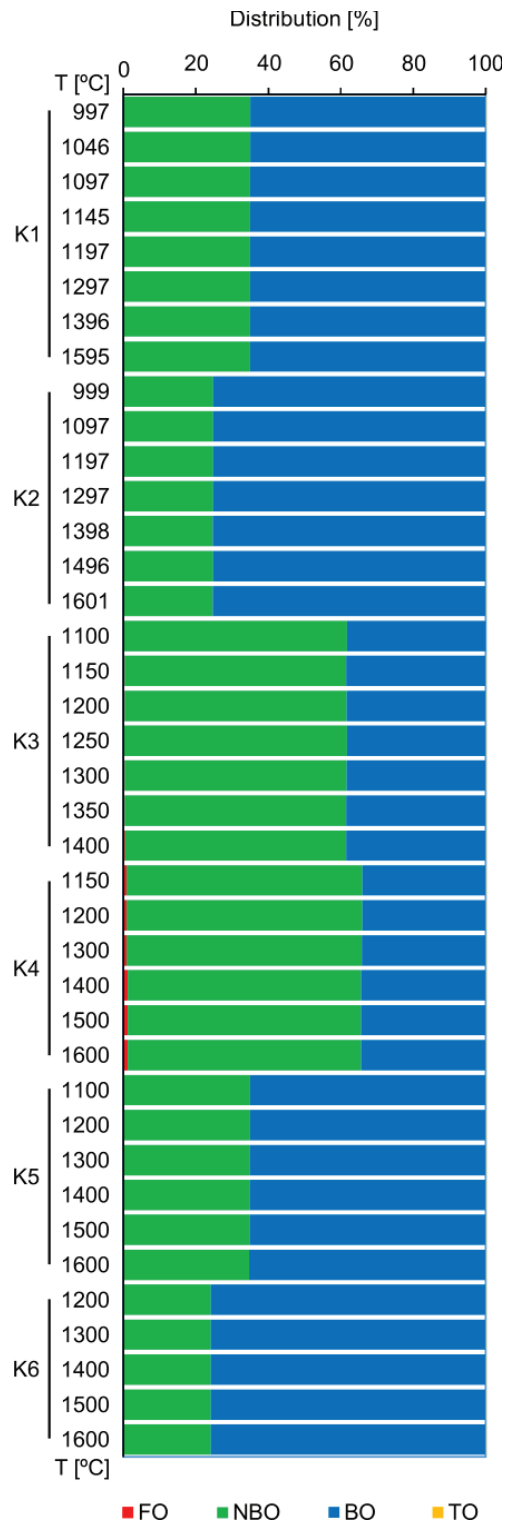
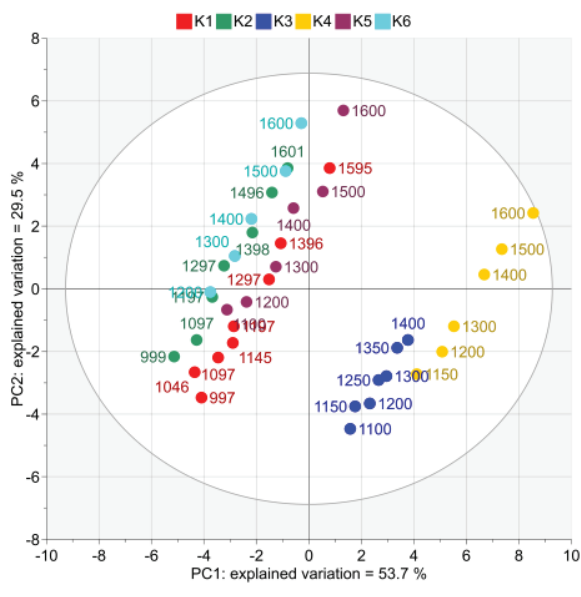


Fig.4: Distribution of oxygen types from the simulations

Multivariate analysis

The PCA score plot of Fig.5a indicates that the structural characteristics enable the cases to be grouped and aligned according to composition and temperature.



(a) Scores

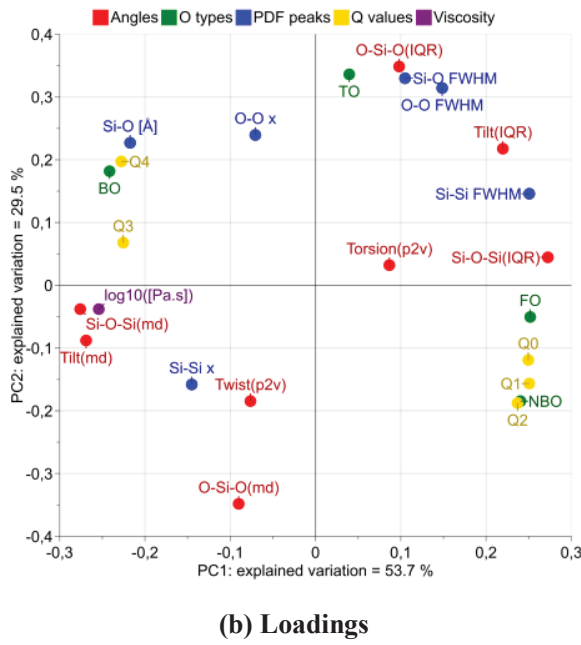
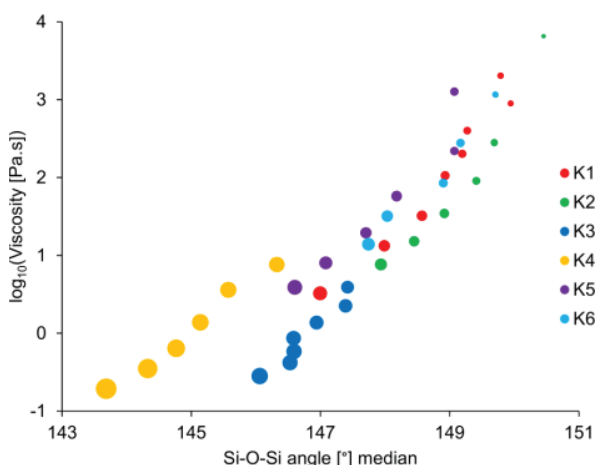


Fig.5: PCA plots of first two components. Based on a 2-component model, the goodness of fitting and prediction (based on cross-validation) are 83.2 % and 79.3 %, respectively.

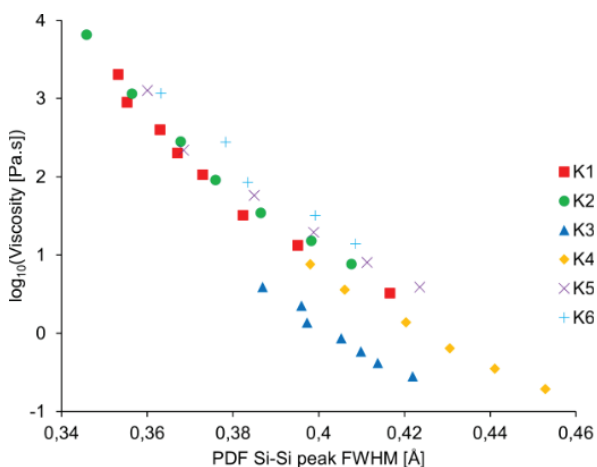
The first principal component (PC1, horizontal axis) is largely aligned to the

structural characteristics that are due to the differences in composition. From the loading plot of Fig.5b, these include mainly those pertaining to Q^n values and oxygen types, as well as a few from PDF and angle attributes. The second principal component (PC2, vertical axis) is largely aligned with the structural characteristics that are due to the differences in temperature. These are almost exclusively those pertaining to PDF and angle attributes. This implies that Q^n values and oxygen types are largely independent of temperature, as exemplified for the former in Fig.4. It is noted that the strong alignment of TO towards PC2 is due to the scaling of variances as part of the PCA, in order to apply equal importance to all variables. The actual share of TOs was well below 0.1 % of all O atoms in all simulations. The loading plot also identifies the structural characteristics that can have strong positive or negative correlations with the reported viscosity values (the variable identified as the purple point with $\log_{10}([\text{Pa.s}])$ label in Fig.5b). The structural characteristics that lie closest (most strongly correlated) are the median Si-O-Si and tilt angles, while those most diametrically opposed (most negatively correlated) are the interquartile ranges of the Si-O-Si angle and Si-Si PDF peak FWHM. These angle and PDF attributes are plotted against viscosity in Fig.6. The median values of Si-O-Si angles show a proportional relationship with the viscosity, in a range comparable to that of quartz and cristobalite. The negative correlation with the interquartile range implies a greater disorder in the silica network that gives lower viscosity. By contrast, the median values and interquartile ranges of the O-Si-O angles are less correlated to viscosity, and their deeper relation with viscosity is beyond the current scope. Nonetheless, taken together with previous discussion, this implies that silicate tetrahedral units are

relatively rigid units that are linked to other units in a relatively flexible manner.



(a) Si-O-Si angle (marker widths: interquartile range 20–25°)



(b) Si-Si peak FWHM

Fig.6: Plots of viscosity against structural characteristic attributes identified in loading plot

Fig.5b to be most correlated or negative correlated.

This is also apparent in the negative correlation of Si-Si FWHM with viscosity. In concordance with the angle variations, the FWHM of the Si-Si peak also implies a more volatile network where the distances between Si atoms are more scattered. Q^n values show less sensitivity to viscosity than the aforementioned structure characteristics, but viscosity tends to increase with increasing shares of Q^3 or higher, and tends to decrease with

increasing shares of Q^2 or lower. Similarly, bridging O atoms tend to be loosely correlated with viscosity, while the inverse is evident in regards to non-bridging and free O atoms. This is expected to be based on the influence that the degree of polymerization has upon viscosity [5]. The O-O PDF attributes of peak location and FWHM do not correlate significantly with viscosity.

4. Conclusion and Outlook

Based on molecular dynamics simulations using a Born-Mayer-Huggins potential function augmented with Morse interactions, the following relations between the structural characteristics of molten $\text{K}_2\text{O}-\text{CaO}-\text{SiO}_2$ slags and their viscosity were elucidated:

- Si and O atoms tend to form stable silicate tetrahedral units that polymerize via bridging O atoms
- The median value of the Si-O-Si angle that links silicate tetrahedral units varies between approximately 143 – 151° and correlates with reported viscosity values between approximately 0.1 – 6500 Pa.s. The extent of variation in this angle (i.e., interquartile range) is also negatively correlated to viscosity.
- Correspondingly, the FWHM of the major peak in the PDF of Si-Si pairs is also negatively correlated with the viscosity
- The silicate tetrahedral units form relatively flexible links between them via O atom network bridges
- Q^n values show less sensitivity to viscosity than the aforementioned structure characteristics, but viscosity tends to increase with increasing shares of Q^3 or higher, and tends to decrease with increasing shares of Q^2 or lower
- Similarly, bridging O atoms tend to be loosely correlated with viscosity, while the inverse was evident in regards to non-bridging and free O atoms.

In future, the structural effects that K and Ca atoms have on the silicate network will be presented, in order to give deeper insights into their effects upon the molten slag viscosity presented herein.

5. Acknowledgements

We thank the Bio4Gasification organisation for the financial support to carry out this study.

6. References

- [1] U. Kleinhans et al., Progress in Energy and Combustion Science **68** (2018) p65
- [2] A. Cormack et al., Glass Physics and Chemistry **27** (2001) p28
- [3] X. Dai et al., Fuel **237** (2019) p163
- [4] C. Jiang et al., Metallurgical and Materials Transactions B: Process Metallurgy and Materials Processing Science **50** (2019) p367
- [5] W. Xuan et al., Fuel **242** (2019) p362
- [6] T. Wu et al., Journal of Non-Crystalline Solids **435** (2016) p17
- [7] G. Fan et al., Material Transactions **56** (2015) p655
- [8] K. Zheng et al., ISIJ International **52** (2012) p342
- [9] M. Chen and B. Zhao, Fuel **180** (2016) p638
- [10] LAMMPS, <https://lammps.sandia.gov/>, 8 Feb 2019
- [11] S. Plimpton, Journal of Computational Physics **117** (1995) p1
- [12] K. Li et al., Chemical Engineering Journal **313** (2017) p1184
- [13] K. Li et al., Energy & Fuels **31** (2017) p13466
- [14] A. Miyake, Mineralogical Journal **20** (1998) p189
- [15] R. Lange, Contributions to Mineralogy and Petrology **130** (1997) p1
- [16] X. Yuan and A. Cormack, Journal Non-Crystalline Solids **319** (2003) p31

Modelling and Simulation Abstracts

Kinetic Modeling of Industrial Plastic Pyrolysis

A.E. Lechleitner^{1*}, T. Schubert¹, M. Lehner¹, W. Hofer²

1. Chair for Process Technology and Industrial Environmental Protection, Montanuniversitaet Leoben,
Franz-Josef-Str. 18, 8700 Leoben, Austria

2. OMV Refining & Marketing GmbH, Mannswoerther Straße 28, 2320 Schwechat, Austria

*corresponding author, andreas.lechleitner@unileoben.ac.at

1. Introduction and Short Description:

Recycling of wastes is one environmental concern of the EU policy to reduce greenhouse gases and substitute raw materials. For this purpose, a co-pyrolysis of polyolefins has been developed in previous works. The process uses a high boiling by-product of the refinery as carrier medium to insert the plastic into pipe reactors for thermal cracking. To investigate the complex reaction scheme of the co-pyrolysis lumped kinetic modeling (LKM) is used. The model will be used to scale up an existing pilot plant to a demo plant.

2. Methodology, Results and Discussion

An integral laboratory plant provides the data for the kinetic model. The plant consists of two serial electrical heated tubular reactors variable in length. The maximum length is 25 meters each. The process temperature can reach up to 500°C and pressures up to 15 bars at flow rates about three kilograms per hour. The feed consists of different types of plastic, such

as low-density polyethylene (LDPE) or polypropylene (PP), mixed with at least 80 wt.% carrier medium. Details of the laboratory plant are described in (Schubert et al. 2019).

The description of the educts and products occurs in lumps. Lumping groups species with similar properties, such as boiling cuts, and thus the reaction system is simplified. A lumped model for the co-pyrolysis is shown in Fig. 1. It consists of four lumps. Plastic is classified in the “Residue” lump by definition and the carrier medium is integrated in the “Residue” and the “Spindle oil” lump. The temperature dependence of the six pseudo first order reactions are described by the Arrhenius equation. As a result, twelve reaction parameters must be determined. Additionally, a collective reaction enthalpy is introduced, so 13 parameters are unknown. The Four Lump System generates four mass balances and one heat balance, which have to be solved simultaneously. To solve this underdetermined equation system the optimization toolbox from Matlab is used.

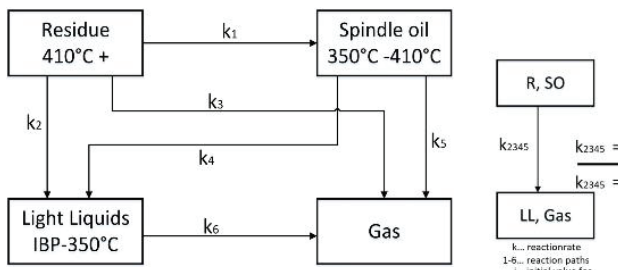


Fig.1: Four lump system with six possible irreversible, monomolecular, first order reactions

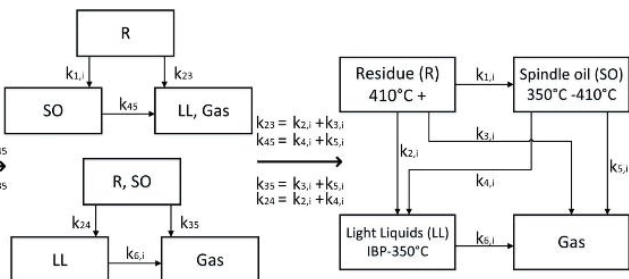


Fig.2: Scheme of the generation process of suitable initial point via total lumping

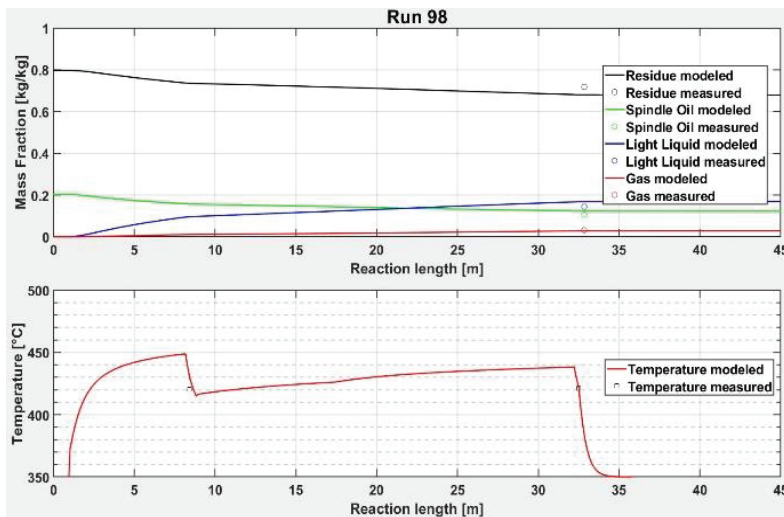


Fig.3: Measured and modeled products and temperature trends over reaction length of an exemplary test run of the pilot plant with 20% PP and 80% carrier medium

To overcome inappropriate starting point at the nonlinear fitting procedure, a total lumping algorithm generates suitable initial values (Fig. 2). (Lechleitner et al. 2019)

Furthermore, the model uses flow patterns to describe the flow regime and the heat transfer. This is necessary because of the two-phase flow in the reactors, which induces different flow velocities and therefore the flow regime has a significant influence on residence times and kinetics. Additionally, determining the heat transfer at different flow patterns is needed to set up the heat balance and identify the reaction enthalpy.

Figs. 3 and 4 present results for the test series of 20% polypropylene and 80% carrier medium.

References

- Lechleitner, Andreas; Schubert, Teresa; Lehner, Markus; Hofer, Wolfgang (2019): Kinetic modeling of pyrolysis within the scope of industrial plastic feedstock recycling. In: 10th International Symposium on Feedstock Recycling of Polymeric Materials. Budapest, 26-29.05.2019, S. 31–33.
- Schubert, Teresa; Lehner, Markus; Karner, Thomas; Hofer, Wolfgang; Lechleitner, Andreas (2019): Influence of reaction pressure on co-pyrolysis of LDPE and a heavy petroleum fraction. In: Fuel Processing Technology 193, S. 204–211. DOI: 10.1016/j.fuproc.2019.05.016.

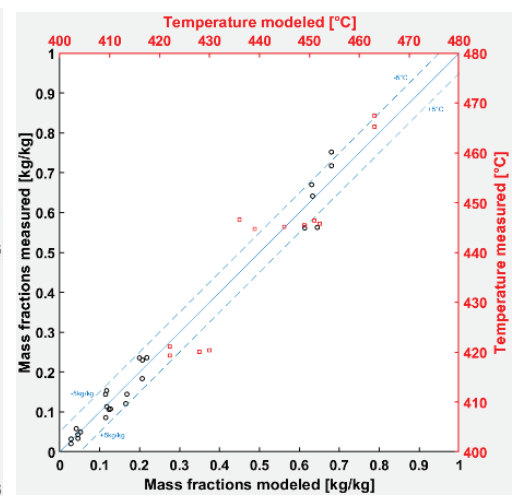


Fig.4: Measured and modeled temperatures (squares) and mass fractions (circles) at the reactor outlet of test runs with 20% PP. The ideal line is at a 45° angle and the ± 5 kg/kg or $\pm 5^\circ\text{C}$ deviation is marked with dashed lines

The standardized mean squared error between measured and modeled temperatures and mass fractions is 0.773%. Hence the fit converges well.

3. Conclusion and Outlook

The existing model can describe the reactors of a novel process at different mixtures of plastics and carrier medium. The kinetic data computed are comparable to literature and fit to observation of other pilot plants.

However, the model will be improved with molar balances, more accurate species data and more experimental data. At the end the model should be linked with a simulation tool, such as PetroSim or HYSYS, to simulate the whole industrial demo plant.

Gas Cleaning and Gas Upgrading Full Papers

Developing an adsorption-based gas cleaning system for a dual fluidized bed gasification process

J. Loipersböck^{1,*}, G. Weber¹, R. Rauch², H. Hofbauer³

1. BIOENERGY 2020+ GmbH,
Inffeldgasse 21b, 8010 Graz, Austria

2. Karlsruhe Institute of Technology, Institute of Chemical, Environmental and Biological Engineering
Engler-Bunte-Ring 1, 76131 Karlsruhe, Germany

3. TU Wien, Institute of Chemical, Environmental and Bioscience Engineering
Getreidemarkt 9/166, 1060 Vienna, Austria

*corresponding author, juergen.loipersboeck@bioenergy2020.eu

Abstract

Biomass can make a major contribution to a renewable future economy. If biomass is gasified a wide variety of products (e.g.: bulk chemicals, hydrogen, methane, alcohols, diesel) can be produced. In each of these processes gas cleaning is a crucial factor. Impurities in the gas can cause catalyst poisoning, pipe plugging, unstable or poisoned end products or harm the environment. Especially aromatic compounds (e.g.: benzene, naphthalene, pyrene) have a huge impact regarding a stable operation of a syngas process. A removal of these compounds can be accomplished either with wet, dry or hot gas cleaning methods. Wet gas cleaning methods tend to produce huge amounts of waste water which needs to be treated separately. Hot gas cleaning methods provide a clean gas, but are often cost intensive due to their high operating temperatures and catalysts used in the system. Another approach is dry or semi dry gas cleaning methods including absorption and adsorption on solid matter. In this work special focus will be laid on adsorption based gas cleaning for syngas applications. Adsorption and desorption test runs were carried out under laboratory conditions using a model gas with aromatic impurities. Adsorption isotherms as well as dynamics were measured with a multi compound model gas. Based on these results a temperature swing adsorption process was designed and tested under laboratory conditions, showing the possibility of replacing the conventional wet gas cleaning by a semi-dry gas cleaning approach.

1. Introduction:

The usage of biomass in sustainable technologies is a key to a renewable future. As it is the only renewable carbon source, a strong focus should be set in the development of renewable processes for the production of carbon based chemicals.

Dual fluidized bed gasification (DFB) is used to produce a high caloric, nitrogen-lean product gas. With this product gas several syntheses like Fischer-Tropsch,

mixed alcohols, methanation and hydrogen production can be realized. Nevertheless, an efficient gas cleaning system is crucial for these downstream processes. Nitrogen based (e.g.: ammonia, hydrocyanic acid), halogen based (e.g.: hydrochloric acid), sulfur based (e.g.: H₂S, COS, mercaptane) impurities as well as higher hydrocarbons (tar) can cause problems in catalysis reaction. Therefore, they have to be removed from the gas before it is applicable in synthesis gas

(syngas) processes. To lower the total amount of tar, DFB gasifiers are operated at higher temperatures, leading to the reduction of the total tar amount, but enhancing the formation of higher aromatics and poly-aromatic hydrocarbons (PAH) due to reduction of oxygen in the structures [1-7]. Hydrogen is well known for tar reduction and reduces the formation of heavier tars. With increasing temperature higher molecular tars are formed. As tar formation is not topic of this work it shall be referred to other authors. [8-12]

To remove these problematic compounds several approaches exist. They can be divided into primary and secondary methods. As primary methods are not scope of this work it shall be referred to the authors cited above. Secondary methods can be divided into wet scrubbing (e.g.: baffle separators, cooling towers or venturi scrubbers), dry or semi dry methods (e.g.: Ab-/adsorption on solids, particle cyclones, cold filters) and hot gas conditioning methods (e.g.: hot filters, thermal and catalytic crackers, steam reformers). [12]

As wet tar removal methods tend to produce high amounts of waste water and hot gas methods are cost intensive this work focuses on dry methods, especially adsorption.

Thiophene removal from an oily phase as well as tar separation during the thiophene syntheses is well studied. Jeevanandam et al. studied the thiophene removal from hydrocarbons by using metal impregnated adsorbents. Yu et al. worked on the desulfurization (especially thiophene and dibenzothiophene) of oil using activated carbon. [13,14]

Edinger et al. investigated the thiophene removal from the gaseous phase using activated carbon as low temperature alternative to the hydro-desulfurization (HDS) at temperatures between 100-200°C. [15]

Several studies concerning the removal of tar from biomass gasifier gas have been done, focusing on the a gas cleaning for heat and electric power production. [16-18]

A comparable gas cleaning technology is employed in the Gothenburg Biogas plant (GoBiGas) were a four-adsorber system is used, to remove heavy tars, BTX and sulphur components to achieve a syngas quality suitable for methanation after a biodiesel scrubber. [19,20]

This paper deals with the development of an adsorption based gas cleaning for the upgrade of a gasifier gas to syngas quality using adsorption technology.

2. Concept and methodology:

In laboratory scale a gas cleaning unit was investigated which focuses on reduction of operating costs by replacing the costly gas scrubbing using biodiesel (RME) by adsorption on activated carbon.

Therefore tar analysis, obtained from industrial DFB gasifiers were used to select model tar components. A classification of tars was introduced to represent each class in the mixture.

With this model tar, experimental research in terms of adsorption and desorption behavior was carried out.

Due to economic considerations, this paper focuses on the fine gas cleaning (substitution of the second biodiesel scrubber, see Fig. 1), as it has a 10 times higher biodiesel consumption as the first biodiesel scrubbing stage [21].

DFB steam gasification

DFB steam gasification is an allothermal gasification technology, using steam as gasification agent. Two reaction zones coupled by a slide and a cyclone are applied for this process. A steam fluidized reactor is used to gasify biomass in a bubbling bed. The fuel reacts with the steam in presence of catalytic active bed material under consumption of heat to the

main gas components hydrogen, carbon monoxide, carbon dioxide and methane [22].

The non-gasified biomass and the bed material are transported over a slide to the combustion zone. There a fast fluidized bed is applied by fluidization with air. The non-gasified biomass is burned there and the bed material is heated up again. Through a cyclone bed material is separated from the flue gas stream and transported back into the gasification reactor. The resulting gasification product is an almost nitrogen-free gas that is well suitable for syngas applications, like hydrogen production, Fischer-Tropsch synthesis or methanation.

For the use in syngas applications impurities have to be removed.

Impurities can be hydrogenated over the water gas shift stage (WGS) or removed by a two staged biodiesel scrubbing unit [23,24], which is the state-of-the-art in biomass to chemical processes.

Figure 1 shows the gas cleaning setup of a Fischer-Tropsch plant based on DFB gasification of wood. The two staged scrubber (biodiesel scrubber “warm” and biodiesel scrubber “cold”) allows an almost complete removal of tar components. The temperature swing adsorption is used to remove high volatile hydrocarbons as well as sulfur components.

Thus, gas cleaning by scrubbing is expensive; a more cost-saving way has yet to be developed.

Table 1 shows the impurity amount in the syngas before and after the first biodiesel scrubber stage (biodiesel scrubber “warm”, Fig. 1). A high removal efficiency of gravimetric tars and a poor removal efficiency of BTX components can be observed. Applying a two staged biodiesel scrubber would lead to high biodiesel consumption, even if the solvent is regenerated [21].

Therefore an adsorption based gas cleaning unit will be developed. First the biodiesel scrubber “cold” and the temperature swing adsorption will be replaced to remove tar and sulfur components more efficient.

To design a temperature swing adsorption (TSA) a detailed investigation regarding the behavior of tars during adsorption and desorption process was carried out.

	Inlet scrubber	Outlet scrubber
H ₂ O [vol-%]	35-45	8-12
Gravimetric tar [g/m ³ _{STP}] (db)	2-5	0-0.2
BTX [g/m ³ _{STP}] (db)	15-20	5-15
Sulfur components [ppm]	175-250	150-250
NH ₃ [ppm]	200-1500	100-400

Tab.1: Impurities before and after the first biodiesel scrubber stage [25-27]

STP... Standard temperature and pressure (273.15 K, 10⁵ Pa)

Classification of tars

Thus characterization of tar has been part of several research projects, a lot of classification systems exist. Baker et al. [28] define tars by their formation in primary, secondary and tertiary tar. However, this characterization does not include chemical properties or specific compound classes, such as organic acids. Furthermore, tar can be defined as organic components with a boiling point higher

than benzene. Additionally, classification distinguishing by gravimetric and GC/MS tar exists. [12,29-32]

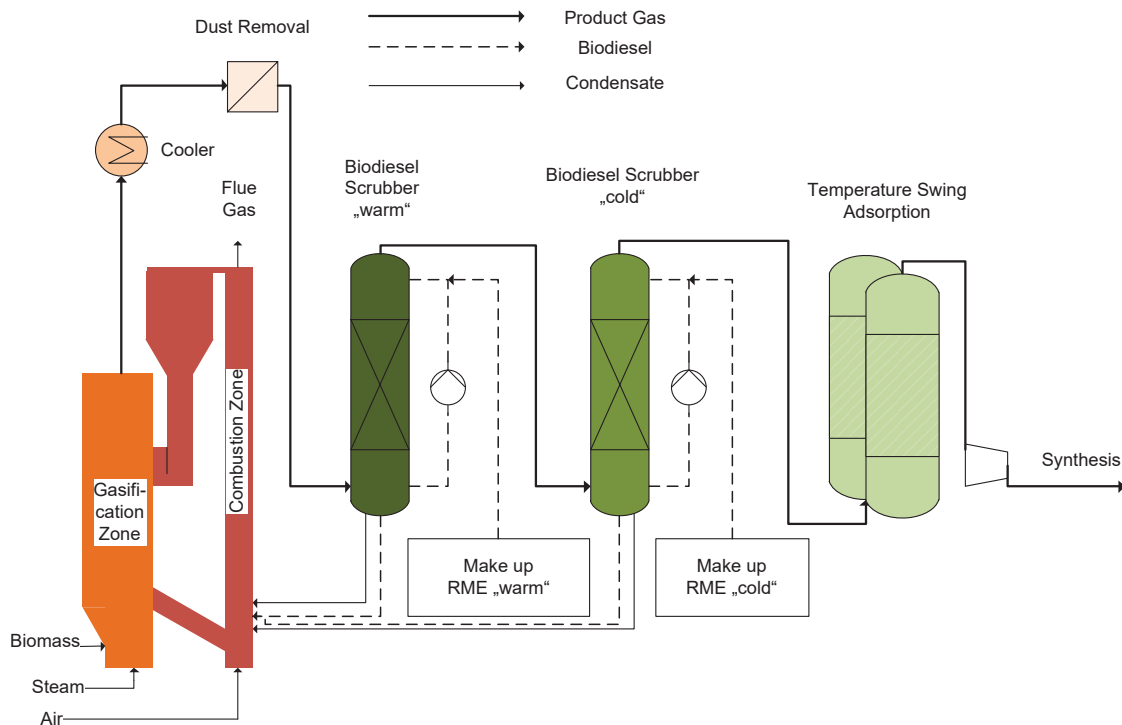


Fig.1: Flow scheme of the gas cleaning of a DFB based syngas plant

Another method for tar classification is the characterization by molecular weight and physical properties, defining five classes. Class 1 tars are described as gravimetric tars. Class 2 tars are heterocyclic tars with a high solubility in water. A typical representative compound for a class 2 tar is phenol. Class 3 tars are light aromatics like toluene. They are described as single ring components. Class 4 tars are light PAH (2-3 ring structures), like naphthalene. Class 5 tars have a poly aromatic structure of 4-7 rings. (e.g.: pyrene). [32]

One of the definitions states that long-chain hydrocarbon compounds having a larger molar mass than benzene (78.1 g / mol) can be referred to as tar. [33]

The tar protocol, defines tar as the total of all organic compounds in the synthesis gas with the exception of permanent gaseous hydrocarbons and benzene. [32-33]

Another definition describes tar as the condensable fraction of organic gasification products and as aromatic hydrocarbons including benzene. [34]

As the aim of this work is to clean up a gas to syngas quality, a removal of benzene due to its condensability during compression is highly recommended. Therefor the classification system using five tar classes [32] including benzene as class 3 tar, will be applied.

Based on the classification approach with five tar classes and the real gas composition after the biodiesel scrubber, a model gas composition was selected.

The model tar after the biodiesel scrubber consists of thiophene, representing aromatics with a hetero atom, toluene representing the BTX fraction (benzene, toluene, xylene), styrene representing aromatics and naphthalene, representing light polycyclic aromatics. Class 5 tars were not considered, as they

are removed in the first biodiesel scrubber stage. Table 2 depicts the model tar composition.

Selection of model tars composition

	Tar composition [%]
Thiophene	0.3
Toluene	85.4
Styrene	7.1
Naphthalene	7.2

Tab.2: Model tar composition after the first biodiesel scrubber stage

This mixture has a tar dew point of 38.9°C, at concentrations of 25.91 g/m³_{STP} which represents the tar dew point of DFB syngas after a one staged biodiesel scrubber. [21]

Activated Carbon

A commercial available activated charcoal was used for the experiments. This coal has a bulk density of 500 kg/m³ and a pellet diameter between 0.5 – 1.6 mm. As measured by BET surface method, an inner surface between 890 - 940 m²/g could be determined for the examined activated carbon. The BJH method gives a pore size between 3.1 to 3.5 nm (adsorption/desorption) for the examined activated carbon. An average pore volume of 0.13 to 0.19 cm³/g (desorption/adsorption) could be determined by BJH the method. The measurements of pore size, pore volume and BET surface were done with a TriStar II 3020 analyzer.

Adsorption setup and design of experiments

To develop an efficient gas cleaning for syngas applications several adsorption

experiments were executed. Figure 2 shows the flow scheme of the adsorption test rig used for the experiments. A mass flow controller (MFC) was applied to adjust a proper carrier gas flow. A syringe pump was used to adjust the amount of water and tars fed into the system. These two streams were mixed in an evaporation column situated in an oven. The mixture was sent to an adsorber, also situated in the oven to guarantee a stable temperature. After the gas left the adsorber several measurements were carried out. Tar components with a higher boiling point than naphthalene were measured by a liquid tar sampling method (according to tar protocol). Tar components with a boiling point of naphthalene and below were measured directly with gas chromatography (FID detector). Sulfur components (thiophene) were also measured by gas chromatography (SCD detector). Adsorption behavior in terms of adsorption isotherms and isobars was determined experimentally. As adsorption reactor a stainless steel cylinder with an inner diameter of 9 mm and a height of 50 mm was used. A superficial velocity of 0.1 m/s was adjusted. Each measuring point was measured multiple times. Adsorption isotherms were established at a standard temperature of 40°C by varying the inlet tar concentration between 1.5 and 50 g/m³_{STP}. Adsorption isobars were measured by adjusting a constant tar concentration of 25 g/m³_{STP} and varying the temperature between 40-220°C.

For both, adsorption isotherms and isobars, the adsorption capacity was calculated after their full loading by equation 1.

$$X_{Ads,Max} = \frac{m_{AC,out} - m_{AC,in}}{m_{AC,in}} \quad (1)$$

To get a more accurate result for the adsorption (respectively desorption) enthalpy the Clausius-Clapeyron equation

(2) was applied. By using the adsorption isothermes the adsorption enthalpy could be calculated. [36]

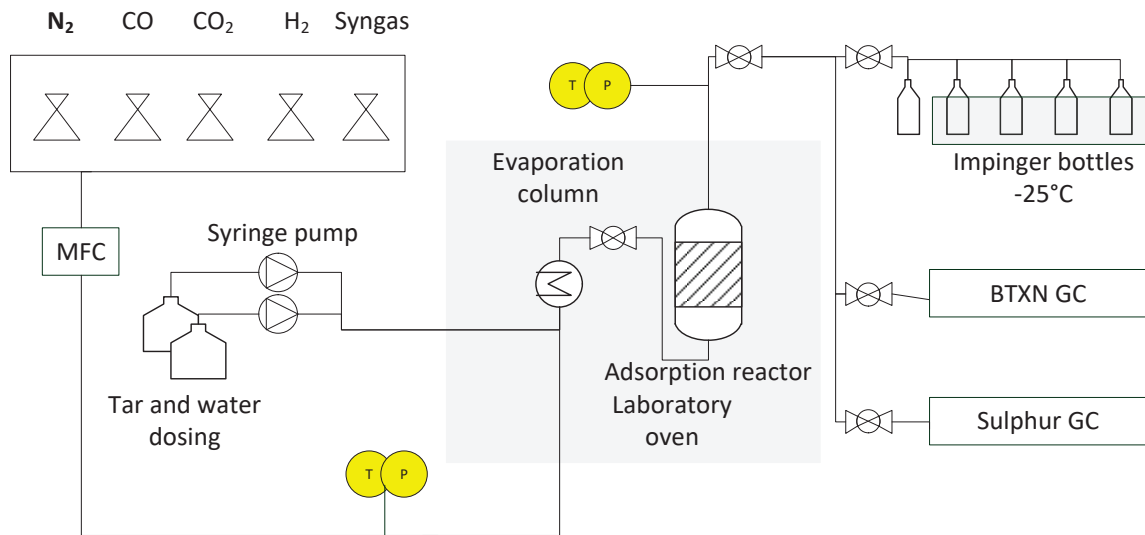


Fig.2: Flow scheme of the lab test setup

$$\ln \frac{p_2}{p_1} = \frac{\Delta H_{Ads}}{R} \left(\frac{1}{T_1} - \frac{1}{T_2} \right) \quad (2)$$

Adsorption dynamics were measured at tar concentrations of 25 g/m³STP by monitoring the total tar amount fed into the system and monitoring the total tar amount leaving the system. The difference between inlet and outlet tar amount was defined as adsorbed tar amount (equation 3).

$$Y(t)_{ads} = Y(t)_{in} - Y(t)_{out} \quad (3)$$

Also the thiophene adsorption dynamics were measured by analyzing the outlet gas in a SCD gas chromatograph.

Based on the adsorption dynamics the specific tar adsorption amount (X_{BT}) was calculated by using the breakthrough time (t_{BT}), the mass of adsorbent (m_{AC}) and the tar inlet concentration (Y_{in}) (equation 4).

$$X_{BT} = \frac{Y_{in} t_{BT}}{m_{AC}} \quad (4)$$

Based on these data, the adsorption part of a temperature swing adsorption was designed.

Desorption setup and design of experiments

To investigate the desorption behavior loaded activated carbon (AC) was used and investigated in a thermo gravimetric analyzer (TGA). In the TGA a temperature ramp was adjusted to measure the mass reduction of the AC over time, respectively the desorption of tars. The temperature, where the highest mass loss occurred was defined as characteristic temperature.

3. Results and discussion

Adsorption

Adsorption isotherms were measured to describe the adsorption behavior of AC used to remove tar components from syngas.

Figure 3 shows the adsorption isotherm measured at 40°C. This isotherm correlates with the pure toluene adsorption at similar temperatures.

A modified Langmuir model was applied to describe the adsorption isotherm. Adsorption isobars were measured at 40°C, 65°C, 85°C and 180°C. Based on these measurements and the fitting Langmuir model, adsorption isotherms for 65°C, 85°C and 180°C were calculated and are shown in Figure 3. These isotherms were validated at other temperatures and show a good correlation at higher tar concentrations (20-30 g/m³STP), and higher deviation at low tar concentrations. A maximum error of 20% could be obtained at low tar concentrations. Based on the adsorption isotherms, the Clausius-Clapeyron equation was used to calculate the adsorption enthalpy. An adsorption enthalpy of 93 kJ/mol could be calculated for the desired process parameters. This value is highly dependent on the process temperature and inlet tar concentration. The measured value correlates with literature data. [35-37]

The adsorption dynamics were measured by a gravimetric approach. The amount (mass) of tar injected into the system was adjusted with a syringe pump. The mass increase of the adsorbent was measured. Figure 4 shows the breakthrough curve measured gravimetrically. It can be seen, that the theoretical mass increase (inlet) and the mass increase of the adsorbent are similar, until a maximum loading of the adsorbent is reached. A maximum adsorption capacity of 0.34 g_{tar}/g_{AC} respectively 34% could be measured. Based on these data a specific tar adsorption amount of 0.30 - 0.33 g_{tar}/g_{AC} could be calculated running several experiments. Nevertheless, this approach gives no information about the outlet concentration of the components itself. So thiophene content was analyzed.

The gravimetric breakthrough curve and the thiophene breakthrough curve

show deviations in terms of breakthrough time. As thiophene is a minor component of the gas, it does not contribute to the gravimetric breakthrough curve in a high amount. A concentration of 25 ppm thiophene was adjusted at the inlet of the system. A complete breakthrough of thiophene could be detected after 50 min, which is similar to the complete saturation time measured by the gravimetric breakthrough approach. However, a further increase beyond the feed concentration could be measured, which indicated displacement effects.

If the thiophene breakthrough curve is compared with the gravimetric breakthrough curve (Figure 4 and Figure 5) it can be seen that thiophene fully breaks through when the activated carbon reaches the maximum loading. Further loading of the AC leads to displacement effects and thiophene is desorbed and replaced by hydrocarbons with a higher evaporation temperature.

Desorption

Desorption behavior was analyzed by TGA experiments. Several temperature ramps, from 20°C to 700°C were measured. Test runs with a heating ramp of 5 K/min, 10 K/min and 20 K/min were carried out. A maximum mass decrease could be observed at a temperature of 152°C. Heating ramps of 10 and 20 K/min showed other results, due to the fast temperature increase. Figure 6 shows the TGA curve including the variation in a temperature range of 30 to 300°C with a heating ramp of 5 K/min.

Based on the characterizing temperature and the adsorption properties a temperature swing adsorption was designed and operated.

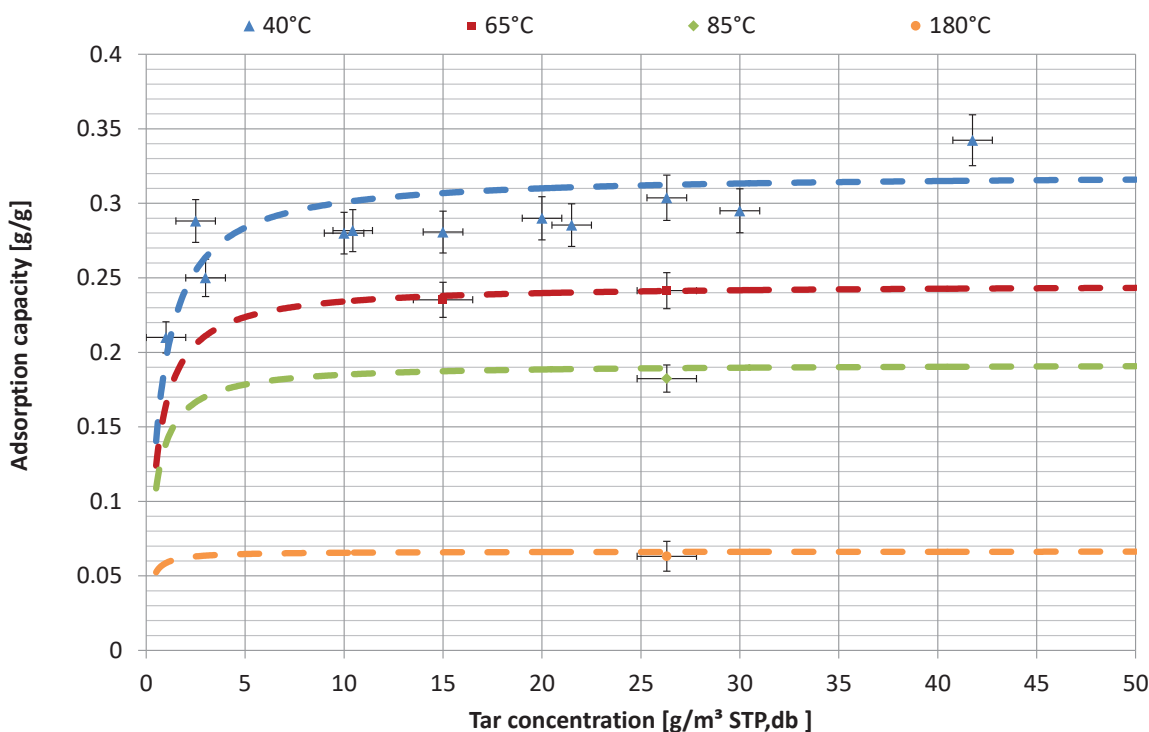


Fig.3: Adsorption isotherms at different temperatures

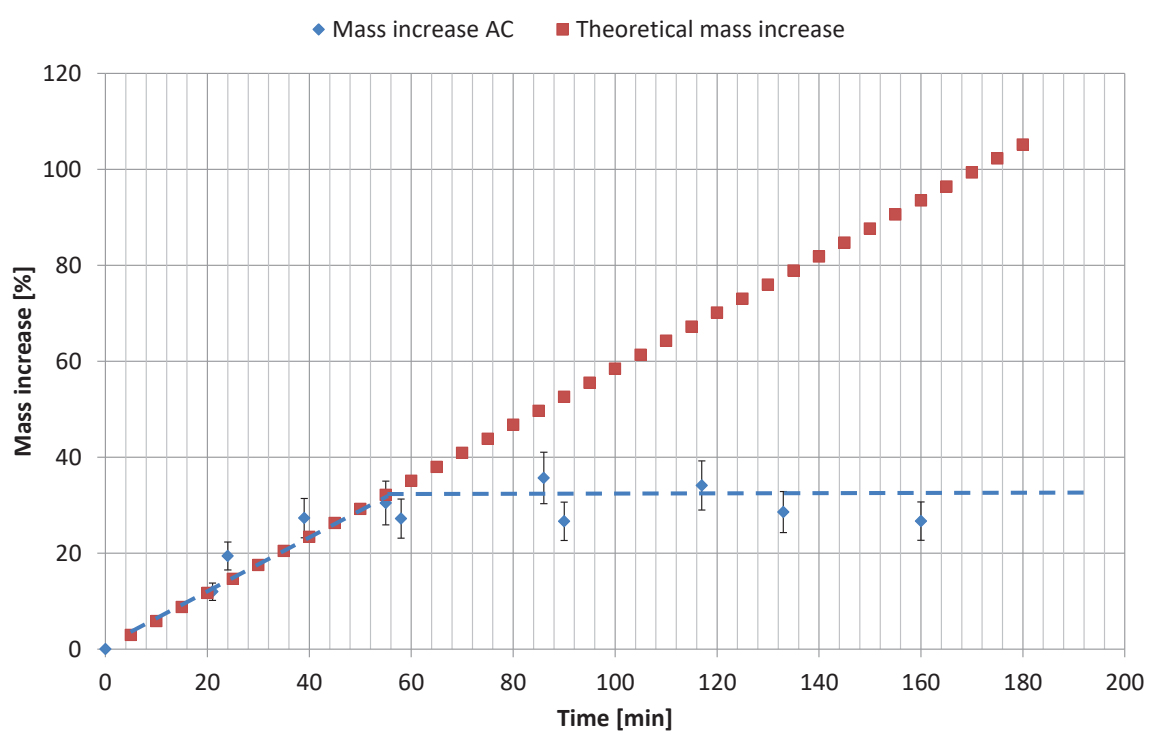


Fig.4: Gravimetric breakthrough curve

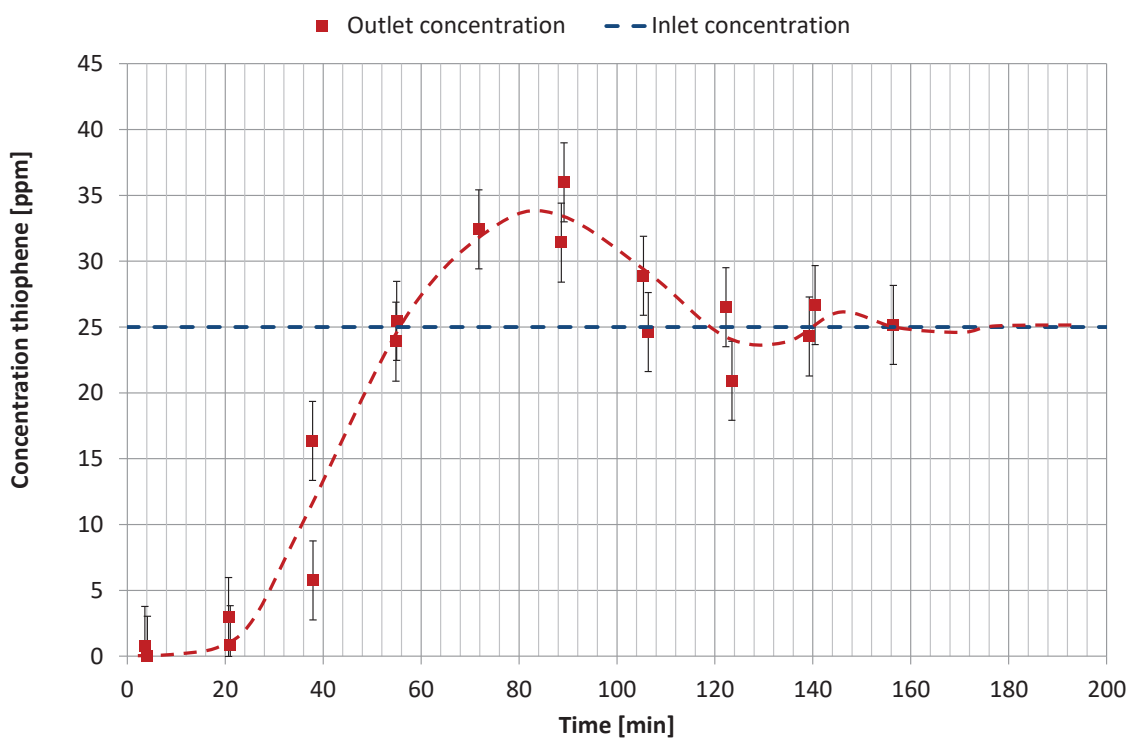


Fig.5: Thiophene breakthrough curve

Temperature swing adsorption

The designed TSA was operated at adsorption temperatures of 40°C and a tar concentration of 25 g/m³STP. Desorption temperatures of 180°C were adjusted for the first test runs, to be comparable to the achieved adsorption isotherms which were also measured at 180°C.

The TSA was operated with the same setup described for the adsorption experiments. The calculated adsorption capacity of 0.3-0.33 g adsorb-able tar per 1 g activated carbon, could be proven throughout several experiments. Figure 7 depicts the tar outlet concentration over 24 hours of operation. It can be clearly seen, that during the desorption phase, operated at 180°C tar components are desorbed and the adsorbent is regenerated. During the adsorption phase (40°C) tar is adsorbed with an efficiency of over 99%. A total of 1.4 m³ of gas per 1 m³ of flush gas (N₂, off-gas) could be cleaned with this setup. However, aging effects of the adsorbent can be observed. Over 200 hours of

continuous TSA operation the adsorption efficiency of the TSA was reduced to 95%. This means further optimizations have to be done.

Displacement effects for the TSA were not considered in this work, as only the sum of tar could be detected.

4. Conclusion and outlook

An adsorption based gas cleaning for the syngas applications has been developed. Due to economic considerations the gas cleaning setup described in Figure 1 was redesigned to replace the “cold” biodiesel scrubber. Adsorption isotherms and isobars were measured to obtain the optimal operation conditions for the expected tar loading in the gas. Desorption experiments were carried out in a TGA to gain the optimal desorption temperature. However this temperature was set higher (from 152 to 180°C) for the first TSA experiments.

Based on these data a TSA was designed and tested in a single reactor

setup, switching between adsorption and desorption operation. First results indicate the possibility of using a two-reactor-setup with a clean gas to flush gas efficiency of $1.4 \text{ m}^3 \text{ clean gas}/\text{m}^3 \text{ flush gas}$.

In further work the replacement effects, observed in this study will be

analyzed in more detail. Also a further optimization of the TSA, regarding a lowering of the desorption temperature and an increase of the clean gas to flush gas ratio will be performed.

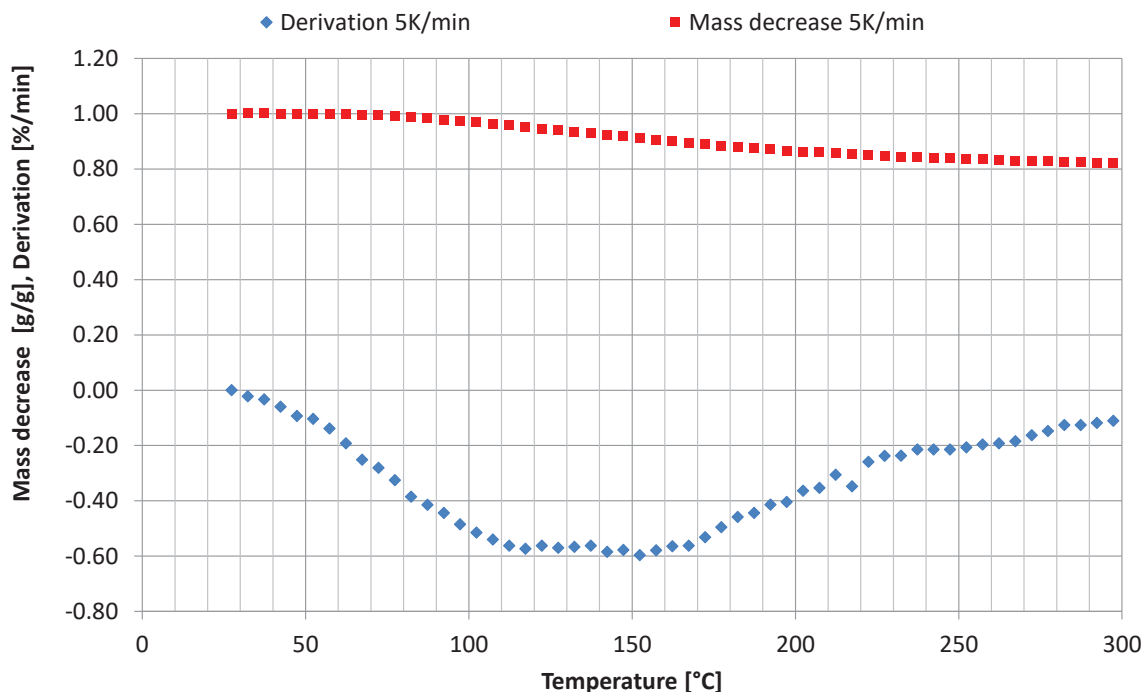


Fig.6: TGA analysis of the loaded AC

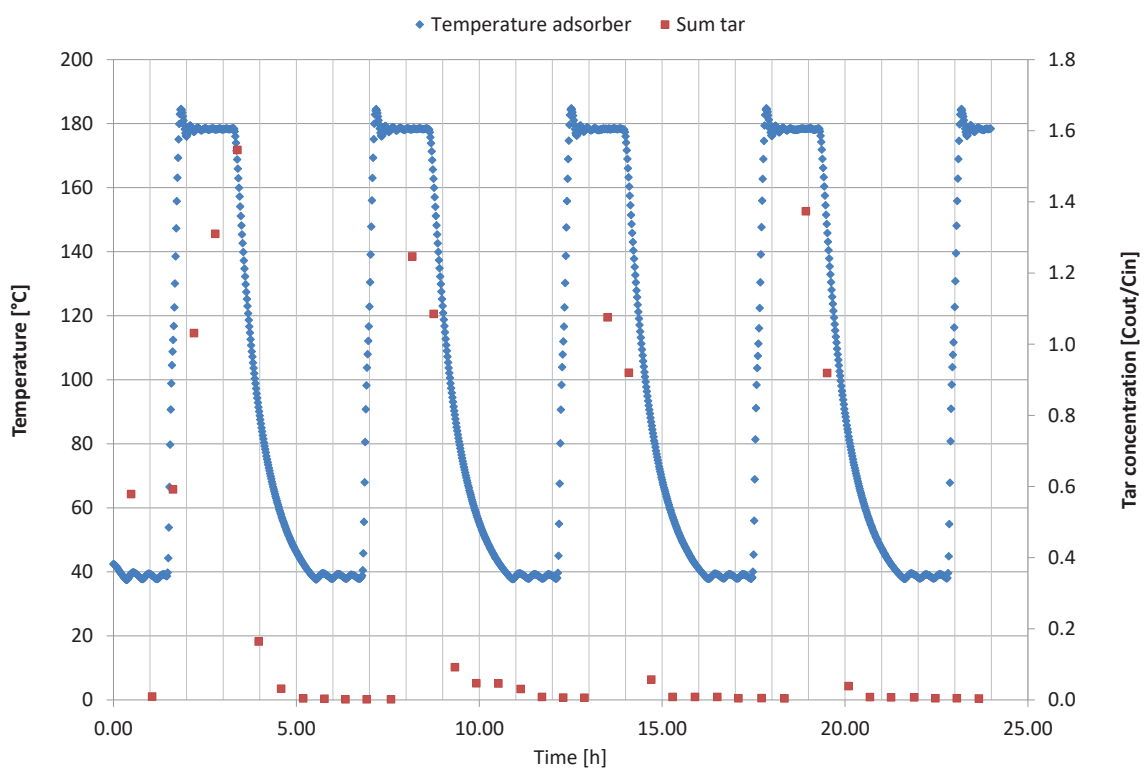


Fig.7: TSA performance over time after 24 hours of operation

5. Acknowledgements

The research leading to these results has received funding from the COMET program managed by the Austrian Research Promotion Agency under grant number 844605. The program is co-financed by the Republic of Austria and the Federal Provinces of Burgenland, Lower Austria and Styria. Co-funding from the industry partners shall be highly acknowledged.

6. References

- [1] C. Li and K. Suzuki, Renewable Sustainable Energy Rev., **13** (2008) p594-604
- [2] H. Nguyen, M. Seemann and H. Thunman, Energy Fuels, **32** (2018) p3499-3509
- [3] J. L. Devi, J. Ptasinksik, K. Janssen and J. J. G. Frans, Biomass Bioenergy, **24** (2003) p125-140
- [4] A. Larsson, M. Seemann, D. Neves and H. Thunman, Fuel Energy, **11** (2013) p6665-6680
- [5] R. J. Evans and T. A. Milne, Springer Dodrecht (1997), p803-816
- [6] R. J. Evans and T. A. Milne, Fuel and Energy Abstracts, **39** (1998)
- [7] P. Morf, P. Hasler and T. Nussbaumer, Fuel, **81** (2002), p843-853
- [8] R. Cypress, Fuel Process. Technol., **15** (1987), p1-15
- [9] P. F. Nelson and K. J. Hüttlinger, Fuel, **65** (1986), p354-361
- [10] W. Wanzl, Chemical Reaction in Thermal Decomposition of Coal, Fuel Process. Technol., **20** (1988), p317-336
- [11] U. Wolfesberger, I. Aigner and H. Hofbauer, Environ. Prog. Sustainable Energy, **28** (2009), p372-379
- [12] T. A. Milne, R. J. Evans and N. Abatzoglou, Biomass Gasifier “Tars”: Their Nature Formation, and Conversion, Technical Report, National Renewable Energy Laboratory (1998)
- [13] P. Jeevanandam, K. J. Klabunde and S. H. Tetzler, Microporous Mesoporous Mater., **79** (2005), p101-110
- [14] C. Yu, J. S. Qiu, Y. F. Sun, X. H. Li, G. Chen and Z. B. Zhao, J. Porous Mater., **15** (2008), p151-157
- [15] P. Edinger, D. Grimekis, K. Panopoulos, S. Karellas and C. Ludwig, J. Environ. Chem. Eng., **5** (2017), p4173-4184
- [16] T. Phuphuakrat, T. Namioka and K. Yoshikawa, Appl. Energy, **87** (2010), p2203-2211
- [17] X. Hu, T. Hanaoka, K. Sakanishi, T. Shinagawa, S. Matsui, M. Tada and T. Iwasaki, J. Jpn. Inst. Energy, **86** (2007), p707-711
- [18] A. M. Mastral, T. Garcia, M. S. Callen, M. V. Navarro and J. Galban, Energy Fuels **15** (2001), p1-7
- [19] H. Thunman, M. Seemann, T. Berdugo Vilches, J. Maric, D. Pallares, H. Ström, G. Berndes, P. Knutsson, A. Larsson, C. Breitholtz and O. Santos, Energy Sci. Eng. **6** (2018), p6-34
- [20] H. Thunman, C. Gustavsson, A. Larsson, I. Gunnarsson and F. Tengberg, Energy Sci. Eng. **7** (2019), p217-229
- [21] R. Bardolf, Optiomierung eines Produktgaswäschers bie der Biomassedampfvergasung im Zweibettwirbelschichtverfahren, PhD thesis (2017), TU Wien
- [22] M. Bolhàr-Nordenkampf, R. Rauch, K. Bosch, C. Aichernig and H. Hofbauer, 2nd Regional Conference on Energy Technology Towards a Clean Environment, Phuket (2002).
- [23] J. Loipersböck, M. Lenzi, R. Rauch and H. Hofbauer, Korean J. Chem. Eng., **34** (2017), p2198-2203
- [24] A. Sauciuc, Z. Abustefi, G. Weber, A. Potetz, R. Rauch H. Hofbauer, G. Schaub and L. Dumitrescu, Biomass Conv. Bioref., **2** (2012), p253-263

- [25] S. Chianese J. Loipersböck, M. Malits, R. Rauch, H. Hofbauer, A. Molino and D. Musmarra, Fuel Process. Technol., **132** (2015), p39
- [26] T. Pröll, I. Siefert, A. Friedl and H. Hofbauer, Ind. Eng. Chem. Res., **44** (2005), p1576
- [27] J. Loipersböck, M. Luisser, S. Müller, H. Hofbauer and R. Rauch, chemengineering, **2** (2018), p61
- [28] E. G. Baker, M. D. Brown, D. C. Elliot and L. K. Mudge, AIChE Summer National Meeting, (1988)
- [29] D. C. Elliot, ACS symposium series, **376** (1988)
- [30] J. Gil, J. Corella, M. P. Aznar and M. A. Caballero, Biomass Bioenergy, **17** (2008), p389-403
- [31] A. Ponzio, S. Kalisz and W. Blasiak, Fuel Process. Technol., **87** (2006), p223-233
- [32] M. Kübel, Teerbildung und Teerkonversion bei der Biomassevergasung – Anwendung der nasschemischen Teerbestimmung nach CENStandard, Cuvillier Verlag, (2007)
- [33] J. P. A. Neeft, H. A. M. Knoef and P. Onaji, Behaviour of tar in biomass gasification system. Tar related problems and their solutions, EWAB Program Report, (1999)
- [34] D. Dayton, A review of the Literature on Catalytic Biomass Tar Destruction, National Renewable Energy Laboratory, (2002)
- [35] D. Bathen, Untersuchungen zur Desorption durch Mikrowellenenergie, VDI-Fortschritt-Bericht Reihe, **3** (1998), VDI Verlag Düsseldorf
- [36] D. M. Ruthven, Principles of Adsorption and Adsorption Processes, John Wiley & Sons, (1984) New York
- [37] U. v. Gemmingen, A. Mersmann and P. Schweighart, Kap. 6 Adsorptionsapparate, in Thermisches Trennen, (1996), Deutscher Verlag für Grundstoffindustrie

Gas Cleaning and Gas Upgrading Abstracts

Secondary tar conversion in a char bed with a real producer gas reducing char deactivation

D. Fuentes-Cano¹, L. von Berg², Israel Pardo-Arias¹, R. Scharler², A. Gómez-Barea¹, A. Anca-Couce^{2*}

1. Universidad de Sevilla, Chemical and Environmental Engineering Department, Bioenergy Group, Camino de los Descubrimientos s/n, 41092 Seville, Spain

2. Graz University of Technology, Institute of Thermal Engineering, Inffeldgasse 21, 8010 Graz, Austria

*corresponding author, anca-couce@tugraz.at

1. Introduction and goals

Fluidized bed gasification is a very promising conversion technology for biomass and waste valorization. However, the high tar content in the produced gas limits its industrial applications. Biomass char can be employed as a catalyst for tar conversion. It has the advantages of being a process byproduct, resistant to sulfur-poisoning and with high activity. However, it has the disadvantage that it tends to deactivate in relatively short times by soot deposition. This deactivation could be delayed by enhancing conditions leading to a higher rate of carbon consumption over the char surface by gasification than carbon deposition from the tars. This has been already proven in experiments with synthetic mixtures of gases and tars [1][2].

The main contribution of this work is to conduct tar conversion experiments with wood char as a catalyst using real gas from a steam-blown fluidized bed biomass gasifier, as compared to most of literature works using simulated syngas [3]. Therefore, the experimental conditions here studied are closer to that expected in a commercial device. The performance of char is analyzed at different temperatures and test duration times, aiming at identifying the conditions enhancing char performance and minimizing deactivation.

2. Methodology and results

The experiments were conducted with the setup shown in Figure 1. The bubbling fluidized bed gasifier was operated with wood pellets as a fuel ($1.5 \text{ kW}_{\text{th}}$), steam as gasification medium (steam-fuel equivalent ratio of 4) and a bed temperature of 750°C . For the tar conversion experiments, the producer gas is directed to the gas conditioning unit, a tubular fluidized bed reactor filled with biomass char. The char temperatures tested were 750, 850 and 875°C for periods up to 6.5 h. The residence time of the gas in contact with char in the hot zone (operated isothermally) of the reactor was around 0.25 s. Tars samples were analysed by means of a GC-FID. The permanent gas composition was measured during tar sampling.

The conversion over time of the GC-detected tars during the tar conversion experiments with char is shown in Figure 2. The experiment at 750°C led to a low tar conversion. The experiments at 850°C and 875°C led to a significant tar conversion and the deactivation over time was limited. This is a highly relevant result due to: 1) A high conversion, particularly at 875°C , was obtained despite the low residence time, and 2) Deactivation was minimized due to the high temperatures and steam concentrations in the reactor, which led to conditions that were at least close to achieving a carbon negative balance ($\text{C gasification rate} > \text{C deposition rate}$).

Moreover, the conversion was higher for tar classes 3 to 5 and lower for benzene. The H_2 content of the gas increased during the tar conversion experiments. The thermal non catalytic

conversion (without char) of tars at 850°C was also tested at the employed residence time, showing to be almost negligible in comparison to the catalytic conversion with char. The results from this work provide useful information to design tar conversion systems from gas produced from biomass gasification using char as catalyst.

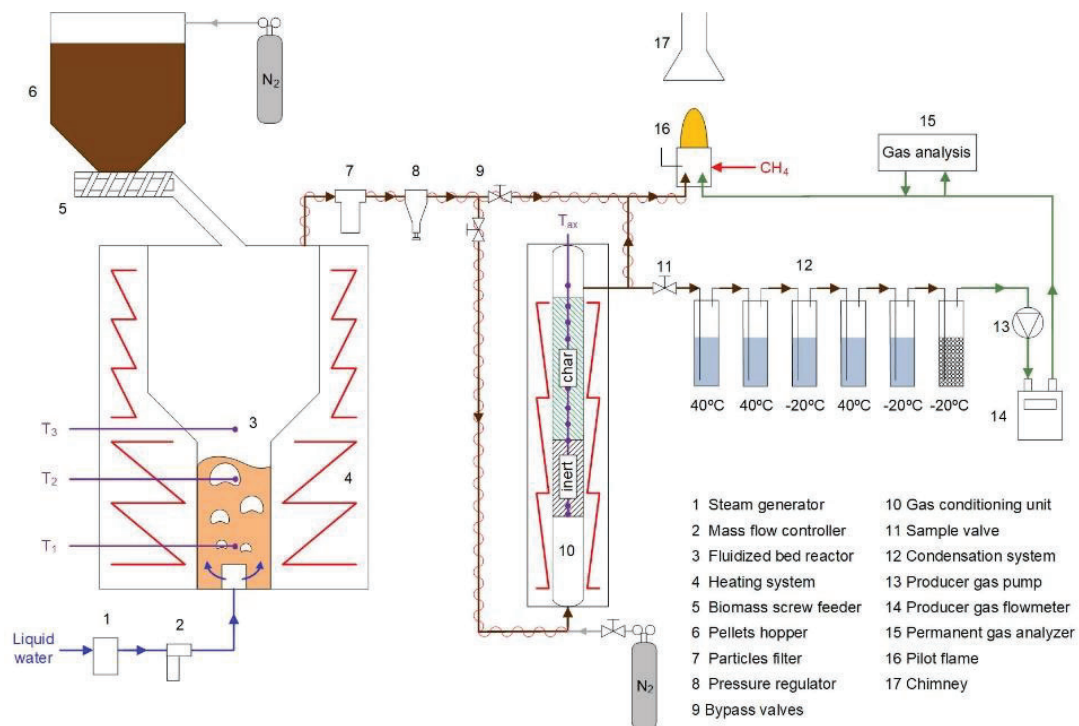


Figure 1: Employed experimental setup

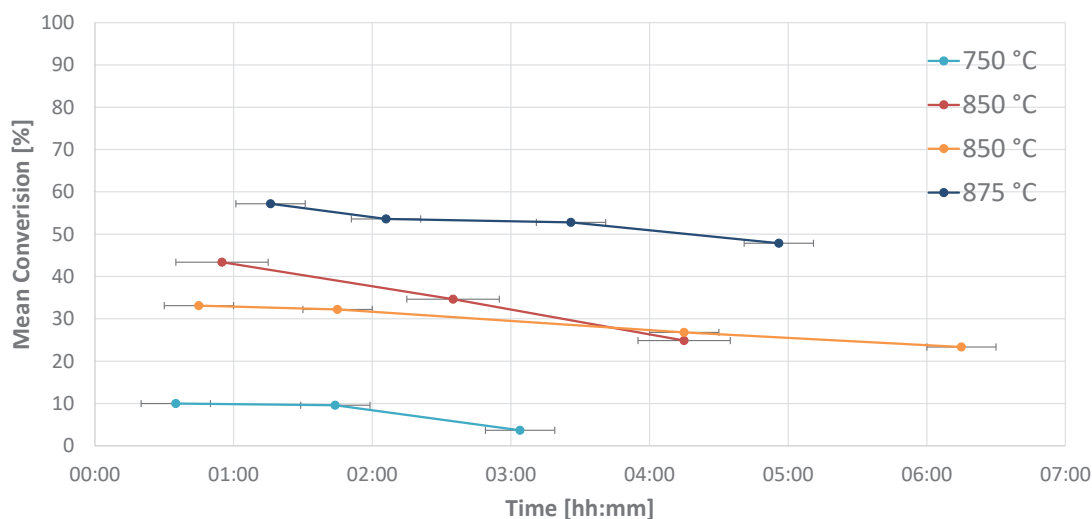


Figure 2: GC-detected tars conversion over time for tar cracking experiments with char at several temperatures. The interval for tar sampling is shown for each measurement point.

[1] Fuentes-Cano, Diego, et al. "Decomposition kinetics of model tar compounds over chars with different internal structure to model hot tar removal in biomass gasification." Chemical Engineering Journal 228 (2013): 1223-1233.

[2] Fuentes-Cano, Diego, et al. "The influence of the char internal structure and composition on heterogeneous conversion of naphthalene." Fuel Processing Technology 172 (2018): 125-132.

[3] G. Ravenni et al.: Activity of chars and activated carbons for removal and decomposition of tar model compounds – A review. Renewable and Sustainable Energy Reviews 94 (2018) 1044–1056.

Decomposition of tars in dual fluidized bed gasification – mechanisms of formation and decomposition in long-term operation

K. Umeki¹, J. Priscak^{2,3}, M. Kuba^{2,3,*}

1. Luleå University of Technology, Energy Engineering, Division of Energy Science, SE-971 87 Luleå, Sweden

2. Bioenergy 2020+ GmbH, Wienerstraße 49, 7540 Güssing, Austria

3. TU Wien, Institute of Chemical, Environmental and Bioscience Engineering (ICEBE),
Getreidemarkt 9/166, 1060 Vienna, Austria

*corresponding author: matthias.kuba @bioenergy2020.eu

1. Introduction and Short Description:

Gasification is a process to convert solid feedstock to a valuable gas, which can be used for various applications. If steam is used as gasifying agent a hydrogen-rich product gas product gas is obtained.

Unlike in case of air gasification, this product gas is not diluted with nitrogen. Due to the generation of a combustible product gas, hydrocarbons are present in this product gas after the gasification reactor.

Hydrocarbons are a product of the pyrolysis step. Larger molecules, especially poly-cyclic aromatic compounds, can be problematic as they condense in downstream equipment, which leads to undesired shut-downs of the power plant. In past studies the influence of different parameters on the formation and reduction of tars in the gasification reactor was investigated.

Several parameters were identified to have a measureable influence on the tar reduction, such as the bed height, the gasification temperature or the moisture content of the fuel.

To successfully reduce the concentration of tars in the product gas the decomposition mechanisms need to be fully understood.

This study aims to deepen the knowledge by further investigating the mechanisms

underlying the formation and decomposition of tars in long-term operation of dual fluidized bed gasification.

2. Methodology, Results and Discussion

Tar sampling was conducted by the Certified Test Laboratory for Combustion Systems at TU Wien, following a method based on the official Tar Guideline. The main principle of the method works as follows:

A gas stream is sampled iso-kinetically for a certain period of time; in this work for 15 min. The product gas passes through a heated sampling line with a cyclone and a filter cartridge before flowing through six impinger bottles filled with toluene as solvent. The impinger bottles are filled in total with 500 mL of toluene (50 mL, 100 mL, 100 mL, 100 mL, 150 mL, and 0 mL for droplet separation) and are situated in a cooling bath of a cryostat with a temperature of -8 °C. The amount of product gas drawn through the impinger bottles was controlled by a diaphragm pump equipped with volume flow measurement.

For every measurement, three samples were taken; the second immediately after the first and the third after a pause of 30 min. Thus, both short-time and long-term variations are statistically covered.

The samples were measured gravimetrically and also with GC-MS. The single tar components from GC-MS measurements were then grouped into an improved characterization scheme (shown in Table 1). Based on this characterization of tars for different operation points, reaction mechanisms were derived and further evaluated.

3. Conclusion and Outlook

The results show decomposition mechanisms based on influencing parameters. The increases in bed height and reaction temperature both led to the reduction of tar content. However, the detailed classification indicated the

different mechanisms for tar reduction by these parameters. All the tar components decreased with larger amount of bed materials although the effect was more significant for mature tar components. High temperature, on the other hand, resulted in lower amount of young tar (PC2 and 3), but increase in benzene and PAH. These results are going to be interpreted with physical analyses of bed materials.

Table 1: Tar classification for each operation point, based on Jarvis et al. [1]

Tar class	Class name	Property
PC1	Pure component 1	Primarily masses assigned to lignin monomers, such as as synapyl alcohol, synapyl aldehyde, coniferyl alcohol, and hemicellulose volatilization products.
PC2	Pure component 2	The peaks in this PC are assigned to cellulose volatilization products. evoglucosan, is a major product from transglycosylation during cellulose pyrolysis
PC3	Pure component 3	This PC contains smaller fragments from the cracking of lignin and carbohydrate pyrolysis products.
PC4	Pure component 4	This PC has a maximum at 725 °C and is devoid of carbohydrate peaks. The products in this PC appear to arise from severely cracked lignin molecules or molecular weight growth
PC5	Pure component 5	The products in this PC are suggestive of molecular weight growth. Possible products include phenol, styrene, indene, fluorene, and cyclopentadien. Peaks associated with PAHs, e.g. naphthalene, acenaphthylene, anthracene, and phenanthrene also begin to form
PC6	Pure component 6	This PC represents a regime dominated by PAHs, with some amount of aliphatic aromatics and permanent gases. Dominant peaks are benzene, naphthalene, acenaphthylene, acetylene, anthracene, phenanthrene, pyrene, fluoranthene, benzacenaphthylene, and phenylacetylene.

[1] Jarvis MW, Haas TJ, Donohoe BS, Daily JW, Gaston KR, Frederick WJ, et al. Elucidation of biomass pyrolysis products using a laminar entrained flow reactor and char particle imaging. Energy and Fuels 2011. doi:10.1021/ef100832d.

Industrial Implementations CCU, Greening the Gas Full Papers

Dual fluidized bed based technologies for carbon dioxide reduction

J. Fuchs^{1*}, A.M. Mauerhofer¹, S. Penthor¹, F. Benedikt¹, A. Bartik¹, M. Hammerschmid¹,
S. Müller¹, H. Hofbauer¹

1. TU Wien, Institute of Chemical, Environmental and Bioscience Engineering (ICEBE),
Getreidemarkt 9/166, 1060 Vienna, Austria
*corresponding author, josef.fuchs@tuwien.ac.at

Abstract

The dual fluidized bed technology offers a broad range of applications for the utilization of CO₂ neutral energy carriers like biomass. This work provides an overview about dual fluidized bed technologies, which could contribute to a more sustainable future. The conventional biomass steam gasification is an already well-known technology. However, an advanced reactor design enables several further processes. These processes could be appropriate for a general CO₂ reduction in the atmosphere.

Based on this technology the **sorption enhanced reforming process (SER)** was developed and enables the in-situ removal of CO₂ from the product gas. Consequently, the chemical equilibrium of the product gas is shifted and a high H₂ content can be obtained in the product gas. Another variation of the DFB process is the **gasification with CO₂** instead of steam as gasification agent. This enables the utilization of a CO₂ stream and the production of a product gas with high carbon content from biomass. Last but not least, a DFB reactor system can also be used for the so-called **chemical looping combustion** process of biomass (**BioCLC**), which has enormous potential for capturing CO₂ due to its low energy demand. The principle is based on the use of a metal oxide as bed material and oxygen carrier. This oxygen carrier is used to burn the gas, which is produced by the gasification reactions of the biomass with steam.

1. Introduction:

In the last decades, fossil energy carriers were established as the main energy source in industrialized countries and all over the world. Decreasing fossil resources and climate change lead to a demand of innovative technologies for decreasing the share of fossil energy carriers.

The dual fluidized bed technology offers a broad range of applications for the utilization of CO₂ neutral energy carriers like biomass. This work provides a review about technologies which are suitable to contribute to a CO₂- neutral future.

The conventional biomass steam gasification is an already well-known technology.

Based on this technology the **sorption enhanced reforming process (SER)** was developed and enables the in-situ removal of CO₂ from the product gas. Consequently, the chemical equilibrium of the product gas is shifted and a high H₂ content can be obtained in the product gas. By applying oxyfuel combustion in the combustion reactor (OxySER), an almost pure CO₂ – stream can be obtained [1]. Thus, both gas streams can contribute to a CO₂ reduction in the atmosphere: On the one hand, a H₂ rich product gas is produced, which can be used directly as a reducing agent in steel industry or as basis for synthesis processes like methanation. On the other hand, a pure CO₂ stream is produced, which either can be stored or,

again, used for synthesis processes like methanation. A scheme of the process can be found in Figure 1.

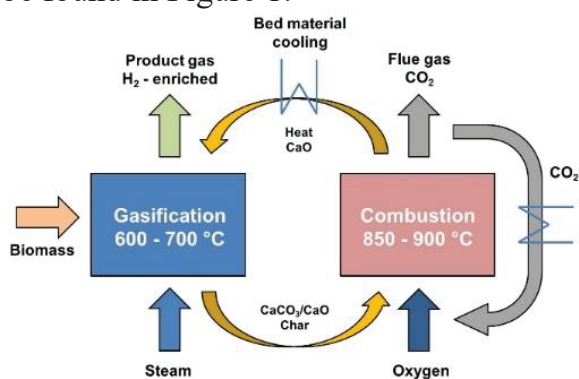


Fig. 1: Sorption enhanced reforming with oxyfuel combustion (OxySER)

Another variation of the DFB process is the **gasification with CO₂** instead of steam (Figure 2). This enables the production of a product gas with a high carbon content from biomass. This seems to be contradictory, since decarbonization is the overall aim of energy intensive industries. Nevertheless, CO₂ is an unavoidable component in many processes and could be used in this way to produce a product gas as basis for synthesis processes with high carbon demand, such as the Dimethyl ether (DME) synthesis.

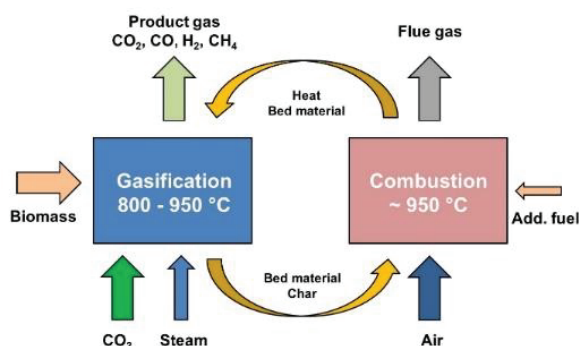


Fig. 2: CO₂/steam gasification within a DFB reactor system

Last but not least, a DFB reactor system can also be used for the so-called **chemical looping combustion of solid biogenic fuels (BioCLC)** process, which has enormous potential for capturing CO₂ due to its low energy demand. The principle of

the chemical looping process is shown in Figure 3 and is based on the use of a metal oxide as bed material and oxygen carrier. This oxygen carrier is used to burn the gas, which is produced by the gasification reactions of the biomass with steam. The oxygen carrier itself is oxidized in the air reactor again. This procedure allows for the production of a N₂-free flue gas.

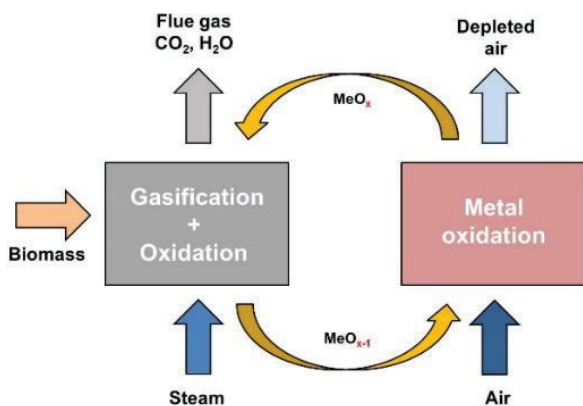


Fig. 3: Chemical looping combustion of solid biogenic fuels within a DFB reactor system

2. Concept and methodology:

Several experimental campaigns have been conducted with the advanced 100 kW_{th} pilot plant at TU Wien to investigate different technologies (OxySER, CO₂ gasification and BioCLC). The pilot plant consists of two reactors (gasification reactor and combustion reactor) with an overall height of about 7 m. More details about the reactor-design can be found in Figure 4 and Figure 5 and were described by Benedikt et al. [2]. The pilot plant facility including a fuel supply equipment, a control room and equipment for gas cooling, cleaning and measurement, covers two floors of around 35 m².

During a test run, the pilot plant is controlled through a programmable logic controller (PLC). The PLC continuously measures and records data of all relevant flow rates, temperatures, pressures as well as the main gas composition of the product gas (H₂, CO, CO₂, CH₄) with a Rosemount

NGA 2000 measurement device. Additionally, C₂H₄ and other higher hydrocarbons are analyzed every 12 min by a gas chromatograph (Perkin Elmer ARNEL - Clarus 500). For analyzing the tar content in the product gas, a standardized arrangement of sampling equipment is used. Single tar components are measured by gas chromatography coupled with mass spectrometry (GCMS). For tar measurements at the advanced pilot plant, toluene is used as solvent instead of isopropanol, because the solubility for tar in toluene is higher and the water content in the gas can be measured continuously. The advanced 100 kW_{th} pilot plant, which is in operation since 2014, is equipped with an enhanced gasification reactor system, which increases the product gas quality significantly. Therefore, an upper gasification reactor with geometrical constrictions leads to an increased hold-up of hot bed material particles and increases the contact time between product gas and hot bed material particles.



Fig. 4: Picture of the control room, 2nd floor and 1st floor of the advanced 100 kW_{th} pilot plant

The enhanced gas-solid contact in these turbulent fluidized zones promotes tar cracking and reforming reactions by the use of a catalytic bed material. Thus, the conversion efficiency is increased. Further, the advanced reactor system allows for the usage of different fuels, bed materials and gasification agents.

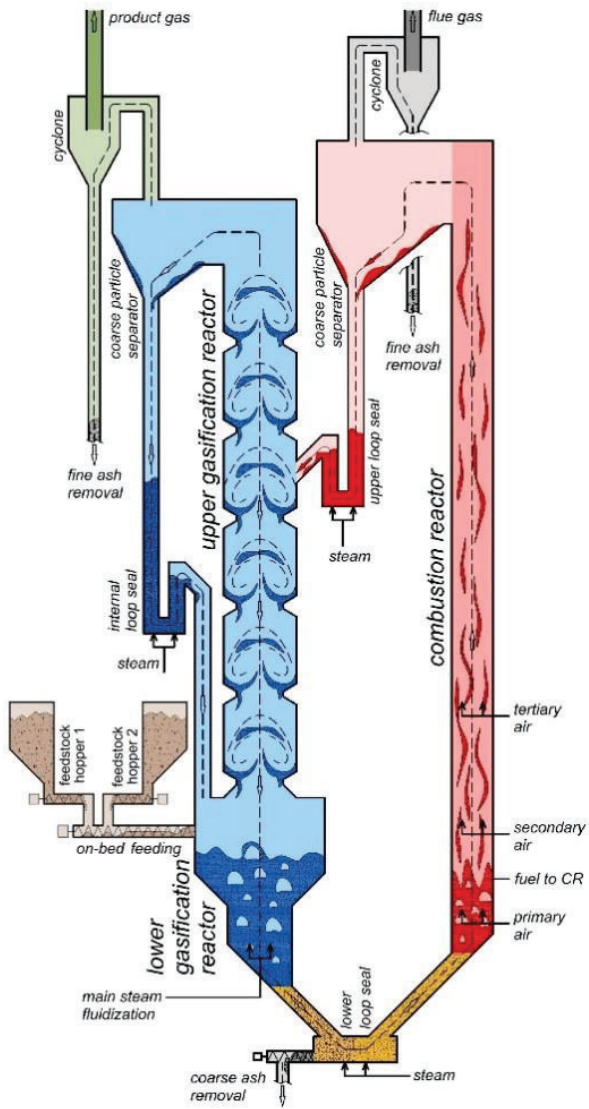


Fig. 5: Scheme of the advanced 100 kW_{th} pilot plant

3. Results and discussion

SER/OxySER

Since hydrogen is regarded as a promising future energy carrier, the SER process aims for the production of a hydrogen rich product gas. On the other hand, carbon is

sequestered in-situ from the gasification process and could be further utilized.

For the SER process the bed material additionally acts as a selective sorbent for CO₂ (Equation 1) when keeping temperatures between 600 and 700 °C in the gasification reactor and temperatures above 830 °C in the combustion reactor (reverse of Equation 1). Typically a calcium based sorbent (limestone, dolomite) is used. Thus, the composition of the product gas is developed towards high H₂ contents and low CO₂ and CO contents. The reason for the strong shift in the product gas composition can be traced back to the water-gas-shift reaction (Equation 2), which is one of the most important reactions in the gasification reactor. A scheme of the principle can be found in Figure 1.



Research on the dependency of the product gas composition on gasification temperature showed, that the highest H₂ content can be reached from 600 °C to 700 °C. The course of the product gas composition up to 800 °C can be found in Figure 5 [3]–[7].

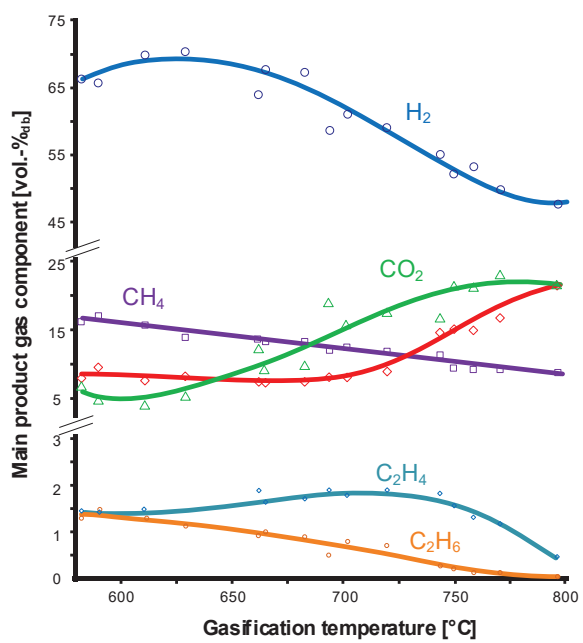


Fig. 5: Dependency of the SER/OxySER process on temperature

Since the gasification temperature influences the CO₂ sorption of the bed material on the one hand, but also the char formation from gasification on the other hand, the carbon balance can be influenced significantly (Figure 6). It can be found, that up to 80% of the total carbon in the fuel can be removed from the gasification reactor and transported to the combustion reactor via char and CO₂ in the bed material (CaCO₃). By applying oxyfuel-combustion in the combustion reactor, a pure CO₂ stream could be obtained and used as raw material for the chemical industry.

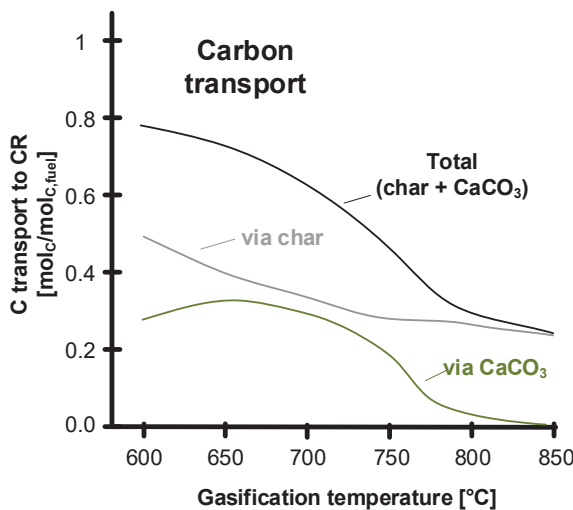


Fig. 6: Dependency of the carbon balance of the SER/OxySER process on temperature

However, the bed material cycle rate in the DFB system was identified as a second influencing factor on the product gas composition [8]. This behavior can be traced back to the change of the residence time of the bed material in the reactors. Recent investigations showed, that the calcination reaction is the limiting factor within the advanced 100 kW_{th} pilot plant.

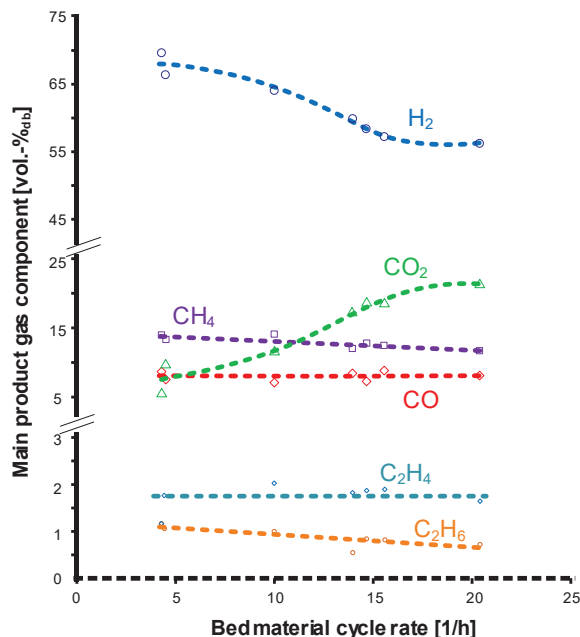


Fig. 7: Dependency of the SER/OxySER process on bed material cycle rate

CO₂ gasification

An option to reduce CO₂ emissions could be the sequestration of CO₂ from different industrial processes and its utilization again for the dual fluidized bed gasification technology. Thus, experimental campaigns [9] regarding CO₂ as gasification agent (together with steam or pure) have been conducted in the advanced 100 kW_{th} pilot plant.

Through the gasification of biomass with CO₂ as gasification agent, a CO-rich product gas could be generated, which could further be processed to valuable synthetic fuels. By increasing the CO₂ content in the gasification agent while decreasing the steam content leads to an increased CO and CO₂ content in the product gas, while the H₂ content is decreasing (Figure 8). This product gas composition was recorded at a gasification temperature around 825 °C.

Further, the process is strongly dependent on gasification temperature (Figure 9). Higher temperatures tend to push the Boudouard reaction (Equation 3) further towards its products CO.

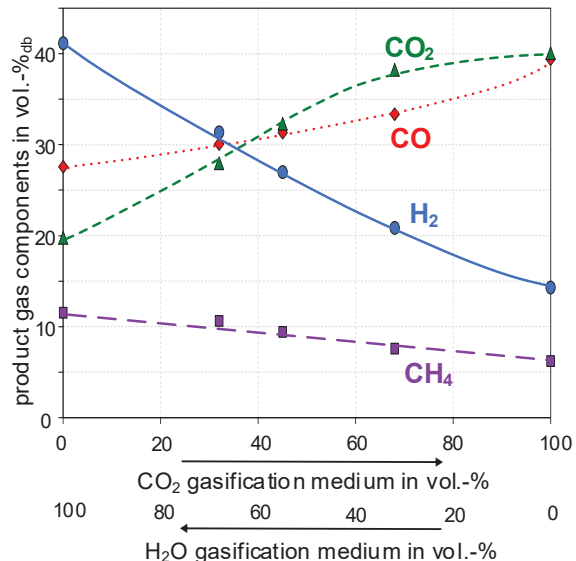


Fig. 8: Dependency of the CO₂ gasification process on gasification agent [9]

Therefore, a higher CO content can be produced with higher gasification temperatures.

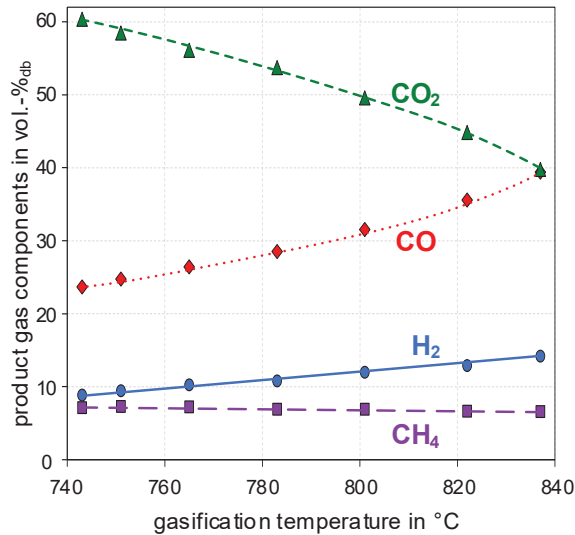


Fig. 9: Dependency of the CO₂ gasification process on temperature

BioCLC

Another process realized using the dual fluidized bed gasification technology is chemical looping combustion of solid biomass [10]. In addition to the steam gasification in the gasification reactor, an in-situ combustion of the produced gas takes place via the bed material, which serves as oxygen carrier (see also principle in Figure 3). Thus, a nearly nitrogen-free flue gas from the gasification reactor (Figure 10) and an oxygen depleted air stream from the combustion reactor are obtained. The bed material (and oxygen carrier) used in such a system could be metal oxides of iron, manganese or copper.

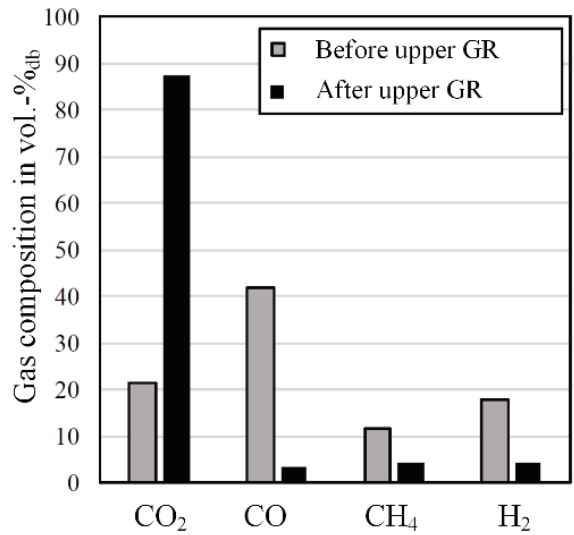


Fig. 10: Flue gas composition of the BioCLC process with ilmenite as oxygen carrier [10]

In contrast to gasification processes, a high CO₂ content in the case of BioCLC means high fuel conversion. Figure 10 shows, that the advanced reactor design leads to a significant improvement of the fuel conversion: The CO₂ content is low before the upper gasification reactor, whereas nearly 90 vol.-%_{db} can be reached after the upper gasification reactor. The improvement of the process can also be seen from the temperature profile in the reactors (Figure 11): The highest temperature can be found in the upper gasification reactor. Thus, heat is released through oxidation of the gas produced from steam gasification via the oxygen carrier (bed material).

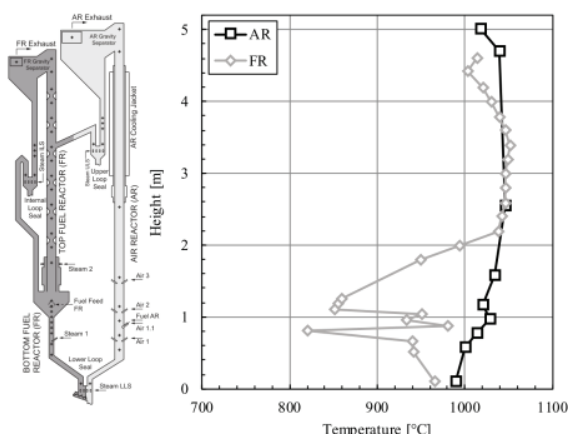


Fig. 11: Temperature profile of the gasification reactor (fuel reactor) and combustion reactor (air reactor) [10]

4. Discussion

Three very different dual fluidized bed technologies are introduced in this work.

However, Table 1 provides an overview about different parameters of these processes. Typically, the gasification processes OxySER and CO₂ gasification produce a product gas which contains chemical energy, whereas the CLC process as a typical combustion process provides heat.

Especially the OxySER process offers advantages, but also disadvantages. On the one hand a H₂ rich product gas is produced, on the other hand carbon from renewable sources (biomass) is sequestered. Since biomass is the only renewable carbon source, the OxySER concept must be implemented wisely. This means the integration in an environment where H₂ on the one hand, but pure CO₂ on the other hand is needed.

Table 1: Comparison of presented processes regarding different parameters

	OxySER	CO ₂ gasification	BioCLC
Product	Chemical Energy + CO ₂ + Heat	Chemical Energy + Heat	Heat + CO ₂
Technical readiness	Pilot scale / test run on industrial scale for SER [11]	Pilot scale	Pilot scale
Advantages	Product gas with high H ₂ content and pure CO ₂ for further utilization	Potential of CO ₂ utilization as gasification agent	Pure CO ₂ for further utilization
Disadvantages	Air separation unit necessary, purity of CO ₂	Low CO ₂ conversion expected	No chemical energy

5. Conclusion and Outlook

The dual fluidized bed technology, which was originally invented for the steam gasification of biomass, is also suitable for various other processes. Especially the advanced reactor design enables several further processes. These processes could

be appropriate for a general CO₂ reduction in the atmosphere, by using biogenic fuels and producing a pure CO₂ stream, which could be further utilized in industry (OxySER and BioCLC) or using a CO₂ stream as gasification agent (CO₂ gasification).

6. References

- [1] S. Müller, "Hydrogen from Biomass for Industry - Industrial Application of Hydrogen Production Based on Dual Fluid Gasification," TU Wien, PhD Thesis, 2013.
- [2] F. Benedikt, J. Fuchs, J. C. Schmid, S. Müller, and H. Hofbauer, "Advanced dual fluidized bed steam gasification of wood and lignite with calcite as bed material," *Korean J. Chem. Eng.*, vol. 34, no. 7, pp. 1–11, 2017.

- [3] J. Fuchs, J. C. Schmid, S. Müller, A. M. Mauerhofer, F. Benedikt, and H. Hofbauer, “The impact of gasification temperature on the process characteristics of sorption enhanced reforming of biomass,” *Biomass Convers. Biorefinery*, 2019.
- [4] G. Soukup, “Der AER – Prozess , Weiterentwicklung in einer Technikumsanlage und Demonstration an einer Großanlage,” TU Wien, PhD Thesis, 2009.
- [5] J. C. Schmid *et al.*, “Sorption Enhanced Reforming with the Novel Dual Fluidized Bed Test Plant at TU Wien,” in *European Biomass Conference and Exhibition (EUBCE)*, 2017, pp. 421–428.
- [6] S. Müller, J. Fuchs, J. C. Schmid, F. Benedikt, and H. Hofbauer, “Experimental development of sorption enhanced reforming by the use of an advanced gasification test plant,” *Int. J. Hydrogen Energy*, vol. 42, no. 50, pp. 29694–29707, 2017.
- [7] J. Fuchs, J. C. Schmid, S. Müller, and H. Hofbauer, “Dual fluidized bed gasification of biomass with selective carbon dioxide removal and limestone as bed material: A review,” *Renew. Sustain. Energy Rev.*, vol. 107, no. March, pp. 212–231, 2019.
- [8] J. Fuchs *et al.*, “The impact of bed material cycle rate on in-situ CO₂ removal for sorption enhanced reforming of different fuel types,” *Energy*, vol. 162, 2018.
- [9] A. M. Mauerhofer, J. Fuchs, S. Müller, F. Benedikt, J. C. Schmid, and H. Hofbauer, “CO₂ gasification in a dual fluidized bed reactor system: Impact on the product gas composition,” *Fuel*, 2019.
- [10] S. Penthör *et al.*, “First results from an 80 kW dual fluidized bed pilot unit for solid fuels at TU Wien,” in *5th International Conference on Chemical Looping, Park City, Utah, USA*, 2018.
- [11] S. Koppatz, “In – situ Produktgaskonditionierung durch selektive CO₂ – Abscheidung bei Wirbelschicht – Dampfvergasung von Biomasse : Machbarkeitsnachweis im industriellen Maßstab,” TU Wien, Master Thesis, 2008.

Evaluation of Two Sorbents for the Sorption-Enhanced Methanation in a Dual Fluidized Bed System

A. Coppola¹, F. Massa¹, P. Salatino^{1,2}, F. Scala^{1,2*}

1. Dipartimento di Ingegneria Chimica, dei Materiali e della Produzione Industriale, Università degli Studi di Napoli Federico II, Piazzale V. Tecchio 80, 80125 Napoli, Italy
2. Istituto di Ricerche sulla Combustione, CNR, Piazzale V. Tecchio 80, 80125 Napoli, Italy

*corresponding author, fabrizio.scala@unina.it

Abstract

The unceasing concern for climate change, closely related to the exploitation of fossil fuels, pushes the scientific community to develop new technologies for CO₂ capture and utilization (CCU). Moreover, the growth and diffusion of solar energy requires new energy storage systems that put solar fuels at the forefront. Methane seems to be a suitable energy vector, which could both store solar energy and exploit fossil fuel derived CO₂. Moreover, methane has the main advantage of an already existing distribution and storage infrastructure.

The methanation reaction from hydrogen and carbon dioxide (or monoxide) is generally carried out in staged adiabatic catalytic fixed beds operated at high pressure in order to overcome thermodynamic limitations. A recently proposed alternative pathway is the sorption-enhanced methanation concept, which is based on the employment of a sorbent able to capture *in situ* the H₂O produced during reaction, to shift equilibrium towards the formation of CH₄.

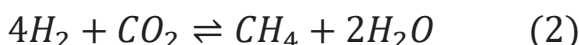
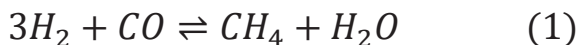
In this work a CaO, derived from natural limestone, and a commercial 3A Zeolite were tested as sorbent materials for H₂O capture in a new configuration for the sorption-enhanced methanation based on the concept of chemical looping in dual interconnected fluidized bed systems. The experimental campaign was aimed at studying the sorbent performance in terms of hydration and dehydration at different operating conditions relevant for catalytic methanation. The results showed that CaO has a good capacity to capture and release steam in the temperature range of interest. Unfortunately, even at the lowest temperatures tested, the sorbent is affected by the presence of CO₂, which worsens its performance in terms of H₂O capture capacity. The zeolite has a more stable behavior than CaO under all investigated conditions. Comparing the performance of the two materials, the zeolite on average has better capture capacity (0.017-0.049 g/g) than CaO (0.006-0.025 g/g) and it is not affected by deactivation during the cycles.

1. Introduction:

Methane is an important energy carrier for many sectors, which features a well-developed distribution and storage infrastructure in many countries, and its massive utilization in the automotive, household and industrial sectors.

Nowadays, natural gas is the main source of methane, however the increasing dispute on global warming related to the exploitation of fossil fuels has moved the interest to alternative and renewable technologies for methane production, such as catalytic and biological methanation processes [1-3].

Specifically, catalytic methanation [4], via CO (Eq.1) or via CO₂ (Eq.2), has several features that make it very interesting if combined with the concepts of solar fuels, chemical storage and CO₂ utilization. Indeed, methane could act as chemical storage carrier of solar energy [2] initially used to convert water into hydrogen by electrolysis [5]. Moreover, CO₂ methanation could be considered as a process for CO₂ utilization in the framework of Carbon Capture and Utilization (CCU) technologies [6-10]. On the other hand, the production of methane from CO could represent the final step after coal or biomass gasification into syngas [11-13].



The typical catalysts able to promote methanation are based on different metals such as Ru, Ni, Co, Fe, and Mo [14], though Ni-based catalysts are considered to provide the best compromise among activity, selectivity and low price [15-17]. Commercial methanators consist of fixed beds, typically operated at high pressure to obtain high methane yields, and arranged in series in order to carry out intermediate cooling steps and recycles to manage the temperature of the process (due to the high exothermicity of the reaction) [1,20]. In particular, the temperature management represents the main issue for the process because it may lead to the deactivation of the catalyst [18]. In addition, the high temperature can promote carbon deposition on the catalyst surface due to the Boudouard reaction [19]. In the last years, many research groups have proposed new solutions, based on new reactor designs (fluidized bed reactors, three-phase reactors), to improve the current methanation process with the goal to have a better temperature control [2].

Recently, Borgschulte et al. [21] and Walspurger et al. [22] investigated the possibility to enhance the methane production by the application of the concept of Sorption-Enhanced Methanation (SEM), where the steam, produced by the methanation reaction, is continuously removed from the reaction environment by means of a suitable regenerable sorbent material, e.g. a zeolite. These studies demonstrated in a lab scale fixed bed apparatus that the SEM process has the potential for high-grade methane production at low pressure using commercial materials, with the consequence of a relevant energy saving for the entire process.

Based on these promising outcomes, in this work an innovative configuration for the SEM process is proposed. This configuration takes advantage of the chemical looping concept where in one reactor (methanator) catalytic methanation occurs simultaneously with the hydration of a suitable sorbent, so as to drive the equilibrium towards product formation, while the regeneration of the sorbent takes place in another reactor (dehydrator). The two reactors are connected each other in a dual-interconnected fluidized beds configuration as shown in Fig. 1. This scheme has the advantage of a steady operation of the plant, thus avoiding the unsteady cyclic operation necessary for sorbent regeneration in fixed bed reactors. In addition, the use of fluidized bed reactors appears to be suitable to achieve good temperature control for highly exothermic reactions like methanation.

In this work, two potential sorbents were tested for their steam capture potential in a lab-scale dual bed fluidized bed apparatus: CaO, derived from natural limestone, and a commercial 3A-zeolite. The main aim was to evaluate the sorbent performance in terms of hydration and dehydration cycles at different operating conditions relevant for catalytic methanation.

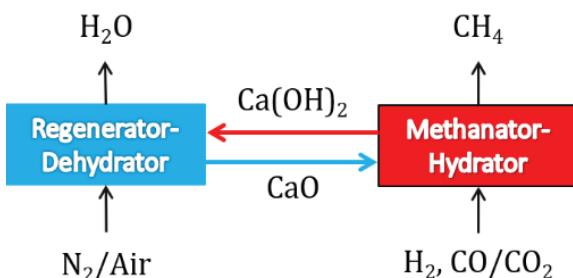


Fig.1: Scheme of the Chemical Looping Sorption-Enhanced Methanation concept

2. Experimental:

Two materials were tested as sorbents for SEM: a CaO and a zeolite. CaO was obtained by calcination of an Italian limestone named Massicci: the material was prepared in a lab-scale fluidized bed at 850°C with air for 20min. The zeolite was a spherical commercial 3A-zeolite.

The experimental apparatus used for the tests, called Twin Beds (Fig.2), consists of two identical lab-scale bubbling fluidized beds connected by a rapid solid transfer line. This system is an ad hoc device used to study looping processes. The two reactors have an inner diameter of 40 mm, and are divided in two sections: a wind box also used as gas preheater; a fluidized bed, separated from the wind box by a perforated plate gas distributor. Both reactors operate separately in batch mode but they are connected each other by a duct (ID 10 mm), partially immersed in both beds, used for fast pneumatic conveying of the sorbent between the two reactors. Transfer of sorbent is accomplished by using a valve system arranged along the duct and at the outlet of the reactors. The solid is injected into the system by a steel hopper connected sideways to the reactor. The apparatus is also equipped with an additional vertical duct, located in the middle between the two beds and connected with the transport duct by means of a 3-way valve; at the bottom of this duct a removable stainless-steel container is placed. The aim of this duct is

to allow a fast discharge of the reactors and to collect the whole bed material into the container at the end of each test. A thorough description of the operating principle of the TB system is reported elsewhere [23].

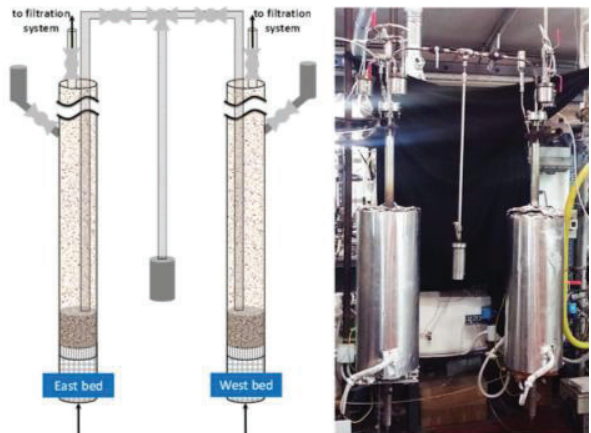


Fig.2: Twin Beds Apparatus

The two reactors were employed as hydrator and dehydrator respectively. The experimental campaign was aimed at evaluating the suitability of the sorbents to capture and release water at different temperatures and reaction environments relevant for methanation. A steam generation system, that permits to produce steam at 200°C, was used to generate the gaseous flow for the hydration step.

The main operating conditions were: hydration with 10% steam (balance air) and dehydration in air. A sensitivity analysis on temperature was carried out varying both the hydration and the dehydration temperature (one at a time, while keeping the other fixed). The temperature range investigated for hydration was 200-300°C, while that for dehydration was 350-450°C. As an example, the acronym M-H25A-D35N is a typical name used to identify one test where the first letter specifies the sorbent (M=Massicci lime; Z=zeolite), H25A indicates the hydration step at 250°C in air, while D35A indicates the dehydration step at 350°C in air. All the conditions investigated are summarized in Table 1.

	Temperature	Fluidizing gas		
		H ₂ O	CO ₂	Balance
X*-H20A-D35A	250/350 (°C)**			
X-H25A-D35A	250/350 (°C)			
X-H25A-D40A	250/400 (°C)			
X-H25A-D45A	250/450 (°C)	10/0 (%vol)	400/400 (ppm)	Air/Air
X-H30A-D35A	300/350 (°C)			
X-H30A-D40A	300/400 (°C)			
X-H30A-D45A	300/450 (°C)			

*X=M for Massicci sorbent, =Z for zeolite sorbent

**the first value (250) refers to the hydration stage, the second one (350) to the dehydration stage

Tab.1: Main operating conditions

The progress of hydration and dehydration reactions was followed during the tests by measuring the steam concentration at the outlet of the reactors by means of a calibrated humidity sensor. Each test consisted of 10 complete cycles, with a fluidization velocity fixed at 0.5m/s, while the time of each hydration or dehydration step was fixed at 10 min. The H₂O capture capacity of the material, during each hydration stage, was evaluated by time-integration of the outlet H₂O profile.

3. Results and discussion

Steam capture tests for Massicci CaO.

Figure 3 reports the steam capture capacity of the sorbent with the number of cycles, expressed as grams of captured H₂O per gram of initial CaO, for all the conditions investigated. In general, the performance of CaO tends to decay with the number of cycles, and to reach an asymptotic value after the 6th-7th cycle. Moreover, the 2nd cycle typically presents a higher value of steam capture than the 1st cycle. This trend is most likely due to the different value of molar density between calcium hydroxide and calcium oxide (which is lower for the first one), with a consequent swelling of the particle during the 1st hydration, which entails an alteration of the sorbent microstructure with the formation of a highly porous CaO after the 1st dehydration step [24].

The decay after the 2nd cycle is the consequence of two effects: the first one is the occurrence of attrition phenomena which imply the removal of sorbent

material leaving as fines from the reactor with the outlet gas; the second effect is caused the irreversible carbonation of the CaO with the CO₂ contained in air, consuming active CaO from the sorbent.

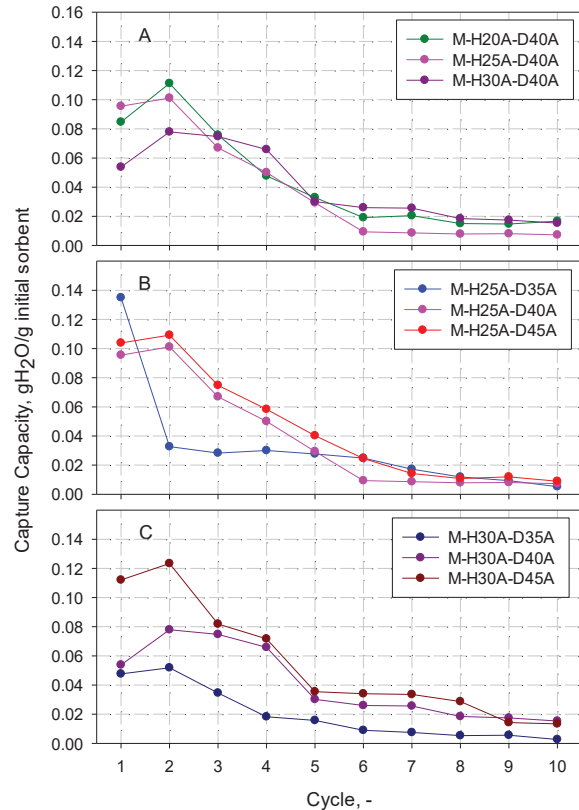


Fig.3: H₂O capture capacity of the sorbent with the number of cycles for Massicci CaO

In Fig. 3-A the results of the tests M-H20A-D40A, M-H25A-D40A and M-H30A-D40A are reported, at a fixed dehydration temperature of 400°C, and for three different hydration temperatures (200, 250 and 300°C). The steam capture capacity decreases with the hydration temperature and this difference is evident during the first cycles and tends to vanish with the increase of the number of cycles. This behavior is related to the higher hydration (and carbonation) kinetics which determines the formation of a plugging layer of Ca(OH)₂ (and CaCO₃) which hinders the diffusion of steam in the particle core. The asymptotic capacity values are similar among the samples and range around 0.008-0.019 g/g.

The effect of the dehydration temperature was investigated setting two different hydration temperatures of 250 and 300°C and varying the dehydration temperature (350, 400 and 450°C). The results are shown in Figs. 3-B and 3-C. In general, the increase of the regeneration (dehydration) temperature improves the steam capture capacity but these differences are only significant during the first cycles and tend to disappear with the increase of the cycle number. Probably, this behavior may be explained by the fact that faster dehydration (at higher temperatures) determines overpressures inside particle that induce a more severe breakage of the particles with the formation of new surface for the subsequent hydration step [25]. However, these effects appear to be more relevant at the highest hydration temperature, in particular during the first cycles (compare Figs. 3-B and 3-C).

Steam capture tests for 3A Zeolite.

Figure 4 (A-C) reports the steam capture capacity of the sorbent with the number of cycles, expressed as grams of captured H₂O per gram of initial zeolite, for all the condition investigated. In general, the behavior of the zeolite is quite stable along the cycles with a slight increase of the capture capacity during the first cycles that indicates a sort of feeble activation.

Similar to CaO, the influence of the hydration temperature was studied fixing the dehydration temperature at 400°C and varying the hydration temperature at 200, 250 and 300°C (Fig. 4-A). It is possible to note a slight negative influence of hydration temperature, in particular for the test Z-H30A-D40A, which shows an average capture value of about 0.022 g/g, compared to 0.044 and 0.049 g/g for Z-H20A-D400A and Z-H25A-D40A, respectively. This effect is due to the worsening of physical absorption of H₂O on the sorbent surface at higher temperatures.

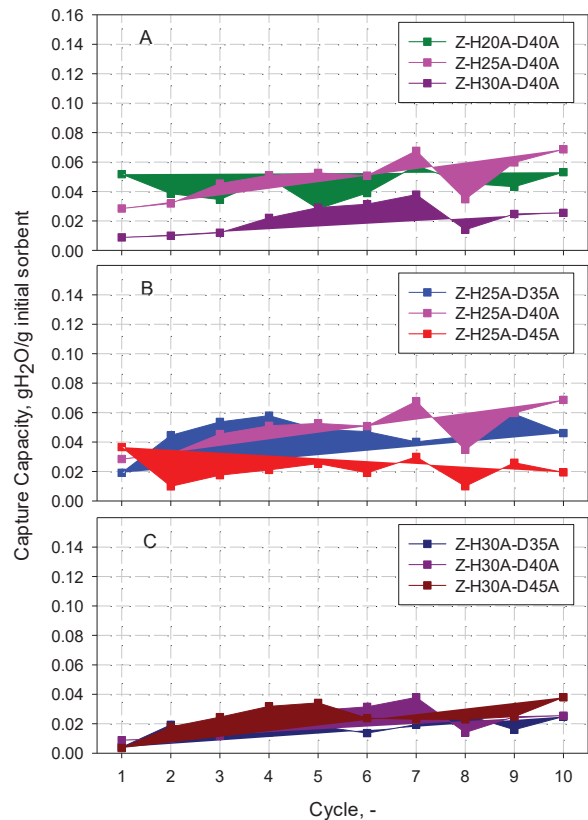


Fig.4: H₂O capture capacity of the sorbent with the number of cycles for 3A Zeolite

In Figs. 4-B and 4-C the effect of the dehydration temperature was examined (350, 400 and 450°C) for two different hydration temperatures (250 and 300°C). In particular, when the hydration temperature was set to 250°C (Fig. 4-B), the increase of the dehydration temperature seems to have a limited effect until 400°C (average values of 0.046 and 0.049 g/g for Z-H25A-D35A and Z-H25A-D40A respectively), while the capture capacity significantly decreases at 450°C (average value of 0.22 g/g for Z-H25A-D45A). This behavior is most likely caused by the chemical degradation of the sorbent at 450°C, probably related to the release of water contained in the zeolite structure.

When the hydration temperature was 300°C, the steam capture capacity records a relevant decay for all investigated dehydration temperatures. As matter of fact, the average capacity values were 0.017, 0.022 and 0.024 g/g for the tests Z-

H30A-D35A, H30A-D40A and H30A-D45A, respectively. Probably, the hydration temperature limits from a thermodynamic point of view the physisorption of water as detected for the tests at different hydration temperatures (see figure 4-A), and this effect is more pronounced when the difference between hydration temperature and dehydration decreases.

4. Conclusions

In this work, the feasibility of two different materials was investigated for their utilization as H_2O sorbents for the Sorption-Enhanced Methanation in an innovative configuration consisting of two interconnected fluidized beds. A calcium oxide, derived from an Italian natural limestone called Massicci, and a commercial 3A zeolite were tested in a lab-scale dual fluidized bed apparatus, called Twin Beds, purposely designed for looping systems. The performance was evaluated in terms of the steam capture capacity and its release in multiple cycle tests of hydration and dehydration. The hydration steps were run in a reaction environment composed by 10% in volume of steam in air, while the dehydration steps in pure air. A sensitivity analysis was carried out at different temperatures of both hydration and dehydration to investigate the effect of these temperatures on both materials.

In general, CaO presents a decay of the steam capture capacity with the number of cycles in all conditions investigated. This decay is likely determined by the combination of chemical deactivation, induced by the irreversible carbonation of the sorbent with CO_2 contained in the air, and the elutriation of fines particles due to attrition phenomena. The increase of the hydration temperature entails a negative effect during the first cycles, which tends to vanish with the increase of the cycle

number. This behavior is probably due to the formation of a plugging external layer of $\text{Ca}(\text{OH})_2$ (and CaCO_3) induced by faster reactions. Conversely, higher dehydration temperatures promote particle breakage with the formation of new surface with the consequent increase of the steam capture capacity.

On the other hand, the zeolite has a more stable behavior than CaO in all conditions investigated, and presents a slight activation during the first cycles. However, the hydration temperature has a similar effect as for CaO, which determines a decrease of the steam capture capacity. The explanation of this trend is due to the less favorable physisorption with the increasing temperature.

Contrary to CaO, the influence of the dehydration temperature on the zeolite seems to be strictly related to the hydration temperature. At low hydration temperature, a negative effect could be observed only at the highest dehydration temperature, probably induced by a modification of the structure of the zeolite. Instead, at higher hydration temperature the steam capture is principally limited by the thermodynamics of physisorption during the hydration stage.

Comparing the performance of the two materials, the zeolite on average has a better asymptotic capture capacity (0.017-0.049 g/g) than CaO (0.006-0.025 g/g) and furthermore it is not affected by deactivation during the cycles. However, this is not the only parameter to be considered for the choice of the best sorbent for the sorption-enhanced methanation, because other features could be important, such as the different cost of the two sorbent, which is in favor of CaO. In addition, another important factor is the attrition resistance of the sorbent in a fluidized bed environment, which will be the subject of future experimental tests. For steady operation in a dual fluidized bed reactor methanator (with continuous

circulation of the sorbent to/from a regenerator reactor), the amount of water removed from the methanation reactor can be regulated by changing the sorbent circulation rate to/from the regenerator or by changing the ratio of sorbent to catalyst loading in the system. It is worth noting that a recent thermodynamic assessment showed that partial water capture might be

preferable with respect to total water removal in order to avoid solid carbon formation (which would lead to catalyst deactivation) [26]. A detailed calculation of the optimal sorbent/catalyst ratio and solids circulation rate would need a preliminary definition of the best operating conditions in terms of the desired fractional amount of captured water.

5. Acknowledgements

N. Vallefuoco, C. De Giacomo, A. Esposito, A. Pace and L. Tregrossi are gratefully acknowledged for their help in performing the tests.

6. References

- [1] A.H. Seifert et al., *Appl. Energy* **132** (2014) p155
- [2] M. Götz et al., *Renew. Energy* **85** (2015) p1371
- [3] S. Rönsch et al., *Fuel* **166** (2016) p276
- [4] P. Sabatier et al., *J. Chem. Soc.* **82** (1902) p333
- [5] G.P. Smestad et al., *Ind. Eng. Chem. Res.* **51** (2012) p11828
- [6] R.M. Cuéllar-Franca et al., *J. CO₂ Utiliz.* **9** (2015) p82
- [7] G. Pleßmann et al., *Energy Procedia* **46** (2014) p22
- [8] H.S.de Boer et al., *Energy* **72** (2014) p360
- [9] J. Newton, in: 14TH ANNUAL APGTF WORKSHOP London, 2014 URL, <http://www.apgtfuk.com/files/workshops/14thWorkshop2014>
- [10] J. Wallbrecht, Int. Gas Union Triennium 2003e2006-Working Committee 2: Underground Gas Storage, Amsterdam, 2006 URL, <http://members.igu.org/html/wgc2006/WOC2database>
- [11] P. Sabatier et al., *Comptes Rendus Des Séances De L'Académie Des Sciences, Section VI – Chimie*. Paris: Imprimerie Gauthier-Villars; 1902.
- [12] W. Boll et al., In: Ullmann's encyclopedia of industrial chemistry. Weinheim: Wiley-VCH Verlag GmbH & Co. KGaA; 2006. p. 85.
- [13] S. Rönsch, Anlagenbilanzierung in der Energietechnik – Grundlagen, Gleichungen und Modelle für die Ingenieurpraxis. 1st ed. Wiesbaden: Springer Vieweg; 2015.
- [14] G.A. Mills et al., *Catal Rev* **8** (1974) p159
- [15] P. Panagiotopoulou et al., *Appl Catal B* **88** (2009) p470
- [16] J.B. Powell et al., *J Catal* **94** (1985) p566
- [17] InfoMine: <http://www.infomine.com/investment/ruthenium/> [download: 04.06.2015].
- [18] M.V. Twigg, Catalyst Handbook, second ed., Manson Publishing Ltd., London, 1996.
- [19] C.H. Bartholomew, *Appl Catal A* **212** (2001) p17
- [20] M. Seemann, PhD thesis. ETH Zurich; 2006.
- [21] A. Borgschulte et al., *Phys. Chem. Chem. Phys.* **15** (2013) p9620
- [22] S. Walspurger et al., *Chem. Eng. J.* **242** (2014) 379–386
- [23] A. Coppola et al., *Powder Technol.* **316** (2017) p585
- [24] A. Coppola et al., *Energy & Fuels* **29** (2015) p4436
- [25] F. Scala et al., *AIChE J.* **43** (1997) p363
- [26] F. Massa et al., *J. CO₂ Utiliz.* (2019) DOI: 10.1016/j.jcou.2019.09.014

Industrial Implementations CCU, Greening the Gas Abstracts

Technoeconomic study of cost driving factors of a gas greening system for steel making based on power-to-gas and biomass gasification

D. C. Rosenfeld ^{*,1}, J. Lindorfer ¹, H. Böhm ¹

1. Energy Institute at the Johannes Kepler University Linz – Department of Energy Technology,
Altenberger Straße 69, 4040 Linz, Austria
^{*}corresponding author, rosenfeld@energieinstitut-linz.at

1. Introduction:

The steel industry is one of the largest greenhouse gas (GHG) emitters in Europe (The Boston Consulting Group, 2013). In 2014, it accounted for 15.6 % of Austria's CO₂ emissions (Umweltbundesamt GmbH, 2016). However, due to the increasing steel demand, it is also one of the most important industry sectors.

To limit global warming to a maximum of 2 °C, the European Commission published a roadmap to a low carbon economy, which intends to reduce CO₂ emissions by 80 to 95 % till 2050, compared to the reference year 1990. As part of this roadmap, the industry sector has to reduce its emissions by 83 to 87 % (European Commission, 2011).

Since the conventional steel making process is highly developed, it can not be expected that a high GHG emission reduction is generated by optimizing operation parameters. Therefore, new technologies and energy carriers have to be used or implemented to reduce the carbon footprint of steel.

One possible implementation of new technologies, would be the utilization of carbon sources from the steel making process – mainly from steel gases, like basic oxygen furnace gas (BOFG), blast furnace gas (BFG) and coke oven

gas (COG) – and upgrade them with renewable hydrogen to synthetic natural gas (SNG). This SNG could substitute the used natural gas and parts of the used PCI (pulverized coal injection) coal.

As part of this work, a potential gas greening system based on power to gas (PtG) and biomass gasification, which should provide renewable hydrogen for methanation of the existing steel gases, was analyzed. For the reference steel plant an annual natural gas consumption of 3 TWh and a steel production of 5 Mt was assumed.

2. Methodology, Results and Discussion

Three implementation and operation scenarios for the mentioned gas greening system were analyzed. One extreme value scenario and two constrained scenarios were defined. In the constrained scenarios, the nominal power of the biomass gasification plant was limited to a maximum of 100 MW_{th}.

All scenarios were included a carbon dioxide reduction potential analysis, a techno economic analysis and a sensitivity analysis. The focus in this work was on showing the potentials for carbon dioxide reduction and gas greening of the three scenarios and how the evaluated SNG generation costs are influenced by factors

such as operation time, cost of electricity input, etc.

The conducted sensitivity analysis has shown that the predominant cost driving factors are the electricity price, the biomass fuel price and the operation time (see Fig. 1).

Furthermore, GHG reduction potentials of more than 800 kt_{CO₂} per year were quantified, in the constrained scenarios additional gas greening potentials of approx. 300 kt_{CO₂} per year were quantified.

3. Conclusion and Outlook

As one essential statement of the evaluation, the currently expected costs of 4 to 10 cent per kWh SNG for 2050 are not competitive to current natural gas prices. As main influencing sources of the SNG generation costs, electricity price, biomass fuel price and operation time were determined.

Further, a possible GHG reduction of 813 kt_{CO₂} per year was concluded. Future research should focus on further sources

that can be substituted by SNG and optimized operation modes of the gas greening system components. Furthermore, a detailed assessment from a techno-economic and technological point of view on N separation implementation will be necessary. If SNG feed into the gas grid is considered as option, the assessment has to further include an evaluation of gas cleaning technologies that are necessary to reach gas grid quality standards.

4. References

- European Commission. (2011). *A Roadmap for moving to a competitive low carbon economy in 2050*. Brussels, Belgium: European Commission.
- The Boston Consulting Group. (2013). *Steel's contribution to a low-carbon europe 2050*. Boston, MA, USA: The Boston Consulting Group, Inc.
- Umweltbundesamt GmbH. (2016). *Klimaschutzbericht 2016*. Vienna, Austria: Umweltbundesamt GmbH.

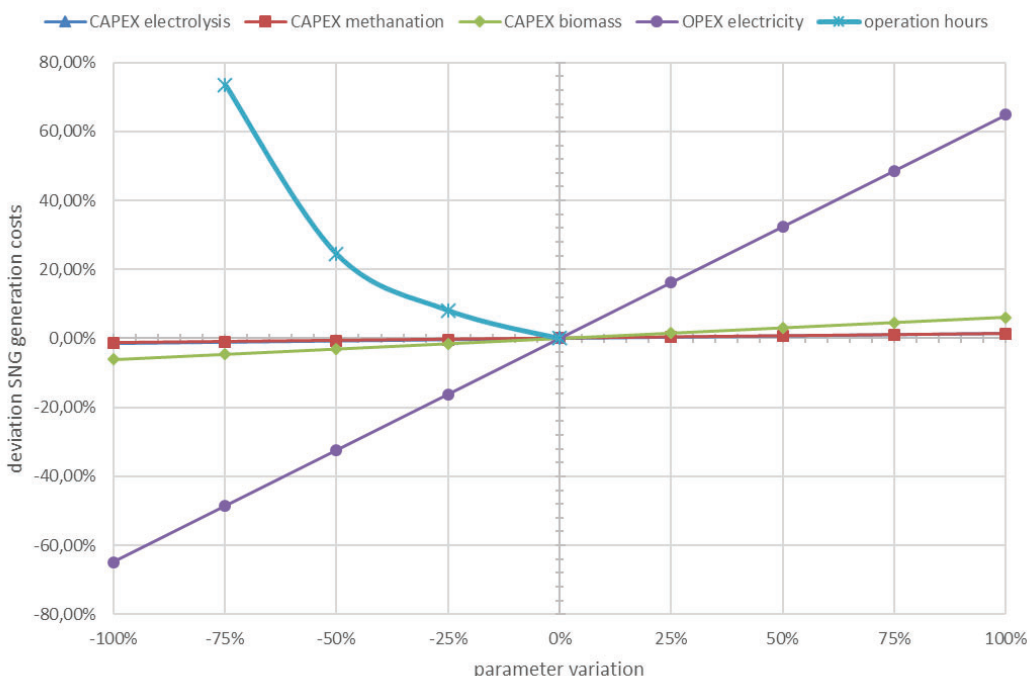


Fig. 1: Sensitivity analysis of one of the constrained scenarios

**Industrial Implementations
Industrial Demonstration
Full Papers**

Thermodynamic Investigation of SNG Production Based on Dual Fluidized Bed Gasification of Biogenic Residues

A. Bartik^{1*}, F. Benedikt¹, A. Lunzer², C. Walcher², S. Müller², H. Hofbauer¹

1. TU Wien, Institute of Chemical, Environmental and Bioscience Engineering,
Getreidemarkt 9/166, 1060 Vienna, Austria
2. Energy & Chemical Engineering GmbH, Pappelstraße 13, 1140 Vienna, Austria

*corresponding author, alexander.bartik@tuwien.ac.at

Abstract

Natural gas is an important commodity in the European energy market. A promising concept for the production of synthetic natural gas on a carbon neutral basis is presented by the gasification of biogenic residues and the further reaction to a methane-rich gas. This paper investigates the thermodynamics of methanation for different product gas compositions of the dual fluidized bed gasification technology. A complete methanation of the carbon oxides is possible by the utilization of a product gas from the sorption enhanced reforming process. For product gases from conventional or carbon dioxide gasification, only partial methanation of carbon monoxide occurs. Additionally, proper handling of carbon depositions through adjustments of feed gas composition and operational parameters in the methanation reactor are essential. Temperature and pressure variations allow a thermodynamically optimized operation, which can reduce energy costs for compression or lower the amount of gas upgrading for grid feed-in. Vice versa, it is shown that the feed gas can be optimally adjusted to the operational parameters of the methanation via the sorption enhanced reforming process.

1. Introduction

Increasing greenhouse gas emissions and the limited availability of primary energy carriers directed the energy policy of the European Union towards sustainable and innovative energy technologies [1]. Natural gas is one of the most important primary energy carriers in Europe, but its availability is heavily dependent on the non-European market. The production of synthetic natural gas (SNG) from biogenic residues offers a promising alternative to the utilization of fossil fuels and represents a novel concept to support the current energy strategy of the European Union [1, 2].

One possible process route is the dual fluidized bed (DFB) gasification, which allows the utilization of locally available residual biogenic or waste resources and

offers possibilities for the production of highly valuable secondary energy carriers on a carbon neutral basis [3, 4]. In combination with sorption enhanced reforming (SER) this technology enables the production of a nitrogen-free product gas with adjustable hydrogen to carbon monoxide and hydrogen to carbon dioxide contents [5].

Before the product gas from the DFB process can be fed to the methanation unit, rigorous gas cleaning is required in order to protect the downstream equipment and the methanation catalyst [6-8].

For the methanation reactor itself, several concepts have been utilized. Adiabatic or cooled fixed bed reactors, fluidized bed reactors, three-phase reactors or micro-reactors. However, only adiabatic fixed bed methanation is commercially available as of today. This variety of reactor types

also explains the wide range of operation conditions. Temperatures from 250 °C to 700 °C and pressures from 1 bar_a to 87 bar_a have been applied. From a thermodynamic point of view the methanation is favored at low temperatures and high pressures [9, 10]. In order to feed the generated gas into the Austrian gas grid, the feed-in regulations must be satisfied [11]. Alternatively, a mixture of CH₄ and H₂, also referred to as hythane, can be generated as a substitute for natural gas in industrial applications [12].

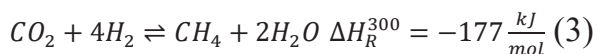
The main chemical species, which are involved in the methanation reaction system, are CH₄, H₂, CO, CO₂ and H₂O. The corresponding reaction equations are the CO-methanation,



the reverse water gas shift reaction, and



the CO₂-methanation (combination of (2) and (1)).



Additionally, the reaction enthalpies at 300 °C (ΔH_R^{300}) are given. Besides these species, the product gas of the DFB gasifier also contains higher hydrocarbons. As the main component ethylene (C₂H₄) is identified and is thus included here [13]. The hydrogenation to methane can be written as:



A deactivation mechanism of the catalyst, which cannot be prevented by gas cleaning steps, is the formation of solid carbon on the catalyst. While adsorbed carbon on the catalyst surface is a necessary reaction intermediate during methanation, the formation of stable deposits leads to catalyst fouling [14]. Thermodynamically,

this deposition can be accounted for by the Boudouard reaction.



The deposited surface carbon can also be hydrogenated to methane,



or undergo gasification with steam [15].



These reactions show that increased amounts of H₂, H₂O or CO₂ in the product gas might prevent the carbon deposition. A different form of deposition can occur through the adsorption of higher hydrocarbons like C₂H₄ on the catalyst surface. Between 500 and 600 °C, this can lead to coke deposits [16].

If kinetic models are considered, all of the above mentioned reaction pathways have to be taken into consideration. The catalytic methanation of syngas is, however, mostly limited by heat and mass transfer and not by kinetics [10]. For temperatures down to 320 °C the gas composition is close to the thermodynamic equilibrium [17, 18]. A thermodynamic calculation thus provides a good estimation of the expected gas composition. Because of the broad variety of possible carbon species, deviations from thermodynamic equilibrium for carbon deposition have to be expected [10]. Nevertheless, graphitic carbon has previously been used to elucidate this issue, since kinetic models are often only valid for specific reaction conditions and catalysts [19].

Extensive studies have been performed on the thermodynamics of methanation [14, 19, 20]. However, for systems with multiple simultaneous reactions, the effect of different product gas mixtures as well as temperature and pressure is not straightforward. Thus, the thermodynamic calculations in this paper are applied to

different product gas mixtures, which have been obtained by the gasification of different biogenic residues with the 100 kW_{th} DFB gasifier at TU Wien. The chosen feed gas compositions for the methanation aim at covering the broad range of product gas compositions, which can be produced by the DFB gasifier.

2. Concept and methodology

In order to calculate the thermodynamic equilibrium, only four of the seven reaction equations (Eq. (1) to Eq. (7)) need to be considered. Otherwise, the system would be overdetermined, because only four equations are linearly independent of each other. For example, the CO₂-methanation reaction can be seen as the reversed water gas shift reaction followed by the CO-methanation.

Thermodynamic calculations are performed with HSC Chemistry and MATLAB. The main focus of this investigation is a low temperature methanation (300 °C) at ambient pressure. These parameter settings result from the current efforts in the design and construction of a lab-scale fluidized bed methanation test rig at TU Wien for the given parameters. Nevertheless, also a temperature variation from 200 °C to 500 °C and a pressure range from 1 bar_a to 10 bar_a are carried out. Graphite is chosen as the prevailing carbon species, since Frick et al. [19] found that the Gibbs free energy is lower than for amorphous carbon and is thus preferentially formed.

In order to classify the feed gas composition the stoichiometric number (*SN*) is defined.

$$SN = \frac{y_{H_2}}{3*y_{CO} + 4*y_{CO_2} + 2*y_{C_2H_4}} \quad (8)$$

SN gives the ratio between the molar fraction of H₂ (*y*_{H₂}) to the molar fractions of the carbonaceous species in the feed gas which react to CH₄. If *SN* is equal to one,

there is a stoichiometric amount of H₂ available according to Eqs. 1, 3 and 4. Because the regarded pressures in this study are relatively low, it is safe to assume ideal gas behavior. Molar fraction are thus equal to volume fractions. This definition of *SN* is not unambiguous, because the chemical equilibrium is influenced by all available species and therefore also by CH₄ and H₂O. Nevertheless, it allows an approximate classification of the feed gas mixture. Typical product gases from the DFB gasification show similar CH₄ concentrations. Water concentrations in the feed gases are assumed zero. This is attributed to the required gas cleaning which is conventionally carried out at low temperatures [21]. If similar CH₄ concentrations and a water free feed gas are assumed, the implementation of *SN* is justified.

Additionally, the CH₄ yield (*Y*_{CH₄}),

$$Y_{CH_4} = \frac{\dot{n}_{CH_4,eq}}{\sum_i N_i \dot{n}_{i,feed}} * 100 \quad (9)$$

the carbon yield (*Y*_C),

$$Y_C = \frac{\dot{n}_{C,eq}}{\sum_i N_i \dot{n}_{i,feed}} * 100 \quad (10)$$

the CO conversion (*X*_{CO}), and

$$X_{CO} = \frac{\dot{n}_{CO,feed} - \dot{n}_{CO,eq}}{\dot{n}_{CO,feed}} * 100 \quad (11)$$

the CO₂ conversion (*X*_{CO₂}) are defined.

$$X_{CO_2} = \frac{\dot{n}_{CO_2,feed} - \dot{n}_{CO_2,eq}}{\dot{n}_{CO_2,feed}} * 100 \quad (11)$$

Index *i* refers to the carbonaceous species in the feed (*i* = CH₄, CO, CO₂, C₂H₄).

Gas cleaning is not within the scope of this study. The feed gas mixture for the methanation is assumed free of impurities and other minor components. Besides, kinetics or heat and mass transfer phenomena are not considered.

Tab. 1: Investigated feed gases

Parameter	Unit	Feed gas number					
		1	2	3	4	5	6
Source	-	[5]	[3]	[22]	[23]	[24]	[25]
Gasification agent	-	H ₂ O	H ₂ O	H ₂ O	H ₂ O	CO ₂ /H ₂ O ^a	H ₂ O
Feedstock	-	BA	BA	LI	SS	RSC	SW
Bed material	-	L	L	O	O/L ^b	O	L
Gasification temperature	°C	625	761	789	800	840	582-797
Combustion temperature	°C	820	998	945	945	938	830-1041
Feed gas composition (water free feed)							
H ₂	vol.-%	68.3	52.4	42.6	35.6	25.8	71.1-47.6
CO	vol.-%	6.5	18.4	21.2	13.7	32.1	7.3-21.6
CO ₂	vol.-%	8.9	21.3	21.8	36.5	33.7	4.1-23
CH ₄	vol.-%	14.5	7.3	12.0	11.7	7.3	17.4-8.8
C ₂ H ₄	vol.-%	1.9	0.6	2.4	2.5	1.1	1.9-0.5

^a CO₂/H₂O = 68/32 vol.-%

^b O/L = 80/20 wt.-%

3. Results and discussion

In Tab. 1 the investigated feed gas compositions for the methanation are shown. Feed gas no. 1 shows a typical SER gas with high hydrogen content. Limestone (L) is used as bed material at lower temperatures and bark (BA) is chosen as the feedstock. Feed gases no. 2-no. 4 present product gases from conventional gasification. With feed gas no. 2 the same fuel and bed material is used but the gasification temperature is higher which results in lower H₂ and higher CO and CO₂ contents. For feed gas no. 3 lignin (LI) is used as fuel and olivine (O) as bed material. Sewage sludge (SS) and an olivine/limestone mixture (O/L) are the basis for feed gas no. 4, which results in low H₂ and high CO₂ contents. For feed gas no. 5, a CO₂/H₂O mixture is used as gasification agent and rapeseed cake (RSC) and O as fuel and bed materials, respectively. This results in even lower H₂ and high CO and CO₂ concentrations. Feed gas no. 6 shows a temperature variation for SER gasification. This is included to demonstrate the adaptability of the DFB gasifier to the requirements of the methanation process (also see Fig. 4). Data

for this variation is only available for softwood (SW) as feedstock.

In Fig. 1 results of chemical equilibrium calculations at 300 °C and 1 bar_a are shown for feed gas nos. 1-5. The volume fractions of the dry gas components after methanation (referred to as raw-SNG) and the water content of the raw-SNG are depicted. C₂H₄ is not displayed in any of the figures, because it is completely converted under all investigated conditions. CO is not shown in Fig. 1, because only trace amounts remain in the raw-SNG. Additionally, Tab. 2 lists some key figures as defined in Eqs. 8-11.

Almost complete conversion of CO and CO₂ to CH₄ can be reached with the SER feed gas (feed gas no. 1). The CH₄ yield is

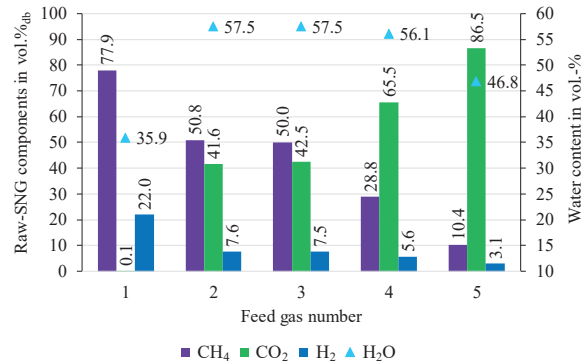


Fig. 1: Raw-SNG gas composition for feed gas nos. 1-5 at 1 bar_a and 300 °C

Tab. 2: Key figure results of the equilibrium calculations

Par.	Unit	Feed gas number				
		1	2	3	4	5
SN	-	1.16	0.37	0.27	0.19	0.11
Y_{CH_4}	%	99.9	29.4	24.6	14.4	5.2
Y_C	%	0	46.5	54.5	52.8	50.9
X_{CO}	%	100	99.9	99.9	99.8	99.9
X_{CO_2}	%	99.7	45.4	42.7	39.9	2.2

99.9 % and no carbon formation is thermodynamically expected. However, 22 vol.-%_{db} of H₂ are still in the raw-SNG and would have to be separated before grid feed-in below 4 vol.-%. Feed gas nos. **2** and **3** show similar results to each other. About 50 vol-%_{db} CH₄ can be expected. CO is almost completely transformed, whereas less than 50% of the CO₂ is converted. Thermodynamically, severe carbon deposition can occur with about half of the feed carbon being separated from the gas stream. The raw-SNG from the SS product gas (feed gas no. **4**) shows a CH₄ yield of only 14.4 %. The rest of the gas is mainly CO₂. If a product gas from CO₂ gasification is used (feed gas no. **5**), 86.5 vol.-%_{db} of the raw-SNG consists of CO₂ and only 10.4 vol.-%_{db} are CH₄. This is equal to a methane yield of 5.2 % and a CO₂ conversion of 2.2%, respectively.

For feed gas nos. **2-5** the SN is below one. Since all feed gases are dry, this correlates with the carbon deposition. CO is almost completely converted for all feed gases. However, even small amounts of CO might exceed the allowed threshold level for grid feed-in on the one hand. On the other hand, CO₂ methanation is found to be kinetically hindered even for very low CO concentrations [26]. For feed gas no. **1** 7 ppm_{v,db} of CO remain in the raw-SNG in the thermodynamic equilibrium. At least 580-750 ppm_{v,db} need to be expected for feed gas nos. **2-5**.

Investigation of the sewage sludge product gas

In the following section a more in-depth discussion of the SS product gas follows (feed gas no. **4**). Because of the expected carbon deposition for this feed gas composition, H₂O should be added if a long catalyst lifetime and a high conversion efficiency are aimed at. Fig. 2 depicts the raw-SNG gas composition after the addition of H₂O for temperatures from 200-500 °C and pressures of 1, 5 and 10 bar_a (Fig. 2b). The amount of water added corresponds to the minimum amount needed to prevent carbon deposition. This minimum volume fraction of H₂O in the feed gas (H_2O_{feed}) as well as Y_{CH_4} are also displayed (Fig. 2a). With increasing temperature, less CH₄ and CO₂ and more CO and H₂ are present. Accordingly, the CH₄ yield decreases from 41 % to 26 % with increasing temperature

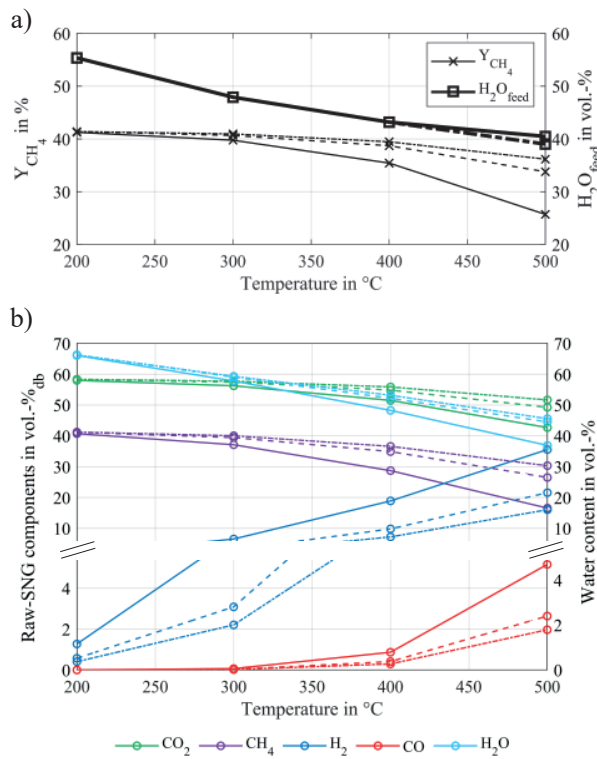


Fig. 2: Temperature and pressure variation for feed gas no. 4 in the thermodynamic equilibrium: 1 bar_a (full line), 5 bar_a (dashed line) and 10 bar_a (dash-dotted line). a) CH₄ yield and feed water content, b) Raw-SNG gas composition

at 1 bar_a. H_2O_{feed} decreases from 55 vol.-% to 40 vol.-% within the displayed temperature range. Nevertheless, the methanation would be preferred at low temperatures from a thermodynamic point of view, if the additionally required steam is not seen as the decisive factor. Especially the strongly rising CO content at higher temperatures makes low temperature methanation attractive. Pressure only has a significant influence on the gas composition at higher temperatures. At 500 °C Y_{CH_4} can be substantially elevated if the pressure is increased to 5 bar_a. A further pressurization only allows a minor improvement of Y_{CH_4} . Whereas, at 200 °C Y_{CH_4} is almost constant for all pressures. For H_2O_{feed} , hardly any influence of pressure can be observed.

A comparison of Fig. 1 and Fig. 2 clarifies the influence of the added feed water at 300 °C and 1 bar_a for the SS product gas. By the addition, the CH₄ content is elevated from 29 to 37 vol.-%_{db}. At the same time, the CO₂ content is lowered from 66 to 56 vol.-%_{db}. H₂ slightly increases from 5.6 to 6.6 vol.-%. The CO concentration is marginally lowered from 714 to 667 ppm_{v,db}. Despite the addition of 48 vol.-% of H₂O to the dry feed gas, the H₂O concentration in the raw-SNG only increases slightly. This can be visualized by the steam gasification reaction (Eq. 7). Most of the steam is needed to gasify the carbon. Because no carbon is present after feed water addition, X_{CO_2} is negative under all displayed conditions. In other words, more CO₂ is formed during methanation than converted.

For grid feed-in the raw-SNG needs to be freed of CO₂. A maximum of only 2 vol.-% is allowed. A H₂ content below the allowed threshold level of 4 vol.-% after CO₂ separation could be achieved by increasing the pressure at 260 °C to

10 bar_a. If the desired commodity is hythane only CO₂ separation is necessary.

Investigation of the SER product gas

Feed gas no. 1 is a typical SER product gas with a high H₂ content. SN is greater than one, which allows a practically complete methanation of the carbon oxides (CO+CO₂) at temperatures below 300 °C with a CH₄ yield of nearly 100 % (Fig. 3). Pressure again only has significant influence on the gas composition at higher temperatures. With pressurization, the decreasing trend of CH₄ and the increasing trends of H₂, CO and CO₂ at higher temperatures can be counteracted. In addition, above 440 °C at 1 bar_a carbon formation is thermodynamically possible. As is shown in Fig. 3a, H₂O needs to be added. At higher pressures, this can be prevented. Below 300 °C there is practically no influence of pressure or temperature on the gas composition.

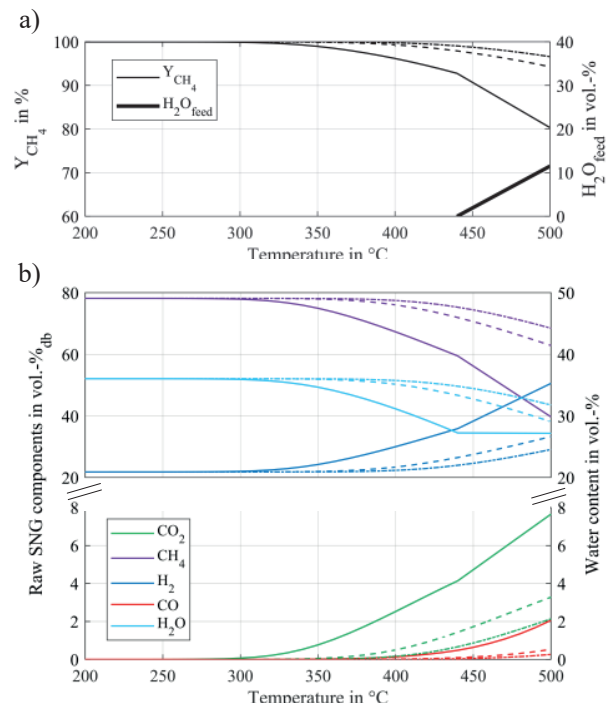


Fig. 3: Temperature and pressure variation for feed gas no. 1 in the thermodynamic equilibrium: 1 bar_a (full line), 5 bar_a (dashed line) and 10 bar_a (dash-dotted line). a) CH₄ yield, b) Raw-SNG gas composition

Methanation around 300 °C and 1 bar_a shows a favorable raw-SNG composition without the need of compression. Lower temperatures would not improve the gas composition, but increase the challenge of employing an active catalyst. For grid feed-in, only H₂ would need to be separated from the raw-SNG. For the application as hythane on the other hand, no further upgrading step is necessary except water condensation.

Besides these advantages, the methanation of SER product gas also comes with drawbacks. The high H₂ content can only be reached by the increased transport of carbon from the fuel to the flue gas. However, the excess carbon (in the form of CO₂), which is still in the raw-SNG in case of conventional gasification, is already removed within the gasification process for the SER product gas. The overall process chain thus shows a low carbon utilization factor. But this lower carbon utilization factor lies primarily in the gasification process and not in the methanation process. Whereas the addition of H₂ from external sources (e.g. electrolysis) would allow the methanation of the leftover CO₂ and yield a high carbon utilization factor for conventional gasification. Another suggestion would be the installation of a water gas shift reactor prior to the methanation reactor, which was demonstrated successfully for hydrogen production from DFB derived wood gas [27].

Investigation of variable product gas compositions of the SER process

Fuchs et al. [25] already described the adaptability of the SER process with regard to the product gas composition. In Fig. 4 the evolution of the product gas components over the gasification temperature of the 100 kW_{th} DFB gasifier at TU Wien is depicted. By temperature variation, the product gas can be adjusted

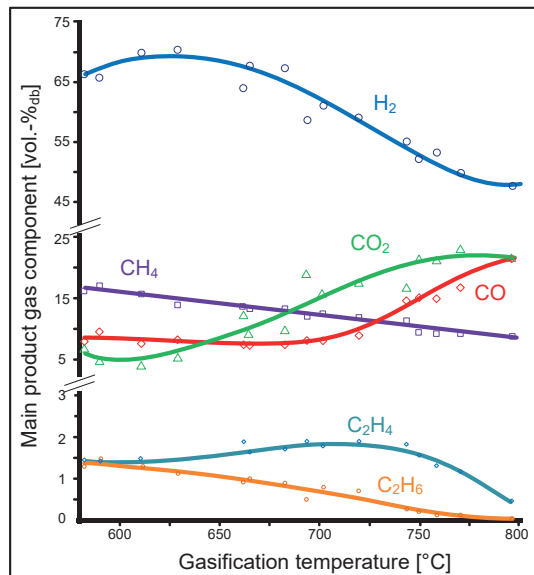


Fig. 4: Product gas composition over gasification temperature for the 100 kW_{th} DFB gasifier at TU Wien for softwood and olivine as fuel and bed material, respectively; from [25]

to the required feed gas for methanation. However, this also adds an additional parameter to the modelling of the methanation reactions.

Fig. 5 displays the composition of the raw-SNG in the thermodynamic equilibrium for all data points of Fig. 4 over SN. Temperature and pressure are again set to 300 °C and 1 bar_a for the methanation process, respectively. In order to assess carbon formation Y_C is given. There is a decreasing trend for CO₂, H₂O and the amount of carbon formed for an increasing SN. CH₄ has a maximum at a SN slightly above one. At the same point carbon formation declines to zero and the small incline in H₂ turns into a sharp increase for higher SN. CO is only present in trace amounts (0.14–614 ppm_{v,db}) and is not displayed here. From a thermodynamic point of view, the feed gas with a SN of 1.09 generates a raw-SNG with the most favorable composition for the methanation at 300 °C and 1 bar_a. A SN of 1.09 corresponds to a gasification temperature of about 680 °C.

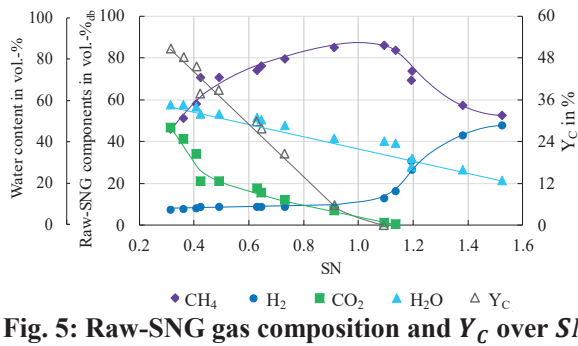


Fig. 5: Raw-SNG gas composition and Y_C over SN for the feed gas compositions according to Fig. 4 at 300 °C and 1 bar_a in the thermodynamic equilibrium

The associated compositions for the feed gas and the raw-SNG as well as the key figures are depicted in Tab. 3. Different operation conditions of the methanation might favor other feed gas compositions from Fig. 4 and vice versa. In order to find the most suitable feed gas composition for deviating methanation conditions, reiterations of the thermodynamic equilibrium calculations would have to be carried out.

Tab. 3: Feed gas and raw-SNG composition and key figures for the feed gas with a SN of 1.09 at 300 °C and 1 bar_a in the thermodynamic equilibrium

Par.	Unit	Feed gas	Raw-SNG
CH ₄	vol.-% _{db}	13.3	86.1
H ₂	vol.-% _{db}	67.8	12.8
CO	vol.-% _{db}	7.3	0.005
CO ₂	vol.-% _{db}	9.8	1.1
C ₂ H ₄	vol.-% _{db}	1.7	0
H ₂ O	vol.-%	0	40.2
Y_{CH_4}	%	98.8	
Y_C	%	0	
X_{CO}	%	100	
X_{CO_2}	%	95.8	

4. Conclusion and Outlook

In this work, the suitability of various product gases from the 100 kW_{th} DFB gasifier for methanation has been evaluated from a thermodynamic point of view. It has been shown, that complete methanation is only possible for SER product gases. For all other gases, only the partial methanation of CO is possible, whereas CO₂ might even constitute the

main raw-SNG component. Additionally, gases from conventional steam gasification or gasification with CO₂ admixture to the gasification agent (H₂O+CO₂) are subject to carbon deposition. Therefore, H₂O needs to be added for a stable operation. Furthermore, the influence of different operation conditions of the methanation on the raw-SNG composition have been visualized. By the careful choice of operation conditions, energy savings and/or less effort for further gas upgrading can be accomplished. A further investigation of the SER product gases has revealed that it is also possible to adapt the gasification process to suit certain methanation conditions optimally. However, if H₂ is available from an external source, conventional gasification can be beneficial because of a higher carbon utilization factor.

It should be noted that all investigations in this paper are based on thermodynamic equilibrium calculations. There are many other parameters, which can influence the performance of the methanation. Catalyst poisoning due to insufficient gas cleaning, the choice of the reactor concept or kinetic limitations necessitate experimental investigations.

Acronyms

BA	bark
DFB	dual fluidized bed
L	limestone
LI	lignin
O	olivine
O/L	olivine/limestone mixture
raw-SNG	synthetic natural gas after methanation/before gas upgrading
RSC	rapeseed cake
SER	sorption enhanced reforming
SNG	synthetic natural gas
SS	sewage sludge

SW	softwood	Y_C	carbon yield in %
vol.-%	volumetric percent	Y_{CH_4}	methane yield in %
wt.-%	weight percent	y_i	molar fraction of species i

Symbols

ΔH_R^{300}	molar reaction enthalpy at 300 °C
H_2O_{feed}	volume fraction of H_2O in the feed in vol.-%
\dot{n}_i	molar flow of species i in mol/s
N_i	number of carbon atoms in species i
SN	stoichiometric number
X_{CO}	carbon monoxide conversion in %
X_{CO_2}	carbon dioxide conversion in %

Indices

a	absolute
C	carbon
CH_4	methane
C_2H_4	ethylene
CO	carbon monoxide
CO_2	carbon dioxide
db	dry basis
eq	equilibrium
feed	in the feed gas
H_2	hydrogen
v	volumetric

5. Acknowledgements

This work is part of the research project ReGas4Industry and receives financial support from the research program “Energieforschung” funded by the Austrian Climate and Energy Fund.

6. References

- [1] European Commission, “Directive (EU) 2018/2001 of the European Parliament and of the Council of 11 December 2018 on the promotion of the use of energy from renewable sources,” *Off. J. Eur. Union*, vol. L 328/82, no. December, p. 128, 2018.
- [2] I. E. A. (IEA), *Gas market report 2018*. 2018.
- [3] F. Benedikt, J. C. Schmid, J. Fuchs, A. M. Mauerhofer, S. Müller, and H. Hofbauer, “Fuel flexible gasification with an advanced 100 kW dual fluidized bed steam gasification pilot plant,” *Energy*, vol. 164, pp. 329–343, 2018.
- [4] A. Sahoo and D. K. Ram, “Gasifier performance and energy analysis for fluidized bed gasification of sugarcane bagasse,” *Energy*, vol. 90, pp. 1420–1425, 2015.
- [5] J. Fuchs, J. C. Schmid, S. Müller, and H. Hofbauer, “Dual fluidized bed gasification of biomass with selective carbon dioxide removal and limestone as bed material: A review,” *Renew. Sustain. Energy Rev.*, vol. 107, no. November 2018, pp. 212–231, 2019.
- [6] M. Asadullah, “Biomass gasification gas cleaning for downstream applications : A comparative critical review,” vol. 40, pp. 118–132, 2014.
- [7] T. Pröll, I. G. Siefert, A. Friedl, and H. Hofbauer, “ Removal of NH_3 from Biomass Gasification Producer Gas by Water Condensing in an Organic Solvent Scrubber,” *Ind. Eng. Chem. Res.*, vol. 44, no. 5, pp. 1576–1584, 2005.
- [8] H. Hofbauer, R. Rauch, S. Fürnsinn, and C. Aichernig, “Energiezentrale Güssing,” 2006.

- [9] J. Kopyscinski, T. J. Schildhauer, and S. M. A. Biollaz, “Production of synthetic natural gas (SNG) from coal and dry biomass - A technology review from 1950 to 2009,” *Fuel*, vol. 89, no. 8, pp. 1763–1783, 2010.
- [10] T. J. Schildhauer and S. M. A. Biollaz, *Synthetic Natural Gas from Coal, Dry Biomass, and Power-to-Gas Applications*. 2016.
- [11] ÖVGW, *Richtlinie G 31-Erdgas in Österreich-Gasbeschaffenheit*. 2001.
- [12] M. Kraussler, P. Schindler, and H. Hofbauer, “An experimental approach aiming the production of a gas mixture composed of hydrogen and methane from biomass as natural gas substitute in industrial applications,” *Bioresour. Technol.*, vol. 237, no. 2017, pp. 39–46, 2017.
- [13] F. Benedikt, M. Kuba, J. Christian, S. Müller, and H. Hofbauer, “Assessment of correlations between tar and product gas composition in dual fluidized bed steam gasification for online tar prediction,” *Appl. Energy*, vol. 238, no. December 2018, pp. 1138–1149, 2020.
- [14] X. Bai, S. Wang, T. Sun, and S. Wang, “Influence of Operating Conditions on Carbon Deposition Over a Ni Catalyst for the Production of Synthetic Natural Gas (SNG) from Coal,” pp. 2157–2166, 2014.
- [15] A. Kambolis, T. J. Schildhauer, and O. Kröcher, “CO Methanation for Synthetic Natural Gas Production,” vol. 69, no. 10, pp. 608–613, 2015.
- [16] S. Rönsch, J. Schneider, S. Matthischke, M. Schlüter, M. Götz, J. Lefebvre, P. Prabhakaran and S. Bajohr, Review on methanation – From fundamentals to current projects,” *Fuel*, vol. 166, pp. 276–296, 2016.
- [17] J. Kopyscinski, T. J. Schildhauer, and S. M. A. Biollaz, “Methanation in a fluidized bed reactor with high initial CO partial pressure : Part II — Modeling and sensitivity study,” *Chem. Eng. Sci.*, vol. 66, no. 8, pp. 1612–1621, 2011.
- [18] J. Kopyscinski, T. J. Schildhauer, F. Vogel, S. M. A. Biollaz and A. Wokaun, “Applying spatially resolved concentration and temperature measurements in a catalytic plate reactor for the kinetic study of CO methanation,” *J. Catal.*, vol. 271, no. 2, pp. 262–279, 2010.
- [19] V. Frick, J. Brelochs, and M. Specht, “Application of ternary diagrams in the design of methanation systems,” vol. 118, pp. 156–160, 2014.
- [20] J. Gao, Y. Wang, Y. Ping, D. Hu, G. Xu, and F. Su, “RSC Advances PAPER: A thermodynamic analysis of methanation reactions of carbon oxides for the production of synthetic natural gas,” pp. 2358–2368, 2012.
- [21] N. Abdoulmoumine, S. Adhikari, A. Kulkarni, and S. Chattanathan, “A review on biomass gasification syngas cleanup,” *Appl. Energy*, vol. 155, pp. 294–307, 2015.
- [22] J. C. Schmid, F. Benedikt, J. Fuchs, A. M. Mauerhofer, S. Müller, and H. Hofbauer, “Syngas for biorefineries from thermochemical gasification of lignocellulosic fuels and residues - 5 years’ experience with an advanced dual fluidized bed gasifier design,” *Biomass Convers. Biorefinery*, 2019.
- [23] J. C. Schmid, A. Bartik, F. Benedikt, A.M. Mauerhofer, J. Fuchs, E. Schanz, S. Reisinger, B. Nowak, F. Bühler, M. Österreicher, A. Lunzer, C. Walcher, S. Müller, M. Fuchs and H. Hofbauer, “Steam gasification of sewage sludge for synthesis processes,” in *ICPS 2019*, 2019.
- [24] A. M. Mauerhofer, S. Müller, F. Benedikt, J. Fuchs, A. Bartik, and H. Hofbauer, “CO₂ Gasification of Biogenic Fuels in a Dual Fluidized Bed Reactor System,” *Submitt. to Biomass Convers. Biorefinery*, 2019.

- [25] J. Fuchs, J. C. Schmid, S. Müller, A. M. Mauerhofer, F. Benedikt, and H. Hofbauer, “The impact of gasification temperature on the process characteristics of sorption-enhanced reforming of biomass,” *Biomass Convers. Biorefinery*, 2019.
- [26] T. Herwijnen, H. Doesburg, and W. A. de Jong, “Kinetics of the Methanation of CO and CO₂ on a Nickel Catalyst,” *J. Catal.*, vol. 28, pp. 391–402, 1973.
- [27] S. Fail, N. Diaz, F. Benedikt, M. Kraussler, J. Hinteregger, K. Bosch, M. Hackel, R. Rauch and H. Hofbauer, “Wood gas processing to generate pure hydrogen suitable for PEM fuel cells,” *ACS Sustain. Chem. Eng.*, vol. 2, no. 12, pp. 2690–2698, 2014.

Evaluating the efficiency of Power-to-X technologies by adapting the VDI-Guideline 4663

N. Eggers¹, J. Böttger¹, L. Kerpen^{2*}, Prof. Dr.-Ing. B. Sankol², Dr.-Ing. T. Birth¹

1. Fraunhofer Institute for Factory Operation and Automation, Department for Convergent Infrastructures,
Sandtorstraße 22, 39106 Magdeburg, Germany

2. Hamburg University of Applied Sciences, Faculty of Engineering and Computer Science
Berliner Tor 11, 20099 Hamburg, Germany

*corresponding author, Lukas.Kerpen@haw-hamburg.de

Abstract

The utilization and conversion of fossil energy sources can be identified as a main reason for greenhouse gas emission. Renewable energy will show a great potential to reduce the need of fossil energy sources, especially if it is combined with Power-to-X technologies. To allow a targeted optimization, the VDI-Guideline 4663 proposes a new method, the Physical Optimum (PhO), to evaluate the efficiency of a process. The basic challenge of this method is the development of an ideal reference process.

This work applies the Physical Optimum on a Power-to-X system and evaluates a component of the system. The paper discusses:

- The method of the Physical Optimum and the resulting PhO-Factor in general
- The implementation of the VDI-Guideline 4663 on complex industrial processes as an indicator of efficiency
- Power-to-X technologies in general and suitable system boundaries for an implementation on Power-to-X systems
- The implementation of the VDI-Guideline 4663 on a heat exchanger as an indicator of efficiency

1. Introduction:

Momentarily, the German public power supply encounters basic changes. The current German Renewable Energy Sources Act (EEG, German: Erneuerbare-Energien-Gesetz) states that 80 % of the electricity supply sector must be based on renewable energy by 2050. [1]

In addition, the international climate agreement of the United Nations Framework Convention on Climate Change (UN-FCCC) plans a cross-sectoral reduction of greenhouse gases by

80 - 95 % by the year 2050, compared to 1990. [2]

Due to the volatility of renewable energy sources, like solar or wind energy, the alteration of the electricity sector faces substantial difficulties considering the power supply flexibility. The drastic reduction of greenhouse gas emissions requires a decarbonization of all energy sectors in Germany, which leads to additional challenges. Especially the electricity, heat, and transportation sector are affected, since they are accountable for a major part of the greenhouse gas emissions. [3]

Figure 1 illustrates the portions of carbon dioxide emissions in various sectors in Germany. The emissions of the year 2015, which amounted to approximately 715 million tons in total, are considered. [3]

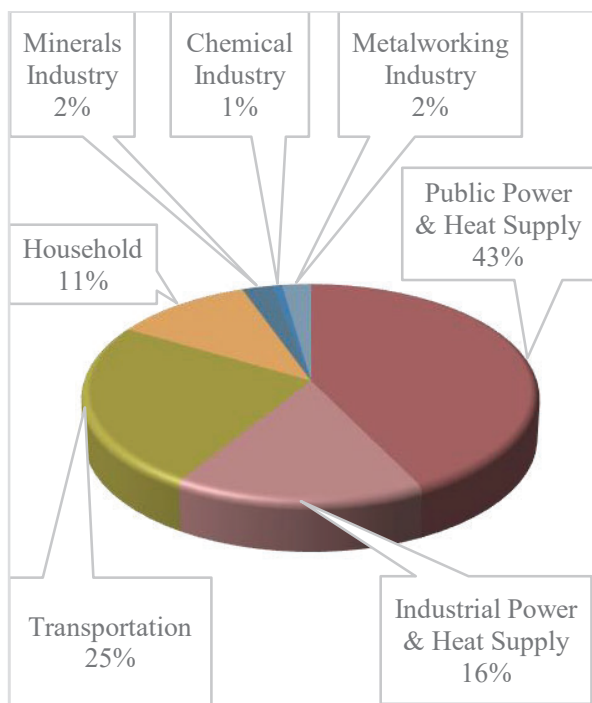


Figure 1: Portions of carbon dioxide emissions in Germany (2015, stated in percent of 715 Mio. tons in total) (Custom illustration following [3])

Currently, the highest carbon dioxide emissions are caused by the power and heat supply, which are assigned to the energy industry. They are followed by mentionable amounts of carbon dioxide emissions by the transportation and household sector. Since the total amount of carbon dioxide emissions by the power and heat supply only cover 69 % [3] of all emissions, it becomes obvious that a decarbonization of the energy sector is not sufficient for compliance with the international climate agreement, but must be extended to the transport, industrial and private sectors.

Power-to-X (PtX) offers several technologies for cross-sector utilization of the greenhouse gas-reducing potential of

renewable energies and thus provides a strategy for both the challenges of the international climate agreement and the goals of the EEG 2017. [4, p.10]

Nevertheless, the economical use of PtX technologies is widely discussed. [5 - 7] Efficiencies indicated in literature differ greatly and are not always completely reproducible.

The Physical Optimum is a promising energy index, that may be helpful in order to evaluate and optimize the operation of PtX-strategies.

2. Power-to-X Strategies

PtX serves as a collective term for almost all technologies of sector coupling except for electromobility³. [8, p.6]

Generally, it includes Power-to-Gas (PtG), Power-to-Liquid (PtL), Power-to-Chemicals (PtC) and Power-to-Heat (PtH) technologies. [9, pp.328]

The strategies may overlap, depending on the definition. For example, the production of liquids (PtL) may occur while a PtC process is running.

Another possibility to differentiate PtX-approaches is the separation into the resulting effective use of the final product, which are Power-to-Heat (PtH), Power-to-Power (PtP), Power-to-Mobility (PtM) and Power-to-Chemicals (PtC). Again, overlapping may occur, since individual end products of the process chain can be used for different purposes. [8, p.7] For example, methanol can be used as feed material in the chemical industry (PtC) or for the production of fuel (PtM). [9, pp.328] Therefore a specific subdivision of the process chains is not possible.

³ In this context, electromobility includes any form of locomotion by storing electrical energy in battery systems and then converting it into mechanical energy. It solely covers so called BEV ("Battery Electric Vehicle"). Therefore, it does not apply to hydrogen- or E-fuel-powered means of transport.

Figure 2 schematically illustrates the technologies with the most important process steps as well as the overlapping of the various strategies.

The starting point for PtX was the PtG approach. For the first time, the use of electricity from renewable energy sources for water electrolysis and a subsequent methanation of hydrogen with the aid of carbon dioxide was discussed. Initially, the basic idea was to link the electricity sector with the natural gas grid. Since the German electricity grid does not have sufficient storage capacities, it was possible to store electrical energy in the form of chemical energy. The natural gas network, which has comparatively high storage capacities in Germany, was used for this purpose. [8, p.6]

Today, PtG does not just include the classic natural gas strategy (Power-to-Methane) but also the direct use or subsequent processing of hydrogen. In addition, the use or processing of synthesis gas, which is produced during the co-electrolysis, is included in PtG. [10, p.2]

Today, PtX involves all processes that offer a solution for cross-sector decarbonization. Consequently, the boundaries of PtX can no longer be defined with such

precision. [8, p.6] For example, it is conceivable to consider the entire chain from power generation to use, such as the conversion back into electrical power. However, this approach does not always make sense, since depending on the final product and the intermediate product, infrastructures such as the natural gas network are used. Thus, it is no longer possible to determine exactly which part of the gas used originates from PtG processes. For this reason, the boundaries of the PtX strategies must be redefined depending on the process chain under consideration.

Figure 2 only portrays examples of the most important usage paths of the PtX strategy and therefore does not describe all possibilities of process interfacing within the scope of PtX.

3. Present deficits in the evaluation of PtX systems

In the course of the discussions about the PtX strategy, the efficiency is fundamental. It is repeatedly pointed out, that the technology is 'too costly' [6] and 'too inefficient' [5]. According to [11], the overall

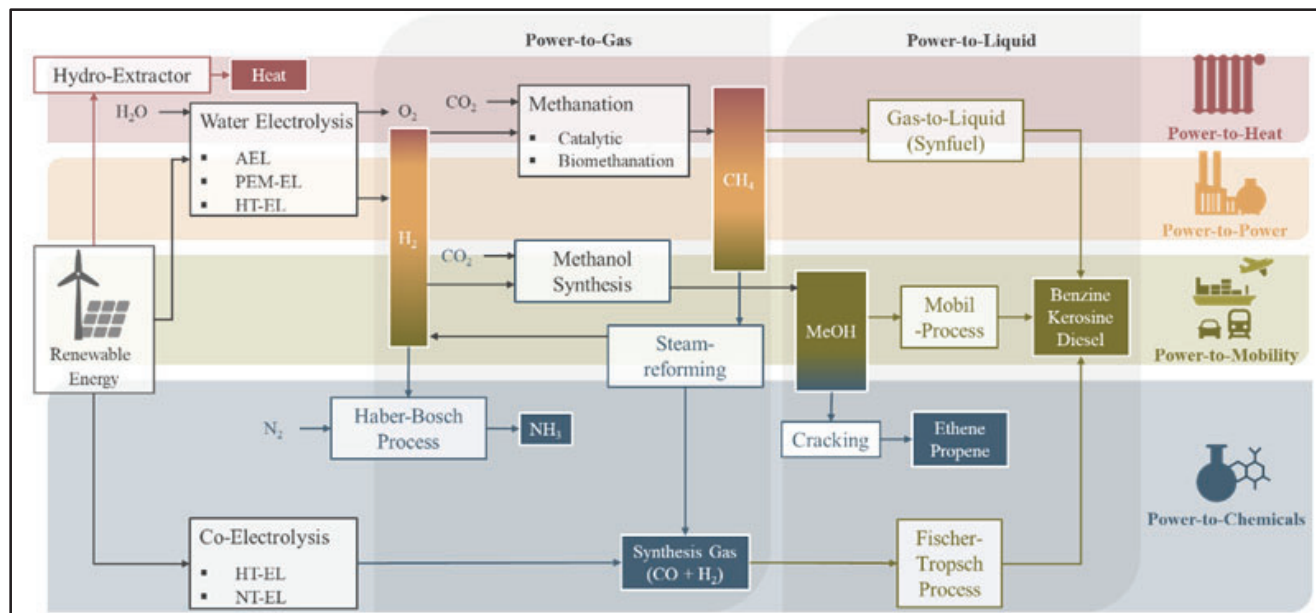


Figure 2: Schematic illustration of the most important paths of the Power-to-X approach (Custom illustration following [8,9])

efficiency of the Power-to-Methane process will be 56 %. [11, p.762] Other sources indicate an efficiency of 46 % to 68 % for the same process. [12, p.9; 13, p.5] Regardless of the climate-related necessity of PtX, the indication of the degree of effectiveness in this form is misleading. Some sources only consider excess electricity for the operation of electrolysis, [11, pp.761] which leads to unsteady partial load operation of the plant. This may result in considerably lower resource and energy efficiency compared to full load operation. Other sources do not specify the operating conditions of the electrolysis cell. [12, 13]

This clarifies, that a comparability of these indices is not guaranteed, even though the process remains identical. The efficiency can only evaluate the process based on the current state of technology, the current political and economic situation and the mode of operation. In conclusion, the potential of an optimization for a planned or existing plant, cannot be determined solely from this data, as long as the optimum is unknown. [14, p.1] Since this problem can be observed in various technical industries, an alternative to conventional rating systems and indices is of necessity.

4. The Physical Optimum:

The Physical Optimum (PhO) was first introduced by D. Volta. It is described as a theoretical, ideal reference process that includes all scientific laws and thus cannot be improved any further. [14, p.32] Hence, it shows the maximum potential of an optimization, while standard cycles do not consider the minimum required effort of a process and therefore only enable an improvement, but never an optimization. [14, p.31]

This ultimate reference point will not be based on the best available technology and is time-independent, if the laws of physics

are considered. A continuous customization of energy indicators, as seen for electric drives or electric domestic appliances (figure 3), can be precluded. [14, p.34]

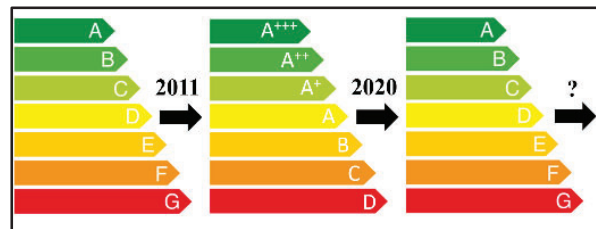


Figure 3: Adjustment of the European Union energy label for refrigerating appliances (Custom illustration following [11, p.43])

Volta first described the PhO-Factor, an energy index that compares a real/measured value with the PhO. This factor allows the adaption of common tools, like the Pareto chart or the Energy Loss Cascade, to specifically optimize a process. Additionally, completely new tools, like the Potential Analysis, were developed.

In his dissertation from 2017, C. Keichel [15] improved the Physical Optimum significantly by introducing a consuming and a demanding perspective of the PhO-Factor. This enabled the applicability of the method to a wide range of users.

The consuming perspective is used to evaluate the efficiency of supplying processes. For example, steam generators use air, combustible material and water to supply steam at a certain pressure and temperature. They are rated by the consuming perspective. It is defined by the energy that is provided in real terms (output) and the energy that is provided under physically optimal conditions (PhO as input). [15, p.42] The demanding perspective is used to evaluate the efficiency of a process that requires energy to operate. Pumps or fans require electrical energy to generate a pressure difference in a fluid flow.

Therefore, they are rated by the demanding perspective. It is defined by the energy that is required by the process in real terms (input) and the energy that would be required under physically optimal conditions (PhO as output). [15, p.42]

The following figure shows both perspectives.

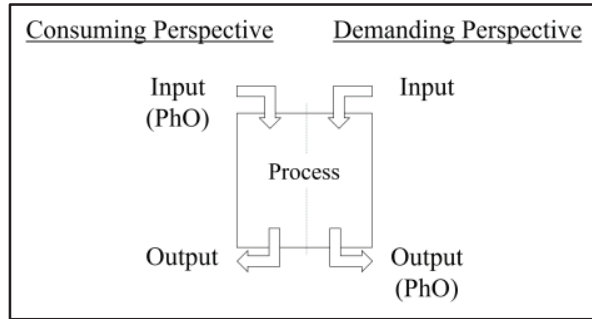


Figure 4: Perspectives of the PhO (Custom illustration following [15, p.43])

The consuming perspective and its boundary are defined as follows: [15, p.43]

$$F_{PhO}^V = \frac{Output}{Input (PhO)} = \frac{V}{V_{PhO}} \leq 1 \quad (1)$$

The demanding perspective and its boundary are defined as follows: [16, p.43]

$$F_{PhO}^B = \frac{Input}{Output (PhO)} = \frac{B}{B_{PhO}} \geq 1 \quad (2)$$

When evaluating industrial processes, usually there will be more than one device, that has an impact on the efficiency of the overall process. In this case, the PhO-Factor must be coupled in order to maintain an index, that shows the maximum potential of optimization. The following figure shows three linked subprocesses.

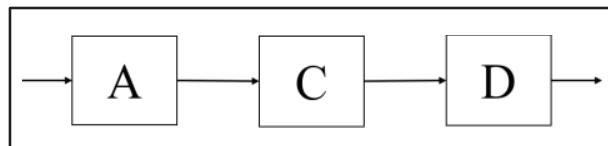


Figure 5: Exemplary subprocesses

Process A is a supplying process and is therefore evaluated by the consuming perspective. Process C and D are subprocesses, that require the energy of process A.

They are evaluated by the demanding perspective. The coupling of the individual values is conducted analogously to the coupling of redundant processes, as described by Keichel. [15, p.73]

$$F_{BC,PhO}^B = \frac{B_C + B_D}{B_{C,PhO} + B_{D,PhO}} \leq 1 \quad (3)$$

The PhO-Factor of the demanding perspective $F_{BC,PhO}^B$ must be coupled with the consuming perspective to define the PhO-Factor of the overall process. [15, p.70]

$$F_{PhO}^{total} = \frac{F_{BC,PhO}^B}{F_{A,PhO}^V} \geq 1 \quad (4)$$

In order to describe transfer processes like heat exchangers, Keichel also describes the capacitive perspective. It compares the energy that is transferred in real terms with the energy that may be transferred under physically optimal conditions. [15, p.99]

$$F_{PhO}^K = \frac{Q_{real}}{Q_{Pho}} \leq 1 \quad (5)$$

While Volta described the PhO-Factor regarding the energy of a process, Keichel also defined the PhO-Factor in terms of power. Considering the power facilitates the identification of inefficient process states, which enables real-time interventions and makes optimizations more efficient. The power-based PhO-Factor is defined by the power in real terms and the power under physically optimal conditions. It may also be described by the derivative of the energy-based PhO-Factor over time: [15, pp.45]

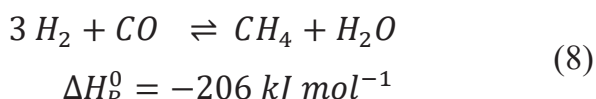
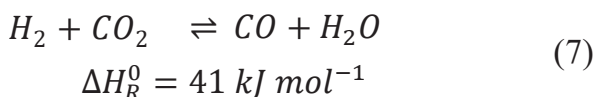
$$f_{Pho}^K = \frac{\dot{Q}_{real}}{\dot{Q}_{Pho}} \leq 1 \quad (6)$$

5. The Power-to-Methane-Concept

For the application of the PhO, the process must be known precisely. For this purpose, as described in Chapter 4, it is first necessary to consider the individual procedures of the process chain. Depending on each procedure, a further partitioning into subsystems may be necessary.

Since an evaluation of the entire PtX strategy would include the assessment of all process steps involved, this paper only applies to the PtG concept, especially the methanation, in an exemplary manner. For the consideration of the entire Power-to-Methane chain, power generation, electrolysis, carbon dioxide capture and methanation must be considered. The further process chain varies depending on the use of the end product and is therefore not taken into account in the Power-to-Methane technology considered in this paper.

With the oldest of the PtX strategies, the hydrogen produced by electrolysis is converted into methane during methanation, by adding carbon dioxide. [16, p.3] The chemical reaction is usually split into the following sub-reactions: [17, p.377]



The total reaction of the methanation is strongly exothermic and shows a negative molar balance. As a result, according to Le Chatelier, it is encouraged at lower temperatures and high pressures. [17, p.377] In addition to methane, by-products such as carbon monoxide, carbon and hydrocarbons can be produced during the reaction. [16, p.18]

The side reactions and the chemical equilibrium are affected by the choice of operating conditions. From a thermodynamic point of view, process control at the highest possible pressure and the lowest possible temperature is the most sensible solution. [16, p.18]

Since the reduction of fully oxidized carbon to methane is an eight-electron reaction, the kinetic barrier is very high. Despite the use of suitable catalysts, a certain amount of activation energy is required. Therefore, the reaction is usually conducted at approximately 300 °C. [16, p.20]

However, in order to encourage the exothermic reaction of the above-mentioned chemical equilibrium, the greatest challenge of the methanation reaction is the efficient release of the reaction heat. For a detailed evaluation of the methanation process, it is therefore advisable to first consider the method of heat control.

6. Evaluating the efficiency of heat transfer processes

Energy conversion in Power-to-Methane processes can run both endo- and exothermically. Regarding electrolysis, energy must be supplied. Simultaneously, since methanation is a strongly exothermic reaction, reliable heat release is essential for successful reaction control (see Chapter 5).

Heat exchangers are used for this purpose. They transfer heat to a heat transfer fluid in exothermic processes. Without appropriate heat release, the PtG process chain would only be viable to a limited extent or not viable at all. Thus, the heat transfer processes must be included in the evaluation of the Power-to-Methane concept.

In the evaluation corresponding to the PhO-Factor, the heat transfer surface, which is theoretically required for this, is called the physically optimal surface A_{PhO} .

It is the surface that is required under optimal conditions in order to transfer the required heat flow. However, since the design of heat exchangers takes the fact into account, that the required transfer capacity is also achieved in case of contamination that reduces the capacity, the heat transfer surface is dimensioned larger (surface A_{VS}). In addition to the contamination-related increase in surface, uncertainties of the calculation model are also included. By applying a factor, the heat transfer surface (surface A_S) is increased. The real heat transfer surface A_{real} (equation (9)) results from the consideration of contamination and uncertainties. The real transfer area is larger than the theoretically necessary area and is thus oversized. [18, p.11]

$$A_{real} = A_{PhO} + A_{VS} + A_S \quad (9)$$

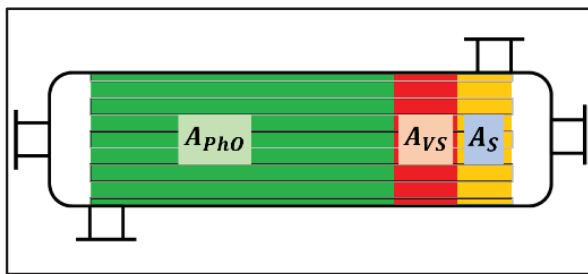


Figure 6: Heat transfer surfaces of a heat exchanger (Custom illustration following [16, p. 96])

The evaluation of heat exchangers in accordance to the VDI-Guideline 4663 is carried out, as per equation (6).

The heat flux in real terms \dot{Q}_{real} and the heat flux under physically optimal conditions \dot{Q}_{PhO} must be determined. The balance of energy only takes the heat exchanger into account. Other components are disregarded.

\dot{Q}_{real} is defined by the mass flux of the fluid \dot{m} , the average specific heat capacity $c_{p,m}$ and the temperature difference in real terms $\Delta\vartheta_{real}$. [19]

$$\dot{Q}_{real} = \dot{m} * c_{p,m} * \Delta\vartheta_{real} \quad (10)$$

The heat flux under physically optimal conditions \dot{Q}_{PhO} is determined with consideration to the conditions. [18, p.22]

$$\dot{Q}_{PhO} = \dot{m} * c_{p,m,PhO} * \Delta\vartheta_{PhO} \quad (11)$$

If it is assumed that the inlet temperatures are constant, the physically optimal outlet temperatures will be the highest or lowest possible temperatures, depending on the considered fluid. This results in apparatus- and operation-specific maximum temperature differences and thus maximum heat flows.

The outlet temperatures under physically optimal conditions will be defined by the operating characteristics, the heat transfer surface A_{ges} and the thermal transmittance coefficient under physically optimal conditions k_{PhO} , if it is assumed, that the heat transfer device is in new conditions.

In case of counter-flow, the temperatures are defined by equation (12) and equation (13). [20]

$$\vartheta'_{1,PhO} =$$

$$\vartheta'_1 - \frac{1 - e^{-(1 - \frac{\dot{C}_1}{\dot{C}_2}) * \frac{k_{PhO} * A_{ges}}{\dot{C}_1}}}{1 - \frac{\dot{C}_1}{\dot{C}_2} * e^{-(1 - \frac{\dot{C}_1}{\dot{C}_2}) * \frac{k_{PhO} * A_{ges}}{\dot{C}_1}}} * (\vartheta'_1 - \vartheta'_2) \quad (12)$$

$$\vartheta''_{2,PhO} =$$

$$\vartheta'_2 - \frac{1 - e^{-(1 - \frac{\dot{C}_2}{\dot{C}_1}) * \frac{k_{PhO} * A_{ges}}{\dot{C}_2}}}{1 - \frac{\dot{C}_2}{\dot{C}_1} * e^{-(1 - \frac{\dot{C}_2}{\dot{C}_1}) * \frac{k_{PhO} * A_{ges}}{\dot{C}_2}}} * (\vartheta'_1 - \vartheta'_2) \quad (13)$$

The thermal transmittance coefficient depends on the operating mode of the heat exchanger and is described by the heat transfer coefficients α_i and the thermal conductivity. The heat transfer coefficients characterize the heat transfer's intensity at boundary surfaces. They are described by the Nusselt number.

Since there is no fouling under physically optimal conditions, fouling is not considered in the definition of k_{PhO} . [21]

$$\frac{1}{k_{PhO}} = \frac{1}{\alpha_1} + \frac{s}{\lambda} + \frac{1}{\alpha_2} \quad (14)$$

With the physically optimal temperature difference $\Delta\vartheta_{PhO}$, which is determined from the inlet and the physically optimal outlet temperature, as well as the energy balance equation (11), the physically optimal heat flow \dot{Q}_{PhO} can be determined and thus the PhO-Factor f_{PhO}^K is formed.

Using \dot{Q}_{real} and \dot{Q}_{PhO} computes the PhO-Factor.

$$f_{PhO}^K = \frac{c_{p,m} * \Delta\vartheta_{real}}{c_{p,m,PhO} * \Delta\vartheta_{PhO}} \leq 1 \quad (15)$$

Due to losses, the physically optimal heat flux cannot be achieved under real terms. Hence, the factor is generally suitable for a targeted optimization.

7. Optimizing an industrial process based on the Physical Optimum

By using an ultimate reference point, the PhO is a very suitable tool to improve a process. When optimizing a complex industrial process, several subprocesses must be considered. The following elaboration lists methods, that allow a targeted selection of the subprocess to be optimized.

In order to optimize such a complex process, the PhO of all subprocesses must be known. By comparing the required power with the power required under physically optimal conditions, the maximum amount of power that could be saved by an optimization, is defined for each subprocess. This may be applied to the consuming (16) and the demanding perspective (17).

$$\Delta\dot{V}_{max,i} = \dot{V}_{PhO,i} - \dot{V}_i \quad (16)$$

$$\Delta\dot{B}_{max,i} = \dot{B}_i - \dot{B}_{PhO,i} \quad (17)$$

The values can be determined analogously using the PhO-Factor. Equation (18) applies to the consuming perspective, while equation (19) applies to the demanding perspective.

$$\Delta\dot{V}_{max,i} = (1 - f_{PhO,i}^V)\dot{V}_{PhO,i} \quad (18)$$

$$\Delta\dot{B}_{max,i} = (f_{PhO,i}^B - 1)\dot{B}_{PhO,i} \quad (19)$$

In terms of energy, the subprocess with the highest value of $\Delta\dot{V}_{max}$ and $\Delta\dot{B}_{max}$ should be optimized. If necessary, the forms of the primary energy must be considered in order to prevent falsification of the evaluation. [14, pp.63]

However, $\Delta\dot{V}_{max}$ and $\Delta\dot{B}_{max}$ offer additional possibilities. For example, by determining the emission of CO₂ that is incurred per Watt, the subprocess with the highest potential of CO₂ savings can be identified by including an according factor.

$$\Delta m_{CO_2,max,i} = \Delta\dot{B}_{max,i} * \frac{kg_{CO_2}}{W} \quad (20)$$

Factors that take other evaluation criteria into account, such as costs, are also conceivable. The subprocess with the greatest savings potential should be optimized.

By applying the indirect PhO-Factor, single subprocesses can be optimized. The indirect PhO-Factor is based on the indirect efficiency. The input of a process is determined by the output and occurring losses. [22]

$$Input = Output + Losses \quad (21)$$

Inserting equation (21) in equation (2) defines the indirect PhO-Factor

$$f_{PhO,ind.}^B = 1 + \sum_{i=1}^n \frac{Loss_i}{Output_{ges}} \geq 1 \quad (22)$$

In terms of energy, the specific loss to be optimized is the maximum ratio of dissipated power to the overall output. Again, an optimization regarding costs or emissions is possible analogously to equation (20).

8. Conclusion and Outlook

This paper identifies basic regulations, that are valid for PtX strategies. Different strategies and challenges in the evaluation of PtX efficiency were discussed. An alternative energy index, the PhO-Factor, was described in this work. Exemplary, the index was developed for an essential component of methanation. Finally, a procedure for targeted process optimization based on the PhO is presented.

The optimization of complex industrial processes must be analyzed even further. It might be possible, that optimizing one sub-process improves its efficiency, while the efficiency of the main process decreases. It should also be verified whether the procedure can be applied analogously to heat ex-changers. For a verification and further development, findings from the current WIPANO research project geoKEMS are used. Additional laboratory experiments will be conducted.

9. Symbols used

A	[m ²]	Surface
B	[e.g. W]	Demand
C	[WK ⁻¹]	Heat capacity flow
c _p	[Jkg ⁻¹ K ⁻¹]	Specific heat capacity
F	[-]	PhO-Factor
f		
k	[Wm ⁻² K ⁻¹]	Thermal transmittance coefficient
m	[kg]	Masse
Q	[W]	Heat
s	[m]	Length
V	[e.g. W]	Consumption

10. Greek symbols

α	[Wm ⁻² K ⁻¹]	Heat transfer coefficient
λ	[Wm ⁻¹ K ⁻¹]	Thermal conductivity
ϑ	[K]	Temperature

11. Sub- and superscript

ges	Total
i	Value related to subprocess i
K	Capacity
m	Average
PhO	Physical Optimum
S	Safety
VS	Fouling

12. Abbreviations

AEL	Alkaline Electrolysis
CHP	Combined Heat and Power
EEG	German Renewable Energy Sources Act
PEM	Proton Exchange Membrane Electrolysis
PhO	Physical Optimum
PtC	Power-to-Chemicals
PtG	Power-to-Gas
PtH	Power-to-Heat
PtL	Power-to-Liquid
PtM	Power-to-Mobility
PtX	Power-to-X
UN-	United Nations Framework
FCCC	Convention on Climate Change
VDI	Association of German Engineers

13. Acknowledgements

Some of the results presented in this paper were developed within the framework of the WIPANO project greoKEMS. In this context, the authors would like to thank the participating partners of CIECH Soda Deutschland GmbH & Co. KG, Envidatec GmbH, HOBUM Oleochemicals GmbH, Schott AG, Tchibo GmbH, Verein Deutscher Ingenieure e.V. and especially the team of Fraunhofer IFF and HAW Hamburg for their support.

14. References

- [1] Erneuerbare-Energien-Gesetz, §1, Absatz 2
- [2] United Nations Framework Convention on Climate Change, art. 4, § 2b) (2017)
- [3] Umweltbundesamt, Nationale Trendtabellen für die deutsche Berichterstattung atmosphärischer Emissionen (2017),
<https://www.umweltbundesamt.de/dokument/nationale-trendtabellen-fuer-die-deutsche-2> (accessed on June 27, 2009)
- [4] C. Schenuit, R. Heuke, J. Paschke, Potentialatlas Power to Gas (2016)
- [5] F. Urbansky, Power to Gas bleibt zu ineffizient (2017),
<https://www.springerprofessional.de/energiespeicher/energiebereitstellung/power-to-gas-bleibt-zu-ineffizient/12499670#> (accessed on June 6, 2019)
- [6] U. Dämgen, BWK – Das Energie-Fachmagazin, 70, 9 (2018) p.41
- [7] M. Grünewald, BWK – Das Energie-Fachmagazin, 71 (2019) p.3
- [8] M. Sterner, Energiewirtschaftliches Kurzgutachten, Notwendigkeit und Chancen für Power-to-X-Technologien (2017)
- [9] U. Bünger, J. Michalsky, P. Schmidt, W. Weindorf, Wasserstoff – Schlüsselement von Power-to-X, Wasserstoff und Brennstoffzelle, 2 (2017)
- [10] Kopernikus-Projekt, Öffentlicher Statusbericht (2018)
- [11] W. Viktor, T. Schabbach, T. Link, J. Fischer, Handbuch Regenerative Energietechnik, 3 (2017)
- [12] G. Müller-Syring, Fachtagung „Erdgas Umwelt Zukunft“ (Leipzig, 02.02.2011), Energiespeicherung in Erdgasnetzen (2011)
- [13] Zukunft ERDGAS GmbH, Delphi-Kurzstudie: Praxis und Potenzial von Power-to-Gas (2017)
- [14] D. Volta, Das Physikalische Optimum als Basis von Systematiken zur Steigerung der Energie- und Stoffeffizienz von Produktionsprozessen (2014)
- [15] C. Keichel, Methode der grenzwertorientierten Bewertung (2017)
- [16] K. Ghaib, Das Power-to-Methane-Konzept (2017)
- [17] M. Sterner, Energiespeicher, 2 (2017)
- [18] Verein Deutscher Ingenieure e. V., VDI 4663 Blatt 1 Bewertung von Energie- und Stoffeffizienz (2019)
- [19] H. D. Baehr, K. Stephan, Wärme- und Stoffübertragung, 9 (2016) p.69
- [20] B. Glück, Mittlere Temperaturdifferenz bei Wärmeübertragern, Raumheizflächen und Behälteraufheizung, (2017) p.16
- [21] P. von Böckh, T. Wetzel, Wärmeübertragung - Grundlagen und Praxis, 7 (2017) p.20
- [22] K.-H. Grote, J. Feldhusen, H. Dubbel, DUBBEL Taschenbuch für den Maschinenbau, 25, (2014) pp. L. 68

Industrial Implementations Industrial Demonstration Abstracts

Dynamic methanation of by-product gases from the steel industry in the scope of the project i³upgrade

A. Hauser^{1*}, M. Weitzer¹, S. Gunsch¹, M. Neubert¹, J. Karl¹

1. Friedrich-Alexander University Erlangen-Nürnberg, Chair of Energy Process Engineering,
Fürther Str. 244f, 90429 Nürnberg, Germany
*corresponding author, alexander.hauser@fau.de

1. Introduction and Short Description

The steel production via the integrated blast furnace route produces carbon- and energy-rich by-product gases in the process steps of coke production in the coke ovens, the pig iron production in the blast furnace and the steel production in the converter. Nowadays, these gases contribute, together with additional fossil fuels, to the energy needs of the steel works (Fig. 1 left). In the light of the European climate protection goals, efforts are made to reduce the CO₂ emissions of the steel production process. As the process operates close to the thermodynamic optimum, a further reduction by process optimization is not

feasible. Another approach is to integrate renewable energies into steel works.

The EU project i³upgrade addresses the integration of (renewable) hydrogen into a steel works without changing or affecting the steel production process and its associated auxiliary systems itself. The carbonaceous by-product gases serve as carbon source for subsequent syntheses with renewable hydrogen (e.g. from electrolysis). Methane synthesis can reduce the purchase of fossil fuels and methanol synthesis forms a valuable feedstock for the chemical industry out of the steel works' by-product gases (Fig. 1 right).

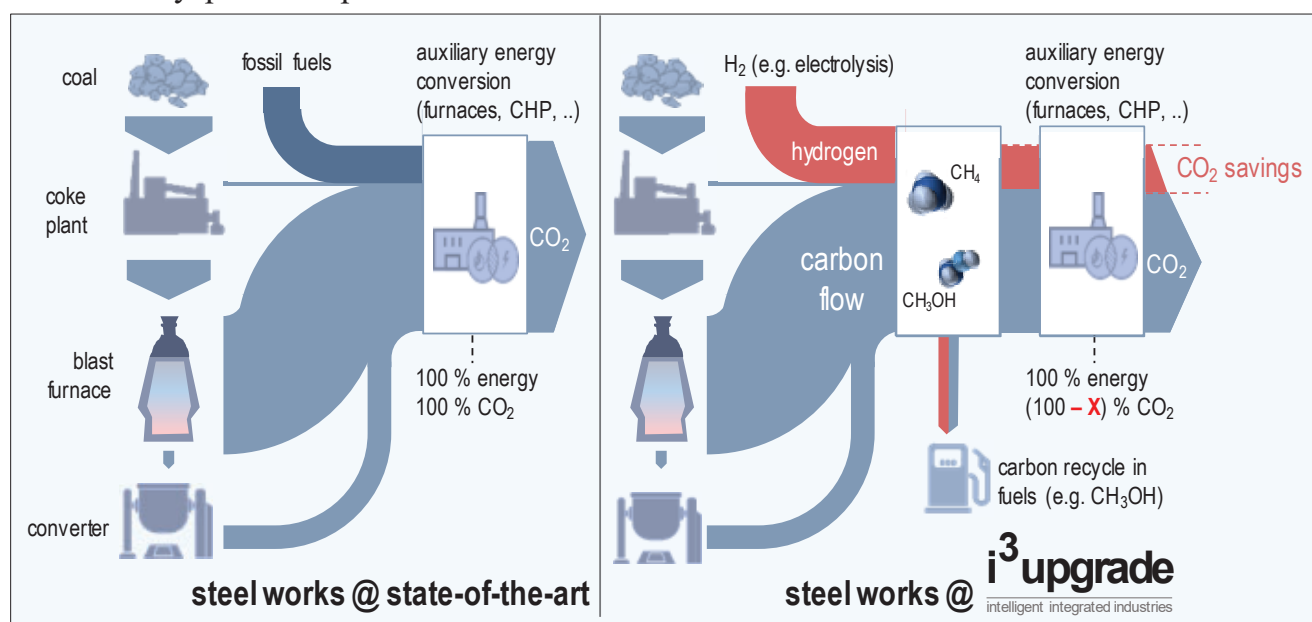


Fig. 1: Overall approach of i³upgrade: Comparison of schematic carbon flows inside an integrated steel works at the state-of-the-art (left) and the approach in i³upgrade (right) with carbon upgrade through hydrogen-intensified syntheses

The focus of this contribution lies on the experimental investigation of the dynamic synthesis of methane from different by-product gas mixtures from the steel industry (bottle mixed feed gases). The results from dynamic operation of a heat pipe cooled structured methanation reactor are compared to steady-state operating points. Special focus lies on the temperature level and distribution in the reactor, the thermodynamics and the conversion and yield.

2. Methodology, Results and Discussion

The used lab-scale methanation test rig with its novel heat pipe cooled reactor concept [1] is presented and the achieved results are illustrated by temperature profiles of the structured reactor. Further results show the impact of the dynamic variation of key process parameters on the conversion and yield of the methanation. Fig. 2 gives a representative result of the experiments with blast furnace gas during the hydrogen-intensified methanation of blast furnace gas. The periodic alteration of the syngas power in step attempts causes jumps of ~30 K at the hot spot measured in a thermowell (see Fig. 3). The temperatures at the reaction channel's surface and in the reactor block

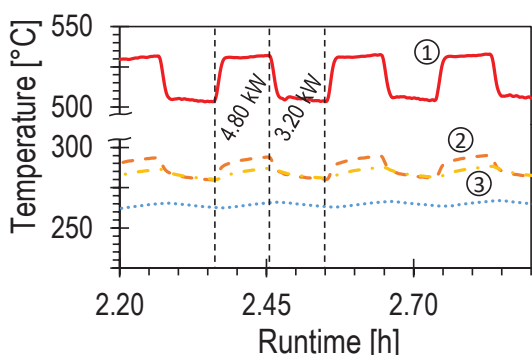


Fig. 2: Timely resolved temperature profiles during hydrogen-intensified methanation of blast furnace gas (drawn through: hot spot temperature; dashed: temperature at edge of reaction channel near reaction zone; dot-dashed: block temperature near reaction zone; dotted: heat pipe working temperature)

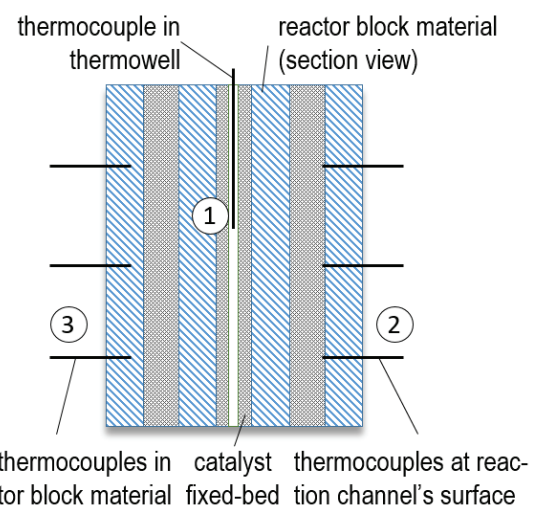


Fig. 3: Very simplified sketch of the heat pipe cooled structured reactor (section view) with the positioning of the thermocouples

(for positioning see Fig. 3) show a damped behaviour and the heat pipe working temperature (measured in a thermowell inside of a heat pipe; not indicated in Fig. 3) fluctuates only minimally.

3. Conclusion and Outlook

The contribution highlights the experimental results from the dynamic catalytic methanation of different bottle mixed steel works' by-product gases in comparison to steady-state operating points.

Acknowledgement

The project i³upgrade has received funding from the Research Fund for Coal and Steel under grant agreement No 800659.

www.i3upgrade.eu

Literature

- [1] Neubert, M., Hauser, A., et al. (2018). Experimental evaluation of a heat pipe cooled structured reactor as part of a two-stage catalytic methanation process in power-to-gas applications. *Applied energy*, 229, 289-298.

Industrial Implementations
Integrated Concepts
Full Papers

Hybridization of biomass steam gasification in dual fluidized bed reactor with concentrated solar energy

A. Gomez-Barea^{1,5*}, M. Suarez-Almeida^{1,5}, M. Silva², C. Pfeifer³, J. Karl⁴, A. Ghoniem⁵

1. Chemical and Environmental Engineering Department, Escuela Técnica Superior de Ingeniería, University of Seville, Camino de los Descubrimientos s/n, 41092 Seville, Spain

2. Energy Engineering Department, Escuela Técnica Superior de Ingeniería, University of Seville, Camino de los Descubrimientos s/n, 41092 Seville, Spain

3 Department of Material Sciences and Process Engineering, University of Natural Resources and Life Sciences, 1190 Vienna, Austria

4 Department of Chemical and Biological Engineering, Friedrich-Alexander Universität Erlangen-Nürnberg, Fürther Strasse 244f, 90429 Nuremberg, Germany

5 Department of Mechanical Engineering, Massachusetts Institute of Technology, 77 Massachusetts Avenue, Cambridge, Massachusetts 02139-4307, United States

*corresponding author, agomezbarrea@us.es

Abstract

Production of syngas from biomass gasification using concentrated solar energy is an attractive technology to produce storable renewable energy and CO₂ reduction. Although many solar gasification reactors have been conceptually developed during the last decades, none has reached commercial status yet. Several challenges have hindered the deployment of the technology due to difficulties derived from: high temperature and/or large reactor volume required for complete fuel conversion; producing a steady syngas output independent on solar radiation variation; achieving effective rate of heat supply to the gasifier when scaling-up. In this paper, a new approach to conduct allothermal gasification of biomass with steam using concentrating solar energy with the potential to overcome the aforementioned technical challenges is presented. It is based on the use of solid particles as thermal energy carrier and storage media. The great advantage of this configuration is that the solar receiver and the reactor are uncoupled, while thermal integration is highly efficient since carrier particles are directly used in the reactor. This paper reviews the state of the art of the most important aspects to develop the technology and presents a model to preliminary analyze the performance of the reactor under various configurations.

1. Introduction

The use of solar energy as external heat source for steam reforming of fuels has been recognized as highly attractive method for increasing the share of renewable energy and reduction of CO₂ emissions. The generation of energy vectors carrying the energy from the sun and the biomass, is an encouraging concept towards full renewable energy production and energy storage. Solar

steam gasification of biomass is one of the most attractive technologies considered for the achievement of such objectives.

Steam gasification of biomass proposed until now are either autothermal (the heat is supplied by partial burning of the fuel) or just laboratory studies where the heat is supplied by electrical heaters. The external heat source would be ideally carried out by transferring all the energy available in the fuel into the produced syngas (instead of

burning part of the fuel to provide the heat), hence raising the yield significantly and improving the overall energy efficiency of the process. However, it is yet to be determined how to supply the solar heat to industrial scale reactors. Various conceptual strategies to hybridize solar energy into steam gasification of biomass have been recently proposed by the authors [1], examining how to implement continuous allothermal gasification using solid particles to carry and store the solar energy.

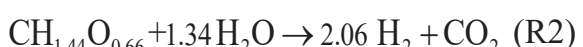
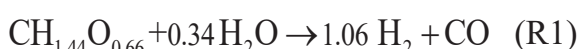
The objective of this paper is to examine the progress on the solar gasification design based on the new concept. A model for new gasification system is developed based on a previous model for conventional fluidized bed gasifiers (FBG) [2] and first calculations are presented to analyze optimal operational conditions. The results are useful to identify the main challenges, shedding light on the next steps for the design of the first generation of reactors based on this concept.

2. Background

Prior to introducing the new concept, the state of the art of solar and non-solar steam gasification and concentrating solar thermal energy for high temperature applications based on solid particle receivers is given in order to justify the new prototype.

2.1. Steam gasification of biomass

The steam gasification of biomass (dry and ash free, termed as “bio” with general formula $\text{CH}_{1.44}\text{O}_{0.66}$) to yield syngas (H_2/CO) or (H_2/CO_2) can be represented by [3]:



The standard heat of reaction at 298 K of R1 and R2 are, respectively, 102.5 and 61.3 kJ/mol_{bio} or 4.27 and 2.55 MJ/kg_{bio}. Therefore, gasification is an endothermal process, requiring significant input to drive the reactions. In addition, because of equilibrium and kinetic reasons, the process must be conducted at high temperature, in the range of 800-1100 °C depending on the fuel and reactor type.

Gasification technologies include allothermal steam gasification, using heat from an external source to drive the process, and autothermal gasification, in which part of the fuel is burnt to generate the necessary heat to maintain the process, using pure oxygen or air. Since in autothermal gasification part of the fuel is consumed to provide thermal heat, the efficiency is lower than in allothermal gasification.

Despite a great number of allothermal steam gasifiers has been developed at laboratory or bench scale (some of the reviewed in [3,4] none has been scale up or commercialized due to practical problem derived from steady production of syngas in spite of solar radiation variation as well as implementation of heat transfer at large scale.

Therefore, steam (non-solar) gasification has been implemented at scale by the use of indirect air-steam dual fluidized bed (DFBG) technology [4], i.e. by autothermal gasification using air. In this arrangement, the biomass is devolatilized in a bubbling FBG where volatiles are released, and char is partially gasified (\approx 5-30% depending on the fuel) with large excess of steam. The process is thermally driven by the circulating hot material from the circulating FB combustor (where the char transported from gasifier and an additional fuel, if necessary, are burnt to heat the sand material). The bubbling FBG

unit is allothermal since the heat from sand comes from the combustor unit (external to the gasifier), although the “gasification system” as a whole (gasifier+combustor) is autothermal. As a result, only about 70% of the energy (and 2/3 of the carbon) from the fuel is stored as chemical energy in the syngas. This is the usual way to operate the existing DFBG as developed by TUV, ECN or some universities/research centers and commercialized by companies like Repotec or Dahlman, although sometimes these DFBG operated burning also natural gas to elevate the combustion temperature.

In Fig. 1, the possibilities of the classical air-steam DFBG are extended by considering that the system can be balanced thermally by some external heat or additional fuel. For obvious reasons, the most attractive case is when all external energy supplied to the gasifier is renewable (i.e. solar) and the fuel is a biomass. In this case the solar energy is transferred to the bio-syngas and all carbon from the biomass is converted to fuel volatiles (CO and hydrocarbons). In turn, it produces a syngas with roughly 115% of the energy and 100% of the carbon of the fuel. Despite the great advantage of this operational mode, sustaining the gasifier with external heat is of most complexity and has not been developed. The approach proposed in the present paper is to convert the existing conventional design of DFBG to admit external solar heat, maximizing the solar share in the syngas.

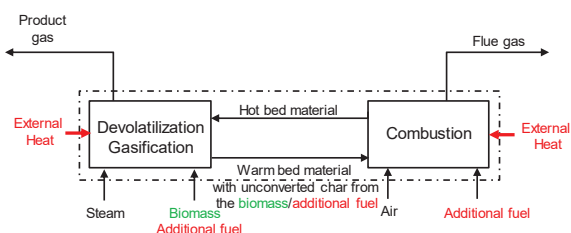


Fig.1: Steam gasification in a dual fluidized bed (DFB) using external heat or fuel

2.2. Solar gasifiers

Solar gasifiers can be classified according to the gas-solid contact (packed bed, fluidized bed, and entrained flow gasifiers) or by the way in which solar radiation contacts the reactants (directly-irradiated, where the solid carbonaceous reactants are directly exposed to radiation, and indirectly-irradiated, where the radiation strokes an intermediate material -opaque wall or energy carrier-). A variety of combinations of gas-solid and solar radiation-reactants contact reactors have been proposed, and some prototypes have been tested at laboratory scale [5,6].

Direct irradiation offers superior heat transfer characteristics and energy efficiency, but the reactor must have a transparent window, which can be fouled by operation. Indirect irradiation, in which an intermediate medium is heated by solar radiation and transported to the gasifier, has less favorable heat transfer but avoids the difficulties with direct-irradiation design [7]. Packed-bed gasifiers are simpler and robust, can accommodate a wide range of feedstock sizes, making them cost effective, but they suffer from mass and heat transfer limitations, ash build-up, and energy losses. Entrained-flow gasifiers exhibit more efficient transport, increasing the syngas throughput significantly, but impose strict requirements on the feedstock size. Both directly- and indirectly- irradiated have been developed for all gas-solid contacts [5,6].

Fluidized-bed reactors achieve high mass and heat transfer rates, overcoming the transport limitations of packed-bed and the particle size needs of entrained-flow reactors, being considered the solar gasifier with highest scaling-up potential although some issues remain to be resolved. An earlier design based on a

conventional bubbling FB was modified into an internally-circulating FB to improve reactor performance, achieving more uniform bed temperature, although the performance was questionable and scaling-up remains unsolved [6]. Indirectly-heated FBG have been proposed to overcome these difficulties, including three approaches to indirectly supply the concentrated solar radiation (CSR) to the reactor: (i) irradiating the reactor external side walls [8]; (ii) using a two-cavity reactor [9]; and (iii) using solid particles as heat transfer carrier [10]. The only reported theoretical investigation based on solar gasifier heated by circulating solids was done in [10,11]. In [10] a hypothetical hybridized DFB gasifier to study the production of Fischer-Tropsch liquid from coal was tentatively considered. In [11] a lift pipe as part of a fluidized-bed was proposed where the bed material and char are heated by heat pipes which are externally irradiated. The gasification proposed in [10] is autothermal since the char and some auxiliary fuel are burnt, decreasing significantly the solar share in the syngas and the syngas yield per unit of fuel input. In addition, no experimental support of this concept has been published.

To sum up, none of aforementioned directly-irradiated gasifiers can be implemented at scale and, in the best cases, only lab-scale devices have been tested to understand the process limits of gasification subjected to solar radiation. The only existing FB solar gasifier reaching the lab-scale is directly-irradiated, but the performance is poor and cannot be applied for large scale applications. The use of solids particles as energy carrier for gasification has theoretically proposed in two earlier works, but has not been experimentally tested.

2.3. Solid particle solar receivers

Solid particles were proposed as heat transfer and thermal storage medium in the early 1980s because of its ability to withstand high temperatures and the straightforward integration of solar energy collection and TES, but the technology plummeted very fast. Only in recent years, driven by the need of achieving higher temperatures and efficient together with cheap TES, solid particle technology has been subject of new research interest [12].

The heat transfer mechanism at the receiver can be either direct or indirect. In the direct type, the solid particles are directly irradiated by CSR, whereas in the indirect type solid particles ‘flow’ inside tubes. Early direct absorption concepts considered a curtain of free-falling particles. Obstructed or impeded flow receivers, rotary kiln and fluidized bed receivers have been proposed to increase residence time of the particles. Regarding indirect heat transfer concepts, flow-in-tube receivers, with and without fluidization, have been tested at small scales. Some technical challenges that must be solved for commercial viability of solid particle technologies [12].

Integration of solar energy conveying by solids particles coming from the hot storage (storing hot particles from the central receiver) is usually conducted by heat exchanger to produce steam or to heat an additional HTF [13]. New solid particle receivers are under development toward more efficient thermodynamic cycles based on gas turbines (Brayton cycle). No thermochemical applications have been considered so far under this operational mode, except the two theoretical studies mentioned [10,11].

2.4. Main conclusions from literature

- Allothermal gasification with external heat from concentrated solar radiation is the most interesting choice for steam gasification of biomass since the syngas produced contains all energy from the biomass and a significant solar share. In addition, it contains most of the carbon of the biomass as combustible species. In spite of this, allothermal steam gasification has been tested only in the laboratory with heat from an external electrical oven.
- The only practical development on steam gasification (no-solar) is the air-steam indirect DFBG. In this technology the heat to the gasifier is achieved by burning part of the fuel (char) and providing this gasifier with external heat has not been considered. As a result, there is not a solar version of the technology.
- Most of solar gasifiers developed up to date are directly-irradiated. They are more efficient than indirectly irradiated gasifiers but scaling-up remains a challenge. As a result, only laboratory devices have been tested. Direct irradiation to the reactor should be avoided in order to overcome all problems hindering application at large scale.
- New technology of solids particle receivers (without reaction) reaching temperatures between 700-900°C has been developed in the last 5 years. Moreover, research under development promises good future perspectives to come up with scalable prototypes reaching 1000°C. The directly-irradiated solar particle, tower-mounted, falling particle cavity receiver is the best choice developed to date and can achieve the thermal requirements of the biomass gasification (800-950°C).

- The solid receiver and the gasifier can be uncoupled using solid particles as energy carrier and storage material. However, excessive storage volume and complications in conveying great amount of solid particles.

The conceptual integration of the solar gasification system and particle receiver is presented in Fig.2. The solids particles act as thermal energy carrier, circulating cyclically between the solar receiver and the gasifier. Two tanks are used to store the particles heated by the receivers and the particle cooled in the gasifier allowing for temporary thermal storage of solar energy. The use of solid particles as energy carrier is attractive since are an excellent thermal energy storage medium, operating at high temperature and low cost.

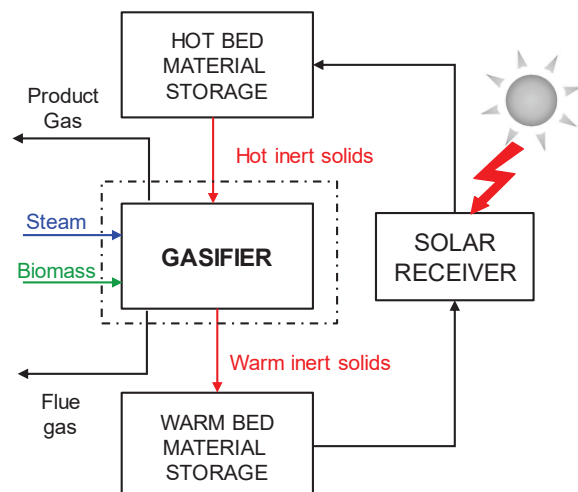


Fig.2: Integration of biomass gasifier in a solar loop with a solid particle receiver

3. Modelling

3.1. Model approach

The stoichiometry of reactions R1 and R2 establishes the amount of reactants involved (steam per unit of biomass or SBR) and products (H_2 and CO/CO_2) generated provided the reactions are complete and stoichiometric. This is not the case in practice because of thermodynamic and kinetic limitations,

yielding a more complex product distribution [2].

Three approaches can be applied to model steam gasification in an FBG: (i) The assumption of equilibrium (EM); (ii) application of kinetics models (KM), taking into account chemical and fluid-dynamics rate considerations; (iii) a combined approach, sometimes called pseudo-equilibrium (PEM). Equilibrium model (EM) is the most universal way to close the calculations but fails in predicting real gas composition and fuel utilization (char conversion). Kinetic model (KM) gives better representation of the process for a specified system (geometry, type of biomass, etc.) but a great deal of inputs is required and the conclusions are system-dependent. Pseudo-equilibrium model (PEM) is based on equilibrium relations together with semiempirical inputs to take into account kinetic- and flow- rate limitations. It is a reasonable compromise between EM and KM using some comprehensive models supported by empirical closures.

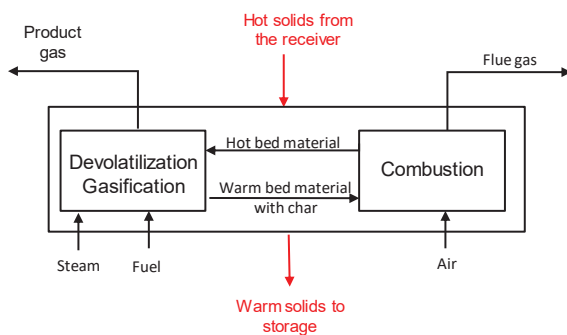


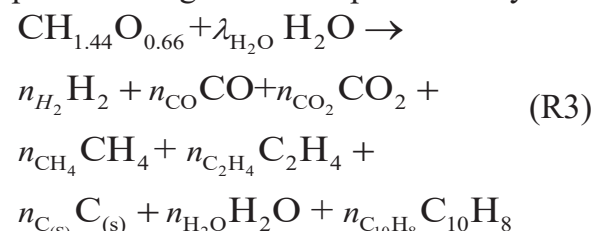
Fig.3: Steam gasification in a solar-heated dual fluidized bed gasifier (sh-DFBG)

The model of the steam gasification of a DFBG using heated solids particles (sh-DFBG) (Fig.3) considers the steam gasification in a FBG and the char burning in the combustor. In both units a circulation of solids (including those coming from the solar loop) flowing in and out must be considered as discussed

below. In this system it is convenient to define two types of solids circulations: internal solids circulation (between reactors) and external circulation (that from the solar loop).

3.2. Model of a solar-heated DFBG

The steam gasification process taking place in the gasifier is represented by



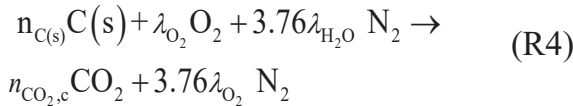
where besides CO and H₂ other components are present in the product gas, such as hydrocarbons (mainly CH₄, and other light hydrocarbons, here lumped into C₂H₄ in R3) and tars (lumped into naphthalene C₁₀H₈ as tar model in R3) as well as solid carbon (char, i.e. C_(s) in R3). In addition, there is always unconverted steam even when feeding it stoichiometrically.

In a stand-alone allothermal steam gasifier it is difficult to fully convert the solid carbon with steam in the gasifier. Operation at high temperature and residence time of the char is required, or the use of catalyst. In a DFBG, in contrast, only a limited fraction of the char generated after fuel devolatilization is converted with steam, being the rest directed to the char combustor, where it is burned with air, generating the heat necessary to balance the system energetically.

The extent of char conversion in any gasifier depends on the carbon-steam gasification rate of the char particles (CO₂-carbon rate is much slower) and the residence time of the char particles in the reactor. On the one hand, the rate of reaction depends on the temperature, the

species concentration (mainly steam, but hydrogen can be also important as it inhibits the carbon-steam reaction rate), the intrinsic reactivity of the char (fuel type and form of char generation) and the quality/extent of gas-solid contact. On the other hand, the residence time of the char particles depends on the rate of solids removal, that can be (i) intentionally made by gas-solid entrainment and elutriation and/or by removing the solids in the case of DFBG to carry the solids to the combustor, or (ii) unintentionally as carbon losses by entrainment of elutriated particles from the bed in a stand-alone gasifier. Theoretically, in a gasifier with any kind of char removal, the residence time of char is infinite and the char conversion is complete, but also the volume of the reactor is very high (infinite for an infinite time of complete carbon conversion in a single particle).

The model of char conversion developed in [2] for a FB is applied in the present reactor model. The char conveys to combustion is burn with air according to



3.3. Process configurations

As said, in a standard (no-solar) DFBG there is only *internal* solids circulation between the units. In contrast, in sh-DFBG besides internal circulation, there is also *external* solids circulation (through the solar loop). Furthermore, in a sh-DFBG there are different possibilities for introducing/extracting the solids in the system as show in Fig.4, and the internal circulation from the gasifier to the combustor can be different to that from the combustor to the gasifier. The biomass spatial time defined as mass of inventory in the gasifier divided by the feed rate of

biomass is always higher in the sh-DFBG compared to conventional DFBG because higher throughput of inert particles (those solids different from fuel and char) passing through the gasifier.

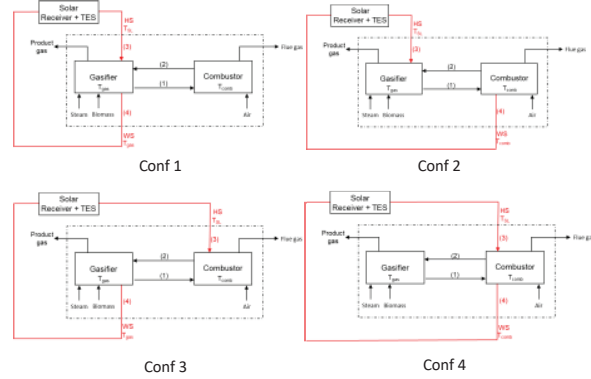


Fig.4: Options for feeding/extracting the solids in an sh-DFBG

3.4. Performance indicators

To quantify the contribution of external solar energy to the system, we define the following parameters:

- *Specific External Heat (SEH)* defined as the solar heat supplied to the system Q_{SL} per unit of biomass input (dry and free of ash), (MJ/k_{daf}).
- *Fraction of external heat supplied* to the system (FEH) defined as the ratio between Q_{SL} and the heat required to thermally-sustain the gasifier Q_g . FEH = Q_{SL}/Q_g .
- *Solar Share (SS)*, defined as ratio between Q_{SL} and the lower heating value of the syngas, expressed in percentage, SS = $(Q_{SL}/LHV_{syngas}) \cdot 100$

4. Results and discussion

Fig. 5 presents the performance of a standard (non-solar) DFBG at different gasification temperatures for fixed combustion temperature, steam equivalence ratio ER_{H2O} (the ratio between the fed and stoichiometric steam), and inlet steam temperature. It is shown that the solids circulation increases as the

gasifier operates at higher temperature. Consequently, lower char residence time is required and lower char conversion is attained in the gasifier (Fig. 5(a)). The yields of syngas and H₂ (Fig. 5(b)) decrease with gasification temperature as a result of the lower char conversion in the gasifier.

Fig. 6 shows the performance of a sh-DFBG operating at fixed gasification temperature with solids addition/removal to/from the gasifier (Confl, see Fig. 4), as a function of the fraction of external heat supplied to the system, FEH. The internal solids circulation decreases significantly with FEH, whereas the biomass spatial time τ_{bio} (larger mass inventory or reactor size for a given biomass flowrate) increases (Fig. 6(a)). Logically, no circulation is necessary when all the heat required to the gasifier is supplied externally (FEH=1). Significant char conversion is reached for reasonable long residence time (80% of char conversion is attained in the gasifier with residence time of 28 min) but higher char conversion requires excessive long residence time and thus reactor volumes (see τ_{bio} in Fig. 6(a)). The syngas produced is improved considerably (Figure 6(c)) as a result of higher steam-char conversion. Fig. 6(d) shows that 15% of solar share can be attained for FEH=1, meaning that 115% of the energy of biomass is transferred to the syngas as compared to 70% in a conventional DFBG, thus a relative increase of 65% ((115-70)/70·100).

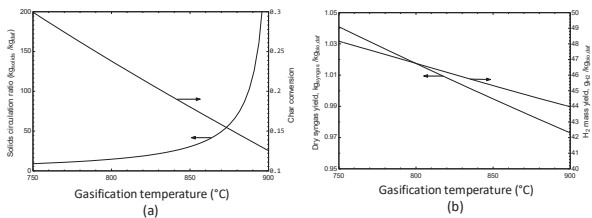


Fig.5: Performance of a standard (no-solar) DFBG as a function of gasification temperature (T_{gas}) for: $T_{\text{comb}}=905$ °C, $ER_{\text{H}_2\text{O}}=2$, biomass type $\text{CH}_{1.4}\text{O}_{0.7}$ and inlet steam temperature 750°C

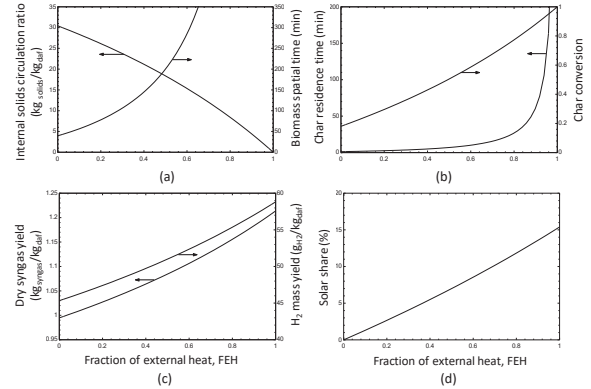


Fig.6: Performance of a sh-DFBG with various levels of external heat ratio (FEH) for Configuration 1 at $T_{\text{gas}}=850$ °C and $T_{\text{SL}}=950$ °C (the rest of operating conditions as in Fig. 5)

Fig. 7 shows the external solids circulation (that circulating through the solar loop) as a function of the specific external heat SEH for the four configurations presented in Fig.4. Configurations with the solids removal in the same unit (Confs 2 and 4 and Confs 1 and 3) present the same value of external solids circulation, as this results from the driving force of temperature between the hot particles and removal point. Therefore, the external solids circulation is higher in Confs 2 and 4, since the driving force is lower.

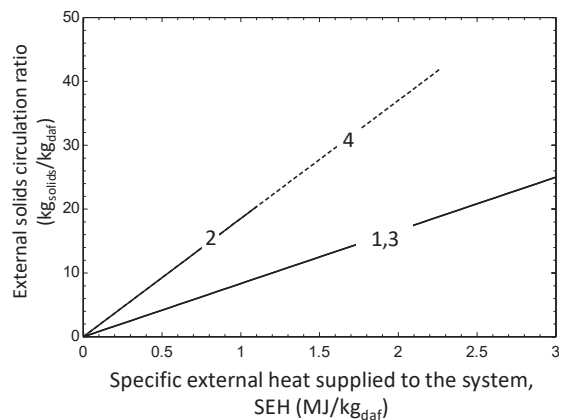


Fig.7: External solids circulation required per unit of biomass input in a sh-DFBG as a function of specific external heat supplied to the system (SEH) for the different configurations (1-4) (operating conditions are the same as in Fig. 6)

Fig.8 compares the internal circulation for the four configurations in Fig.4. Confl requires the lowest internal solids

circulation for equal specific external heat, whereas Conf4 demands the highest one. Confs 2 and 3 present different internal circulations depending on the direction of the solids flow. Moreover, Confs 1 and 3 present the highest external solar heat absorption capacity (the highest SEH), reaching a value of 3 MJ/kg_{bio}, corresponding to a solar share of 15%, as shown in Fig. 6(d) for FEH=1. In Confl the internal solids circulation in the two directions is the same and decreases with SEH, while in Conf3 the solids flow to the gasifier is higher than that to the combustor, and the difference of the two solids flows increases with FEH. The internal solids circulation in Confl becomes zero when the system reaches the maximum solar share, i.e. when it becomes completely allothermal. In this case, all the external solids pass through the gasifier only, full char conversion is attained in it, and the combustor is out of service.

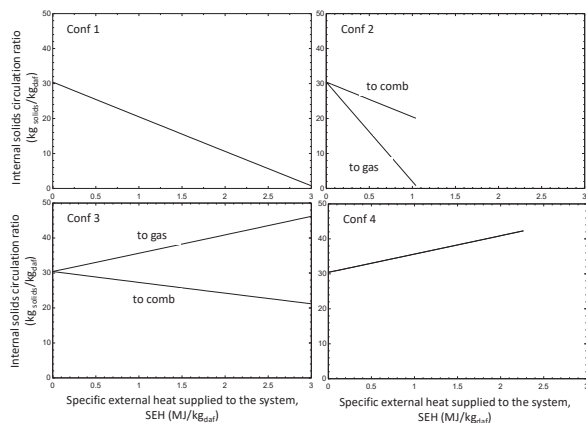


Fig.8: Internal solids circulation in a sh-DFBG as a function of specific external heat supplied to the system (SEH) for different configurations (1-4) (operating conditions are the same as in Fig. 6 and 7). Nomenclature: “to gas” is from combustor to gasifier; “to comb” is from gasifier to combustor

An operational point is identified in Conf2 where the system is saturated to absorb more external solar heat, even if more external hot solids were introduced in the gasifier. At that point ($SEH \approx 1$ MJ/kg_{daf}) part of the char is burnt and char conversion in the gasifier is limited to 0.46

reaching a maximum solar share of about 6%. The maximum SEH attainable in Conf4 is around 2.3 MJ/kg_{daf}, lower than the maximum SEH in Confs 1 and 3 (3 MJ/kg_{daf}). This results from the difference between the driving forces of temperatures (hot particles-combustor, i.e. 950-905=45°C in this simulation) and that (gasifier-combustor, i.e. 905-850=55°C in this simulation). Since the latter temperature driving force is higher than the former, some char is burnt in the combustor to heat up the solids from the gasifier to combustor and the char conversion is lower than unity in the gasifier, resulting in SHE lower than the maximum. For the same driving forces, for instance by taking combustor temperature at 900°C (the two driving force would be 50°C), full char conversion is attained in the gasifier and $SEH = 3$ MJ/kg_{daf}.

From the above analysis (gasification perspective) Confl is the most attractive option. However, additional aspects from solar receiver side have to take into account. Solids removal from the gasifier (Confs1 and 3) will result in reacting particles in the solar loop, which in principle poses new problems (the solid particle receivers currently under developments are mainly based on “open” designs [12]). On the other hand, removal of solids from the combustor (Confs 2 and 4) will make more difficult the solar receiver from the thermal point of view (higher temperature of the hot solids to the receiver) and will increase the circulation of solids between reactors, although it has the advantage of allowing the use of open solid particle receivers. A way to relax the disadvantage of the high thermal level is the cooling of solids from the combustor in an intermediate exchanger before sending them back to the warm solids tank. The heat exchange could generate superheated steam to feed the gasifier, for instance; however, there are other ways to superheat

the steam like exchanging with the produced syngas or flue gas and the options should be considered. The use of heat pipes working between this intermediate exchanger and the gasifier could also benefit the process as should be taken into account as additional alternative. Further research is necessary.

5. Conclusions and future work

A new conceptual integration of solar gasification and particle receiver is presented and analyzed in this paper. The solids particles act as thermal energy carrier, circulating between the solar receiver and the gasifier with intermediate thermal energy storage. The advantage of this configuration is that the solar receiver and the reactor are uncoupled, while thermal integration is highly efficient since carrier particles are directly used in the reactor. The new system can be accomplished with the state-of-the-art technology by considering some new aspects for the particular reactor conditions. Moreover, temperatures in the receiver are realizable using latest developments of solar concentrators, although some specific aspects need to be developed for an efficient matching between the biomass and solar components.

The solids circulation and quality of syngas for different arrangements have been analyzed in this work by development of a model of a solar-heated DFBG. Addition of solids to the gasifier seems to be the most attractive option but limits the operation to close solids particle receiver or enforced carrying out solids separation before sending them to the receiver. However, additional aspects have to take into account and research is underway. Optimization of the system for the different configurations is under study, as well as how to adapt the new gasifier and combustor as more external heat is

added. Criteria for optimization includes taking into account technical viability, thermal efficiency, solar share into syngas, and operational flexibility. The latter criterion includes considering stand-alone operation without solar energy, transient from solar to non-solar mode, hybrid operation and the size of the thermal storage.

6. Acknowledgements

The authors acknowledge the financial support by MINECO of Spanish government (project CTM2016-78089-R), and the grants PRX18/00629 and BES-2017-080653, as well as the Foundation Seed Fund MIT - Spain "la Caixa" (project SOLGASBI).

7. References

- [1] Gómez-Barea et al., Applied Energy “A+B” symposium AEAB2019 (2019) Boston (US)
- [2] Gómez-Barea and Leckner, Fuel 107 (2013) p419
- [3] Florin and Harris, Chemical Engineering Science 63 (2008) p287
- [4] Karl and Pröll. Renewable and Sustainable Energy Reviews 98 (2018) p64
- [5] Alonso and Romero. Renewable Sustainable Energy Rev. 41 (2015) p53
- [6] Kodama et al., Solar Energy 156 (2017) p113
- [7] Nathan et al., Proceedings of the Combustion Institute 36 (2017) p2055
- [8] Flamant et al., Chemical Engineering Science 102 (2013) p567
- [9] Gordillo and Belghit, Fuel Processing Technology 92 (2011) p314
- [10] Guo et al., Energy Fuels 29 (2015) p2738
- [11] Nzihou et al., Energy 42 (2012) p.121
- [12] Ho, Applied Thermal Engineering 109 (2016) p958
- [13] Zhang et al., Progress in Energy and Combustion Science 53 (2016) p1

Integrated Concept for Municipal Solid waste Valorization: Pre-Pilot Experience

K. Kirtania^{1*}, K.B. Kabir¹, A.K.M.K. Aurnob¹, A. Arnob¹, U. Salma¹, M.S. Islam², M.M. Rahman¹

1. Department of Chemical Engineering, Bangladesh University of Engineering and Technology,
Dhaka – 1000, Bangladesh

2. Department of Glass and Ceramic Engineering, Bangladesh University of Engineering and Technology,
Dhaka – 1000, Bangladesh

*corresponding author, kkdwpip@che.buet.ac.bd

Abstract

Municipal solid waste (MSW) is considered to be one of the critical issues in developing countries. To manage this waste in a sustainable way, it is necessary to develop integrated processes to find its multiple utilization pathways. Hydrothermal carbonization (HTC) of MSW integrated with power generation and nutrient recovery could be a plausible solution to the wet waste handling problem in a densely populated country like Bangladesh. In this study, MSW sampled from a landfill of Dhaka city revealed the presence of high amount of organic waste (~ 74 w/w%). This facilitated the concept of waste valorization through nutrient recovery. The heating value of the MSW was found to be 14.7 MJ/kg (on dry basis) making it a suitable source for power generation. HTC experiments on the waste showed a retention of almost ~83% of the energy in biocoal. Based on these results, an integrated biorefinery having a capacity of processing all the MSW generated in Dhaka, can produce 45 MWe power with 3.2 ton/day of K and 0.9 ton/day of Ca as by-product. These results would be further evaluated in a pilot-scale demonstration in 2020.

1. Introduction

Due to rapid economic and population growth, the worldwide generation of solid waste has increased significantly. In the past five years, Bangladesh has also seen a rapid economic growth by becoming a middle-income country resulting in generation of more than 5 million tonnes of municipal solid waste (MSW) annually [1]. This poses a unique threat to the environment along with the health of the people living in urban areas [2]. It is therefore of utmost importance to develop an appropriate and pragmatic concept for processing this large volume of waste. Among the technologies available for waste processing, **hydrothermal**

carbonization (HTC) holds the potential to handle a massive amount of moisture present in the feedstock. Moreover, being a thermochemical process, it has the possibility to process the waste with minimum requirement of land considering a land limited country like Bangladesh. In addition to processing of waste, there are possibilities of recovering nutrients for soil and plants. Biocoal from HTC has been predominantly used for soil amendment in Europe [3]. Biocoal acts as the habitat for the microbes and helps in slow release of K, Ca and phosphorus [4]. In the concept of waste based biorefinery [5], waste is utilized to its maximum potential through multiple product line.

This work assesses the feasibility of an integrated concept for conversion of solid waste to energy through laboratory scale trials to pilot-scale demonstration. This combines state of the art technologies for generating electricity and nutrient recovery for soil amendment. In the proposed process, municipal solid waste will be hydrothermally treated to produce an intermediate product, biocoal, which will be further utilized as feedstock for electricity generation process. By-products from the hydrothermal treatment can be used for the recovery of nutrients. Fig. 1 shows a schematic of the concept.

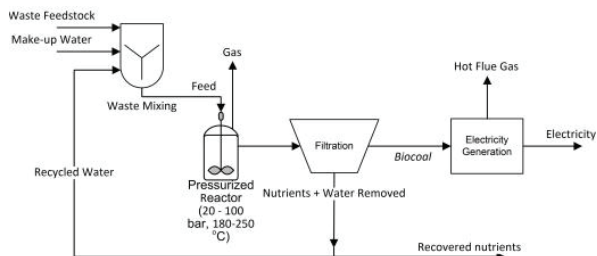


Fig. 1: Integrated concept for waste valorization

2. Concept and Methodology

2.1 MSW Sampling

MSW was conducted for 5 days by collecting 11 samples following ASTM D 5231 from a landfill of Dhaka North City Corporation (DNCC). This ensured the confidence level for the organic waste content in the sample more than 90 % on mass basis. Then the samples were sorted for organic (food) waste, plastic, rubber, wood, metals etc.

2.2 Sample Characterization

The heating values of the different components of the samples were determined using a Parr bomb calorimeter following the method ASTM D 5865. Approximately, around 1 g sample was loaded in a crucible which was placed inside the bomb where the ignition took place through an electric spark. By determining the difference between the

initial and final temperature difference, the amount of heat generated was calculated. Further characterization of the food waste in MSW was carried out using a muffle furnace to determine its organic and ash content following ASTM D 1102 and ASTM E 870. The ash content was then further digested in a solution to determine the Na, K, Ca and Ba in the food waste using a flame photometer.

2.3 HTC experiments

HTC was carried out in an in-house reactor with a volume of 5.7 cm³. The reactor was heated by a heat-gun (Model: VonHaus, 15/181, UK) elevating the inside temperature up to 230 °C. The reactor was closed on both sides using Swagelok fitting to ensure a pressurized environment. N₂ was purged before loading sample inside the reactor. The sample was dried before the HTC experiment to control the water content inside. A water content of 90% was kept constant for all cases. Experiments were performed at a number of temperatures between 190 °C to 230 °C to determine the most suitable condition. The residence time was varied between 20 and 40 min. Finally, characterization of the HTC product, biocoal, was performed to determine the most energy retaining condition.

3. Results and Discussion

3.1 Sampling and Sorting

MSW sampling showed an organic (food waste) fraction of 74.2 % in the parent sample. The rest of the sample consisted of cotton, plastic, mixed paper, wood, leather etc. This means there is significant potential in converting these food waste into value-added products. Food waste is typically rich in organics and metals useful for plant growth. The organic portion holds the energy that could be utilized as

fuel while metals could be recovered as nutrients.

3.2 Energy and Metal Content

In this study, focus was on the energy content and possible nutrient content (i.e. Na, K and Ca) of the assorted food waste. The organic and ash content of the food waste present in the food waste is presented in Tab 1. Based on the analysis of the food waste ash, metal contents under consideration are listed in Tab 2. For HTC, it was observed that up to 40% of the metal content from the parent sample could be found in the liquid phase while 60 % was retained in the solid phase (biocoal) [6]. Therefore, it could be extrapolated to the fact that about 40 % of the metal compounds from the liquid phase may be recovered for further use. If the use of biocoal is beneficial considering its role in soil remediation, partially it could be used for this purpose. It should be noted that biooil from HTC does not have large surface area like the biochar from pyrolysis at a higher temperature [4].

	Wt. Avg. (%)	St. Dev.
Organic content	82.94	5.3
Ash content	17.06	

Tab 1. Analysis of food waste (w/w % dry basis)

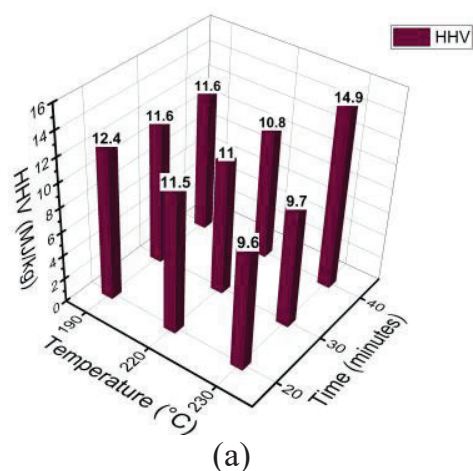
Metals	Amount (w/w %)	St. Dev.
Na	0.35	0.01
K	1.05	0.04
Ca	0.3	0.02

Tab 2. Na, K and Ca content in food waste (w/w % dry basis), weighted average taken on 11 samples

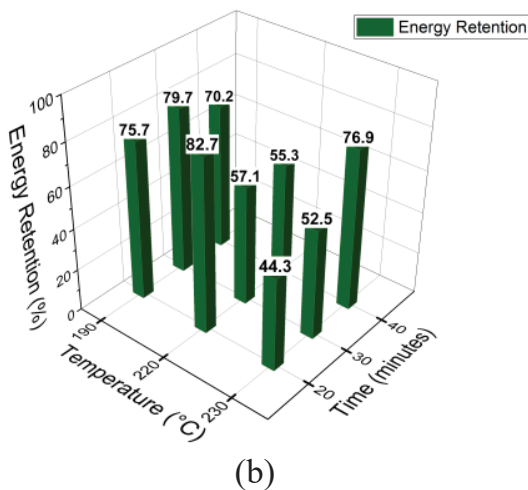
3.3 HTC Biocoal

Biocoal from HTC of food waste resulted in a solid product having a dark color.

Being treated at a temperature range between 190-230 °C, the microbial activities for decomposition was stopped [7]. The reactions that took place during the HTC process partially broke down the bonds among carboxyl, hydroxyl and carbonyl groups [8]. Part of the mass from the parent feedstock was lost as gas from the treatment and partly, some organics was dissolved in the water phase. After losing the oxygen containing groups from the surface, the biocoal becomes denser and more carbonaceous, giving it an appearance like char. The HTC biocoals obtained from different conditions were tested for heating values to find the most energy retaining condition. Based on the solid (biocoal) yields and their heating values, the total energy retained from the parent sample was determined. The heating values of the biocoal varied from 9.6 – 14.9 MJ/kg. The solid yield for biocoal production varied between 50 % and 78 %. Highest solid yield retained the most amount of energy. The most amount of energy is retained at 220 °C and 20 min reaction time with a retention of 83 % of the energy from the parent sample as can be seen from Fig. 2.



(a)



(b)

Fig. 2: HHVs of the HTC biocoals along with their energy retention with respect to parent sample

3.4 Integrated Biorefinery

The integrated concept for biorefinery depends on successful prioritization of products from waste. Section 3.3 described the possibilities of using biocoal as an energy source if food waste is used as feedstock. If we consider a combined feedstock resulting from all types of waste present in MSW, total energy content would become ~ 14.7 MJ/kg. As plastic would not decompose under HTC condition, all other organic fraction could be considered as the biogenic waste retaining $\sim 83\%$ of the energy. This would mean that a biorefinery with a processing capacity of the total MSW generated in Dhaka city (1050 ton/day of dry MSW ~ 178 MW_{th}) [9] would produce 820 ton/day biocoal (~ 148 MW_{th}). Furthermore, it could be possible to recover significant amount of nutrients from the aqueous phase. Considering a 40 % leaching from food waste, 3.2 ton of K and 0.9 ton of Ca would be dissolved in the aqueous phase. In light of the above discussion, the possible outcomes of this integrated concept are described using a block diagram in Fig. 3.

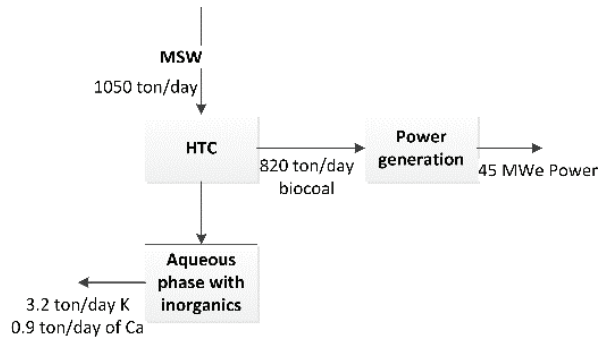


Fig. 3: Possible biorefinery configuration from MSW

It should be noted that the aqueous phase would get contaminated with other metal ions and low boiling point organics. Among other metals, there are possibilities of the presence of heavy metals which need to be dealt with carefully before any application on soil.

4. Conclusion and Outlook

The integrated biorefinery concept has the potential to contribute energy, provide nutrient to soil and reduce environmental stress from waste decomposition simultaneously. With a high energy retention through processing a wet feedstock, HTC was found to be a useful technology.

However, further study is needed on the valorization of MSW including phosphorous and nitrogen retention in the biocoal and in the aqueous phase. This might prove even more useful if significant of phosphorous can be retained as fertilizer. This information will also help in formulating the pilot-scale demonstration of the HTC of MSW in Bangladesh.

Acknowledgements

The authors acknowledge the support of Energy, Power and Research Council (EPRC), Government of People's Republic of Bangladesh for their financial support to carry out this research through the research grant with contract number

EPRC/58-2018-001-01. Also, they like to express their sincere thanks to DNCC staff who provided support with MSW sampling.

References

1. K. M. N. Islam, *J. Renew. Energy.* **2016**, 1–16 (2016).
2. M. Sharholy, K. Ahmad, G. Mahmood, R. C. Trivedi, *Waste Manag.* **28**, 459–467 (2008).
3. A. Wagner, M. Kaupenjohann, *Eur. J. Soil Sci.* **65**, 139–148 (2014).
4. J. A. Libra *et al.*, *Biofuels.* **2**, 71–106 (2011).
5. K. Kirtania, in *Waste Biorefinery - Potential and Perspectives*, T. Bhaskar, A. Pandey, S. V. Mohan, D.J. Lee, S. K. Khanal, Eds. (Elsevier Inc., ed. 1st, 2018; pp. 129–156).
6. T. Wild, PhD thesis, *Universität Dortmund* (2006).
7. I. Pavlovič, Ž. Knez, M. Škerget, *J. Agric. Food Chem.* **61**, 8003–8025 (2013).
8. A. Funke, F. Ziegler, *Biofuels, Bioprod. Biorefining.* **6**, 246–256 (2012).
9. M. Alamgir, M. Ahsan, *Iran. J. Environ. Heal. Sci. Eng.* **4**, 67–76 (2007).

Industrial Implementations Operational Experience Full Papers

Laser-based deposit diagnostic in biomass-fired power plants

F. Graube-Kühne^{1*}, S.Grahl¹, D. Bernhardt¹, M.Beckmann¹

1. Dresden University of Technology, Institute of Process Engineering and Environmental Technology – Energy Process Engineering,
George-Bähr-Str. 3b, 01069 Dresden, Germany
*corresponding author, franziska.graube-kuehne@tu-dresden.de

Abstract

Several components in biomass and waste such as alkali metals result in combustion residues. Part of them form deposits on the walls of superheaters and water walls, leading to corrosion and lower heat output. These deposits are to be removed during operation of the power plant. An adjusted cleaning of the deposits improves the plant's efficiency by increased heat output or enables a higher throughput and leads to reduced maintenance costs. Both the deposit location and the deposit properties affect the efficiency of the cleaning. Thus, measurement setups aim to detect the deposits online and to analyze their properties.

Laser-based diagnostic comprises the detection of deposits and their thickness by measuring wall distances. The system can be used as stand-alone setup or in combination with different measurement setups as well as in combination with balancing tools to predict deposit development of large heat exchanger areas. The established measurement setup is presented followed by the integration of the system into modern monitoring systems.

Afterwards, results are presented that were recorded during a measurement campaign at a German waste power plant. The results are applicable to biomass fired power plants. As part of the study several measurement setups were installed and compared. Topology plots recorded with the laser distance sensor and an assessment of their usefulness regarding cleaning optimization follow, both as single measurement setup and as part of a monitoring concept.

1. Introduction:

In the combustion process residues like chlorine, alkali metals, silicates, sulfates and others emerge [1–4]. They may form deposits on water walls and superheater surfaces. Problematically, these deposits both limit the heat output and may act corrosively. [5] The lower heat output reduces the energy generation of the plant. The corrosion can result in higher maintenance costs and plant outage. As a result, the plant efficiency decreases, respectively. To avoid these inconveniences, a removal of the deposits is necessary which increases the

throughput and reduces maintenance costs. [6]

Unpropitiously, the deposits differ in thickness and have different properties dependent on their location within the boiler, the fuel and the process control [5, 7]. Additionally, the deposits affect the temperature profile of the boiler. The lower heat output results in higher temperatures on the flue gas pass, which again affects the deposit growth. Thus, the deposits have to be removed online and the cleaning needs to be adjusted appropriately to the location and the properties of the deposits [8]. The

adjustment of the cleaning must consider the appropriate time, appropriate place and the appropriate cleaning setup, e.g. the water pressure or the residence time.

To realize such a cleaning, a monitoring concept is necessary. Several sensors are on the market that can be part of such a concept, namely heat flux sensors [9], infrared cameras [10], pyrometers [11] and others. The before-mentioned sensor systems are all adequate for a qualitative evaluation. The application of combined systems or the simultaneous measurement of location and thickness extends the qualitative evaluation and, hence, enables target-oriented cleaning.

2. Deposit Thickness Measurement

Deposit thickness measurement makes local deposit evaluation feasible by analyzing the degree of deposition. The deposit thickness measurement setup consists of a laser distance sensor combined with a motorized mirror. The setup is depicted in Figure 1.

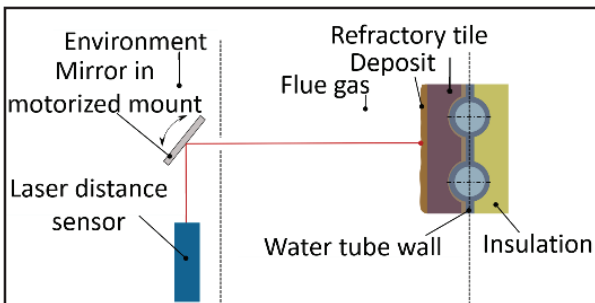


Fig.1: Setup for deposit thickness measurement with a laser distance sensor [12]

The laser distance sensor is simultaneously transmitter and receiver. The laser beam is aligned with the mirror. The mirror directs the laser beam through an orifice into the boiler, where the Laser-spot focusses on the opposite boiler wall. By motorizing the mirror two angles are adjustable, so that the mirror can be tilted in two spatial directions. The advantage of the setup is the spatially adjustable measurement spot.

The position is recorded in Cartesian coordinates and related to the mean distance value. The mirror systematically grades the surfaces. [13] As a result, the sensor delivers topology plots as shown in Figure 2.

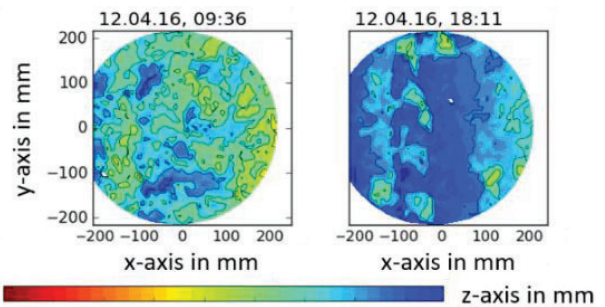


Fig.2: Topology plots before and after a cleaning [12]

The sensor was developed and proven in a cleaning project. The topology plots in Figure 2 were recorded during that project before and after a cleaning. Dark blue color represents clean walls, bright blue deposits have a thickness up to 10 mm. Green color indicates a deposit thickness of 20 mm, yellow parts have already 28 mm deposit layer. The left side shows dense deposits on the walls. Most parts in the measurement area are covered with deposits up to 20 mm; on the right part even stronger deposits are visible. Almost all deposits are removed after the successful cleaning and the edge of the refractory tile is visible at the left side.

The calibration of the laser distance sensor must be realized on the clean boiler wall. The distance decreases through the deposit growth. Boiler movements are considered, but the results show no influence of the boiler wall movement, because the movement in small boilers is below the minimum value of the measurement setup. 98 % of all measured values spread within +/- 1 mm around the mean value. Possibly, this is different for larger boilers. At current state, the system is only usable for biomass- and waste-fired boilers through

the high particle load in the flue gas of pulverized coal fired boilers and the large boiler sizes. [13]

The laser distance sensor is applicable as standalone system for the measurement of the degree of fouling. In combination with other sensors properties are also measurable. The following chapter presents the combination of the laser distance sensor with the deposit sensor, followed by a chapter concerning the integration of the laser distance sensor in a monitoring concept using an online balancing program.

3. Integration into deposit diagnostics

The measurement of the deposit thickness shows the amount of deposits on the water walls. Still, the adjustment of the cleaning is difficult due to missing knowledge of the deposit properties. Therefore, the sensor may be combined with other measurement systems to improve the knowledge of deposits. The combination of the laser distance sensor with heat flux sensors and a pyrometer or an infrared camera allows the simultaneous measurement of the thickness, the thermal conductivity and the heat capacity of the deposit. The combination of heat flux sensors with a pyrometer or infrared camera and the further assessment of the data is called deposit sensor [12]. The setup of the sensor is visualized in Figure 3.

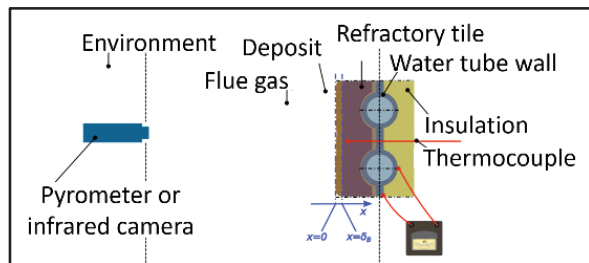


Fig.3: Setup of Deposit Sensor [14]

The signal of both the pyrometer or infrared camera and the heat flux sensors

are compared regarding time shift and damping of the signal as they are deposit dependent. The analysis of the signal results in the thermal effusivity b , which depends on the deposit's thermal conductivity λ and the thermal diffusivity a [15].

$$b = \frac{\lambda}{\sqrt{a}}$$

Figure 4 shows the comparison of a pyrometer signal and a heat flux signal. The heat flux signal (green) follows the pyrometer signal (blue) and appears like a filtered signal because of a lower fluctuation. Due to that estimation of some deposit properties, like porosity and thermal conductivity, is possible.

The combination of the two sensors enables not just the estimation, but rather the measurement of the thermal conductivity. The different deposit properties are connected. Hence, knowledge of some properties helps classifying the deposits and estimating other properties, e.g. porous deposits are brittle and may be cleaned easily by a high momentum; sintered deposits are very dense and hard to clean.

Not every deposit removal is recommendable. Many operators face erosion problems through too frequent cleaning. Thus, thin deposits, especially when they have a high thermal conductivity, can rest on the walls to protect the tubes as there is no necessity to clean them. An adjusted cleaning needs to detect such cases. Here, detection of deposits only is not target-oriented, assessment of the cleaning necessity is important, too.

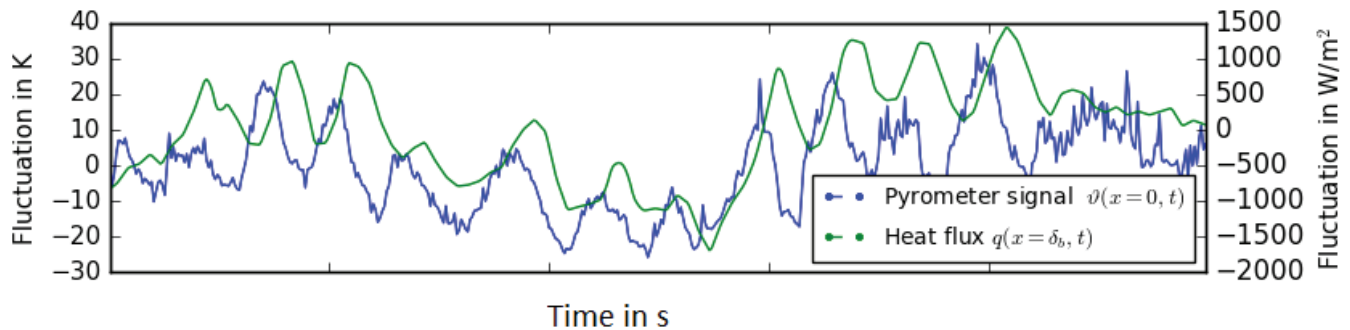


Fig.4: Measured Signal of Heat Flux Sensor and Pyrometer

4. Integration into Monitoring concept

The combination of laser distance sensor with the deposit sensor is not always possible, but another combination is also conceivable – the combination of the deposit distance sensor and an online balancing tool. The online balancing tool is a device to model the boiler as a whole and serves for monitoring all flows. Mass balances and energy conservation equations calculate all mass flows and temperatures all over the boiler using measurement points at selected locations [16]. Integrated are those sensors that are anyways recorded in the process control. Therefore, no extra installation of sensors is necessary. The online balancing tool detects global boiler deposition through temperature shifts and lower heat output, but the global model cannot evaluate local effects. The laser distance sensor reveals the local deposition status. When combining the sensor and the balancing tool, the sensor may feed information into the balancing tool and the online balancing tool is able to evaluate effects of the local deposit growth on the entire boiler efficiency. The combination enables a timely adjusted cleaning with focus on the requested heat output.

5. Results and discussion

Several systems were presented in the previous chapters: the deposit sensor, the laser distance sensor and the online balancing tool. All these systems were combined in a project to evaluate the

usefulness of each system. The project was carried out at the municipal waste incinerator in Coburg with 36.6MW thermal and 10.6MW electrical output. The findings shall be transferred to biomass-fired boilers in follow up projects. The aim of downtime reduction and increase of heat output is for both power plant types factual. Five cleaning cycles were supervised using the following measurement setups:

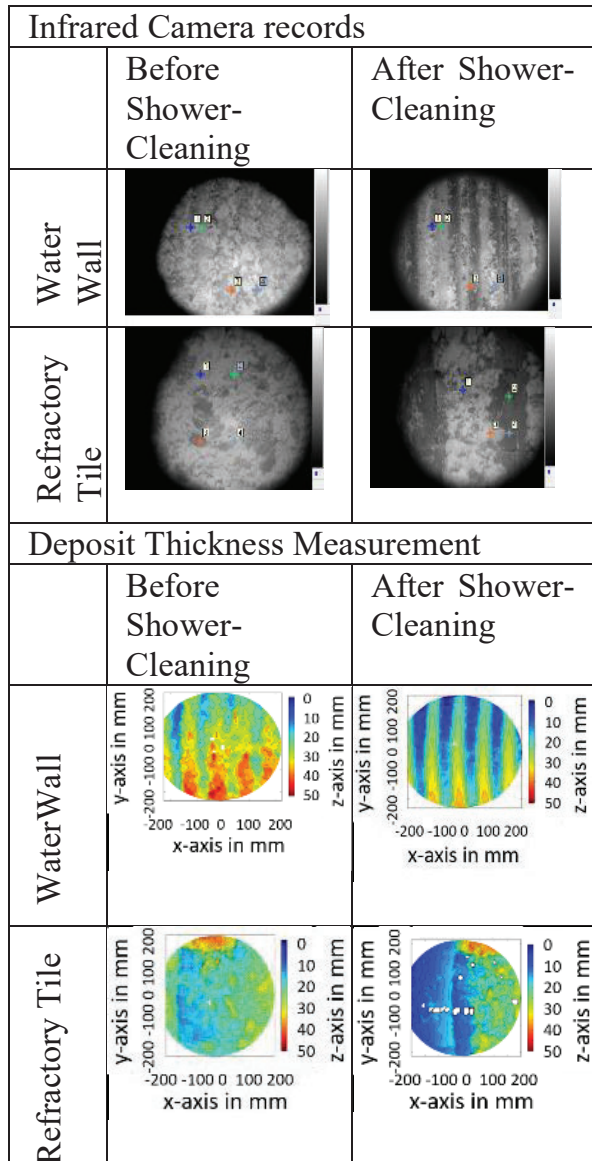
- The deposit sensor
- The laser distance sensor (measured before and after cleaning, not continuously)
- The online balancing tool
- An infrared camera

Table 1 shows the data obtained before and after the cleaning on refractory tiles and the water wall for an infrared camera and the laser distance sensor. The cleaning tests were carried out on refractory tiles and water walls respectively.

Deposits are clearly visible in both records, measured with the infrared camera and the laser distance sensor. Hence, both systems are usable as diagnostic systems for deposits. While the additional information delivered by the infrared camera is the surface temperature – assuming that the emissivity of the deposit is known – the laser distance sensor provides the deposit thickness as additional information. The emissivity of the deposits is often uncertain, making the

laser distance sensor the more reliable system.

Main focus of the project was the cleaning process. Hence, the installed measurement technique was used to evaluate the cleaning parameters. The results of the first three cleaning cycles are summarized in [Table 2](#). The thermal conductivity, the thermal diffusivity and the porosity were obtained from the deposit sensor in combination with the laser distance sensor. The process control provided the flue gas temperature and the volume flow of the cleaning water. The laser distance sensor measured the deposit thickness. The temperature gradient inside the deposit during the cleaning was calculated with aid of the semi-infinite wall model.



Tab.1: Infrared Camera and Laser Distance Plots derived before and after a shower cleaning

The following result was obtained: Both the first and the second cleaning were successful, because the deposits were removed from the walls. Nonetheless, an adjustment of the cleaning was useful, because the high amount of cold water endangered the water wall. This may lead to thermomechanical shocks or erosion through droplets. [8] Thus, when cleaning a third time, although thicker deposits were on the walls less water was used. The cleaning result was similar to the first two cleaning cycles, but the risks of droplet erosion and thermomechanical shock inside the water wall could be reduced. In fact, the monitoring concept helped saving water, because the cleaning time was reduced and the amount of water decreased. Simultaneously, the tubes were protected from thermomechanical shocks and water erosion.

The online balancing tool evaluated the cleaning likewise. Figure [5](#) shows the received results during the three cleaning cycles that are also evaluated in [Table 2](#). To globally evaluate the deposition rate, cleanliness factors are implemented, which indicate the fouling in the first, second and third pass. A high cleanliness factor represents low fouling. Thus, the factors have to raise after each cleaning. Accordingly to the cleaning results measured with the laser distance sensor, all three assessed cleanings are successful. Hence, the cleaning cycles significantly improved the cleanliness of boiler and the local and global results fit together. Observation of the fuel heat output shows, that the rising of the cleanliness factor is not affected through changes of the fuel, but comes from the cleaning only.

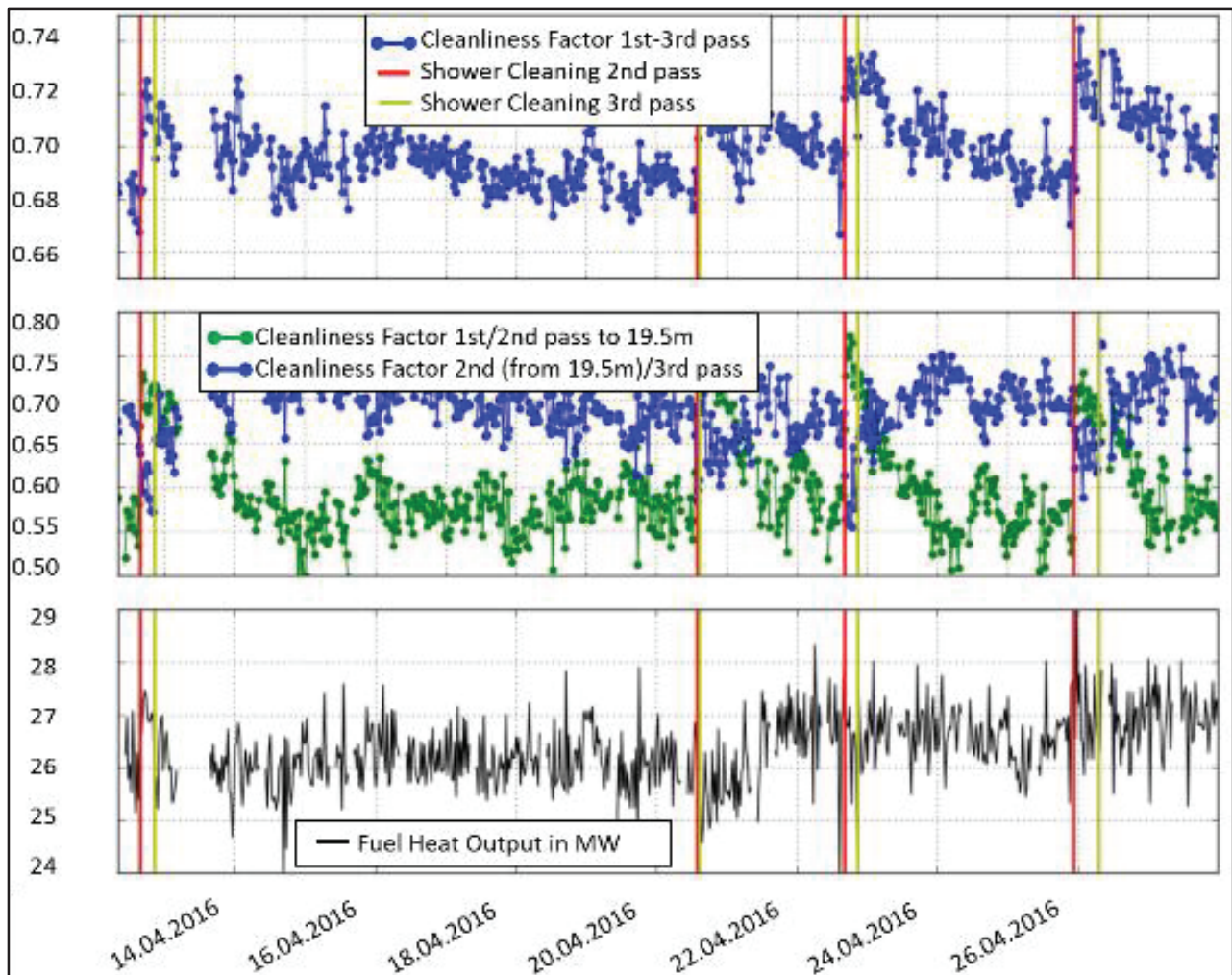
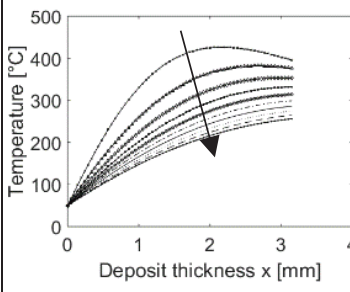
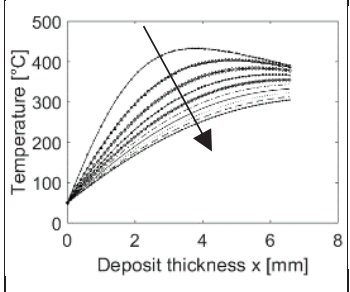
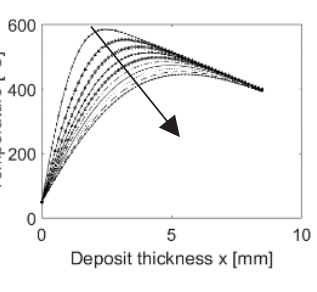
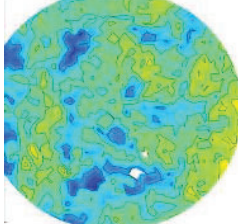
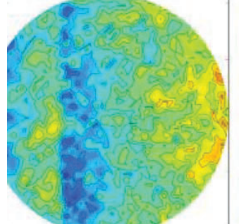
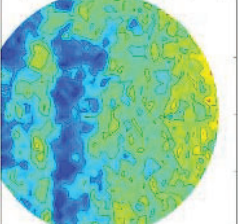
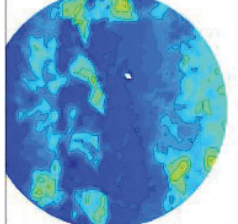
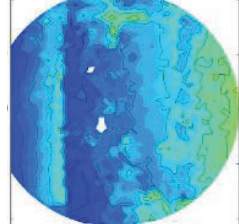
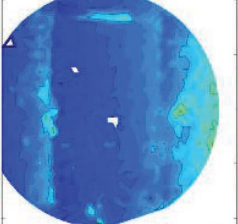


Fig.5: Cleanliness Factors Measured with the Online Balancing Program

6. Further application potential and expectable costs

The presented application is only one example of usage. The deposit thickness measurement is likewise conceivable for measurements of slag thickness and slag distribution in gasifiers. The system is equally applicable for all processes where fouling and deposits may arise, e.g. gas cleaning, chemical processes and so on. Using a standard laser, 5000 € cover the laser and accessories, while the operational costs only involve air for cleaning and the electricity in the mW range for the laser. The experience with

long term measurements are currently very little, but for an application of one month without interruption no cleaning was necessary and no impurification detectable. Not just the price, also the effort for the usage of such a system is low compared to camera systems for example. The tube bending is much smaller and the resolution higher. Especially in waste and biomass fired power plants the cost-performance ratio is not proportionate for large camera systems. Here, the application of laser thickness measurement due to their price is a good option.

	1st cleaning	2nd cleaning	3rd cleaning
Flue gas temperature	780°C	757°C	739°C
Volume flow rate of the cleaning water	0.8 l/s	0.8 l/s	0.61 l/s
Thermal conductivity of the deposit	0.61 W/(m·K)	0.74 W/(m·K)	0.34 W/(m·K)
Porosity of the deposit	45%	41%	59%
Thermal diffusivity of the deposit	$6.4 \cdot 10^{-7} \text{ m}^2/\text{s}$	$7.8 \cdot 10^{-7} \text{ m}^2/\text{s}$	$5.1 \cdot 10^{-7} \text{ m}^2/\text{s}$
Average deposit thickness	3.2 mm	6.6 mm	8.6 mm
Cleaning time	16.8 s	16.8 s	16.8 s
Temperature course during the cleaning process (the arrow shows the temporal progress)			
Deposit thickness plot before the cleaning process			
Deposit thickness plot after the cleaning process			

Tab.2: Results of Three Cleaning Cycles [17]

7. Conclusion and Outlook

The current paper presents a measurement system based on a laser distance sensor, which is able to detect deposits and to measure their thickness. Firstly, the setup was presented, afterwards the integration into deposit diagnostic followed. There are different possible combinations:

1. The combination with the deposit sensor enables the measurement and calculation of some deposit properties, e.g. thermal conductivity, porosity and thermal diffusivity.
2. The sensor may be combined with an online balancing tool. This combination serves as a measure of local effects on the global efficiency of the boiler.

Target is the adjusted handling of deposits respecting their properties. In that scope the laser distance sensor helps detecting deposits and adjusting the cleaning according to their thickness.

The presented systems were combined in a power plant. The measurement systems could be combined to compare their effectiveness and to derive more deposit properties. The results from the investigation of two cleaning cycles were applied to a third cleaning interval. During the third cleaning less water with lower residence time has been used. Comparable cleaning results were achieved. Accordingly, the functionality of the laser distance sensor as standalone system or in combination with other diagnostic instruments could be shown. Actual

studies combine the laser distance sensor and a pyrometer within one casing to simplify the simultaneous use of both the distance sensor and the deposit sensor. Furthermore, the sensors shall be fed with mathematical models that analyze both the deposit and the cleaning setup to improve the cleaning recommendations, here operators can control the cleaning success. Future perspective is the integration of the laser thickness sensor or the combined measurement systems into expert systems, looking further ahead an automation of the cleaning system based on sensors is conceivable. This would be beneficial for waste-fired, biomass-fired and co-fired power plants, because the optimized cleaning leads to corrosion based downtime reduction.

8. Acknowledgements

We are obliged to staff members of CheMin GmbH, Martin GmbH and “Zweckverband für Abfallwirtschaft in Nordwest-Oberfranken” for the valuable help and data provided by them. We are grateful to Dipl.-Ing. M. Reiche for his prior work.

9. References

- [1] Y. Shao, J. Wang, F. Preto, J. Zhu, and C. Xu, “Ash Deposition in Biomass Combustion or Co-Firing for Power/Heat Generation,” *Energies*, vol. 5, no. 12, pp. 5171–5189, 2012.
- [2] J. Sandberg, *Fouling in biomass fired boilers*. Västerås: Department of Public Technology, Mälardalen University, 2007.
- [3] P. A. Jensen, M. Stenholm, and P. Hald, “Deposition Investigation in Straw-Fired Boilers,” *Energy Fuels*, vol. 11, no. 5, pp. 1048–1055, 1997.
- [4] A. Zbogar, F. Frandsen, P. A. Jensen, and P. Glarborg, “Shedding of ash deposits,” *Progress in Energy and Combustion Science*, vol. 35, no. 1, pp. 31–56, 2009.
- [5] R. W. Bryers, “Fireside slagging, fouling, and high-temperature corrosion of heat-transfer surface due to impurities in steam-raising fuels,” *Progress in Energy and Combustion Science*, vol. 22, no. 1, pp. 29–120, 1996.
- [6] J. Harpeng, S. Vodegel, and R. Warnecke, “Beurteilung der Online-Belagsreinigung durch Rußbläser und Klopfer [Assessment of Online Deposit Removal through Soot Blowers and Knocking Devices],” Jun. 2005.
- [7] W. Gumz, H. Kirsch, and M.-T. Mackowsky, *Schlackenkunde [Slagging theory]*. Berlin/ Göttingen/ Heidelberg: Springer-Verlag, 1958.

- [8] F. Graube, S. Grahl, S. Rostkowski, and M. Beckmann, “Optimisation of water-cannon cleaning for deposit removal on water walls inside waste incinerators,” (eng), *Waste Management & Research*, vol. 34 // 2, pp. 139–147, 2016.
- [9] S. Krüger, *Wärmestrommessung an Membranwänden von Dampferzeugern [Heat Flux Measurement on Water Tube Walls of Steam Generators]*. Zugl.: Dresden, Techn. Univ., Diss., 2009 u.d.T.: Krüger, S.: Wärmestromdichtemessung an Membranwänden von Dampferzeugern. Neuruppin: TK-Verl. Thomé-Kozmiensky, 2009.
- [10] R. Koschack, G. Hoven, and B. Sobotta, “Method and apparatus for monitoring the formation of deposits in furnaces,” US20080298426A1.
- [11] S. Bohnes, S. Wirtz, and V. Scherer, “Einfluss von Belägen in Hochtemperaturprozessen: Simultane Messung der Wärmeleitfähigkeit und der stofflichen Eigenschaften [Influence of Deposits in high temperature processes: simultaneous measurement of thermal conductivity and deposit properties],” Ruhr-Universität Bochum, LEAT, 2008.
- [12] M. Reiche, S. Grahl, and M. Beckmann, “Advanced monitoring of the fouling process on water walls,” *Fuel*, vol. 216, pp. 436–444, 2018.
- [13] M. Reiche, S. Grahl, M. Beckmann, M. Kaiser, and W. Spiegel, “Verschmutzungsmonitoring von Dampferzeugern durch neuartige Sensorkonzepte für eine verbesserte Anlagenfahrweise und Online-Reinigung [Fouling Monitoring of Steam Generators through novel Sensor Concepts for improved operation mode and Online Cleaning],” Darmstadt, 06. und Sep. 7 2017.
- [14] M. Reiche *et al.*, “Verschmutzung und optimierte Abreinigung der Heizflächen in der Abfallverbrennungsanlage Coburg [Deposition and optimized cleaning of heating surfaces in the waste incinerator Coburg],” in *Energie aus Abfall*, K. J. Thomé-Kozmiensky and M. Beckmann, Eds., Neuruppin: TK Verlag Karl Thomé-Kozmiensky, 2016, pp. 173–188.
- [15] S. Grahl, F. Graube, and M. Beckmann, “In-situ method for determining the fire-side slagging and fouling behavior on steam generator water walls,” in *10th European Conference on Industrial Furnaces and Boilers: INFUB ; Gaia (Porto), Hotel Holiday Inn Gaia, Portugal, 7 - 10 April 2015*, Gaia (Porto), 2015.
- [16] M. Beckmann *et al.*, “Possibilities of Process Optimization in Municipal Solid Waste Incineration Plants by an Online Balancing Program,” in *Proceedings of International Conference on Incineration and Thermal Treatment Technologies - IT3*.
- [17] F. Graube, S. Grahl, M. Reiche, and M. Beckmann, “Methods for optimized on-line cleaning,” in *Waste management*, K. J. Thomé-Kozmiensky, S. Thiel, and L. Pelloni, Eds., Neuruppin: TK-Verl., 2018, pp. 231–244.

Industrial Implementations Operational Experience Abstracts

A Review Study on Chinese Domestic Gasification Technologies

Yin Pang^{1*}, Dominik Müller¹, Jürgen Karl¹

1. Chair of Energy Process Engineering, Friedrich-Alexander-University Erlangen-Nürnberg,
Fuerther Str. 244f, 90429 Nuremberg, Germany
*corresponding author, yin.pang@fau.de

1. Introduction

After the import of foreign gasification technologies (e.g. Siemens GSP, GE Texaco, Shell, Lurgi) for (mainly) chemicals production in China, the own domestic gasification technologies are rapidly developed in the last decades. However, only a few information is available at the international level. The first part of this work reports the motivation regarding to national energy resources. The major part presents the development of entrained-flow, fluidized-bed and fixed-bed gasification technologies with respect to their technology owners, technical details and industrial applications. The technical information from the individual commercial technology owners will be highlighted if it is validated by operation experiences. In the final part, the authors will forecast possible future focuses of technology development.

2. Entrained-Flow Gasification Technologies

The report of entrained-flow gasifiers includes OMB, HT-L, Shenning, TPRI, TUOSG, MCGS, SE, JE, Jinhua, WHG, LongKing and Qiyao-LiuHua [1-3].

According to feed type and number of working burners, the industrial gasification processes can be categorized into:

- Slurry-feed, single burner (MCGS)

- Slurry-feed, multiple burners (OMB)
- Dry-feed, single burner (HT-L; Shenning; SE)
- Dry-feed, multiple burners (TPRI; TUOSG; WHG; JE)

The corresponding processes have been partially indicated above. The Fig. 1 shows the simplified gasifier geometry of selected entrained-flow processes. In the full paper and in the presentation, the authors will elaborate the individual process with their characteristics, process parameters, system behaviors and industrial applications.

3. Fluidized-Bed Gasification Technologies

The industrial Chinese fluidized-bed gasification processes will include Huang-tai, AFB, Tai-shi, Keda, KSY, Tian-wo, SG, Tsinergy, Ende and Changyuan [4,5].

4. Fixed-bed Gasification Technologies

The domestic moving-bed technologies including Sedin and Yun-Mei will be reported [6,7].

5. Conclusion and Outlook

The full paper will contain a systematic review concerning all types of gasification processes. Besides, the industrial applications based on published information will be tabularly summarized. The possible domestic future focuses will

be predicted according to governmental policies and environmental aspects.

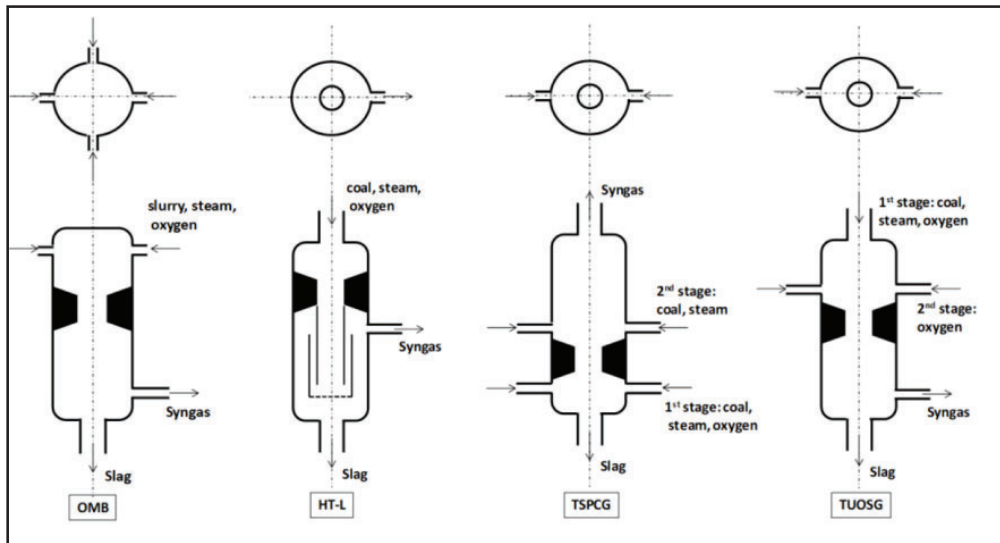


Fig. 1: Simplified Geometries of Chinese Domestic Entrained-Flow Gasifiers (work in progress)

6. Literature

- [1] F. Wang, Z. Zhou, Z. Dai, X. Gong, G. Yu, H. Liu, Y. Wang, Z. Yu, *Front. Energy Power Eng. China* 2007, 1, 251–258.
- [2] X. Guo, Z. Qin, *M-Sized Nitrogenous Fertil. Process* 2017, 1, 17–21.
- [3] K. Chen, *Shandong Ind. Technol.* 2018, 7, 92.
- [4] J. Cao, Z. Cheng, Y. Fang, H. Jing, J. Huang, Y. Wang, *Powder Technol.* 2008, 183, 127–132.
- [5] H. Chen, Y. Fang, J. Huang, Y. Xu, J. Yang, J. Zhang, Y. Wang, *Coal Convers.* 2000, 23, 56–60.
- [6] F. Liu, J. Bi, *Shanxi Chem. Ind.* 2017, 5, 84–87.
- [7] F. Liu, J. Bi, *Coal Chem. Ind.* 2017, 45, 8–12.

Heat-to-Fuel Workshop Full Papers

Influence of Pressure and CO₂ in Fluidized Bed Gasification of Waste Biomasses

M. Szul^{1*}, K. Słowik, K. Głów, T. Iluk

Instytut Chemicznej Przeróbki Węgla,

Zamkowa 1, 41-803 Zabrze, Poland

*corresponding author, mszul@ichpw.pl

Abstract

An autothermal fluidized bed reactor was used to carry out research on the influence of pressure on gasification process of different types of biomasses. The gasified feedstocks were bark, lignin and softwood pellet as a reference material. The gasification was done with a mixture of O₂/CO₂/H₂O. The impact of the application of CO₂ on yield of H₂ in syngas was determined. Resulting high content of CO makes use of the syngas in chemical synthesis applications very difficult without pretreatment. On the other hand, the CO₂ proved to improve Carbon Conversion Efficiency of the gasification and to be an option for its chemical sequestration (negative carbon footprint). Moreover, a slight variation of conventional indices used to evaluate efficiencies of gasification systems (Carbon Conversion Efficiency and Steam/Carbon ratio) was proposed to take into account the impact of the additional source of carbon. Increasing system pressure led to syngas changes in line with predictions of the Le Chatelier's principle. The changes were seen primarily by higher yields of CH₄ and lower overall production of syngas. For higher hydrocarbons (C_xH_y) the trend was unclear. For each pressure level and a standard 850°C gasification temperature, a set of stable gasification parameters were achieved with the exception of lignin at 2 bar_g.

Keywords: O₂/CO₂/H₂O, gasification, biomass, biogenic residues, pressure, ash agglomeration

1. Introduction:

Pressurized gasification is the state-of-art technology for highly-efficient production of chemical intermediates or fuels from primary sources of energy. However, when the feedstock is changed to renewable sources like biomass, the need for use of pressurized reactors is highly debated. The impulse for development of pressure systems for gasification of biomass has been recognized by many influential agencies. For renewable production of fuels and chemicals, International Renewable Energy Agency and Internal Energy Agency have prioritized the

following goals:

- 1) to develop BtL routes for the production of biodiesel and DME from black liquor gasification;
- 2) to mature pressurized gasification plants to produce bio-SNG, as in the Bio2G project;
- 3) to study hybrid biochemical and thermochemical conversion routes.

The first two goals are directly related to development of pressurized biomass gasification systems.

Noteworthy, from the principle for thermodynamics gasification of biogenic feedstocks at higher operating pressures

may be beneficial from several perspectives. Firstly, biomass gasification at elevated pressures provides higher reaction efficiencies and kinetics. Secondly, when the syngas is produced for the purpose of chemical synthesis, the overall process efficiency can be increased by avoiding the step of gas compression, which always incurs energy and exergy losses. Nonetheless, drawbacks are operational challenges related to complexity of the system, its construction and control.

To assess the effect of pressure on kinetics of gasification reactors often thermogravimetric (TG) approaches are applied. Currently, TG lack the possibility to exactly map the process conditions of a fluidized bed (FB), where volatilization and gasification happen quickly one after the other at the same temperature and pressure conditions. For most biomasses 4-7 bar is said to be the maximum gasification pressure which provides an optimum ratio of kinetic-gain to process-complexity-loss. Thus, it is often suggested that operation at 4-5 bars should be optimal for biomass (1-2, 5).

Another approach is thermodynamic equilibrium calculations and modelling. With equilibrium models it has been shown that rising pressure and temperature leads to lower H₂ and CO production, while yields of CO₂ and CH₄ increase [4-5].

Looking into syngas changes, contradictory results of FB pressure gasification can be found. Generally it is agreed that with increasing pressure also overall gas yields and tar yields increase. The subject of char production remains disputable. In autothermal steam blown gasification studies it has been proven that methane yield increases by up to 38% with pressure increase from 2-10 bars [15]. This indicates higher needs for catalytic syngas shift and conversion after pressurized gasification. The changes in yields of

gaseous compounds with pressure can be partly explained by the influence of pressure on gas phase reactions (acceleration of water-gas shift kinetics and change in hydrocarbon reactions) that act in line with the Le Chatelier's principle. The increase of methane yield with pressure is suggested also to be partially linked to a change in secondary pyrolysis reactions scheme that takes place under high pressures.

Another aspect of biomass gasification is utilization of CO₂ as a gasifying agent. CO₂ can take part in gasification systems similar to steam and thus act as both fluidizing and active gasification agent. Usage of CO₂ shifts equilibrium of both Boudouard's reaction as well as gas-shift reaction in favour of CO. CO₂ also has higher specific heat capacity and hence tendency to lower temperature of gasification, hence higher equivalence ratios (ER) are needed. The concept of using CO₂ for increasing C conversion and lowering C footprint is known and has been subjected to research in coal gasification and oxy-combustion studies. For biomass, use of CO₂ can make a unit C negative which is very interesting for the future. To this point only limited amount of data can be found on CO₂ gasification of biomass [18-21].

The article presents results of experimental research on pressurized gasification of wastes biomass in FB reactor. Two waste feedstocks (wood bark and lignin from production of bio-ethanol) were compared with a reference fuel (softwood pellet, SWP) for their gasification efficiency figures. The tests were performed in autothermal mode with use of O₂/CO₂/H₂O mixture as gasifying agent. The operational data on FB gasification of waste biomasses, process efficiency and syngas quality figures were validated with mass and energy balances.

For good design of gasification experiments it is necessary to set a precise range of control variables that can be followed. For O₂/CO₂/H₂O gasification process the encountered opposing action of CO₂ and H₂O makes the use of conventional indices problematic. Thus, few validated process and efficiency indices are presented here in order to help to describe the CO₂ gasification runs. Analysis of obtained results provides answers in the field of production of FT fuels from CO₂ gasification of waste biomasses.

2. Concept and methodology:

Research installation

The experiments were carried out on a bench-scale experimental stand presented in Fig. 1. Main part of the unit is a fluidised-bed gasifier with an in-bed feeding system. The reactor is electrically heated during start-up. Its upper part is a water-jacket design which is used for

excess heat removal. This design enables quick start-up as well as long term stable operation with good control of process temperature. The internal part of the reactor is made of a heat-resistant steel tube with internal diameter of 105 mm and height of 1500 mm. Bottom part of the reactor is 300 mm long and has conical shape which tapers to the diameter of 75 mm at the distributor level. Fluidization medium is distributed within the reactor with use of a perforated plate of ca. 4% open area. Temperature measurements inside the reactor and the freeboard are carried out with use of five vertically mounted K-type thermocouples. Three bottom thermocouples are placed within the bed while the remaining two indicate temperature profile of the freeboard. The fuel feeding system consists of three storage tanks. Two of them are equipped with knife gate valves which enable fuel

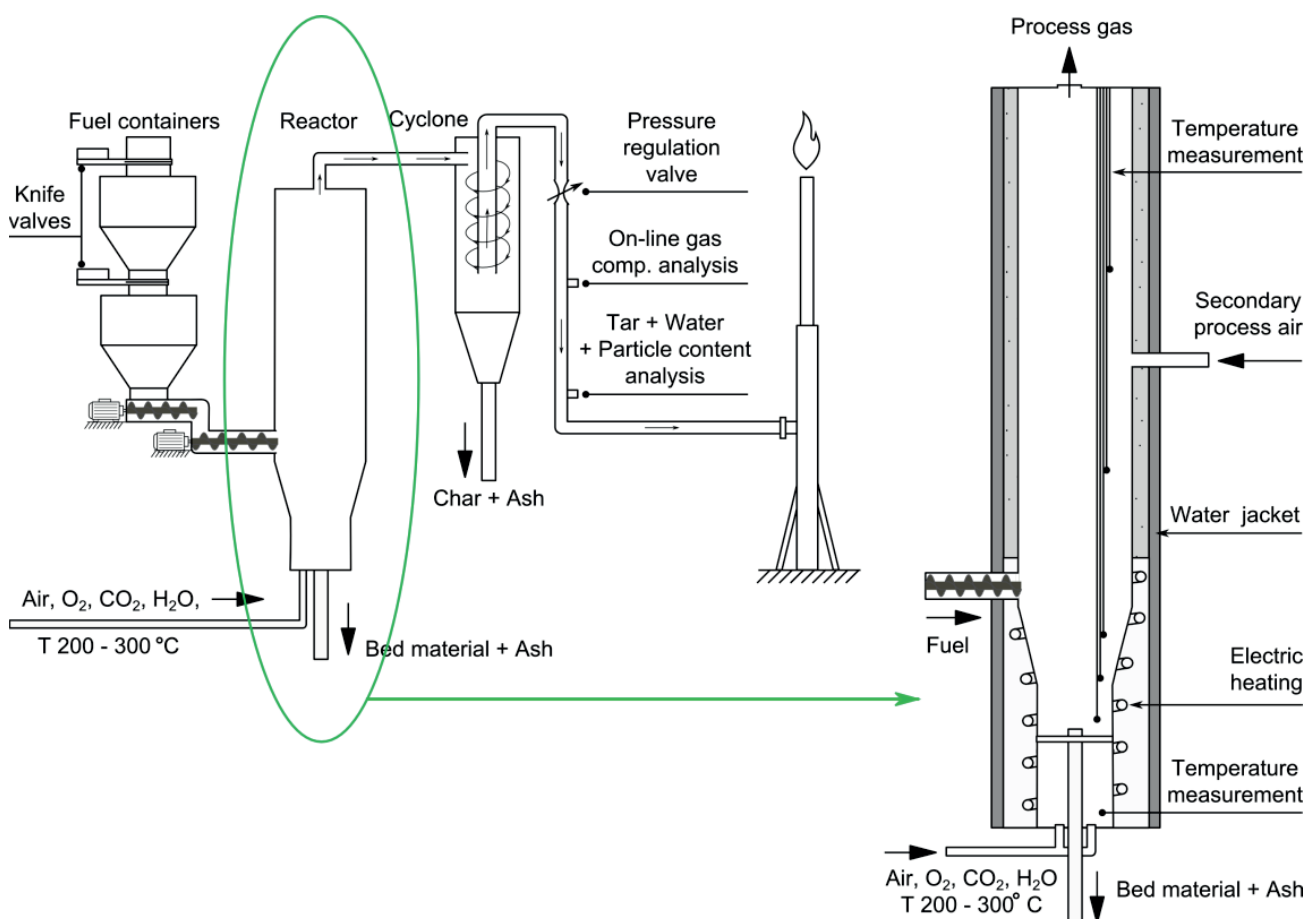


Fig. 1: Process scheme of the lab scale gasification installation

loading while the experiments are conducted in over pressure. The biomass flow is regulated by changing rotational speed of the upper screw feeders. From the fuel dosing tanks, the fuel is fed into a drop tube. The drop tube ends with a high capacity in-bed screw feeder which is equipped with an additional water jacket. This technical solution prevents heating-up of the stored fuel and its uncontrolled pyrolysis during intermittent phases of reactor's operation. For safety reasons, the feeding system is continuously purged with small quantities of nitrogen.

Downstream of the reactor, syngas reaches a cyclone where particles of the entrained char, ash and bed material are recovered. Syngas after dedusting is directed through a pressure relief valve towards a flare. After reduction of pressure, the syngas is sampled for analyses. Gasification agent mixture is prepared from gas cylinders (arranged into bundles with separate pressure regulators) containing technical grade O₂, N₂, CO₂. The flow rate of each agent is measured independently by means of a dedicated Bronkhorst EL-FLOW SELECT mass flow controller. The gas mixture flow lines are electrically heated up to 320°C. The steam flow rate is regulated by FWT di Tommaso Commonara water dosing pump (max. flow - 4dm³/h) positioned upstream of the steam generator and steam preheater.

Feedstocks

The conducted research was focused on the use of two waste biomass feedstocks of high ash content and demanding chemical composition. Feedstocks before use were pelletized (6mm diameter) to improve their density and homogeneity. However, due to small size of screw feeders used in this small-scale unit, the fuel pellets needed to be crushed and sieved before use. Average particle size

		SWP	Bark	Lignin
Moisture	wt.% ar.	5.28	3.51	10.80
Ash	wt.% a.	0.216	9.868	4.372
Volatile matter	wt.% a.	84.8	71.7	66.7
C	wt.% a.	48.1	44.9	52.7
H	wt.% a.	5.379	4.452	4.863
N	wt.% a.	0.065	0.482	1.410
S	wt.% a.	0.022	0.033	0.208
HHV	kJ/kg	20,799	17,986	22,428
Characteristic ash melting temp.	IDT/ ST/ HT/ FT, °C	660/ 900/ 1420/ 1560	760/ 1500/ 1530/ 1540	600/ 690/ 1310/ 1540
Bulk density	kg/m ³	502.8	797.9	777.6
>3.15 mm	wt.%	31.41	11.65	4.49
3.15–2mm	wt.%	35.13	35.97	25.29
2-1.4mm	wt.%	25.57	19.49	31.15
1.4–1mm	wt.%	5.84	9.54	15.31
1-0.8mm	wt.%	1.14	4.10	6.17

Tab. 1: Physicochemical characteristic of gasified feedstocks

distribution and bulk density of the feedstocks after size reduction were measured. Physicochemical properties of the gasified biomasses are shown in Tab. 1. The feedstocks ashes were analysed with visual method against their thermal behaviour in half-reducing atmosphere. The procedure followed CEN/TS 15370-1. Primary bed material used in the research was olivine, obtained from Magnolithe GmbH.

Determination of syngas composition and content of contaminants

Samples of the syngas were collected in Tedlar bags and analysed with GC in order to determine the exact composition. The GC analyses were done using a Varian CP3800 coupled with Flame Ionization Detector and Thermal Conductivity Detector and Pulse Flame Photometric Detector. The qualitative and quantitative analyses were performed using the external gas standard method. Moreover, syngas was sampled to determine its content of water, tar and solid particles. The sampling system consisted

of a probe, two impinger bottles and a tube filled with cotton wool. The probe was introduced axially into syngas line after the pressure relief valve. The end of the probe was connected to two impinger bottles containing about 50 ml of isopropanol at ambient temperature. In these two bottles most tar and dust is collected. The glass tube filled with cotton wool, fitted at the end of the probing set, acts as a droplet collector. The syngas was sucked by a pump coupled with a flow regulator.

For determination of water content in syngas, Karl-Fischer method was applied. Mass of gravimetric tars was measured after evaporation of solvent under reduced pressure (0.1 bar, 80°C) and final drying until constant mass was reached. Conditions of the above mentioned treatment, stand for definition of tars adapted for this research.

Dust particles collected in the isopropanol solution were filtered off, washed with additional portion of isopropanol and dried until constant mass was reached. The total amount of solids after the gasifier was determined by addition of the weight of solids from the isopropanol probing and from the stream of solids separated in the cyclone. For mass balancing and efficiency calculations the recovered solids were used for proximate and ultimate analysis.

Method and operating conditions of the reactor

After initial electrical preheating of the reactor up to 700 °C, combustion process was started with air and small amount of steam. When temperature in the bed reached 750 °C the air was replaced by carbon dioxide and oxygen mixture. Flowrates of gas and fuel were adjusted to obtain steady combustion parameters and good control over heating-up of the bed up to starting temperature of the process (840°C). Usually the longitudinal profile

of temperatures in freeboard zone stabilized between 600°C and 750°C. If the conditions in the reactor/installation (i.e. temperature, pressures etc.) were sufficient, the fuel stream was further increased to initiate the gasification process. Set point of total pressure was regulated manually by adjusting the pressure-relieve valve.

For all feedstocks a baseline gasification temperature has been set to 850°C. The temperature was controlled by adjusting the flowrate of oxygen, fuel and water fed into reactor' jacket. Reactor pressure has been varied between 0, 1 and 2 bar_g.

The influence of steam added to the process was determined in the range 0.55 – 1.2 H₂O/C, where the index can be calculated as:

$$\frac{H_2O}{C} = \frac{\dot{m}_{Steam,fa} + \dot{m}_{H_2O,fuel}}{\dot{m}_{C,fuel}} \quad (1)$$

In terms of fluidization number, the tests were conducted at the level of U/U_{mf} = 8.5±1.5, with the exception of lignin.

FB gasification indices

In conventional gasification systems where air/H₂O or O₂/H₂O mixtures are used as gasifying agent the conversion efficiency indices are well established and successfully allow comparing different reactors and process conditions. Primary attention has been paid here towards Cold Gas Efficiency (CGE), Carbon Conversion Efficiency (CCE) and H₂O/Carbon (H₂O/C).

CGE gives direct information about the amount of useful chemical energy of fuel transformed into syngas. It can be calculated based on either higher or lower heating values and is not sensitive for the composition of gasifying agent. In the article Eq. 2 was used to calculate reactor' CGE.

$$CGE = \frac{(HHV_{syn} + i_{syn})\dot{m}_{syn} \times 100\%}{(HHV_{fuel} + i_{fuel})\dot{m}_{fuel}} \quad (2)$$

CCE is an index that gives information regarding the efficiency of a process/reactor in conversion of feedstock's carbon into syngas rather than to tars or chars. It is based on C balance of the system and can be calculated through the use of the following equation:

$$\varphi_{C,fuel \rightarrow C,syn} = \frac{x_{C,syn} \dot{m}_{syn} \times 100\%}{x_{C,fuel} \dot{m}_{fuel}} \quad (3)$$

Eq. 3 does not take into account the additional source of C introduced in feed with CO₂. Hence, it evaluates process efficiencies of over 100%. To counteract this fact the CCE needs to be fitted with additional term related to the fed CO₂. For this reason equation Eq. 4 was devised. It is a direct C balance equation which takes into account the additional substrate - CO₂. Part of the CO₂ reacts with fuel and influences the CO and H₂ yields in syngas, while rest leaves as a ballast gas which influences the composition of syngas.

$$\varphi_{C,in \rightarrow C,syn} = \frac{x_{C,syn} \dot{m}_{syn} \times 100\%}{x_{C,fuel} \dot{m}_{fuel} + \dot{m}_{CO2,fa}} \quad (4)$$

Eq. 4 is proposed as the best simple approximation of the logic behind the conventional CCE index for later studies on CO₂ gasification.

The same reasoning was applied towards determination of a correct way to define an index based on H₂O/C, which would serve the purpose of relating the amount of steam used as a fluidizing agent, to the amount of carbon fed with fuel and CO₂. Similarly to CCE, usefulness of H₂O/C finds limits when CO₂ is introduced into a gasifier. In a gasifier, CO₂ acts as a substrate in CO₂ related reforming reaction while being a product of water-gas shift reactions. The most important steam and CO₂ gasification reactions were collated in Tab. 2. Boudouard's reaction is the main pathway through which CO₂ influences gasification systems. This reaction

Irreversible reactions	
$C + O_2 \rightarrow CO_2$	$Q = -405 \frac{kJ}{mol}$ Complete oxidation of C
$H_2 + \frac{1}{2}O_2 \rightarrow H_2O$	$Q = -242 \frac{kJ}{mol}$ Oxidation of H ₂
Reversible reactions	
$C + H_2O \rightleftharpoons CO + H_2$	$Q = 131 \frac{kJ}{mol}$ Water - gas reaction
$CO + H_2O \rightleftharpoons CO_2 + H_2$	$Q = -41 \frac{kJ}{mol}$ Water - gas shift reaction
$C_xH_y + xH_2O \rightleftharpoons xCO + \frac{(y+2x)}{2}H_2$	$Q = +(endo.)$ General steam reforming reaction
$C + CO_2 \rightleftharpoons 2CO$	$Q = 172 \frac{kJ}{mol}$ Boudouard's reaction
$C_xH_y + xCO_2 \rightleftharpoons 2xCO + \frac{y}{2}H_2$	or $C_xH_y + \frac{y}{4}CO_2 \rightleftharpoons \left(x + \frac{y}{4}\right)C + \frac{y}{2}H_2O$ $Q = +(endo.)$ General CO ₂ reforming reaction

Tab. 2: Collation of most important gasification reactions impacted by partial pressure of H₂O and CO₂.

is more endothermic than water-gas shift and produces CO which pushes the water-gas reaction towards the side of substrates. In equilibrium models, CO₂ addition increases yields of CO with simultaneous drop in production of H₂. To follow the combined influence of CO₂ and H₂O a number of indices have been analysed. The most reliable and clear to evaluate results have been found when the index H₂O/(C+CO₂) was calculated:

$$\frac{H_2O}{(C+CO_2)} = \frac{\dot{m}_{Steam,fa} + \dot{m}_{H2O,fuel}}{\dot{m}_{C,fuel} + \dot{m}_{CO2,fa}} \quad (5)$$

The expression can be calculated with both mass and molar values. However, usefulness of the obtained results differs.

Design of experiment

When conducting gasification experiments in FB reactors it is vitally important to keep similarity of process conditions alike between each test (U/U_{mf} , ER, CO_2/C , $\text{H}_2\text{O}/\text{C}$, m_{fuel} etc.). This goal becomes difficult to reach in situations when reactor pressures are varied. The level of complexity rises even further when mixture of $\text{O}_2/\text{CO}_2/\text{H}_2\text{O}$ is used for gasification. To simplify the amount of strategies, which can be used to design a FB research, two most commonly applied strategies are described below. For any FB research, the fundamental condition is to keep hydrodynamic parameters of the bed constant. Following is the stream of fuel which can either be kept constant (constant heat input) or rise with increasing pressure in a linear or exponential function (varying heat input). For biomasses the rise in reactor's output power can be approximated to change linearly with increasing pressure (up to 8 bar). In the constant heat input case, it is impossible to keep the relations between the amount of $\text{H}_2\text{O}/\text{CO}_2$ and the feedstock (carbon in fuel) constant. Either H_2O or CO_2 needs to be used as the excess fluidizing gas needed to keep the hydrodynamic conditions of the bed stable between different pressures. On the other hand, when a variable heat input is applied, the relations between fluidizing gas composition and the feedstocks can be kept constant, but in this case another source of problem stems up from the increasing amount of ash material present in the system. On one hand ash agglomerates can influence the gasification kinetics while on the other it can lead to severe agglomeration problems. In this research the variable heat input strategy has been applied.

3. Results and discussion

Goal of this research was to perform screening tests in order to search for optimal gasification conditions and to set limits for tests that will be carried out in later stages of the project. Results of the gasification runs where stable process conditions were achieved are presented in Tab. 3. For each pressure value, at standard 850°C FB temperature, a set of stable gasification parameters were achieved with the exception of gasification of lignin at 2 bar_g. For lignin also experiments at 2 bar_g and temperatures of 830°C and 800°C always led to quicker or slower defluidization of the bed.

From all the feedstocks, lignin stood out as the most difficult one for gasification. Its atmospheric gasification showed that high amount of fuel stayed in the bed and that it did not fluidize well (high temperatures difference in FB). Here also the freeboard temperatures were lower than for other feedstocks. On the other hand, when at 1 bar fluidization number was slightly reduced, lignin exhibited high tendency for fragmentation, and large portion of the fuel was elutriated from the bed. Hence, higher freeboard temperatures were noticed. To assess if this property is characteristic for lignin, bark was also gasified at higher in-bed gas velocities. However, no signs of feedstock fragmentation, heterogeneous bed behaviour, or tendencies for defluidization were noticed. For bark and SWP the variable heat input design of experiment was successful and gave good comparison of obtained results. Also, no conditions were determined when the FB would defluidize.

In relation to gas yield, lignin produced much higher amounts of gas species in relation to other feedstocks, mainly with regard to CO. Furthermore, a general trend was noticed where for all tested feedstocks, increase in pressure led to

Fuel	Softwood pellet			Oak bark			Lignin		
Run number	1	2	3	4	5	6	7	8	9
In bed temp. [°C]	852.8	843.6	853.6	853.3	853.7	854.9	852.0	853.9	-
Reactor pressure (MPa _g)	0.0	1.0	1.9	0.0	1.0	2.0	0.0	1.0	2.0
Fuel ar. [kg/h; kW]	2.52	5.64	7.35	2.95	5.73	8.51	2.62	5.37	-
Composition of the fluidizing agent [kg/h]:									
O ₂	1.02	1.81	2.77	1.08	2.14	3.04	1.28	2.58	-
CO ₂	2.90	2.74	6.62	3.18	4.95	4.95	4.36	5.33	-
H ₂ O	0.73	2.48	3.70	0.60	2.49	3.86	0.70	2.70	-
Syngas composition [vol. %]:									
H ₂	11.88	15.16	13.21	14.21	15.60	19.66	12.13	18.00	-
CO	21.62	24.00	23.56	24.18	27.01	25.10	24.91	26.04	-
CO ₂	53.41	42.44	48.84	49.71	44.39	43.12	52.00	44.45	-
CH ₄	4.67	8.76	8.70	4.21	4.77	6.05	3.18	4.21	-
C ₂ H ₄	2.46	3.32	2.60	1.59	1.41	1.52	1.01	1.00	-
C ₂ H ₆	0.26	0.37	0.27	0.14	0.16	0.31	0.18	0.09	-
HHV [kJ/Nm ³]*	8.42	11.41	10.27	8.15	8.78	9.72	7.08	8.38	-
Syngas yield [Nm ³ /kg _{daf}]	1.607	1.305	1.570	1.741	1.631	1.554	2.263	1.942	-
H ₂ O [g/Nm ³]	228.1	364.0	383.0	161.0	306.0	309.0	172.8	312.0	-
Tar [g/Nm ³]**	5.50	5.29	4.34	0.64	5.20	5.60	1.62	4.95	-
Solids [g/Nm ³]	4.54	3.30	2.60	68.76	54.77	52.52	10.51	7.87	-
FB gasification parameters:									
U/U _{mf} [-]	8.93	7.99	7.31	8.87	9.84	8.79	11.57	11.39	-
ER [-]	0.30	0.24	0.30	0.29	0.29	0.28	0.34	0.33	-
H ₂ O/C [g/g]	0.67	1.00	1.15	0.55	0.99	1.03	0.73	1.21	-
H ₂ O/(C+CO ₂) [mol/mol]	0.2744	0.5248	0.5101	0.2241	0.4402	0.5138	0.2584	0.5258	-
H/CO [vol.%/vol.%]	0.55	0.63	0.56	0.59	0.58	0.78	0.49	0.69	-
Gasification efficiency parameters [%]:									
CGE – Eq. 2	70.91	77.43	73.05	76.80	78.28	79.22	76.17	75.05	-
CCE – Eq. 3	160.54	125.23	148.64	158.37	145.52	129.54	185.75	150.85	-
CCE – Eq. 4	98.40	98.67	98.97	97.20	97.27	97.13	98.73	98.58	-

* syngas in dry state with CO₂

** tar measurement and definition described above

Tab. 3: Results experimental test runs CO₂ gasification, Process efficiency parameters, Process indices.

subsequent increase in yield of CH₄. For higher hydrocarbons (C_xH_y) the trend was unclear.

To perform synthesis of chemicals from syngas it is necessary to assure a certain ratio of H₂/CO. For FT the ratio should reach values in excess of 2. With conventional O₂/H₂O gasification and with use of mildly catalytic bed material such as olivine this goal is often attainable with-

out use of additional water-gas shift reactors. However, in the performed experiments it has been shown that addition of even small amounts of CO₂ into a gasification system has a detrimental effect on the yield of H₂. The highest ratio of H₂/CO = 0.78 was obtained for gasification of bark when the H₂O/(C+CO₂) was equal to 0.51 (H₂O/C = 1.03). For lignin the same tend was

noticed where the ratio of $H_2O/C=1.2$, yielded only $H_2/CO=0.69$ (here $H_2O/(C+CO_2) = 0.53$).

When process efficiency is concerned, the highest CGE of over 76% has been reached for bark. Consecutively lignin and SWP gave lower CGE, yet still above the level of 70%. Recurrent picture can be seen where gasification of lignin was done with lower CGE and higher CCE in relation to bark. No clear information could be determined as to the impact of pressure on CCE. However, for bark a stable rise in CGE was noticed.

Bed agglomeration propensity

Even though for all tested feedstocks, the gasification runs were conducted at the same temperature level the amount of observed bed agglomeration differed greatly. For all SWP tests no signs of bed agglomerations could be found. Gasification of bark led to formation of a small amount of very fine agglomerates in the bed (sieve analysis >1mm). However, for no process conditions did the agglomeration of bark ash led to the point of bed defluidization. Finally, even though many experiments were performed, no stable operation at 2 bar_g could be reached for lignin. From equilibrium calculations it is known that pressure should have little or no effect on agglomeration behaviour of the tested biomasses. Still, performed tests show that when the amount of fuel fed into a FB is increased, situations where the bed does not fluidize stably are encountered often. Origins of this behaviour may lie in maldistribution of the fluidizing gas due to the increasing amount of char material present in FB or reaching the critical concentration of ash.

4. Conclusion and Outlook

The presented experimental research was conducted for 3 pressures, changing rate of fed fuel (variable heat input) and similar fluidization conditions. This mode of experiment design gave good compara-

bility of results between tests conducted at very broad spectrum of gasifying agent compositions and feedstocks. Hence, it is proposed for future research on pressure gasification with use of CO₂. Important though is to take into consideration the impact of increasing ash material present in bed to avoid its defluidization.

For the tested waste biomasses, bark was determined to give the best overall gasification behaviour with good yields and quality of syngas, high CGE and CCE. Connecting this with the fact that for bark' gasification runs were very stable, makes the feedstock very promising for future research. SWP used here as reference material provided worse characteristics of produced syngas and CGE to both bark and lignin. However, it was also the only feedstock which showed no signs of ash agglomeration in FB.

On the other hand, it was found that lignin gasification was prone to lead to bed defluidization with increasing stream of fuel and system pressure. It can be argued that bed fluidization occurred here through a mechanism which involves a combined influence of the chemical characteristic of lignin's ash material as well as a certain limiting amount of the ash that is possible to be present in a FB. Experience gained during the trials indicates that lignin is a difficult, but promising feedstock for gasification. Due to its abundance, waste character and stable annual availability, it should be treated as a viable choice for diversification of the group of applicable waste feedstocks.

The conducted experiments show that the concept of chemical sequestration of CO₂ is technically feasible option in biomass gasification reactors. However, influence of the applied CO₂ on the composition of yielded syngas is very high and may deem its utilization for the purpose of chemical synthesis impractical.

Due to the fact that addition of CO₂ into a gasification system changes the usefulness of commonly applied process efficiency indicators it is important to adapt them in a way which would not

influence highly their original meaning. For this reason the adapted CCE (Eq. 4) and H₂O/(C+CO₂) (Eq. 5) indices were proposed.

5. Acknowledgements

This work was supported by the European Union's Horizon 2020 research and innovation programme under grant agreement number 764675 (Heat-to-Fuel).

6. References

- [1] I. Lopes Motta et al., *Ren. and Sust. En. Rev.* **94** (2018) p998
- [2] C. Wu et al., *Biotechnology Advances*. **27** (2009) p588
- [3] C. Pfeifer et at., *Biomass Conversion and Biorefinery*. **1** (1) p39.
- [4] G. Xu et al., *Particuology* **6** (2008) p376
- [5] E. Kurkela et al., *Environ Prog Sustain Energy*, **33** (2014) p681
- [6] Y. Xiang et al., *Energy* **179** (2019) p571
- [7] J.J. Huang et al., *Energy Fuels* **17** (2003) p1474
- [8] J. Li et al., *Fuel* **220** (2018) p80
- [9] H. H. Bui et al., *Fuel Processing Technology* **152** (2016) p207
- [10] R. S.Xu et al., *Chemical Engineering Research and Design*, **107** (2016) p34
- [11] S. Tuomi et al., *Fuel* **158** (2015) p293
- [12] J. Fermoso et al., *Journal of Analytical and Applied Pyrolysis* **85** (2009)
- [13] T.R McLendon et al., *Biomass and Bioenergy* **26** (2004) p377
- [14] M. Mayerhofer et al., *Fuel* **99** (2012) p204
- [15] S. Valin et al., *Fuel Processing Technology* **91** (2010) p1222
- [16] L. J. Wang et al., *Biomass and Bioenergy* **32** (2008) p573
- [17] D. C. Elliott, et al., Chapter 52 in *Fundamentals of Thermochemical Biomass Conversion* (1985).
- [18] M. Jeremiáš et al., *Fuel* **210** (2017) p605
- [19] M. Jeremiáš et al., *Applied Energy* **217** (2018) p361
- [20] S. Valin et al., *Fuel* **177** (2016) p288
- [21] Y. Cheng et al., *Powder Technology* **296** (2016) p87
- [22] M. Balland, *Waste and Biomass Valorization* **8** (2017) p2823

Heat-to-Fuel Workshop Abstracts

Modeling, design and assessment of a milli structured reactor for Fischer Tropsch reaction

G.Geffraye(*), A.Bengaouer, A.Chappaz, M.Jouve

CEA, Commissariat à l'Energie Atomique et aux Energies Alternatives
LITEN, DTBH 17 avenue des Martyrs, 38000 Grenoble Cedex 9, FRANCE
*corresponding author, genevieve.geffraye@cea.fr

1. Introduction and Short Description

Heat to Fuel (HtF) aims at delivering the next generation of biofuel production technologies towards the decarbonisation of the transportation sector. Fischer Tropsch (FT) is a promising technology for the efficient production of 2nd generation fuels. Among all the existing reactor technologies, the milli structured one has been selected to be investigated and implemented in the HtF system process.

This paper discusses:

- The state of the art of the FT reactors technology and R&D on intensified reactors
- The design process of an optimized FT milli structured reactor for HtF.
- Simulation and experimental results obtained at CEA

2. State of the art of FT reactors

Various FT technologies are already available and industrially operational at large scale (production capacity from 10000 to 100000bbl/day) for Coal to Liquid (CtL) or Gas to Liquid (GtL) applications. According to the level of operating temperature, the technologies differ. High Temperature Fischer Tropsch (HTFT) reactors (300-350°C) are mainly Circulating Fluidized Bed reactors (CFB) and Fixed Fluidized Bed reactors (FFB). Low Temperature FT (LTFT) reactors (200-240°C) are of two kinds, Multi Tubular Fixed Bed reactors and Slurry reactors. In the 2000s, small scale (about 1000bbl/day) intensified reactors have been developed for GtL and Biomass to Liquid (BtL) applications. Beginning of 2017, Velocys built a GtL unit for ENVIA.

3. R&D on intensified reactors

Research studies are mainly on long chain hydrocarbons production with low temperature reactions (<240°C) in catalytic (Co or Fe) fixed bed reactors. Most of the studies are performed on milli structured or micro structured fixed bed reactors and on monolith reactors and aim at enhancing the catalyst efficiency by reducing diffusion lengths and increasing mass and heat transfers.

4. Design process of an optimized millistructured fixed bed reactor for HtF

Here, the final objective is to provide an optimized large scale millistructured fixed bed reactor (~ 1.5Nm³/h) filled with an innovative catalyst for a system integration.

Starting from a mini scale FT reactor (millistructured reactor prototype of 0.1Nm³/h) and from a reference catalyst (Co on alumina), the upscaling of the reactor is proceeded step by step, based on experimental tests and on simulation results and in parallel to the improvement of the catalyst. Two reference catalysts, 16% Co/α alumina and 18% Co/γ alumina, are considered.



Manufactured millistructured reactor (mini scale)

5. Millistructured FT reactor modeling and simulations

A large bibliographic survey has been performed providing a state-of-the art on FT modeling.

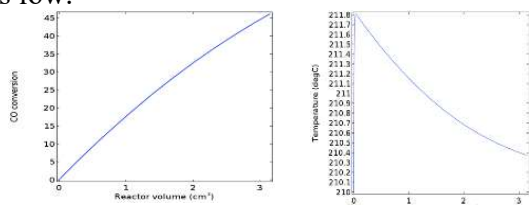
Several kinetic models have been implemented and compared against existing conversion data. The kinetic model of Ma et al, 2011 [1], gives

[1] Mal et al, 'Fischer Tropsch synthesis : support and cobalt cluster size effects on kinetics over Co/Al₂O₃ and Co/SiO₂ catalysts', Fuel n°90,2011, pp756-765

accurate results and has been selected and adjusted.

A heat transfer model has been developed (based on a literature review) taking into account the radial dispersion in the bed and the convection between the wall and the bed.

Those correlations have been implemented in different models; a 1D plug flow model, with a simplified heat balance and no mass diffusion, and a 2D model, with heat and mass diffusion. The preliminary simulation results show that 1 pass conversion of 50% seems achievable for lab scale reactor at high Space Velocity (SV). The temperature rise along the bed is in the range of 2-5K. The pressure drop along the bed is low.

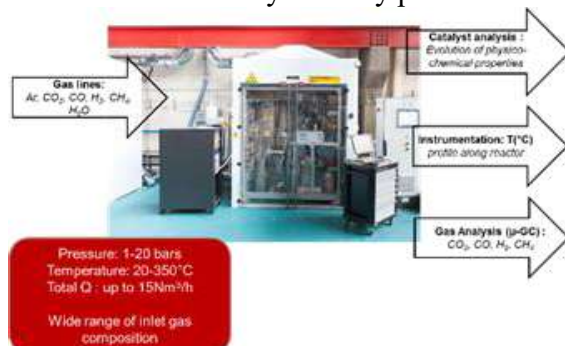


Plug Flow simulation. Evolution of the CO conversion and temperature along the bed for SV 4.3 Nm³/kg*h, 210°C, 20 bar, diameter of particle=0.5 mm

A more accurate model is being developed and will be assessed on the experimental data obtained on CEA bench tests. This accurate model will allow to design the large scale reactor to be implemented in the HtF system with confidence.

6. Experimentation characterization and first results

CEA has an experimental platform devoted to the study of FT synthesis, used for both, reactor assessment and catalysts study performances.

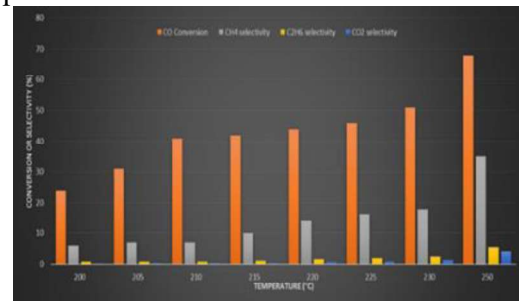


The available gases are H₂, CO, CO₂, CH₄ through gas lines and possibly other gases through bottles, which allow a wide range of gas composition. The inlet total flowrate may reach up to 3.6Nm³/min. The working pressure range is 1-70 bars. Gases can be heated up to 350°C. Analysis of the resulting products are realized on site: outlet gases analysis with a μ-

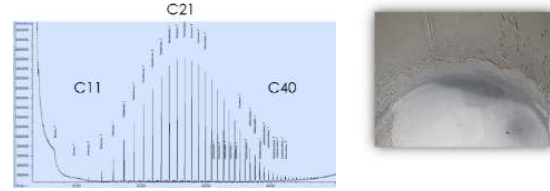
GS, Liquid Hydrocarbons analysis with a GC-MS, possible catalyst post analysis (evolution of physico-chemical properties).

A large series of tests has been performed on the mini scale reactor for both reference catalysts, with sensitivity tests to several parameters: inlet temperature from 200 to 250°C; SV from 3.5 to 15Nm³/kg*h, gas compositions at the inlet (presence of CH₄ and CO₂ additionally to H₂ and CO)

As examples of the obtained results, figures below show the sensitivity of the performances to the temperature for the CO/α alumina catalyst, and the GC-MS analysis the heavy liquids and wax condensed under 150°C.



Sensitivity to the temperature:
CO Conversion, CH4, C2H6 and CO2 selectivities for CO/α catalyst



Collected heavy liquid and wax and GC-MS analysis

The CO conversion decreases with the SV increase and increases with inlet gases temperature. Also, the maximum temperature increases. For T=250°C, the observed gradient is about 5°C, which is still acceptable. But the CH₄ selectivity increases which is not favorable. The recommended temperature is 210°C with an observed increase temperature of 2°C. There is a large impact of the composition on XCO and SCH₄. Comparing both reference catalysts, CO/α alumina catalyst seems more stable and performant compared to CO/γ alumina catalyst. IREC proposed CO/γ alumina catalyst improvement.

7. Conclusion

To provide an optimized FT millistructured reactor to be implemented in the HtF system an iterative and interactive process is underway. It is based on simulations results assessed on experimental data. Results obtained show that 50% CO conversion can be obtained at 210°C with low temperature increase and low CH₄

selectivity. Those conditions are proposed as FT reactor optimal operational conditions in the HtF system.

Aqueous phase reforming of Fischer-Tropsch water fraction

Giulia Zoppi¹, Giuseppe Pipitone¹, Hannes Gruber^{2,3}, Gerald Weber², Alexander Reichhold³, Raffaele Pirone¹, Samir Bensaid^{1*}

1 Department of Applied Science and Technology, Politecnico di Torino, Corso Duca degli Abruzzi 24, 10129, Turin, Italy;

2. Bioenergy 2020+ GmbH, Wienerstraße 49, Güssing, 7540, Austria

3 Institute of Chemical, Environmental & Biological Engineering, TU Wien, Vienna, Austria, Getreidemarkt 9/166, 1060 Vienna, Austria

* Corresponding author: samir.bensaid@polito.it

1. Introduction and Short Description:

The need of a sustainable and renewable production of fuels promoted the study of alternative processes to the conventional oil-based refinery. Among many technologies, Fischer-Tropsch (FT) reaction can convert CO and H₂ to transportation fuels. Despite its known performance, one of the economic bottlenecks is the production of large amounts of carbon-laden wastewater. As a consequence, it is necessary to treat the water fraction or recover the dissolved oxygenates, both for economic and environmental issues. Aqueous phase reforming is a catalytic process carried out at 230-270 °C and 30-60 bar with the aim of obtaining a gas mixture rich in hydrogen, according to the following reaction stoichiometry.



It has been greatly studied with model compounds (alcohols and polyalcohols), but very few studies have been referred to mixture, and it is even negligible the available literature for real industrial phase.

2. Methodology, Results and Discussion

In the present work, methanol, ethanol, 1-propanol, 2-propanol, butanol and acetic acid were tested as representative compounds for FT water; an actual liquid phase coming from a low temperature FT process has been tested at different reaction temperatures (230-270 °C) and time (0-4 hours) with a developmental 5% Pt/C catalyst.

Together with the gas phase, a thorough characterization of the liquid phase was performed to determine key intermediates/by-products present at the end of the reaction.

The catalytic tests have been performed in a Parr bench top reactor, equipped with a temperature controller. The screening of the model compounds was performed at equal carbon concentration (0.9 wt.%). At the end of the reaction, the gas phase was collected in a sampling syringe and the analysis performed by an SRA μGC. The liquid phase was characterized by HPLC Shimadzu system, equipped with a Rezex ROA organic acid column. The quantification of the compounds was performed via external calibration.

In Figure 1 the HPLC chromatogram of the FT water is reported; the main compounds present are C1-C4 alcohols and the corresponding carboxylic acids.

Among the obtained results, it is highlighted in Figure 2 the influence of reaction time on the FT water APR studied

at 270 °C, that was found to be the temperature with the highest hydrogen yield. It was observed that ethanol and propanol were readily converted during the heating time, while methanol was less reactive. Moreover, acetic acid did not convert at all, in agreement with previous results.

In the gas phase it is highlighted the constant increase of hydrogen and carbon dioxide, while the amount of alkanes was almost constant, after that 270 °C was reached (i.e. 0 hour in the graph). This is directly linked to the complete conversion of ethanol and propanol that lead to methane and ethane respectively. Indeed, from the APR of the representative compounds it is possible to ascribe the produced gases to the single alcohols present in the FT water.

3. Conclusion and Outlook

Water-soluble oxygenates in the aqueous effluent of Fischer-Tropsch are not easily recoverable, as they can form complex azeotropes, and are often in low concentration. While the wastewater treatment is the most used option, we proposed to investigate the catalytic route of aqueous phase reforming to produce

hydrogen as valuable by-product, solving at the same time environmental and economic concerns.

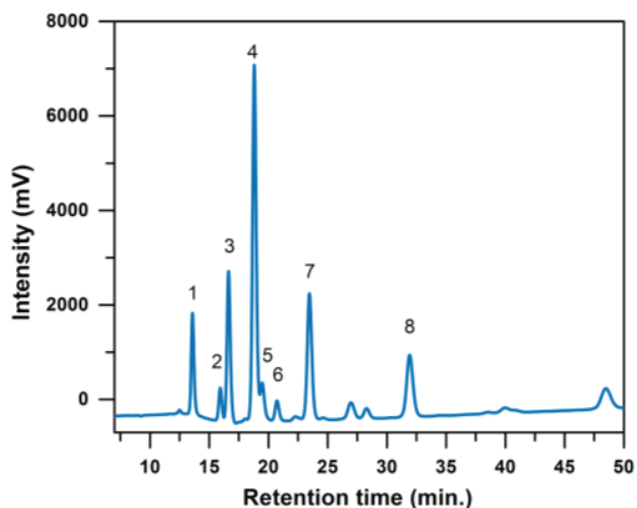


Fig. 1: HPLC chromatogram of FT water (1: acetic acid, 2: propionic acid, 3: methanol, 4: ethanol, 5: butanoic acid, 6: 2-propanol, 7: 1-propanol, 8: butanol)

Acknowledgement

This work was supported by the European Union's Horizon 2020 research and innovation programme under grant agreement number 764675.

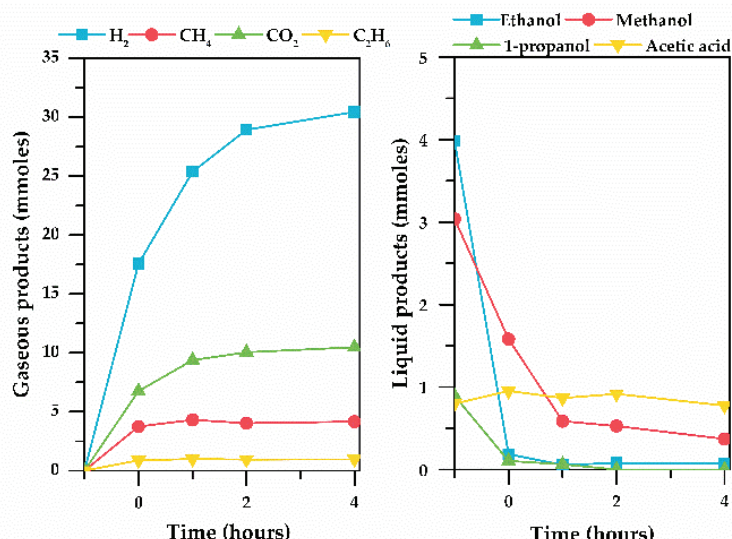


Fig. 2: Influence of reaction time on the aqueous phase reforming of FT water. Reaction conditions: 270 °C, 0.375 g Pt/C, 75 mL FT solution.

Poster Session Full Papers

Investigation of the upgrading of Fischer-Tropsch waxes through hydroprocessing

P. Neuner^{1*}, N. Netsch¹, R. Rauch¹

1. Karlsruhe Institute of Technology, Engler-Bunte-Institute – Fuel Chemistry and Technology,
Engler-Bunte-Ring 1, 76131 Karlsruhe, Germany

*corresponding author, philipp.neuner@kit.edu

Abstract

Through the increasing role of renewable fuels in our daily lives their production and their improvement is a necessary step. Fischer-Tropsch synthesis based on renewable resources is one way to achieve this. The upgrading of its intermediates, known as Fischer-Tropsch waxes (FTW) can help to increase the economic viability of such a process by converting the waxes to pharmaceutical products or high value fuel additives. For each desired product regulations have to be reached (European Pharmacopoeia), certain benchmarks must be fulfilled, this ranges from viscosity to boiling point to the degree of isomerisation and the amount of byproducts in the mixtures. Especially aromatic components can pose a problem for pharmaceutical usage of the waxes. In this paper, the conversion of FTW via hydroprocessing was investigated, using a semi batch stirred-tank reactor. The focus lies on the conversion, the successiveness of the occurring reactions, the isomer content and the amount of formed aromatic compounds.

1. Introduction:

Renewable fuels are becoming increasingly relevant. Therefore, the production and upgrading of it is a necessary step towards emission free energy consumption and fossil fuel divestment. One possibility is the use of regenerative carbon sources and hydrogen from electrolysis to produce synthesis gas and subsequent Fischer-Tropsch synthesis to produce transportation fuels. One group of byproducts are paraffins with high molecular weights (Fischer-Tropsch waxes). One of the research projects at the Engler-Bunte-Institute is the upgrading of these waxes through hydroprocessing. In this particular case, it only connotes to isomerisation and cracking of long chain paraffins. Hydroprocessing is not a single-stage process [1]. It consists of a multitude

of chemical reactions and equilibria of intermediates which need to be transported within the different catalytic sides [2]. Commercial catalysts usually operate with two different active species [3] and are therefore called bifunctional catalysts. Each catalytic side fulfils a critical role (Fig. 1). The first one is for hydrogenation on the metallic side. Its function is for dehydrating. They are a necessary component for the acidic function, providing olefins and inhibiting the formation of coke on the surface [3]. On acidic active sides the formation of carbenium ions takes place. Cracking and isomerisation happens at formed carbenium ions [4]. Bouchy et. al described multiple different mechanisms of cracking and isomerisation and their reaction rates. In Fig. 2 are two example mechanisms presented. The upper one

shows formation of a new isomer and the lower one the cracking mechanism. Both require a carbenium ion to be present. According to this study the reaction rate of isomerisation is usually higher, then the reaction rate of the scission of the carbon-carbon bonds. Compared to each other only the scission of tertiary carbon ions (Fig. 2, bottom) have a higher reaction rate then isomerisation [4]

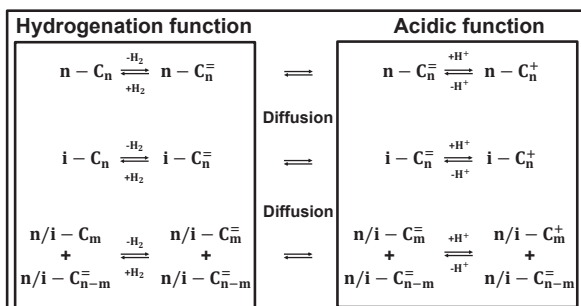


Fig. 1: reaction network of hydroprocessing of long-chain paraffins in a heterogenous catalysed reaction [4]

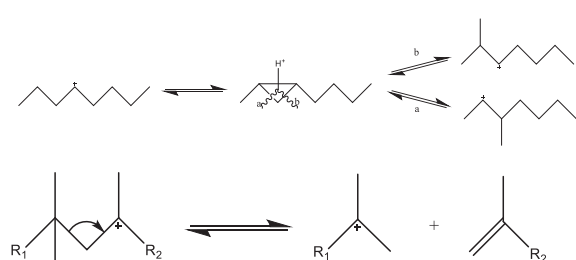


Fig. 2: isomerisation (top) and cracking mechanism (bottom) during hydroprocessing of long-chain paraffins [4]

A high degree of isomerisation is necessary for fast cracking reactions. Making the hydroprocessing essentially a two-stage process, with isomerisation taking place before cracking. The goal of this research is to understand the differences in product properties during and after hydroprocessing and to take a closer look at the mechanism proposed in the literature. In this paper, the focus is on the liquid product fraction.

2. Concept and methodology:

The overall aim is to enhance the economic value of the wax via tuning the isomer content, viscosity or boiling point. Therefore both reaction mechanisms and their influence on each other need to be understood. The focus lies mostly on isomer content, viscosity or boiling point curves. These properties can be adjusted through cracking and isomerisation, and the ratio between those. To examine these reactions, a slurry reactor was used in semibatch mode (Fig. 3). The reactor was chosen to increase byproduct formation for easier detection via NMR. It consisted of a gastight and heatable reaction vessel with a volume of 1 litre and a maximum temperature of 400 °C. The gas flow was regulated, using mass flow controllers for argon and hydrogen. During running experiments gas was continuously and directly dispersed into the liquid phase and discharged through the exhaust gas stream. With this setup, it was possible to maintain a constant hydrogen partial pressure over the duration of the whole reaction. Prior to the start of each experiment, wax was poured directly into the reactor and mixed with the catalyst particles ($CoMo/Al_2O_3$, $d_p = 100-200 \mu m$, $m_{Wax} = 512,58 \text{ g}$, $m_{cat} = 9,426 \text{ g}$).

Table 1: Process parameters of the residence time experiment. Parameters were kept constant over the course of the experiment

Process parameters		
p_{abs}	30	bar
T_R	380	°C
T_{HS}	100	°C
T_{CS}	20	°C
$\dot{V}_{H_2}(20^\circ, 1 \text{ bar})$	248	ml/min
$\dot{V}_{Ar}(20^\circ, 1 \text{ bar})$	35	ml/min
$m_{cat}(CoMo/Al_2O_3)$	9,43	g
d_p	100-200	μm

A liquid sampling station was set up for extracting wax without removing catalyst. It consisted of a pipe with a sintered metal plate on the end, reaching almost the bottom of the reactor. The sample flow out of the reaction zone was controlled via needle valve. In this publication the focus lies on one experiment conducted over 72 hours with samples being regularly extracted from the reactor. The process parameters and overall mass balances are presented in Table 1 and Table 2.

Due to the big difference of the molar mass of the monitored products and educts and therefore their physio-chemical properties, various byproducts, like light gases or gasoline are produced. Small amounts will be carried out of the reactor by the gas flow. To collect these, the gas was led through two separation vessels on different temperatures ($100\text{ }^{\circ}\text{C}$ and room temperature). With the above described setup, the product stream was separated into three different fractions. The first is the liquid wax directly out of the reactor, the second and third phases are condensed

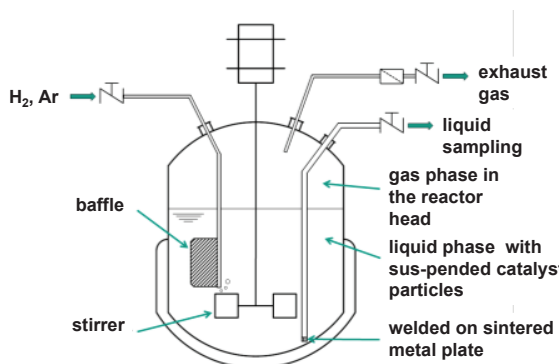


Fig. 3: Schemata of the slurry reactor used for the hydroprocessing experiments [5]

products at different temperatures. Due to the necessity of extracting samples during running experiments, the liquid products were extracted at reaction temperature of $380\text{ }^{\circ}\text{C}$. Which led to evaporation during the extraction and therefore to an overall loss of 21,4 wt% of the injected educt.

This was one of the main disadvantages of the slurry reactor (Table 2).

Table 2: Total mass balance of the performed residence time experiment at the end of the run

Mass balance	[g]	[%]
Educt	512,6	100
Removed mass	287,8	56,1
Hot separator	35,9	7,0
Cold separator	79,4	15,5
Sum	403,1	78,6
Loss	109,5	21,4

The liquid products were analysed via gas chromatography, using a simulated distillation (SimDist). With this method, it was possible to detect the n- and iso-paraffins in the C₉-C₆₀ range. The analysis was done in an external laboratory from Bioenergy2020+ in Güssing (Austria).

3. Results and discussion

Each product stream was evaluated on its own. The main reactions of the wax were cracking and isomerisation. Despite focussing only on the product fraction in the reactor (excluding the liquids from the separators), a change in the chain-length distribution to overall shorter chains could be observed. These results are depicted in Fig. 4 (top). It also showed an almost ideal hydrocracking behaviour (Fig. 4, top, 28,8 h) on the C₂₁ mark [4]. Shifting the longer chains from above this threshold to shorter chains. The integrated versions of the SimDist results can be separated into product fractions with different chain lengths, as seen in Fig. 4 (bottom).

With increasing residence time in the reactor, the liquid phase shows a decrease of long chains (C₃₁-C₅₀) and a significant formation of medium-sized chains

(C₂₁-C₃₀). This indicates the consecutive character of hydroprocessing reactions.

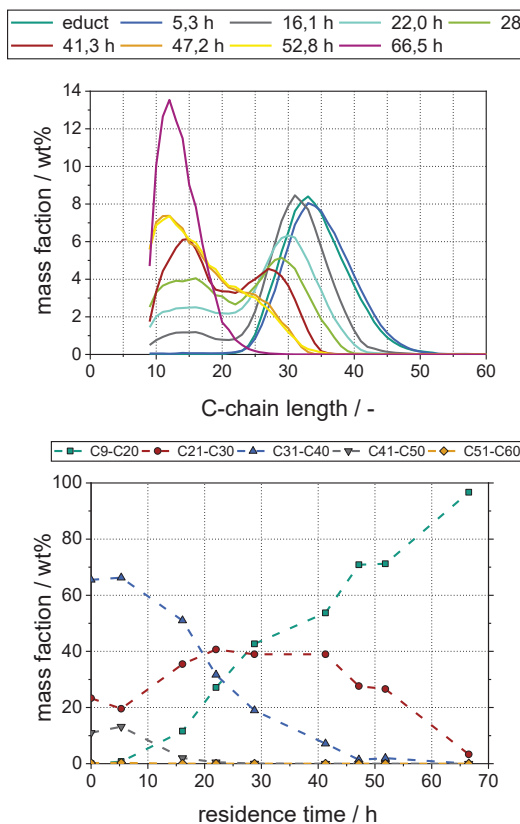


Fig. 4: Mass fraction of the liquid phase inside the slurry reactor during hydroprocessing (top) and product yield distribution with increasing residence time (bottom) ($T_R=380$ °C, $p_{abs}=30$ bar, $p_{H_2}=26,3$ bar)

With scission being more likely in the centre of the molecules than terminal scission. This is due to the fact, that carbenium formation is more stable on larger paraffins [4]. With the reaction advancing, and more secondary cracking occurring, a large portion of short chain molecules of C₉-C₂₀ is formed. Smaller molecules are evaporated and carried out of the reactor, via the constant gas flow. The evaporation, in combination with the continuous removal of product increased the catalyst/wax-ratio over time, making the reaction faster towards the end. The residue in the hot separator (HS) and cold separator (CS) were analysed after other

experiments. A symmetrical chain length distribution between C₅ and C₁₅ was detected [5].

To evaluate the difference between isomerisation and cracking a definition for the conversion had to be found. A common approach in the literature is to set a certain chain length as threshold [6]. Because of the almost ideal hydrocracking behaviour at the C₂₁ mark, this was chosen for the calculations for the conversion of the cracking reactions (Eq. 1). For the isomerisation the whole isomer content in the mixture was examined (Eq. 2).

$$X_{\text{Cracking}} = \frac{w_{FTW,C_{21+}} - w_{C_{21+}}(t)}{w_{FTW,C_{21+}}} \quad (\text{Eq. 1})$$

$$X_{\text{Iso}} = \frac{w_{FTW,n} - w_n(t)}{w_{FTW,n}} \quad (\text{Eq. 2})$$

The results are depicted in Fig. 5. It shows that the isomerisation starts before the cracking process. The isomerisation reaching its steady state after approximately 30 hours on stream.

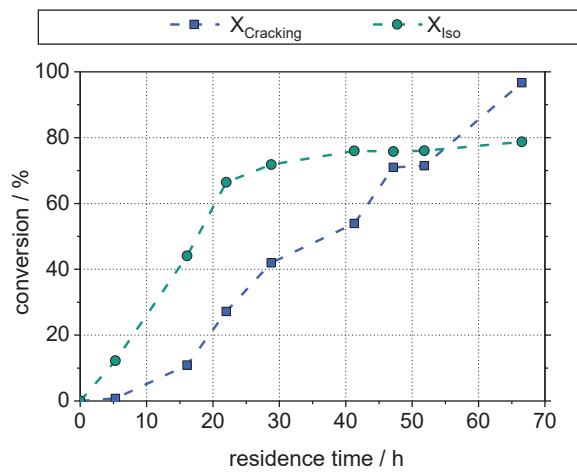


Fig. 5: Conversion of long-chain paraffins to short-chain n-paraffins and isomers ($T_R=380$ °C, $p_{abs}=30$ bar, $p_{H_2}=26,3$ bar)

The conversion for the cracked products reaches almost 100 %, so after a given reaction time and secondary cracking

reactions taking over, there are no molecules bigger than C₂₀ in the liquid phase inside the reactor. These results reiterate that these reactions have also to be considered as a consecutive reaction pathway with reaction steps from paraffin to olefin to isomer to cracked products. This reinforces the assumptions made by Bouchy et al., who stated that the carbenium ion formation is more stable on highly isomerised paraffins [4]. With higher carbenium ion concentration, the cracking reaction will become more frequent.

The used SimDist-Method, made it possible to detect isomers even in waxes with high molecular weights. Therefore, a comparison of the mass fractions of these two components was done (Fig. 6). It showed an equilibrium between isomers and n-paraffins, independent from chain length (>C₉). The equilibria can be observed after the process reaches a steady state after approximately 30 h. This indicates that the isomerisation inside the liquid product reaches a saturated status

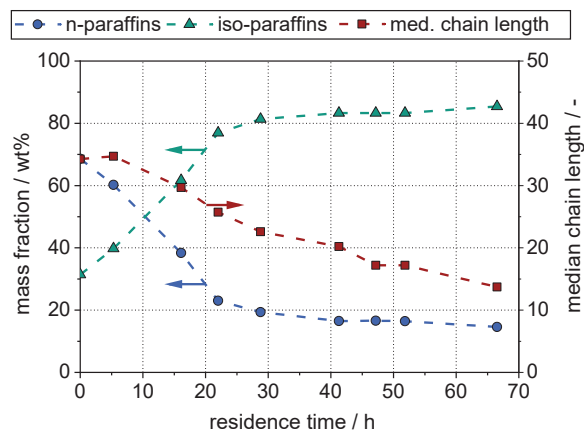


Fig. 6: Mass fraction of isomers, n-paraffins and chain length of the liquid phase inside the slurry reactor during hydroprocessing ($T_R=380\text{ }^\circ\text{C}$, $p_{abs}=30\text{ bar}$, $p_{H_2}=26,3\text{ bar}$)

after a given reaction time. On chains lower than C₉, the degree of isomerisation would fall off, due to the limited possibilities to form isomers on the shorter chains [4]. This equilibrium is to be further

investigated in future studies. Especially towards its dependence on reaction temperature, and pressure.

While analysing cracked Fischer-Tropsch waxes via gas chromatography, it is relatively easy to detect the n-paraffins in the mixture. This can be done by measuring the retention time of defined n-paraffin mixtures. It becomes more difficult to distinguish the byproducts in between the n-paraffins due to similar elution times, which result in the sum of multiple overlapping peaks (Fig. 7).

They consist of isomers, olefins and aromatics. A reasonable approach to evaluate the data had to be chosen. The solution was, to differentiate only between n-paraffins and their isomers, disregarding the amount of olefins and aromatics in the mixture.

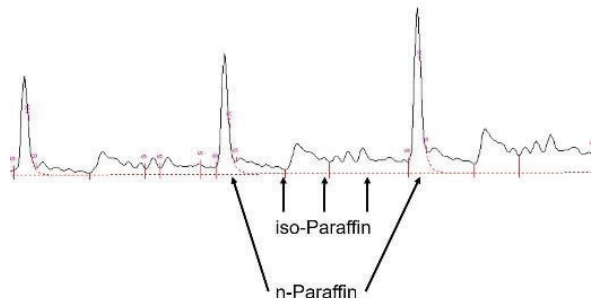


Fig. 7: extract of a typical GC-spectrum of long chain paraffins after hydroprocessing [5]

To evaluate the validity of this approach the cracked waxes were examined using ¹H-NMR spectroscopy. Here the content of all of the above mentioned components could be identified (Fig. 8). On the top graph there are the two peaks enhanced. Those are the ones for presumably the n- and iso- paraffins. The n-paraffin peak decreases, while the isomer peak increases with the reaction time. In the expected areas for olefins and aromatics there are no visually detectable peaks. If these areas are enhanced, the aromatics and olefins become visible. Both component fractions

grow with increased reaction time, but are negligible compared to the amount of

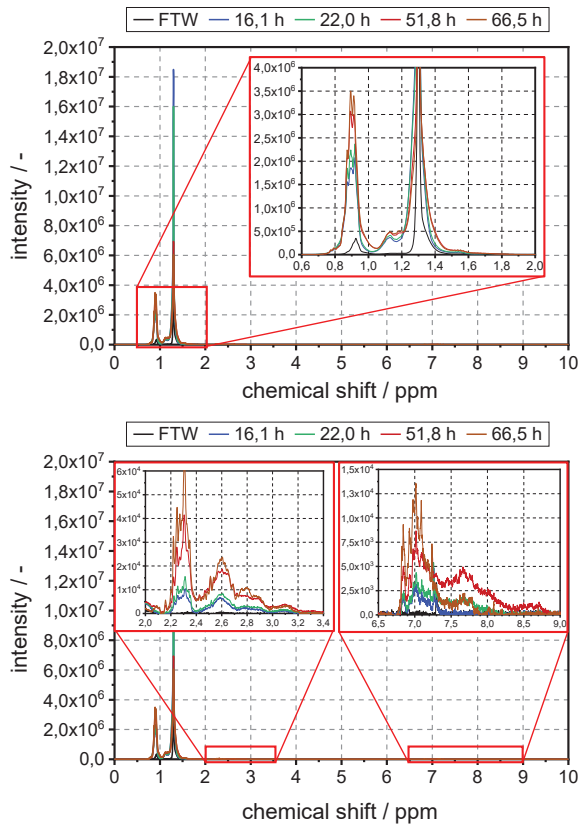


Fig. 8: NMR measurements of long-chain paraffins after hydroprocessing at different residence times ($T_R=380\text{ }^{\circ}\text{C}$, $p_{abs}=30\text{ bar}$, $p_{H_2}=26,3\text{ bar}$) [5]

Table 3: 1H-NMR shift of organic compounds[7,8]

Various C-Bonds	0,0 – 2,0 ppm
CH ₃ on hetero atom	1,8 – 2,5 ppm
CH ₃ on aromatic compound	1,8 – 2,5 ppm
CH ₃ on olefin	1,8 – 2,5 ppm
CH on aromatic compound	6,0 – 9,5 ppm
CH on hetero aromatic compound	6,0 – 9,5 ppm

n-and iso- paraffins (peak maxima are 60 up to 250 times lower). With these measurements, it was possible to validate the above-mentioned approach of classifying everything but n-paraffins as isomers.

4. Conclusion and Outlook

Our current research shows, in accordance with known literature, a prove of concept for hydroprocessing of Fischer-Tropsch waxes in a semi-batch slurry reactor. We were able to describe the whole process with occurring intermediates due to the consecutiveness of the reaction from long-chain paraffins over olefins to isomers to short chain paraffins. We also stated an equilibrium of n- and iso-paraffins after reaching a steady state. Similar equilibria were observed on different studies [4]. With 1H- NMR spectroscopy, we could detect a negligible amount of byproducts besides isomers and n-paraffins. This allows to rely exclusively on a SimDist method to analyze the product composition of hydroprocessed waxes.

5. Acknowledgements

We want to express our gratitude towards our colleagues at Bioenergy2020+ for providing us with the necessary measurements and expertise of the simulated distillation of long chain hydrocarbons.

used acronyms	
T_R	Temperature reactor
T_{HS}	temperature hot separator
T_{CS}	temperature cold separator
d_p	particle size
m_{wax}	mass wax
m_{cat}	mass catalyst
$X_{Cracking}$	Cracking conversion
X_{Iso}	Isomerisation conversion
$w_{FTW,n}$	mass fraction of n-Paraffins in the FTW
$w_{FTW, C21+}$	mass fraction of Paraffins with greater chain lenght then C20 in the FTW
$w_{C21+}(t)$	mass fraction of product with greater chain lenght then C20 after a given reaction time (t)
$w_n(t)$	mass fraction of n-Paraffins in the product after a given reaction time (t)

6. References

- [1] Coonradt, H. et al. Mechanism of Hydrocracking. Reactions of Paraffins and Olefins. I&EC Process Design and Development, 1964, (Vol 3. No. 1).
- [2] Reschetilowski, W. Einführung in die Heterogene Katalyse, 2015.
- [3] Regali, F. Hydroconversion of model Fischer-Tropsch wax over noble metal/silica-alumina catalysts. Doctoral Thesis in Chemical Engineering, 2013.
- [4] Bouchy, C., Hastoy, G., Guillon, E., Martens, J.A. Fischer-Tropsch Waxes Upgrading via Hydrocracking and Selective Hydroisomerization. Oil & Gas Science and Technology - Revue de l'IFP, 2009, 64(1), 91-112.
- [5] Netsch, N. Experimentelle Untersuchung der Katalysatordesaktivierung und der Endprodukteigenschaften bei mildem Hydroprocessing von Fischer-Tropsch-Wachsen. Masterarbeit. Karlsruher Institut für Technologie, 2019.
- [6] Leckel, D. Low-Pressure Hydrocracking of Coal-Derived Fischer–Tropsch Waxes to Diesel. Energy & Fuels, 2007, 21(3), 1425-1431.
- [7] Breitmaier, E. Vom NMR-Spektrum zur Strukturformel organischer Verbindungen. 3. überarbeitete und erweiterte Auflage. Weinheim: Wiley-VCH, 2012. ISBN 3-527-31499-7.
- [8] Bruker Corporation, Protonen- NMR- Chemische Verschiebung. <http://www2.chem.uic.edu/nmr/downloads/bruker/en-US/html/Avance%20Beginners%20Guide/de/18014398879165963.html> [Zugriff am: 12.07.2019]

Concept for the ideal 16MW_{th} biomass gasification system to feed a synthetic natural gas production process

C. Walcher^{1,2*}, S. Müller³, H. Hofbauer³, M. Fuchs⁴

1. Verto Engineering GmbH, Franz-Josefs Kai 53/131010 Vienna, Austria
2. Energy & Chemical Engineering GmbH, Pappelstrasse 13, 1140 Vienna, Austria
3. TU Wien, Institute of Chemical, Environmental and Bioscience Engineering, Getreidemarkt 9/166, 1060 Vienna, Austria
4. Federal Ministry for Sustainability and Tourism, Stubenring 1, 1010 Wien

*corresponding author, cw@vertö-engineering.com

Abstract: Biological, synthetic natural gas (SNG) prepared to fulfill the necessary grid feeding guidelines has the potential to keep up with the rising energy demands. Common production technologies for the extraction of natural gas from fossil sources cause relevant carbon dioxide (CO₂) emissions. Biological, synthetic natural gas from renewable energy sources is discussed as an alternative option to replace the traditional extraction process and can therefore be part of a low carbon energy system. This paper describes an optimized process for a biomass gasification system to feed a synthetic natural gas production process. The described investigations include the state of knowledge and the state of the art technology of large scale plants, simulation results from the software IPSEpro, economic analysis, and suggestions for an optimized equipment. The economic analysis shows promising results as well as measures to enable positive revenue surpluses for the optimized novel process concept. Furthermore, a guideline for an overall economic operation of an 16MW_{th} biomass gasification system to feed a synthetic natural gas production process can be derived from the economic analysis. The max. investment costs may not exceed 36 mio. Euros while the operational costs, for the optimized process concept, should be reduced by 50%. The highest share of the operational costs is represented by the fuel costs and so the most challenging task will be, to find an appropriate low-cost or negative-cost opportunity fuel available the whole year with low compositional fluctuations. Facing the challenges of climate change in general respectively on a global level the implementation of the Clean Energy for all Europeans Package on a more regional level the optimization of developed technologies needs to gain more effort.

Keywords: biomass - gasification - synthetic natural gas - SNG – process concept

1. Introduction

The worldwide coverage of electricity, heat and fuels demands further research on alternative feedstocks and technologies to enable a sustainable production in the future [1]. Thus, the thermo - chemical conversion of biogenic fuels with the dual fluid gasification technology provides a unique method for the production of eco - friendly and sustainable energy supply [2]. Furthermore, the dual fluid gasification

technology has the potential to make another step forward to meet the **European political agenda** for circular economy and renewable energy strategies and therefore, can be named as a promising technology to support the set energy and bioeconomy strategies [3]. Traditional dual fluid gasification enables in comparison with other gasification technologies a favorable product gas composition and so supports various

utilization possibilities like hydrogen-rich gas, Fischer-Tropsch fuel, mixed alcohols and synthetic natural gas [4]. The methanation process enables a further improvement of the gas composition and leads to a high share of methane in the product gas stream. The methanation process itself demands very high product gas qualities and less catalyst harming impurities [5].

For the realization of a low carbon energy system, the development of new energy carriers is needed because most energy carriers today are based upon fossil energy sources. For this reason, synthetic natural gas produced from renewable energy sources is discussed as an alternative to fossil energy carriers [6]. The production of synthetic natural gas by the usage of the dual fluid gasification technology, has the potential to bind biogenic renewable carbon (C). Synthetic natural gas can be used as an energy carrier, for energy storage applications, to feed the gas grids or as fuel for combustion engines.

Previous experimental setups, test works, demonstration plants and large scale plants for the production of synthetic natural gas had to deal with certain problems. The desired fuel flexibility combined with the high product gas quality demand, especially forced the attention on the product gas cleaning and upgrading technology. The goal is to provide a product gas suitable to feed a synthetic natural gas production process. Therefore, the following important question occurs:

What does the ideal industrial scale biomass gasification system to feed a synthetic natural gas production process look like?

The following paper contains a novel process concept based on important technical, commercial and legal aspects.

As a part of this precise evaluation the paper discusses:

- the state of knowledge and the state of the art technology of large-scale plants,
- simulation results from the software IPSEpro investigating the energy and mass balances for the novel process concept,
- equipment improvements to further enhance the performance of traditional used equipment,
- an economic analysis of the dual fluid gasification with a subsequent methanation.

2. Concept and methodology

The following investigations describe the evaluation of a biomass gasification concept to feed a synthetic natural gas production process. Therefore, the most important technical, commercial and legal aspects were taken in account and harmonized. For this purpose, a comprehensive literature research was made first. This research contains the most important information of the gasification technology as well as the state of knowledge and the state of the art technology of large - scale plants. The investigations focus in particular on increasing fuel flexibility and the associated increased need for gas cleaning and preparation utilities.

For the calculation of the gasification plant parameters, the simulation software IPSEpro has been used. IPSEpro has proven its reliability in many process design simulations in the past. IPSEpro enables an efficient and quick calculation of mass and energy balances for a modeled process design.

The applied process design to feed a synthetic natural gas production process is basing on reported experiences with

biomass gasification in Güssing, Oberwart, Senden and Gothenburg. The biomass gasification power plant Güssing represents the first industrial scale power plant using the dual fluidized gasification technology. In 2008 the construction of the Bio – SNG process and development unit (PDU) was finished. The first production of synthetic natural gas was demonstrated [7]. A sufficient gas cleaning and preparation strategy was developed and applied. The three main units were a two stages product gas scrubber based on methyl ester (ME), an activated char coal guard and a zinc oxide (ZnO) bed [5]. The construction of the biomass gasification power plant Oberwart was encouraged by promising results from the demonstration power plant Güssing. In Oberwart a novel cooling concept for the exhaust gas route was developed and demonstrated. Furthermore, some reasonable heat exchanger construction design changes were developed to deal with the high loads of fines [8]. The biomass gasification power plant in Senden is mentioned due to its high availability level. Senden uses new biomass fuel mixtures but nevertheless high availability levels are reached, and even higher availability levels are predicted due to modifications. Therefore, the process concept for the Senden plant represents a favorable strategy to deal with the desire for more fuel flexibility. Especially the fuel preparation and supply equipment represent a sophisticated technology [9]. The construction of the bio synthetic natural gas plant Gothenburg in Sweden was encouraged by the promising results and findings from the bio synthetic natural gas process and development unit (PDU) in Güssing. The Bio - SNG plant Gothenburg represents the first of its kind plant for industrial scale production of advanced biofuels from woody biomass, whereby methane was identified as the desired end product due to local conditions. In **Table 1** and the main

operational data from Gothenburg can be seen. The operational results show that 20 MW of synthetic natural gas with high purity can be produced from 32 MW of biomass (based on lower heating value) together with additional electricity and operational resources like lime, scrubber solvent, fresh bed material and natural gas [10].

Table 1: Gothenburg input values [10]

Plant input		
Thermal fuel power	32	MW
Biomass fuel (WP)	6250	kg_{db}/h
Biomass water content	50	wt.-%
Electricity consumption	2	MW
Scrubber solvent	70	kg/h
Nitrogen purge gas	4	Nm^3/h
Limestone	110	kg/h
Fresh bed material	65	kg/h
Active carbon	2.7	kg/h
Natural gas	100	Nm^3/h

Table 2: Gothenburg output values [10]

Plant output		
Product gas to methanation	24.5	MW
Synthetic natural gas	20	MW
	1980	Nm^3/h
District heating gasification	2.5	MW
District heating methanation	1.3	MW

Furthermore, an equipment specification by target costing combined with an economic analysis was used to evaluate the developed novel gasification concept to feed a synthetic natural gas production process. As economic analysis tool the net present value calculation method was used. The net present value calculation considers a time span of 20 years and breaks the investment decisions down to a

payment in the presence. The target costing results were used as input values for the optimized option.

3. Results and discussion

Figure 1 shows the IPSEpro simulation sheet for the investigated biomass power plant to feed a synthetic natural gas production process. The IPSEpro simulation sheet was developed out of existing process simulation sheets which origin from the winddiesel_klienIF project and related simulation tasks [11]. These simulation sheets have been continually further developed by various past projects and experiments on this topic and now contain very important and valuable empirical data for the gasification technology process simulation. Thus, the steady growing IPSEpro simulation sheet itself contains a high-quality source for set values. The following main changes compared to the conventional process routes, in terms of the process interconnections, have been made:

- Saturated steam from the methanation process enters the gasification process and is used to heat up the drying air and powers the district heating system.
- The gasification process also provides steam at an elevated pressure level for the methanation process. Therefore, the power demand of the steam generator is high compared to other simulation results from gasification process units. The steam output to the methanation process is realized directly after the steam generator. Subsequently, the raised pressure is relaxed in an expansion valve to the desired steam super heater input pressure.
- A warm water pressure circuit is intended to power the vaporizer and steam generator by using excess

energy from the product gas route and the exhaust gas route. In order to prevent tar condensation in the product gas route as well as vaporization in the warm water circuit itself a pressure of 36 bara is used. These conditions require a narrow temperature window between 200 to 244°C and lead to a correspondingly high circulation flow.

Table 3 shows the used input values for the IPSEpro simulation. The foreseen biogenic fuel includes increased levels of sulfur (S), chlorine (Cl) and nitrogen (N) which leads to an increased formation of hydrogen sulfide (H_2S), hydrochloric acid (HCl) and ammonia (NH_3). This measure is intended to represent the use of low-cost or negative-cost opportunity fuels.

Table 3: IPSEpro simulation input values

Plant input		
Thermal fuel power	16	MW
Biogenic fuel	3250	kg _{db} /h
Initial water content	42	wt.-%
Water content post dryer	20	wt.-%
Scrubber solvent	45	kg/h
Limestone	17.5	kg/h
Fresh bed material	50	kg/h

Table 4 shows the output values for the IPSEpro simulation.

Table 4: IPSEpro simulation output values

Plant output		
Product gas to methanation	11.2	MW
	3265	Nm ³ /h
Initial water content	42	wt.-%
District heating gasification	1.1	MW

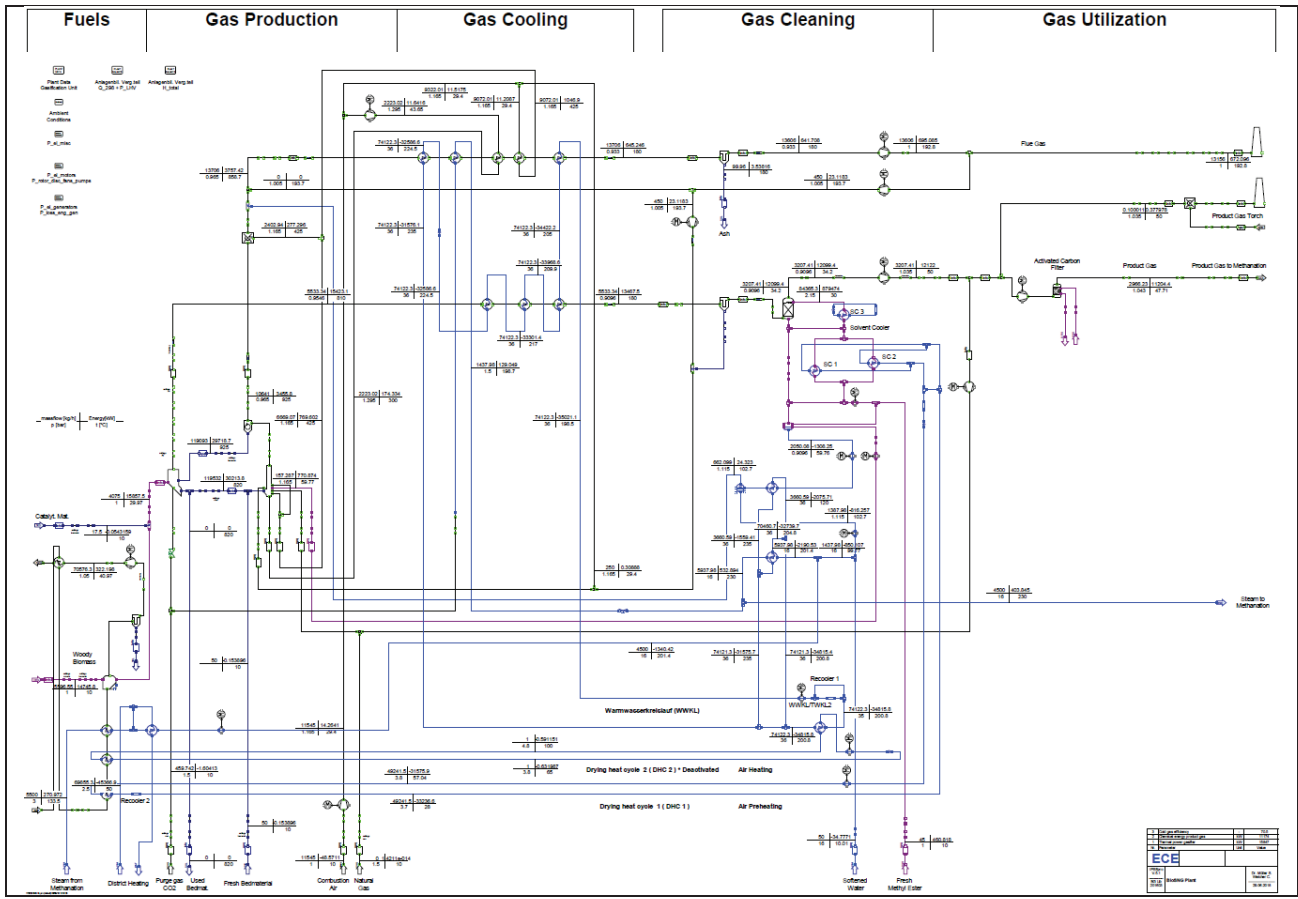


Figure 1: Flow sheet gasification unit to feed the methanation process in IPSEpro

Table 5 shows IPSEpro simulation results across the product gas route including main parameters. The SNG values are derived from the process and development unit (PDU) in Güssing [5] and the SNG output amount originates from the experimental data of Gothenburg [10]. It can be seen that 10 MW of synthetic natural gas can be produced from 16 MW of biomass which indicates an efficiency of approx. $\eta = 64\%$.

Table 5: Product gas route data for the 16MW_{th} biomass gasification system

16MW _{th} gasification unit - product gas route						
	Gasifier out	Filter out	Scrubber out	A-Carb out	SNG	Unit
Chemical energy	12083	12083	12083	11186	10000	kW
Volume flow	6174	6174	3526	3265	990	Nm ³ /h
Water content (H ₂ O)	46.3	46.3	5.9	5.9	0	vol%
Hydrogen (H ₂)	38.6	38.6	38.6	38.6	0.78	vol% _{db}
Carbon monoxide (CO)	24.0	24.0	24.0	24.0	0.13	vol% _{db}
Carbon dioxide (CO ₂)	23.3	23.3	23.3	23.3	0.03	vol% _{db}
Methane (CH ₄)	10.0	10.0	10.0	10.0	94.4	vol% _{db}
Ethene (C ₂ H ₄)	2.5	2.5	2.5	2.5	0	vol% _{db}
Hydrogen sulfide (H ₂ S)	0.05	0.05	0.05	0.0001	0	vol% _{db}
Hydrochloric acid (HCl)	0.01	0.01	0.01	0.001	0	vol% _{db}
Ammonia (NH ₃)	0.3	0.3	0.3	0.0001	0	vol% _{db}
Tar	5.0	4.5	0.1	0.1	0	g/Nm ³

Figure 2 shows the basic flow sheet for the desired process concept to feed a synthetic natural gas production process. The green area marks the biogenic fuel supply to the gasifier. In order to deal with the desired fuel flexibility an appropriate fuel storage, drying, discharge and conveying concept needs to be implemented. As already mentioned, low-cost or negative-cost opportunity fuels lead to the formation of undesired

components in the gasifier. Therefore, the product gas route in blue needs an improved product gas cleaning and preparation strategy. The flue gas route in red has to deal with the mostly increased dust contents of cheaper fuels. The overall target is to produce high quality product gas which has a sufficient H₂ to CO ratio and not contain any catalyst harming substances to feed the subsequent methanation process.

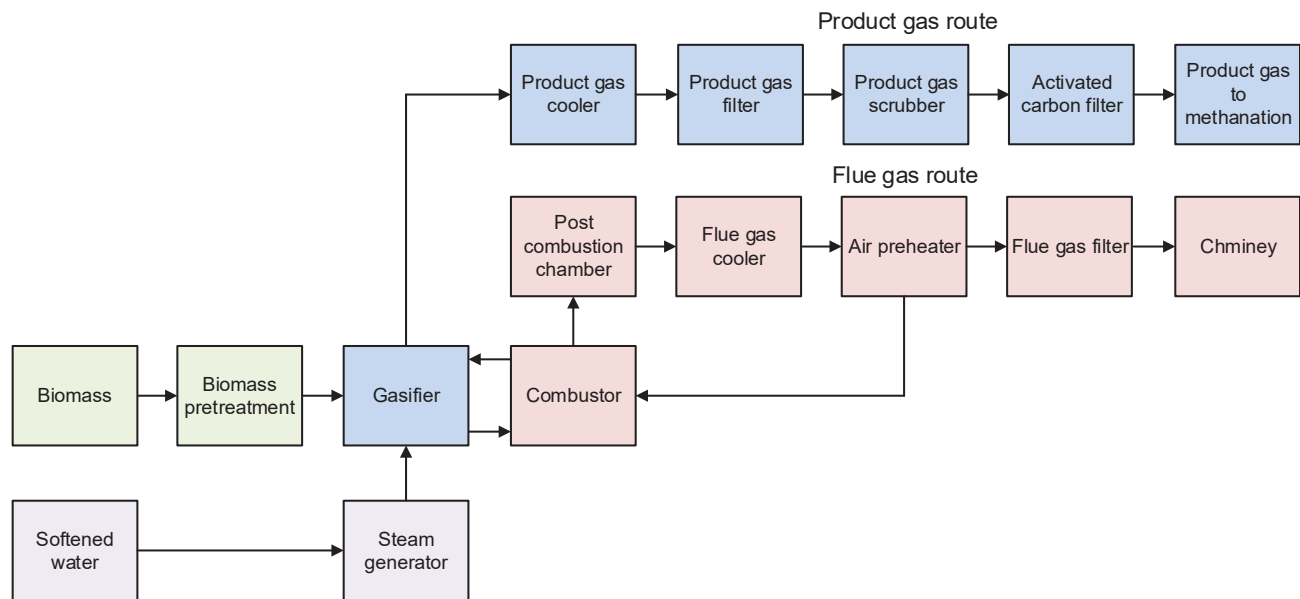


Figure 2: Basic flow sheet

The economic analysis is based on the development strategy, the target costing goals, the mass and energy balances and evaluated cost rates. The development strategy for the novel process concept, marked as “optimized”, contains ambitious goals. The total investment costs, for the combined gasification unit and methanation unit are reduced to 15 mio. Euros while the fuel costs, maintenance costs, insurance costs, labor costs and operation supply costs were decreased by 50%. The ash disposal costs were increased by 25% to consider the usage of low-cost or negative-cost opportunity fuels. These measures were derived out of the target costing goals, discussed in internal meetings with the TU

Wien. **Table 6** shows the net present value calculation for the economic analysis. A reference period of 20 years has been set and a cumulative present value factor of 10 was used. Six options were taken in account for the economic evaluation:

- Option 0: In this case the purchase of natural gas was considered.
- Option 1: The standard SNG powerplant was considered.
- Option 2: The optimized SNG process concept was considered.
- Option 3: The max. investment costs for the optimized concept and 50% fuel costs were calculated.

- Option 4: The max. investment costs for the optimized concept and 67% fuel costs were calculated.
- Option 5: The max. investment costs for the optimized concept and 84% fuel costs were calculated.
- Option 6: The max. investment costs for the optimized concept and 100% fuel costs were calculated.

As can be seen in **Table 6** option 1 cannot compete with option 0. Option 2 has a significantly better result than option 1 and reaches a positive net present value. The reason for this is the novel process concept with the determined improvement ambitions out of the development strategy and the target costing goals.

For Option 3, 4, 5 and 6 the investment costs were raised at different fuel cost levels until the result was equal to Option 0. Thereby the maximum investment costs for the optimized process concept and 50%

fuel costs were calculated with 36 mio. Euros. Increased fuel costs decrease the max. possible invest. costs. Option 3 serves as guideline for an overall economic operation of a gasification unit in combination with a subsequent methanation process unit. Maximum investment costs up to 36 mio. Euros and 50% reduction for the fuel costs, maintenance costs, labor costs and operation supply costs can be derived. The highest share from the reduction of the operational costs is covered by the fuel costs. Therefore, in addition to achieve the given investment costs, the most important task will be to achieve the desired fuel flexibility by the use of low-cost or negative-cost opportunity fuels. It is important to find a biogenic fuel which is available over the whole year and is not subject to high costs and compositional fluctuations. In addition, mixtures of traditional fuels and cheaper fuels could also be considered.

Table 6: Economic analysis

Economic analysis								
Parameter	Unit	Natural gas	SNG	SNG	SNG	SNG	SNG	SNG
		Option 0	Option 1	Option 2	Option 3	Option 4	Option 5	Option 6
Boundaries								
Natural gas demand	MWh/a	77 770						
Wood chips demand	MWh/a		112 000	112 000	112 000	112 000	112 000	112 000
Investment costs incl. Interests	€	0	37 500 000	15 000 000	35 990 970	33 736 233	31 481 496	29 359 391
Expenses								
Fuel costs (Natural gas)	€/a	1 944 250						
Fuel costs (Woodchips or alternatives)	€/a		2 520 000	1 260 000	1 260 000	1 688 400	2 116 800	2 520 000
Sum fuel costs	€/a	1 944 250	2 520 000	1 260 000	1 260 000	1 688 400	2 116 800	2 520 000
Maintenance, insurance, admin., tax	€/a		3 375 000	1 350 000	3 239 187	3 036 261	2 833 335	2 642 345
Labor costs	€/a		490 000	245 000	245 000	245 000	245 000	245 000
Operating supplies	€/a		1 793 327	896 663	896 663	896 663	896 663	896 663
Ash disposal costs	€/a		93 870	117 338	117 338	117 338	117 338	117 338
Sum Operation & Maintenance costs	€/a		5 752 197	2 609 001	4 498 188	4 295 262	4 092 335	3 901 346
Earnings								
District heating	€/a		343 035	343 035	343 035	343 035	343 035	343 035
SNG earnings	€/a		7 070 000	7 070 000	7 070 000	7 070 000	7 070 000	7 070 000
Costs								
Sum (Expenses - Earnings)	€/a	1 944 250	859 162	- 3 544 034	- 1 654 847	- 1 429 373	- 1 203 900	- 991 689
Net present value calculation								
Cumulative present value factor	-	10	10	10	10	10	10	10
Additional investment costs	€	0	37 500 000	15 000 000	35 990 970	33 736 233	31 481 496	29 359 391
Operating expenses savings	€/a	0	1 085 089	5 488 284	3 599 097	3 373 623	3 148 150	2 935 939
Net present value	€	0	-26 649 115	39 882 843	0	0	0	0

4. Conclusion and Outlook

The present work was carried out to investigate the ideal concept for a 16 MW_{th} biomass gasification system to feed a synthetic natural gas production process. Therefore, the most important technical, commercial and legal aspects were taken in account and harmonized. For this purpose, a comprehensive literature research was made first. This research contains the most important information of the gasification technology as well as the state of knowledge and the state of the art technology of large - scale plants. This resulted in the novel process concept. The presented novel process concept provides a good basis for the development of future large-scale biomass power plants to feed a synthetic natural gas production process. Furthermore, the desired fuel flexibility was also investigated and included in the conceptual design. The new concept serves as a further achievement in the long development process chain of the dual fluid gasification technology and may can provide another performance enhancement towards to an overall economic operation. The economic analysis shows that positive net present values can be reached by the novel process concept and that positive revenue surpluses can also be expected. It should be noted, however, that this analysis is based on an ambitious development strategy and target goals and the used expenses and investment costs should be seen as a guideline to achieve an overall economic performance for the dual fluid gasification technology to feed a subsequent synthetic natural gas production process. In particular the total investment costs for a 16MW_{th} biomass gasification system and a subsequent

methanation unit to feed a synthetic natural gas production process, may not exceed 36 mio. Euros while the operational costs should be reduced by 50%. The highest share of the operational costs is represented by the fuel costs and so the most challenging task will be, to find an appropriate low-cost or negative-cost opportunity fuel available the whole year with low compositional fluctuations.

Nevertheless, the thermo-chemical conversion of biogenic fuels still provides a unique method to produce eco-friendly and sustainable energy supply and therefore the technology should be further pushed forward, especially in times of climate change and rising energy demands. Future projects on this topic should further focus on low-cost or negative-cost opportunity fuels to highly valuable synthesis products via gasification. At this point the recently started project ReGas4Industry may be mentioned due to its current research topics in the field of opportunity fuels to highly valuable synthesis products [12]. Furthermore, the development of modern software solutions which can transfer the desired project parameters directly into a finished process conception should be pushed too. Especially the further political strategies, as mentioned the European bioeconomy strategy, offers the opportunity to bring together not only a CO₂ reduced energy source but also a waste treatment facility and a fuel provider for the needed logistics. Indeed, a systemic and more holistic approach is needed to find solutions also for the undoubtable still present economic challenges of this technology.

5. References

- [1] OECD/IEA (2018); World Energy Outlook 2018, IEA.
- [2] Kaltschmitt M., Hartmann H., Hofbauer H., (2009); Energie aus Biomasse: Grundlagen, Technik und Verfahren”, 2 Auflage, Springer-Verlag, Heidelberg, Germany.
- [3] Lazarevic, D., & Valve, H., (2017); Narrating expectations for the circular economy: Towards a common and contested European transition. Energy research & social science, pp60ff.
- [4] Bolhar-Nordenkampf M., (2004); Techno-Economic Assessment on the Gasification of Biomass on the Large Scale for Heat and Power Production, Dissertation, Institute of Chemical Engineering, Vienna University of Technology, p51ff.
- [5] Rehling B., (2012); Development of the 1MW Bio-SNG plant, evaluation on technological and economical aspects and upscaling considerations, p25ff.; p36ff.; p55f.
- [6] Claasen P, Vrije T, Koukious E, Niel E, Eroglu I, Modigell M, Friel A, Wukovits W, Ahrer W., (2010); Non-thermal production of pure hydrogen from biomass—hyvolution. J Clean Prod p1ff.
- [7] Pröll T., (2004); Dissertation, Potenziale der Wirbelschichtdampfvergasung fester Biomasse-Modellierung und Simulation auf Basis der Betriebserfahrung am Biomassekraftwerk Güssing p39ff.
- [8] Kuba M., He H., Kirnbauer F., Boström D., Öhman M., Hofbauer H., (2015); Deposit build-up and ash behavior in dual fluid bed steam gasification of logging residues in an industrial power plant, in Elsevier, Research article, p7ff.
- [9] Kuba M., Kraft S., Kirnbauer F., Maierhans F., Hofbauer H., (2017); Influence of controlled handling of solid inorganic materials and design changes on the product gas quality in dual fluid bed gasification of woody biomass, in Elsevier, Research article, p232ff.
- [10] Thunman H., Seemann M., Berdugo Vilches T., Maric J., Pallares D., Ström H., Derndes G.; Knutsson P., Larsson A., Breitholtz C., Santos O., (2018); Paper: Advanced biofuel production via gasification – lessons learned from 200 man – years of research activity with Chalmers’research gasifier and the GoBiGas demonstration plant, Division of Energy Technology, Chalmers University of Technology, Göteborg Sweden, p7ff.
- [11] Müller, S., Groß, P., Rauch, R., Zweiler, R., Aichernig, C., Fuchs, M., & Hofbauer, H. (2018). Production of diesel from biomass and wind power–Energy storage by the use of the Fischer-Tropsch process. *Biomass Conversion and Biorefinery*, 8(2), 275–282.
- [12] ReGas4Industry, project number: 871732, Energy research project, project partners: TU Wien, Energy & Chemical Engineering GmbH, SMS Group Process Technologies GmbH

Poster Session Abstracts

Hot Metal Production with Reduced Fossil Carbon Usage

S. Müller^{1,*}, L. Theiss¹, M. Hammerschmid¹, J. Fuchs¹,
D.C. Rosenfeld², M. Lehner³, H. Hofbauer¹

1. TU Wien, Institute of Chemical Environmental and Bioscience Engineering; 2. Johannes Kepler Universität Linz, Department of Energy Technology; 3. Montanuniversität Leoben, Department of Environmental and Energy Process Engineering; *corresponding author: stefan.mueller@tuwien.ac.at

Abstract:

The present work describes the results achieved during a study aiming at the full replacement of the natural gas demand of an integrated hot metal production. A novel approach for the implementation of a biomass gasification plant combined with an electrolysis unit was used to substitute the present natural gas demand of an integrated raw iron production plant. Therefore, a simulation platform, including mathematical models for all relevant process units, enabling the calculation of all relevant mass and energy balances was created. As a result, the calculations show that a natural gas demand of about 385 MW can be replaced and additional 100 MW hydrogen-rich reducing gas can be produced by the use of 132 MW of biomass together with 571 MW electricity produced from renewable energy sources.

1. Introduction and Short Description:

The **energy strategy** of the European Union for the future aims at pretending secure, safe and affordable energy. Furthermore, the energy strategy includes the utilization of local available resources, a reduction of greenhouse gas emissions and the development of new innovative energy technologies, as new high performance low-carbon technologies. [1], [2] The production of iron causes significant fossil carbon dioxide emissions. Therefore, numerous researchers investigate the replacement of fossil energy carriers for iron production. Hereby, the replacement of fossil energy carriers should not impair the quality of final products or lead to a reduced availability of the applied production process. So far, following question: Which changes in a hot metal production process would enable the most reasonable reduction of fossil carbon usage based on available technologies? has not been answered. The present work describes the results of investigations aiming at reasonable changes with respect to the

reduction of fossil carbon usage of a hot metal production process. Within the present work a description of the production process is carried out. Furthermore, the present paper discusses:

- the **used concept** for the reduction of fossil-based carbon emissions,
- the **simulation results** achieved,
- and an interpretation of the achieved results with respect to a **large-scale implementation**.

2. Methodology, Results and Discussion

Figure 1 shows the used concept for the creation of an industrial plant model enabling a full replacement of the natural gas supply of a hot metal production. As can be seen, the proposed concept consists of a biomass gasification system, an electrolysis unit, a carbon dioxide removal unit, and a methanation unit. The used **biomass gasification system** is operated as dual fluidized bed gasification system converting woody biomass into a hydrogen-rich gas. Besides, the used operation mode enables the production of

a carbon dioxide-rich gas to follow a carbon capture perspective and enable further utilization, which has been investigated intensively in the last years. [3-5] A detailed description of the used so-called OxySER process can be found in literature. [6], [10] The electrolysis unit is used to provide hydrogen to the overall process allowing **methanation** according to stoichiometric ideal conditions accounting present biogenic carbon as well as recycled **carbon dioxide** from a blast furnace. A carbon dioxide removal unit is used to recycle carbon dioxide from the CO₂-rich blast furnace gas as a feedstock for the methanation process. A detailed description of the process units can be found elsewhere. [7] [8] [9]

3. Conclusion and Outlook

Figure 1 shows the main result of the present work. It was executed to determine possible modifications to enable a significant reduction of fossil carbon dioxide emissions of a hot metal production. The carried-out calculations show that:

- 50 t/h of woody biomass,
- 60 t/h of water,
- and 571 MW of electricity

would be necessary to replace fossil natural gas of the analyzed hot metal production plant. It can be added that 50 t/h of woody biomass would represent about 1% of the primary energy usage of biomass in the energy sector in Austria. [11] Besides, the recycling of 20 000 Nm³/h of carbon dioxide (CO₂) is required to operate the proposed process configuration. The created simulation model indicates valuable data for the design of proposed modifications.

Up-scaling of OxySER to 150 MW, Up-scaling of electrolysis to 600 MW, and long-term methanation test with real gas from hot metal production are recommended to be executed before an implementation at a larger scale. It can be said that a quick acceleration of accompanying implementation steps would be necessary, if there should be any chance to reach the climate targets from the latest Paris Agreement.

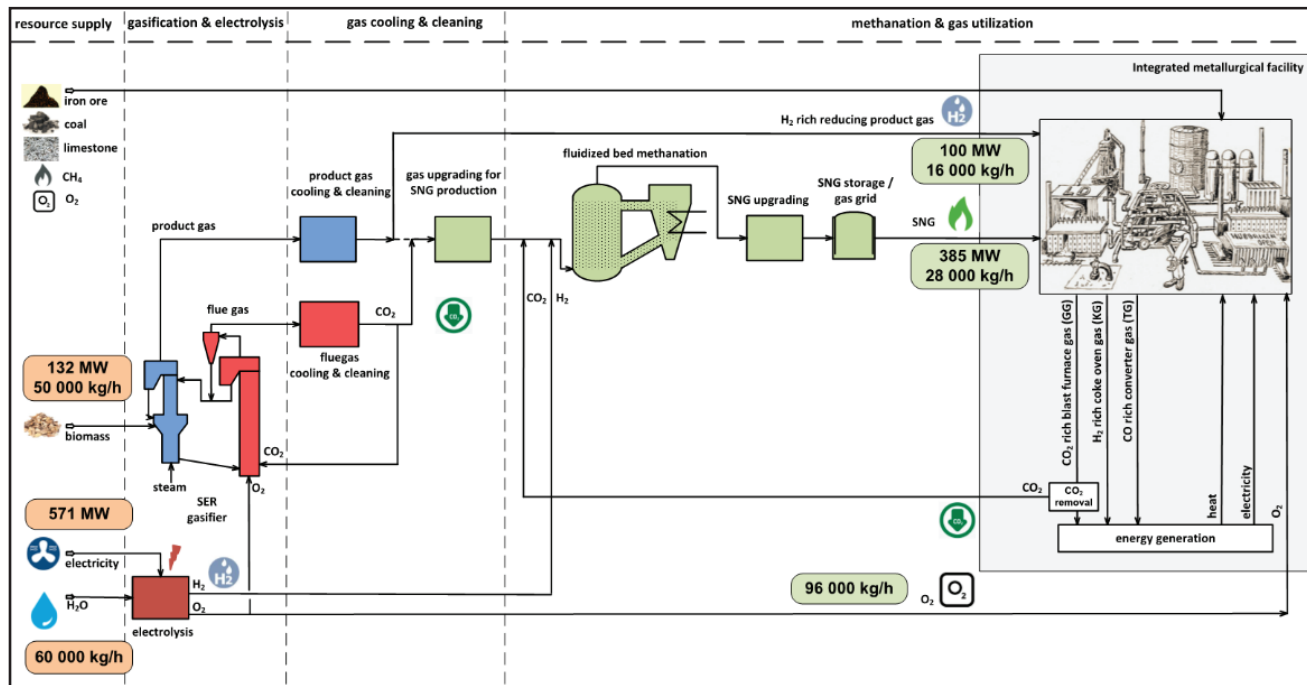


Fig. 1: Hot Metal Production with Reduced Fossil Carbon Usage

Acknowledgement

The present work is part of the research project “Renewable Steel Gases” in cooperation with voestalpine Stahl GmbH, voestalpine Stahl Donawitz GmbH, K1-MET GmbH, JKU Linz and Montanuniversität Leoben. “Renewable Steel Gases” receives financial support by the research program “Energieforschung” funded by the “Austrian Climate and Energy Fund”.

References

- [1] http://europa.eu/legislation_summaries/energy/index_en.htm (read at July 1st, 2019)
- [2] Hofbauer, H., Müller, S., 2018, "Thermochemical conversion of biomass residues to green fuels, electricity and heat", at: COP24 - Katowice Climate Change Conference (UNFCCC), Katowice, December 2018
- [3] Fuchs, J., Schmid, J.C., Müller, S., Mauerhofer, A. M., Benedikt, F., Hofbauer, H., 2019, "The impact of gasification temperature on the process characteristics of sorption enhanced reforming of biomass," Biomass Convers. Biorefinery
- [4] Fuchs, J., Schmid, J.C., Benedikt, F., Müller, S., Hofbauer, H., Stocker, H., Kieberger, N., Bürgler, T., 2018, "The impact of bed material cycle rate on in-situ CO₂ removal for sorption enhanced reforming of different fuel types," Energy, vol. 162, pp. 35–44.
- [5] Fuchs, J., Müller, S., Schmid, J.C., Hofbauer, H., 2019, "A kinetic model of carbonation and calcination of limestone for sorption enhanced reforming of biomass," Int. J. Greenhous Gas Control, vol. 90, no. June, p. 102787, 2019.
- [6] Hammerschmid M., Müller S., Fuchs J., Hofbauer H.; Evaluation of Sorption Enhanced Reforming in Combination with Oxyfuel-Combustion for the sequestration of CO₂, to be published in: Proceedings International Conference on Polygeneration Strategies, 18th – 20th November, Vienna 2019
- [7] Götz, M., Lefebvre, J., Mörs, F., McDaniel, K.A., Graf, F., Bajohr, S., Kolb, T., 2015, Renewable Power-to-Gas: a technological and economic review. Renew Energy 85:1371–1390. <https://doi.org/10.1016/j.renene.2015.07.066>
- [8] Schildhauer, T.J.; Methanation for Synthetic Natural Gas Production – Chemical Reaction Engineering Aspects, in: Synthetic Natural Gas from Coal, Dry Biomass, and Power-to-Gas Applications. New Jersey: John Wiley & Sons Verlag, 2016
- [9] Schöny, G.; Post Combustion CO₂ Capture based on Temperature Swing Adsorption – from Process Evaluation to Continuous Bench Scale Operation, PhD thesis, Institute of Chemical Environmental and Bioscience Engineering, TU Wien 2015
- [10] Fuchs, J., Schmid, J.C., Müller, S., Hofbauer, H., "Dual fluidized bed gasification of biomass with selective carbon dioxide removal and limestone as bed material: A review", Renewable and Sustainable Energy Reviews, Vol. 107 (2019), pp 212-231, <https://doi.org/10.1016/j.rser.2019.03.013>
- [11] Brauner, G.; Systemeffizienz bei regenerativer Stromerzeugung - Strategien für effiziente Energieversorgung bis 2050. Wien: Springer Verlag, 2019, <https://doi.org/10.1007/978-3-658-24854-3>, ISBN 978-3-658-24853-6

Biogas to SNG Demonstration Plant

K.Salbrechter¹, A.R. Medved¹, A. Krammer¹, P. Wolf-Zöllner¹, M. Lehner¹

1. Montanuniversität Leoben, Chair for Process Technology and Industrial Environmental Protection
Franz-Josef-Strasse 18, 8700 Leoben, Austria
*corresponding katrin.salbrechter@unileoben.ac.at

1. Introduction

Following the European climate strategy #mission 2030 Austria will cover 100 % of the national total electricity consumption from renewable energies. The shift from carbon-based energy sources to renewables is indicated through a high increase of wind power and photovoltaic. These technologies require long-term storage options due to the high volatility. The key systems for the storage of fluctuating renewable energies are hydrogen and synthetic natural gas (SNG). Green energy from wind power and photovoltaic is used in water electrolysis for hydrogen production and its subsequent methanation of carbon dioxide for the production of the SNG.

An existing biogas plant in the southern region of Austria is currently operating at half capacity. Coupling it with a load-flexible methanation plant can optimize the generation, storage and utilization of renewable energies. The experimental results of a laboratory scale plant already showed a 100% CO₂ conversion from the input gas to methane and water. [1] [2] [3]

The Renewable Gasfield project combines the hydrogen production via electrolysis and the load-flexible methanation plant on a large scale and its SNG product distribution. For the synthetic natural gas production, ceramic honeycomb nickel catalysts are used. (Fig. 1) To prevent catalyst poisoning the raw

biogas requires pretreatment by adsorption, saving the usually necessary and cost-intensive CO₂ separation.

2. Methodology

In the laboratory methanation plant at the MU Leoben investigations on the necessary stationary operation parameters for the highest possible CO₂ conversion are being explored. Three fixed-bed reactors connected in serial offer a variation of test conditions concerning the composition of the input gas, amount and the material of catalyst, pressure and the flow rate.

Experiments at a pressure level from 7.5 to 10 bar (which corresponds to the optimum pressure for the methanation) with a H₂ surplus from 0 to 10 % and different flow rates are being conducted. All tests are being done with the coated ceramic honeycomb catalysts whereas comparison tests are performed by using a commercial nickel bulk catalyst under the aforementioned conditions.

3. Conclusion and Outlook

The poster will introduce the Renewable Gasfield Project. The first performance results for the methanation process are obtained with a commercial bulk catalyst. For the utilization of wash coated honeycomb catalysts these results constitute an important indication and facilitate the identification of the optimum

operation parameters like pressure level, H₂ surplus and flow rate.

[2]

Kirchbacher f. et al.: Energy 146 (2018) 34-46; doi: 10.1016/j.energy.2017.05.026

4. References

- [1] Biegger P. et al. Energies 2018, 11,1679; doi:10.3390/en11071679

[3]

Kirchbacher et al. ChemEngTrans 52 (2016) 1231-1236; doi: 10.3303/CET1652206

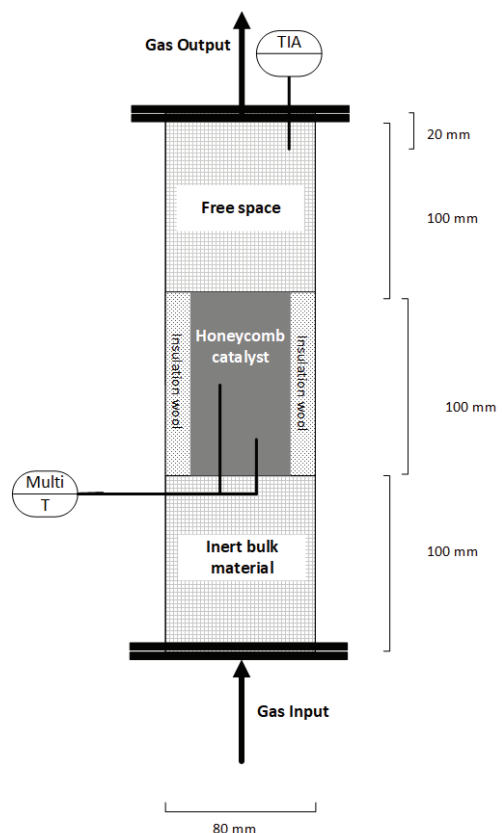


Fig. 1: Scheme of a reactor with honeycomb catalyst loading

Optimization of industrial Bio-SNG production from low-grade fuels

M. Veress^{1*}, A. Bartik¹, F. Benedikt¹, S. Müller¹, H. Hofbauer¹

1. Vienna University of Technology, Institute of Chemical Engineering - Future Energy Technology,
Getreidemarkt 9/166, 1060 Vienna, Austria

*corresponding author, marton.veress@student.tuwien.ac.at

1. Introduction and Short Description:

In the course of the rising energy demand of the world and the simultaneous need for the reduction of harmful emissions, the question arises how mankind can ensure a global sustainable development for the (near) future. With a view to the ambitious target of the Paris Agreement to hold the increase of global average temperature to well below 2°C compared to pre-industrial levels, innovative energy technologies have to be developed to provide safe and affordable energy.

Dual fluid gasification can be named as a promising technology to support the targeted energy strategy. By means of this process solid feedstock can be converted to a mid-calorific product gas with a favorable composition to produce a large variety of end products, such as synthetic natural gas (SNG), Fischer-Tropsch diesel, mixed alcohols, methanol, basic chemicals and hydrogen.

Research and process development on the production of SNG from syngas has been carried out for over 100 years. Still, the process has not proven to be economically competitive, if conventional expensive fuels, like wood, are used. Therefore, the focus of research lies on a successful development of the conversion of residuals and waste materials into a high-value product. However, these cheap alternative fuels, such as sewage sludge, usually show rather unfavorable properties for

gasification and thus lead to technical challenges and limitations.

The aim of this work is to elaborate an optimal process route for Bio-SNG production from low-grade fuels for an industrial plant.

Hence, the discussion and evaluation of the following points are the object of this work:

- the **state of knowledge** for gas cleaning and SNG production
- suggestion of an **optimal process route**
- **simulation results** displaying mass and energy balances
- interpretation of achieved results

2. Methodology, Results and Discussion

The investigations in this work are based on an intensive literature study, operation data from the 100kW_{th} dual fluidized bed pilot plant at TU Wien as well as other commercial plants, and simulation results obtained by the software package IPSEpro.

3. Conclusion and Outlook

The full paper will contain broad results which will be used to evaluate the suggested process route in terms of technical feasibility and economic performance compared to conventional ways of SNG-production.

Modeling steam gasification of biomass with Mathcad 15 via two reaction stages

B. Wojnicka^{1*}, M. Ściążko², J.C. Schmid³

1. AGH University of Science and Technology, 30 Mickiewicza Av., 30-0589 Cracow, Poland

2. Institute for Chemical Processing of Coal, ul. Zamkowa 1, 41-803 Zabrze

3. SMS group Process Technologies GmbH, Daffingerstraße 4, 1030 Vienna, Austria

*corresponding author, bar.wojnicka@gmail.com

1. Introduction

The use of biomass as renewable fuel gives an opportunity to decrease the carbon footprint of the energy sector. Novel gasification technologies ensure the flexible and efficient utilization of different biogenic fuel types. Dual fluidized bed (DFB) gasification is a fast progressing technology for allothermal steam gasification of biomass, developed at TU Wien. [1]

To enable technology scale-up, a model is beneficial, which can deliver reliable process data for reactor design. Therefore, the authors propose a model of biomass steam gasification for a DFB reactor system. The developed model predicts the process gas composition and gasification product yields based on fuel ultimate and proximate analysis and process conditions. The model bases on a closed mass and energy balance. The algorithm was written in Mathcad 15 [2]. It allows for the calculation of heat demand of the gasification reactor and serves as a tool for predicting performance indicating key parameters of the gasification process. The model is validated by experimental results of gasification test runs conducted with the advanced 100 kW_{th} DFB pilot plant at TU Wien [3].

In the DFB reactor system, chips or pellets of biomass are rapidly heated after entering the steam blown gasification

reactor. Before the fuel particles reach the reactor's temperature, they undergo drying and pyrolysis. The pyrolysis process of biomass typically occurs within the temperature range of 250-650 °C. In any case, pyrolysis is already finished when biomass reaches the typical operation temperature of the fluidized bed gasification reactor (ca. 850 °C). The degassed fuel particles end up as solid char. At the same time, the tar produced during pyrolysis starts to decompose with higher temperatures [4]. Gasification of the char from the pyrolysis with steam is the rate-limiting reaction of the entire process in gasification reactor. Steam gasification of char occurs preferably at higher temperatures [5]. In addition, the water-gas-shift reaction and steam reforming of hydrocarbons take place. In a fluidized bed reactor operating at steady-state conditions, all kind of single sub-reaction pathways take place in parallel and influence each other. The overall gasification process inside a fluidized bed is highly complex. Thus, it was aspired to develop a chemical model as simple as possible, nevertheless enabling meaningful results.

2. Model development

The developed model approach of DFB steam gasification of biomass is presented in Figure 1. The proposed model involves two subsequent stages: i) pyrolysis of fuel particles considered as a non-isothermal

process with very high heating rate in the order of thousands of Kelvins per minute, and ii) gasification of the pyrolysis products (char, tar and gaseous components) considered as an isothermal process occurring at the temperature of the gasification reactor. The total heat demand for the process in gasification reactor (Q_t) is the sum of heat demand for the pyrolysis stage (Q_p) and the heat demand for steam gasification of pyrolysis products (Q_g). The oxidation of unconverted residue char in the combustion reactor, serves as the heat source for the overall process in the gasification reactor. The two reactors are connected via circulating solid heat carrier (bed material).

Pyrolysis of biomass is described according to first order devolatilization reaction kinetics extended to describe particular pyrolysis products formation. The pyrolysis model also covers a secondary decomposition of produced tar components. Products of the pyrolysis reactions include pyrolytic gases, steam, benzene, toluene and xylene (BTX), tar and residue char including ash. The model of biomass pyrolysis was based on algorithm for coal pyrolysis developed by Sciazko M. [6].

Primary and secondary pyrolysis products are inputs for the **second stage of gasification**, during which unreacted char, remaining tar, and reactive gaseous components (CO , CO_2 , H_2O , H_2) together with steam are involved in gasification reactions. Three gasification reactions are taken into account: water gas reaction, water gas shift reaction and tar steam reforming according to arbitrary assumed stoichiometry. A pseudo-equilibrium model is applied for calculations – the expressions for equilibrium constants of chosen reactions are corrected by using empirical coefficients accounting for the difference between equilibrium and the

actual state in the reactor. This approach can be considered as an analysis of quasi stationary states. For the sake of model simplicity all other compounds not considered in gasification reactions are assumed to be inert and they are bypassed around the gasification reactions stage. The final process gas is a physical mixture of gaseous components released during pyrolysis and bypassed around gasification reactions stage and those formed or transformed during gasification reactions.

The heat demand for the gasification reactor is calculated as a difference between the total enthalpy of products and the total enthalpy of substrates.

3. Results

Table 1 presents simulation results. The calculated values are validated by measurement results from a gasification test run with a 100 kW dual fluidized bed steam gasifier, wood pellets as fuel, and a catalytic active olivine-limestone mixture as bed material. The relative errors between the simulation and the measurements are below 10% in most cases. The model has a higher error in predicting the tar and BTX contents in the process gas. Nevertheless the main process gas composition is predicted with good accuracy. Moreover, model can serve as a tool for quick and accurate estimation of key parameters indicating process performance (e.g. process gas yield, H_2O conversion, cold gas efficiency, H_2 to CO ratio) for given fuel and process conditions. In addition to the presented validation, also results with other bed material types and gasification temperature were investigated.

4. Conclusion

The proposed model of DFB steam gasification of biomass comprising combination of non-isothermal, kinetic pyrolysis stage and isothermal pseudo-equilibrium stage of pyrolysis products gasification with bypass for some gaseous components presents innovative approach to biomass gasification modeling. It allows for obtaining meaningful results with relatively simple model structure which corresponds to actual process pathway in DFB gasification reactor. The model gives an insight into the process flow by delivering mass and energy balance of all considered stages.

The pyrolysis phase of the model can be used autonomously and serves to predict biomass pyrolysis products yields and the process energy balance.

The pseudo-equilibrium approach in the gasification reactions stage is a good compromise between more detailed but also tedious and complex kinetic models and easy to apply but limited due to

divergence between equilibrium state and the actual state in gasification reactor equilibrium models.

Choosing Mathcad 15 as a simulation tool gives an advantage of flexibility and good control over each step of modeling process. It also favors better understanding of the applied approach, since the entire calculation algorithm has to be introduced equation after equation.

The developed model has a high potential for practical applications. It is a good tool for quick and accurate prediction of yields and compositions of gasification products and estimation of key parameters indicating process performance based on fuel ultimate and proximate analysis and process conditions. However it has limitations regarding prediction of BTX and tar compounds in the process gas stream.

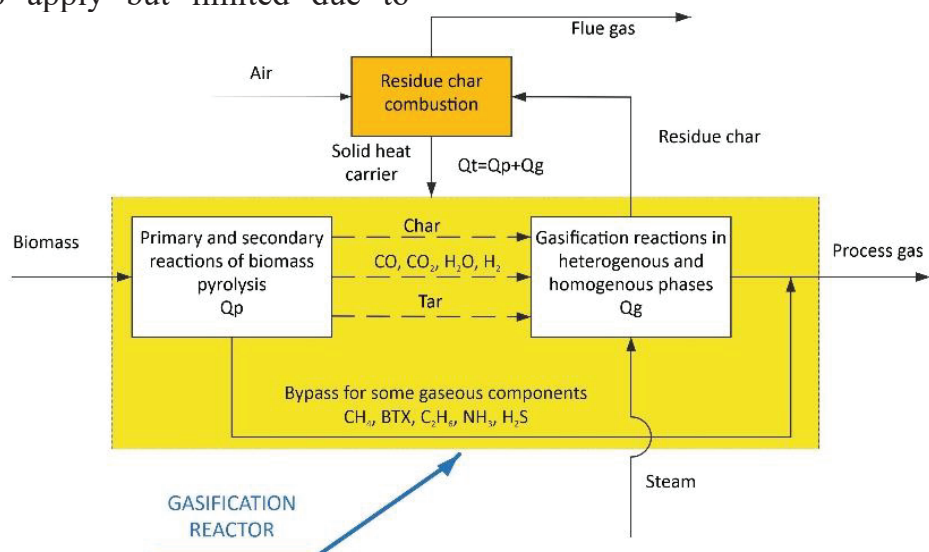


Fig. 1: Model approach of dual fluidized bed steam gasification of biomass (modified from [2])

Table 1 Comparison of experimental and simulation results generated for gasification of soft wood using a mixture (50/50 wt. %) of olivine and calcite as bed material.

Parameter	Unit	Experiment	Simulation	Relative error (%)
H ₂	vol. % dry	43.8	45.1	3.0
CO	vol. % dry	20.9	22.1	5.7

CO₂	vol. % dry	20.8	22.4	7.7
CH₄	vol. % dry	9.43	9.13	-3.2
C_xH_y	vol. % dry	1.03	1.05	1.9
Water in the gas stream	vol. %	31	32	3.2
Dry process gas volume flow	Nm ³ /h	28	28	0.0
Dry process gas yield	Nm ³ /kg _{bio, daf}	1.42	1.40	-1.4
Steam-related H₂O conversion	kg _{H2O} / kg _{H2O}	0.32	0.35	9.4
Fuel-related H₂O conversion	kg _{H2O} / kg _{bio,daf}	0.24	0.28	16.7
Dry process gas lower heating value	MJ/Nm ³	11.4	11.6	1.8
Process gas power	kW	89	89	0.0
Cold gas efficiency	%	87	86	-1.1
Process gas H₂ to CO ratio	-	2.1	2.0	-4.8
Tar content in the dry gas stream	g/Nm ³	3.6	4.0	11.1
BTX content in the dry gas stream	g/Nm ³	15.2	6.8	-55.3
Heat demand for gasification reactor	kW	-	19.34	-

5. References

- [1] Hofbauer H. (2019), “Large Scale Biomass Gasification for Electricity and Fuels”, in: Energy from Organic Materials (Biomass), Springer.
- [2] Wojnicka B. (2018), “Steam gasification with an advanced dual fluidized bed pilot plant at TU Wien” (Master’s Thesis), AGH University of Science and Technology, Cracow, Poland.
- [3] Benedikt F. et al. (2018), “Fuel flexible gasification with an advanced 100 kW dual fluidized bed steam gasification pilot plant”, Energy, Vol.164.
- [4] Schmid J.C. et al., (2016), “First Scientific Results with the Novel Dual Fluidized Bed Gasification Test Facility at TU Wien”, in: Proceedings EUBCE 2016, Amsterdam, Netherlands.
- [5] Di Blasi C., (2009) “Combustion and Gasification Rates of Lignocellulosic Chars”, Progress in Energy and Combustion Science, Vol.35.
- [6] Ściążko M., (2010) “Modele klasyfikacji węgla w ujęciu termodynamicznym i kinetycznym” Wydawnictwa Akademii Górnictwo-Hutniczej im. Stanisława Staszica w Krakowie, Kraków

ISBN 978-3-9503671-1-9

www.icps-conference.org

